GERMINAL CENTERS IN LYMPHOID AND NON-LYMPHOID TISSUES: ADAPTIVE AND EVOLVING STRUCTURES

EDITED BY: Said Aoufouchi, Michel Cogne and Thierry Fest
PUBLISHED IN: Frontiers in Immunology

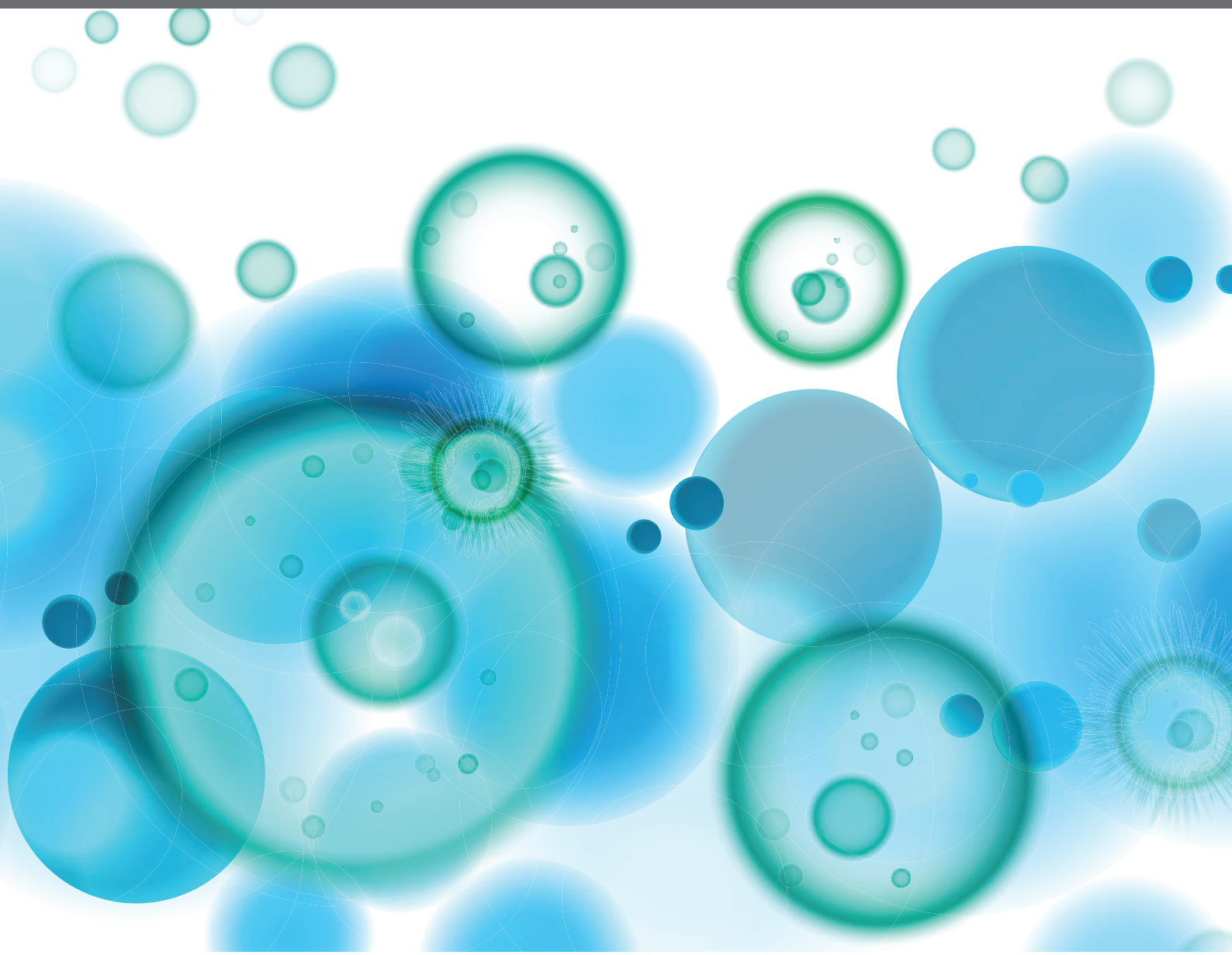

frontiers Research Topics

frontiers

ISSN 1664-8714
ISBN 978-2-88974-959-1
DOI 10.3389/978-2-88974-959-1

About Frontiers

Frontiers is more than just an open-access publisher of scholarly articles: it is a pioneering approach to the world of academia, radically improving the way scholarly research is managed. The grand vision of Frontiers is a world where all people have an equal opportunity to seek, share and generate knowledge. Frontiers provides immediate and permanent online open access to all its publications, but this alone is not enough to realize our grand goals.

Frontiers Journal Series

The Frontiers Journal Series is a multi-tier and interdisciplinary set of open-access, online journals, promising a paradigm shift from the current review, selection and dissemination processes in academic publishing. All Frontiers journals are driven by researchers for researchers; therefore, they constitute a service to the scholarly community. At the same time, the Frontiers Journal Series operates on a revolutionary invention, the tiered publishing system, initially addressing specific communities of scholars, and gradually climbing up to broader public understanding, thus serving the interests of the lay society, too.

Dedication to Quality

Each Frontiers article is a landmark of the highest quality, thanks to genuinely collaborative interactions between authors and review editors, who include some of the world's best academicians. Research must be certified by peers before entering a stream of knowledge that may eventually reach the public - and shape society; therefore, Frontiers only applies the most rigorous and unbiased reviews.
Frontiers revolutionizes research publishing by freely delivering the most outstanding research, evaluated with no bias from both the academic and social point of view. By applying the most advanced information technologies, Frontiers is catapulting scholarly publishing into a new generation.

What are Frontiers Research Topics?

Frontiers Research Topics are very popular trademarks of the Frontiers Journals Series: they are collections of at least ten articles, all centered on a particular subject. With their unique mix of varied contributions from Original Research to Review Articles, Frontiers Research Topics unify the most influential researchers, the latest key findings and historical advances in a hot research area! Find out more on how to host your own Frontiers Research Topic or contribute to one as an author by contacting the Frontiers Editorial Office: frontiersin.org/about/contact

GERMINAL CENTERS IN LYMPHOID AND NON-LYMPHOID TISSUES: ADAPTIVE AND EVOLVING STRUCTURES

Topic Editors:
Said Aoufouchi, UMR 9019 Intégrité du Génome et Cancers, France
Michel Cogne, University of Rennes 1, France
Thierry Fest, University of Rennes 1, France

Citation: Aoufouchi, S., Cogne, M., Fest, T., eds. (2022). Germinal Centers in Lymphoid and Non-Lymphoid Tissues: Adaptive and Evolving Structures. Lausanne: Frontiers Media SA. doi: 10.3389/978-2-88974-959-1

Table of Contents

frontiers in Immunology

EDITORIAL
published: 29 March 2022
doi: 10.3389/fimmu.2022.880733

Editorial: Germinal Centers in Lymphoid and Non-Lymphoid Tissues: Adaptive and Evolving Structures

Michel Cogné[1,2], *Thierry Fest*[2,3] *and Said Aoufouchi*[4,5,6]*

[1] University of Limoges, Limoges, France, [2] University of Rennes 1, Rennes, France, [3] INSERM UMR1236 Microenvironnement, Différenciation cellulaire, Immunologie et Cancer, Rennes, France, [4] UMR 9019 Intégrité du Génome et Cancers, Centre National de la Recherche Scientifique, Villejuif, France, [5] Université Paris-Saclay, Saint Aubin, France, [6] Institut Gustave Roussy, Villejuif, France

Keywords: germinal center (GC) B cell, affinity maturation, humoral immune response, Tertiary Lymphoid Structures (TLS), GC B cell outcomes, cell fate decision, B and T cell interactions, B cell lymphoma

Editorial on the Reseacrh Topic

Germinal Centers in Lymphoid and Non-Lymphoid Tissues: Adaptive and Evolving Structures

Germinal centers (GC) are central places for the development of adaptive immune responses. While their development follows a first wave of extra-follicular activation, they uniquely contribute to the development of long-term responses including both diversified memory B cells with strong ability to activate and differentiate upon antigen re-challenge, and long-lived plasma cells producing high-affinity class-switched antibodies. They are central to protective immune responses against microbial or tumor-associated antigens, but they are also major sites where dealing with peripheral tolerance to autoantigens, programmed cell death and with the hazardous outcomes of DNA lesions inflicted to B-cells.

There is currently no definitive model accounting for all the outcomes of GC formation, since these evolving structures integrate stimulating and inhibitory signals from multiple origins, including antigens, chemokines, cytokines, specific antibody level and they dynamically evolve so that the very same factors initially promoting GC development can later contribute to GC resolution.

In contexts of chronic local inflammation, "GC-like" tertiary lymphoid structures (TLS) have long been reported within some non-lymphoid tissues and they recently received strong attention for their contribution to tumor immunology. They share structural and functional characteristics with GC that form in the secondary lymphoid organs. TLS are induced by persistent infection, autoimmune disorders and cancer. Interestingly in many cancer types, a good correlation has been reported between richness in TLS in tumor site and prolonged patient survival (1, Trüb et al.). The cellular and molecular signals that govern the induction and the fate of TLS in such pathological situations are not well-understood, but are among the hotest research questions in this emerging TLS-Cancer topic with potential for new discovery in B cell focused immunotherapies. We therefore believe that classical GC and TLS structures are the two sides of the general mechanism of immune response and immune surveillance.

In this Research Topic of Frontiers in Immunology, Kennedy and Clark from Chicago University, review the general compartments and connections at work in GCs. In a perspective paper notably commenting conflicting data about the role of hypoxia within the GC, Boothby et al. propose

OPEN ACCESS

Edited and reviewed by:
Harry W. Schroeder, University of Alabama, United States

***Correspondence:**
Said Aoufouchi
said.aoufouchi@gustaveroussy.fr

Specialty section:
This article was submitted to B Cell Biology, a section of the journal Frontiers in Immunology

Received: *21 February 2022*
Accepted: *07 March 2022*
Published: *29 March 2022*

Citation:
Cogné M, Fest T and Aoufouchi S (2022) Editorial: Germinal Centers in Lymphoid and Non-Lymphoid Tissues: Adaptive and Evolving Structures. Front. Immunol. 13:880733. doi: 10.3389/fimmu.2022.880733

standards for analyzing and reporting data sets from GC cells differentiated under variable immunization constraints. This Research Topic additionally reports a multiscale model in which Tejero et al. combine the expected effects of both asymetric divisions of B cells, the network of their cellular interactions and the strength of affinity-based CD40-signalling for determining the outcome of B-cell activation towards either memory MBC) or plasma cells (PC). In this regard, Nakagawa and Calado review the conditions mediating positive selection of light zone(LZ) B-cells and instructing them to be selected as either PCs, MBCs or persistent GC-B cells reentering the dark zone. Santamaria et al. present new experimental data in human showing that this cell fate decision is also impacted by a threshold of IL-4/STAT6 signaling making GC LZ B cells either proliferate and transiently express a MYC-dependent transcriptional program or rather up-regulate BLIMP and instructively progress towards PC differentiation when CD23-dependent signaling becomes lower. Lemarié et al. also show induction of the unfolded protein response genes as a very early event at the pre-plasmablastic stage.

Going deeper into the diversity of cell interactions, Lu and Craft review recent evidence about the contribution of Tfr cells in the balance between productive immune responses and B cell memory and the maintenance of homeostasis for avoiding immunopathology.

Rivas et al., analyzing both murine models and data from human DLBCL patients, provide new evidence about the caretaker role of the cohesin complex in genomic stability of GC B-cells. They notably show that cohesin ATPase subunit Smc3 haploinsufficiency favors malignant transformation, through gene repression and impaired enhancer-promoter interactions, with loss of epigenetic modifiers (TET2 or KMT2D) preventing B-cell exit from the GC reaction and their commitment to plasma cell differentiation.

Schmiedel et al., using a Brg-1 deficient model, also provide data showing that ATPase, Brg1 and the BAF chromatin remodeling complex, are required for enhancer-promoter interactions which promote cell cycle-related gene expression during GC formation.

Dauba and Khamlichi review into much details the long -range promoter-enhancer interactions within the IgH locus which promotes chromatin remodeling and synapses between target switch sequences in a B-cell stimulation-dependent manner in order to support CSR. Dalloul et al. additionally provide new evidence that the process of Cclass switch recombination (CSR) can initiate even in the absence of the activation induced cytidine deaminase (AID) enzyme as an intrinsic ability of an appropriately conformed IgH locus to undergo recombination, so that AID is rather catalyzing and boosting CSR rather than initiating CSR in GC B-cells. Fuertes et al. finally review the role of multiple microRNAs (miRNAs) in the regulation of Tfh and GC B-cell responses as well as in B cell neoplasia and GC response dysregulation.

It altogether appears that cell fate decisions from GC B cells integrate both the quality and the cumulative amounts of signals that they have received from the Ag and their local microenvironment, following an instructive model, and their intrinsic ability to be committed to proliferation or differentiation, with cell death as another major fatal outcome of B cell activation and AID induction (2–4).

AUTHOR CONTRIBUTIONS

All authors listed have made a substantial, direct, and intellectual contribution to the work, and approved it for publication.

REFERENCES

1. Sautès-Fridman C, Verneau J, Sun C-M, Moreira M, Chen TW-W, Meylan M, et al. Tertiary Lymphoid Structures and B Cells: Clinical Impact and Therapeutic Modulation in Cancer. *Semin Immunol* (2020) 48:101406. doi: 10.1016/j.smim.2020.101406
2. Péron S, Laffleur B, Denis-Lagache N, Cook-Moreau J, Tinguely A, Delpy L, et al. AID-Driven Deletion Causes Immunoglobulin Heavy Chain Locus Suicide Recombination in B Cells. *Science* (2012) 336:931–4. doi: 10.1126/science.1218692
3. Dalloul I, Boyer F, Dalloul Z, Pignarre A, Caron G, Fest T, et al. Locus Suicide Recombination Actively Occurs on the Functionally Rearranged IgH Allele in B-Cells From Inflamed Human Lymphoid Tissues. *PLoS Genet* (2019) 15: e1007721. doi: 10.1371/journal.pgen.1007721
4. Mayer CT, Gazumyan A, Kara EE, Gitlin AD, Golijanin J, Viant C, et al. The Microanatomic Segregation of Selection by Apoptosis in the Germinal Center. *Science* (2017) 358. doi: 10.1126/science.aao2602

Conflict of Interest: The authors declare that the research was conducted in the absence of any commercial or financial relationships that could be construed as a potential conflict of interest.

frontiers in Immunology

ORIGINAL RESEARCH
published: 05 February 2021
doi: 10.3389/fimmu.2020.620716

Multiscale Modeling of Germinal Center Recapitulates the Temporal Transition From Memory B Cells to Plasma Cells Differentiation as Regulated by Antigen Affinity-Based Tfh Cell Help

Elena Merino Tejero[1‡], Danial Lashgari[1‡], Rodrigo García-Valiente[1], Xuefeng Gao[2], Fabien Crauste[3], Philippe A. Robert[4†], Michael Meyer-Hermann[4,5], María Rodríguez Martínez[6], S. Marieke van Ham[7,8], Jeroen E. J. Guikema[9], Huub Hoefsloot[10] and Antoine H. C. van Kampen[1,10]*

[1] Bioinformatics Laboratory, Epidemiology and Data Science, Amsterdam Public Health Research Institute, Amsterdam Institute for Infection and Immunity, Amsterdam, Netherlands, [2] Department of Hematology and Oncology, International Cancer Center, Shenzhen University General Hospital, Shenzhen University Health Science Center, Shenzhen, China, [3] Université de Paris, CNRS, MAP5 UMR 8145, Paris, France, [4] Department for Systems Immunology and Braunschweig Integrated Centre of Systems Biology, Helmholtz Centre for Infection Research, Braunschweig, Germany, [5] Institute for Biochemistry, Biotechnology and Bioinformatics, Technische Universität Braunschweig, Braunschweig, Germany, [6] IBM Research Europe, Zürich, Switzerland, [7] Department of Immunopathology, Sanquin Research and Landsteiner Laboratory, Amsterdam UMC, University of Amsterdam, Amsterdam, Netherlands, [8] Swammerdam Institute for Life Sciences, University of Amsterdam, Amsterdam, Netherlands, [9] Department of Pathology, Lymphoma and Myeloma Center Amsterdam (LYMMCARE), Amsterdam University Medical Centers, Amsterdam, Netherlands, [10] Biosystems Data Analysis, Swammerdam Institute for Life Sciences, University of Amsterdam, Amsterdam, Netherlands

Germinal centers play a key role in the adaptive immune system since they are able to produce memory B cells and plasma cells that produce high affinity antibodies for an effective immune protection. The mechanisms underlying cell-fate decisions are not well understood but asymmetric division of antigen, B-cell receptor affinity, interactions between B-cells and T follicular helper cells (triggering CD40 signaling), and regulatory interactions of transcription factors have all been proposed to play a role. In addition, a temporal switch from memory B-cell to plasma cell differentiation during the germinal center reaction has been shown. To investigate if antigen affinity-based Tfh cell help recapitulates the temporal switch we implemented a multiscale model that integrates cellular interactions with a core gene regulatory network comprising BCL6, IRF4, and BLIMP1. Using this model we show that affinity-based CD40 signaling in combination with asymmetric division of B-cells result in switch from memory B-cell to plasma cell generation during the course of the germinal center reaction. We also show that cell fate division is unlikely to be (solely) based on asymmetric division of Ag but that BLIMP1 is a more important factor. Altogether, our model enables to test the influence of molecular

OPEN ACCESS

Edited by:
Thierry Fest,
University of Rennes 1, France

Reviewed by:
Masaki Hikida,
Akita University, Japan
Paolo Casali,
University of Texas Health Science Center at San Antonio, United States

***Correspondence:**
Antoine H. C. van Kampen
a.h.vankampen@amsterdamumc.nl

†Present address:
Philippe A. Robert,
Department of Immunology,
University of Oslo, Oslo, Norway

‡*These authors share first authorship*

Specialty section:
This article was submitted to B Cell Biology, a section of the journal Frontiers in Immunology

Received: *23 October 2020*
Accepted: *21 December 2020*
Published: *05 February 2021*

Citation:
Merino Tejero E, Lashgari D, García-Valiente R, Gao X, Crauste F, Robert PA, Meyer-Hermann M, Martínez MR, van Ham SM, Guikema JEJ, Hoefsloot H and van Kampen AHC (2021) Multiscale Modeling of Germinal Center Recapitulates the Temporal Transition From Memory B Cells to Plasma Cells Differentiation as Regulated by Antigen Affinity-Based Tfh Cell Help. Front. Immunol. 11:620716. doi: 10.3389/fimmu.2020.620716

modulations of the CD40 signaling pathway on the production of germinal center output cells.

Keywords: multiscale model, plasma cell differentiation, T follicular helper cell, CD40 signaling, germinal center

INTRODUCTION

Germinal centers (GCs) are anatomical structures located inside B-cell follicles within secondary lymphoid organs that play an important role in the adaptive immune system (1, 2). Through subsequent rounds of cell proliferation, somatic hypermutation (SHM) and positive selection the B-cell receptor (BcR) is optimized for antigen (Ag) binding in a process called affinity maturation. This eventually results in the development of memory B-cells (MBCs) and plasma cells (PCs) that produce high affinity antibodies (Abs), which provide an effective immune protection. GCs comprise two functional zones. In the dark zone (DZ) centroblasts (CBs) rapidly proliferate and accumulate SHMs in the genes that encode their BcR. The light zone (LZ) is mainly characterized by the presence of centrocytes (CCs), follicular dendritic cells (FDCs) that present Ag in the form of immune complexes to GC B cells (3), and T follicular helper (Tfh) cells. CCs capture and internalize Ag through their BcR in an affinity-dependent manner triggering survival signals. Subsequently, the Ag is processed by the CCs resulting in class II MHC-peptide complexes (pMHCII) presented to the Tfh cells. Hence, B cells compete in an affinity-dependent way for interaction with Tfh cells, facilitating CD40 and cytokine signaling to become positively selected. Positively selected CCs may return to the CB state and recycle to the DZ to undergo further rounds of proliferation and SHM. Alternatively, positively selected CCs may differentiate to MBCs or PCs (4–8). Recently, it was also shown that GC B-cell migration influences PC development (9) The cellular and molecular mechanisms that regulate PC and MBC differentiation remain largely unknown, while such knowledge would crucially advance our understanding of GC-associated diseases such as B-cell lymphomas and autoimmune disorders. In this research we present a multiscale computational model (MSM) integrating molecular and cellular mechanisms to investigate PC differentiation.

In vivo studies in which Tfh-dependent positive selection of CCs was triggered in a BcR-independent fashion using the DEC205 surface lectin indicated that the interaction of CCs with Tfh cells critically determines positive selection and subsequent generation of PCs (10, 11) Other studies suggested that BcR signaling, but not Tfh interaction, initiates PC differentiation (12–15). The role of BcR signaling in PC differentiation is supported by the observation that long-lived PCs in bone marrow produce high-affinity Abs that contain many SHMs (13, 16–18). Smith and co-workers showed that the extend of affinity maturation of MBCs and PCs differs for NP hapten-specific B-cell responses typically resulting in high-affinity PCs and low-affinity MBCs (18). Other work suggested a temporal switch during the GC reaction resulting in the production of MBCs primarily during the early GC phase while long-lived bone-marrow (BM) PCs are generated at later stages (19). In support, Shinnakasu and co-workers showed that lower affinity cells at earlier stages of the GC reaction are favored to enter the MBC compartment and also suggested that high-affinity GC B cells are preferentially selected to enter the cell-cycle and undergo PC differentiation (20).

Previously, an agent-based model (ABM) was developed that assumes that all CCs positively selected by Tfh cells subsequently recycle to the DZ for further proliferation, mutation and differentiation (2). Experimental evidence for this model was in part provided by demonstrating PC precursors in the DZ (13, 21, 22). This computational model was dubbed LEDA (LEave the GC through the DArk zone) and distributes the captured Ag asymmetrically during cell division to the daughter cells. The Ag-retaining cells differentiate into PCs and leave the GC (2). Other models were investigated in this paper, such as LEDAX, in which the decision about differentiation is already taken during the interaction with Tfh cells in the LZ irrespective of asymmetric division. A probabilistic decision is made after symmetric division in the DZ to decide if the B-cell differentiates to an output cell or heads for another round of selection. Nevertheless, we wanted to test the effect of asymmetric division on PC differentiation and, therefore, we used the LEDA model as a starting point. However, direct experimental evidence that asymmetric division determines cell fate is lacking.

A large body of research focuses on the molecular mechanisms underlying PC and MBC differentiation including epigenetics (23–25), the role of various transcription factors (TFs), and gene regulatory networks (GRN) [e.g., (26–29)]. Our MSM is built on a core GRN comprising three TFs (BCL6, IRF4, and BLIMP1) that are directly involved in PC differentiation. The TF B lymphocyte induced maturation protein 1 (BLIMP1) is essential for PC differentiation and regulates a large number of target genes required for the function of these cells (30). For example, BLIMP1 represses class II transactivator (CIITA) and activation-induced cytidine deaminase (AID), thereby inhibiting Ag presentation and GC associated AID-dependent Ig gene diversifications, respectively (30, 31). BLIMP1, however, may not initiate PC differentiation which has been suggested to start by down-regulation of the Paired Box 5 (PAX5) and B-cell lymphoma 6 (BCL6) proteins, which supports the theory that BcR signaling, resulting from BcR – Ag interaction, initiates this process (13). BcR signaling results in the repression of BCL6 (32), which is an important factor for BcR diversification and sustained cell proliferation. However, other studies have shown that Interferon regulatory factor 4 (IRF4) initiates plasmablast (PB) differentiation by inducing expression of BLIMP1 (33, 34). This does not exclude the possibility that BcR signals are involved in increasing IRF4

levels. CD40 signaling, resulting from CC – Tfh interaction, upregulates IRF4, which subsequently activates BLIMP1 and leads to PC differentiation. In PCs, IRF4 can also bind to its own promoter to create a positive feedback mechanism that maintains high IRF4 expression and, consequently, BLIMP1 expression (35). BLIMP1 is generally considered to repress gene expression but it may also induce gene expression of IRF4 and other genes (30). BCL6 is highly expressed in GC B cells and inhibits both the expression of BLIMP1 and IRF4. BCL6 binds to its own promoter to inhibit its own transcription thereby resulting in an autoregulatory negative feedback loop (36). In turn, BLIMP1 and IRF4 repress BCL6, which is down-regulated in PC differentiation.

It is challenging to integrate the cellular and molecular mechanisms involved in PC differentiation since details about the effect of cellular interactions through signaling on the underlying molecular networks are not known in full detail. Conversely, the effect of GRN states on cell behavior or phenotype also remains to be elucidated in more detail. Moreover, these mechanisms operate at different time scales. One way of proceeding is to model (affinity dependent) signals resulting from cellular interactions that affect the underlying GRN, which in turn determines cell fate. We present a MSM integrating molecular and cellular mechanisms to investigate PC differentiation. In particular, we integrate two pre-existing and published computational models: the cell-based LEDA model (2) and a differential equation-based GRN including BCL6, IRF4, and BLIMP1 (37). This GRN model considers BcR and CD40 signals delivered to the B cells but it assumes that only the CD40 signal initiates and progresses differentiation. Other (cytokine-driven) signals during B/T-cell interactions are neglected in our model. Our MSM integrates and investigates asymmetric division and (affinity-based) CD40 signaling in PC differentiation.

Using this model we show that affinity-based CD40 signaling in combination with asymmetric division result in MBC and PC generation in accordance with the temporal switch. In contrast, a constant strong CD40 signal does only result in PCs, while a constant weak signal results in MBC output throughout the GC reaction. We also conclude that cell fate division is unlikely to be (solely) based on asymmetric division of Ag since this does not result in the differentiation of all high-level BLIMP1 B-cells. Vice versa, PCs differentiated on the basis of high BLIMP1 levels are a mixture of cells with and without internalized Ag indicating that not only Ag retaining cells engage in differentiation. We propose experiments to validate our computational findings. Altogether, our model enables to test the influence of molecular modulations of CD40 signaling pathway onto the production of MBC and PCs.

METHODS

Computational Model at the Cellular Level

The MSM that we developed is an extension of the pre-existing "hyphasma" model, which is a detailed ABM of the GC that simulates the behavior of individual GC cells and their interactions (**Figure 1A**) (2, 38). Under the so-called LEDA hypothesis it assumes that output cells exit the GC from the DZ after asymmetric division. Here, we summarize the relevant

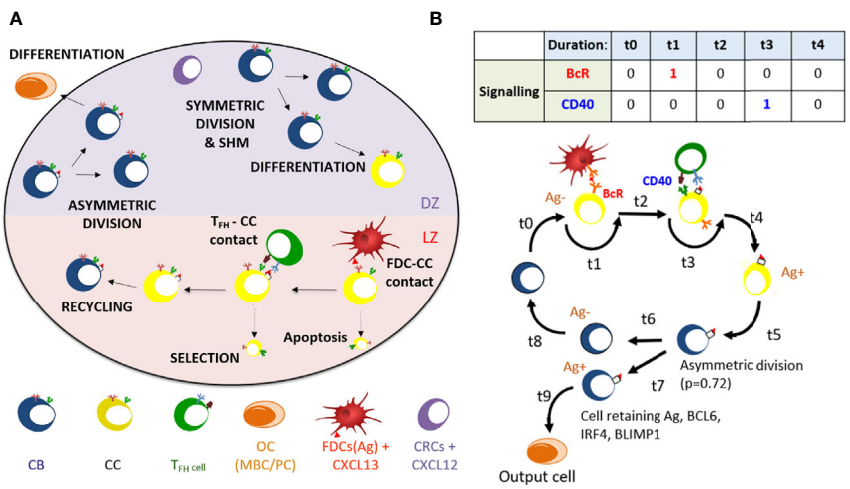

FIGURE 1 | **(A)** Overview of cellular processes in the ABM. In an established GC a dark zone (DZ) and a light zone (LZ) are distinguished. CBs and CCs prefer to move in the direction of the CXCL12 and CXCL13 chemokines produced by the CRCs and FDCs respectively. Tfh cells prefer to move towards the LZ. FDCs carry Ag that can be captured by CCs. CCs may be positively selected through interaction with Tfh cells after which they can recycle to the dark. In the DZ the CB will (a) symmetrically divide. After cell division, an output cell is produced, or the cell differentiates to a CC. Cells die through apoptosis if they do not interact with the FDC and Tfh cells. **(B)** Schematic overview of the BcR and CD40 signaling events during the GC reaction. Durations *t* indicate non-fixed time intervals (cell states). At the end of each interval the concentrations of BCL6, IRF4, and BLIMP1 are updated using the differential equations. A CB (Ag–; blue cell) differentiates to a CC (Ag–; yellow cell) within a time duration *t0*. The CC interacts with the FDC for a time duration *t1* during which BcR signaling occurs. Subsequently, CD40 signaling is active for duration *t3* during B-cell – Tfh interaction. Successful interaction will result in an Ag+ cell. Asymmetric division occurs with a probability p=0.72. Differentiation of CB to a CC always initializes the CC to Ag–.

aspects of this model. The model simulates a GC reaction for 21 days (504 h) at a time resolution of 0.002 h (7.2 s). Parameters for the ABM in our simulations are provided as **Supplementary Files** (parameters 1–5.txt). The GC is represented as a three-dimensional sphere of grid points with N=64 grid points in each direction (lattice constant = 5 μm). This grid hosts agents that represent CCs, CBs, Tfh cells, and FDCs. In addition, pre-calculated gradients of CXCL12 and CXCL13 chemokines are imposed on this grid. Originally, the ABM was initiated with a fixed number of three founder B cells (2). However, in our simulations we assumed a continuous influx of, on average, 2 cells per hour in the first 96 h resulting in approximately 100 founder cells accounting for the observation that early GCs are highly polyclonal (39, 40). The behavior in terms of division, differentiation, interaction, and cell death between these cells is defined by a set of rules. CBs, CCs and Tfh cells move according to persistent random-walk based on chemokine gradients, while FDCs have a fixed position on the grid. The affinity of the BcR is defined as the Manhattan distance (L1 norm) between the BcR and the Ag within a four dimensional "shape space" (41, 42). This distance represents the minimum number of SHMs required for the BcR to acquire maximum affinity for the Ag. Hence, the BcR sequence is not explicitly encoded but rather the shape space position of a B-cell determines its BcR affinity. SHM moves the BcR one step in the shape space thereby increasing or decreasing the distance to the Ag, which is converted to an affinity value between 0 and 1 using a Gaussian weight function. The discrete nature of the shape space translates to 25 discrete affinity values (**Supplementary Figures 1** and **2**).

In the model, B cells (CBs) proliferate in the DZ while accumulating BcR mutations, and migrate as CCs to the LZ where they can interact with FDCs to capture Ag with a rate depending on the BcR affinity. This provides survival signals to the CCs and rescues them from apoptosis. Higher affinity CCs will capture more Ag and, subsequently, will outcompete lower affinity CCs for Tfh interaction to become positively selected. If the Tfh interacts with many B cells at a time it will signal to the one with highest amount of internalized Ag. The positively selected CCs are recycled into CBs and migrate to the DZ for further rounds of division and SHM. The number of divisions of recycled CBs depends on the amount of captured Ag during the selection process. During cell division the Ag is asymmetrically distributed in 72% of the cell divisions (43). Daughter cells that receive the captured Ag differentiate to output cells after one or more divisions and exit the GC. Daughter cells that did not receive Ag cycle back to the LZ as CCs. Daughter cells of CBs that divide symmetrically receive half of the Ag and both become CCs.

Computational Model at the Molecular Level

Martinez and co-workers developed a computational model representing a core GRN involved in PC differentiation (**Figure 2A**) (37). This model includes three TFs, i.e., BCL6, BLIMP1 and IRF4 that are modeled by ordinary differential equations (ODEs). The level of these genes is controlled by the BcR and CD40 signals (**Supplementary Information**, Equations 1 to 5; **Supplementary Table 1** lists the parameter values for the model). This GRN represents a bistable system with one state (BCL6 high, BLIMP1/IRF4 low) denoting the CBs/CCs and a second state (BLIMP1/IRF4 high, BCL6 low) representing PCs (**Figure 2B**).

GC B cells integrate upstream signals from BcR and CD40 signaling pathways. When a BcR signal is induced through binding with the Ag, then BCL6 is degraded. However, its level is rapidly restored to the initial steady state (BCL6 high) when the signal is removed (unbinding of Ag). The CD40 signal induced during interaction with a Tfh cell increases transcription of IRF4 which in turn increases the level of BLIMP1. This results in the PC phenotype (BLIMP1+) This

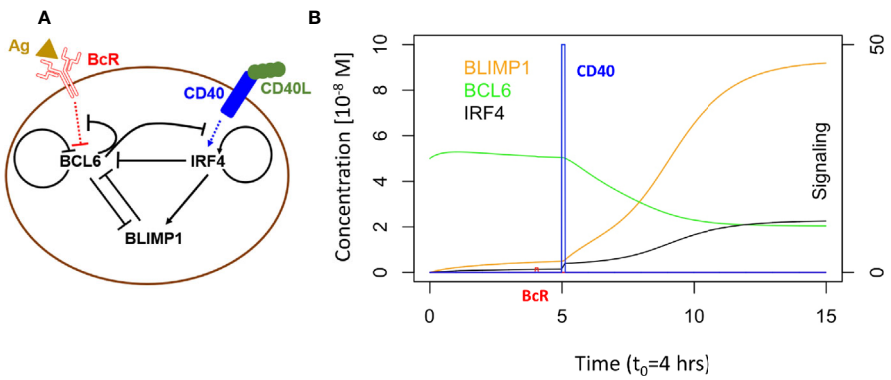

FIGURE 2 | **(A)** B-cell with GRN and signaling events. Arrows indicate activation. Bar-headed lines denote inhibition. BCL6 is inhibited upon binding of the Ag to the BcR. IRF4 is activated upon binding of CD40L to CD40 during Tfh – B-cell interaction. **(B)** GRN temporal dynamics upon binding of Ag and CD40L. Each time unit represents 4 h. The protein levels of BCL6 (blue), IRF4 (black), and BLIMP1 (orange) have units of 10^{-8} M and are shown over an interval of 60 h. The BcR signal (red) and CD40 signal (green) are present for a short duration (*t1* and *t3* in **Figure 1B**). BcR signaling results in a slight temporary change in TF concentrations. In contrast, CD40 signaling results in a switch of all TF levels going from a B-cell to a PC (BLIMP1+) phenotype (in approximately 40 h in this example). CD40 signal intensity in the multiscale model varies between 0 and 50. BcR signal is fixed to 1.

state is irreversible due to the positive autoregulatory feedback of IRF4 and the cooperative binding of the TFs to the DNA.

Multiscale Model

To enable the investigation of cellular and molecular mechanisms involved in PC differentiation we integrated the ABM and the GRN through the embedding of the GRN (set of ODEs) in each individual B-cell and output cell of the ABM (**Figure 3**). This was achieved by adding additional properties (ODEs (initial) TF levels, and BcR/CD40 signal) to each agent (cell) of the ABM.

Founder cells and daughter cells resulting cell division are initialized with the same initial concentrations for BCL6, IRF4, and BLIMP1. The cell-based ABM and the GRN model operate at different time scales, e.g., weeks and hours respectively. Consequently, the relatively fast changes in the GRN affect the longer term outcome on the cell level. This is accomplished by updating the TF concentrations at every time step (7.2 s) of the ABM while taking into account transcription and degradation rates, and using the levels of the TFs of the previous time point as initial values for the ODEs. If a CC binds to the FDC (**Figure 1B**) it receives a constant BcR signal (bcr0 = 1 in the ODE) for the duration *t1* of binding. If the CC binds to a Tfh cell it will receive a CD40 signal (see below) for the duration *t3* of binding. BcR and CD40 signals never occur simultaneously because binding to the Tfh cell only occurs after detaching from the FDC.

It has been shown that TFs may distribute unequally in daughter CBs after division (44). Consequently, it has been hypothesized that asymmetric division may affect cell fate. Therefore, the MSM allows for asymmetric division of both Ag and the TFs with a probability of 0.72 (2, 43). Following asymmetric division, the TF concentrations become zero in one daughter cell while the other daughter cell assumes the concentration from the parent cell. In a symmetric division the TF and Ag concentrations in both daughter cells are set to half the concentrations of the parent cell.

Tfh Facilitated CD40 Signaling

The MSM considers a constant or an affinity-based CD40 signal by defining cd40 (see **Supplementary Information Equations 1–5; Supplementary Table 1**). The magnitude of the constant signal was set to 50 to ensure that after Tfh contact the BLIMP1 level of the B-cell sufficiently increases to eventually differentiate to a PC while also maintaining typical GC dynamics (e.g., CB and CC cell count profiles). For the affinity-based signal we assume that higher affinity B cells capture more Ag and present more pMHCII to Tfh cells resulting in an increased Tfh – B-cell interaction and, therefore, an increased CD40 signaling. The affinity-based CD40 signal was defined by setting cd40=affinity*50. Since affinity assumes values between 0 and 1, the CD40 signal has a strength between 0 and 50. This ensures that at maximum affinity the B-cell will always differentiate into a

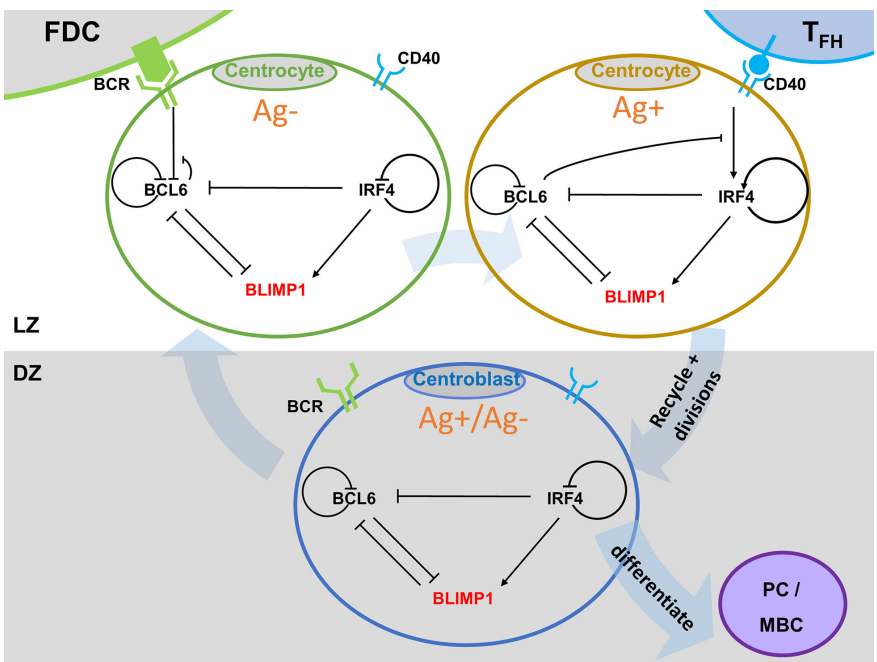

FIGURE 3 | Multiscale model for PC differentiation. The cellular model (ABM) and molecular GRN (ODE) models are integrated by embedding the GRN in each B-cell and output cell of the ABM. Signals through the BcR (FDC interaction) and CD40 (Tfh interaction) change the state (TF concentrations) of the GRN which is updated at every time step of the ABM. A positively selected CC becomes Ag+ by definition. In scenario 1 simulations an Ag+ cell differentiates to an output cell after asymmetric cell division. In scenario 2, sufficient CD40 signaling may increase BLIMP1 levels to obtain a PC phenotype (BLIMP1+). For precise cell type definitions see **Table 2** and **Supplementary Figures 6–8, 20**.

PC while at lower affinities MBCs will be produced (see below). Note that in simulations 3 and 4 (see below) higher values of the CD40 signal results in PC differentiation even after symmetric division (which reduces the BLIMP1 level by 50%) because the BLIMP1 level will rapidly return to its high-level equilibrium value due to the positive autoregulatory feedback of IRF4 that also remains at a relatively high level (**Supplementary Figures 3–5**).

Simulations

Table 1 shows the five simulations that were performed. The parameters for each simulation are provided as **Supplementary Files**. Scenario 1 simulations 1 and 2 represent a model in which asymmetric division of Ag determines cell fate. The Ag-retaining daughter cell (Ag+) differentiates to an output cell. In these simulations we tracked the CD40 signaling and the levels of the TFs but the GRN does not affect the fate of the B-cell and, therefore, does not affect the outcome of the simulation. However, after completion of scenario 1 simulations we inspect the BLIMP1 level of the output cells to define a PC and MBC subset (see cell definitions below and **Supplementary Figure 20**). Scenario 2 simulations 3, 4, and 5 represent the model in which we use the BLIMP1 level to decide on cell fate. In these simulations cells with a high BLIMP1 concentration will differentiate to PCs regardless of the Ag state (Ag+ or Ag–) of the cell. For both cell-fate decision rules we compare results obtained with a constant and affinity-based CD40 signal. In simulation 5 we use a constant CD40 signaling with cd40 = 10. All simulations are terminated after 21 days. In the result section we present the outcome of these 5 individual simulations. However, we also repeated simulation 3 and 4 30 times with different random seeds, which shows that the amount of variability observed in the temporal dynamics (**Supplementary Figures 16–19**) is limited. Also the resulting variability in the reported percentages is very low (standard error <0.01, most standard deviations <1%; **Supplementary Tables 3** and **4**). Scenario 1 simulations were not repeated but a similar amount of variability is expected.

Definition of (output) Cells

Table 2 shows the definition of cell types in scenario 1 (Ag+ decision rule) and scenario 2 (BLIMP1+ decision rule) simulations. **Supplementary Figures 6 to 8** and **20** provide further explanation. In scenario 2, we do not explicitly discriminate between MBCs and PCs but define "output" cells solely on the basis of its Ag status, i.e., the daughter cells that retains the Ag after asymmetric division (Ag+ cell) differentiates to an output cell (2). In a post-simulation step we use the BLIMP1 level to classify the output cells to PCs (Ag+ and BLIMP1+; $\geq 8 \times 10^{-8}$ M) and MBCs (Ag+ and BLIMP1–; $<8 \times 10^{-8}$ M). We have defined MBCs in this way because a BLIMP1– cell does not represent a PC while in this model an Ag+ cell was defined as an output cell. Although this is not an ideal MBC definition it correctly recapitulates the MBC dynamics as observed in Weisel and co-workers (19). In the MSM a recycled CB is, by definition, Ag+ and goes through one or multiple rounds of divisions prior to differentiation to an output cell. Consequently, Ag+ cells represent a mixture of recycled CBs, dividing cells, and output cells. In scenario 1, dividing Ag+ cells that have the potential to become a PC (i.e., Ag+/BLIMP1+) are annoted as PBs to allow a further discrimination between cell states in the model. In scenario 1, Ag– output cells are non-existent by definition and, hence, all Ag– cells are CBs or CCs. In scenario 2, cells may become a PC if they are BLIMP1+ irrespective of its Ag status and, consequently, PCs may either be Ag+ or Ag–. BLIMP1+ cells that are not (yet) output cells are annotated as PB (Ag+ or Ag–). In scenario 2, Ag+/BLIMP1– output cells are considered to be MBCs.

TABLE 1 | Definition of simulations.

		CD40 signal	
		Constant	**Affinity-based**
Decision rule for differentiation	**Ag inheritance** (scenario 1)	Simulation 1 (CD40 = 50)	Simulation 2
	BLIMP1 level (scenario 2)	Simulation 3 (CD40 = 50) Simulation 5 (CD40 = 10)	Simulation 4

TABLE 2 | Definition of cell types based on Ag status and BLIMP1.

		Scenario 1		Scenario 2	
		BLIMP1+	**BLIMP1–**	**BLIMP1+**	**BLIMP1–**
Output cell	**Ag+**	PC	MBC	PC	MBC
Not output cell	**Ag+**	PB	CB	PB	CB
Output cell	**Ag–**	NA	NA	PC	NA
Not output cell	**Ag–**	CB/CC	CB/CC	PB	CB/CC

NA, not applicable.

Software

The MSM was implemented in C++ and simulations were done on a MacOS Mojave 10.14.5 operation system. Run times of a single simulation take approximately 8 h on a single core of an Intel Core i7 processor. Model repetitions were carried out on the Dutch national e-infrastructure with the support of SURF Cooperative (www.surfsara.nl). Output files of the simulation were analyzed in R (Core Team, 2019) version 3.5.3 using various libraries: forcats (0.5.0), purr (0.3.4), tidyr (1.0.3), tibble (3.0.1), ggplot(2_3.3.0), tidyverse (1.3.0), viridis (0.5.1), viridisLite (0.3.0), ggnewscale (0.4.1), readr (1.3.1), dplyr (0.8.5). The MSM is available from GitHub (https://github.com/EDS-Bioinformatics-Laboratory/MSM_PCdifferentiation).

RESULTS

Ag Inheritance-Based GC Output with Constant and Strong CD40 Signal Exclusively Produces PCs (Scenario 1)

We wondered how the levels of BLIMP1 compared to internalized-Ag status (Ag+ or Ag–) in GC B-cell population when CD40 signal

was constant and strong. This served as a reference for scenario 2 simulations (**Table 1**). The scenario 1 model is based on the hypothesis that Ag-retaining (Ag+) cells differentiate to a mixture of PC and MBC output cells. This theory in which asymmetric division drives PC differentiation resulting in PCs from the earliest stages of the GC reaction seems incompatible with the experimentally observed temporal switch (19). **Figure 4A** shows the overall dynamics of simulation 1. The CB and CC counts show a typical GC response with the total cell count approximating about 3800 cells at 142 h (6 days). **Figure 4B** shows the DZ-to-LZ ratio, which fluctuates around 2 in agreement with *in vivo* experiments (11). **Figure 5A** shows the number of PCs during the GC reaction, which by definition emerge from the very initial stages of the GC reaction. **Figure 5C** shows that the affinity of these PCs increases during the course of the GC reaction.

Table 3 shows the percentages of (output) cells at day 21 of the simulation. The full tables and cell counts are listed in the **Supplementary File Counts_and_Percentages.xlsx**. Inspection of the BLIMP1 level of the output cells facilitates post-simulation differentiation between PCs (Ag+/BLIMP1+) and MBCs (Ag+/BLIMP1−). During the GC reaction, about 5% (15,136 cells) of all CCs (290,291) differentiate to a PC (Ag+/BLIMP1+) while no MBCs (Ag+/BLIMP1−) are generated because the constant but strong CD40 signaling enforces high BLIMP1 levels for Ag+ cells. A fraction of PB (Ag+/BLIMP1+) cells do not develop into output cells due to symmetric cell division, which generates two Ag− daughter cells (**Supplementary Figure 7**). The subset of Ag− cells (CBs and CCs), which are not output cells nor PBs comprise a mixture of BLIMP1+ and BLIMP1− representing 12 and 62% of all cells respectively. Consequently, an additional maximum of 12% (36,124 cells) could potentially have developed into a PC if BLIMP1 level was considered as a criterion for differentiation. **Figure 6A** shows the distribution of PCs (Ag+/BLIMP1+), PBs (Ag+), and CCs/CBs (Ag−/BLIMP1−, Ag−/BLIMP1+). No MBCs are produced. CCs and CBs are distributed over all affinity classes and have BLIMP1 levels below the threshold ($<8 \times 10^{-8}$ M) that defines PCs. PCs (high BLIMP1 level) emerge from the early stages but their number and affinity increases with time. Finally, the figure shows an increasing number of Ag+ cells that increase in affinity over time but do are not output cells. About 79% of the subset of Ag+ cells did not develop into output cells despite their high BLIMP1 levels. In addition, about 17% of the Ag− cells are BLIMP1+.

In summary, the scenario 1 model with constant CD40 signaling simulation produces PCs of low to high affinities but no MBCs due to the strong CD40 signal. Approximately 75% of the PCs are generated after the peak response of the output cells (**Figure 5A**; **Supplementary Figure 9**) and are of relatively high affinity due to ongoing affinity maturation (**Figure 5C**). A large fraction of the Ag+ cells are BLIMP1+ while most Ag− cells are BLIMP1−. Considering BLIMP1 levels of the Ag− cells, a larger number of PCs should potentially have been generated.

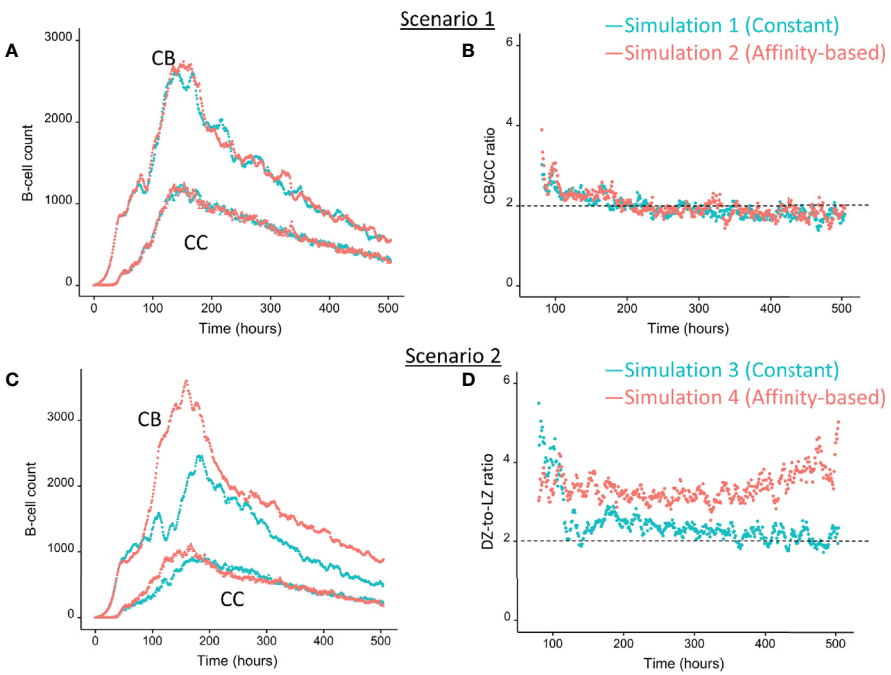

FIGURE 4 | Overall GC dynamics with constant CD40 signal (CD40 = 50; blue) and affinity-based CD40 signal (red). **(A)** Scenario 1. Number of CBs (top curves) and CCs (bottom curves). **(B)** Scenario 1. DZ-to-LZ ratio calculated from CB and CC counts. **(C)** Scenario 2. Number of CBs (top curves) and CCs (bottom curves). **(D)** Scenario 2. DZ-to-LZ ratio calculated from CB and CC counts.

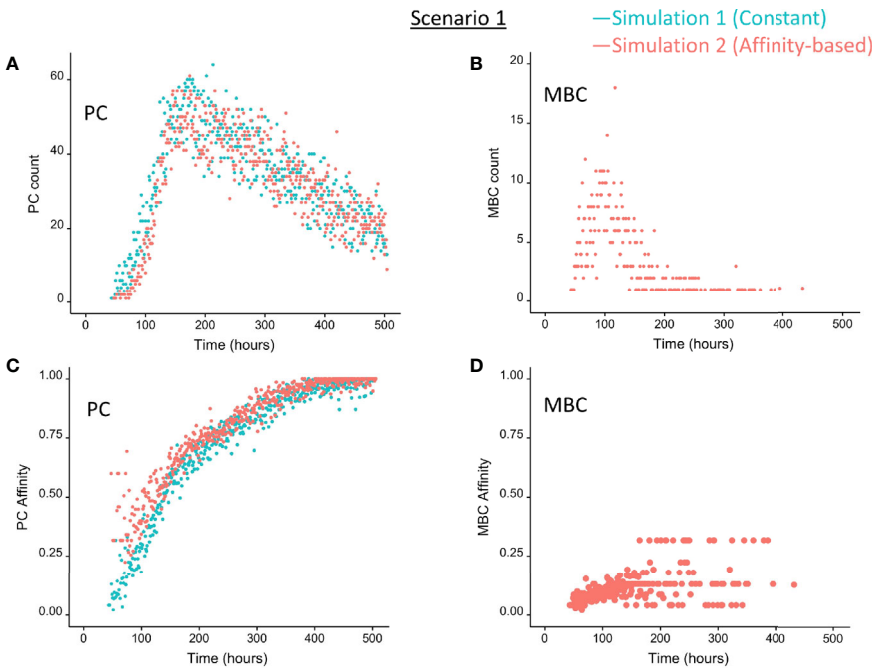

FIGURE 5 | Output cells for scenario 1 simulations with a constant CD40 signal (CD40 = 50; blue) or affinity-based CD40 signal (red). **(A)** Number of PCs, **(B)** number of MBCs, **(C)** PC affinity, and **(D)** MBC affinity during GC reaction. Post-simulation inspection of BLIMP1 levels of the output cells (Ag+) allows to discriminate between PCs (Ag+/BLIMP1+) and MBCs (Ag+/BLIMP1−). No MBCs are produced with a constant CD40 signal.

TABLE 3 | Percentages of cell types at day 21.

	Scenario 1		Scenario 2		
	Constant CD40 = 50	Affinity-based	Constant CD40 = 50	Affinity-based	Constant CD40 = 10
PC	5	5	14	13	3
PB	20	19	28	26	18
MBC	0	0.3	0	0.3	2
CB/CC	75	76	58	61	77
	100.0	100.0	100.0	100.0	100.0

Ag Inheritance-Based GC Output With a Strong Affinity-Based CD40 Signal Enables the Production of Both PCs and MBCs (Scenario 1)

Since no MBCs (Ag+/BLIMP1−) were generated in simulation 1, we wanted to investigate the effect on output cell subsets (post-simulation) when applying an affinity-based CD40 signal to control the levels of BLIMP1. In this simulation (simulation 2), the generation of output cells is still fully determined by Ag inheritance after asymmetric division and, consequently, CD40 signaling nor BLIMP1 level affects the cell fate or GC reaction. Consequently, the overall dynamics of this simulation is approximately the same as for the first simulation (**Figure 4**). Difference in overall dynamics result from stochasticity in the model. **Figures 5A, C** show the number of PCs and corresponding affinity during the GC reaction. **Figures 5B, D** show the number of MBCs (Ag+/BLIMP1−) and affinity respectively. In contrast to simulation 1, low affinity MBCs are generated during the earlier phase of the GC response and generation of PCs seems slightly delayed although stochasticity in the model prevents a firm conclusion. The number of PCs at the end of the GC reaction is similar to simulation 1 (5% of all cells corresponding to 14,303 cells; **Table 3**). In addition, 833 (0.3%) MBCs were generated. The number of PBs, CCs, and CBs is similar to simulation 1. Also in this simulation an additional 35,159 Ag− cells (12% of all cells) could potentially have developed into a PC if the BLIMP1 level was used as a decision rule for PC differentiation during the simulation. **Figure 6B** shows that MBCs are of low affinity, have BLIMP1 levels below the PC threshold ($<8 \times 10^{-8}$ M) and are generated during the early phase of the GC response. Increased affinity abolished MBCs as a result of increasing BLIMP1 level resulting in a transition to PCs with BLIMP1 levels above the threshold. We also observe that at affinity=0.25 a larger number of Ag+ cells with intermediate BLIMP1 levels occur, which is a consequence of affinity-based signaling in which cells that have weaker CD40 signaling more slowly increase their BLIMP1 levels. About 75% of the subset of Ag+ cells did not develop into output cells despite high BLIMP1 levels. In addition, about 16% of the Ag− cells are BLIMP1+.

In summary, affinity-based CD40 signaling simulation produces a mixture of early lower affinity MBCs followed by

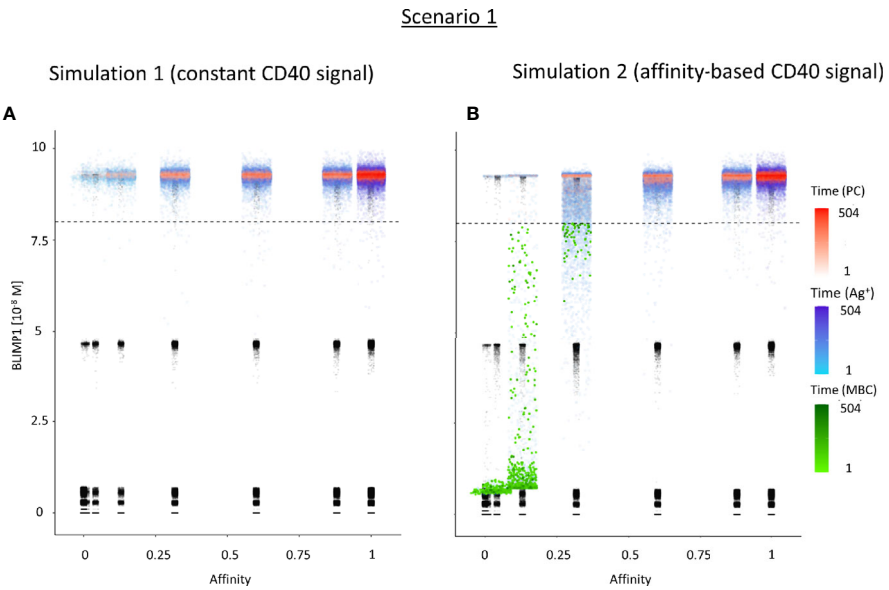

FIGURE 6 | Distribution of PCs, MBCs, and Ag+ (but not PC/MBC) cells with respect to their affinity, BLIMP1 level, and time of generation for scenario 1 simulations. **(A)** Simulation 1 with a constant CD40 signal (CD40 = 50). All output cells are PCs (no MBCs are generated). **(B)** Simulation 2 with an affinity-based CD40 signal. Output cells are mainly MBCs during the early GC reaction for B cells with affinity levels between 0 and 0.25. As the GC reaction progresses and B-cell affinity increases, BLIMP1 levels consequently rise above the threshold leading to a switch in the GC output towards mainly PCs for affinity levels between 0.25 and 1. Each dot represents a cell. Black dots represent cells other than PCs, MBCs, Ag+. Color gradient represents time from 1 to 504 h. Affinity assumes discrete values. Dotted line represents the BLIMP1 threshold (8×10^{-8}M) for PC differentiation. Intermediate BLIMP1 levels arise mainly due to symmetric division of cells with high BLIMP1 level. Since values are recorded only in case of an event (e.g., cell division, Tfh interaction, differentiation) and because of steep curve of the BLIMP1 profile after Tfh-cell contact, BLIMP1 levels seem restricted to particular values but are not. Low and high BLIMP1 levels represent steady-states. Jittering of affinity values has been applied to prevent too many overlapping data points but causes some overlap of the lower affinity classes.

later higher affinity PCs. Approximately 76% of the PCs are generated after the peak response of the output cells (**Figure 5A**) while 85% of the MBCs are produced prior to the peak response (**Figure 5B**; **Supplementary Figure 11**). This temporal shift is in agreement with recent findings (19). Overall, we see that a large fraction of Ag+ non-output cells are BLIMP1+ and, therefore, a larger number of PCs should potentially have been generated.

BLIMP1 and Ag-Defined Fate Decisions Do Not Lead to MBC Generation Under Strong Constant CD40 Signal (Scenario 2)

We then wondered whether we could determine cell fate based on the coupling of BLIMP1 level and Ag status under a strong constant CD40 signal. In this simulation (simulation 3), the generation of PCs is fully based on BLIMP1 levels and does not take Ag status into account, i.e., subsequent to a series of cell divisions the CBs with high BLIMP1 levels (≥8 M) differentiate to PCs (Ag+BLIMP1+ or Ag–BLIMP1+). In addition, Ag-retaining cells with low BLIMP1 levels (<8M) differentiate to MBCs (Ag+BLIMP1–). **Figure 4C** shows the overall GC dynamics, which is similar to scenario 1 simulations but the DZ-to-LZ ratio slightly increased (**Figure 4D**). The effect of stochasticity on the overall GC dynamics and the DZ-to-LZ ratio is limited as shown from repeated simulations in **Supplementary Figures 16** and **17**. **Figures 7A, C** show the number of PCs and corresponding affinity. No MBCs are produced in this simulation due to strong CD40 signaling that enforces high BLIMP1 levels and, consequently, only PCs are generated. This was not surprising considering simulation 1. However, the number of PCs at the end of the GC reaction is about a factor 3 larger compared to simulation 1 (14% of all cells corresponding to 38,684 cells; **Table 3**). The number of PBs is slightly larger compared to the simulation 1 while the number of CBs and CCs are slightly reduced. Approximately 33% of all BLIMP1+ cells (115,310) differentiate to PCs and about two-third of these cells are Ag–. The distribution of PCs, and Ag+ cells (**Figure 8A**) is similar compared to simulation 1 (**Figure 6A**) but PCs now assume BLIMP1 levels ranging from 8 to about 9 while in simulation 1 all Ag+ output cells assumed the highest possible BLIMP1 level (i.e., ~9). The bimodal distribution is observed since some CBs will differentiate immediately when the BLIMP1 level passes the threshold while other cells may engage in one or more cell divisions giving BLIMP1 additional time to reach its maximum value.

In summary, the MSM allows to couple the decision for differentiation based on both BLIMP1 level and Ag status. With a constant strong CD40 signaling the scenario 2 simulation produces only PCs of low to high affinities but no MBCs. Substantially more PCs are generated in comparison to simulation 1 and 72% of these PCs are generated after the peak response of the output cells (**Figure 7A**; **Supplementary Figure 10**), which are of relatively high affinity (**Figure 7C**). The

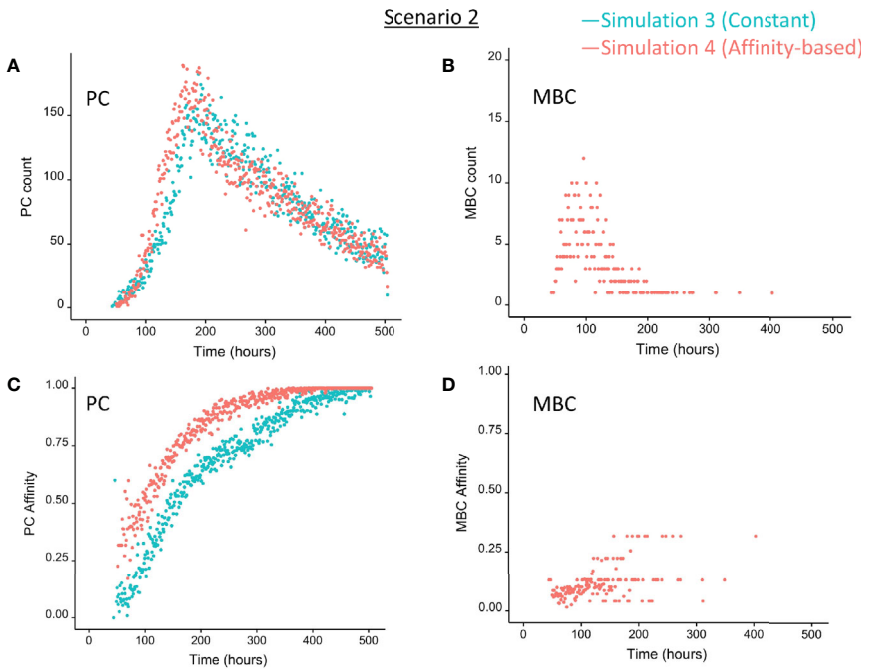

FIGURE 7 | Output cells for scenario 2 simulations with a constant CD40 signal (CD40 = 50; blue) or affinity-based CD40 signal (red). **(A)** Number of PCs (Ag+ BLIMP1+, Ag–BLIMP1+), **(B)** number of MBCs (Ag+BLIMP1–), **(C)** PC affinity, and **(D)** MBC affinity during GC reaction. No MBCs are produced with a constant CD40 signal.

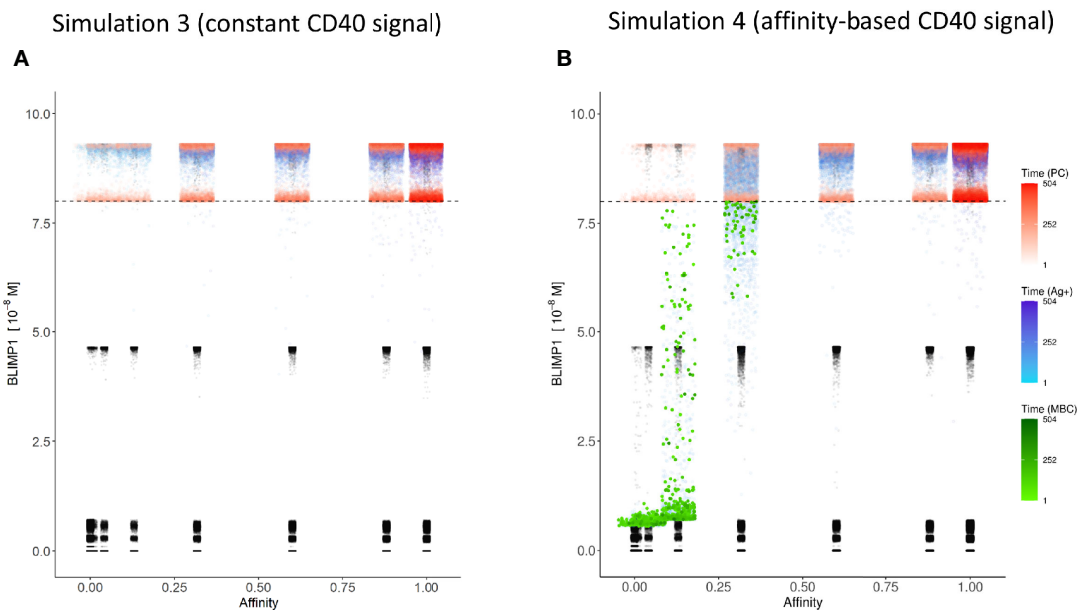

FIGURE 8 | Distribution of PCs, MBCs, and Ag+ (but not PC/MBC) cells with respect to their affinity, BLIMP1 level, and time of generation for scenario 2 simulations. **(A)** Simulation 1 with a Constant CD40 signal (CD40 = 50). All output cells are PCs (no MBCs are generated). **(B)** Simulation 2 with an affinity-based CD40 signaling. Output cells are mainly MBCs during the early GC reaction, which then switches to PC production. For a further description see **Figure 6**. In **(A)** and **(B)** PCs (red) are generated accross all affinity levels.

slight increase in DZ-to-LZ ratio implies that the transzone migration rates in scenario 2 are no longer in full agreement with the patterns observed in (11).

BLIMP1– and Ag-Defined Fate Decisions Under a Strong Affinity-Based CD40 Signal Produce MBCs and Show a Temporal Switch (Scenario 2)

Considering no MBCs were generated under strong constant CD40 signal we wondered whether the decision for differentiation based on BLIMP1 level and Ag status under an affinity-based CD40 signal produces both PCs and MBCs. The overall GC dynamics of this simulation (simulation 4) is shown in **Figure 4C** which are clearly different from simulation 3 in which a constant CD40 signal was used. The number of CCs is similar, but the number of CBs largely increased resulting in an increased DZ-to-LZ ratio to approximately 3 to 4 (**Figure 4D**). The effect of stochasticity in the model on GC dynamics and DZ-to-LZ ratio is shown in **Supplementary Figures 18 and 19** for 30 repetitions. **Figure 7A** shows that the number of PCs in simulation 3 (38,684 cells) and simulation 4 (35,670) is similar but, overall, the PCs have a higher affinity (**Figure 7C**). Affinity-based signaling results in the generation of MBCs of low affinity mostly during the early phase of the GC response (**Figures 7B, C**). The number of PCs at the end of the GC reaction is approximately a factor 2.5 larger compared to simulation 2 that also involved affinity-based signaling (13% of all cells; **Table 3**). The percentage of MBCs (0.3%; 781 cells) is comparable to simulation 2. This corresponds to 0.5% of all BLIMP1– cells. Similar to simulation 3, approximately 33% of all BLIMP1+ cells (107,943) differentiate to a PC and about two-third of these cells are Ag–. The distribution of PCs, MBCs, and Ag+ cells is shown in **Figure 8B**.

In summary, in scenario 2, the affinity-based CD40 signaling simulation produces PCs and a small fraction of MBCs. However, substantially more PCs are generated in comparison to scenario 1. 75% of these PCs are generated after the peak response of the output cells while 89% of the MBCs are produced prior to this peak and are of lower affinity. (**Figure 7**; **Supplementary Figure 12**). Although we now observed a temporal shift there is a significant increase in the DZ-to-LZ ratio indicating transzone migration rates that are not in agreement with (11). We also observed that a substantial fraction of the PCs are Ag– indicating that the decision for PC differentiation should not (fully) be based on Ag status.

BLIMP- and Ag-Defined Fate Decisions Under Weak Constant CD40 Signal Produce MBCs But Fail to Show a Temporal Switch (Scenario 2)

In simulation 3, we used a strong and constant CD40 signal (cd40 = 50) that prevented the generation of MBCs because Tfh cell help will always sufficiently increase the BLIMP1 level to exclusively result in PC differentiation. In contrast in simulation 4 we allowed the CD40 signal to vary with affinity resulting in a temporal switch from MBCs to PCs. Since an constant high-level is not realistic (i.e., no MBCs are produced) we questioned if we could generate both MBCs and PCs by using a constant but lower CD40 signal (cd40 = 10; simulation 5). In this simulation the overall GC dynamics is similar to the other simulations (**Supplementary Figure 14A**). The DZ-to-LZ ratio fluctuates around a value of 2 (**Supplementary Figure 14B**). The total number of cells during the course of the GC reaction is comparable to the other simulations. Compared with simulation 3, a constant and weak CD40 signaling indeed results in the generation of MBCs and even increased five-fold (2%; 5,048 cells) at the expense of a lower number of PCs (3%; 10,204 cells; **Supplementary file Counts_and_Percentages.xlsx**). However, since the CD40 signal strength does not change over time this simulation does not result in a temporal switch but a steady but low production of MBCs throughout the GC reaction (**Supplementary Figure 13**). We also observe that only Ag+ BLIMP1+ and no Ag–BLIMP1+ PCs are generated reflecting that cells that divided symmetrically result in daughter cells with BLIMP1 and IRF4 concentrations that are never high enough to return to the BLIMP1+ state. **Figure 9** shows the distribution of the PCs, MBCs and Ag+ cells. About 73% of the PCs are produced after the peak of the output cell production and also the majority of the MBCs (74%) are produced after the peak (**Supplementary Figure 15**). In **Figure 10**, we show an example of the temporal dynamics of B-cell lineage during the GC reaction starting with a founder cell that eventually results in PC differentiation. It shows how BLIMP1 level, Ag status, and affinity evolve as a result of the synergistic interaction between the molecular and cellular level at different events in the MSM.

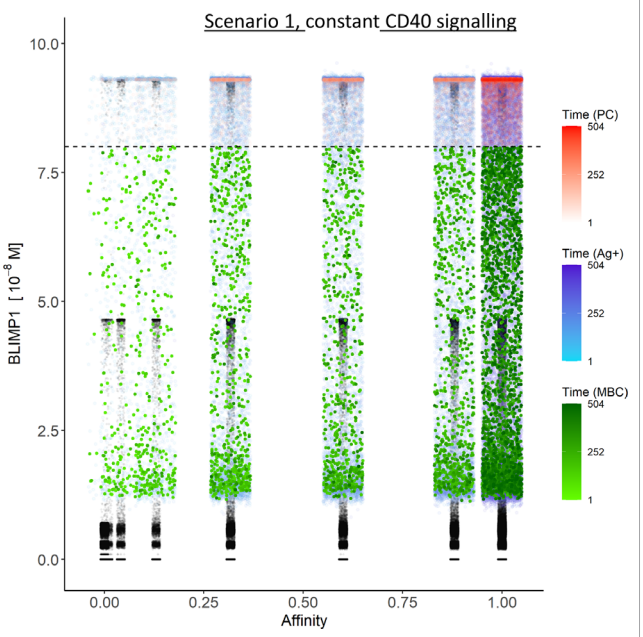

FIGURE 9 | Distribution of PCs, MBCs, and Ag+ (but not PC/MBC) cells with respect to their affinity, BLIMP1 level, and time of generation for scenario 2 simulations. Constant CD40 signaling (CD40 = 10). For a further description see **Figure 6**.

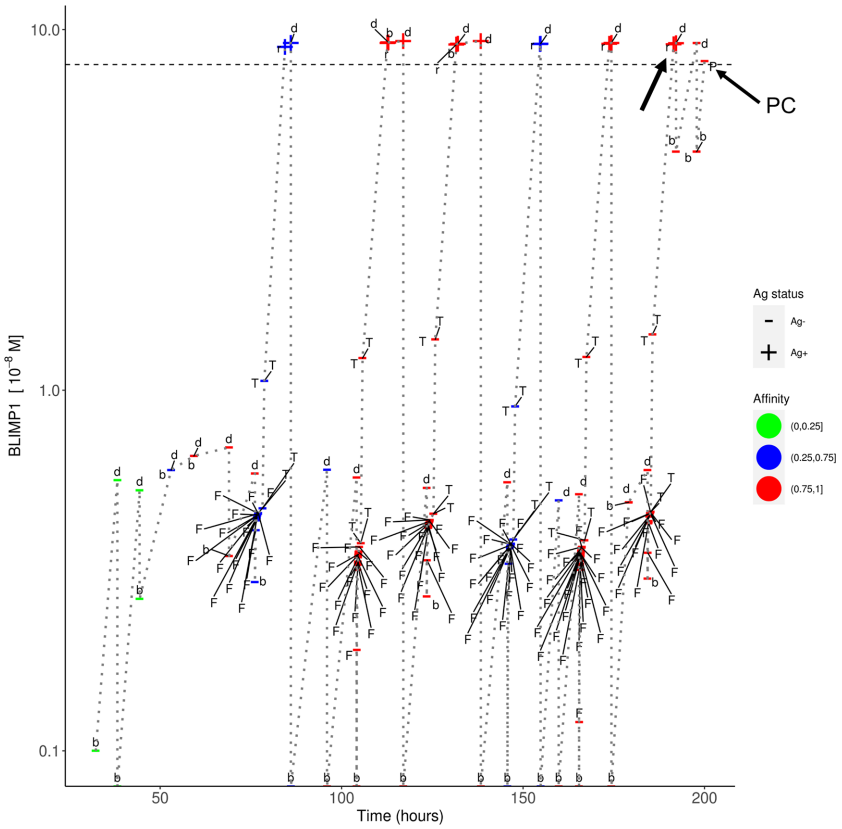

FIGURE 10 | Temporal dynamics of B-cell lineage for scenario 2, affinity-based CD40 signaling (simulation 4). The dotted lines traces the lineage of a single founder B_cell entering at the initial phase of the GC reaction up to a PC differentiation event at about 200 h. At each event (d, division; b, born, F, FDC contact; T, Tfh interaction; r, recycle to DZ; P, PC differentiation) the BLIMP1 level, Ag status (Ag+/Ag–), and affinity (low, medium high) is shown. The horizontal dotted line represents the BLIMP1 threshold for PC differentiation. CBs go through one or more cell divisions (d, b) before differentiating to CCs to have interaction with the FDC and Tfh cells. The affinity of the B-cells in this lineage shows an overall increase although SHM may also decrease affinity (red to blue color). Ag– cells are created from asymmetric division. BLIMP1 level varies in time as a result of transcriptional activity and (a)symmetric division. After interaction with a Tfh cell, the BLIMP1 level increases due to CD40 signaling. Asymmetric division may leave the BLIMP1 level unchanged or reduce it to 0. Symmetric division reduces the concentration with 50%. In this particular lineage we observe that a Ag+BLIMP1+ cell (indicated by the arrow) asymmetrically divides resulting in a Ag–BLIMP1– cell, which subsequently increases its BLIMP1 level again in subsequent divisions, and final differentiates to a PC (Ag–BLIMP1+).

In summary, a constant and weak CD40 signaling strength is able to produce MBCs throughout the GC reaction at the expense of PCs and, consequently, no temporal switch is observed.

DISCUSSION

We presented a multiscale computational model integrating cellular and molecular mechanisms, operating at different time scales, to investigate output cell differentiation based on Ag status and/or BLIMP1 level. In this paper we compared these mechanisms for cell-fate determination under various instances of CD40 signaling.

An important insight from our model (simulations 2 and 4) is the observation that regulation of the BLIMP1 level through affinity-dependent but not constant CD40 signaling, results in the occurrence of a temporal transition from MBC to PC output during the GC reaction (19, 45). In addition, simulation 2 showed that the LEDA theory (i.e., a mechanism in which the decision for output cell differentiation is solely based on asymmetric division but not on BLIMP1 level) does not exclude a temporal transition. However, scenario 1 simulations produce BLIMP1+ cells of which approximately 33% are Ag– showing that a decision for differentiation solely based on Ag status is not adequate since this will exclude a large number of BLIMP1+ cells from PC differentiation. Inspection of the PCs (BLIMP1+ cells) of the scenario 2 simulations shows that these are a mixture of Ag+ (~11%) and Ag– (~22%) cells. This also argues against asymmetric inheritance as sole mechanism for PC differentiation. It is known that high affinity GC B cells present more pMHCII molecules to Tfh cells resulting in increased expression of CD40L and hence stronger CD40 signaling which determines cell phenotype (21, 46–49) and results in faster and more cell divisions in the DZ (17, 21, 50, 51).

The lack of experimental data to support our findings is clearly a weakness of our work and complementary experiments

are required to validate the results from our simulations. In particular, we propose experiments to generate data about the (1) average number of PCs and MBCs that leave a single GC during its life time; (2) extend and and/or role of (a)symmetric division of Ag and TFs in relation to cell fate; (3) quantitative relationship between BcR affinity, CD40 signaling strength and BLIMP1 level.

One other apparent weakness of the MSM concerns the definition of MBCs as Ag+BLIMP1− cells. Although mechanisms of MBC differentiation are even less understood than for PC differentiation, we needed a route to generate both MBCs and PCs to make the model more realistic. Noticeably, lack of MBCs would have had a (small) effect on the overall GC dynamics. In favor of our approach is the observation that MBCs have indeed low BLIMP1 levels (8) and the observation of a temporal switch with low affinity MBCs and higher affinity PCs. The current definition, however, implies that Ag status (Ag+) is one of the determinants in MBC differentiation and that also MBCs leave the GC through the DZ. However, there is no experimental evidence to support this assumption at this stage. The generation of MBCs could be improved by modeling of the BTB domain and CNC homolog 2 [BACH2; (20, 52)] and the contribution of the CD40 pathway to MBC differentiation. Inclusion of the BACH2 in the GRN is, however, not sufficient as was recently shown in another model (53). One way forward is to model different cell fate (apoptosis, MBC/PC differentiation, and DZ recycling) for different levels of Tfh cell help, and to include MYC, FOXO1, IL-4, and IL-21 (Laidlaw and Cyster (54) Nat Rev Immunol; Luo et al. (55) Immunity]. However, the work of Krautler and co-workers seems to support the conclusion that Tfh-cell acts *via* signals other than CD40. Moreover, the stochastic selection of low-affinity B cells has been proposed as yet another mechanism to produced MBCs (18, 45, 56) or PCs (56–59).

One assumption in the MSM concerns the asymmetric division of TFs. It has been shown that BCL6 and IRF4 may distribute unequally in daughter CBs after division (44, 60), and it has been hypothesized that this may affect cell fate. To the best of our knowledge, neither symmetric nor asymmetric distribution of BLIMP1 during division has been reported.

Results from our simulations show that approximately 15,000 – 35,000 PCs and 800 MBCs are produced in a single GC reaction corresponding to about 5 – 14% and 0.3% respectively of all GC cells. Although data is available regarding numbers of PCs and MBCs generated spleen and bone marrow during an immune response [e.g., Sugimoto-Ishige et al. (61), Kishi et al. (62) J. Imm., 185, 211, Weisel et al. (19)], these numbers always represent percentages of observed PCs/MBCs from total number of splenic or bone marrow cells, which are impossible to translate to number of output cells from a single GC and, therefore, not directly comparable with our results.

In a recent study, it was shown that both BcR signaling and help from Tfh cells are required for positive selection of CCs, as signaling pathways that emanate from the BcR and CD40 ligation are rewired in GC B cells. In contrast to naïve B cells, GC B cells require both signals to induce the c-Myc transcription factor, which is a critical mediator of GC B-cell survival, cell-cycle reentry, and a marker of positive selection (55). These results indicate that CCs compete for Tfh-cell help in a BcR affinity-dependent fashion. It also has been proposed that c-Myc^{+}Bcl6^{lo}IRF4^{+} cells are most likely PC precursors while Myc^{+}Bcl6^{hi}IRF4^{-} will recycle to the DZ (7). However, cells with low BCL6 and higher IRF4 or BLIMP1 expression have also been found in the DZ, which supports the recycling model our MSM (13, 21). In support for our model, it has been shown that DZ B cells displayed a more prominent PC gene signature than LZ B cells (12, 13). Similarly, high-affinity LZ B cells showed a strong PC signature including a high expression of IRF4 in high-affinity CCs. Their experiments indicated that PC differentiation is initiated by signals delivered to high-affinity B cells in the LZ with subsequent transition to a late PC phenotype occurring after migration to the DZ.

These and other, sometimes contradicting studies, on MBC and PC differentiation clearly show the need for additional research to unravel mechanisms underlying cell-fate decisions in the GC. Further extensions of our MSM are expected to contribute to this.

DATA AVAILABILITY STATEMENT

The original contributions presented in the study are included in the article/**Supplementary Material**. Further inquiries can be directed to the corresponding author.

AUTHOR CONTRIBUTIONS

EM, HH, XG, FC, JG, and AK designed the study. MRM designed the GRN. EM, DL, MM-H, and PR implemented the software. EM, DL, and AK carried out the simulation and analyses. All authors were involved in the interpretation of results. JG, HH, and AK supervised the study. All authors contributed to the article and approved the submitted version.

FUNDING

This work is supported by a CASyM Exchange Research Grant, COSMIC (www.cosmic-h2020.eu) which has received funding from the European Union's Horizon 2020 research and innovation program under the Marie Skłodowska-Curie grant agreement no 765158, and by the Human Frontier Science Program 570 (RGP0033/2015).

ACKNOWLEDGMENTS

We thank Olivier Gandrillon (Ens, Lyon) for his contribution to the multiscale model. We thank Barbera van Schaik to setup a Virtual Machine provided by the Dutch national e-infrastructure with the support of SURF Cooperative, to process large output files.

SUPPLEMENTARY MATERIAL

The Supplementary Material for this article can be found online at: https://www.frontiersin.org/articles/10.3389/fimmu.2020.620716/full#supplementary-material

REFERENCES

1. De Silva NS, Simonetti G, Heise N, Klein U. The diverse roles of IRF4 in late germinal center B-cell differentiation. *Immunol Rev* (2012) 247(1):73–92. doi: 10.1111/j.1600-065X.2012.01113.x
2. Meyer-Hermann M, Mohr E, Pelletier N, Zhang Y, Victora GD, Toellner KM. A theory of germinal center b cell selection, division, and exit. *Cell Rep* (2012) 2(1):162–74. doi: 10.1016/j.celrep.2012.05.010
3. Allen CDC, Cyster JG. Follicular dendritic cell networks of primary follicles and germinal centers: phenotype and function. *Semin Immunol* (2008) 20: (1):14–25. doi: 10.1016/j.smim.2007.12.001
4. Ionescu L, Urschel S. Memory B Cells and Long-lived Plasma Cells. *Transplantation* (2019) 103(5):890–8. doi: 10.1097/TP.0000000000002594
5. Higgins BW, McHeyzer-Williams LJ, McHeyzer-Williams MG. Programming Isotype-specific Plasma Cell Function. *Trends Immunol* (2019) 40(4):345–57. doi: 10.1016/j.it.2019.01.012
6. Shlomchic MJ, Luo W, Weisel FJ. Linking Signaling and Selection in the Germinal Center. *Physiol Behav* (2019) 176(1):139–48. doi: 10.1111/imr.12744
7. Ise W, Kurosaki T. Plasma cell differentiation during the germinal center reaction. *Immunol Rev* (2019) 288(1):64–74. doi: 10.1111/imr.12751
8. Suan D. Plasma cell and memory B cell differentiation from the germinal center. *Curr Opin Immunol* (2017) 45:97–102. doi: 10.1016/j.coi.2017.03.006
9. Reimer D, Meyer-Hermann M, Rakhymzhan A, Steinmetz T, Tripal P, Thomas J, et al. B Cell Speed and B-FDC Contacts in Germinal Centers Determine Plasma Cell Output via Swiprosin-1/EFhd2. *Cell Rep* (2020) 32 (6):108030. doi: 10.1016/j.celrep.2020.108030
10. Shulman Z, Gitlin AD, Weinstein JS, Lainez B, Esplugues E, Flavell R, et al. Germinal centers: Dynamic signaling by T follicular helper cells during germinal center B cell selection. *Science (80-)* (2014) 345(6200):1058–62. doi: 10.1126/science.1257861
11. Victora GD, Nussenzweig MC. Germinal center dynamics revealed by multiphoton microscopy with a photoactivatable fluorescent reporter. *Cell* (2010) 143(4):592–605. doi: 10.1016/j.cell.2010.10.032
12. Arpin C, Julie D, Kooten C, Merville P, Grouard G, Francine B, et al. Generation of memory B cells and plasma cells in vitro. *Science (80-)* (1995) 268(5211):720–2. doi: 10.1126/science.7537388
13. Kräutler N, Suan D, Butt D, Bourne K, Hermes JR, Chan TD, et al. Differentiation of germinal center B cells into plasma cells is initiated by high-affinity antigen and completed by Tfh cells. *J Exp Med* (2017) 214 (5):1259–67. doi: 10.1084/jem.20161533
14. Luo W, Hawse W, Conter L, Trivedi N, Weisel F, Wikenheiser D, et al. The AKT kinase signaling network is rewired by PTEN to control proximal BCR signaling in germinal center B cells. *Nat Immunol* (2019) 20(6):736–46. doi: 10.1038/s41590-019-0376-3
15. Shlomchik MJ, Luo W, Weisel F. Linking signaling and selection in the germinal center. *Immunol Rev* (2019) 288(1):49–63. doi: 10.1111/imr.12744
16. Chan TD. Affinity-based selection and the germinal center response. *Immunol Rev* (2012) 1):11–23. doi: 10.1111/j.1600-065X.2012.01118.x
17. Phan. High affinity germinal center B cells are actively selected into the plasma cell compartment. *J Exp Med* (2006) 203(11):2419–24. doi: 10.1084/jem.20061254
18. Smith KGC, Light A, Nossal GJV, Tarlinton DM. The extent of affinity maturation differs between the memory and antibody-forming cell compartments in the primary immune response. *EMBO J* (1997) 16 (11):2996–3006. doi: 10.1093/emboj/16.11.2996
19. Weisel FJ, Zuccarino-catania GV, Chikina M, Shlomchik MJ, Weisel FJ, Zuccarino-catania GV, et al. A Temporal Switch in the Germinal Center Determines Differential Output of Memory B and Plasma Cells. *Immunity* (2016) 44(1):116–30. doi: 10.1016/j.immuni.2015.12.004
20. Shinnakasu R, Inoue T, Kometani K, Moriyama S, Adachi Y, Nakayama M, et al. Regulated selection of germinal-center cells into the memory B cell compartment. *Nat Immunol* (2016) 17(7):861–9. 2016/05/10. doi: 10.1038/ni.3460
21. Ise W, Fujii K, Shiroguchi K, Ito A, Kometani K, Takeda K, et al. T Follicular Helper Cell-Germinal Center B Cell Interaction Strength Regulates Entry into Plasma Cell or Recycling Germinal Center Cell Fate. *Immunity* (2018) 48 (4):702–715.e4. doi: 10.1016/j.immuni.2018.03.027
22. Steiniger BS, Raimer L, Ecke A, Stuck BA, Cetin Y. Plasma cells, plasmablasts, and AID+/CD30+ B lymphoblasts inside and outside germinal centres: details of the basal light zone and the outer zone in human palatine tonsils. *Histochem Cell Biol* (2020) 154(1):55–75. doi: 10.1007/s00418-020-01861-1
23. Fujii K, Tanaka S, Hasegawa T, Narazaki M, Kumanogoh A, Koseki H, et al. Tet DNA demethylase is required for plasma cell differentiation by controlling expression levels of IRF4. *Int Immunol* (2020) 32(10):683–90. doi: 10.1093/intimm/dxaa042
24. Azagra A, Marina-Zárate E, Ramiro AR, Javierre BM, Parra M. From Loops to Looks: Transcription Factors and Chromatin Organization Shaping Terminal B Cell Differentiation. *Trends Immunol* (2020) 41(1):46–60. doi: 10.1016/j.it.2019.11.006
25. Herviou L, Jourdan M, Martinez AM, Cavalli G, Moreaux J. EZH2 is overexpressed in transitional preplasmablasts and is involved in human plasma cell differentiation. *Leukemia* (2019) 33(8):2047–60. doi: 10.1038/s41375-019-0392-1
26. Nutt SL, Taubenheim N, Hasbold J, Corcoran LM, Hodgkin PD. Seminars in Immunology The genetic network controlling plasma cell differentiation. *Semin Immunol* (2011) 23:341–9. doi: 10.1016/j.smim.2011.08.010
27. Roy K, Mitchell S, Liu Y, Ohta S, Lin Ys, Metzig MO, et al. A Regulatory Circuit Controlling the Dynamics of NFκB cRel Transitions B Cells from Proliferation to Plasma Cell Differentiation. *Immunity* (2019) 50(3):616–628.e6. doi: 10.1016/j.immuni.2019.02.004
28. Liu GJ, Jaritz M, Wöhner M, Agerer B, Bergthaler A, Malin SG, et al. Repression of the B cell identity factor Pax5 is not required for plasma cell development. *J Exp Med* (2020) 217(11). doi: 10.1084/jem.20200147
29. Davidzohn N, Biram A, Stoler-Barak L, Grenov A, Dassa B, Shulman Z. Syk degradation restrains plasma cell formation and promotes zonal transitions in germinal centers. *J Exp Med* (2020) 217(3). doi: 10.1084/jem.20191043
30. Minnich M, Tagoh H, Bonelt P, Axelsson E, Fischer M, Cebolla B, et al. Multifunctional role of the transcription factor Blimp-1 in coordinating plasma cell differentiation. *Nat Immunol* (2016) 17(3):331–43. 2016/01/19. doi: 10.1038/ni.3349
31. Piskurich JF, Lin KI, Lin Y, Wang Y, Ting JPY, Calame K. BLIMP-1 mediates extinction of major histocompatibility class II transactivator expression in plasma cells. *Nat Immunol* (2000) 1(6):526–32. doi: 10.1038/82788
32. Basso K, Dalla-Favera R. BCL6: master regulator of the germinal centerreaction and key oncogene in B cell lymphomagenesis. *Adv Immunol* (2010) 105:193–210. doi: 10.1016/S0065-2776(10)05007-8
33. Kwon H, Thierry-Mieg D, Thierry-Mieg J, Kim HP, Oh J, Tunyaplin C, et al. Analysis of Interleukin-21-Induced Prdm1 Gene Regulation Reveals Functional Cooperation of STAT3 and IRF4 Transcription Factors. *Immunity* (2009) 31(6):941–52. doi: 10.1016/j.immuni.2009.10.008
34. Zhang TT, Gonzalez DG, Cote CM, Kerfoot SM, Deng S, Cheng Y, et al. Bach2 represses plasma cell gene regulatory network in B cells to promote antibody class switch. *Immunity* (2016) 45(1):49–63. 2003/12/03. doi: 10.1038/emboj.2010.257
35. Shaffer AL, Emre NC, Romesser PB, Staudt LM. IRF4: Immunity. Malignancy! Therapy? *Clin Cancer Res* (2009) 15(9):2954–61. 2009/04/23. doi: 10.1158/1078-0432.CCR-08-1845
36. Basso K, Dalla-Favera R. Germinal centres and B cell lymphomagenesis. *Nat Rev Immunol* (2015) 15(3):172–84. doi: 10.1038/nri3814
37. Martínez MR, Corradin A, Klein U, Álvarez MJ, Toffolo GM, Di Camillo B, et al. Quantitative modeling of the terminal differentiation of B cells and mechanisms of lymphomagenesis. *Proc Natl Acad Sci USA* (2012) 109 (7):2672–7. doi: 10.1073/pnas.1113019109
38. Robert PA. How to simulate a Germinal Center. *Methods Mol Biol* (2017) 1623:303–34. doi: 10.1007/978-1-4939-7095-7_22
39. Tas JMJ, Mesin L, Pasqual G, Targ S, Jacobsen JT, Mano YM, et al. Visualizing antibody affinity maturation in germinal centers. *Sci (80-)* (2016) 351 (6277):1048–54. doi: 10.1126/science.aad3439
40. Meyer-Hermann M, Binder SC, Mesin L, Victora GD. Computer simulation of multi-color brainbow staining and clonal evolution of B cells in germinal centers. *Front Immunol* (2018) 9. doi: 10.3389/fimmu.2018.02020
41. Meyer-Hermann M, Deutsch A, Or-Guil M. Recycling Probability and Dynamical Properties of Germinal Center Reactions. *J Theor Biol* (2001) 210(3):265–85. doi: 10.1006/jtbi.2001.2297

42. Perelson AS, Oster GF. Theoretical studies of clonal selection minimal antibody repertoire size and reliability of self non self discrimination. *J Theor Biol* (1979) 81(4):645–70. doi: 10.1016/0022-5193(79)90275-3
43. Thaunat O, Granja AG, Barral P, Filby A, Montaner B, Collinson L, et al. Asymmetric Segregation of Polarized Antigen on B Cell Division Shapes Presentation Capacity. *Science* (2012) 335:475–80. doi: 10.1126/science.1214100
44. Lin WH, Adams WC, Nish SA, Chen Y-H, Yen B, Rothman NJ, et al. Asymmetric PI3K Signaling Driving Developmental and Regenerative Cell Fate Bifurcation. *Cell Rep* (2015) 13(10):2203–18. doi: 10.1016/j.celrep.2015.10.072
45. Pélissier A, Akrout Y, Jahn K, Kuipers J, Klein U, Beerenwinkel N, et al. Computational Model Reveals a Stochastic Mechanism behind Germinal Center Clonal Bursts. *Cells* (2020) 9(6):1–25. doi: 10.3390/cells9061448
46. Jaiswal AI, Croft M. CD40 ligand induction on T cell subsets by peptide-presenting B cells: implications for development of the primary T and B cell response. *J Immunol* (1997) 159(5):2282–91.
47. Koike T, Harada K, Horiuchi S, Kitamura D. The quantity of CD40 signaling determines the differentiation of B cells into functionally distinct memory cell subsets. *Elife* (2019) 8:1–25. doi: 10.7554/eLife.44245
48. Schwickert TA, Lindquist RL, Shakhar G, Livshits G, Skokos D, Kosco-Vilbois MH, et al. In vivo imaging of germinal centres reveals a dynamic open structure. *Nature* (2007) 446(7131):83–7. doi: 10.1038/nature05573
49. Schwickert TA, Victora GD, Fooksman DR, Kamphorst AO, Mugnier MR, Gitlin AD, et al. A dynamic T cell-limited checkpoint regulates affinity-dependent B cell entry into the germinal center. *J Exp Med* (2011) 208(6):1243–52. doi: 10.1084/jem.20102477
50. Gitlin AD, Shulman Z, Nussenzweig MC. Clonal selection in the germinal center by regulated proliferation and hypermutation. *Bone* (2014) 23(1):1–7. doi: 10.1038/nature13300
51. Gitlin AD, Mayer CT, Oliveira TY, Shulman Z, Jones MJK, Koren A, et al. T cell help controls the speed of the cell cycle in germinal center B cells. *Physiol Behav* (2015) 176(1):139–48. doi: 10.1126/science.aac4919
52. Ochiai K, Muto A, Tanaka H, Takahashi S, Igarashi K. Regulation of the plasma cell transcription factor Blimp-1 gene by Bach2 and Bcl6. *Int Immunol* (2008) 20(3):453–60. doi: 10.1093/intimm/dxn005
53. Thomas MJ, Klein U, Lygeros J, Martínez MR. A probabilistic model of the germinal center reaction. *Front Immunol* (2019) 10:1–11. doi: 10.3389/fimmu.2019.00689
54. Laidlaw BJ, Cyster JG. Transcriptional regulation of memory B cell differentiation. *Nat Rev Immunol* (2020). doi: 10.1038/s41577-020-00446-2
55. Luo W, Weisel F, Shlomchik MJ. B Cell Receptor and CD40 Signaling Are Rewired for Synergistic Induction of the c-Myc Transcription Factor in Germinal Center B Cells. *Immunity* (2018) 48(2):313–26. doi: 10.1016/j.immuni.2018.01.008
56. Duffy KR, Wellard CJ, Markham JF, Zhou JHS, Holmberg R, Hawkins ED, et al. Stochastic Competition. *Sci (80-)* (2012) 279(January):338–41. doi: 10.1126/science.1213230
57. Dustin ML, Meyer-Hermann M. Antigen feast or famine. *Science* (2012) 335(6067):408–9. doi: 10.1126/science.1218165
58. Hasbold J, Corcoran LM, Tarlinton DM, Tangye SG, Hodgkin PD. Evidence from the generation of immunoglobulin G-secreting cells that stochastic mechanisms regulate lymphocyte differentiation. *Nat Immunol 2003/12/03* (2004) 5(1):55–63. doi: 10.1038/ni1016
59. Zhou JHS, Markham JF, Duffy KR, Hodgkin PD. Stochastically timed competition between division and differentiation fates regulates the transition from B lymphoblast to plasma cell. *Front Immunol* (2018) 9(SEP):1–15. doi: 10.3389/fimmu.2018.02053
60. Barnett BE, Ciocca ML, Goenka R, Barnett LG, Wu J, Laufer TM, et al. Asymmetric B cell division in the germinal center reaction. *Sci (80-)* (2012) 335(6066):342–4. doi: 10.1126/science.1213495
61. Sugimoto-Ishige A, Harada M, Tanaka M, Terooatea T, Adachi Y, Takahashi Y, et al. Bim establishes the B-cell repertoire from early to late in the immune response. *Int Immunol* (2020). (September). doi: 10.1093/intimm/dxaa060
62. Kishi Y, Aiba Y, Higuchi T, Furukawa K, Tokuhisa T, Takemori T, et al. Augmented Antibody Response with Premature Germinal Center Regression in CD40L Transgenic Mice. *J Immunol* (2010) 185(1):211–9. doi: 10.4049/jimmunol.0901694

Conflict of Interest: MR was employed by the company IBM.

The remaining authors declare that the research was conducted in the absence of any commercial or financial relationships that could be construed as a potential conflict of interest.

frontiers in Immunology

MINI REVIEW
published: 31 March 2021
doi: 10.3389/fimmu.2021.661678

Positive Selection in the Light Zone of Germinal Centers

Rinako Nakagawa[1*†] *and Dinis Pedro Calado*[1,2*†]

[1] *Immunity and Cancer Laboratory, The Francis Crick Institute, London, United Kingdom,* [2] *Peter Gorer Department of Immunobiology, School of Immunology & Microbial Sciences, King's College London, London, United Kingdom*

Germinal centers (GCs) are essential sites for the production of high-affinity antibody secreting plasma cells (PCs) and memory-B cells (MBCs), which form the framework of vaccination. Affinity maturation and permissive selection in GCs are key for the production of PCs and MBCs, respectively. For these purposes, GCs positively select "fit" cells in the light zone of the GC and instructs them for one of three known B cell fates: PCs, MBCs and persistent GC-B cells as dark zone entrants. In this review, we provide an overview of the positive selection process and discuss its mechanisms and how B cell fates are instructed.

Keywords: positive selection, cMyc, affinity maturation, permissive selection, clonal diversity

OPEN ACCESS

Edited by:
Thierry Fest,
University of Rennes 1, France

Reviewed by:
Claude-Agnes Reynaud,
Université Paris Descartes, France
Steven M. Kerfoot,
Western University, Canada

****Correspondence:***
Rinako Nakagawa
rinako.nakagawa@crick.ac.uk
Dinis Pedro Calado
dinis.calado@crick.ac.uk

†These authors share senior authorship

Specialty section:
This article was submitted to B Cell Biology, a section of the journal Frontiers in Immunology

Received: *31 January 2021*
Accepted: *16 March 2021*
Published: *31 March 2021*

Citation:
Nakagawa R and Calado DP (2021) Positive Selection in the Light Zone of Germinal Centers. Front. Immunol. 12:661678. doi: 10.3389/fimmu.2021.661678

INTRODUCTION

Germinal centers (GCs) are sites where antibody affinity for the antigen (Ag) is improved and Ag-activated B cells differentiate, hence they are important for host defense and clearance of exogenous pathogens. This specialized microstructure transiently forms within the B cell follicles of secondary lymphoid organs during the course of T cell-dependent immune responses. The process of increasing antibody affinity is known as affinity maturation (1, 2) and results from somatic hypermutation (SHM) of immunoglobulin (Ig) genes in GC-B cells and clonal selection (3). GCs include two distinct regions, light zone (LZ) and dark zone (DZ) (4). SHM is mediated by activation-induced cytidine deaminase (AID) (5) and occurs in the DZ where GC-B cells extensively proliferate. In the LZ, GC-B cells are selected in an Ag and T cell-dependent manner. LZ-B cells retrieve Ag on follicular dendritic cells (FDCs) that can uniquely retain and display Ag in the form of immune complex (ICs) (6). B cell receptor (BCR) binding of Ag by LZ-B cells results in internalization of BCR-Ag and subsequent presentation of Ag in the form of Ag-specific-peptide-major histocompatibility II (pMHCII), which enables them to receive help from T follicular helper cells (TFHs). These positively selected LZ-B cells induce cMyc, a critical regulator for GC maintenance and proliferation, and cMyc positivity transiently marks "licensed" GC-B cells (7, 8). $cMyc^+$ GC-B-cells in the LZ re-start the cell cycle and travel to the DZ for further cell division (7–9). GC-B cells undergo iterative rounds of mutation and selection through a migration cycle between LZ and DZ. Eventually, GC reactions produce high-affinity antibody secreting plasma cells (PCs) and memory-B cells (MBCs). In this review, we summarize and discuss studies illustrating how positive selection of GC-B cells are triggered, what molecular and cellular events that GC-B cells undergo during the process of positive selection, and how B cell fate decisions are coordinated during positive selection.

MECHANISMS BY WHICH GCs POSITIVELY SELECT LZ-B CELLS

Current Models for Affinity-Dependent Positive Selection

In response to signals from BCR engagement and TFHs, a fraction of LZ-B cells are positively selected and results in evasion of apoptosis partially in a microRNA-155-dependent manner (10, 11). cMyc is induced upon positive selection and its expression effectively defines positively selected GC-B cells (7, 8). In the currently favored model, positive selection occurs in an affinity-dependent manner (12, 13). LZ-B cells capture FDC-bound Ags through their BCRs, process and present them in the form of pMHCII and signals downstream of BCR-Ag engagement allow survival. Higher-affinity GC-B cells more effectively receive helper signals from TFHs because they acquire more Ag, present pMHCII at higher levels and thereby induce greater TFH activation, this is in line with studies from early B cell responses *in vivo* (14) and *in vitro* (15). For promoting efficient positive selection, recycling GC-B cells reset their BCRs and MHCII before reentering the LZ (16, 17). Contact duration between cognate T cells and GC-B cells is shorter than that between T cell and Ag-activated B cells before GC formation (12, 18, 19). Moreover, only a limited proportion of T cells in GCs appear to actively interact with GC-B cells that are significantly more numerous than TFHs within the time window of confocal microscopic analysis (12, 18). These observations suggest that interactions between GC-B cells and TFHs are strictly controlled and therefore GC-B cells may compete for cognate T cell help. Together with a mathematical simulation model (20), these findings support that T cells are a limiting factor and positive selection can occur in a T cell-driven selection mechanism (12, 21). This selection mechanism is further supported by studies using a DEC-205-antibody-based Ag delivery approach (22). DEC-205 is an endocytic receptor that is primarily expressed in dendritic cells but also in B cells and directs captured Ag to Ag-processing compartments (23). Administration of Ag coupled to anti-DEC205 antibody allows delivering the Ag to endosomal compartments independently of BCR *via* a DEC205 receptor in GC-B cells (24) and results in greatly enhanced presentation of Ag peptide regardless of the nature of BCR (25). DEC-205-antibody-mediated Ag delivery prolongs interactions between GC-B cells and TFHs (26) and enables GC-B cells to gain more help from TFHs (9, 13, 24). Consequently, transcript levels of cMyc are considerably increased in the DEC205 agent-treated GC-B cells in a dose dependent manner (7, 27). The series of experiments demonstrate that providing strong T cell help to the total GC-B cell population during GC responses greatly potentiates positive selection process and resultant proliferation (24, 27–29). These findings underscore essential roles of T cell help in positive selection. However, a recent report has shown that by interrogating NP-specific GC-B cell responses in MHCII haploinsufficient mice in which both MHCII and pMHCII are halved compared to WT mice, the density of pMHCII is not as critical for selection in established GCs as in naive B cells (30). This finding suggests that other factors also play a role in an affinity-dependent positive selection, such as BCR signaling.

Strong BCR signaling through soluble Ag binding eliminates Ag-specific GC-B cells by inducing apoptosis predominantly in LZ-B cells within hours of engagement (31–33), thus enhanced BCR signaling is deleterious for GC-B cells. In agreement with this, canonical BCR signaling pathways are attenuated in GC-B cells compared to those in naïve B-cells (34–37) due to negative feedback by the activation of negative regulators for BCR signaling in a phosphate and tensin homolog (PTEN)-dependent manner (38). Nonetheless, GC-B cells can transmit PI3K-mediated signaling through BCR in a Syk-dependent manner to restrict the activity of forkhead Box O1 (FoxO1) (39), a critical transcription factor for the DZ transcriptional program (25, 40, 41). This occurs through synaptic interactions between GC-B cells and FDCs in which GC-B cells can respond to membrane-bound Ags more efficiently than naïve B cells in an affinity-dependent manner (36, 37, 42). Using an adoptive transfer system, the propagation of donor derived GC-B cells is investigated upon restimulation with sub-saturating T cell help provided by DEC205 agent in the presence or absence of simultaneous Ag injection. Restimulation with Ag in the presence of T cell help enhances GC responses compared to T cell help only (29), suggesting that BCR signaling could potentiate positive selection synergistically with T cell help. Transient BCR signals prime B cells and alter their nature for forthcoming contact with T cells prior to GC formation (43, 44). Similar alterations might occur in GC-B cells upon reception of BCR signals.

Potential Alternative Mechanisms of Permissive Positive Selection and the Beyond.

The permissive environment of GCs confers clonal breadth in MBCs that is effective for viral clearance (45, 46). Recent findings underpin that GCs permit retaining cells with varied affinities for the antigen (47–49). Permissive positive selection cannot be well explained only by affinity-dependent models and there could be an alternative mechanism that is not well understood. We recently identified cMyc$^+$ LZ-B cell subpopulations that arise at different times following the reception of positive selection signals. Analysis of the cMyc$^+$ LZ-B cell subpopulations revealed that a significantly large fraction of low-affinity cells is initially positively selected, but are mostly outcompeted by more proliferative higher-affinity cells before DZ migration (50). This mechanism partially explains how low-affinity GC-B cells can be retained in GCs because positively selected GC-B cells can avoid apoptosis in GCs (10, 50). In our observations, rather than selecting only higher-affinity cells from the beginning of positive selection, GCs permit selection of low-affinity cells at the beginning of each round of positive selection, thus selection is relatively independent of BCR affinity. This mode of positive selection continues for a period of time during the height of GC reactions (50). However, the differential strength of signals between low-affinity and higher-affinity cells eventually leads to differential proliferation rate of positively selected cells. As a

result, higher-affinity cells proliferate better and are enriched in cMyc$^+$ LZ-B cells compared to cMyc$^-$ LZ-B cells (7, 50). Following Ag-mediated activation, over time Ag may become more limited with GC-B cells having more competition for antigen-induced survival signals. If GC-B cells are fit enough despite carrying low-affinity BCRs, they could compete effectively for Ag and acquire Ag successfully.

We noted that CD40 expression is elevated in the cMyc$^+$ LZ-B cell subpopulation emerging soon after positive selection compared to the cMyc$^-$ LZ compartment that contains GC-B cells before positive selection; although this subpopulation largely comprises low-affinity cells at a similar level to that of cMyc$^-$ LZ-B cells (50). Increased CD40 expression might allow these GC-B cells to gain more T cell help by these two mechanisms; i) inducible T cell co-stimulator ligand (ICOSL), a ligand for ICOS that is one of the co-stimulatory receptors expressed on TFHs, is induced on GC-B cells through CD40 engagement with CD40L on TFHs and potentiates GC-TFH interactions (51, 52); ii) these cells may have an increased chance of interacting with IL-4 expressing TFHs that express CD40L at a higher level than IL-21/IL-4 expressing TFHs or IL-21 expressing TFHs (53). Alternatively, reduction of the engagement of Herpesvirus entry mediator (HVEM) on GC-B cells with a ligand, B- and T-lymphocyte attenuator (BTLA) on TFHs leads to increased expression of CD40L in TFHs (54). Thus, reduced expression of negative regulators such as HVEM on GC-B cells can also lead to an increased amount of T cell help. The underlying mechanisms for upregulation of CD40 in these GC-B cells are unknown, but they perhaps receive additional signals prior to, or at the initiation of, receiving cMyc-inducing signals to upregulate the molecule. CD40 expression on B cells is shown to be enhanced *in vitro* by B cell-activating factor (BAFF) (55) which can be secreted by FDCs (56, 57). Under the condition that only a limited amount of Ag is available, GC-B cells that successfully acquire Ag could receive survival signals from FDCs *via* contact-based interaction and/or *via* trophic factors independently of BCR affinity. This could provide an advantage for GC-B cells to undergo positive selection [functions of FDCs during GC responses are extensively discussed elsewhere (58–60)]. In such case, modulation of FDCs' functions by other factors, such as Toll-like-receptor (TLR) 4 ligands (61), may play a role in permissive selection.

The concept that higher-affinity cells are favorably selected from the beginning of the positive selection process is supported by *in vitro* microscopic observations that the higher-affinity cells can form more stable contacts with the membrane, better resist the pulling force required to capture Ag without causing cell rupture, transmit stronger BCR signals and acquire a larger amount of Ag to present to T cells compared to low-affinity cells (36, 37, 42, 62). However, the proportion of higher-affinity cells in the cMyc$^+$ subpopulation that appears soon after positive selection is similar to that of cMyc$^-$ LZ compartment before positive selection (50). This suggests that low-affinity cells can be selected at a comparable level as higher-affinity cells at the beginning of positive selection. The discrepancy could be caused by the method of Ag presentation by FDCs, since multimerized Ag on FDCs can impact the GC selection process (59, 63) and also by the availability of complement proteins (such as C3d) that are required for bridging the Ag bound to BCR and the BCR coreceptor complex. The BCR co receptor complex consisting of CD19, CD21 (a.k.a. complement receptor type 2, CR2) and CD81 can augment BCR signaling and Ag processing, to lower the Ag threshold and quicken Ag presentation (64–66). Potentially, the differential expression of BCR coreceptor complexes and/or negative regulators such as HVEM on low-affinity cells may allow them to be more competitive with higher-affinity cells by enhancing BCR signaling and T cell help (**Figure 1**). More investigation is required to elucidate mechanisms allowing low-affinity B cells to be positively selected.

Recent reports have shown that DEL-OVA (duck egg lysozyme-ovalbumin) *ex vivo* pulsed DEL-specific HyHEL-10 B cells can join existing GCs elicited by OVA (i.e., DEL has not been deposited on FDCs) and contribute to GC responses at a comparable level to DEL-OVA-immunized recipients (44, 67). In these experiments, the HyHEL-10 B cells that were exposed to DEL-OVA *ex vivo* for 5 min were transferred into recipient mice that had been immunized with OVA for 3 or more days. This may be interpreted as single Ag acquisition by B cells is sufficient for them to participate in GC responses without any further Ag acquisition; alternatively, the HyHEL-10 B cells pulsed for 5 min might somehow deliver un-internalized Ag to FDCs and the deposited Ag may have been used for robust GC responses. It has been controversial whether retention of immune complex (ICs) on FDCs is essential for GC formation and positive selection (68–71), while reports have shown that ICs deposited on FDCs during GC responses contribute to optimum affinity maturation (72–74). Nonetheless, the results using HyHEL10 B cell adoptive transfer system suggest two possibilities; i) GC-B cells can survive and proliferate with very little Ag if B cells have taken up Ag adequately during initial activation; and ii) B cells activated by a dissimilar Ag to the original GC initiating Ag may take over the GC if the newcomer B cells receive cognate T cell help (in this case, transferred DEL-specific B cells can present OVA-peptide and thus can receive T cell help from OVA-specific T cells in OVA-elicited GCs). Inter-GC trafficking of B cells into neighboring GCs is suggested by long-term observations of single GCs using intravital microscopy technique (47). Since GCs are dynamic open structures and TFHs can emigrate into neighboring GCs (75, 76), it is still possible that a GC-B clone recognizing an Ag re-seeds in neighboring GCs whose reactions are elicited by another Ag (or cryptic epitopes) if cognate T cells also migrate. A recent report has shown that GCs elicited by complex Ags somehow permit B cells that do not detect the original Ag (48). Retention of varied clones in GCs may be attained by a combination of inter-GC trafficking and intra-clonal permissive selection.

MOLECULAR EVENTS DURING POSITIVE SELECTION AND B CELL FATE INSTRUCTION

The cMyc$^+$ GC-B cell compartment is suggested to be heterogeneous due to differential signal activation (25, 41) and

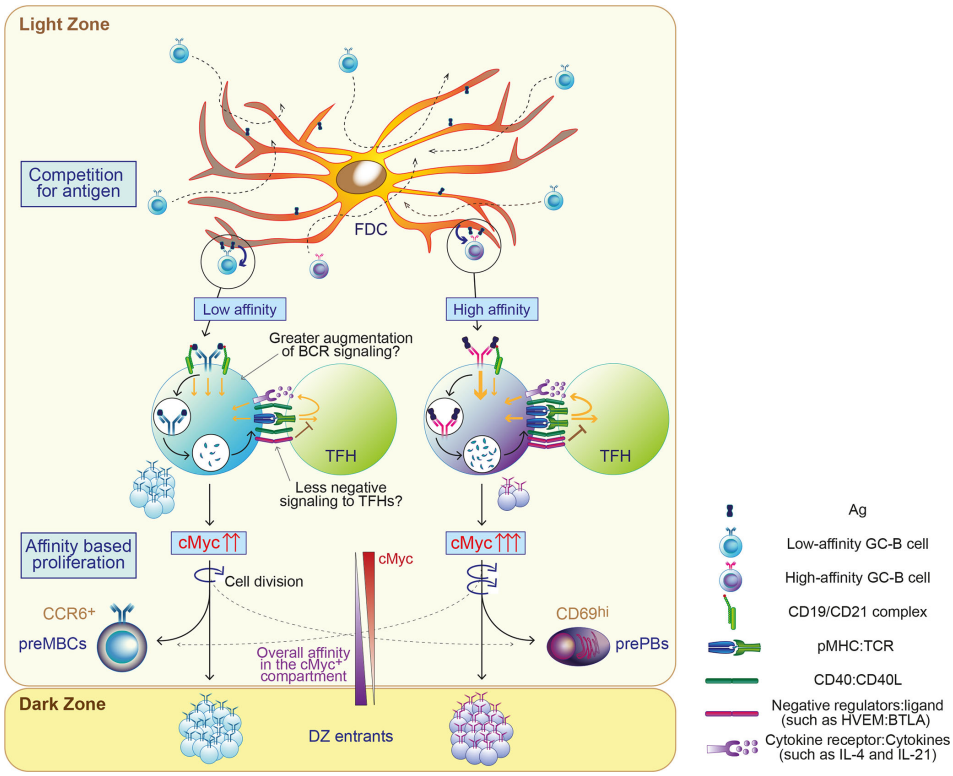

FIGURE 1 | Proposed model of permissive positive selection in GCs. GC-B cells compete for antigen when only limited amount of antigen (Ag) is available. Fit cells retrieve Ag deposited on follicular dendritic cells (FDCs) relatively independently of BCR affinity and receive survival signals from FDCs through contact-based interaction and/or trophic factors. Both high and low-affinity cells process Ag and present differing levels of Ag in the form of peptide-MHCII complex (pMHC) in proportion to its affinity. Low-affinity cells may augment the level of signaling above a threshold with potentially undefined mechanisms, such as favorably augmented signals and/or less negative feedback. GC-B cells received sufficient signals for positive selection proliferate mainly based on their BCR affinity. Their fates are also instructed, generally depending on their BCR affinity. cMyc^{+} GC-B cells divide in the LZ and cMyc expression in GC-B cells is reduced accordingly. The width of the arrows in GC-B cells and TFH depicts the signal strength.

as a result gives rise to heterogeneous populations containing future PBs/PCs, DZ-entrants and future MBCs (24, 50, 77).

Fate 1: Plasmablasts/Plasma Cells (PBs/PCs)

Increased TFH help drives GC-B cells to differentiate into PBs/PCs (24, 29, 77) with enhanced NF-κB signaling *via* CD40-CD40L ligation (39, 78, 79). Consistent with these findings, PB/PC precursors in GCs defined as cMyc^{+} CD69^{hi} Bcl6^{lo} LZ-B cells express relatively high levels of IRF4 (50, 77) which is a critical transcription factor for PC differentiation and induced by NF-κB signaling (80). These distinct precursors consist of high-affinity GC-B cells in agreement with previous findings (81, 82) and become detectable soon after positive selection (50, 77). Stable contact between TFHs and GC-B cells as a consequence of greater pMHC presentation in GC-B cells induces Ca^{2+}-dependent expression of IL-21 and IL-4 in TFHs (26). Thus, stronger T cell help inducing signals promote PB/PC differentiation from GC-B cells by producing cytokines that support PC differentiation (53). However, some GC-B cells persistently remain as GC-B cells (i.e., become DZ-entrants) instead of differentiating into PBs/PCs upon receiving exogenous strong T cell help by DEC205 agent (24, 28), suggesting that there is still a missing component for the PB/PC fate instruction other than TFH help. Recent reports have shown that signaling induced by Ag-BCR engagement contributes to PB/PC differentiation from GC-B cells (29, 44, 81, 83, 84). Strong BCR signaling in conjunction with CD40 signaling can upregulate IRF4 by degrading the E3 ubiquitin ligases Cbl that ubiquitinates IRF4 for degradation in GC-B cells (84). PB/PC output is largely influenced by Ag valency that reduces Ag affinity threshold in extrafollicular PC responses (85, 86), thus multivalent Ag presentation on FDCs may also play a role in PB/PC differentiation from GC-B cells.

Fate 2: Memory-B Cells (MBCs)

In contrast to PBs/PCs, MBC precursors predominantly contain lower-affinity cells and appear to require only minimal amount of help from TFHs (87, 88). Together with the observations that MBC precursors are relatively quiescent (87–89), it is broadly assumed that MBCs arise from "non-positively-selected" LZ-B-cells. However, this concept cannot explain these three points; i) how the specificity of the BCR can be checked before positive selection, ii) how cell survival can be assured without positive

selection, and iii) how high-affinity clones can be selected for MBC differentiation from a pool of GC-B cells with varied affinity. To understand the origin of MBCs, extensive single cell transcriptomic analysis identified a preMBC subset in mouse spleens (90) and human tonsils (91). These preMBC subsets are characterized by the expression of *Ccr6* (90, 91) as expected from a previous report (88). Unexpectedly the mouse preMBC subset has relatively higher *Mki67* expression than MBC subsets (90) and the human preMBC subset exhibits a similar level of *Myc* expression to subsets containing positively selected cells (91), which is counter-intuitive considering the relatively quiescent nature of MBC precursors as previously reported (87–89). These findings suggest that $CCR6^+$ preMBCs could receive sufficient signals from TFHs to induce cMyc and divide before fully differentiating into MBCs. In agreement with these findings, we identified MBC precursors within $cMyc^+$ positively selected GC-B cells that are less proliferative than other $cMyc^+$ LZ-B cells but still dividing (50). Stronger TFH help induces differentiation of $CD80^{hi}$ MBCs whose Ig genes accumulate mutations compared to those of $CD80^-$ MBCs (92, 93), and resultantly $CD80^{hi}$ MBCs comprise relatively high-affinity clones (93). A very small fraction of high-affinity cells within the $cMyc^+$ MBC precursor subpopulation (defined as $cMyc^+$ $CD23^{hi}$ $CCR6^+$ LZ-B cells) (50) might differentiate into $CD80^{hi}$ MBCs following reception of robust T cell help. For the MBC fate instruction, interplay between transcription factors exerts functions that regulate MBC differentiation from $cMyc^+$ GC-B cells. Myc-interacting zinc finger protein-1 (MIZ-1) is expressed in most $cMyc^+$ LZ-B cells and the transcriptional activator Miz-1 switches to a transcriptional repressor upon cMyc binding (94, 95). The cMyc/Miz-1 complex represses Miz-1 target genes and results in restricting positively selected GC-B cells from forming MBCs to favor GC-B cell fate as DZ-entrants (94). A transcription factor, hematopoietically-expressed homeobox protein (Hhex) that is expressed in MBC precursors and promotes MBC differentiation (50, 90) can interact with cMyc to decrease its activity, including cell proliferation and metabolism in tumors (96). Reception of differential signals for positive selection induces these transcription factors at varied levels in positively selected GC-B cells (97), which most likely play a part in MBC differentiation. However, the overall nature of the signaling network for transition from GC-B cell to MBCs remains unknown.

Fate 3: DZ Entrants

The remaining positively selected LZ-B cells other than cells instructed to PB/PC and MBC fates transit to the DZ for further proliferation as DZ-entrants. BCR signals downregulate FoxO1 and cyclin D3, which are essential for maintenance and proliferation of DZ-B cells, respectively (25, 39–41, 98, 99). Strongly induced cMyc expression in positively selected LZ-B cells in turn activates activating enhancer binding protein 4 (AP-4) that contribute to the induction of cyclin D3 (100). Hence, positively selected cells are likely to turn on the DZ-proliferation program when BCR-induced signals are weakened in the LZ, which is concordant with previous observations about the co-expression of FoxO1 and/or cyclin D3 together with cMyc in positively selected LZ-B cells (41, 98, 100).

CONCLUDING REMARKS

Clonal breadth achieved by permissive selection is particularly useful for protection from viruses that constantly mutate. Understanding the underlying mechanisms of permissive selection followed by B cell differentiation will guide vaccine design and improve their efficacy in the future.

AUTHOR CONTRIBUTIONS

RN and DC wrote the manuscript. All authors contributed to the article and approved the submitted version.

FUNDING

This work was supported by the Francis Crick Institute, which receives its core funding from Cancer Research UK (FC001057), the UK Medical Research Council (FC001057), and Wellcome Trust (FC001057) to DC and by the UK Medical Research Council (grant reference MR/J008060) to DC.

ACKNOWLEDGMENTS

We thank H. Purvis for critically reviewing the manuscript.

REFERENCES

1. Berek C, Berger A, Apel M. Maturation of the immune response in germinal centers. *Cell* (1991) 67(6):1121–9. doi: 10.1016/0092-8674(91)90289-B
2. Jacob J, Kelsoe G, Rajewsky K, Weiss U. Intraclonal generation of antibody mutants in germinal centres. *Nature* (1991) 354(6352):389–92. doi: 10.1038/354389a0
3. Cyster JG, Allen CDC. B Cell Responses: Cell Interaction Dynamics and Decisions. *Cell* (2019) 177(3):524–40. doi: 10.1016/j.cell.2019.03.016
4. Kepler TB, Perelson AS. Cyclic re-entry of germinal center B cells and the efficiency of affinity maturation. *Immunol Today* (1993) 14(8):412–5. doi: 10.1016/0167-5699(93)90145-B
5. Muramatsu M, Kinoshita K, Fagarasan S, Yamada S, Shinkai Y, Honjo T, et al. Class switch recombination and hypermutation require activation-induced cytidine deaminase (AID), a potential RNA editing enzyme. *Cell* (2000) 102(5):553–63. doi: 10.1016/S0092-8674(00)00078-7
6. Heesters BA, Myers RC, Carroll MC. Follicular dendritic cells: dynamic antigen libraries. *Nat Rev Immunol* (2014) 14(7):495–504. doi: 10.1038/nri3689
7. Dominguez-Sola D, Victora GD, Ying CY, Phan RT, Saito M, Nussenzweig MC, et al. The proto-oncogene MYC is required for selection in the germinal center and cyclic reentry. *Nat Immunol* (2012) 13(11):1083–91. doi: 10.1038/ni.2428
8. Calado DP, Sasaki Y, Godinho SA, Pellerin A, Kochert K, Sleckman BP, et al. The cell-cycle regulator c-Myc is essential for the formation and maintenance

of germinal centers. *Nat Immunol* (2012) 13(11):1092–100. doi: 10.1038/ni.2418
9. Mesin L, Ersching J, Victora GD. Germinal Center B Cell Dynamics. *Immunity* (2016) 45(3):471–82. doi: 10.1016/j.immuni.2016.09.001
10. Mayer CT, Gazumyan A, Kara EE, Gitlin AD, Golijanin J, Viant C, et al. The microanatomic segregation of selection by apoptosis in the germinal center. *Science* (2017) 358(6360):eaao2602. doi: 10.1126/science.aao2602
11. Nakagawa R, Toboso-Navasa A, Schips M, Young G, Bhaw-Rosun L, Llorian-Sopena M, et al. MicroRNA-155 controls affinity-based selection by protecting c-MYC+ B cells from apoptosis. *J Clin Invest* (2016) 126(1):377–88. doi: 10.1172/JCI82914
12. Allen CD, Okada T, Cyster JG. Germinal-center organization and cellular dynamics. *Immunity* (2007) 27(2):190–202. doi: 10.1016/j.immuni.2007.07.009
13. Victora GD, Nussenzweig MC. Germinal centers. *Annu Rev Immunol* (2012) 30:429–57. doi: 10.1146/annurev-immunol-020711-075032
14. Schwickert TA, Victora GD, Fooksman DR, Kamphorst AO, Mugnier MR, Gitlin AD, et al. A dynamic T cell-limited checkpoint regulates affinity-dependent B cell entry into the germinal center. *J Exp Med* (2011) 208 (6):1243–52. doi: 10.1084/jem.20102477
15. Batista FD, Neuberger MS. Affinity dependence of the B cell response to antigen: a threshold, a ceiling, and the importance of off-rate. *Immunity* (1998) 8(6):751–9. doi: 10.1016/S1074-7613(00)80580-4
16. Bannard O, McGowan SJ, Ersching J, Ishido S, Victora GD, Shin JS, et al. Ubiquitin-mediated fluctuations in MHC class II facilitate efficient germinal center B cell responses. *J Exp Med* (2016) 213(6):993–1009. doi: 10.1084/jem.20151682
17. Stewart I, Radtke D, Phillips B, McGowan SJ, Bannard O. Germinal Center B Cells Replace Their Antigen Receptors in Dark Zones and Fail Light Zone Entry when Immunoglobulin Gene Mutations are Damaging. *Immunity* (2018) 49(3):477–489 e7. doi: 10.1016/j.immuni.2018.08.025
18. Allen CD, Okada T, Tang HL, Cyster JG. Imaging of germinal center selection events during affinity maturation. *Science* (2007) 315(5811):528–31. doi: 10.1126/science.1136736
19. Okada T, Miller MJ, Parker I, Krummel MF, Neighbors M, Hartley SB, et al. Antigen-engaged B cells undergo chemotaxis toward the T zone and form motile conjugates with helper T cells. *PloS Biol* (2005) 3(6):e150. doi: 10.1371/journal.pbio.0030150
20. Meyer-Hermann ME, Maini PK, Iber D. An analysis of B cell selection mechanisms in germinal centers. *Math Med Biol* (2006) 23(3):255–77. doi: 10.1093/imammb/dql012
21. De Silva NS, Klein U. Dynamics of B cells in germinal centres. *Nat Rev Immunol* (2015) 15(3):137–48. doi: 10.1038/nri3804
22. Bonifaz L, Bonnyay D, Mahnke K, Rivera M, Nussenzweig MC, Steinman RM. Efficient targeting of protein antigen to the dendritic cell receptor DEC-205 in the steady state leads to antigen presentation on major histocompatibility complex class I products and peripheral CD8+ T cell tolerance. *J Exp Med* (2002) 196(12):1627–38. doi: 10.1084/jem.20021598
23. Jiang W, Swiggard WJ, Heufler C, Peng M, Mirza A, Steinman RM, et al. The receptor DEC-205 expressed by dendritic cells and thymic epithelial cells is involved in antigen processing. *Nature* (1995) 375(6527):151–5. doi: 10.1038/375151a0
24. Victora GD, Schwickert TA, Fooksman DR, Kamphorst AO, Meyer-Hermann M, Dustin ML, et al. Germinal center dynamics revealed by multiphoton microscopy with a photoactivatable fluorescent reporter. *Cell* (2010) 143 (4):592–605. doi: 10.1016/j.cell.2010.10.032
25. Inoue T, Shinnakasu R, Ise W, Kawai C, Egawa T, Kurosaki T. The transcription factor Foxo1 controls germinal center B cell proliferation in response to T cell help. *J Exp Med* (2017) 214(4):1181–98. doi: 10.1084/jem.20161263
26. Shulman Z, Gitlin AD, Weinstein JS, Lainez B, Esplugues E, Flavell RA, et al. Dynamic signaling by T follicular helper cells during germinal center B cell selection. *Science* (2014) 345(6200):1058–62. doi: 10.1126/science.1257861
27. Finkin S, Hartweger H, Oliveira TY, Kara EE, Nussenzweig MC. Protein Amounts of the MYC Transcription Factor Determine Germinal Center B Cell Division Capacity. *Immunity* (2019) 51(2):324–336 e5. doi: 10.1016/j.immuni.2019.06.013
28. Gitlin AD, Mayer CT, Oliveira TY, Shulman Z, Jones MJ, Koren A, et al. HUMORAL IMMUNITY. T cell help controls the speed of the cell cycle in germinal center B cells. *Science* (2015) 349(6248):643–6. doi: 10.1126/science.aac4919
29. Turner JS, Ke F, Grigorova IL. B Cell Receptor Crosslinking Augments Germinal Center B Cell Selection when T Cell Help Is Limiting. *Cell Rep* (2018) 25(6):1395–403 e4. doi: 10.1016/j.celrep.2018.10.042
30. Yeh CH, Nojima T, Kuraoka M, Kelsoe G. Germinal center entry not selection of B cells is controlled by peptide-MHCII complex density. *Nat Commun* (2018) 9(1):928. doi: 10.1038/s41467-018-03382-x
31. Han S, Zheng B, Dal Porto J, Kelsoe G. In situ studies of the primary immune response to (4-hydroxy-3-nitrophenyl)acetyl. IV. Affinity-dependent, antigen-driven B cell apoptosis in germinal centers as a mechanism for maintaining self-tolerance. *J Exp Med* (1995) 182(6):1635–44. doi: 10.1084/jem.182.6.1635
32. Pulendran B, Kannourakis G, Nouri S, Smith KG, Nossal GJ. Soluble antigen can cause enhanced apoptosis of germinal-centre B cells. *Nature* (1995) 375 (6529):331–4. doi: 10.1038/375331a0
33. Shokat KM, Goodnow CC. Antigen-induced B-cell death and elimination during germinal-centre immune responses. *Nature* (1995) 375(6529):334–8. doi: 10.1038/375334a0
34. Khalil AM, Cambier JC, Shlomchik MJ. B cell receptor signal transduction in the GC is short-circuited by high phosphatase activity. *Science* (2012) 336 (6085):1178–81. doi: 10.1126/science.1213368
35. Mueller J, Matloubian M, Zikherman J. Cutting edge: An in vivo reporter reveals active B cell receptor signaling in the germinal center. *J Immunol* (2015) 194(7):2993–7. doi: 10.4049/jimmunol.1403086
36. Nowosad CR, Spillane KM, Tolar P. Germinal center B cells recognize antigen through a specialized immune synapse architecture. *Nat Immunol* (2016) 17 (7):870–7. doi: 10.1038/ni.3458
37. Kwak K, Quizon N, Sohn H, Saniee A, Manzella-Lapeira J, Holla P, et al. Intrinsic properties of human germinal center B cells set antigen affinity thresholds. *Sci Immunol* (2018) 3(29):eaau6598. doi: 10.1126/sciimmunol.aau6598
38. Luo W, Hawse W, Conter L, Trivedi N, Weisel F, Wikenheiser D, et al. The AKT kinase signaling network is rewired by PTEN to control proximal BCR signaling in germinal center B cells. *Nat Immunol* (2019) 20(6):736–46. doi: 10.1038/s41590-019-0376-3
39. Luo W, Weisel F, Shlomchik MJ. B Cell Receptor and CD40 Signaling Are Rewired for Synergistic Induction of the c-Myc Transcription Factor in Germinal Center B Cells. *Immunity* (2018) 48(2):313–326 e5. doi: 10.1016/j.immuni.2018.01.008
40. Dominguez-Sola D, Kung J, Holmes AB, Wells VA, Mo T, Basso K, et al. The FOXO1 Transcription Factor Instructs the Germinal Center Dark Zone Program. *Immunity* (2015) 43(6):1064–74. doi: 10.1016/j.immuni.2015.10.015
41. Sander S, Chu VT, Yasuda T, Franklin A, Graf R, Calado DP, et al. PI3 Kinase and FOXO1 Transcription Factor Activity Differentially Control B Cells in the Germinal Center Light and Dark Zones. *Immunity* (2015) 43(6):1075–86. doi: 10.1016/j.immuni.2015.10.021
42. Akkaya M, Kwak K, Pierce SK. B cell memory: building two walls of protection against pathogens. *Nat Rev Immunol* (2020) 20(4):229–38. doi: 10.1038/s41577-019-0244-2
43. Damdinsuren B, Zhang Y, Khalil A, Wood WH 3rd, Becker KG, Shlomchik MJ, et al. Single round of antigen receptor signaling programs naive B cells to receive T cell help. *Immunity* (2010) 32(3):355–66. doi: 10.1016/j.immuni.2010.02.013
44. Turner JS, Marthi M, Benet ZL, Grigorova I. Transiently antigen-primed B cells return to naive-like state in absence of T-cell help. *Nat Commun* (2017) 8:15072. doi: 10.1038/ncomms15072
45. Purtha WE, Tedder TF, Johnson S, Bhattacharya D, Diamond MS. Memory B cells, but not long-lived plasma cells, possess antigen specificities for viral escape mutants. *J Exp Med* (2011) 208(13):2599–606. doi: 10.1084/jem.20110740
46. Takahashi Y, Kelsoe G. Role of germinal centers for the induction of broadly-reactive memory B cells. *Curr Opin Immunol* (2017) 45:119–25. doi: 10.1016/j.coi.2017.03.002
47. Firl DJ, Degn SE, Padera T, Carroll MC. Capturing change in clonal composition amongst single mouse germinal centers. *Elife* (2018) 7:e33051. doi: 10.7554/eLife.33051

48. Kuraoka M, Schmidt AG, Nojima T, Feng F, Watanabe A, Kitamura D, et al. Complex Antigens Drive Permissive Clonal Selection in Germinal Centers. *Immunity* (2016) 44(3):542–52. doi: 10.1016/j.immuni.2016.02.010
49. Tas JM, Mesin L, Pasqual G, Targ S, Jacobsen JT, Mano YM, et al. Visualizing antibody affinity maturation in germinal centers. *Science* (2016) 351 (6277):1048–54. doi: 10.1126/science.aad3439
50. Nakagawa R, Toboso-Navasa A, Schips M, Young G, Bhaw-Rosun L, Llorian-Sopena M, et al. Permissive selection followed by affinity-based proliferation of GC light zone B cells dictates cell fate and ensures clonal breadth. *Proc Natl Acad Sci USA* (2021) 118(2):e2016425118. doi: 10.1073/pnas.2016425118
51. Liu D, Xu H, Shih C, Wan Z, Ma X, Ma W, et al. T-B-cell entanglement and ICOSL-driven feed-forward regulation of germinal centre reaction. *Nature* (2015) 517(7533):214–8. doi: 10.1038/nature13803
52. Wan Z, Lin Y, Zhao Y, Qi H. TFH cells in bystander and cognate interactions with B cells. *Immunol Rev* (2019) 288(1):28–36. doi: 10.1111/imr.12747
53. Weinstein JS, Herman EI, Lainez B, Licona-Limon P, Esplugues E, Flavell R, et al. TFH cells progressively differentiate to regulate the germinal center response. *Nat Immunol* (2016) 17(10):1197–205. doi: 10.1038/ni.3554
54. Mintz MA, Felce JH, Chou MY, Mayya V, Xu Y, Shui JW, et al. The HVEM-BTLA Axis Restrains T Cell Help to Germinal Center B Cells and Functions as a Cell-Extrinsic Suppressor in Lymphomagenesis. *Immunity* (2019) 51 (2):310–323 e7. doi: 10.1016/j.immuni.2019.05.022
55. Zhang F, Song SS, Shu JL, Li Y, Wu YJ, Wang QT, et al. BAFF upregulates CD28/B7 and CD40/CD154 expression and promotes mouse T and B cell interaction in vitro via BAFF receptor. *Acta Pharmacol Sin* (2016) 37(8):1101–9. doi: 10.1038/aps.2016.15
56. Munoz-Fernandez R, Blanco FJ, Frecha C, Martin F, Kimatrai M, Abadia-Molina AC, et al. Follicular dendritic cells are related to bone marrow stromal cell progenitors and to myofibroblasts. *J Immunol* (2006) 177(1):280–9. doi: 10.4049/jimmunol.177.1.280
57. Nishikawa Y, Hikida M, Magari M, Kanayama N, Mori M, Kitamura H, et al. Establishment of lymphotoxin beta receptor signaling-dependent cell lines with follicular dendritic cell phenotypes from mouse lymph nodes. *J Immunol* (2006) 177(8):5204–14. doi: 10.4049/jimmunol.177.8.5204
58. Allen CD, Cyster JG. Follicular dendritic cell networks of primary follicles and germinal centers: phenotype and function. *Semin Immunol* (2008) 20(1):14–25. doi: 10.1016/j.smim.2007.12.001
59. El Shikh ME, El Sayed RM, Sukumar S, Szakal AK, Tew JG. Activation of B cells by antigens on follicular dendritic cells. *Trends Immunol* (2010) 31 (6):205–11. doi: 10.1016/j.it.2010.03.002
60. Vinuesa CG, Linterman MA, Goodnow CC, Randall KL. T cells and follicular dendritic cells in germinal center B-cell formation and selection. *Immunol Rev* (2010) 237(1):72–89. doi: 10.1111/j.1600-065X.2010.00937.x
61. Garin A, Meyer-Hermann M, Contie M, Figge MT, Buatois V, Gunzer M, et al. Toll-like receptor 4 signaling by follicular dendritic cells is pivotal for germinal center onset and affinity maturation. *Immunity* (2010) 33(1):84–95. doi: 10.1016/j.immuni.2010.07.005
62. Tolar P. Cytoskeletal control of B cell responses to antigens. *Nat Rev Immunol* (2017) 17(10):621–34. doi: 10.1038/nri.2017.67
63. Aydar Y, Sukumar S, Szakal AK, Tew JG. The influence of immune complex-bearing follicular dendritic cells on the IgM response, Ig class switching, and production of high affinity IgG. *J Immunol* (2005) 174(9):5358–66. doi: 10.4049/jimmunol.174.9.5358
64. Carroll MC, Isenman DE. Regulation of humoral immunity by complement. *Immunity* (2012) 37(2):199–207. doi: 10.1016/j.immuni.2012.08.002
65. Cherukuri A, Cheng PC, Pierce SK. The role of the CD19/CD21 complex in B cell processing and presentation of complement-tagged antigens. *J Immunol* (2001) 167(1):163–72. doi: 10.4049/jimmunol.167.1.163
66. Fearon DT, Carroll MC. Regulation of B lymphocyte responses to foreign and self-antigens by the CD19/CD21 complex. *Annu Rev Immunol* (2000) 18:393–422. doi: 10.1146/annurev.immunol.18.1.393
67. Turner JS, Z.L B, Grigorova IL. Antigen Acquisition Enables Newly Arriving B Cells To Enter Ongoing Immunization-Induced Germinal Centers. *J Immunol* (2017) 199(4):1301–7. doi: 10.4049/jimmunol.1700267
68. Boes M, Esau C, Fischer MB, Schmidt T, Carroll M, Chen J. Enhanced B-1 cell development, but impaired IgG antibody responses in mice deficient in secreted IgM. *J Immunol* (1998) 160(10):4776–87.
69. Haberman AM, Shlomchik MJ. Reassessing the function of immune-complex retention by follicular dendritic cells. *Nat Rev Immunol* (2003) 3(9):757–64. doi: 10.1038/nri1178
70. Hannum LG, Haberman AM, Anderson SM, Shlomchik MJ. Germinal center initiation, variable gene region hypermutation, and mutant B cell selection without detectable immune complexes on follicular dendritic cells. *J Exp Med* (2000) 192(7):931–42. doi: 10.1084/jem.192.7.931
71. Kosco-Vilbois MH. Are follicular dendritic cells really good for nothing? *Nat Rev Immunol* (2003) 3(9):764–9. doi: 10.1038/nri1179
72. Phan TG, Green JA, Gray EE, Xu Y, Cyster JG. Immune complex relay by subcapsular sinus macrophages and noncognate B cells drives antibody affinity maturation. *Nat Immunol* (2009) 10(7):786–93. doi: 10.1038/ni.1745
73. van der Poel CE, Bajic G, Macaulay CW, van den Broek T, Ellson CD, Bouma G, et al. Follicular Dendritic Cells Modulate Germinal Center B Cell Diversity through FcgammaRIIB. *Cell Rep* (2019) 29(9):2745–2755 e4. doi: 10.1016/j.celrep.2019.10.086
74. Wu Y, Sukumar S, El Shikh ME, Best AM, Szakal AK, Tew JG. Immune complex-bearing follicular dendritic cells deliver a late antigenic signal that promotes somatic hypermutation. *J Immunol* (2008) 180(1):281–90. doi: 10.4049/jimmunol.180.1.281
75. Schwickert TA, Lindquist RL, Shakhar G, Livshits G, Skokos D, Kosco-Vilbois MH, et al. In vivo imaging of germinal centres reveals a dynamic open structure. *Nature* (2007) 446(7131):83–7. doi: 10.1038/nature05573
76. Shulman Z, Gitlin AD, Targ S, Jankovic M, Pasqual G, Nussenzweig MC, et al. T follicular helper cell dynamics in germinal centers. *Science* (2013) 341 (6146):673–7. doi: 10.1126/science.1241680
77. Ise W, Fujii K, Shiroguchi K, Ito A, Kometani K, Takeda K, et al. T Follicular Helper Cell-Germinal Center B Cell Interaction Strength Regulates Entry into Plasma Cell or Recycling Germinal Center Cell Fate. *Immunity* (2018) 48 (4):702–715 e4. doi: 10.1016/j.immuni.2018.03.027
78. Heise N, De Silva NS, Silva K, Carette A, Simonetti G, Pasparakis M, et al. Germinal center B cell maintenance and differentiation are controlled by distinct NF-kappaB transcription factor subunits. *J Exp Med* (2014) 211 (10):2103–18. doi: 10.1084/jem.20132613
79. Saito M, Gao J, Basso K, Kitagawa Y, Smith PM, Bhagat G, et al. A signaling pathway mediating downregulation of BCL6 in germinal center B cells is blocked by BCL6 gene alterations in B cell lymphoma. *Cancer Cell* (2007) 12 (3):280–92. doi: 10.1016/j.ccr.2007.08.011
80. Nutt SL, Hodgkin PD, Tarlinton DM, Corcoran LM. The generation of antibody-secreting plasma cells. *Nat Rev Immunol* (2015) 15(3):160–71. doi: 10.1038/nri3795
81. Krautler NJ, Suan D, Butt D, Bourne K, Hermes JR, Chan TD, et al. Differentiation of germinal center B cells into plasma cells is initiated by high-affinity antigen and completed by Tfh cells. *J Exp Med* (2017) 214 (5):1259–67. doi: 10.1084/jem.20161533
82. Phan TG, Paus D, Chan TD, Turner ML, Nutt SL, Basten A, et al. High affinity germinal center B cells are actively selected into the plasma cell compartment. *J Exp Med* (2006) 203(11):2419–24. doi: 10.1084/jem.20061254
83. Davidzohn N, Biram A, Stoler-Barak L, Grenov A, Dassa B, Shulman Z. Syk degradation restrains plasma cell formation and promotes zonal transitions in germinal centers. *J Exp Med* (2020) 217(3):jem.20191043. doi: 10.1084/jem.20191043
84. Li X, Gadzinsky A, Gong L, Tong H, Calderon V, Li Y, et al. Cbl Ubiquitin Ligases Control B Cell Exit from the Germinal-Center Reaction. *Immunity* (2018) 48(3):530–541 e6. doi: 10.1016/j.immuni.2018.03.006
85. Kato Y, Abbott RK, Freeman BL, Haupt S, Groschel B, Silva M, et al. Multifaceted Effects of Antigen Valency on B Cell Response Composition and Differentiation In Vivo. *Immunity* (2020) 53(3):548–563 e8. doi: 10.1016/j.immuni.2020.08.001
86. Paus D, Phan TG, Chan TD, Gardam S, Basten A, Brink R. Antigen recognition strength regulates the choice between extrafollicular plasma cell and germinal center B cell differentiation. *J Exp Med* (2006) 203(4):1081–91. doi: 10.1084/jem.20060087
87. Shinnakasu R, Inoue T, Kometani K, Moriyama S, Adachi Y, Nakayama M, et al. Regulated selection of germinal-center cells into the memory B cell compartment. *Nat Immunol* (2016) 17(7):861–9. doi: 10.1038/ni.3460
88. Suan D, Krautler NJ, Maag JLV, Butt D, Bourne K, Hermes JR, et al. CCR6 Defines Memory B Cell Precursors in Mouse and Human Germinal Centers,

Revealing Light-Zone Location and Predominant Low Antigen Affinity. *Immunity* (2017) 47(6):1142–1153 e4. doi: 10.1016/j.immuni.2017.11.022
89. Wang Y, Shi J, Yan J, Xiao Z, Hou X, Lu P, et al. Germinal-center development of memory B cells driven by IL-9 from follicular helper T cells. *Nat Immunol* (2017) 18(8):921–30. doi: 10.1038/ni.3788
90. Laidlaw BJ, Duan L, Xu Y, Vazquez SE, Cyster JG. The transcription factor Hhex cooperates with the corepressor Tle3 to promote memory B cell development. *Nat Immunol* (2020) 21(9):1082–93. doi: 10.1038/s41590-020-0713-6
91. Holmes AB, Corinaldesi C, Shen Q, Kumar R, Compagno N, Wang Z, et al. Single-cell analysis of germinal-center B cells informs on lymphoma cell of origin and outcome. *J Exp Med* (2020) 217(10):e20200483. doi: 10.1084/jem.20200483
92. Anderson SM, Tomayko MM, Ahuja A, Haberman AM, Shlomchik MJ. New markers for murine memory B cells that define mutated and unmutated subsets. *J Exp Med* (2007) 204(9):2103–14. doi: 10.1084/jem.20062571
93. Koike T, Harada K, Horiuchi S, Kitamura D. The quantity of CD40 signaling determines the differentiation of B cells into functionally distinct memory cell subsets. *Elife* (2019) 8:e44245. doi: 10.7554/eLife.44245
94. Toboso-Navasa A, Gunawan A, Morlino G, Nakagawa R, Taddei A, Damry D, et al. Restriction of memory B cell differentiation at the germinal center B cell positive selection stage. *J Exp Med* (2020) 217(7):e20191933. doi: 10.1084/jem.20191933
95. Wiese KE, Walz S, von Eyss B, Wolf E, Athineos D, Sansom O, et al. The role of MIZ-1 in MYC-dependent tumorigenesis. *Cold Spring Harb Perspect Med* (2013) 3(12):a014290. doi: 10.1101/cshperspect.a014290
96. Marfil V, Blazquez M, Serrano F, Castell JV, Bort R. Growth-promoting and tumourigenic activity of c-Myc is suppressed by Hhex. *Oncogene* (2015) 34 (23):3011–22. doi: 10.1038/onc.2014.240
97. Laidlaw BJ, Cyster JG. Transcriptional regulation of memory B cell differentiation. *Nat Rev Immunol* (2020). doi: 10.1038/s41577-020-00446-2
98. Ramezani-Rad P, Chen C, Zhu Z, Rickert RC. Cyclin D3 Governs Clonal Expansion of Dark Zone Germinal Center B Cells. *Cell Rep* (2020) 33 (7):108403. doi: 10.1016/j.celrep.2020.108403
99. Pae J, Ersching J, Castro TBR, Schips M, Mesin L, Allon SJ, et al. Cyclin D3 drives inertial cell cycling in dark zone germinal center B cells. *J Exp Med* (2021) 218(4):e20201699. doi: 10.1084/jem.20201699
100. Chou C, Verbaro DJ, Tonc E, Holmgren M, Cella M, Colonna M, et al. The Transcription Factor AP4 Mediates Resolution of Chronic Viral Infection through Amplification of Germinal Center B Cell Responses. *Immunity* (2016) 45(3):570–82. doi: 10.1016/j.immuni.2016.07.023

Conflict of Interest: The authors declare that the research was conducted in the absence of any commercial or financial relationships that could be construed as a potential conflict of interest.

frontiers in Immunology

MINI REVIEW
published: 31 March 2021
doi: 10.3389/fimmu.2021.659151

Compartments and Connections Within the Germinal Center

Domenick E. Kennedy[*†] *and Marcus R. Clark*[*]

Gwen Knapp Center for Lupus and Immunology Research, Section of Rheumatology, Department of Medicine, University of Chicago, Chicago, IL, United States

Protective high affinity antibody responses emerge through an orchestrated developmental process that occurs in germinal centers (GCs). While GCs have been appreciated since 1930, a wealth of recent progress provides new insights into the molecular and cellular dynamics governing humoral immunity. In this review, we highlight advances that demonstrate that fundamental GC B cell function, selection, proliferation and SHM occur within distinct cell states. The resulting new model provides new opportunities to understand the evolution of immunity in infectious, autoimmune and neoplastic diseases.

Keywords: B cell, germinal center, transcription, epigenetics, T cell help, tingible body macrophage, somatic hypermutation, affinity maturation

OPEN ACCESS

Edited by:
Ann M. Haberman,
Yale University, United States

Reviewed by:
Claude-Agnes Reynaud,
Université Paris Descartes, France
Julia Jellusova,
TU München, Germany

****Correspondence:***
Marcus R. Clark
mclark@uchicago.edu
Domenick E. Kennedy
domenick.kennedy@abbvie.com

†Present address:
Domenick E. Kennedy,
Drug Discovery Science and Technology, AbbVie, North Chicago, IL, United States

Specialty section:
This article was submitted to B Cell Biology, a section of the journal Frontiers in Immunology

Received: *27 January 2021*
Accepted: *15 March 2021*
Published: *31 March 2021*

Citation:
Kennedy DE and Clark MR (2021) Compartments and Connections Within the Germinal Center. Front. Immunol. 12:659151. doi: 10.3389/fimmu.2021.659151

INTRODUCTION

Since the histologic identification in 1930, almost a century of investigation has revealed the central importance of germinal centers (GCs) in humoral immunity (1). Fundamental to GC function is the orchestration of the molecular programs of immunoglobulin gene somatic hypermutation (SHM), selection for antibody affinity and specificity, and proliferative expansion of selected cells. Within the GC, these processes are coordinated with remarkable rapidity such that a B cell transits through these processes in four to six hours allowing for numerous rounds of selection and immune amplification during the course of a typical acute GC reaction of 14 to 21 days (2, 3). From the GC circuit both plasma cells (PCs) and memory B cells (MBCs) are produced ensuring both acute and durable antigen-specific immunity.

The importance of GCs in infection and vaccine responses has been demonstrated in numerous studies (3–5). However, the molecular nature of the GC incurs risk. One risk is that, through stochastic SHM, autoreactive and potentially pathogenic antibodies arise. However, elegant studies have demonstrated that GCs strongly select against autoreactivity (6). Indeed, selection against autoreactivity appears to have primacy over selection for affinity. The mechanisms by which GCs purge the antigen-selected repertoire of autoreactivity remain unclear.

The other risk of ongoing SHM and proliferation is neoplastic transformation. The GC B cell molecular program establishes a state that promotes survival in the presence of increased genomic stress (7, 8). This both enables SHM and increases the risk of lymphoma (9, 10). Indeed, GC B cells are precursors for large B cell lymphoma, follicular lymphoma, and Burkitt lymphoma (11, 12). Transformation has been linked to off-target AID activity (13). Studies in humans and mice have revealed multiple genetic, epigenetic and signaling mechanisms that individually mitigate the risk of neoplastic transformation inherit to the GC response. Recent studies are providing insights into how these mechanisms are coordinated with those that drive affinity maturation (14–16).

In this review, we will discuss the current understanding of how SHM, selection and proliferation are coordinated within the GC. We will first discuss the cellular architecture of the GC and then what is known about underlying molecular programs. Finally, we will propose a model that segregates fundamental GC molecular functions into separate cell states and niches in a way that enables effective adaptive immunity and mitigates the risks of neoplastic transformation.

GC CELLULAR EVOLUTION

The initial histological description of GCs noted characteristic dark and light zones (DZ and LZ respectively). Live cell imaging, and other complementary approaches, have provided remarkable insights into how GCs form and polarize into these two zones that perform very different functions. However, as described below, it has become clear that simple division of cells into DZ and LZ populations obscures underlying molecular GC functions.

Germinal Center Initiation

Activation of naïve B cells in primary follicles induces migration to interfollicular areas and conjugates with antigen-specific T cells. B cells then present antigens to T cells and receive help through CD40-CD40L signals that promote B cell survival (5, 17, 18). Based on intravital microscopy experiments, these B-T cell conjugates can be found within a day after immunization (19, 20). NF-κB signaling is critical downstream of BCR activation to form GCs (21). However, while GCs do not form in mice with impaired NF-κB signaling, responding B cells are still able to migrate to the B-T cell border and present antigen to T cells. Instead, NF-κB signaling regulates expression of the transcription factors (TFs) IRF4 and BCL6, which are critical for both the GC and PC developmental programs (18, 20, 22, 23).

The formation of B-T cell conjugates is followed by T cells entering the B cell follicle on day 3. Subsequently, on day 4, B cells re-enter the B cell follicle and proliferate to form early GCs (18–20). Contrary to these distinct cellular events, the molecular regulation underlying the early events after antigen encounter is still being defined. Recent studies suggest there are multiple pre-GC B cell states leading up to commitment to the GC B cell program (24). Some of these are controlled by the transcriptional repressor BCL6 (20, 25). BCL6 is upregulated in the outer follicle after antigen encounter and is important for forming B-T cell conjugates prior to GC commitment (20). Within early and mature GCs, BCL6 controls B cell positioning within the B cell follicle (20, 23, 26–28). It also enhances GC B cell proliferation by making them more tolerant of DNA damage (7, 8). Ultimately, BCL6 drives the GC B cell program and prevents PC differentiation through inhibition of *Prdm1* (BLIMP) (29).

Recent studies further reinforce the importance of BCL6 in GC B cell commitment. By modulating the amount of Bcl6 expression in transgenic mice, one study found that $Bcl6^{hi}$ B cells responding to immunization were more likely to commit to the GC program (30). In complementary studies, Zhang et al. found that while T-B cell conjugates are important to generate GC B cell precursors, increasing the time of T-B cell conjugates or CD40 signaling reduces progression to a $Bcl6^{hi}$ state and favors plasmablast (PB) differentiation in the extrafollicular region (24).

Class Switch Recombination Occurs During the GC Initiation Phase

In 2019, it was discovered that class switch recombination (CSR), the process by which B cells perform DNA rearrangements at the heavy chain locus to replace IgM and IgD, for IgA, IgG, or IgE, occurs during the GC initiation phase (31). Most studies on CSR have been performed *in vitro* and focused on the molecular mechanism, reviewed (32). However, strong evidence for when CSR occurs *in vivo* was lacking. Through a combination of imaging and molecular experiments Roco et al. found that CSR occurs in the first few days after activation and prior to GC commitment (31). Evidence for this included the observation of predominantly IgM^+ GCs as well as the visualization of CSR prior to mature GC formation. This study resolved a critical question in the field placing CSR in the early events during GC initiation, and validated earlier evidence that CSR might occur prior to mature GCs (33, 34). The transcriptional states associated with CSR have now been resolved at the single cell level, further accelerating our understanding of early events in the GC reaction (35).

Mature GC Cellular Dynamics

By day 4 after immunization, GCs precursors begin to expand and polarize to form LZ and DZ areas by day 7 (18, 36). The LZ contains more sparse populations of B cells that capture antigen from follicular dendritic cells (FDCs) and receive help from cognate T follicular helper (T_{FH}) cells (37). B cells in the LZ are selected based on their competency to present antigen to T_{FH} cells as well as BCR signal strength (38–40). These B cell interactions with T_{FH} cells guide the major known GC fates which include cyclic re-entry, cell death as well as PC and MBC differentiation (37). Tingible body macrophages (TBMs), which lie within the DZ, clear dying B cells and thereby likely prevent inflammation and autoimmunity (37, 41).

A wealth of data assign both proliferation and somatic hypermutation to the DZ (3, 18, 37). However, genomic mutation, and the attendant genotoxic stress are incompatible and indeed antagonistic to proliferation. It is possible that mechanisms intrinsic to genotoxic stress, such as the sensing of DNA breaks by p53, segregate proliferation from SHM within the DZ (42). However, as discussed below, these incompatible processes occur in different cell populations each occupying a unique niche within the GC.

A Paradox

An extensive body of literature has revealed that the LZ and DZ perform very different functions and that this is associated with great molecular complexity. However, when LZ ($CD83^{hi}CXCR4^{low}$) and DZ($CD83^{lo}CXCR4^{hi}$) cells are isolated and characterized for RNA expression and genomic accessibility, they are remarkably similar (14, 38, 43). Taken at face value, these data suggest that primarily post-transcriptional

mechanisms regulate cycling through the dark and light zones. This seems attractive as it could provide for very rapid cell fate transitions. Alternatively, it is possible that simply dividing GC B cells into two populations obscures important underlying molecular dynamics.

There are data supporting the latter possibility. In addition to driving affinity maturation, the GC selects for differentiation into both PCs and MBCs. Precursors of these populations must exist in the GC and, indeed, some have been identified (16, 44, 45). However, these populations are not observed upon simple division of the GC into two populations.

Given the rapidity of the GC cycle, it is also possible that B cells are always in transition (46). This is suggested by available single cell RNA-Seq studies, where GC B cells do not resolve into discrete cell populations (14–16). However, some cell fate decisions are discrete and are associated with definitive checkpoints. A cell either undergoes mitosis or it does not. Likewise for apoptosis. It is possible that SHM occurs along a gradient of cell states. However, we would argue that such a strategy would incur unnecessary genomic risk. Furthermore, during B lymphopoiesis genomic recombination and proliferation are segregated into very different cell populations (47, 48). As described below, this strategy is recapitulated in the GC.

Division of the DZ Into Two Discrete Cell States

The canonical DZ encompasses a gradient of CXCR4 and CD83 surface expression. Differing levels of CXCR4 raises the possibility that these cells could occupy different niches within the DZ and therefore be imbued with different functions. Remarkably, when we split the DZ into two populations ($CXCR4^{hi}CD83^{+}$ and $CXCR4^{+}CD83^{-}$), and therefore GC B cells into three populations, there were striking differences in RNA and protein expression (14). It became clear that proliferation was restricted to the $CXCR4^{hi}CD83^{+}$ population. More specifically, these cells were the site of mitosis marked by increased cell size, enrichment of cells in G2/M and high expression of the mitotic factor Cyclin B1. Previous work has indicated that GC B cells can transit the G1/S checkpoint in any compartment (49, 50). Our data indicate that mitosis occurs in a discrete cell state, which we refer to as proliferative DZ cells or DZp cells.

Conversely, $CXCR4^{+}CD83^{-}$ cells have features of cells undergoing SHM. These include high expression of *Aicda* and genotoxic stress genes as well as induced phosphoproteomic pathways of DNA damage response. These cells were also in the G1 phase of the cell cycle where AID activity is known to occur (14, 51). We refer to this DZ subset as DZd for DZ differentiation. While immunoglobulin gene transcription, which is necessary for AID targeting (52), is induced in DZd, it was effectively repressed in DZp cells. These and other data indicate that both positive and repressive mechanisms ensure segregation of mitosis and SHM into different cell states.

Comparison across RNA expression and proteomic data sets indicated a cyclic progression in which cells selected in the LZ transit to the DZp for mitosis and then to the DZd for SHM (14). These data also revealed how the molecular programs in one cell state primes for functions in the next. Myc provides an example. The *Myc* locus displayed increased genome accessibility and transcription in LZ B cells compared to the DZ populations. However, phosphorylated MYC protein was observed in LZ and DZp B cells, with the downstream MYC program uniquely high in DZp cells.

These data, in conjunction with scRNA-Seq data (14, 15) indicate that expression across each stage is dynamic and that the initiation of transcriptional programs rapidly induces proteomic and functional programs as cells transit through each stage. Overall, these data help explain the rapidity of the GC cycle (2, 3, 38, 50, 53–57).

Remarkably, ATAC-Seq of the LZ, DZp and DZd revealed enhancer accessibility was also very dynamic across the three cell states (14). These differences were not only quantitative but also qualitative with characteristic TF binding motifs becoming accessible in each GC B cell state. In fact, the most enriched TF binding motifs found in each subpopulation were for TFs known to have importance within the GC. These included CTCF in the DZd, OCT2 in the DZp, and SpiB and PU.1 in the LZ (58–62). OCT2 is required for GC B cell proliferation and is dysregulated in B cell lymphomas (62). While OCT2 binding motifs were enriched in DZp accessible regions, *Oct2* expression did not change between subsets. Instead, expression of *Pou2af1* (binding partner of OCT2) was increased in DZp cells (14, 63–65). These data suggest that epigenetic mechanisms play important and complementary roles to TFs in regulating GC B cell fate. We propose that, by mechanisms yet to be defined, GC B cells integrate regulatory mechanisms across the whole vertical pathway of protein expression to affect rapid cell fate decisions.

A New GC Model

Our analysis revealed several markers of the DZp population that allowed identification of distinct clusters of DZp cells within the larger DZd pool (14). These clusters did not arise solely from clonal proliferative expansion. Rather, cells appear to migrate to these DZp niches to undergo mitosis. Why would mitosis occur in a distinct niche? Subsequent analysis demonstrated that DZp cells are intimately intertwined with TBMs. Furthermore, within these cellular aggregates are GC DZp cells that are apoptotic and appear to be undergoing engulfment by TBMs. Integration of these and molecular data suggests a new model of GC compartmentalization (**Figure 1**).

As well described, selection for antigen receptor affinity occurs within the LZ with coordinated collaboration between GC LZ B cells, FDCs and T_{FH} cells (**Figure 1A**). Interactions between LZ B cells and T_{FH} cells are critical to determine GC B cell fate. Our data suggest that those LZ B cells that have been successively selected, and also those that have not, migrate to the DZp niche (**Figure 1B**). Those fated for apoptosis are then eliminated by TBMs, which are the principal macrophage cell population within the GC (37, 66). The mechanisms by which TBMs identify dying B cells is not fully understood. However, it is known that FDCs secrete a molecule called MFGE8, which labels apoptotic cells for phagocytosis (67, 68). This labeling

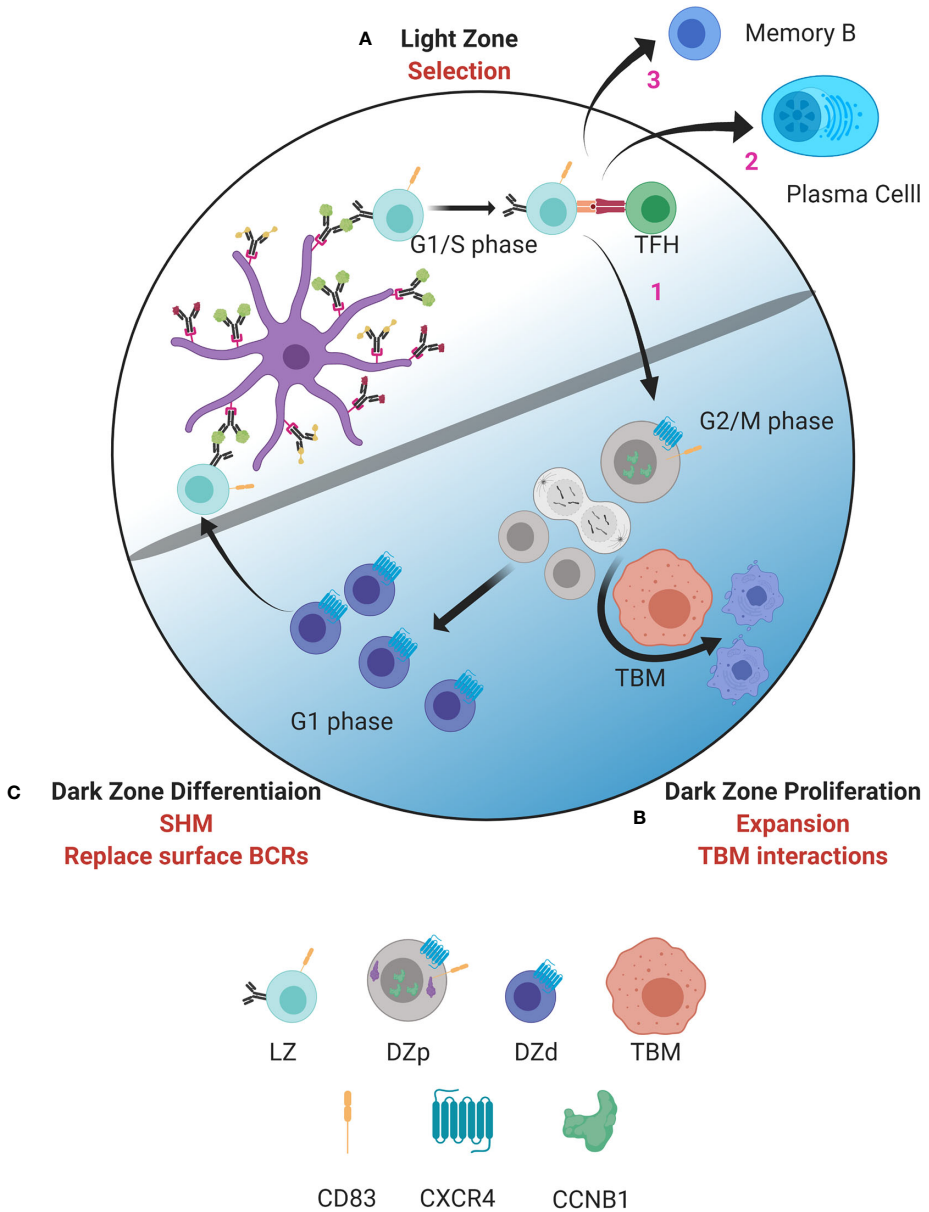

FIGURE 1 | Model of germinal center dynamics and compartmentalization. GC B cells progress through a series of molecular states compartmentalizing key functions to distinct spatial niches. **(A)** GC B cell selection occurs in the LZ. B cells entering the LZ from the DZd first attempt to capture antigen deposited on follicular dendritic cells (FDC). This is followed by antigen processing and presentation to T_{FH} cells in the context of MHC class II. Interactions between LZ B cells and T_{FH} determine if B cells are fated to differentiate into MBCs or PBs, undergo cyclic re-entry into the DZp, or initiate apoptosis. Cells selected for cyclic re-entry migrate to the DZp **(B)**. We propose that B cells that initiate apoptosis in the LZ are cleared by TBMs in the DZp niche. Those cells that are successfully selected in the LZ, and therefore are not cleared by TBMs, undergo mitosis. **(C)** After one or more rounds of cell division, GC B cells transit to the DZd compartment where differentiative functions, such as SHM and replacing old BCRs with newly mutated BCRs, are proposed to occur. B cells that successfully complete processes in the DZd migrate to the LZ to undergo selection. Figure created with BioRender.com.

occurs by binding phosphatidylserine that is externalized on the surface of cells undergoing apoptosis (69). Recently, a molecule called decay accelerating factor (DAF) has also been proposed to regulate GC B cell phagocytosis (70). Such signals likely help TBMs distinguish between healthy B cells and B cells undergoing apoptosis. We propose that B cells that have been successfully selected in the LZ, and are not cleared by TBMs, can then undergo mitosis.

Why would clearance of apoptotic cells be coordinated with mitosis? Apoptosis is the usual pathway of GC cell death (37). However, when apoptotic cells attempt division it can result in mitotic catastrophe and necrosis (71). Therefore, by positioning

TBMs within the DZp niche, necrosis, and the attendant inflammation, would be prevented. Many factors affect the G1/S checkpoint and the decision to initiate proliferation (72). Our data suggest that the main quality check for cell cycle progression is at G2/M.

One of the main controllers of proliferation within the DZp is Myc. B cells selected for cyclic re-entry typically divide on average twice in the DZ (49, 50). The number of divisions is dependent on the strength of signal received from T_{FH} cells. This, in turn, correlates with Myc protein levels implicating Myc in controlling the extent of proliferation (73). In this model, selection in the LZ determines the magnitude of Myc expression. Proliferation then continues until Myc levels are sufficiently diluted by cell division (73–75).

Upon completing one or more rounds of mitosis, GC B cells transition to the DZd stage (**Figure 1C**) where cell cycle exit is coordinated with induction of immunoglobulin gene transcription, which is required for AID targeting. Furthermore, dissolution of the nuclear membrane, as occurs when cells undergo mitosis, facilitates AID entering the nucleus (51). These mechanisms are predicted to restrict AID-mediated SHM to DZd cells. Indeed, these cells bear features of genotoxic stress and DNA repair associated with SHM (14). Our findings are consistent with studies suggesting that SHM occur in G1 phase cells (51, 76–79). Therefore, proliferation and SHM appear to occur in sequential and mutually exclusive cell states, DZp and DZd respectively, that ensure cells have exited cell cycle before initiating SHM. In this way, the attendant risks of gene mutation are mitigated.

B cells undergoing SHM-associated DNA damage and repair undergo an additional checkpoint prior to transit to the LZ. Upon completion of SHM, GC B cells replace old surface BCRs with the newly mutated BCR (80). B cells that generated nonfunctional BCRs due to SHM are fated for apoptosis prior to LZ entry. Thus, there are two levels of BCR selection per GC cycle, structural competency followed by relative affinity. We would postulate that those cells that express an incompetent BCR in the DZd might undergo retrograde GC cycling to be cleared by TBMs, the only known macrophage resident in the DZ (37, 66).

In our model, cells transit from the DZd to LZ without intervening proliferation. Therefore, only mutations that immediately arise on the DNA coding strand would be selected. Mutations on the non-coding strand must also be selected. However for these mutations to be selected, we predict that must arise during the preceding GC cycle and previous transit through the DZd. This would allow these single stranded mutations to be "fixed" by DNA replication in the DZp and therefore become "visible" for subsequent selection in the LZ. Alternatively, it is possible that a minor fraction of DZd cells migrate back to the DZp for proliferation and fixing of non-coding strand mutations.

Selection in the LZ Also Determines Differentiation to PC and MB Cell Fates

In addition to cyclic re-entry into the DZ, LZ B cell interactions with T_{FH} govern GC exit into the PB or MBC fates (18, 81–83). While the LZ population that induces Myc contains cells destined for cyclic re-entry, this B cell pool also contains PB and MBC precursors (45, 84). PB precursors are $BCL6^{lo}CD69^{hi}IRF4^{+}$ and express high-affinity BCRs (38, 45, 85). Commitment to the PC fate is associated with stable B:T_{FH} cell conjugates suggesting strong T cell help instructs PC differentiation (45).

In contrast MBCs develop from low-affinity B cell clones that receive low strength signals from T_{FH} (5, 86–88). Weak T cell help also results in low Myc and mTORC1 activation, which also predisposes to differentiation into MBCs (44). Overall, these studies indicate that high affinity BCRs and strong T_{FH} interactions predispose to PC differentiation while low affinity BCRs, and poor T cell help, leads to differentiation into MBCs.

CONCLUSION

Here we provide a three-compartment model that segregates each fundamental GC B cell function, selection, proliferation and SHM, into distinct, separate cell states. This both mitigates the risk of SHM and allows coordination of molecular processes specific to each function. Furthermore, analysis of these three populations reveal just how molecularly dynamic the GC subsets are with large differences in genomic accessibility, transcription, protein expression and protein phosphorylation across each cell state. Therefore, it is likely that many regulatory mechanisms vertically integrate across the biosynthetic pathway to both drive and maintain the integrity of the GC response. Understanding these mechanisms, and how they integrate to regulate GCs, will provide opportunities to better treat a wide breadth of infectious, autoimmune and neoplastic diseases.

AUTHOR CONTRIBUTIONS

DK and MC wrote and edited the manuscript. All authors contributed to the article and approved the submitted version.

FUNDING

This work is supported by the US National Institutes of Health, National Institute of Allergy and Infectious Diseases grant R01AI143778.

REFERENCES

1. Röhlich K. Beitrag zur Cytologie der Keimzentren der Lymphknoten. *Z Mikrosk Anat Forsch* (1930) 20:287–97. doi: 10.3389/fimmu.2017.01639
2. Mayer CT, Gazumyan A, Kara EE, Gitlin AD, Golijanin J, Viant C, et al. The microanatomic segregation of selection by apoptosis in the germinal center. *Science* (2017) 358(6360):eaao2602. doi: 10.1126/science.aao2602
3. Mesin L, Ersching J, Victora GD. Germinal Center B Cell Dynamics. *Immunity* (2016) 45(3):471–82. doi: 10.1016/j.immuni.2016.09.001

4. Singh A. Eliciting B cell immunity against infectious diseases using nanovaccines. *Nat Nanotechnol* (2021) 16(1):16–24. doi: 10.1038/s41565-020-00790-3
5. Cyster JG, Allen CDC. B Cell Responses: Cell Interaction Dynamics and Decisions. *Cell* (2019) 177(3):524–40. doi: 10.1016/j.cell.2019.03.016
6. Burnett DL, Langley DB, Schofield P, Hermes JR, Chan TD, Jackson J, et al. Germinal center antibody mutation trajectories are determined by rapid self/foreign discrimination. *Science* (2018) 360(6385):223–6. doi: 10.1126/science.aao3859
7. Basso K, Saito M, Sumazin P, Margolin AA, Wang K, Lim WK, et al. Integrated biochemical and computational approach identifies BCL6 direct target genes controlling multiple pathways in normal germinal center B cells. *Blood* (2010) 115(5):975–84. doi: 10.1182/blood-2009-06-227017
8. Huang C, Geng H, Boss I, Wang L, Melnick A. Cooperative transcriptional repression by BCL6 and BACH2 in germinal center B-cell differentiation. *Blood* (2014) 123(7):1012–20. doi: 10.1182/blood-2013-07-518605
9. Mlynarczyk C, Fontan L, Melnick A. Germinal center-derived lymphomas: The darkest side of humoral immunity. *Immunol Rev* (2019) 288(1):214–39. doi: 10.1111/imr.12755
10. Fernando TM, Marullo R, Pera Gresely B, Phillip JM, Yang SN, Lundell-Smith G, et al. BCL6 Evolved to Enable Stress Tolerance in Vertebrates and Is Broadly Required by Cancer Cells to Adapt to Stress. *Cancer Discov* (2019) 9(5):662–79. doi: 10.1158/2159-8290.CD-17-1444
11. Kuppers R, Klein U, Hansmann ML, Rajewsky K. Cellular origin of human B-cell lymphomas. *N Engl J Med* (1999) 341(20):1520–9. doi: 10.1056/NEJM199911113412007
12. Wright GW, Huang DW, Phelan JD, Coulibaly ZA, Roulland S, Young RM, et al. A Probabilistic Classification Tool for Genetic Subtypes of Diffuse Large B Cell Lymphoma with Therapeutic Implications. *Cancer Cell* (2020) 37(4):551–68 e14. doi: 10.1016/j.ccell.2020.03.015
13. Kuppers R, Dalla-Favera R. Mechanisms of chromosomal translocations in B cell lymphomas. *Oncogene* (2001) 20(40):5580–94. doi: 10.1038/sj.onc.1204640
14. Kennedy DE, Okoreeh MK, Maienschein-Cline M, Ai J, Veselits M, McLean KC, et al. Novel specialized cell state and spatial compartments within the germinal center. *Nat Immunol* (2020) 21:660–70. doi: 10.1038/s41590-020-0660-2
15. Milpied P, Cervera-Marzal I, Mollichella ML, Tesson B, Brisou G, Traverse-Glehen A, et al. Human germinal center transcriptional programs are de-synchronized in B cell lymphoma. *Nat Immunol* (2018) 19(9):1013–24. doi: 10.1038/s41590-018-0181-4
16. Holmes AB, Corinaldesi C, Shen Q, Kumar R, Compagno N, Wang Z, et al. Single-cell analysis of germinal-center B cells informs on lymphoma cell of origin and outcome. *J Exp Med* (2020) 217(10):e20200483. doi: 10.1084/jem.20200483
17. Goodnow CC, Vinuesa CG, Randall KL, Mackay F, Brink R. Control systems and decision making for antibody production. *Nat Immunol* (2010) 11(8):681–8. doi: 10.1038/ni.1900
18. De Silva NS, Klein U. Dynamics of B cells in germinal centres. *Nat Rev Immunol* (2015) 15(3):137–48. doi: 10.1038/nri3804
19. Kerfoot SM, Yaari G, Patel JR, Johnson KL, Gonzalez DG, Kleinstein SH, et al. Germinal center B cell and T follicular helper cell development initiates in the interfollicular zone. *Immunity* (2011) 34(6):947–60. doi: 10.1016/j.immuni.2011.03.024
20. Kitano M, Moriyama S, Ando Y, Hikida M, Mori Y, Kurosaki T, et al. Bcl6 protein expression shapes pre-germinal center B cell dynamics and follicular helper T cell heterogeneity. *Immunity* (2011) 34(6):961–72. doi: 10.1016/j.immuni.2011.03.025
21. Jacque E, Schweighoffer E, Visekruna A, Papoutsopoulou S, Janzen J, Zillwood R, et al. IKK-induced NF-kappaB1 p105 proteolysis is critical for B cell antibody responses to T cell-dependent antigen. *J Exp Med* (2014) 211(10):2085–101. doi: 10.1084/jem.20132019
22. Ochiai K, Maienschein-Cline M, Simonetti G, Chen J, Rosenthal R, Brink R, et al. Transcriptional regulation of germinal center B and plasma cell fates by dynamical control of IRF4. *Immunity* (2013) 38(5):918–29. doi: 10.1016/j.immuni.2013.04.009
23. Huang C, Gonzalez DG, Cote CM, Jiang Y, Hatzi K, Teater M, et al. The BCL6 RD2 domain governs commitment of activated B cells to form germinal centers. *Cell Rep* (2014) 8(5):1497–508. doi: 10.1016/j.celrep.2014.07.059
24. Zhang TT, Gonzalez DG, Cote CM, Kerfoot SM, Deng S, Cheng Y, et al. Germinal center B cell development has distinctly regulated stages completed by disengagement from T cell help. *Elife* (2017) 6:e19552. doi: 10.7554/eLife.19552
25. Basso K, Schneider C, Shen Q, Holmes AB, Setty M, Leslie C, et al. BCL6 positively regulates AID and germinal center gene expression via repression of miR-155. *J Exp Med* (2012) 209(13):2455–65. doi: 10.1084/jem.20121387
26. Cinamon G, Matloubian M, Lesneski MJ, Xu Y, Low C, Lu T, et al. Sphingosine 1-phosphate receptor 1 promotes B cell localization in the splenic marginal zone. *Nat Immunol* (2004) 5(7):713–20. doi: 10.1038/ni1083
27. Gatto D, Paus D, Basten A, Mackay CR, Brink R. Guidance of B cells by the orphan G protein-coupled receptor EBI2 shapes humoral immune responses. *Immunity* (2009) 31(2):259–69. doi: 10.1016/j.immuni.2009.06.016
28. Pereira JP, Kelly LM, Xu Y, Cyster JG. EBI2 mediates B cell segregation between the outer and centre follicle. *Nature* (2009) 460(7259):1122–6. doi: 10.1038/nature08226
29. Tunyaplin C, Shaffer AL, Angelin-Duclos CD, Yu X, Staudt LM, Calame KL. Direct repression of prdm1 by Bcl-6 inhibits plasmacytic differentiation. *J Immunol* (2004) 173(2):1158–65. doi: 10.4049/jimmunol.173.2.1158
30. Robinson MJ, Ding Z, Pitt C, Brodie EJ, Quast I, Tarlinton DM, et al. The Amount of BCL6 in B Cells Shortly after Antigen Engagement Determines Their Representation in Subsequent Germinal Centers. *Cell Rep* (2020) 30(5):1530–41 e4. doi: 10.1016/j.celrep.2020.01.009
31. Roco JA, Mesin L, Binder SC, Nefzger C, Gonzalez-Figueroa P, Canete PF, et al. Class-Switch Recombination Occurs Infrequently in Germinal Centers. *Immunity* (2019) 51(2):337–50 e7. doi: 10.1016/j.immuni.2019.07.001
32. Xu Z, Zan H, Pone EJ, Mai T, Casali P. Immunoglobulin class-switch DNA recombination: induction, targeting and beyond. *Nat Rev Immunol* (2012) 12(7):517–31. doi: 10.1038/nri3216
33. Pape KA, Kouskoff V, Nemazee D, Tang HL, Cyster JG, Tze LE, et al. Visualization of the genesis and fate of isotype-switched B cells during a primary immune response. *J Exp Med* (2003) 197(12):1677–87. doi: 10.1084/jem.20012065
34. Cunningham AF, Gaspal F, Serre K, Mohr E, Henderson IR, Scott-Tucker A, et al. Salmonella induces a switched antibody response without germinal centers that impedes the extracellular spread of infection. *J Immunol* (2007) 178(10):6200–7. doi: 10.4049/jimmunol.178.10.6200
35. King HW, Orban N, Riches JC, Clear AJ, Warnes G, Teichmann SA, et al. Single-cell analysis of human B cell maturation predicts how antibody class switching shapes selection dynamics. *Sci Immunol* (2021) 6(56):eabe6291. doi: 10.1126/sciimmunol.abe6291
36. MacLennan IC. Germinal centers. *Ann Rev Immunol* (1994) 12:117–40. doi: 10.1146/annurev.iy.12.040194.001001
37. Victora GD, Nussenzweig MC. Germinal centers. *Ann Rev Immunol* (2012) 30:429–57. doi: 10.1146/annurev-immunol-020711-075032
38. Victora GD, Schwickert TA, Fooksman DR, Kamphorst AO, Meyer-Hermann M, Dustin ML, et al. Germinal center dynamics revealed by multiphoton microscopy with a photoactivatable fluorescent reporter. *Cell* (2010) 143(4):592–605. doi: 10.1016/j.cell.2010.10.032
39. Luo W, Weisel F, Shlomchik MJ. B Cell Receptor and CD40 Signaling Are Rewired for Synergistic Induction of the c-Myc Transcription Factor in Germinal Center B Cells. *Immunity* (2018) 48(2):313–26 e5. doi: 10.1016/j.immuni.2018.01.008
40. Shulman Z, Gitlin AD, Weinstein JS, Lainez B, Esplugues E, Flavell RA, et al. Dynamic signaling by T follicular helper cells during germinal center B cell selection. *Science* (2014) 345(6200):1058–62. doi: 10.1126/science.1257861
41. Baumann I, Kolowos W, Voll RE, Manger B, Gaipl U, Neuhuber WL, et al. Impaired uptake of apoptotic cells into tingible body macrophages in germinal centers of patients with systemic lupus erythematosus. *Arthritis Rheumatol* (2002) 46(1):191–201. doi: 10.1002/1529-0131(200201)46:1<191::AID-ART10027>3.0.CO;2-K
42. Kastenhuber ER, Lowe SW. Putting p53 in Context. *Cell* (2017) 170(6):1062–78. doi: 10.1016/j.cell.2017.08.028
43. Yoshida H, Lareau CA, Ramirez RN, Rose SA, Maier B, Wroblewska A, et al. The cis-Regulatory Atlas of the Mouse Immune System. *Cell* (2019) 176(4):897–912 e20. doi: 10.1016/j.cell.2018.12.036
44. Inoue T, Shinnakasu R, Kawai C, Ise W, Kawakami E, Sax N, et al. Exit from germinal center to become quiescent memory B cells depends on metabolic

reprograming and provision of a survival signal. *J Exp Med* (2021) 218(1): e20200866. doi: 10.1084/jem.20200866
45. Ise W, Fujii K, Shiroguchi K, Ito A, Kometani K, Takeda K, et al. T Follicular Helper Cell-Germinal Center B Cell Interaction Strength Regulates Entry into Plasma Cell or Recycling Germinal Center Cell Fate. *Immunity* (2018) 48 (4):702–15 e4. doi: 10.1016/j.immuni.2018.03.027
46. Dufaud CR, McHeyzer-Williams LJ, McHeyzer-Williams MG. Deconstructing the germinal center, one cell at a time. *Curr Opin Immunol* (2017) 45:112–8. doi: 10.1016/j.coi.2017.03.007
47. Clark MR, Mandal M, Ochiai K, Singh H. Orchestrating B cell lymphopoiesis through interplay of IL-7 receptor and pre-B cell receptor signalling. *Nat Rev Immunol* (2014) 14(2):69–80. doi: 10.1038/nri3570
48. Mandal M, Okoreeh MK, Kennedy DE, Maienschein-Cline M, Ai J, McLean KC, et al. CXCR4 signaling directs Igk recombination and the molecular mechanisms of late B lymphopoiesis. *Nat Immunol* (2019) 20(10):1393–403. doi: 10.1038/s41590-019-0468-0
49. Gitlin AD, Mayer CT, Oliveira TY, Shulman Z, Jones MJ, Koren A, et al. HUMORAL IMMUNITY. T cell help controls the speed of the cell cycle in germinal center B cells. *Science* (2015) 349(6248):643–6. doi: 10.1126/science.aac4919
50. Gitlin AD, Shulman Z, Nussenzweig MC. Clonal selection in the germinal centre by regulated proliferation and hypermutation. *Nature* (2014) 509 (7502):637–40. doi: 10.1038/nature13300
51. Wang Q, Kieffer-Kwon KR, Oliveira TY, Mayer CT, Yao K, Pai J, et al. The cell cycle restricts activation-induced cytidine deaminase activity to early G1. *J Exp Med* (2017) 214(1):49–58. doi: 10.1084/jem.20161649
52. Storb U. Why does somatic hypermutation by AID require transcription of its target genes? *Adv Immunol* (2014) 122:253–77. doi: 10.1016/B978-0-12-800267-4.00007-9
53. Allen CD, Okada T, Tang HL, Cyster JG. Imaging of germinal center selection events during affinity maturation. *Science* (2007) 315(5811):528–31. doi: 10.1126/science.1136736
54. Beltman JB, Allen CD, Cyster JG, de Boer RJ. B cells within germinal centers migrate preferentially from dark to light zone. *Proc Natl Acad Sci U S A* (2011) 108(21):8755–60. doi: 10.1073/pnas.1101554108
55. Schwickert TA, Lindquist RL, Shakhar G, Livshits G, Skokos D, Kosco-Vilbois MH, et al. In vivo imaging of germinal centres reveals a dynamic open structure. *Nature* (2007) 446(7131):83–7. doi: 10.1038/nature05573
56. Meyer-Hermann M, Mohr E, Pelletier N, Zhang Y, Victora GD, Toellner KM. A theory of germinal center B cell selection, division, and exit. *Cell Rep* (2012) 2(1):162–74. doi: 10.1016/j.celrep.2012.05.010
57. Hauser AE, Junt T, Mempel TR, Sneddon MW, Kleinstein SH, Henrickson SE, et al. Definition of germinal-center B cell migration in vivo reveals predominant intrazonal circulation patterns. *Immunity* (2007) 26(5):655–67. doi: 10.1016/j.immuni.2007.04.008
58. Perez-Garcia A, Marina-Zarate E, Alvarez-Prado AF, Ligos JM, Galjart N, Ramiro AR. CTCF orchestrates the germinal centre transcriptional program and prevents premature plasma cell differentiation. *Nat Commun* (2017) 8:16067. doi: 10.1038/ncomms16067
59. Song S, Cao C, Choukrallah MA, Tang F, Christofori G, Kohler H, et al. OBF1 and Oct factors control the germinal center transcriptional program. *Blood* (2021). doi: 10.1182/blood.2020010175
60. Willis SN, Tellier J, Liao Y, Trezise S, Light A, O'Donnell K, et al. Environmental sensing by mature B cells is controlled by the transcription factors PU.1 and SpiB. *Nat Commun* (2017) 8(1):1426. doi: 10.1038/s41467-017-01605-1
61. Carotta S, Willis SN, Hasbold J, Inouye M, Pang SH, Emslie D, et al. The transcription factors IRF8 and PU.1 negatively regulate plasma cell differentiation. *J Exp Med* (2014) 211(11):2169–81. doi: 10.1084/jem.20140425
62. Hodson DJ, Shaffer AL, Xiao W, Wright GW, Schmitz R, Phelan JD, et al. Regulation of normal B-cell differentiation and malignant B-cell survival by OCT2. *Proc Natl Acad Sci U S A* (2016) 113(14):E2039–46. doi: 10.1073/pnas.1600557113
63. Strubin M, Newell JW, Matthias P. OBF-1, a novel B cell-specific coactivator that stimulates immunoglobulin promoter activity through association with octamer-binding proteins. *Cell* (1995) 80(3):497–506. doi: 10.1016/0092-8674(95)90500-6
64. Gstaiger M, Knoepfel L, Georgiev O, Schaffner W, Hovens CM. A B-cell coactivator of octamer-binding transcription factors. *Nature* (1995) 373 (6512):360–2. doi: 10.1038/373360a0
65. Luo Y, Roeder RG. Cloning, functional characterization, and mechanism of action of the B-cell-specific transcriptional coactivator OCA-B. *Mol Cell Biol* (1995) 15(8):4115–24. doi: 10.1128/MCB.15.8.4115
66. Brink R, Phan TG. Self-Reactive B Cells in the Germinal Center Reaction. *Annu Rev Immunol* (2018) 36:339–57. doi: 10.1146/annurev-immunol-051116-052510
67. Hanayama R, Tanaka M, Miyasaka K, Aozasa K, Koike M, Uchiyama Y, et al. Autoimmune disease and impaired uptake of apoptotic cells in MFG-E8-deficient mice. *Science* (2004) 304(5674):1147–50. doi: 10.1126/science.1094359
68. Kranich J, Krautler NJ, Heinen E, Polymenidou M, Bridel C, Schildknecht A, et al. Follicular dendritic cells control engulfment of apoptotic bodies by secreting Mfge8. *J Exp Med* (2008) 205(6):1293–302. doi: 10.1084/jem.20071019
69. Birge RB, Boeltz S, Kumar S, Carlson J, Wanderley J, Calianese D, et al. Phosphatidylserine is a global immunosuppressive signal in efferocytosis, infectious disease, and cancer. *Cell Death Differ* (2016) 23(6):962–78. doi: 10.1038/cdd.2016.11
70. Dernstedt A, Leidig J, Holm A, Kerkman PF, Mjosberg J, Ahlm C, et al. Regulation of Decay Accelerating Factor Primes Human Germinal Center B Cells for Phagocytosis. *Front Immunol* (2020) 11:599647. doi: 10.3389/fimmu.2020.599647
71. Vitale I, Galluzzi L, Castedo M, Kroemer G. Mitotic catastrophe: a mechanism for avoiding genomic instability. *Nat Rev Mol Cell Biol* (2011) 12(6):385–92. doi: 10.1038/nrm3115
72. Bertoli C, Skotheim JM, de Bruin RA. Control of cell cycle transcription during G1 and S phases. *Nat Rev Mol Cell Biol* (2013) 14(8):518–28. doi: 10.1038/nrm3629
73. Finkin S, Hartweger H, Oliveira TY, Kara EE, Nussenzweig MC. Protein Amounts of the MYC Transcription Factor Determine Germinal Center B Cell Division Capacity. *Immunity* (2019) 51(2):324–36 e5. doi: 10.1016/j.immuni.2019.06.013
74. Calado DP, Sasaki Y, Godinho SA, Pellerin A, Kochert K, Sleckman BP, et al. The cell-cycle regulator c-Myc is essential for the formation and maintenance of germinal centers. *Nat Immunol* (2012) 13(11):1092–100. doi: 10.1038/ni.2418
75. Dominguez-Sola D, Victora GD, Ying CY, Phan RT, Saito M, Nussenzweig MC, et al. The proto-oncogene MYC is required for selection in the germinal center and cyclic reentry. *Nat Immunol* (2012) 13(11):1083–91. doi: 10.1038/ni.2428
76. Khair L, Guikema JE, Linehan EK, Ucher AJ, Leus NG, Ogilvie C, et al. ATM increases activation-induced cytidine deaminase activity at downstream S regions during class-switch recombination. *J Immunol* (2014) 192(10):4887–96. doi: 10.4049/jimmunol.1303481
77. Schrader CE, Guikema JE, Linehan EK, Selsing E, Stavnezer J. Activation-induced cytidine deaminase-dependent DNA breaks in class switch recombination occur during G1 phase of the cell cycle and depend upon mismatch repair. *J Immunol* (2007) 179(9):6064–71. doi: 10.4049/jimmunol.179.9.6064
78. Petersen S, Casellas R, Reina-San-Martin B, Chen HT, Difilippantonio MJ, Wilson PC, et al. AID is required to initiate Nbs1/gamma-H2AX focus formation and mutations at sites of class switching. *Nature* (2001) 414 (6864):660–5. doi: 10.1038/414660a
79. Sharbeen G, Yee CW, Smith AL, Jolly CJ. Ectopic restriction of DNA repair reveals that UNG2 excises AID-induced uracils predominantly or exclusively during G1 phase. *J Exp Med* (2012) 209(5):965–74. doi: 10.1084/jem.20112379
80. Stewart I, Radtke D, Phillips B, McGowan SJ, Bannard O. Germinal Center B Cells Replace Their Antigen Receptors in Dark Zones and Fail Light Zone Entry when Immunoglobulin Gene Mutations are Damaging. *Immunity* (2018) 49(3):477–89 e7. doi: 10.1016/j.immuni.2018.08.025
81. Akkaya M, Kwak K, Pierce SK. B cell memory: building two walls of protection against pathogens. *Nat Rev Immunol* (2020) 20(4):229–38. doi: 10.1038/s41577-019-0244-2
82. Merino Tejero E, Lashgari D, Garcia-Valiente R, Gao X, Crauste F, Robert PA, et al. Multiscale Modeling of Germinal Center Recapitulates the Temporal Transition From Memory B Cells to Plasma Cells Differentiation as Regulated by Antigen Affinity-Based Tfh Cell Help. *Front Immunol* (2020) 11:620716. doi: 10.3389/fimmu.2020.620716

83. Liu B, Lin Y, Yan J, Yao J, Liu D, Ma W, et al. Affinity-coupled CCL22 promotes positive selection in germinal centres. *Nature* (2021). doi: 10.1038/s41586-021-03384-8
84. Nakagawa R, Toboso-Navasa A, Schips M, Young G, Bhaw-Rosun L, Llorian-Sopena M, et al. Permissive selection followed by affinity-based proliferation of GC light zone B cells dictates cell fate and ensures clonal breadth. *Proc Nat Acad Sci U S A* (2021) 118(2):e2016425118. doi: 10.1073/pnas.2016425118
85. Phan TG, Paus D, Chan TD, Turner ML, Nutt SL, Basten A, et al. High affinity germinal center B cells are actively selected into the plasma cell compartment. *J Exp Med* (2006) 203(11):2419–24. doi: 10.1084/jem.20061254
86. Shinnakasu R, Inoue T, Kometani K, Moriyama S, Adachi Y, Nakayama M, et al. Regulated selection of germinal-center cells into the memory B cell compartment. *Nat Immunol* (2016) 17(7):861–9. doi: 10.1038/ni.3460
87. Viant C, Weymar GHJ, Escolano A, Chen S, Hartweger H, Cipolla M, et al. Antibody Affinity Shapes the Choice between Memory and Germinal Center B Cell Fates. *Cell* (2020) 183(5):1298–311 e11. doi: 10.1016/j.cell.2020.09.063
88. Palm AE, Henry C. Remembrance of Things Past: Long-Term B Cell Memory After Infection and Vaccination. *Front Immunol* (2019) 10:1787. doi: 10.3389/fimmu.2019.01787

Conflict of Interest: The authors declare that the research was conducted in the absence of any commercial or financial relationships that could be construed as a potential conflict of interest.

frontiers in Immunology

MINI REVIEW
published: 19 April 2021
doi: 10.3389/fimmu.2021.660450

microRNA Fine-Tuning of the Germinal Center Response

Teresa Fuertes[1], *Irene Salgado*[2] *and Virginia G. de Yébenes*[2,3]*

[1] B Lymphocyte Biology Lab, Centro Nacional de Investigaciones Cardiovasculares, Madrid, Spain, [2] Department of Immunology, Ophthalmology and ENT, Universidad Complutense de Madrid School of Medicine, Madrid, Spain, [3] Inmunología Linfocitaria Lab, Hospital 12 de Octubre Health Research Institute (imas12), Madrid, Spain

Germinal centers (GCs) are complex multicellular structures in which antigen-specific B cells undergo the molecular remodeling that enables the generation of high-affinity antibodies and the differentiation programs that lead to the generation of plasma–antibody-secreting cells and memory B cells. These reactions are tightly controlled by a variety of mechanisms, including the post-transcriptional control of gene expression by microRNAs (miRNAs). Through the development of animal models with B cell-specific modified miRNA expression, we have contributed to the understanding of the role of miRNAs in the regulation of GC responses and in B cell neoplasia. Here, we review recent advances in the understanding of the role of miRNAs in the regulation of B cell and T follicular helper physiology during the GC response and in the diseases associated to GC response dysregulation.

Keywords: microRNA, germinal center, antibodies, autoimmunity, neoplasia

OPEN ACCESS

Edited by:
Thierry Fest,
University of Rennes 1, France

Reviewed by:
Paolo Casali,
University of Texas Health Science Center at San Antonio, United States
Masaki Hikida,
Akita University, Japan

****Correspondence:***
Virginia G. de Yébenes
vgarciay@ucm.es

Specialty section:
This article was submitted to B Cell Biology, a section of the journal Frontiers in Immunology

Received: *29 January 2021*
Accepted: *31 March 2021*
Published: *19 April 2021*

Citation:
Fuertes T, Salgado I and de Yébenes VG (2021) microRNA Fine-Tuning of the Germinal Center Response. Front. Immunol. 12:660450. doi: 10.3389/fimmu.2021.660450

INTRODUCTION

The germinal center (GC) response is a key B lymphocyte maturation and differentiation program essential for the generation of competent protective immunity. The GC response is initiated in mature B lymphocytes after antigen encounter and leads to the generation of memory B cells and plasma antibody-secreting cells that produce antibodies with high antigen affinity and with different immunoglobulin (Ig) isotypes, conferring the Ig molecule with the ability to orchestrate different immune effector responses (1, 2). At the molecular level, these reactions are initiated by the activity of activation induced deaminase (AID), an enzyme that deaminates cytosines in the Ig genes, triggering somatic hypermutation (SHM) and class switch recombination (CSR), processes respectively responsible for the changes in affinity and isotype in the Ig genes. At the cellular level, initiation of the GC reaction requires the cognate interaction of antigen-activated B-lymphocytes with a specialized subset of GC T CD4 cells, the follicular T helper (Tfh) cells. Tfh-GC B cell interactions are dependent on a number of molecule interactions that signal for full B and Tfh cell differentiation together with cellular localization in follicles. These interactions include T-cell receptor recognition of B cell peptide-MHC complexes as well as CD40 and ICOS ligand co-receptor interactions (3). Developing Tfh and B GC cells are influenced by changing cytokine, chemokine and cellular environments through the induction of specific transcriptional programs (4). Gene transcription in Tfh and B cells is regulated by key GC transcription factors such as BCL6, as well as by RNA-binding proteins and microRNAs (miRNAs) (3, 5). miRNAs are small non-coding RNA molecules that drive post-transcriptional negative regulation of gene expression by

promoting the degradation or translational blockade of partially complementary target mRNAs. Mature miRNAs are 21-24-nucleotide RNA molecules processed from longer RNA precursors in two consecutive cleavage steps mediated by the RNase III enzymes Drosha and Dicer (6). Ablation of miRNAs in miRNA-processing-enzyme deletion knockout models has demonstrated that miRNAs play essential roles in diverse developmental, cellular, and physiological processes (7, 8). miRNAs fine-tune cellular gene expression networks and have emerged as essential regulators of GC differentiation responses.

miRNAs IN PHYSIOLOGICAL GC REGULATION

Studies of global miRNA depletion in GC B and T cell-specific models showed that miRNAs are essential for proper GC formation (9, 10). Dicer-mediated miRNA depletion after AID expression in early activated GC B cells impaired the production of high-affinity class-switched antibodies and the generation of memory B and long-lived plasma cells after T cell-dependent immunization due to defects in B cell proliferation and survival (9). Likewise, DGCR8-Drosha complex-mediated miRNA depletion in CD4 T cells showed that CD4 T cell-expressed miRNAs are essential for the differentiation of Tfh cells and the induction of GC B cells during T cell-dependent immunizations (10). Interestingly, miRNAs are not only required to regulate Tfh and GC B cell function in a cell intrinsic manner, but are also important contact-independent mediators of T-B cellular communication (**Figure 1**). This communication occurs through the transfer to B cells of a restricted set of T cell-derived miRNAs in extracellular vesicles and modulates the efficiency of GC generation and antibody secretion in response to immunization (11).

miRNAs in the Regulation of B Cells in the GC

The most extensively studied GC B cell miRNA is miR-155, whose expression is upregulated after mature B cell activation and in GC B cells (12–15). Infection of miR-155-deficient mice with pathogenic bacteria showed that miR-155 expression is required to control pathogen-induced disease (16). Characterization of the response to T cell-dependent immunizations in miR-155$^{-/-}$ loss-of-function and miR-155^{KI} gain-of-function mouse models revealed that miR-155 expression is required for efficient adaptive immune responses, including the generation of GC B cells and the secretion of antigen-specific antibodies (12, 16). miR-155 is a positive regulator of the GC response, and deficiency in miR-155 expression leads to reduced cytokine production, IgG1 secretion, impaired affinity maturation, and plasmablast B cell generation in a B cell autonomous manner (12, 17, 18). miR-155 controls affinity-based selection, at least in part, by protecting light zone (LZ) GC c-MYC^{+} B cells from apoptosis (19).

Transcriptome studies showed that miR-155 regulates the expression of numerous mRNAs in B cells (17, 18), although the functional consequences of miR-155-dependent mRNA regulation in GC B cells has been characterized for only a few miR-155 targets. The transcription factor PU.1 is a direct miR-155 target implicated in miR-155 mediated effects on CSR (17). PU.1 is encoded by *Sfpi1*, and the consequences of disrupting miR-155–*Sfpi1* mRNA interaction *in vivo* were determined by generating knock-in mice with a mutation in the miR-155 recognition site in the *Sfpi1* mRNA 3'UTR. miR-155-mediated PU.1 post-transcriptional regulation was shown to be required for efficient terminal plasma B cell differentiation and antigen-specific immunoglobulin (Ig) secretion through the downregulation of *Pax5* expression and genes involved in adhesion and B-T cell interactions (20).

The other well characterized miR-155 target in GC B cells is activation-induced deaminase (AID), the enzyme responsible for the molecular remodeling of Igs in the GC. Knock-in mice with a disruption of the miR-155 recognition site in the *Aicda* mRNA 3'UTR demonstrated that miR-155 expression in GC B cells is needed to limit AID expression, allow proper affinity maturation, and restrict oncogenic AID-mediated MYC-IgH chromosomal translocations (21, 22). GC tolerance of DNA damage is multilayered and temporally regulated (23), and miR-155 expression is in turn limited by the expression of BCL6 (24, 25), an important transcriptional regulator and proto-oncogene that inhibits the DNA damage response in GC B cells (26). In addition, miR-155 negatively regulates the expression of *Socs1*, a P53 activator important for the DNA damage response (27). miR-155 thus plays a dual role in modulating the accumulation of DNA double-strand breaks (DSB) associated with the GC reaction, regulating P53 activity by controlling the expression levels of *Aicda* and *Socs1*.

AID expression is directly regulated in B cells by yet other miRNAs in B cells. miR-361 is another BCL6-downregulated miRNA that targets *Aicda*, presumably in light-zone GC B cells (25). miR-181b, which is highly expressed in mature resting B cells and whose expression diminishes upon B cell activation, targets *Aicda* directly through the binding of several partly complementary sequences found in its mRNA 3'UTR (28). Thus, AID levels are controlled by different miRNAs at different stages of B cell activation.

Another miRNA that positively regulates the GC response upon its induction during B cell activation and in GC B cells is miR-217. Using gain- and loss-of-function mouse models, we showed that miR-217 promotes the generation of GC B cells and increases the generation of class-switched antibodies and the frequency of somatic hypermutation in B cells. We found that miR-217 regulates a DNA damage response and repair gene network that stabilizes BCL6 expression in GC B cells (29). Thus, miR-217 downregulates a network of genes that sense and repair genotoxic events on DNA, which in turn can increase GC B cell tolerance to DNA damage in the context of AID activity, very much like BCL6. Notably, we found that miR-217 protects BCL6 from previously described genotoxic stress-induced degradation (23), suggesting that both molecules form part of the same network that renders GC cells permissive to genomic instability and prone to malignant transformation.

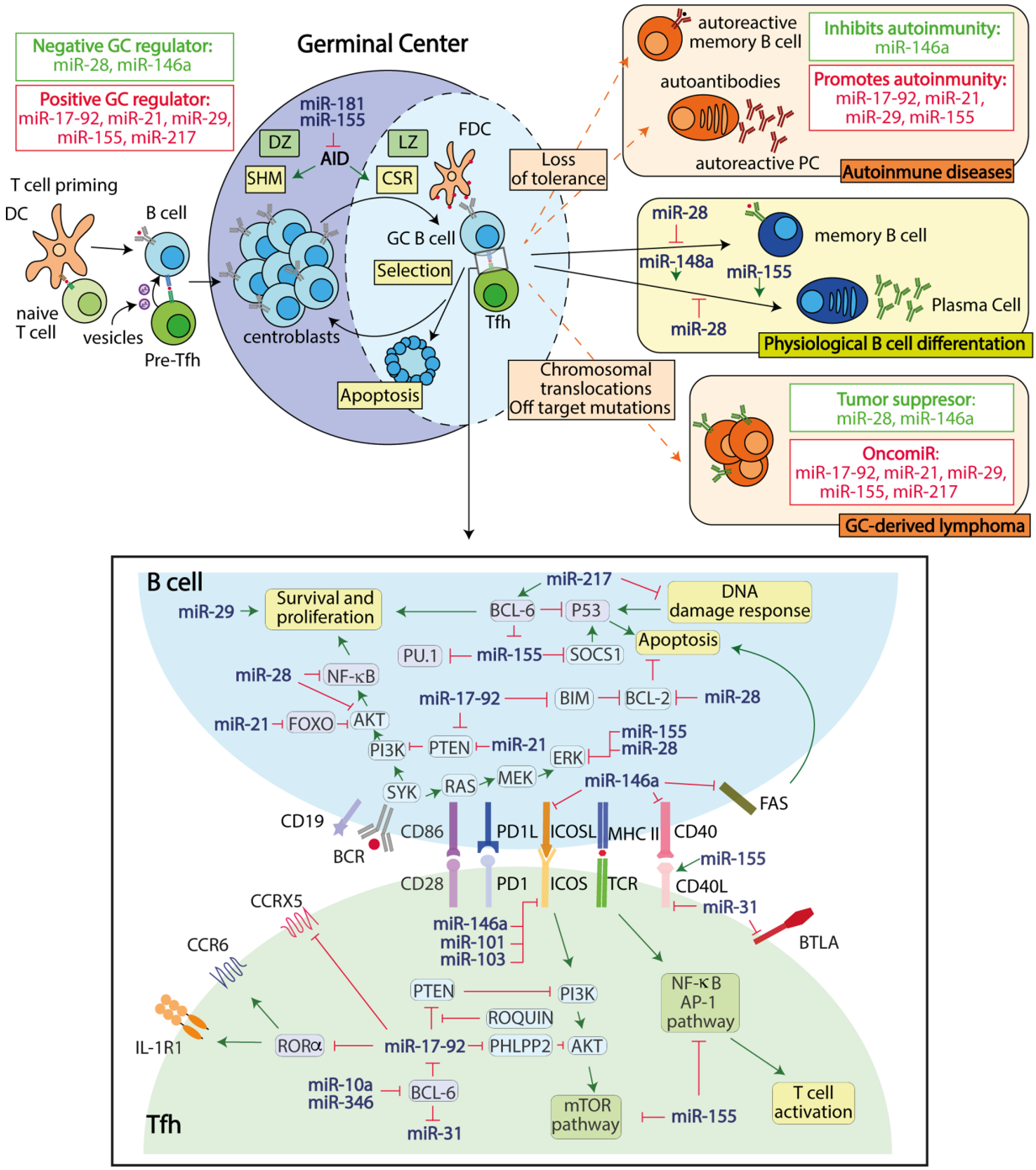

FIGURE 1 | miRNAs regulate gene expression in B and Tfh germinal center cells. Regulated miRNA expression is required to regulate B-Tfh cell interactions and ensure proper GC responses. GC-derived dysfunctions caused by miRNA alterations can lead to the development of autoimmunity and/or B cell neoplasia through the disruption of post-transcriptional control mechanisms required for the maintenance of GC homeostasis.

Positive regulation of terminal post-GC plasma B cell differentiation has been suggested to be regulated by other miRNAs. A likely candidate is miR-148a, the most abundant miRNA in human and murine plasma cells, which has been shown to promote plasma cell differentiation and survival *in vitro*. Importantly, miR-148a expression was shown to downregulate the expression of the GC transcription factors *Mitf* and *Bach2*, which block premature plasma cell maturation

and favor cell death (30). Definition of the role of miR-148a as a regulator of GC-dependent plasma cell differentiation *in vivo* would require the development of gain- or loss-of-function miR-148a B cell-specific mouse models.

GC miRNAs can also act as regulators that restrict the GC response, the best-characterized negative regulators of GC responses being miR-28 and miR-146a. miR-28 is a GC-specific miRNA (14, 15) whose expression is lost in numerous mature B-cell neoplasms (31–33). By combining gain- and loss-of-function approaches, we showed that miR-28 negatively regulates CSR and immunization-triggered GC and post-GC plasma and memory B cell generation. Combined transcriptome and proteome analysis upon inducible re-expression of miR-28 in B cells revealed that miR-28 expression induces the coordinated downregulation of the key BCR signaling gene network regulating B-cell proliferation and cell death (33), thus supporting the notion that miR-28 limits the strength of BCR signaling and regulates proliferation and survival of GC B cells.

miR-146a is expressed in B cells upon stimulation and within GC B cells (15), and loss of miR-146a causes a B cell-intrinsic increase in the GC response to immunization (34), spontaneous GC generation in aged mice, and increased production of anti-double–stranded DNA (dsDNA) auto-antibodies (35). miR-146a was shown to limit B cell GC functional responses by downregulating B cell expression of signaling pathway components involved in GC B Tfh cellular interactions, such as ICOSL (34) and CD40 (35).

Other miRNAs have also been suggested to negatively regulate terminal post-GC plasma and memory B cell differentiation. miR-125b, a miRNA highly expressed in dividing centroblasts in GC B cells (36), has been shown to inhibit plasma cell generation and antibody secretion *in vitro* (37, 38). Importantly, direct mRNA targeting by miR-125b was shown to downregulate the expression of BLIMP-1 and IRF-4 transcription factors, which are essential for plasma cell differentiation (36–39). *Prdm1*, the gene encoding BLIMP-1, is a direct target of other highly expressed GC B cell miRNAs, including miR-9, miR-30a, and let-7 family miRNAs (40–43). Interestingly, the expression of miR-30a and miR-125b is regulated epigenetically in B cells and can be modulated using histone deacetylase inhibitors to inhibit BLIMP-1 expression in the context of antibody responses and GC-derived diseases (44–46). Memory B cell generation is associated to changes in chromatin accessibility and miRNA expression, and miR-181 has been recently identified as a major gene expression regulator during memory B cell differentiation (47).

Overall, these studies have identified a set of miRNAs that are required to promote or limit the GC reaction through post-transcriptional gene expression regulation in B cells (**Figure 1** and **Table 1**).

miRNAs in the Regulation of Follicular Helper T Cells

The induction of the GC reaction is critically dependent on the colocalization of B cells with Tfh cells and interaction between the two. This GC B-Tfh cell interaction and the resulting intracellular signaling are also controlled by miRNAs expressed in Tfh cells. Remarkably, miR-146a downregulates the inducible costimulatory *Icos* expression in Tfh cells (34), and thus the expression of the two interacting molecules (ICOS and ICOSL) of this costimulatory pathway are negatively controlled in both cell subsets by the same miRNA. ICOS directly controls the migration of $CD4^+$ T cells from the T cell-B cell border into the B cell follicles of peripheral lymphoid organs (77). Importantly, ICOS signaling in T cells was shown to be important for miR-146a mediated Tfh and GC regulation (34). *Icos* expression is also negatively regulated by two other miRNAs whose expression is downregulated during Tfh differentiation, miR-101 and miR-103 (78, 79). Thus, ICOS co-stimulatory receptor expression is redundantly regulated by miRNAs in Tfh cells presumably to limit or end the GC reaction.

GC B-Tfh derived ICOS signaling is mediated by the PI3K/AKT pathway (80) and inhibited by PTEN phosphatase activity in Tfh cells (81). This key signaling pathway for Tfh activation and differentiation (3) is additionally regulated at different levels in Tfh cells by miRNAs from the miR-17-92 cluster. miR-17-92 cluster expression is induced early in T cell activation (48) and is repressed by BCL6, the critical transcriptional factor that regulates Tfh differentiation (82). T cell-specific miR-17-92 gain- and loss-of function mouse models showed that the microRNAs of the cluster are critical promoters of Tfh and GC B cell differentiation and antigen-specific antibody generation during both T-cell dependent immune responses and chronic viral infection (10, 48, 49). miR-17-92 cluster miRNAs regulate the ICOS-PI3K signaling pathway in Tfh cells through the simultaneous targeting of different pathway inhibitory components. miR-17-92 inhibits PTEN phosphatase expression upstream of AKT (10, 48, 51) as well as the downstream AKT phosphatase PHLPP2 (48). This pathway is additionally regulated in Tfh cells by Roquin, an RNA-binding protein that recognizes specific stem-loop structures in the 3'UTRs of target mRNAs and which interferes with miR-17-92 binding to an overlapping binding site in the *Pten* mRNA 3'UTR (83). Important miR-17-92 targets mediating other aspects of the Tfh differentiation program include the transcription factor RORα; responsible for the induction of IL-1R1 and CCR6 expression in Tfh cells (10), and CXCR5, a hallmark Tfh molecule that influences Tfh cell localization to follicles in which the ligand CXCL13 is expressed (82).

BCL6 represses the expression of a significant fraction of the miRNAs expressed in mouse $CD4^+$ T cells (82); however, the functional contribution of this repression to the Tfh cell transcriptional program has been characterized for few miRNAs outside the miR-17-92 cluster. BCL6 represses miR-31 expression in human Tfh cells through direct binding to its promoter (84). miR-31 inhibits the expression of CD40L, SAP, and BTLA, which are crucial for Tfh cell helper activity and cross-talk with B cells (85–87). Accordingly, Tfh cells forced to express miR-31 display decreased B-helper activity (84). Although BCL6 controls Tfh activity in humans and mice, the role of miR-31 is restricted to human Tfh cell differentiation, reflecting a species specificity on the action of some miRNAs.

Bcl6 gene expression is also regulated by miRNAs in $CD4^+$ T cells, and this regulation influences the generation of Tfh cells

TABLE 1 | Identified roles of miRNAs in the regulation of physiological GC responses and in GC-derived dysfunctions.

GC regulation miRNA	Role in GC physiology	Role in B cell neoplasia	Role in autoimmunity	Molecular mechanisms and targets
miR-17-92 polycistron (miR-17, miR-18a, miR-19a, miR-20a, miR-19b, and miR-92a)	**Positive GC regulator**. Promotes GC responses, Tfh and GC B cell generation (10, 48, 49).	**OncomiR.** Promotes B cell GC-derived lymphoma (50)	**Promotes autoimmunity.** miR-17-92 expression in lymphocytes promotes spontaneous accumulation of Tfh and GC B cells, IgG anti-dsDNA antibodies and fatal immunopathology (48, 51).	Promotes proliferation and survival in lymphocytes by inhibiting the expression of *Pten* and *Bim* (51). Regulates differentiation and enhances ICOS-PI3K signaling by downregulating *Pten* and *Phlpp2* phosphatase gene expression in Tfh cells (10, 48, 49).
miR-155	**Positive GC regulator** Promotes GC responses and Tfh and GC B cell generation (12, 16, 52)	**OncomiR** Induces preB and mature B cell lymphomas (53–56)	**Promotes autoimmunity** miR-155 expression promotes autoimmunity in autoimmune mouse models of collagen-induced arthritis (57), systemic lupus erythematosus Fas^{lpr} (58, 59), and age-dependent miR-146a deficiency (52).	Regulates the GC reaction *via* B cell-intrinsic (12, 17, 18) and T cell-intrinsic mechanisms (52). Prevents LZ GC c-MYC^+ B cell apoptosis by downregulating *Jarid2* (19). Targets *Sfpi1* (17, 60) and *Aicda* (21, 22, 44) mRNAs and prevents P53 (27) and ERK activation through the inhibition of SHIP-1 (58) in B cells. Promotes *Prmd1*/BLIMP-1 expression and plasma cell differentation through PU.1-*Pax5* downregulation in B cells (20, 60). Regulates Tfh development and autoimmunity by modulating NF-κB, AP-1, and mTOR pathways (52) and promotes Tfh cellular proliferation and CD40L expression by repressing *Peli1* (61). Targets *S1pr1* in B cells from Fas^{lpr} lupus-like mice, and its expression is decreased in SLE patients (57, 59). Inhibits *Pu.1* in rheumatoid arthritis B cells (60). Promotes age-dependent inflammation associated to accumulation of Tfh, GC B cells and the generation of autoantibodies in miR146a deficient mice (62).
miR-217	**Positive GC regulator** Promotes GC B cell generation and GC responses (29).	**OncomiR** Overexpression in B cells leads to clonal GC-derived lymphomas (29).	NA	Downregulates DNA damage and repair response through *Nbs1*, *Xrcc2*, *Lig4*, and *Pds5b* gene expression downregulation and BCL6 stabilization (29).
miR-29	**Positive GC regulator** Promotes GC B cell generation after T-cell dependent immunization (63)	**OncomiR** Overexpression in B cells leads to B-cell chronic lymphocytic leukemia (B-CLL) development (64)	**Promotes autoimmunity** Promotes autoimmunity in collagen-induced arthritis (63)	Promotes B-cell proliferation (63, 64). Downregulates the expression of *Ddk6*, *Dnmt3a*, and the P53-responsive and tumor suppressor gene *Pxdn* (64).
miR-21	**Positive GC regulator** Promotes GC responses, Tfh and GC B cell generation (Schell SL J Immunol 2019, 202 (1 Supplement) 121.12; (Abstr) (65). Expression inhibited by BLIMP-1 during plasma cell differentiation (66).	**oncomiR** Induces B lymphomas dependent on continuous miR-21 expression (67).	**Promotes autoimmunity** miR-21 inhibition ameliorates disease in a lupus model (68)	Promotes B cell activation and proliferation. Activates the PI3K–AKT–mTOR pathway. Inhibits expression of *Pten*, *Pdcd4* (69), *Foxo* (70), *Fas* (65), and *Pdcd4* (68).
miR-28	**Negative GC regulator** Impairs CSR and memory B and plasma cell differentiation (33).	**Tumor suppressor** Efficiently inhibits tumor growth after intratumor or systemic administration of miR-28 synthetic mimics in various DLBCL and BL xenograft models and in a primary mouse BL (33).	NA	Inhibits BCR signaling and impairs B-cell proliferation and survival. Inhibits *MAD2L1, BAG1, RAP1B, p-AKT, p-ERK, NFKB2, IKKB* and *BCL2* gene expression (32, 33).

(Continued)

TABLE 1 | Continued

GC regulation miRNA	Role in GC physiology	Role in B cell neoplasia	Role in autoimmunity	Molecular mechanisms and targets
miR-146a	**Negative GC regulator** Limits Tfh and GC B cell generation and GC responses in T and B cells (34, 35, 52)	**Tumor suppressor** miR-146a knockout mice spontaneously develop B cell lymphomas and myeloid malignancies (71, 72). miR-146b and miR-146a knockout mice develop histologically distinct B cell lymphomas (73). miR-146a deficiency accelerates c-MYC-induced B cell lymphoma development (74).	**Inhibits autoimmunity** Loss of miR-146a in immune cells promotes autoimmunity (72) (52). Loss of miR-146a causes a B cell-intrinsic increase in anti- dsDNA auto-antibody production and spontaneous GC reactions (35).	Immunosuppressive roles in innate and adaptive immunity (72, 75). Downregulates the expression of signaling pathway components involved in GC B-Tfh cellular interactions, such as ICOSL-ICOS (34) and CD40-CD40L (35). Limits Tfh numbers by downregulating *Stat1* expression (75) and counterregulates miR-155 targets in Tfh cells, which is relevant to inhibit the generation of autoantibodies associated to age-dependent inflammation (52). Dysregulated overexpression promotes a lymphoproliferative syndrome and GC B cell expansion *via Fas* expression downregulation in GC B cells (76).

NA, not analyzed.

from T cell precursors. miR-10a, a miRNA highly expressed in mouse regulatory T cells (T_{reg}), has been proposed to attenuate the conversion of inducible T_{regs} to Tfh cells through *Bcl6* repression in mice (88). miR-346 has been suggested to repress *BCL6* gene expression in human Tfh cells (62).

Another key miRNA regulator of both CG B and Tfh cells is the positive GC regulator miR-155. Immunization of T cell-specific miR-155-deficient *Cd4*-Cre miR155$^{fl/fl}$ mice revealed impaired in GC B and Tfh cell generation and antigen-specific antibody production (52), revealing that miR-155 expression regulates Tfh development during immunization responses through T cell intrinsic mechanisms. The same study showed that miR-155 regulates different Tfh-cell targets important for Tfh development and autoimmunity in the NF-κB, AP-1 and mTOR pathways. Interestingly, miR-155 promotes Tfh cell accumulation during chronic, low-grade inflammation by counteracting the effect of miR-146a in Tfh cells (52). A later study showed that miR-155 promotes Tfh cell proliferation and CD40L expression by repressing expression of *Peli1*, a ubiquitin ligase that promotes the degradation of the NF-κB family transcription factor c-REL (61). These data suggest that miR-155 contributes to increased Tfh-mediated GC B activation through increased CD40L–CD40 interaction, which is known to be a limiting step in B cell clonal expansion, GC formation, isotype switching, affinity maturation, and the generation of long-lived plasma cells (89, 90).

Thus, miRNAs regulate Tfh cellular differentiation and interaction with B cells in the GC at multiple levels and through multilayer regulatory molecular circuits (**Figure 1**).

miRNAs IN GC-DERIVED B CELL NEOPLASIA AND AUTOIMMUNE DISEASES

Defects in GC regulation lead to immune diseases such as autoimmunity and mature B-cell neoplasia. These diseases are ultimately caused by the dysregulation of two distinct GC checkpoints; a breakdown of immune tolerance in autoimmunity and a surpassing of the DNA damage-tolerance threshold associated with Ig remodeling during CSR and SHM in B cell neoplasia. However, both diseases share a contribution from some of the mechanisms that promote GC dysfunction, including lymphoproliferative aberrant GC persistence, abnormal cellular components, and abnormal cellular signaling (91–93).

Recent studies addressing the contribution of miRNAs to these two GC-derived diseases revealed that dysregulated miRNA expression in GC B or Tfh cells can trigger B cell neoplasia or autoimmunity (**Figure 1**). Interestingly, several miRNAs that positively regulate the GC response also promote autoimmunity and B cell neoplasia (**Table 1**). For instance, miR-155, which promotes GC responses through T and B cell intrinsic mechanisms (12, 16, 52), also promotes autoimmune diseases characterized by switched auto-antibodies (52, 57–60, 94) and B cell neoplasia (53–56), likely through multilayer mechanisms that can lead to aberrant GC persistence due to increased

proliferation, reduced cell death and altered cellular signaling of Tfh and GC B cells (**Table 1**). Similarly, the miR-17-92 polycistron, which promotes GC responses by enhancing Tfh and B lymphocyte proliferation and survival by inhibiting the expression of *Pten* and *Bim* (10, 48, 49, 51), when overexpressed in different mouse models promotes the generation of spontaneous GCs, IgG anti-double–stranded DNA (dsDNA) autoantibodies linked to fatal immunopathology (48, 51), and B cell GC-derived lymphoma (50). Accordingly, miR-155 and miR-17-92 are upregulated in mature B cell neoplasia and GC-derived autoimmune diseases (95–97), suggesting their involvement in the enhancement of GC-derived human diseases. Other miRNAs that positively regulate GC responses and have been found to promote both autoimmunity and B-cell derived neoplasia include miR-29 and miR-21 (**Table 1**). Further studies are required to establish whether the switched autoantibodies generated in the context of positive GC miRNA regulator overexpression are derived from GC-derived plasma cells or are also generated from extrafollicular plasma cells.

Several miRNAs that negatively regulate the GC reaction have the opposite effect on B cell neoplasia and autoimmunity development, limiting the generation of GC-derived diseases (**Table 1**). miR-28 and miR-146a, well-characterized negative regulators of GC responses (33–35, 52), have both been found to exert tumor suppressor activity in B cell lymphoma development by limiting cell proliferation, promoting cell death and regulating cell signaling (33, 71, 73, 74) (**Table 1**). However, protection against autoimmune diseases has only been explored for miR-146a, which inhibits autoimmunity, anti-dsDNA autoantibody production (72), and spontaneous GC reactions (52) counterregulating miR-155 targets in Tfh cells (62) and through B cell-intrinsic mechanisms, likely by targeting CD40 signaling pathway components (35). Nevertheless, GC B cell miR-146a expression needs to be tightly regulated because forced overexpression promotes a lymphoproliferative syndrome *via Fas* downregulation (76). Thus, both super abundant or insufficient miR-146a expression are harmful for GC homeostasis.

Overall, these studies show that regulated miRNA expression is required to ensure proper GC responses and that GC-derived dysfunctions caused by miRNA alterations frequently lead to the development of both autoimmunity and B cell neoplasia through the disruption of post-transcriptional control mechanisms required for the maintenance of GC homeostasis, regulated cell signaling, cell death and proliferation. Further studies are needed to characterize with more detail the molecular mechanisms leading to both neoplastic transformation and autoimmunity caused by miRNA-dependent GC gene expression dysregulation.

CONCLUSIONS AND PERSPECTIVE

Studies by many groups in the field have shown that miRNAs play a key role in GC-response regulation and are required to prevent GC-derived autoimmunity and B cell neoplasia. The description of the role of dysregulated miRNAs in mature B cell oncogenic transformation and GC-derived autoimmunity has led to the clinical use of miRNAs as disease biomarkers with prognostic and predictive value and to the identification of targets for miRNA-based therapy (97, 98). The mechanisms leading to dysregulated miRNA expression in GC cells are poorly understood, and their characterization will likely provide new opportunities for therapeutic intervention. Strategies to restore or inhibit dysregulated miRNA expression have already established the therapeutic potential of miRNA modulation in *in vivo* models of GC-derived B cell neoplasia and autoimmunity (33, 44, 56, 68, 99–105). Moreover, synthetic miRNA mimics or anti-miR molecules are suitable for the generation of miRNA-based drugs that can be coupled to different types of nanocarriers and conjugates for effective delivery [reviewed in (106)].

The unique molecular features of miRNAs make them attractive tools for the development of miRNA-based therapies, and miRNA-based drugs are currently being tested in clinical trials for several diseases, including different types of cancer [reviewed in (97)]. This emerging and promising field faces a number of challenges regarding the clinical translation of miRNA-based therapies for B cell neoplasia and autoimmunity. Major challenges include i) the development of cell-type specific miRNA-based drug targeting approaches to improve specificity and reduce toxicity derived from miRNA delivery to healthy cells and ii) the development of models of human mature B cell neoplasia and GC-derived autoimmunity that faithfully recapitulate human disease to improve pre-clinical testing. The rapid pace of research in the field ensures the continuing excitement and expectations in building the path from basic science to translational miRNA-mediated GC regulation.

AUTHOR CONTRIBUTIONS

TF, IS and VY contributed substantially to the content and structure of this review. All authors contributed to the article and approved the submitted version.

FUNDING

Our work is supported by the Spanish Ministerio de Ciencia e Innovación (PID2019-107551RB-I00). TF is supported by a PhD fellowship from the Spanish Ministerio de Ciencia, Innovacion y Universidades (BES-2017-079759), VY by funding from the Universidad Complutense de Madrid, and IS by a student research grant from the Ministerio de Educación y Formación Profesional.

ACKNOWLEDGMENTS

We thank Simon Bartlett for English editing.

REFERENCES

1. Victora GD, Nussenzweig MC. Germinal Centers. *Annu Rev Immunol* (2012) 30:429–57. doi: 10.1146/annurev-immunol-020711-075032
2. Mesin L, Ersching J, Victora GD. Germinal Center B Cell Dynamics. *Immunity* (2016) 45:471–82. doi: 10.1016/j.immuni.2016.09.001
3. Vinuesa CG, Linterman MA, Yu D, MacLennan IC. Follicular Helper T Cells. *Annu Rev Immunol* (2016) 34:335–68. doi: 10.1146/annurev-immunol-041015-055605
4. Stebegg M, Kumar SD, Silva-Cayetano A, Fonseca VR, Linterman MA, Graca L. Regulation of the Germinal Center Response. *Front Immunol* (2018) 9:2469. doi: 10.3389/fimmu.2018.02469
5. Song S, Matthias PD. The Transcriptional Regulation of Germinal Center Formation. *Front Immunol* (2018) 9:2026. doi: 10.3389/fimmu.2018.02026
6. Gebert LFR, MacRae IJ. Regulation of Microrna Function in Animals. *Nat Rev Mol Cell Biol* (2019) 20:21–37. doi: 10.1038/s41580-018-0045-7
7. Guo WT, Wang Y. Dgcr8 Knockout Approaches to Understand Microrna Functions in Vitro and in Vivo. *Cell Mol Life Sci* (2019) 76:1697–711. doi: 10.1007/s00018-019-03020-9
8. Park CY, Choi YS, McManus MT. Analysis of Microrna Knockouts in Mice. *Hum Mol Genet* (2010) 19:R169–75. doi: 10.1093/hmg/ddq367
9. Xu S, Guo K, Zeng Q, Huo J, Lam KP. The Rnase III Enzyme Dicer is Essential for Germinal Center B-Cell Formation. *Blood* (2012) 119:767–76. doi: 10.1182/blood-2011-05-355412
10. Baumjohann D, Kageyama R, Clingan JM, Morar MM, Patel S, de Kouchkovsky D, et al. The Microrna Cluster Mir-17 Approximately 92 Promotes TFH Cell Differentiation and Represses Subset-Inappropriate Gene Expression. *Nat Immunol* (2013) 14:840–8. doi: 10.1038/ni.2642
11. Fernandez-Messina L, Rodriguez-Galan A, de Yebenes VG, Gutierrez-Vazquez C, Tenreiro S, Seabra MC, et al. Transfer of Extracellular Vesicle-Microrna Controls Germinal Center Reaction and Antibody Production. *EMBO Rep* (2020) 21:e48925. doi: 10.15252/embr.201948925
12. Thai TH, Calado DP, Casola S, Ansel KM, Xiao C, Xue Y, et al. Regulation of the Germinal Center Response by Microrna-155. *Science* (2007) 316:604–8. doi: 10.1126/science.1141229
13. Tam W. Identification and Characterization of Human BIC, a Gene on Chromosome 21 That Encodes a Noncoding RNA. *Gene* (2001) 274:157–67. doi: 10.1016/S0378-1119(01)00612-6
14. Basso K, Sumazin P, Morozov P, Schneider C, Maute RL, Kitagawa Y, et al. Identification of the Human Mature B Cell Mirnome. *Immunity* (2009) 30:744–52. doi: 10.1016/j.immuni.2009.03.017
15. Kuchen S, Resch W, Yamane A, Kuo N, Li Z, Chakraborty T, et al. Regulation of Microrna Expression and Abundance During Lymphopoiesis. *Immunity* (2010) 32:828–39. doi: 10.1016/j.immuni.2010.05.009
16. Rodriguez A, Vigorito E, Clare S, Warren MV, Couttet P, Soond DR, et al. Requirement of Bic/Microrna-155 for Normal Immune Function. *Science* (2007) 316:608–11. doi: 10.1126/science.1139253
17. Vigorito E, Perks KL, Abreu-Goodger C, Bunting S, Xiang Z, Kohlhaas S, et al. Microrna-155 Regulates the Generation of Immunoglobulin Class-Switched Plasma Cells. *Immunity* (2007) 27:847–59. doi: 10.1016/j.immuni.2007.10.009
18. Arbore G, Henley T, Biggins L, Andrews S, Vigorito E, Turner M, et al. Microrna-155 is Essential for the Optimal Proliferation and Survival of Plasmablast B Cells. *Life Sci Alliance* (2019) 2(3):e201800244. doi: 10.26508/lsa.201800244
19. Nakagawa R, Leyland R, Meyer-Hermann M, Lu D, Turner M, Arbore G, et al. Microrna-155 Controls Affinity-Based Selection by Protecting C-MYC + B Cells From Apoptosis. *J Clin Invest* (2016) 126:377–88. doi: 10.1172/JCI82914
20. Lu D, Nakagawa R, Lazzaro S, Staudacher P, Abreu-Goodger C, Henley T, et al. The Mir-155-PU.1 Axis Acts on Pax5 to Enable Efficient Terminal B Cell Differentiation. *J Exp Med* (2014) 211:2183–98. doi: 10.1084/jem.20140338
21. Teng G, Hakimpour P, Landgraf P, Rice A, Tuschl T, Casellas R, et al. Microrna-155 is a Negative Regulator of Activation-Induced Cytidine Deaminase. *Immunity* (2008) 28:621–9. doi: 10.1016/j.immuni.2008.03.015
22. Dorsett Y, McBride KM, Jankovic M, Gazumyan A, Thai TH, Robbiani DF, et al. Microrna-155 Suppresses Activation-Induced Cytidine Deaminase-Mediated Myc-Igh Translocation. *Immunity* (2008) 28:630–8. doi: 10.1016/j.immuni.2008.04.002
23. Phan RT, Saito M, Kitagawa Y, Means AR, Dalla-Favera R. Genotoxic Stress Regulates Expression of the Proto-Oncogene Bcl6 in Germinal Center B Cells. *Nat Immunol* (2007) 8:1132–9. doi: 10.1038/ni1508
24. Phan RT, Dalla-Favera R. The BCL6 Proto-Oncogene Suppresses P53 Expression in Germinal-Centre B Cells. *Nature* (2004) 432:635–9. doi: 10.1038/nature03147
25. Basso K, Schneider C, Shen Q, Holmes AB, Setty M, Leslie C, et al. BCL6 Positively Regulates AID and Germinal Center Gene Expression Via Repression of Mir-155. *J Exp Med* (2012) 209:2455–65. doi: 10.1084/jem.20121387
26. Basso K, Dalla-Favera R. Roles of BCL6 in Normal and Transformed Germinal Center B Cells. *Immunol Rev* (2012) 247:172–83. doi: 10.1111/j.1600-065X.2012.01112.x
27. Bouamar H, Jiang D, Wang L, Lin AP, Ortega M, Aguiar RC. Microrna 155 Control of P53 Activity is Context Dependent and Mediated by Aicda and Socs1. *Mol Cell Biol* (2015) 35:1329–40. doi: 10.1128/MCB.01446-14
28. de Yebenes VG, Belver L, Pisano DG, Gonzalez S, Villasante A, Croce C, et al. Mir-181b Negatively Regulates Activation-Induced Cytidine Deaminase in B Cells. *J Exp Med* (2008) 205:2199–206. doi: 10.1084/jem.20080579
29. de Yebenes VG, Bartolome-Izquierdo N, Nogales-Cadenas R, Perez-Duran P, Mur SM, Martinez N, et al. Mir-217 is an Oncogene That Enhances the Germinal Center Reaction. *Blood* (2014) 124:229–39. doi: 10.1182/blood-2013-12-543611
30. Porstner M, Winkelmann R, Daum P, Schmid J, Pracht K, Corte-Real J, et al. Mir-148a Promotes Plasma Cell Differentiation and Targets the Germinal Center Transcription Factors Mitf and Bach2. *Eur J Immunol* (2015) 45:1206–15. doi: 10.1002/eji.201444637
31. Iqbal J, Shen Y, Huang X, Liu Y, Wake L, Liu C, et al. Global Microrna Expression Profiling Uncovers Molecular Markers for Classification and Prognosis in Aggressive B-Cell Lymphoma. *Blood* (2015) 125:1137–45. doi: 10.1182/blood-2014-04-566778
32. Schneider C, Setty M, Holmes AB, Maute RL, Leslie CS, Mussolin L, et al. Microrna 28 Controls Cell Proliferation and is Down-Regulated in B-Cell Lymphomas. *Proc Natl Acad Sci USA* (2014) 111:8185–90. doi: 10.1073/pnas.1322466111
33. Bartolome-Izquierdo N, de Yebenes VG, Alvarez-Prado AF, Mur SM, Lopez Del Olmo JA, Roa S, et al. Mir-28 Regulates the Germinal Center Reaction and Blocks Tumor Growth in Preclinical Models of Non-Hodgkin Lymphoma. *Blood* (2017) 129:2408–19. doi: 10.1182/blood-2016-08-731166
34. Pratama A, Srivastava M, Williams NJ, Papa I, Lee SK, Dinh XT, et al. Microrna-146a Regulates ICOS-ICOSL Signalling to Limit Accumulation of T Follicular Helper Cells and Germinal Centres. *Nat Commun* (2015) 6:6436. doi: 10.1038/ncomms7436
35. Cho S, Lee HM, Yu IS, Choi YS, Huang HY, Hashemifar SS, et al. Differential Cell-Intrinsic Regulations of Germinal Center B and T Cells by Mir-146a and Mir-146b. *Nat Commun* (2018) 9:2757. doi: 10.1038/s41467-018-05196-3
36. Malumbres R, Sarosiek KA, Cubedo E, Ruiz JW, Jiang X, Gascoyne RD, et al. Differentiation Stage-Specific Expression of Micrornas in B Lymphocytes and Diffuse Large B-Cell Lymphomas. *Blood* (2009) 113:3754–64. doi: 10.1182/blood-2008-10-184077
37. Gururajan M, Haga CL, Das S, Leu CM, Hodson D, Josson S, et al. Microrna 125b Inhibition of B Cell Differentiation in Germinal Centers. *Int Immunol* (2010) 22:583–92. doi: 10.1093/intimm/dxq042
38. Tsai DY, Hung KH, Lin IY, Su ST, Wu SY, Chung CH, et al. Uncovering Microrna Regulatory Hubs That Modulate Plasma Cell Differentiation. *Sci Rep* (2015) 5:17957. doi: 10.1038/srep17957
39. Morelli E, Leone E, Cantafio ME, Di Martino MT, Amodio N, Biamonte L, et al. Selective Targeting of IRF4 by Synthetic Microrna-125b-5p Mimics Induces Anti-Multiple Myeloma Activity in Vitro and in Vivo. *Leukemia* (2015) 29:2173–83. doi: 10.1038/leu.2015.124
40. Nie K, Gomez M, Landgraf P, Garcia JF, Liu Y, Tan LH, et al. Microrna-Mediated Down-Regulation of PRDM1/Blimp-1 in Hodgkin/Reed-Sternberg Cells: A Potential Pathogenetic Lesion in HODGKIN

Lymphomas. *Am J Pathol* (2008) 173:242–52. doi: 10.2353/ajpath.2008.080009
41. Nie K, Zhang T, Allawi H, Gomez M, Liu Y, Chadburn A, et al. Epigenetic Down-Regulation of the Tumor Suppressor Gene PRDM1/Blimp-1 in Diffuse Large B Cell Lymphomas: A Potential Role of the Microrna Let-7. *Am J Pathol* (2010) 177:1470–9. doi: 10.2353/ajpath.2010.091291
42. Zhang J, Jima DD, Jacobs C, Fischer R, Gottwein E, Huang G, et al. Patterns of Microrna Expression Characterize Stages of Human B-Cell Differentiation. *Blood* (2009) 113:4586–94. doi: 10.1182/blood-2008-09-178186
43. Huang X, Zhou X, Wang Z, Li F, Liu F, Zhong L, et al. CD99 Triggers Upregulation of Mir-9-Modulated PRDM1/BLIMP1 in Hodgkin/Reed-Sternberg Cells and Induces Redifferentiation. *Int J Cancer* (2012) 131: E382–94. doi: 10.1002/ijc.26503
44. White CA, Pone EJ, Lam T, Tat C, Hayama KL, Li G, et al. Histone Deacetylase Inhibitors Upregulate B Cell Micrornas That Silence AID and Blimp-1 Expression for Epigenetic Modulation of Antibody and Autoantibody Responses. *J Immunol* (2014) 193:5933–50. doi: 10.4049/jimmunol.1401702
45. Shen T, Sanchez HN, Zan H, Casali P. Genome-Wide Analysis Reveals Selective Modulation of Micrornas and Mrnas by Histone Deacetylase Inhibitor in B Cells Induced to Undergo Class-Switch DNA Recombination and Plasma Cell Differentiation. *Front Immunol* (2015) 6:627. doi: 10.3389/fimmu.2015.00627
46. Moroney JB, Chupp DP, Xu Z, Zan H, Casali P. Epigenetics of the Antibody and Autoantibody Response. *Curr Opin Immunol* (2020) 67:75–86. doi: 10.1016/j.coi.2020.09.004
47. Moroney JB, Vasudev A, Pertsemlidis A, Zan H, Casali P. Integrative Transcriptome and Chromatin Landscape Analysis Reveals Distinct Epigenetic Regulations in Human Memory B Cells. *Nat Commun* (2020) 11:5435. doi: 10.1038/s41467-020-19242-6
48. Kang SG, Liu WH, Lu P, Jin HY, Lim HW, Shepherd J, et al. Micrornas of the Mir-17 Approximately 92 Family are Critical Regulators of T(FH) Differentiation. *Nat Immunol* (2013) 14:849–57. doi: 10.1038/ni.2648
49. Wu T, Wieland A, Lee J, Hale JS, Han JH, Xu X, et al. Cutting Edge: Mir-17-92 is Required for Both CD4 Th1 and T Follicular Helper Cell Responses During Viral Infection. *J Immunol* (2015) 195:2515–9. doi: 10.4049/jimmunol.1500317
50. Jin HY, Oda H, Lai M, Skalsky RL, Bethel K, Shepherd J, et al. Microrna-17~92 Plays a Causative Role in Lymphomagenesis by Coordinating Multiple Oncogenic Pathways. *EMBO J* (2013) 32:2377–91. doi: 10.1038/emboj.2013.178
51. Xiao C, Srinivasan L, Calado DP, Patterson HC, Zhang B, Wang J, et al. Lymphoproliferative Disease and Autoimmunity in Mice With Increased Mir-17-92 Expression in Lymphocytes. *Nat Immunol* (2008) 9:405–14. doi: 10.1038/ni1575
52. Hu R, Kagele DA, Huffaker TB, Runtsch MC, Alexander M, Liu J, et al. Mir-155 Promotes T Follicular Helper Cell Accumulation During Chronic, Low-Grade Inflammation. *Immunity* (2014) 41:605–19. doi: 10.1016/j.immuni.2014.09.015
53. Costinean S, Zanesi N, Pekarsky Y, Tili E, Volinia S, Heerema N, et al. Pre-B Cell Proliferation and Lymphoblastic Leukemia/High-Grade Lymphoma in E(Mu)-Mir155 Transgenic Mice. *Proc Natl Acad Sci USA* (2006) 103:7024–9. doi: 10.1073/pnas.0602266103
54. Costinean S, Sandhu SK, Pedersen IM, Tili E, Trotta R, Perrotti D, et al. Src Homology 2 Domain-Containing Inositol-5-Phosphatase and CCAAT Enhancer-Binding Protein Beta are Targeted by Mir-155 in B Cells of Emicro-Mir-155 Transgenic Mice. *Blood* (2009) 114:1374–82. doi: 10.1182/blood-2009-05-220814
55. Pedersen IM, Otero D, Kao E, Miletic AV, Hother C, Ralfkiaer E, et al. Onco-Mir-155 Targets SHIP1 to Promote Tnfalpha-Dependent Growth of B Cell Lymphomas. *EMBO Mol Med* (2009) 1:288–95. doi: 10.1002/emmm.200900028
56. Babar IA, Cheng CJ, Booth CJ, Liang X, Weidhaas JB, Saltzman WM, et al. Nanoparticle-Based Therapy in an in Vivo Microrna-155 (Mir-155)-Dependent Mouse Model of Lymphoma. *Proc Natl Acad Sci USA* (2012) 109:E1695–704. doi: 10.1073/pnas.1201516109
57. Kurowska-Stolarska M, Alivernini S, Ballantine LE, Asquith DL, Millar NL, Gilchrist DS, et al. Microrna-155 as a Proinflammatory Regulator in Clinical and Experimental Arthritis. *Proc Natl Acad Sci USA* (2011) 108:11193–8. doi: 10.1073/pnas.1019536108
58. Thai TH, Patterson HC, Pham DH, Kis-Toth K, Kaminski DA, Tsokos GC. Deletion of Microrna-155 Reduces Autoantibody Responses and Alleviates Lupus-Like Disease in the Fas(Lpr) Mouse. *Proc Natl Acad Sci USA* (2013) 110:20194–9. doi: 10.1073/pnas.1317632110
59. Xin Q, Li J, Dang J, Bian X, Shan S, Yuan J, et al. Mir-155 Deficiency Ameliorates Autoimmune Inflammation of Systemic Lupus Erythematosus by Targeting S1pr1 in Faslpr/Lpr Mice. *J Immunol* (2015) 194:5437–45. doi: 10.4049/jimmunol.1403028
60. Alivernini S, Kurowska-Stolarska M, Tolusso B, Benvenuto R, Elmesmari A, Canestri S, et al. Microrna-155 Influences B-Cell Function Through PU.1 in Rheumatoid Arthritis. *Nat Commun* (2016) 7:12970. doi: 10.1038/ncomms12970
61. Liu WH, Kang SG, Huang Z, Wu CJ, Jin HY, Maine CJ, et al. A Mir-155-Peli1-C-Rel Pathway Controls the Generation and Function of T Follicular Helper Cells. *J Exp Med* (2016) 213:1901–19. doi: 10.1084/jem.20160204
62. Chen J, Tian J, Tang X, Rui K, Ma J, Mao C, et al. Mir-346 Regulates CD4(+) CXCR5(+) T Cells in the Pathogenesis of Graves' Disease. *Endocrine* (2015) 49:752–60. doi: 10.1007/s12020-015-0546-5
63. van Nieuwenhuijze A, Dooley J, Humblet-Baron S, Sreenivasan J, Koenders M, Schlenner SM, et al. Defective Germinal Center B-Cell Response and Reduced Arthritic Pathology in Microrna-29a-Deficient Mice. *Cell Mol Life Sci* (2017) 74:2095–106. doi: 10.1007/s00018-017-2456-6
64. Santanam U, Zanesi N, Efanov A, Costinean S, Palamarchuk A, Hagan JP, et al. Chronic Lymphocytic Leukemia Modeled in Mouse by Targeted Mir-29 Expression. *Proc Natl Acad Sci USA* (2010) 107:12210–5. doi: 10.1073/pnas.1007186107
65. Yan Y, Deng X, Ning X, Li F, Cao J. Pathogenic Mechanism of Mir-21 in Autoimmune Lymphoid Hyperplasia Syndrome. *Oncol Lett* (2017) 13:4734–40. doi: 10.3892/ol.2017.6039
66. Barnes NA, Stephenson S, Cocco M, Tooze RM, Doody GM. BLIMP-1 and STAT3 Counterregulate Microrna-21 During Plasma Cell Differentiation. *J Immunol* (2012) 189:253–60. doi: 10.4049/jimmunol.1101563
67. Medina PP, Nolde M, Slack FJ. Oncomir Addiction in an in Vivo Model of Microrna-21-Induced Pre-B-Cell Lymphoma. *Nature* (2010) 467:86–90. doi: 10.1038/nature09284
68. Garchow BG, Bartulos Encinas O, Leung YT, Tsao PY, Eisenberg RA, Caricchio R, et al. Silencing of Microrna-21 in Vivo Ameliorates Autoimmune Splenomegaly in Lupus Mice. *EMBO Mol Med* (2011) 3:605–15. doi: 10.1002/emmm.201100171
69. Gu L, Song G, Chen L, Nie Z, He B, Pan Y, et al. Inhibition of Mir-21 Induces Biological and Behavioral Alterations in Diffuse Large B-Cell Lymphoma. *Acta Haematol* (2013) 130:87–94. doi: 10.1159/000346441
70. Go H, Jang JY, Kim PJ, Kim YG, Nam SJ, Paik JH, et al. Microrna-21 Plays an Oncogenic Role by Targeting FOXO1 and Activating the PI3K/AKT Pathway in Diffuse Large B-Cell Lymphoma. *Oncotarget* (2015) 6:15035–49. doi: 10.18632/oncotarget.3729
71. Zhao JL, Rao DS, Boldin MP, Taganov KD, O'Connell RM, Baltimore D. NF-Kappab Dysregulation in Microrna-146a-Deficient Mice Drives the Development of Myeloid Malignancies. *Proc Natl Acad Sci USA* (2011) 108:9184–9. doi: 10.1073/pnas.1105398108
72. Boldin MP, Taganov KD, Rao DS, Yang L, Zhao JL, Kalwani M, et al. Mir-146a is a Significant Brake on Autoimmunity, Myeloproliferation, and Cancer in Mice. *J Exp Med* (2011) 208:1189–201. doi: 10.1084/jem.20101823
73. Mitsumura T, Ito Y, Chiba T, Matsushima T, Kurimoto R, Tanaka Y, et al. Ablation of Mir-146b in Mice Causes Hematopoietic Malignancy. *Blood Adv* (2018) 2:3483–91. doi: 10.1182/bloodadvances.2018017954
74. Contreras JR, Palanichamy JK, Tran TM, Fernando TR, Rodriguez-Malave NI, Goswami N, et al. Microrna-146a Modulates B-Cell Oncogenesis by Regulating Egr1. *Oncotarget* (2015) 6:11023–37. doi: 10.18632/oncotarget.3433
75. Wang H, Li X, Li T, Wang L, Wu X, Liu J, et al. Multiple Roles of Microrna-146a in Immune Responses and Hepatocellular Carcinoma. *Oncol Lett* (2019) 18:5033–42. doi: 10.3892/ol.2019.10862

76. Guo Q, Zhang J, Li J, Zou L, Zhang J, Xie Z, et al. Forced Mir-146a Expression Causes Autoimmune Lymphoproliferative Syndrome in Mice Via Downregulation of Fas in Germinal Center B Cells. *Blood* (2013) 121:4875–83. doi: 10.1182/blood-2012-08-452425
77. Xu H, Li X, Liu D, Li J, Zhang X, Chen X, et al. Follicular T-Helper Cell Recruitment Governed by Bystander B Cells and ICOS-Driven Motility. *Nature* (2013) 496:523–7. doi: 10.1038/nature12058
78. Yu D, Tan AH, Hu X, Athanasopoulos V, Simpson N, Silva DG, et al. Roquin Represses Autoimmunity by Limiting Inducible T-Cell Co-Stimulator Messenger RNA. *Nature* (2007) 450:299–303. doi: 10.1038/nature06253
79. Athanasopoulos V, Barker A, Yu D, Tan AH, Srivastava M, Contreras N, et al. The ROQUIN Family of Proteins Localizes to Stress Granules Via the ROQ Domain and Binds Target Mrnas. *FEBS J* (2010) 277:2109–27. doi: 10.1111/j.1742-4658.2010.07628.x
80. Gigoux M, Shang J, Pak Y, Xu M, Choe J, Mak TW, et al. Inducible Costimulator Promotes Helper T-Cell Differentiation Through Phosphoinositide 3-Kinase. *Proc Natl Acad Sci USA* (2009) 106:20371–6. doi: 10.1073/pnas.0911573106
81. Rolf J, Bell SE, Kovesdi D, Janas ML, Soond DR, Webb LM, et al. Phosphoinositide 3-Kinase Activity in T Cells Regulates the Magnitude of the Germinal Center Reaction. *J Immunol* (2010) 185:4042–52. doi: 10.4049/jimmunol.1001730
82. Yu D, Rao S, Tsai LM, Lee SK, He Y, Sutcliffe EL, et al. The Transcriptional Repressor Bcl-6 Directs T Follicular Helper Cell Lineage Commitment. *Immunity* (2009) 31:457–68. doi: 10.1016/j.immuni.2009.07.002
83. Essig K, Hu D, Guimaraes JC, Alterauge D, Edelmann S, Raj T, et al. Roquin Suppresses the PI3K-Mtor Signaling Pathway to Inhibit T Helper Cell Differentiation and Conversion of Treg to Tfr Cells. *Immunity* (2017) 47:1067–82.e12. doi: 10.1016/j.immuni.2017.11.008
84. Ripamonti A, Provasi E, Lorenzo M, De Simone M, Ranzani V, Vangelisti S, et al. Repression of Mir-31 by BCL6 Stabilizes the Helper Function of Human Follicular Helper T Cells. *Proc Natl Acad Sci USA* (2017) 114:12797–802. doi: 10.1073/pnas.1705364114
85. Deenick EK, Ma CS. The Regulation and Role of T Follicular Helper Cells in Immunity. *Immunology* (2011) 134:361–7. doi: 10.1111/j.1365-2567.2011.03487.x
86. Cannons JL, Qi H, Lu KT, Dutta M, Gomez-Rodriguez J, Cheng J, et al. Optimal Germinal Center Responses Require a Multistage T Cell:B Cell Adhesion Process Involving Integrins, SLAM-Associated Protein, and CD84. *Immunity* (2010) 32:253–65. doi: 10.1016/j.immuni.2010.01.010
87. Kashiwakuma D, Suto A, Hiramatsu Y, Ikeda K, Takatori H, Suzuki K, et al. B and T Lymphocyte Attenuator Suppresses IL-21 Production From Follicular Th Cells and Subsequent Humoral Immune Responses. *J Immunol* (2010) 185:2730–6. doi: 10.4049/jimmunol.0903839
88. Takahashi H, Kanno T, Nakayamada S, Hirahara K, Sciume G, Muljo SA, et al. TGF-Beta and Retinoic Acid Induce the Microrna Mir-10a, Which Targets Bcl-6 and Constrains the Plasticity of Helper T Cells. *Nat Immunol* (2012) 13:587–95. doi: 10.1038/ni.2286
89. Quezada SA, Jarvinen LZ, Lind EF, Noelle RJ. CD40/CD154 Interactions At the Interface of Tolerance and Immunity. *Annu Rev Immunol* (2004) 22:307–28. doi: 10.1146/annurev.immunol.22.012703.104533
90. Perez-Melgosa M, Hollenbaugh D, Wilson CB. Cutting Edge: CD40 Ligand is a Limiting Factor in the Humoral Response to T Cell-Dependent Antigens. *J Immunol* (1999) 163:1123–7.
91. Vinuesa CG, Sanz I, Cook MC. Dysregulation of Germinal Centres in Autoimmune Disease. *Nat Rev Immunol* (2009) 9:845–57. doi: 10.1038/nri2637
92. Elsner RA, Shlomchik MJ. Germinal Center and Extrafollicular B Cell Responses in Vaccination, Immunity, and Autoimmunity. *Immunity* (2020) 53:1136–50. doi: 10.1016/j.immuni.2020.11.006
93. Mlynarczyk C, Fontan L, Melnick A. Germinal Center-Derived Lymphomas: The Darkest Side of Humoral Immunity. *Immunol Rev* (2019) 288:214–39. doi: 10.1111/imr.12755
94. Wen Z, Xu L, Chen X, Xu W, Yin Z, Gao X, et al. Autoantibody Induction by DNA-Containing Immune Complexes Requires HMGB1 With the TLR2/Microrna-155 Pathway. *J Immunol* (2013) 190:5411–22. doi: 10.4049/jimmunol.1203301
95. Kuo G, Wu CY, Yang HY. Mir-17-92 Cluster and Immunity. *J Formos Med Assoc* (2019) 118:2–6. doi: 10.1016/j.jfma.2018.04.013
96. Leng RX, Pan HF, Qin WZ, Chen GM, Ye DQ. Role of Microrna-155 in Autoimmunity. *Cytokine Growth Factor Rev* (2011) 22:141–7. doi: 10.1016/j.cytogfr.2011.05.002
97. Fuertes T, Ramiro AR, de Yebenes VG. Mirna-Based Therapies in B Cell Non-Hodgkin Lymphoma. *Trends Immunol* (2020) 41:932–47. doi: 10.1016/j.it.2020.08.006
98. Long H, Wang X, Chen Y, Wang L, Zhao M, Lu Q. Dysregulation of Micrornas in Autoimmune Diseases: Pathogenesis, Biomarkers and Potential Therapeutic Targets. *Cancer Lett* (2018) 428:90–103. doi: 10.1016/j.canlet.2018.04.016
99. Zhang Y, Roccaro AM, Rombaoa C, Flores L, Obad S, Fernandes SM, et al. LNA-Mediated Anti-Mir-155 Silencing in Low-Grade B-Cell Lymphomas. *Blood* (2012) 120:1678–86. doi: 10.1182/blood-2012-02-410647
100. Zhu FQ, Zeng L, Tang N, Tang YP, Zhou BP, Li FF, et al. Microrna-155 Downregulation Promotes Cell Cycle Arrest and Apoptosis in Diffuse Large B-Cell Lymphoma. *Oncol Res* (2016) 24:415–27. doi: 10.3727/096504016X14685034103473
101. Cheng CJ, Bahal R, Babar IA, Pincus Z, Barrera F, Liu C, et al. Microrna Silencing for Cancer Therapy Targeted to the Tumour Microenvironment. *Nature* (2015) 518:107–10. doi: 10.1038/nature13905
102. Leone E, Morelli E, Di Martino MT, Amodio N, Foresta U, Gulla A, et al. Targeting Mir-21 Inhibits in Vitro and in Vivo Multiple Myeloma Cell Growth. *Clin Cancer Res* (2013) 19:2096–106. doi: 10.1158/1078-0432.CCR-12-3325
103. Su YL, Wang X, Mann M, Adamus TP, Wang D, Moreira DF, et al. Myeloid Cell-Targeted Mir-146a Mimic Inhibits NF-Kappab-Driven Inflammation and Leukemia Progression in Vivo. *Blood* (2020) 135:167–80. doi: 10.1182/blood.2019002045
104. Zhang J, Jia G, Liu Q, Hu J, Yan M, Yang B, et al. Silencing Mir-146a Influences B Cells and Ameliorates Experimental Autoimmune Myasthenia Gravis. *Immunology* (2015) 144:56–67. doi: 10.1111/imm.12347
105. Casali P, Shen T, Xu Y, Qiu Z, Chupp DP, Im J, et al. Estrogen Reverses HDAC Inhibitor-Mediated Repression of Aicda and Class-Switching in Antibody and Autoantibody Responses by Downregulation of Mir-26a. *Front Immunol* (2020) 11:491. doi: 10.3389/fimmu.2020.00491
106. Rupaimoole R, Slack FJ. Microrna Therapeutics: Towards a New Era for the Management of Cancer and Other Diseases. *Nat Rev Drug Discovery* (2017) 16:203–22. doi: 10.1038/nrd.2016.246

Conflict of Interest: A European Patent Application titled 'miRNA compositions for the treatment of mature B cell neoplasms' EP16722679, EP17382740 was filed on March 3 2017.

frontiers in Immunology

REVIEW
published: 29 April 2021
doi: 10.3389/fimmu.2021.671998

Early Emergence of Adaptive Mechanisms Sustaining Ig Production: Application to Antibody Therapy

Maud Lemarié[1], *Fabrice Chatonnet*[1,2], *Gersende Caron*[1,2] *and Thierry Fest*[1,2]*

[1] Université de Rennes 1, INSERM, Établissement Français du Sang de Bretagne, UMR_S1236, Rennes, France,
[2] Laboratoire d'Hématologie, Pôle de Biologie, Centre Hospitalier Universitaire, Rennes, France

Antibody therapy, where artificially-produced immunoglobulins (Ig) are used to treat pathological conditions such as auto-immune diseases and cancers, is a very innovative and competitive field. Although substantial efforts have been made in recent years to obtain specific and efficient antibodies, there is still room for improvement especially when considering a precise tissular targeting or increasing antigen affinity. A better understanding of the cellular and molecular steps of terminal B cell differentiation, in which an antigen-activated B cell becomes an antibody secreting cell, may improve antibody therapy. In this review, we use our recently published data about human B cell differentiation, to show that the mechanisms necessary to adapt a metamorphosing B cell to its new secretory function appear quite early in the differentiation process i.e., at the pre-plasmablast stage. After characterizing the molecular pathways appearing at this stage, we will focus on recent findings about two main processes involved in antibody production: unfolded protein response (UPR) and endoplasmic reticulum (ER) stress. We'll show that many genes coding for factors involved in UPR and ER stress are induced at the pre-plasmablast stage, sustaining our hypothesis. Finally, we propose to use this recently acquired knowledge to improve productivity of industrialized therapeutic antibodies.

Keywords: UPR, ER stress, B cell differentiation, mAbs, RNA-seq

OPEN ACCESS

Edited by:
Lars Nitschke,
University of Erlangen Nuremberg, Germany

Reviewed by:
Ronald B. Corley,
Boston University, United States
Julia Jellusova,
TU München, Germany
Dirk Mielenz,
University of Erlangen Nuremberg, Germany

***Correspondence:**
Thierry Fest
thierry.fest@univ-rennes1.fr

Specialty section:
This article was submitted to B Cell Biology, a section of the journal Frontiers in Immunology

Received: *24 February 2021*
Accepted: *12 April 2021*
Published: *29 April 2021*

Citation:
Lemarié M, Chatonnet F, Caron G and Fest T (2021) Early Emergence of Adaptive Mechanisms Sustaining Ig Production: Application to Antibody Therapy. Front. Immunol. 12:671998. doi: 10.3389/fimmu.2021.671998

ON THE ROAD TO BECOME AN INGENIOUS SECRETED-ANTIBODY FACTORY: DIFFERENTIATION STEPS FROM B TO PLASMA CELL

Plasma cells (PCs) secrete huge amount of immunoglobulin molecules (Igs) subsequently to antigen entry into the body. Before becoming high-affinity antibody secreting cells (ASCs), B cells undergo several steps of differentiation. First, inside the bone marrow, precursor B cells edit a B-cell receptor (BCR) (or surface-attached IgM, an-antigen specific Ig of the first line of defence with poor affinity towards the antigen). At this point, they produce Ig but only intended to be transmembrane receptors. Naive B cells (NBCs) are in a resting state in peripheral blood or secondary lymphoid organs until their activation by a foreign antigen. Once activated by circulating antigens, NBCs reach a secondary

lymphoid organ and move towards the B: T interface where they receive help from specialized CD4+ T cells called follicular helper T cells (Tfh) *via* efficient B: T synapses (1–3). B cells need interaction with several co-activators, including CD40L and the delivery of cytokines including IL-21 and IL-4, to undergo their differentiation into fully mature effectors. The terminal steps of the differentiation occur in a microanatomical specialized area of secondary lymphoid organs called germinal centers (GCs) which are created by B cells themselves in response to *BCL6* expression. In this context, IL-21 represents the main upstream cytokine responsible for BCL6 maximal expression and GCs maintenance (4). GCs are organized into two separated territories - called light zone and dark zone – between which the B cell continuously moves until reaching a high affinity for targeted antigens (1–3). At first, B cells proliferate in the dark zone where cells undergo AID-driven somatic hypermutation (SHM) of variable regions of their Ig gene loci. The second step takes place into the light zone where B cell clones carrying a modified variable region of Ig are tested for its antigen affinity by follicular dendritic cells with the help of Tfh cells. Clonal B cells go through this step with 4 different outcomes based on the strength of BCR signal (antigen affinity) and the amount of Tfh help received: (i) a low-affinity and no help leads to apoptosis of the clone; (ii) mid-affinity and low Tfh help leads to the formation of a long-lived memory cell, (iii) higher affinity and T cell help leads to another round of SHM in the dark zone and (iv) highest levels of both signal leads to the differentiation into a long-lived plasma cell (PC) (2, 3, 5). This B cell maturation is completed by the Ig class-switch recombination (CSR), allowing cells to produce and secrete IgM, IgG, IgE or IgA, each class offering specific functions to adapt the antibody response to the context.

In our lab, we developed and standardized an *in vitro* model system of human NBCs differentiation into plasmablasts (PBs) (**Figure 1**). Starting from blood donor buffy coat we purify NBCs and then culture them with IL-2, CD40L, CpG and anti-IgM Fab'2 in order to activate cells *via* a transcriptional burst (6). As soon as day-1, B cells are fully activated and referred hereafter as day-1 ActB. Beyond day-4 (day-4 ActB), culture conditions are modified and cells maintained only with IL-2, IL-4 and IL-10 stimulation for 2 or 3 additional days in order to complete the PB differentiation. We showed recently that committed B cells that differentiate into PBs present an extinction of both IL-4/STAT6 signaling and CBLB ubiquitin ligase expression, concomitant to IRF4 induction (7). As a surrogate marker of this commitment, membrane surface expression of CD23 disappears due to IL-4/STAT6 extinction. We showed that day-5 $CD23^-$ post-ActB cells contain precursors of plasmablasts (pre-PBs) which present the capacity to enter the cell cycle, while the $CD23^+$ counterparts are unable to differentiate and stay in an activated state (7, 8). After nearly 7-8 days of culture, some PBs start to express the PC-specific CD138 marker which points out the generation of early PCs. PB and PC differentiated *in vitro* secrete high amounts of Igs; they display morphological and transcriptomic features of their *in vivo* counterpart and represent an useful tool to explore normal human PB and PC biology (8–10).

While becoming a PC and therefore fully efficient for Ig secretion, cells experience massive organelles modifications including membrane amplification and trafficking. The endoplasmic reticulum structure reaches its maximum of protein production during this stage (11) and cells are subject to an intensive and continuous stress that needs to be controlled to escape from cell death.

EARLY APPEARANCE OF ADAPTIVE MECHANISMS TO HIGH THROUGHPUT IG SECRETION

General Mechanisms of ER Stress and Unfolded Protein Response (UPR)

In every tissue, cells continuously produce proteins in their cytoplasm to meet their needs and to respond to

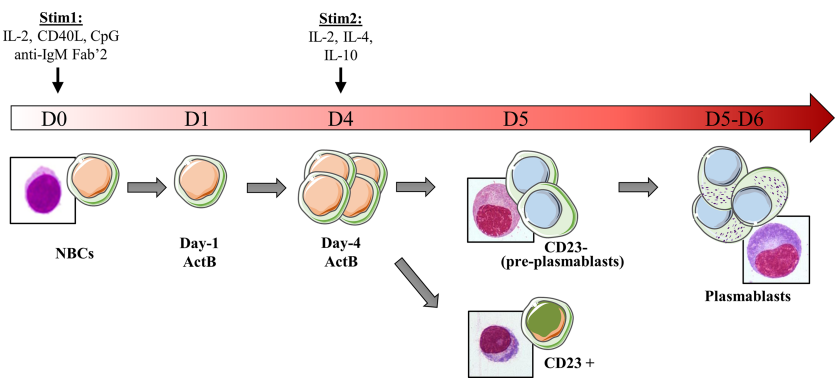

FIGURE 1 | Schematic representation of the *in vitro* model of B cells differentiation used in our laboratory. Peripheral NBCs from blood donors are stained with a cell-tracer then stimulated with IL-2, CD40L, CpG and anti-IgM Fab'2. Day-1 activated cells are referred as day-1 ActB. After 4 days, activated B cells that have proliferated (Day-4 ActB) are selected according cell-tracer dilution and stimulated with IL-2, IL-4 and IL-10 to induce their differentiation into plasmablasts. The day after (D5), three populations are detected: (i) CD23+ cells that are stuck in an activated state and unable to differentiate, (ii) CD23- population, containing precursors of plasmablasts (pre-PB) which give rise to (iii) differentiated plasmablasts (PB). The increase in the cytoplasm/nucleus ratio, characteristic of the development of the Ig production machinery in PB, is early detected in the pre-PB stage. RNA-seq data are available for NBC, Day-1 ActB, Day-4 ActB, CD23+, CD23- and PB subsets.

microenvironment signals. Igs are part of the transmembrane and secreted proteins. After being transcribed, mRNA is pushed to the surface of the endoplasmic reticulum (ER) to be processed by the ER-attached ribosomes and translated into the ER lumen. As the translation occurs in the ER, proteins enter the lumen in their misfolded form. From here, Igs produced in naive B cells start their journey through multiple organelles in order to be well-processed and then bound to the membrane. After antigen activation, IgGs that are produced in PBs/PCs are aimed to be secreted outside of the cell.

After antigen encounter and B cell differentiation into PC, a metabolic switch occurs and a sharp increase in nutrient uptake is necessary to meet the growing need (reviewed in (12)). Ig processing is overwhelmed into the ER lumen, leading to an unfolded and misfolded protein (hereafter designated un/misfolded protein) rate increase and an ER high-stress state. The unfolded protein response (UPR) is then engaged in these cells to meet the increasing needs for protein processing, folding and secretion, and to protect them from apoptosis. Three well-characterized UPR axes have been described as involved in ER stress response: (i) inositol-requiring transmembrane kinase/endonuclease 1α (IRE1α)/X-box binding protein (XBP) - 1, (ii) protein kinase RNA-like endoplasmic reticulum kinase (PERK) and (iii) activating transcription factor 6 (ATF6) pathways (13, 14). In resting conditions, the ATPase Ig-binding protein (BiP) - a resident-ER chaperone - binds to each of them. Stress signals then lead to a BiP UPR first-line of response to ensure activation of ER transmembrane IRE1α, PERK and ATF6 elements. Indeed, BiP dissociates from IRE1α and PERK proteins to release them and then binds to un/misfolded proteins (15). Importantly, BiP association/dissociation cycle with IRE1α and PERK is governed by an ADP-ATP cycle. ATP-bound BiP preferentially binds to ER transmembrane elements (16). When ER stress is increasing, DnaJ-like co-factors (ERdj) bind to un/misfolded proteins and accompany their transfer to the ATP-bound BiP, leading subsequently to ATP hydrolysis (17, 18). As a consequence, BiP dissociates from ER elements and then associates with un/misfolded proteins under its ADP-binding state, stably sequestering clients to prevent aggregation in the ER lumen and accompanying for folding (18, 19). BiP-clients complex dissociation, induced by Nucleotide Exchange Factors (NEF) which remove ADP from BiP, is then required to properly complete folding process and secretion. BiP consequently returns to its initial position with ER elements, meaning that ER stress is under control (20, 21). ATF6 is also released from BiP during ER stress (22) but needs an additional step to be fully activated. Hence, the released ATF6 is then cleaved in the Golgi apparatus by Site-1 and Site-2 proteases (encodes by *MBTPS1* and *MBTPS2*, respectively) before being translocated back to the nucleus to induce the expression of UPR genes such as *XBP1* (23–26) (**Figure 2**).

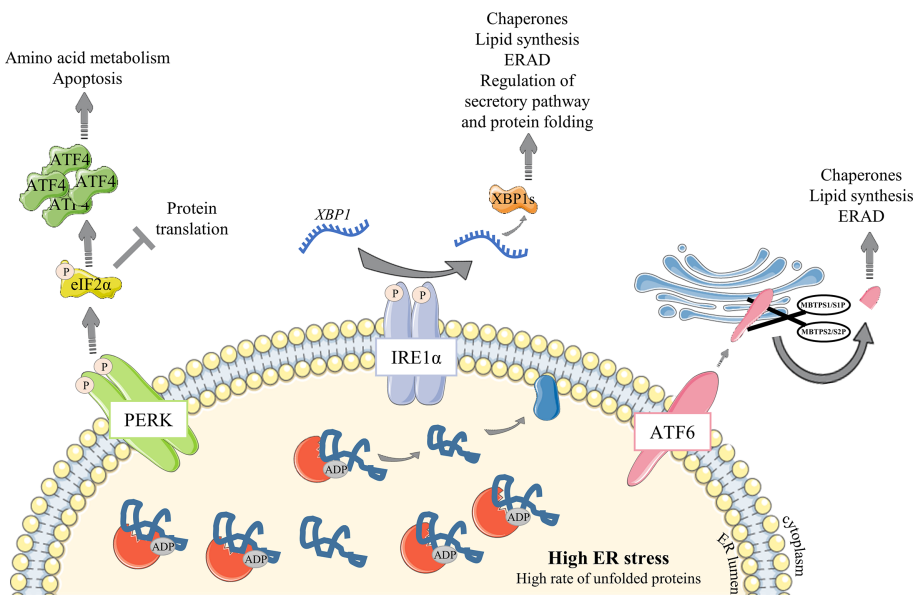

FIGURE 2 | Overview of the UPR signaling pathway under ER stress conditions. Unfolded Protein Response is engaged to respond to increasing amount of proteins in the ER. (1) The ER-resident chaperone BiP binds to unfolded and misfolded proteins and consequently releases the sequestrated IRE1α, PERK and ATF6 ER sensors, leading to their activation following (i) dimerization and auto-phosphorylation of IRE1α and PERK elements or (ii) *MBTPS1*/S1P and *MBTPS2*/S2P – mediated cleavage of ATF6α in the Golgi apparatus. Activated ATF6α then translocates into the nucleus and upregulates chaperones expression and factors involved in lipid synthesis and ERAD. Activated PERK phosphorylates eIF2α which represses global protein translation except for ATF4 whose translation is enhanced. ATF4 then upregulates amino acid metabolism and apoptosis. IRE1α, *via* XBP-1 transcription factor, leads to a broader range of responses with upregulation of many factors including chaperones and those important for lipid synthesis and ERAD. IRE1α regulates as well the factors important for protein folding and secretory functions. Particularly, *XBP1* mRNA requires IRE1α to be spliced and efficient as a transcription factor.

Early Appearance and Temporal Regulation of ER Stress and UPR Factors

ER stress responses seem to be engaged well before PCs massively produce antibodies. A preparation to morphological and genomic modifications that NBCs undergo to become ASCs is probably needed. During B cell differentiation, BLIMP-1 (encoded by *PRDM1*), the major regulator of the antibody-secretory function of PCs, represses the B cell identity transcriptional program including genes encoding for BCL6 and PAX5 (27), and enhances *XBP1* expression (28). Activation of this latter factor is one of the most important events and is maintained essentially by BLIMP-1. Interestingly, BLIMP-1 positively controls the activity of mammalian target of rapamycin (mTORC1) (29), which is described as a key metabolic factor since it controls proteins, nucleotides and lipids synthesis (30). mTORC1 has also been well characterized in B cell development (31, 32) but its role in ER stress has emerged only in the last decade with a few studies showing its importance for a sustainable Ig production. mTORC1 inhibition in mature murine PCs leads to a decrease in serum IgM and IgG levels and a failure to induce BiP protein expression (33, 34). More recently, mTORC1 was defined as a precocious factor in the UPR response to Ig production and secretion. In fact, two separated studies unveiled crucial aspects of mTORC1 function in murine PCs. Double knock-out of XBP-1 and TSC1, a mTOR inhibitor, leads to an increase of Ig production and the differentiation into PCs was maintained even in absence of XBP-1 (33). These results suggest the existence of an alternative UPR response independent of the IRE1α/XBP-1 and ATF6 pathways. Additional studies indicate that UPR-, protein production- and secretion-affiliated gene expressions - such as *Hspa5*, *Pdia6*, *Ero1l*, encoding respectively for BiP, for a protein disulfide isomerase and for an ER-resident oxidase, increased in activated B cells dependently of mTORC1. Interestingly, this upregulation is observed well before the activation of BLIMP1-dependent PC program and *Xbp1* gene expression in mice (35). RNA-seq data obtained throughout our *in vitro* differentiation model of human B cells (7) support these results and show an UPR response well before cells are secreting antibodies. Hence, bio-informatic analyses of the RNA-seq dataset segregated genes linked to UPR by GO annotations into 4 clusters according to gene expression modifications during the differentiation steps: 1) stable from NBCs to PB stage; 2) upregulated as early as the day-1 ActB stage, 3) downregulated right after B cell activation, and 4) upregulated in pre-PB and maintained in PBs (**Figure 3A**). Indeed, the comparison between NBCs, day-1 ActB, day-4 ActB, post-ActB, pre-PB cells, and PB cells shows that UPR-affiliated genes seem to be only partially influenced by the *XBP-1* and *PRDM1* expression levels. Since cluster 4 includes XBP-1, IRE1α and ATF6α factors, we hypothesized that UPR-associated genes specifically upregulated in pre-PB are IRE1α/XBP-1- or ATF6-dependent which is not the case for genes from cluster 2. The main functions associated with each cluster were then evaluated by the DAVID pathway enrichment software in order to find differences between ER stress response governed or not by IRE1α/XBP-1 or ATF6. Thus, genes from cluster 4 whose expression is specifically upregulated in Pre-PB and PB stages are mainly associated with IRE1α - and ATF6- mediated UPR, protein folding and transport, and apoptosis inhibition. For genes involved in cluster 2 whose expression appears as soon as day-1 of the culture, they are mainly associated with ER to Golgi vesicle-mediated transport, ER stress suppression and IRE1α -mediated UPR (a few genes compared to cluster 4). Overall, both UPR and ER stress responses are activated early in B cells engaged in PC differentiation and in at least two separate phases with different molecular requirements.

A Specific Inhibition of the PERK Pathway Throughout B Cell Differentiation

In contrast to insulin-secreting pancreas cells (36–38) and collagen-secreting chondrocytes (39), Ig secretion is described as using a PERK-independent ER stress response (40–42). In our *in vitro* model, *EIF2AK3* (which encodes PERK itself) but also well-characterized *DDIT3* (also known as CHOP) and *ATF4*, both pro-apoptotic PERK target genes, are all included in cluster 3. Interestingly, when the gene expressions in ActB and PB populations are compared to NBCs we noticed that in addition to *EIF2AK3* and *ATF4*, other specific genes of the PERK pathway such as *ATF3* and *PPP1R15A* are part of the cluster 3 (**Figure 3A** and **Table S1**). Their expressions are 2 to 10 times higher in NBCs compared to the more mature stages (**Figure 3B**). In contrast, the IRE1α/ATF6 target gene, *HSPA5* (from cluster 4) maintains high levels of expression from NBC to ActB stages and even increases its expression (by more than 3 times) at pre-PB stage (**Figures 3B**). Altogether, these data show that PERK-pathway gets inactivated as soon as NBCs are stimulated and remains inhibited in PC.

Characterization of the factors involved in the suppression of the PERK pathway during PC differentiation has long been elusive. However, two recent studies demonstrated the role of UFBP1 (Ufm1 binding protein 1; issued from the gene *DDRGK1* presents in cluster 2) in this process. Indeed, UFBP1-mediated ufmylation of IRE1α protein protects from IRE1α degradation, leading to its stabilization and the suppression of the PERK pathway (43). In addition, the UFBP1-mediated suppression of PERK leads to the active promotion of PC differentiation and therefore ER expansion (44). Since the expression of *DDRGK1* occurs in cluster 2 in our *in vitro* model, we speculate that UFBP1-mediated PERK inhibition is primarily IRE1α/XBP-1 and ATF6 independent (**Figures 3**, **4** and **Table S1**). However, *DDRGK1* expression increases slightly in pre-PB and PB populations suggesting that a delayed IRE1α/XBP-1 and ATF6 effect may exist and participate in *DDRGK1* expression at latter stages of differentiation.

The PERK pathway is also actively suppressed by the $P58^{IPK}$ protein in many cell types. Mechanistically, $P58^{IPK}$ binds directly to the kinase domain of PERK, which impedes its activity and further activation of its targets (45). $P58^{IPK}$ is encoded by *DNAJC3*, a member of the DnaJ family acting downstream of the ATF6 and IRE1α/XBP-1 pathways (28, 45–50). Although no clear evidence exist so far for its role in B cells, some studies

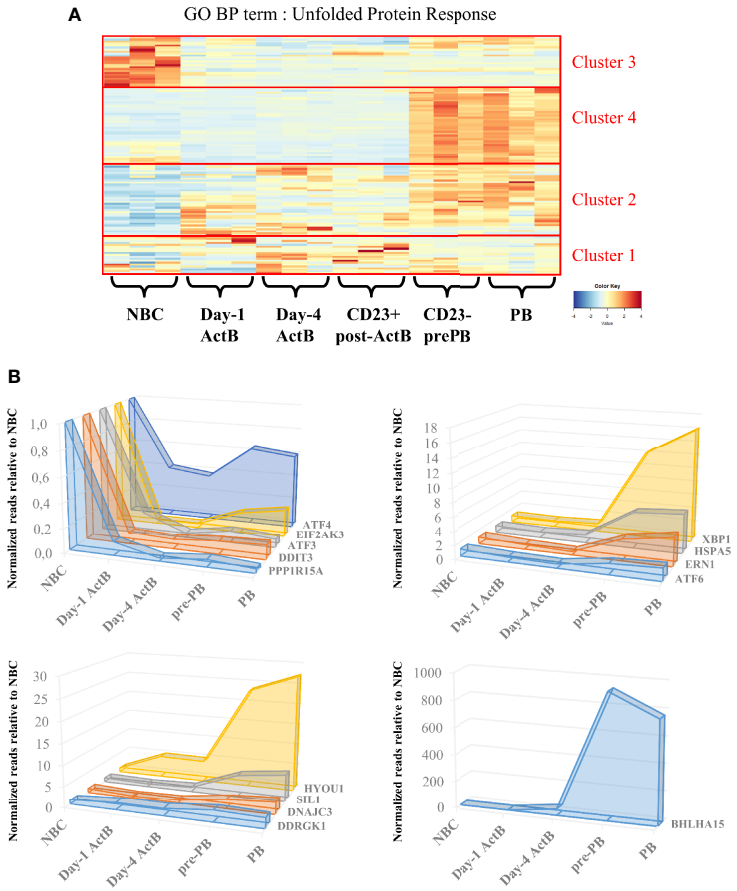

FIGURE 3 | Unfolded protein response is temporally regulated during the transition from naive B cells to plasmablasts. **(A)** Genes belonging to the Gene Ontology – Biological Processes term "Unfolded Protein Response" were selected and their expression in our RNA-seq data was submitted to an unsupervised hierarchical clustering analysis. The resulting heatmap is shown here, delineating four different expression clusters: (1) stable expression, (2) genes upregulated from Day-1, (3) genes upregulated in NBC and (4) genes upregulated in Pre-PB and PB. **(B)** Means of normalized reads obtained from 3 different experiments at Day-1 ActB, Day-4 ActB, pre-PB and PB stages were compared to the NBC counterpart, whose mean is reduced to 1. Left upper panel shows genes related to the PERK pathway. Right upper panel shows genes related to the IRE1α and ATF6 pathways and lower panels show potential genes which are either implicated (i) in the PERK regulation or (ii) in endoplasmic reticulum modifications related to stress. All of the selected genes are addressed in this review.

showed that $p58^{IPK}$ protein expression increased rapidly after stimulation of murine B cells with LPS (41, 42) or CpG (35), while the expression of PERK downstream targets decreased. In our model of human B cell differentiation, the expression of *DNAJC3* increases strongly in cluster 4 in pre-PB and PB populations compared to ActB cells. This is in agreement with Gaudette et al. study in mice (35), which suggested that $P58^{IPK}$ could partially contribute to the inhibition of the PERK pathway in ASCs, as soon as in the pre-PB stage (**Figures 3**, **4** and **Table S1**).

Similarly, SIL1, a nucleotide exchange factor, could represent another potential inhibitor of PERK since the *SIL1* knockdown in HeLa cells showed an activation of the PERK pathway (51). In our model, *SIL1* expression was strongly induced in pre-PB and PB (around 5-fold increase) compared to the earlier differentiation stages. Although *SIL1* does not belong to the GO term UPR in Biological Processes (BP), we found it in the RE Cellular Component (CC) annotation. A similar temporal clustering of our RNA-seq data performed on genes of this GO term showed that *SIL1* belongs to a cluster of genes over-expressed specifically in pre-PBs and PBs (GO CC: RE; cluster 3) (**Figures 3B**, **S1** and **Table S2**). Interestingly, SIL1 has been described as a co-chaperone of BiP required for the release of BiP-clients in the ER lumen (20, 21) after sequestration with BiP. However, the knockdown mouse model of Ichhaporia et al. demonstrated that SIL1 was unnecessary for the release of BiP from un/misfolded Ig and for subsequent production of Ig (52). Recently, ChIP-sequencing data done in human PBs (GSE142493 (53);) revealed an enrichment of XBP-1 in *SIL1* promoter, suggesting a potential role of SIL1 in cell differentiation. This result, together with the HeLa data described above and our model of B cell differentiation strongly suggests that SIL may play a role in the inhibition of the PERK pathway in human ASCs (**Figure 4**). In addition,

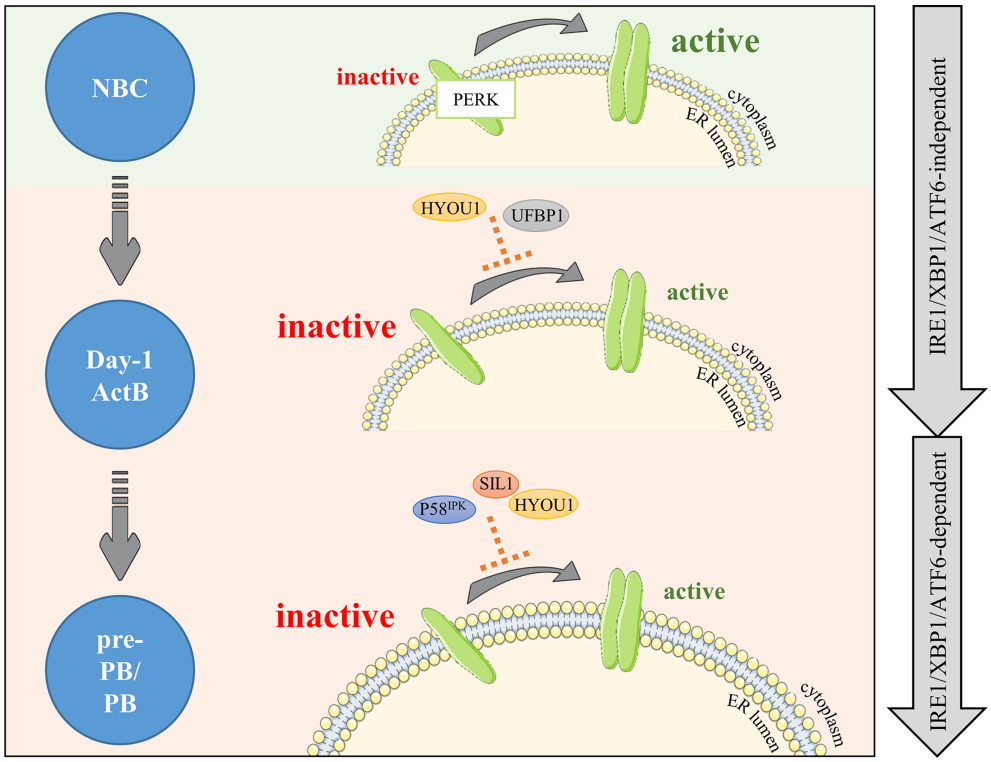

FIGURE 4 | PERK is negatively regulated right after B cell activation and maintained under negative control during differentiation. PERK signaling is upregulated in NBCs (light green background). In activated B cells, PERK needs to be dampened by factors limiting PERK activity (light orange background). Our RNA-seq analysis combined with literature emphases on two new potential negative factors: HYOU1 and UFBP1. Then, differentiation (pre-PB/PB) involves important changes including increased production of Ig, which critically increases ER stress and risks of apoptosis; hence, PERK signaling repression needs to be reinforced. Factors potentially involved in this control are part of the ADP/ATP BiP regulation cycle: the DnaJ protein $P58^{IPK}$ and the nucleotide exchange factors SIL1 and HYOU1. The first wave of negative control is IRE1α/XBP-1/ATF6-independent and the second wave is IRE1α/XBP-1/ATF6-dependent (right gray arrows).

HYOU1 (also known as ORP150) which is another nucleotide exchange factor for BiP, can substitute for SIL1 (54–56) and has been described in the literature as a cyto-protective factor against ER stress (57, 58). In our system, *HYOU1* (which, unlike *SIL1*, is included in the GO BP UPR term) belongs to the cluster 4 and its expression is (i) higher than for *SIL1* and (ii) strongly upregulated in pre-PB and PB stages (**Figure 3** and **Table S1**). Then, given that HYOU1 can substitute for SIL1 in its functions, HYOU1 could represent an alternative factor of suppression of PERK, active in the last stages of B cell differentiation (**Figure 4**).

Taken together, these data provide support to a better understanding of PERK suppression in ASCs. Consistent with previous studies (35, 42), we found that the PERK pathway is inhibited early in the process of B cell differentiation by the specific repression of some of its genes. Two phases of repression seem to exist: (i) a strong first wave of repression, IRE1α/XBP-1 and ATF6 independent which appears right after NBC activation, and (ii) a second wave, dependent on IRE1α/XBP-1 and ATF6 occurring when Ig production is at its highest level (**Figure 3B**). ASCs are constantly in a state of prolonged and elevated ER stress and therefore at a constant risk of apoptosis. Even though the implication of apoptosis mediated by the PERK and IRE1α/XBP-1 pathways in the resolution of acute ER stress is controversial (31, 59–70), prolonged PERK signaling promotes apoptosis in contrast to a sustained IRE1α response which improves cell survival (71). Therefore, in order to achieve successful antibody secretion in ASCs, it appears that PERK signaling needs to be restricted. In addition, previous studies suggested that while PERK could be partially activated in stimulated B cells, the subsequent signal appears not to be sufficient to induce target genes (41, 42).

Interestingly, the expression pattern of *HYOU1* is bimodal with the first and second peak of expression corresponding, respectively, to the first and second wave of PERK inhibition (**Figures 3B** and **4**). Since XBP-1 and ATF6 have been reported as critical inductors of *Hyou1* expression in murine B cells and fibroblasts, respectively, we hypothesise that both factors may contribute to HYOU1-mediated PERK inhibition in the late stage of B cell differentiation (35, 49). However, to date, no mechanism of action has been highlighted regarding either HYOU1 or SIL1 suppression of PERK pathway and further investigations are required to clarify this point. Altogether, HYOU1, in addition to provide ER stress protection (72–74),

may exhibit critical repressor control of PERK in ASCs together with UFBP1 and P58^{IPK}.

Focus on MIST1, a Factor Involved in IRE1α/XBP-1/ATF6 Response

In the literature, XBP-1 appears to be a central factor governing the UPR response in PC differentiation and Ig secretion. To be actively efficient under ER-stress conditions, XBP-1 mRNA needs to be spliced by IRE1α which is previously released from BiP and then activated after auto-phosphorylation (75). Among potential XBP-1 target genes identified in murine PCs, MIST1 (encoded by *Bhlha15*) is a factor which has already been documented as important in secretory functions of some cells (76–80). *Bhlha15* promoter is bound by XBP-1 in murine PCs (76) and its expression is under XBP-1 dependence in several cell types including PCs (76, 81, 82). The study published by Capoccia et al. (83) ascribed a potential role of MIST1 in ER stress occurring in PCs. By transcriptome comparison between day-3 LPS-treated PCs obtained from *Bhlha15*$^{-/-}$ and WT mice, they found among the 218 differentially expressed genes specific functional annotations for endoplasmic reticulum and molecules transport. PCs associated with the small intestine have shown dilated and unorganized rough ER supporting the fact that MIST1 plays a critical role in ER stress despite its lack of involvement in PC differentiation (83).

In mice, the expression of *Bhlha15* like *Xbp1* is strongly induced in PCs compared to NBCs, MBCs and GC B cells (83, 84) (GSE 4142). In addition, *Bhlha15*$^{-/-}$ mice present a significant decrease of specific antibodies secretion in the serum 7 days after immunization (84). Overall, MIST1 and its respective functions have only been studied in the late stages of PC differentiation. Our RNA-seq data give a more precise picture on the regulation of *BHLHA15* expression during normal human B cell differentiation and notably by showing an expression as soon as day-4 of the culture (**Figure 3B**), prompting for further studies about its function in ER-stress and UPR management during B cell differentiation.

USING B CELL DIFFERENTIATION MECHANISMS TO IMPROVE IMMUNOGLOBULIN PRODUCTION

Production of recombinant protein has been well studied for the past few decades and research continues to constantly improve this engineered production. Among recombinant proteins, monoclonal antibodies (mAbs) production reports largely to the pharmaceutical industry. The first industrialized mAb was approved in 1997 and used for non-hodgkin's lymphoma patients. Rituxan®, better known as Rituximab, was employed to recognize CD20 on B cells as an antigen. Almost 80 approved therapeutic mAbs were developed since, such as Humira® (Adalimumab/anti-TNFα), Xolair® (Omalizumab/anti-IgE), Opdivo® (Nivolumab/blocks PD-L1 binding to PD-1 and PD-2) or more recently Sarclisa® (Isatuximab/anti-CD38) and Imfinzi® (Durvalumab/blocks PD-L1 binding to PD-1 and CD80). Each of them involved an intensive work mainly focused on how to efficiently increase mAb productivity (mAb titer and quality), a major concern in industrial settings.

Chinese Hamster Ovary (CHO) cells are the main producing cell line for engineered monoclonal antibody production. CHO cells are easy to manipulate and enable post-translational modifications important for Igs functions, such as glycosylation. Production is organized as (i) CHO cell line generation, consisting in the development of the vector for recombinant protein expression and its transfection into CHO cells, (ii) selection/purification of clones which integrated the vector, (iii) large scale bioproduction and (iv) final formulation to appropriately administrate mAbs into the patient. Continuous productivity improvement could be achieved by modifying cell culture conditions (85–87) and editing genes involved in protein translation, folding and secretion.

Massive production of recombinant proteins in CHO cells leads to an important ER stress requiring control to attain a production with high stability and quality. Uncontrolled ER stress generates less secreted proteins (mainly due to apoptosis of overstressed clones), but can be regulated by inducing autophagy (88). It also leads to a final product of poor quality (aggregates and subvisible particles coming from protein folding and assembly dysfunctions) (89), which, for the latter, represents issues for further clinical use (90). Hence, recent works proposed to control factors involved in the UPR pathway since some of them were described as able to monitor and control ER stress during Ig production. For instance, Talbot et al. (91) proposed to monitor ER stress in order to control aggregates concentration into the final product. To this end, they used two different culture conditions based on the presence or absence of specific nutrients for production of two different Ig subtypes. The deprivation condition induced a higher and earlier ER stress. The increase in the relative gene expression of several UPR-specific genes was assessed throughout culture and revealed a specific signature assigned to each Ig subtype and culture condition. Using this signature to monitor cell cultures, the authors obtained a significant decrease in aggregates and subvisible particles for IgG1 mAbs, unlike what was observed for IgG2 mAbs. In the case of IgG1 production, *HSPA5* was induced later than for IgG2 while *DERL3*, an ER-associated degradation (ERAD)-specific gene which helps for un/misfolded protein degradation (92–94) is induced earlier. This protected cells from overwhelmed UPR and allowed an extended time of culture. With the support of other studies, detailing ER biomarkers profiling during of CHO cell lines culture (95–97), they finally proposed to include a UPR genes signature to the quality parameters of mAbs production, providing culture conditions labelled as "ER stress under control". As an example, *HERPUD1*, another ERAD-specific gene, is described as an early indicator of ER stress response (96, 97) and then could be used to predict production efficiency and stability. Interestingly, this gene is included in the cluster 2 of our study, indicating that it is an early UPR marker during the B cell differentiation process. Hence, our RNA-seq dataset supports conclusions of published data (95–97) and provides new potential factors to detect i) when ER stress is

precociously managed, with genes such as *VCP* or *MBTPS2* (both in cluster 2), and ii) UPR intensity during culture of high recombinant protein expressing cell lines with *SYVN1*, *SSR1, DERL1, DERL2, MBTPS1* or *WFS1* (all included in cluster 4).

The UPR activation is cell line-dependent but appears to be also clone-dependent. In fact, producing high-proliferative clones with high quality specificities is possible but relays on their proper ability to activate UPR and to escape from apoptosis. Therefore, a clonal selection process is necessary to select for clones with the best performance in terms of mAb titers, cell mass and viability. To this aim, UPR can be monitored with different UPR-inducible systems in CHO cells by (i) using promoters containing all three UPR responsive elements (UPRE, ERSE, and ACGT) (98), (ii) using native promoters of ER-stress induced factors such as BiP (99) or (iii) using a fluorescent reporter which produce specific fluorescence based on *XBP-1* splicing by activated IRE1α (96). Although those systems allow for selection of clones with the best performance, Poulain et al. (100) showed recently that during selection, the lower the expression of the protein of interest is in a pool of cells, the higher will be the frequency of clones with high productivity in this pool. To show this, they transduced a CHO

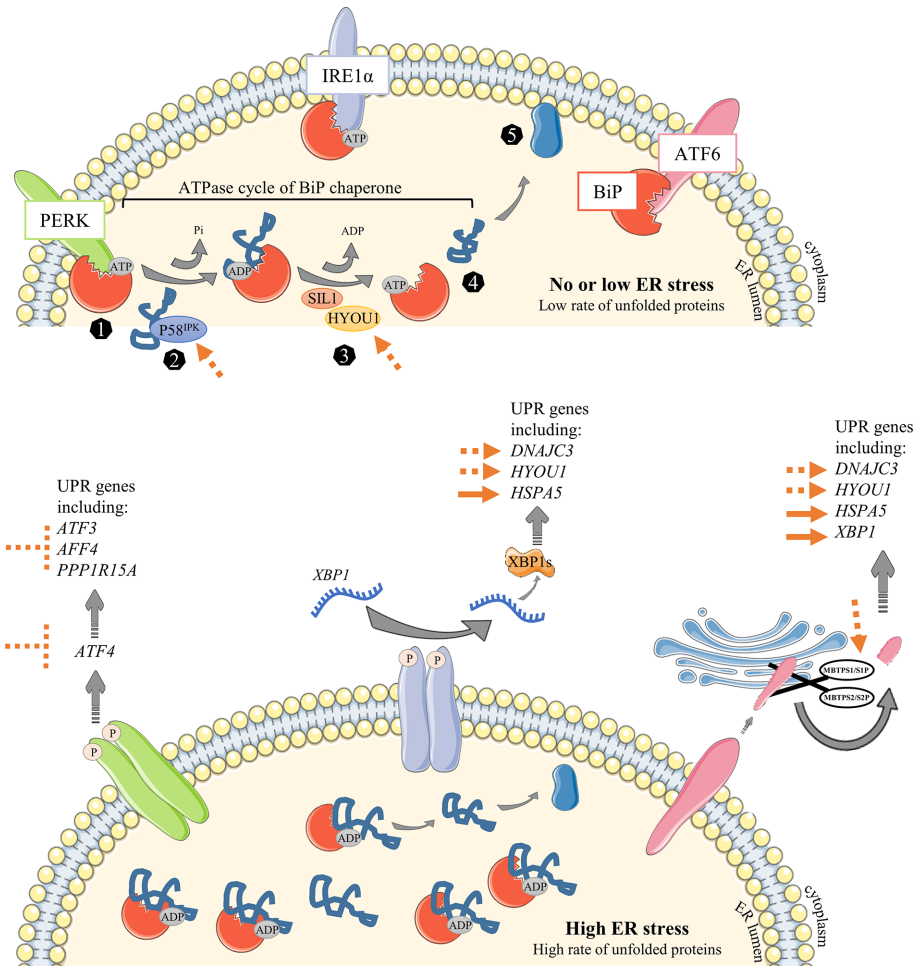

FIGURE 5 | Overview of known or suggested strategies to improve Ig production in CHO cells. In the first steps of NBC activation, a low rate of proteins is processed into the ER leading to no or negligible stress conditions (upper panel). When cells undergo the following steps of differentiation that will result in the generation of highly-producing secreted Ig PBs/PCs, mass of their ER is getting bigger and associated with an important stress. Unfolded Protein Response is then engaged to cope with the increasing amount of proteins in the ER. (1) The ER-resident chaperone BiP binds to unfolded and misfolded proteins and consequently releases the sequestrated IRE1α, PERK and ATF6 ER sensors, leading to their activation following (i) dimerization and auto-phosphorylation of IRE1α and PERK elements or (ii) *MBTPS1*/S1P and *MBTPS2*/S2P – mediated cleavage of ATF6α in the Golgi apparatus. (2) DnaJ family members such as $P58^{IPK}$ (encoded by *DNAJC3*) bind directly to unfolded and misfolded proteins to guide their transfer onto an ATP-bound BiP. Given the ATPase activity of BiP, an inorganic phosphate (Pi) is instantly released from BiP, leading to a conformational modification which stabilizes protein into the ADP-bound BiP (3). Thereafter, nucleotide-exchange factors (NEFs) such as SIL1 and HYOU1 facilitate the release of ADP from BiP and the rebinding of ATP. 4-5) As a consequence, client is released and then processed to be secreted outside of the cell. The main strategies already proposed to improve Ig production in CHO cells are represented as full orange arrows. The strategies discussed in this review are represented as repressive or permissive dotted orange arrows.

cell line containing an inducible expression system called cumate-gene switch with an inducible plasmid containing the gene of interest. This system allowed to study the impact of high- versus low-expressing ones on final productivity. Therefore, reducing expression of recombinant proteins in CHO cells combined with selection of clones with higher capacities to deploy UPR, increases final recombinant protein titers and stability.

Decreasing ER stress during recombinant protein production has been one of the main concerns in mAb research since a few years. Therefore, controlling ER stress could represent a complementary aspect to the monitoring one. Work mainly focused on UPR-specific genes activation has been successfully done with factors such as IRE1α (101), BiP (102, 103) or XBP-1 (104). PDIs (protein disulfite isomerases) which are upregulated during Ig production (such as *PDIA5* and *PDIA6* in cluster 4; **Figure 3A**) have also been shown to increase the protein secretion rate in CHO cells when overexpressed (105, 106).

As previously described in this review, BiP, XBP-1, IRE1α and PDI are part of the cluster 4 in the dataset. Importantly, many other factors whose expression follows cluster 4 pattern are UPR sensors. Among them, $P58^{IPK}$, MIST1 (both described in chapter 2), DERL1, WFS1, or even MBTPS1/S1P (**Figure 5**) could represent new targets to improve ER stress response during the production of mAbs. As previously shown, some pathways relative to ER stress responses are engaged very early after B cell activation, as shown by the cluster 2 in **Figure 3A**. Therefore, it would be advantageous to study genes from cluster 2 such as *DDRGK1* (UFBP1 protein, described in chapter 2), *PIGBOS1*, *HERPUD1*, *DCTN1*, *MBTPS2/S2P* or *ERO1A* in order to increase the number of potential novel engineering targets. HYOU1, whose expression pattern has been discussed in this review, could be another interesting target (**Figure 5**), since its overexpression was shown to improve ER stress responses in liver cells from obese diabetic mice (74) or neurons under hypoxia (72, 73).

Nonetheless, inhibiting UPR suppressors such as ATF6β (107) could also represent an alternative way to increase mAbs productivity. Our analysis identifies *DNAJB9* from cluster 4 as a potential new target since it acts by inhibiting activation of IRE1α (108). Moreover, playing with PERK signaling could offer new strategies to improve productivity. Thus, the control of PERK downstream targets such as *ATF3*, *DDIT3* or directly *ATF4* or *EIF2AK3* in CHO cells can protect cells from apoptosis (**Figure 5**). In accordance with our hypothesis, Roy et al. (96) observed a PERK inhibition feedback coupled with IRE1α activation in cells with high levels of IgG secretion after several days of culture and argued that a mechanism may exists in PCs to decrease apoptosis risk over production time.

CONCLUSION

The model used in our laboratory facilitates the study of B cell development from NBCs to the plasmablast stage and allows to visualize at molecular level any modifications occurring either early or late during the maturation process (6–8, 109–111). Indeed, this paper brings new elements concerning the regulation of PERK and some factors that could have an impact on the productivity of mAbs. PERK regulation is poorly studied in B cells and our present study merges RNA-sequencing with already published data regarding ER stress response in other cell types to unveil new mechanisms that need to be further studied in B cells. Additionally, despite the fact that research in mAbs engineering has been intensive over the past decades, here we have opened up new perspectives for the optimization of mAbs production.

AUTHOR CONTRIBUTIONS

ML performed the literature search, wrote and revised the manuscript, designed the figures and analysed the clusters with the DAVID bio-informatic tool. FC analysed the RNA-sequencing dataset, generated heatmaps and revised the manuscript. GC and TF revised the manuscript. All authors contributed to the article and approved the submitted version.

FUNDING

This study was funded by Agence Nationale de la Recherche (ANR) number: ANR-19-CE15-0020-01.

SUPPLEMENTARY MATERIAL

The Supplementary Material for this article can be found online at: https://www.frontiersin.org/articles/10.3389/fimmu.2021.671998/full#supplementary-material

REFERENCES

1. Shapiro-Shelef M, Calame K. Regulation of Plasma-Cell Development. *Nat Rev Immunol* (2005) 5:230–42. doi: 10.1038/nri1572
2. Victora GD, Schwickert TA, Fooksman DR, Kamphorst AO, Meyer-Hermann M, Dustin ML, et al. Germinal Center Dynamics Revealed by Multiphoton Microscopy With a Photoactivatable Fluorescent Reporter. *Cell* (2010) 143:592–605. doi: 10.1016/j.cell.2010.10.032
3. De Silva NS, Klein U. Dynamics of B Cells in Germinal Centres. *Nat Rev Immunol* (2015) 15:137–48. doi: 10.1038/nri3804
4. Linterman MA, Beaton L, Yu D, Ramiscal RR, Srivastava M, Hogan JJ, et al. IL-21 Acts Directly on B Cells to Regulate Bcl-6 Expression and Germinal Center Responses. *J Exp Med* (2010) 207:353–63. doi: 10.1084/jem.20091738
5. Laidlaw BJ, Cyster JG. Transcriptional Regulation of Memory B Cell Differentiation. *Nat Rev Immunol* (2020) 21:209–20. doi: 10.1038/s41577-020-00446-2
6. Le Gallou S, Caron G, Delaloy C, Rossille D, Tarte K, Fest T. IL-2 Requirement for Human Plasma Cell Generation: Coupling Differentiation and Proliferation by Enhancing MAPK-ERK Signaling. *J Immunol* (2012) 189:161–73. doi: 10.4049/jimmunol.1200301
7. Pignarre A, Chatonnet F, Caron G, Haas M, Desmots-Loyer F, Fest T. Plasmablasts Derive From CD23-Negative Activated B Cells After the Extinction of IL-4/STAT6 Signaling and IRF4 Induction. *Blood* (2020) 137:1166–80. doi: 10.1182/blood.2020005083

8. Caron G, Hussein M, Kulis M, Delaloy C, Chatonnet F, Pignarre A, et al. Cell-Cycle-Dependent Reconfiguration of the DNA Methylome During Terminal Differentiation of Human B Cells Into Plasma Cells. *Cell Rep* (2015) 13:1059–71. doi: 10.1016/j.celrep.2015.09.051
9. Kassambara A, Rème T, Jourdan M, Fest T, Hose D, Tarte K, et al. GenomicScape: An Easy-to-Use Web Tool for Gene Expression Data Analysis. Application to Investigate the Molecular Events in the Differentiation of B Cells Into Plasma Cells. *PloS Comput Biol* (2015) 11: e1004077. doi: 10.1371/journal.pcbi.1004077
10. Jourdan M, Cren M, Robert N, Bolloré K, Fest T, Duperray C, et al. IL-6 Supports the Generation of Human Long-Lived Plasma Cells in Combination With Either APRIL or Stromal Cell-Soluble Factors. *Leukemia* (2014) 28:1647–56. doi: 10.1038/leu.2014.61
11. Tagliavacca L, Anelli T, Fagioli C, Mezghrani A, Ruffato E, Sitia R. The Making of a Professional Secretory Cell: Architectural and Functional Changes in the ER During B Lymphocyte Plasma Cell Differentiation. *Biol Chem* (2003) 384:1273–7. doi: 10.1515/BC.2003.141
12. Lam WY, Bhattacharya D. Metabolic Links Between Plasma Cell Survival, Secretion, and Stress. *Trends Immunol* (2018) 39:19–27. doi: 10.1016/j.it.2017.08.007
13. Todd DJ, Lee A-H, Glimcher LH. The Endoplasmic Reticulum Stress Response in Immunity and Autoimmunity. *Nat Rev Immunol* (2008) 8:663–74. doi: 10.1038/nri2359
14. Brewer JW, Hendershot LM. Building an Antibody Factory: A Job for the Unfolded Protein Response. *Nat Immunol* (2005) 6:23–9. doi: 10.1038/ni1149
15. Bertolotti A, Zhang Y, Hendershot LM, Harding HP, Ron D. Dynamic Interaction of BiP and ER Stress Transducers in the Unfolded-Protein Response. *Nat Cell Biol* (2000) 2:326–32. doi: 10.1038/35014014
16. Sou SN, Ilieva KM, Polizzi KM. Binding of Human BiP to the ER Stress Transducers IRE1 and PERK Requires ATP. *Biochem Biophys Res Commun* (2012) 420:473–8. doi: 10.1016/j.bbrc.2012.03.030
17. Lin HY, Masso-Welch P, Di YP, Cai JW, Shen JW, Subjeck JR. The 170-kDa Glucose-Regulated Stress Protein is an Endoplasmic Reticulum Protein That Binds Immunoglobulin. *Mol Biol Cell* (1993) 4:1109–19. doi: 10.1091/mbc.4.11.1109
18. Kityk R, Kopp J, Mayer MP. Molecular Mechanism of J-Domain-Triggered ATP Hydrolysis by Hsp70 Chaperones. *Mol Cell* (2018) 69:227–37.e4. doi: 10.1016/j.molcel.2017.12.003
19. Misselwitz B, Staeck O, Rapoport TA. J Proteins Catalytically Activate Hsp70 Molecules to Trap a Wide Range of Peptide Sequences. *Mol Cell* (1998) 2:593–603. doi: 10.1016/S1097-2765(00)80158-6
20. Behnke J, Feige MJ, Hendershot LM. BiP and Its Nucleotide Exchange Factors Grp170 and Sil1: Mechanisms of Action and Biological Functions. *J Mol Biol* (2015) 427:1589–608. doi: 10.1016/j.jmb.2015.02.011
21. Bracher A, Verghese J. The Nucleotide Exchange Factors of Hsp70 Molecular Chaperones. *Front Mol Biosci* (2015) 2:48–56. doi: 10.3389/fmolb.2015.00010
22. Shen J, Chen X, Hendershot L, Prywes R. ER Stress Regulation of ATF6 Localization by Dissociation of BiP/GRP78 Binding and Unmasking of Golgi Localization Signals. *Dev Cell* (2002) 3:99–111. doi: 10.1016/S1534-5807(02)00203-4
23. Haze K, Yoshida H, Yanagi H, Yura T, Mori K. Mammalian Transcription Factor ATF6 is Synthesized as a Transmembrane Protein and Activated by Proteolysis in Response to Endoplasmic Reticulum Stress. *Mol Biol Cell* (1999) 10:3787–99. doi: 10.1091/mbc.10.11.3787
24. Yoshida H, Matsui T, Yamamoto A, Okada T, Mori K. XBP1 mRNA Is Induced by ATF6 and Spliced by IRE1 in Response to ER Stress to Produce a Highly Active Transcription Factor. *Cell* (2001) 107:881–91. doi: 10.1016/S0092-8674(01)00611-0
25. Chen X, Shen J, Prywes R. The Luminal Domain of ATF6 Senses Endoplasmic Reticulum (ER) Stress and Causes Translocation of ATF6 From the ER to the Golgi. *J Biol Chem* (2002) 277:13045–52. doi: 10.1074/jbc.M110636200
26. Shen J, Prywes R. Dependence of Site-2 Protease Cleavage of ATF6 on Prior Site-1 Protease Digestion Is Determined by the Size of the Luminal Domain of ATF6. *J Biol Chem* (2004) 279:43046–51. doi: 10.1074/jbc.M408466200
27. Shaffer AL, Lin K-I, Kuo TC, Yu X, Hurt EM, Rosenwald A, et al. Blimp-1 Orchestrates Plasma Cell Differentiation by Extinguishing the Mature B Cell Gene Expression Program. *Immunity* (2002) 17:51–62. doi: 10.1016/S1074-7613(02)00335-7
28. Shaffer AL, Shapiro-Shelef M, Iwakoshi NN, Lee A-H, Qian S-B, Zhao H, et al. XBP1, Downstream of Blimp-1, Expands the Secretory Apparatus and Other Organelles, and Increases Protein Synthesis in Plasma Cell Differentiation. *Immunity* (2004) 21:81–93. doi: 10.1016/j.immuni.2004.06.010
29. Tellier J, Shi W, Minnich M, Liao Y, Crawford S, Smyth GK, et al. Blimp-1 Controls Plasma Cell Function Through the Regulation of Immunoglobulin Secretion and the Unfolded Protein Response. *Nat Immunol* (2016) 17:323–30. doi: 10.1038/ni.3348
30. Shimobayashi M, Hall MN. Making New Contacts: The mTOR Network in Metabolism and Signalling Crosstalk. *Nat Rev Mol Cell Biol* (2014) 15:155–62. doi: 10.1038/nrm3757
31. Iwata TN, Ramírez JA, Tsang M, Park H, Margineantu DH, Hockenbery DM, et al. Conditional Disruption of Raptor Reveals an Essential Role for mTORC1 in B Cell Development, Survival, and Metabolism. *J Immunol* (2016) 197:2250–60. doi: 10.4049/jimmunol.1600492
32. Li B, Li Z, Wang P, Huang Q, Xu L, He R, et al. Mammalian Target of Rapamycin Complex 1 Signalling is Essential for Germinal Centre Reaction. *Immunology* (2017) 152:276–86. doi: 10.1111/imm.12767
33. Benhamron S, Pattanayak SP, Berger M, Tirosh B. mTOR Activation Promotes Plasma Cell Differentiation and Bypasses XBP-1 for Immunoglobulin Secretion. *Mol Cell Biol* (2015) 35:153–66. doi: 10.1128/MCB.01187-14
34. Jones DD, Gaudette BT, Wilmore JR, Chernova I, Bortnick A, Weiss BM, et al. mTOR has Distinct Functions in Generating Versus Sustaining Humoral Immunity. *J Clin Invest* (2016) 126:4250–61. doi: 10.1172/JCI86504
35. Gaudette BT, Jones DD, Bortnick A, Argon Y, Allman D. mTORC1 Coordinates an Immediate Unfolded Protein Response-Related Transcriptome in Activated B Cells Preceding Antibody Secretion. *Nat Commun* (2020) 11:723. doi: 10.1038/s41467-019-14032-1
36. Harding HP, Zeng H, Zhang Y, Jungries R, Chung P, Plesken H, et al. Diabetes Mellitus and Exocrine Pancreatic Dysfunction in Perk–/– Mice Reveals a Role for Translational Control in Secretory Cell Survival. *Mol Cell* (2001) 7:1153–63. doi: 10.1016/S1097-2765(01)00264-7
37. Zhang W, Feng D, Li Y, Iida K, McGrath B, Cavener DR. PERK EIF2AK3 Control of Pancreatic β Cell Differentiation and Proliferation is Required for Postnatal Glucose Homeostasis. *Cell Metab* (2006) 4:491–7. doi: 10.1016/j.cmet.2006.11.002
38. Sowers CR, Wang R, Bourne RA, McGrath BC, Hu J, Bevilacqua SC, et al. The Protein Kinase PERK/EIF2AK3 Regulates Proinsulin Processing Not Via Protein Synthesis But by Controlling Endoplasmic Reticulum Chaperones. *J Biol Chem* (2018) 293:5134–49. doi: 10.1074/jbc.M117.813790
39. Hisanaga S, Miyake M, Taniuchi S, Oyadomari M, Morimoto M, Sato R, et al. PERK-Mediated Translational Control is Required for Collagen Secretion in Chondrocytes. *Sci Rep* (2018) 8:773. doi: 10.1038/s41598-017-19052-9
40. Zhang K, Wong HN, Song B, Miller CN, Scheuner D, Kaufman RJ. The Unfolded Protein Response Sensor IRE1α is Required At 2 Distinct Steps in B Cell Lymphopoiesis. *J Clin Invest* (2005) 115:268–81. doi: 10.1172/JCI200521848
41. Gass JN, Jiang H-Y, Wek RC, Brewer JW. The Unfolded Protein Response of B-lymphocytes: PERK-Independent Development of Antibody-Secreting Cells. *Mol Immunol* (2008) 45:1035–43. doi: 10.1016/j.molimm.2007.07.029
42. Ma Y, Shimizu Y, Mann MJ, Jin Y, Hendershot LM. Plasma Cell Differentiation Initiates a Limited ER Stress Response by Specifically Suppressing the PERK-dependent Branch of the Unfolded Protein Response. *Cell Stress Chaperones* (2010) 15:281–93. doi: 10.1007/s12192-009-0142-9
43. Liu J, Wang Y, Song L, Zeng L, Yi W, Liu T, et al. A Critical Role of DDRGK1 in Endoplasmic Reticulum Homoeostasis Via Regulation of IRE1α Stability. *Nat Commun* (2017) 8:14186. doi: 10.1038/ncomms14186
44. Zhu H, Bhatt B, Sivaprakasam S, Cai Y, Liu S, Kodeboyina SK, et al. Ufbp1 Promotes Plasma Cell Development and ER Expansion by Modulating Distinct Branches of UPR. *Nat Commun* (2019) 10:1084. doi: 10.1038/s41467-019-08908-5

45. Yan W, Frank CL, Korth MJ, Sopher BL, Novoa I, Ron D, et al. Control of PERK eIF2 Kinase Activity by the Endoplasmic Reticulum Stress-Induced Molecular Chaperone P58IPK. *Proc Natl Acad Sci* (2002) 99:15920–5. doi: 10.1073/pnas.252341799
46. van Huizen R, Martindale JL, Gorospe M, Holbrook NJ. P58IPK, a Novel Endoplasmic Reticulum Stress-Inducible Protein and Potential Negative Regulator of eIF2α Signaling. *J Biol Chem* (2003) 278:15558–64. doi: 10.1074/jbc.M212074200
47. Lee A-H, Iwakoshi NN, Glimcher LH. XBP-1 Regulates a Subset of Endoplasmic Reticulum Resident Chaperone Genes in the Unfolded Protein Response. *Mol Cell Biol* (2003) 23:7448–59. doi: 10.1128/MCB.23.21.7448-7459.2003
48. Yamamoto K, Sato T, Matsui T, Sato M, Okada T, Yoshida H, et al. Transcriptional Induction of Mammalian ER Quality Control Proteins is Mediated by Single or Combined Action of ATF6α and XBP1. *Dev Cell* (2007) 13:365–76. doi: 10.1016/j.devcel.2007.07.018
49. Wu J, Rutkowski DT, Dubois M, Swathirajan J, Saunders T, Wang J, et al. ATF6α Optimizes Long-Term Endoplasmic Reticulum Function to Protect Cells From Chronic Stress. *Dev Cell* (2007) 13:351–64. doi: 10.1016/j.devcel.2007.07.005
50. Roobol A, Roobol J, Bastide A, Knight JRP, Willis AE, Smales CM. p58IPK is an Inhibitor of the eIF2α Kinase GCN2 and its Localization and Expression Underpin Protein Synthesis and ER Processing Capacity. *Biochem J* (2015) 465:213–25. doi: 10.1042/BJ20140852
51. Capone V, Clemente E, Restelli E, Di Campli A, Sperduti S, Ornaghi F, et al. PERK Inhibition Attenuates the Abnormalities of the Secretory Pathway and the Increased Apoptotic Rate Induced by SIL1 Knockdown in HeLa Cells. *Biochim Biophys Acta Mol Basis Dis* (2018) 1864:3164–80. doi: 10.1016/j.bbadis.2018.07.003
52. Ichhaporia VP, Sanford T, Howes J, Marion TN, Hendershot LM. Sil1, a Nucleotide Exchange Factor for BiP, is Not Required for Antibody Assembly or Secretion. *Mol Biol Cell* (2015) 26:420–9. doi: 10.1091/mbc.E14-09-1392
53. Cocco M, Care MA, Saadi A, Al-Maskari M, Doody G, Tooze R. A Dichotomy of Gene Regulatory Associations During the Activated B-Cell to Plasmablast Transition. *Life Sci Alliance* (2020) 3:e202000654. doi: 10.26508/lsa.202000654
54. Weitzmann A, Volkmer J, Zimmermann R. The Nucleotide Exchange Factor Activity of Grp170 may Explain the Non-Lethal Phenotype of Loss of Sil1 Function in Man and Mouse. *FEBS Lett* (2006) 580:5237–40. doi: 10.1016/j.febslet.2006.08.055
55. Zhao L, Rosales C, Seburn K, Ron D, Ackerman SL. Alteration of the Unfolded Protein Response Modifies Neurodegeneration in a Mouse Model of Marinesco–Sjögren Syndrome. *Hum Mol Genet* (2010) 19:25–35. doi: 10.1093/hmg/ddp464
56. Kusaczuk M, Cechowska-Pasko M. Molecular Chaperone ORP150 in ER Stress–Related Diseases. *Curr Pharm Des* (2013) 19:2807–18. doi: 10.2174/1381612811319150016
57. Jung TW, Kyung EJ, Kim H-C, Shin YK, Lee SH, Park ES, et al. Protectin DX Ameliorates Hepatic Steatosis by Suppression of Endoplasmic Reticulum Stress Via AMPK-Induced ORP150 Expression. *J Pharmacol Exp Ther* (2018) 365:485–93. doi: 10.1124/jpet.117.246686
58. Jung TW, Park HS, Choi GH, Kim D, Ahn SH, Kim D-S, et al. Maresin 1 Attenuates Pro-Inflammatory Reactions and ER Stress in HUVECs Via PPARα-Mediated Pathway. *Mol Cell Biochem* (2018) 448:335–47. doi: 10.1007/s11010-018-3392-y
59. Zinszner H, Kuroda M, Wang X, Batchvarova N, Lightfoot RT, Remotti H, et al. CHOP is Implicated in Programmed Cell Death in Response to Impaired Function of the Endoplasmic Reticulum. *Genes Dev* (1998) 12:982–95. doi: 10.1101/gad.12.7.982
60. Harding HP, Zhang Y, Bertolotti A, Zeng H, Ron D. Perk Is Essential for Translational Regulation and Cell Survival During the Unfolded Protein Response. *Mol Cell* (2000) 5:897–904. doi: 10.1016/S1097-2765(00)80330-5
61. Lee A-H, Iwakoshi NN, Anderson KC, Glimcher LH. Proteasome Inhibitors Disrupt the Unfolded Protein Response in Myeloma Cells. *Proc Natl Acad Sci* (2003) 100:9946–51. doi: 10.1073/pnas.1334037100
62. Lu PD, Jousse C, Marciniak SJ, Zhang Y, Novoa I, Scheuner D, et al. Cytoprotection by Pre-Emptive Conditional Phosphorylation of Translation Initiation Factor 2. *EMBO J* (2004) 23:169–79. doi: 10.1038/sj.emboj.7600030
63. Lee A-H, Chu GC, Iwakoshi NN, Glimcher LH. XBP-1 is Required for Biogenesis of Cellular Secretory Machinery of Exocrine Glands. *EMBO J* (2005) 24:4368–80. doi: 10.1038/sj.emboj.7600903
64. Lin JH, Li H, Yasumura D, Cohen HR, Zhang C, Panning B, et al. IRE1 Signaling Affects Cell Fate During the Unfolded Protein Response. *Science* (2007) 318:944–9. doi: 10.1126/science.1146361
65. Han D, Upton J-P, Hagen A, Callahan J, Oakes SA, Papa FR. A Kinase Inhibitor Activates the IRE1α RNase to Confer Cytoprotection Against ER Stress. *Biochem Biophys Res Commun* (2008) 365:777–83. doi: 10.1016/j.bbrc.2007.11.040
66. Lange PS, Chavez JC, Pinto JT, Coppola G, Sun C-W, Townes TM, et al. ATF4 is an Oxidative Stress–Inducible, Prodeath Transcription Factor in Neurons In Vitro and In Vivo. *J Exp Med* (2008) 205:1227–42. doi: 10.1084/jem.20071460
67. Tokutake Y, Yamada K, Hayashi S, Arai W, Watanabe T, Yonekura S. IRE1-XBP1 Pathway of the Unfolded Protein Response is Required During Early Differentiation of C2C12 Myoblasts. *Int J Mol Sci* (2019) 21:182. doi: 10.3390/ijms21010182
68. McCarthy N, Dolgikh N, Logue S, Patterson JB, Zeng Q, Gorman AM, et al. The IRE1 and PERK Arms of the Unfolded Protein Response Promote Survival of Rhabdomyosarcoma Cells. *Cancer Lett* (2020) 490:76–88. doi: 10.1016/j.canlet.2020.07.009
69. Shi Z, Xu L, Xie H, Ouyang R, Ke Y, Zhou R, et al. Attenuation of Intermittent Hypoxia-Induced Apoptosis and Fibrosis in Pulmonary Tissues Via Suppression of ER Stress Activation. *BMC Pulm Med* (2020) 20:92. doi: 10.1186/s12890-020-1123-0
70. Zhou R, Ma Y, Tao Z, Qiu S, Gong Z, Tao L, et al. Melatonin Inhibits Glucose-Induced Apoptosis in Osteoblastic Cell Line Through PERK-eIF2α-ATF4 Pathway. *Front Pharmacol* (2020) 11:602307. doi: 10.3389/fphar.2020.602307
71. Lin JH, Li H, Zhang Y, Ron D, Walter P. Divergent Effects of PERK and IRE1 Signaling on Cell Viability. *PloS One* (2009) 4:e4170. doi: 10.1371/journal.pone.0004170
72. Kuwabara K, Matsumoto M, Ikeda J, Hori O, Ogawa S, Maeda Y, et al. Purification and Characterization of a Novel Stress Protein, the 150-kDa Oxygen-regulated Protein (ORP150), From Cultured Rat Astrocytes and Its Expression in Ischemic Mouse Brain. *J Biol Chem* (1996) 271:5025–32. doi: 10.1074/jbc.271.9.5025
73. Tamatani M, Matsuyama T, Yamaguchi A, Mitsuda N, Tsukamoto Y, Taniguchi M, et al. ORP150 Protects Against Hypoxia/Ischemia-Induced Neuronal Death. *Nat Med* (2001) 7:317–23. doi: 10.1038/85463
74. Nakatani Y, Kaneto H, Kawamori D, Yoshiuchi K, Hatazaki M, Matsuoka T, et al. Involvement of Endoplasmic Reticulum Stress in Insulin Resistance and Diabetes. *J Biol Chem* (2005) 280:847–51. doi: 10.1074/jbc.M411860200
75. Cox JS, Walter P. A Novel Mechanism for Regulating Activity of a Transcription Factor That Controls the Unfolded Protein Response. *Cell* (1996) 87:391–404. doi: 10.1016/S0092-8674(00)81360-4
76. Acosta-Alvear D, Zhou Y, Blais A, Tsikitis M, Lents NH, Arias C, et al. XBP1 Controls Diverse Cell Type- and Condition-Specific Transcriptional Regulatory Networks. *Mol Cell* (2007) 27:53–66. doi: 10.1016/j.molcel.2007.06.011
77. Kowalik AS, Johnson CL, Chadi SA, Weston JY, Fazio EN, Pin CL. Mice Lacking the Transcription Factor Mist1 Exhibit an Altered Stress Response and Increased Sensitivity to Caerulein-Induced Pancreatitis. *Am J Physiol Gastrointest Liver Physiol* (2007) 292:G1123–32. doi: 10.1152/ajpgi.00512.2006
78. Alahari S, Mehmood R, Johnson CL, Pin CL. The Absence of MIST1 Leads to Increased Ethanol Sensitivity and Decreased Activity of the Unfolded Protein Response in Mouse Pancreatic Acinar Cells. *PloS One* (2011) 6:e28863. doi: 10.1371/journal.pone.0028863
79. Hess DA, Strelau KM, Karki A, Jiang M, Azevedo-Pouly AC, Lee A-H, et al. MIST1 Links Secretion and Stress as Both Target and Regulator of the Unfolded Protein Response. *Mol Cell Biol* (2016) 36:2931–44. doi: 10.1128/MCB.00366-16
80. Lo H-YG, Jin RU, Sibbel G, Liu D, Karki A, Joens MS, et al. A Single Transcription Factor is Sufficient to Induce and Maintain Secretory Cell Architecture. *Genes Dev* (2017) 31:154–71. doi: 10.1101/gad.285684.116
81. Huh WJ, Esen E, Geahlen JH, Bredemeyer AJ, Lee A-H, Shi G, et al. XBP1 Controls Maturation of Gastric Zymogenic Cells by Induction of MIST1 and

Expansion of the Rough Endoplasmic Reticulum. *Gastroenterology* (2010) 139:2038–49. doi: 10.1053/j.gastro.2010.08.050
82. Metzler MA, Venkatesh SG, Lakshmanan J, Carenbauer AL, Perez SM, Andres SA, et al. A Systems Biology Approach Identifies a Regulatory Network in Parotid Acinar Cell Terminal Differentiation. *PloS One* (2015) 10:e0125153. doi: 10.1371/journal.pone.0125153
83. Capoccia BJ, Lennerz JKM, Bredemeyer AJ, Klco JM, Frater JL, Mills JC. Transcription Factor MIST1 in Terminal Differentiation of Mouse and Human Plasma Cells. *Physiol Genomics* (2011) 43:174–86. doi: 10.1152/physiolgenomics.00084.2010
84. Bhattacharya D, Cheah MT, Franco CB, Hosen N, Pin CL, Sha WC, et al. Transcriptional Profiling of Antigen-Dependent Murine B Cell Differentiation and Memory Formation. *J Immunol* (2007) 179:6808–19. doi: 10.4049/jimmunol.179.10.6808
85. Sandadi S, Ensari S, Kearns B. Heuristic Optimization of Antibody Production by Chinese Hamster Ovary Cells. *Biotechnol Prog* (2005) 21:1537–42. doi: 10.1021/bp0501266
86. Kelly PS, Alarcon Miguez A, Alves C, Barron N. From Media to Mitochondria–Rewiring Cellular Energy Metabolism of Chinese Hamster Ovary Cells for the Enhanced Production of Biopharmaceuticals. *Curr Opin Chem Eng* (2018) 22:71–80. doi: 10.1016/j.coche.2018.08.009
87. Yin B, Wang Q, Chung C-Y, Ren X, Bhattacharya R, Yarema KJ, et al. Butyrated ManNAc Analog Improves Protein Expression in Chinese Hamster Ovary Cells. *Biotechnol Bioeng* (2018) 115:1531–41. doi: 10.1002/bit.26560
88. Braasch K, Kryworuchko M, Piret JM. Autophagy-Inducing Peptide Increases CHO Cell Monoclonal Antibody Production in Batch and Fed-Batch Cultures. *Biotechnol Bioeng* (2021) 118:bit.27703. doi: 10.1002/bit.27703
89. Ishii Y, Murakami J, Sasaki K, Tsukahara M, Wakamatsu K. Efficient Folding/Assembly in Chinese Hamster Ovary Cells is Critical for High Quality (Low Aggregate Content) of Secreted Trastuzumab as Well as for High Production: Stepwise Multivariate Regression Analyses. *J Biosci Bioeng* (2014) 118:223–30. doi: 10.1016/j.jbiosc.2014.01.013
90. Matucci A, Nencini F, Pratesi S, Maggi E, Vultaggio A. An Overview on Safety of Monoclonal Antibodies. *Curr Opin Allergy Clin Immunol* (2016) 16:576–81. doi: 10.1097/ACI.0000000000000315
91. Talbot NE, Mead EJ, Davies SA, Uddin S, Smales CM. Application of ER Stress Biomarkers to Predict Formulated Monoclonal Antibody Stability. *Biotechnol J* (2019) 14:1900024. doi: 10.1002/biot.201900024
92. Hiller MM, Finger A, Schweiger M, Wolf DH. ER Degradation of a Misfolded Luminal Protein by the Cytosolic Ubiquitin-Proteasome Pathway. *Science* (1996) 273:1725–8. doi: 10.1126/science.273.5282.1725
93. Oda Y, Okada T, Yoshida H, Kaufman RJ, Nagata K, Mori K. Derlin-2 and Derlin-3 are Regulated by the Mammalian Unfolded Protein Response and are Required for ER-associated Degradation. *J Cell Biol* (2006) 172:383–93. doi: 10.1083/jcb.200507057
94. Belmont PJ, Chen WJ, San Pedro MN, Thuerauf DJ, Gellings Lowe N, Gude N, et al. Roles for Endoplasmic Reticulum–Associated Degradation and the Novel Endoplasmic Reticulum Stress Response Gene Derlin-3 in the Ischemic Heart. *Circ Res* (2010) 106:307–16. doi: 10.1161/CIRCRESAHA.109.203901
95. Prashad K, Mehra S. Dynamics of Unfolded Protein Response in Recombinant CHO Cells. *Cytotechnology* (2015) 67:237–54. doi: 10.1007/s10616-013-9678-8
96. Roy G, Zhang S, Li L, Higham E, Wu H, Marelli M, et al. Development of a Fluorescent Reporter System for Monitoring ER Stress in Chinese Hamster Ovary Cells and its Application for Therapeutic Protein Production. *PloS One* (2017) 12:e0183694. doi: 10.1371/journal.pone.0183694
97. Maldonado-Agurto R, Dickson AJ. Multiplexed Digital mRNA Expression Analysis Profiles System-Wide Changes in mRNA Abundance and Responsiveness of UPR-Specific Gene Expression Changes During Batch Culture of Recombinant Chinese Hamster Ovary Cells. *Biotechnol J* (2018) 13:1700429. doi: 10.1002/biot.201700429
98. Du Z, Treiber D, McCoy RE, Miller AK, Han M, He F, et al. Non-Invasive UPR Monitoring System and its Applications in CHO Production Cultures. *Biotechnol Bioeng* (2013) 110:2184–94. doi: 10.1002/bit.24877
99. Kober L, Zehe C, Bode J. Development of a Novel ER Stress Based Selection System for the Isolation of Highly Productive Clones. *Biotechnol Bioeng* (2012) 109:2599–611. doi: 10.1002/bit.24527
100. Poulain A, Mullick A, Massie B, Durocher Y. Reducing Recombinant Protein Expression During CHO Pool Selection Enhances Frequency of High-Producing Cells. *J Biotechnol* (2019) 296:32–41. doi: 10.1016/j.jbiotec.2019.03.009
101. Koskela EV, Gonzalez Salcedo A, Piirainen MA, Iivonen HA, Salminen H, Frey AD. Mining Data From Plasma Cell Differentiation Identified Novel Genes for Engineering of a Yeast Antibody Factory. *Front Bioeng Biotechnol* (2020) 8:255. doi: 10.3389/fbioe.2020.00255
102. Damasceno LM, Anderson KA, Ritter G, Cregg JM, Old LJ, Batt CA. Cooverexpression of Chaperones for Enhanced Secretion of a Single-Chain Antibody Fragment in Pichia Pastoris. *Appl Microbiol Biotechnol* (2007) 74:381–9. doi: 10.1007/s00253-006-0652-7
103. Ha TK, Hansen AH, Kildegaard HF, Lee GM. BiP Inducer X: An ER Stress Inhibitor for Enhancing Recombinant Antibody Production in CHO Cell Culture. *Biotechnol J* (2019) 14:1900130. doi: 10.1002/biot.201900130
104. Tigges M, Fussenegger M. Xbp1-based Engineering of Secretory Capacity Enhances the Productivity of Chinese Hamster Ovary Cells. *Metab Eng* (2006) 8:264–72. doi: 10.1016/j.ymben.2006.01.006
105. Mohan C, Park SH, Chung JY, Lee GM. Effect of Doxycycline-Regulated Protein Disulfide Isomerase Expression on the Specific Productivity of Recombinant CHO Cells: Thrombopoietin and Antibody. *Biotechnol Bioeng* (2007) 98:611–5. doi: 10.1002/bit.21453
106. Borth N, Mattanovich D, Kunert R, Katinger H. Effect of Increased Expression of Protein Disulfide Isomerase and Heavy Chain Binding Protein on Antibody Secretion in a Recombinant CHO Cell Line. *Biotechnol Prog* (2008) 21:106–11. doi: 10.1021/bp0498241
107. Pieper LA, Strotbek M, Wenger T, Olayioye MA, Hausser A. ATF6β-Based Fine-Tuning of the Unfolded Protein Response Enhances Therapeutic Antibody Productivity of Chinese Hamster Ovary Cells: ATF6β-Based CHO Cell Engineering. *Biotechnol Bioeng* (2017) 114:1310–8. doi: 10.1002/bit.26263
108. Amin-Wetzel N, Saunders RA, Kamphuis MJ, Rato C, Preissler S, Harding HP, et al. A J-Protein Co-Chaperone Recruits Bip to Monomerize IRE1 and Repress the Unfolded Protein Response. *Cell* (2017) 171:1625–37.e13. doi: 10.1016/j.cell.2017.10.040
109. Dalloul I, Boyer F, Dalloul Z, Pignarre A, Caron G, Fest T, et al. Locus Suicide Recombination Actively Occurs on the Functionally Rearranged IgH Allele in B-cells From Inflamed Human Lymphoid Tissues. *PloS Genet* (2019) 15:e1007721. doi: 10.1371/journal.pgen.1007721
110. Jourdan M, Caraux A, Caron G, Robert N, Fiol G, Rème T, et al. Characterization of a Transitional Preplasmablast Population in the Process of Human B Cell to Plasma Cell Differentiation. *J Immunol* (2011) 187:3931–41. doi: 10.4049/jimmunol.1101230
111. Hipp N, Symington H, Pastoret C, Caron G, Monvoisin C, Tarte K, et al. IL-2 Imprints Human Naive B Cell Fate Towards Plasma Cell Through ERK/ELK1-mediated BACH2 Repression. *Nat Commun* (2017) 8:1443. doi: 10.1038/s41467-017-01475-7

Conflict of Interest: The authors declare that the research was conducted in the absence of any commercial or financial relationships that could be construed as a potential conflict of interest.

frontiers in Immunology

PERSPECTIVE
published: 10 May 2021
doi: 10.3389/fimmu.2021.664249

Over-Generalizing About GC (Hypoxia): Pitfalls of Limiting Breadth of Experimental Systems and Analyses in Framing Informatics Conclusions

Mark R. Boothby[1], Ariel Raybuck[1], Sung Hoon Cho[1], Kristy R. Stengel[2], Volker H. Haase[3], Scott Hiebert[2] and Jingxin Li[4]*

[1] Department of Pathology, Microbiology & Immunology, Molecular Pathogenesis Division, Vanderbilt University Medical Center and School of Medicine, Nashville, TN, United States, [2] Department of Biochemistry, Vanderbilt University School of Medicine, Nashville TN, United States, [3] Department of Medicine, Nephrology Division, Vanderbilt University Medical Center and School of Medicine, Nashville, TN, United States, [4] Medical Scientist Training Program, Perelman School of Medicine, University of Pennsylvania, Philadelphia, PA, United States

OPEN ACCESS

Edited by:
Thierry Fest, University of Rennes 1, France

Reviewed by:
Masaki Hikida, Akita University, Japan
Fabrice Chatonnet, Centre Hospitalier Universitaire (CHU) de Rennes, France

***Correspondence:**
Mark R. Boothby
mark.boothby@vumc.org

Specialty section:
This article was submitted to B Cell Biology, a section of the journal Frontiers in Immunology

Received: *04 February 2021*
Accepted: *14 April 2021*
Published: *10 May 2021*

Citation:
Boothby MR, Raybuck A, Cho SH, Stengel KR, Haase VH, Hiebert S and Li J (2021) Over-Generalizing About GC (Hypoxia): Pitfalls of Limiting Breadth of Experimental Systems and Analyses in Framing Informatics Conclusions. Front. Immunol. 12:664249. doi: 10.3389/fimmu.2021.664249

Accumulating evidence suggests that many immune responses are influenced by local nutrient concentrations in addition to the programming of intermediary metabolism within immune cells. Humoral immunity and germinal centers (GC) are settings in which these factors are under active investigation. Hypoxia is an example of how a particular nutrient is distributed in lymphoid follicles during an antibody response, and how oxygen sensors may impact the qualities of antibody output after immunization. Using exclusively a bio-informatic analysis of mRNA levels in GC and other B cells, recent work challenged the concept that there is any hypoxia or that it has any influence. To explore this proposition, we performed new analyses of published genomics data, explored potential sources of disparity, and elucidated aspects of the apparently conflicting conclusions. Specifically, replicability and variance among data sets derived from different naïve as well as GC B cells were considered. The results highlight broader issues that merit consideration, especially at a time of heightened focus on scientific reports in the realm of immunity and antibody responses. Based on these analyses, a standard is proposed under which the relationship of new data sets should be compared to prior "fingerprints" of cell types and reported transparently to referees and readers. In light of independent evidence of diversity within and among GC elicited by protein immunization, avoidance of overly broad conclusions about germinal centers in general when experimental systems are subject to substantial constraints imposed by technical features also is warranted.

Keywords: hypoxia, intermediary metabolism, Germinal center (GC) B cells, RNA-Seq, polyclonal preimmune repertoire, BCR transgenic mice

INTRODUCTION

In the March 2020 issue of *Nature Immunology*, Weisel, Shlomchik, and co-workers presented interesting data pioneering the use of flow-purified B cells from BCR knock-in mice to explore substrate utilization and metabolic features of B lymphocytes (1). These included naïve B cells - in some but not all comparisons - and a population of germinal center (GC)-phenotype B cells recovered from recipients with a monomorphic B cell population designed to avoid inclusion of other B cells into GC (1–3). Comparisons also involved B cells after T-independent activation *in vivo* (1). In light of the limits to using bio-informatic data to reach conclusions about biological systems, the new evidence about fatty acid oxidation (1) advances insights beyond gene expression profiles comparing naïve and GC B cells (4). However, the paper evoked a need to evaluate the conclusive statement that the "GCBC transcriptome is not commensurate with [….] hypoxia" and similar broad conclusions of the text. This claim seems connected to a view of the authors that RNA-Seq data with GCBC do not contain evidence of enrichment for genes encoding glycolytic enzymes, or that such increases relative to naïve B cells would necessarily show up in a metabolomics analysis with ^{13}C-labeled glucose. These issues prompted examination of these and other data sets in GEO. The results of the analyses point to limits to the conclusions as stated in (1); they also raise a broader question about the system used for this work.

Several papers (4–6) have documented results from intravital labeling with imidazole compounds that covalently modify cellular constituents when the mitochondria of viable cells operate under reductive conditions due to intracellular hypoxia (7–9). Work under controlled conditions has shown that a meaningful signal above background is obtained only when the ambient pO_2 is below about 1-1.5%, levels sufficient to yield HIF stabilization (7–9). Indeed, direct evidence of increased HIF-1α has been presented for both GC B cells (4, 5) and their Tfh counterparts (10), suggesting that many GC light zones are hypoxic. Of note, any issue of HIF function requires understanding that BCR engagement and TLR stimulation cause sustained HIF-1α and HIF-2α stabilization, which presents a drawback to comparing activated versus GC B cells. It might formally be possible that duration of the hypoxia, BCR signaling, and HIF stabilization failed to yield changes in mRNA concentrations large enough for enough gene products to yield a "statistically significant" result in a gene set enrichment analysis (GSEA) algorithm. Indeed, using a gene signature derived with the human breast cancer-like cell line MCF7 (11), the authors' analysis of their purified GC B cells suggested that neither hypoxia-related nor HIF-1 target genes were enriched under their conditions of experimentation (1). Our previous published work had used GSEA with a gene signature indicative of biologically significant hypoxia (12) and scored the result of 2-fold normalized enrichment as statistically significant (4). In contrast, application of this gene signature to the data sets of (1) yielded a balanced mix of increased versus decreased mRNA and was not "statistically significant". This difference along with other disparities of the data prompted us to compare the informatic findings while also using additional benchmarks that could test each report for independent replication.

METHODS AND TECHNICAL LOG

Datasets comparing RNA expression data from "naïve" (IgD+ or Follicular) versus immunization-induced GC B cells were mined from the GEO depositions of raw sequencing data, all of which were generated with Illumina Hi-Seq 2000 or 2500 instruments. For a bespoke pipeline, sequences were trimmed using the fastp FASTQ preprocessor for overrepresented sequences and to remove any sequence with a quality score <10 (13). Trimmed sequences were aligned to the mm10 mouse genome using the STAR sequence aligner of Dobin et al. (14). Aligned sequences were then quality-tested using Qualimap (15) software, and counted using featurecounts in Rsubread (16). To cross-check results and to use a commercial platform readily accessible to anyone seeking to re-analyze the data herein, the RNA-Seq platform within the suites of Basepair Technologies were used. Processing of the gene expression and PCA were cross-checked by using the commercial pipeline of Basepair Technologies as applied to the primary data for naïve and GC B cells of the papers cited as (1, 4, 17, 18).

For heatmap generation (**Figures 2A, B**) *via* the Basepair Technology platform, first the raw read counts generated using STAR aligner and featurecounts were normalized using the DESeq2 package. DESeq2 (19) performs an internal normalization where geometric mean is calculated for each gene across all samples. The counts for a gene in each sample are then divided by this mean. The median of these ratios in a sample is the size factor for that sample. After this, a Z-score normalization is performed on the normalized read counts across samples for each gene, so that Z-scores are computed on a gene-by-gene (row-by-row) basis by subtracting the mean and then dividing by the standard deviation. Computed Z scores were then used to plot heatmaps in which each row represents one gene. There were no substantive differences between different data sets in the quality [for naïve and GC B cell RNA respectively, 92% and 91-92%, 95% and 94-95%, 94% and 93%, and 87% and 91% for the papers referenced in the main text as (1, 4, 13, and 14, respectively) *via* the in-house pipeline uniformly applied to all samples. Comparable values, all above 90%, were generated by the Basepair Technologies pipeline and STAR alignment algorithms. Length scoring also was indistinguishable among the different datasets, two of which [the papers cited as (1) and (18) in the main text] were generated by paired-end sequencing. These steps were followed by multi-factor differential expression analysis in which deposited datasets as well as "naïve" *vs.* "GCB" expression data were compared using DESeq2 (20). Effect size shrinkage of differential expression data was normalized using the *apeglm* method published by Zhu et al. (21). Euclidean distances and Spearman correlation coefficients were derived by applying a standard "dist" function

in R to the data described above. Gene set enrichment analyses were carried out using the GSEA program of the Broad Institute (22, 23) and gene sets derived from published literature, the Rat Genome database ("RGD"), and the Broad KEGG database. As a technical and data note, the informatics pipeline reported in (1) used voom instead of DESeq2, followed by rankSumTestWithCorrelation instead of GSEA. As expected from the technical literature (19, 24–27), the results from each pipeline did not materially differ when applied to the GEO-deposited data of (1). For **Figure 2D** display of count data in a manner that reduces dependence on the variance of the mean for low count data, blinded dispersion estimation using the variance stabilizing transform, VST (28), was conducted on the DESeq2 count data followed by generation of a heat map in which the count data are displayed rather than relative expression.

RESULTS

GC hypoxia was observed with several types of immunization, including with NP-carrier (ovalbumin) (6), but only one paper (4), by Cho, Boothby, et al., had RNA-Seq data for comparisons. However, contemporaneous (2016, 2017) papers with data deposited in GEO had replicate data on naïve and bulk GC B cells (i.e., unfractionated mixtures of all of the diverse types of GC B cell, **Figure 1A**) in a similar time frame (7-10 d) after immunization with the same immunogen (SRBC) (17, 18). We analyzed the sequencer output data for all four papers (1, 4, 17, 18) using the same two parallel pipelines (one assembled in-house, detailed in a technical log appended to this Perspective; a second *via* Basepair Technologies, Inc for an independent framework).

Several salient observations emerged from these comparisons. Unsupervised clustering with Spearman correlation analyses

A

Citation #		GCB	Naïve B
1	**Weisel/ Shlomchik**	CD19+ Fas+ CD38-	CD19+ CD93-
13	**Busslinger**	B220+ GL7+	B220+ GL7-
14	**Melnick**	CD19+ B220+ Fas+ GL7+	CD19+ B220+ IgD+
4	**Cho / Boothby**	B220+ Fas+ GL7+	B220+ Fas- GL7− IgD+

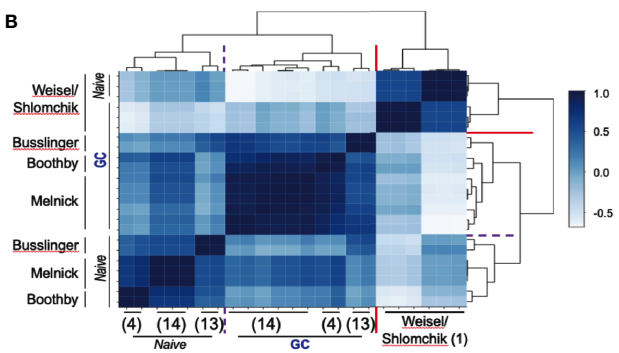

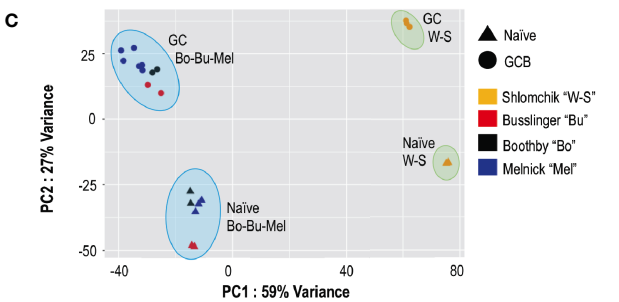

FIGURE 1 | Quantitative comparisons of the overall RNA-Seq data for naïve and GC B cells in the transgenic and non-transgenic systems. Raw RNA-Seq data for naïve and GC B cells were downloaded from the GEO deposits for the papers cited as (1), "W-S" (17);, "Bu" (4);, "Bo" (18); "Mel", and put through each of two separate analysis pipelines applied uniformly to all data (detailed in the Methods and technical log). **(A)** A tabulation of the surface markers used to purify naïve (or naïve follicular) and total germinal center B cells in the papers analyzed. **(B)** Self-organizing map from unsupervised clustering based on Spearman correlation coefficients across the data sets of the papers cited as (1, 4, 17, 18). Darker blue represents strong positive correlation (1.0 = identical across the RNA-Seq data); lightest blues are anti-correlated. **(C)** Shown here, a PCA plot depicting results across the datasets for the indicated conditions (triangles, naïve; circles, GC B cells) and datasets (color-coded as to the paper linked to each GEO data set according to the Legend) generated using the bespoke analysis pipeline detailed in the *Methods and Technical Log* (below). X- and Y- axes are defined by PC1 and PC2, accounting for 59% and 27% of the variance across the datasets, respectively. The results match those derived by the fully independent analysis using the default settings in Basepair Technologies' pipeline (not shown).

(**Figure 1B**), Principal Components analyses (**Figure 1C**), and the Euclidean distances among the different types of samples, revealed that the results from (1) differ substantially from the data of (3), (17), and (18). *First*, the mRNA expression pattern of GC B cells generated after transferring large numbers of B cells [apparently, 10^6 - (2) as cited in (1)] biased toward a single specificity BCR (B1-8^i Vκ -/-) into recipient mice with a monomorphic B cell population specific for Ig (AM14-Tg × V_κ8R-KI BALB/c mice, i.e., specific for allotype-disparate IgG2a^b) differed substantially from the other samples. A measure of overall differences between naïve and GC B cells was less in (1) (mean Euclidean distances of 126.3 ± 0.69) than the difference between the GC B cells of the transferred B1-8i, Vκ-/- cells (1) and the polyclonal GCBC (4, 17, 18) (mean Euclidean distances of 170.3 ± 10.3; $p<0.01$) as well as those of non-transgenic naïve versus GC B cells (147.6 ± SEM of 3.3; $p<0.05$). *Second*, the GC B cells from mice with a normal pre-immune repertoire (4, 17, 18) were substantially more similar to one another in comparing among three independent analyses (correlation coefficients in the range of +0.41 to +0.92) as opposed to anti-correlation of the B1-8i-derived GCBC, (correlation coefficients of -0.05 to -0.32). Although each of the independent data sets with the non-transgenic C57Bl/6 (B6) system differed somewhat – internally and from each other - the RNA-Seq "fingerprints" of naïve B cells in the polyclonal system were quite similar. Thus, the data were replicable when comparing independent SRBC immunizations of mice with no restrictions of the repertoire or BCR. In contrast, even the naïve B1-8^i Vκ-/- B cells were quite distinct from the clusters of polyclonal naïve B cells (**Figures 1B, C**). Relative to the data from (18) as well as (4), the changes were more modest in (1). The similarities and differences among independent data sets can also be parsed by heat maps of differentially expressed genes among the data sets, analyzing either the total set thereof or highlighting specific genes that are known to encode major determinants of B cell positioning, signal initiation during activation, of differentiation into GC B or plasma cells (**Figures 2A, B**). In practice, the collective data (**Figures 1B, C; 2B**) indicate that the GCBC generated after adoptive transfers of B cells with a restricted repertoire into mice whose endogenous B cells will contribute little to the GC are qualitatively distinct from a polyclonal response that evolved from a polyclonal repertoire.

Turning to the question, are there hypoxia-related gene signatures in GC B cells when taking into account other work with a polyclonal repertoire, GSEA algorithms were applied using several different gene sets for hypoxia (**Figure 2C**). A further facet of what the analyses revealed is that with some hypoxia modules, even the RNA-Seq data of (1) show significant enrichment in GSEA (**Figure 2C**). These increases can also be appreciated in data with the actual counts when displaying all naïve and GC B cell data (**Figure 2D**). Moreover, RNA-Seq data with GC from NP-CGG-immunized mice with a normal pre-immune landscape (29) also show enrichment for a functional hypoxia signature (**Figure 2C**, data from the Pernis lab), and divergence from the B1-8i data. Metabolism rather than hypoxia was the central point of (1), a part of which was indirect evidence about glycolytic rates - perhaps on the view that if HIF were stabilized, expression of glycolytic genes should be increased. Prior work had provided evidence that the "glycolysis", "mitochondrial respiration/oxidation" and "FAO" transcriptomes were increased in GCBC when compared to naïve B cells (4). Although this analysis was not evident in the Figure presented in (1) using the B1-8i system, a GSEA comparing naïve and GCBC with the RNA-Seq data in (1) found significant increases in glycolysis-related gene expression (**Figure 2C**), which also applied to each of the other data sets. Indeed, expression of genes encoding enzymes along the glycolysis pathway increased in GC B cell data sets of (1) as well as the polyclonal B6 GC B cells when compared to naïve B cells (**Figure 2D**).

DISCUSSION

The data presented here underscore that what is measured for an overall population of GC B cells is influenced by the structure of the experiment and the inputs analyzed. Key findings are that the cells analyzed in (1) were distinct from and changed less from naïve to GC phenotype than what is found in reproducible data with B cells that derived from a normal polyclonal repertoire (1, 17, 18). B1-8i, Vκ-/- B cells started out with substantial differences in activation markers such as *Nr4a1* and differentiation-related genes, i.e., *Prdm1* and *Irf4*. Of note, the differences do not relate to the particular informatic tools but instead to the selection of inputs. Thus, the pipelines used here yield similar results to those of (1) if, and only if, the analyses are restricted to those data sets and only use the selections in that work. Several factors may be involved in the differences between GC B cells in (1) from those in analyses published several years previously (4, 17, 18). Akin to findings with T cells (30), the experiments in (1) may involve the intra-clonal competition shown to result from using hundreds of thousands of transferred antigen receptor-transgenic cells (31, 32) - as already documented for B1-8i (31). In addition, the metabolic environments of highly diverse GC may differ from the secondary follicles that ensued with the transfer system used in (1). These factors warrant investigation, but the differences emphasize why it is vital that stated conclusions be restricted by limitations of the approach – not least when the approach is quite artificial.

GC are quite heterogeneous (33, 34). This point suggests that caution is warranted from the outset, militating against framing conclusions as blanket generalizations to apply across all GC. In terms of hypoxia or HIF gene signatures, prior work reported (4) that as many as 20% of splenic GC had no signal of intravital hypoxia, a variegation observed in parallel by others (J. Jellusova, personal communication). An integrative possibility is that hypoxia and/or its influence are reduced in GC designed to minimize bystander B cell involvement and dominated by a single specificity, as in (1–3). One technical issue is that there is no validated universal 'hypoxia' or 'HIF' module for activated lymphocytes, let alone a unitary module that includes GC B cells. Hypoxia and HIF responses are protean, but three decades of

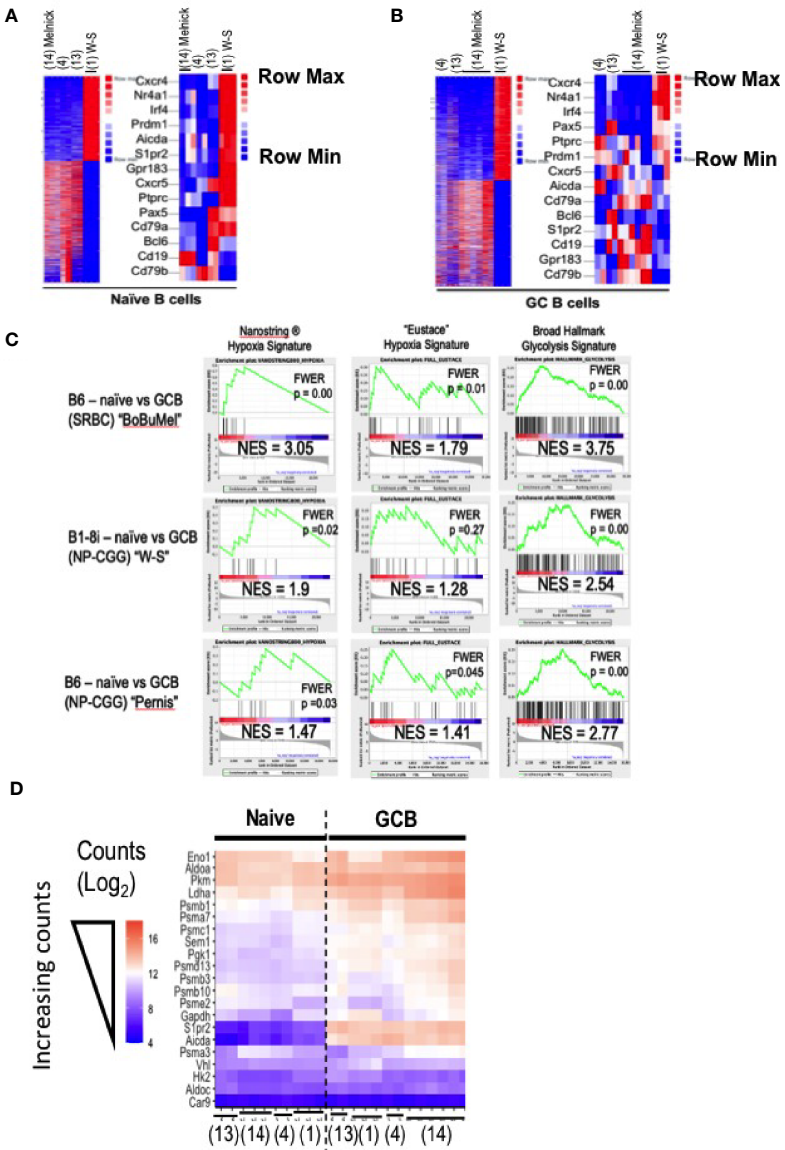

FIGURE 2 | Comparisons of condition-dependent differential gene expression. As in **Figure 1**, GEO data deposits were downloaded for the papers cited as (1), "W-S" (17);, "Bu" (4);, "Bo" (18); "Mel" and processed by trimming, alignment, generation of normalized counts (FPKM), and quantification of differential expression using each of two independent pipelines (i.e., both bespoke and Basepair Technologies'). **(A, B)** Heat maps generated in the Basepair Technologies platform and derived from differential expression analyses comparing the groups "SRBC-immunized B6 mice" versus the BALB/c B1-8i, Vk -/- system are shown for **(A)** naïve and **(B)** GC B cells. In each panel, all differentially expressed genes (16% and 14% of totals, respectively, i.e., 3214/22,843 and 3461/21,327 genes differentially expressed >2-fold with p-adjusted < 0.05) are displayed. To the right, a subset of B lineage-specific or other genes functionally relevant in GC biology are shown. In these heat maps, entries that are dark red are upregulated and those that are blue are downregulated. Since the rows (genes) are Z-Score scaled, the maps report differences in expression of single genes across the samples. **(C)** Gene Set Enrichment Analyses (GSEA) were performed using the Broad algorithm as detailed in the Methods log. Analyses were performed both with data derived by the bespoke pipeline (shown here) and with the expression data exported from the Basepair pipeline, which yielded congruent results to those shown here. Inset values show the normalized enrichment score (NES) and p value after compensation for multiple comparisons (FWER), as indicated. Each panel displays results for a separate analysis in which ranked differential expression data were processed using the Broad Institute's GSEA software. The three columns represent outputs obtained using the indicated gene signatures: Hypoxia Signature as established by Nanostring Technologies ®, the hypoxia gene signature of Eustace et al. [as in references (4, 12)], and the Broad Institute's Hallmark Glycolysis gene set. The rows of panels identify the RNA-Seq data sets that were analyzed in comparisons of GC to naïve B cells: (i) data from like samples in (4, 17, 18); (ii) data from (1); and (iii) data from (29), all of which were processed through the same pipeline with same parameters. **(D)** A heatmap of the blinded variance-stabilizing transformed (VST) count data for selected genes encoding glycolytic enzymes or hypoxia-related genes in all samples [naïve and GC B cells of (1, 4, 17, 18)], benchmarked against two genes (*Aicda*; *S1pr2*) known to be highly expressed in GC B cells. Color coding from lowest (darker purple) counts to highest (deepest peach) is as indicated. Columns position (placement and order) was the computational result of self-organizing mapping, with expected separationi of naïve from GC B cells. Citations below the heat map indicate the publication sourcing of each column's data.

papers address cell type-specific functionality of a transcription factor. Thus, some restraint may be warranted before concluding that a GC transcriptome is not commensurate with hypoxia or conflating HIF with a particular magnitude of increased expression of genes encoding the enzymes of glycolysis or glycolytic flux. The issues connected to these questions take on added currency in considering antibody diversification during the persistent hypoxemia of many patients with severe CoVID-2019 infection. Thus, a great challenge will be to assess if human GC (in which questions about hypoxia, HIF, and *in situ* metabolism) exhibit effects such as those uncovered in mice (4–6) - either in normoxemic people or during concurrent hypoxemia.

Of course, such studies may rely heavily on scRNA-Seq and informatics analyses – conflicting or not – cannot settle secondary issues such as glucose uptake and utilization. Translation efficiency, post-translational modifications, and complex but unknown aspects of nutrient supplies, substrate concentrations, and substrate competition along webs of interconnected pathways all are downstream from the mRNA in question. That simply means that direct rigorous biochemical assays of glucose uptake per cell [e.g., ^{3}H-2-deoxyglucose (DG), since 2-NBDG is known not necessarily to correlate with glucose entry rates (35)] and of glucose oxidation are needed before stating or accepting broad conclusions about germinal center B cells based on a single or special case as in (1). In this respect, normalizing a measure such as uptake to cell size – which is distinct from suitable compensation for autofluorescence in flow cytometry - lacks rigor. Normalization to size is analogous to concluding that a 160 kg person eating 4400 kCal/d has the same energy intake as one who is 80 kg and eats 2200 kCal/d, or claiming that a truck does not consume more fuel than a compact sedan if the size-normalized fuel consumption is the same. With respect to conclusions based solely on informatics, it is proposed that a reasonable standard is to (a) compare new RNA-Seq data sets to independent entries in GEO, and (b) quantify the correlation to - or difference from - those that are in GEO and readily comparable (i.e., not micro-array to RNA-Seq). Of essential importance, some restraint in statement of conclusions, along with openness about limitations, is vital at a time when the societal landscape is roiled by consequences of how scientists frame their work or evidence.

DATA AVAILABILITY STATEMENT

The datasets presented in this study can be found in online repositories. The names of the repository/repositories and accession number(s) can be found in the article/**Supplementary Material**.

AUTHOR CONTRIBUTIONS

MB wrote the text and guided analyses along with getting presubmission input from three independent faculty/PIs. AR led the primary informatic analyses, prepared figures, drafted portions of text, and edited the overall text. SC, KS, and JL performed analyses and provided insights into the RNA-Seq data and gene sets in the papers meta-analyzed. VHH provided input and guidance to SHC and MB; SHC provided input and guidance to KS and MB. All authors contributed to the article and approved the submitted version.

FUNDING

Departmental Funds - Department of Pathology, Microbiology, & Immunology, Vanderbilt University Medical Center.

SUPPLEMENTARY MATERIAL

The Supplementary Material for this article can be found online at: https://www.frontiersin.org/articles/10.3389/fimmu.2021.664249/full#supplementary-material

REFERENCES

1. Weisel FJ, Mullett SJ, Elsner RA, Menk AV, Trivedi N, Luo W, et al. Germinal Center B Cells Selectively Oxidize Fatty Acids for Energy While Conducting Minimal Glycolysis. *Nat Immunol* (2020) 21:331–42. doi: 10.1038/s41590-020-0598-4
2. Zuccarino-Catania GV, Sadanand S, Weisel FJ, Tomayko MM, Meng H, Kleinstein SH, et al. CD80 and PD-L2 Define Functionally Distinct Memory B Cell Subsets That are Independent of Antibody Isotype. *Nat Immunol* (2014) 15:631–7. doi: 10.1038/ni.2914
3. Weisel FJ, Zuccarino-Catania GV, Chikina M, Shlomchik MJ. A Temporal Switch in the Germinal Center Determines Differential Output of Memory B and Plasma Cells. *Immunity* (2016) 44:116–30. doi: 10.1016/j.immuni.2015.12.004
4. Cho SH, Raybuck AL, Stengel K, Wei M, Beck TC, Volanakis E, et al. Germinal Centre Hypoxia and Regulation of Antibody Qualities by a Hypoxia Response System. *Nature* (2016) 537:234–8. doi: 10.1038/nature19334
5. Jellusova J, Cato MH, Apgar JR, Ramezani-Rad P, Leung CR, Chen C, et al. Gsk3 is a Metabolic Checkpoint Regulator in B Cells. *Nat Immunol* (2017) 18:303–12. doi: 10.1038/ni.3664
6. Abbott RK, Thayer M, Labuda J, Silva M, Philbrook P, Cain DW, et al. Germinal Center Hypoxia Potentiates Immunoglobulin Class Switch Recombination. *J Immunol* (2016) 197:4014–20. doi: 10.4049/jimmunol.1601401
7. Koch CJ, Evans SM, Lord EM. Oxygen Dependence of Cellular Uptake of EF5 [2-(2-Nitro-1H-Imidazol-1-Yl)-N-(2,2,3,3,3-pentafluoropropyl) Acetamide]: Analysis of Drug Adducts by Fluorescent Antibodies vs Bound Radioactivity. *Br J Cancer* (1995) 72:869–74. doi: 10.1038/bjc.1995.426
8. Mahy P, De Bast M, Gallez B, Gueulette J, Koch CJ, Scalliet P, et al. In Vivo Colocalization of 2-Nitroimidazole EF5 Fluorescence Intensity and Electron Paramagnetic Resonance Oximetry in Mouse Tumors. *Radiother Oncol* (2003) 67:53–61. doi: 10.1016/S0167-8140(03)00028-8
9. Koch CJ. Importance of Antibody Concentration in the Assessment of Cellular Hypoxia by Flow Cytometry: EF5 and Pimonidazole. *Radiat Res* (2008) 169:677–88. doi: 10.1667/RR1305.1
10. Cho SH, Raybuck AL, Blagih J, Kemboi E, Haase VH, Jones RG, et al. Hypoxia-Inducible Factors (HIF) in CD4^{+} T Cells Promote Metabolism, Switch Cytokine Secretion, and T Cell Help in Humoral Immunity. *PNAS U S A* (2019) 116:8975–84. doi: 10.1073/pnas.1811702116
11. Schödel J, Oikonomopoulos S, Ragoussis J, Pugh CW, Ratcliffe PJ, Mole DR. High-Resolution Genome-Wide Mapping of HIF-binding Sites by Chip-Seq. *Blood* (2011) 117:e207–17. doi: 10.1182/blood-2010-10-314427

12. Eustace A, Mani N, Span PN, Irlam JJ, Taylor J, Betts GN, et al. A 26-Gene Hypoxia Signature Predicts Benefit From Hypoxia-Modifying Therapy in Laryngeal Cancer But Not Bladder Cancer. *Clin Cancer Res* (2013) 19:4879–88. doi: 10.1158/1078-0432.CCR-13-0542
13. Chen S, Zhou Y, Chen Y, Gu J. Fastp: An Ultra-Fast All-in-One FASTQ Preprocessor. *Bioinformatics* (2018) 29(17):i884–90. doi: 10.1093/bioinformatics/bty560
14. Dobin A, Davis CA, Schlesinger F, Drenkow J, Zaleski C, Jha S, et al. STAR: Ultrafast Universal RNA-seq Aligner. *Bioinf (Oxford England)* (2013) 29 (1):15–21. doi: 10.1093/bioinformatics/bts635
15. Okonechnikov K, Conesa A, Garcia-Alcalde F. Qualimap 2: Advanced Multi-Sample Quality Control for High-Throughput Sequencing Data. *Bioinformatics* (2015) 32(2):292–4. doi: 10.1093/bioinformatics/btv566
16. Liao Y, Smyth GK, Shi W. The R Package *Rsubread* is Easier, Faster, Cheaper and Better for Alignment and Quantification of RNA Sequencing Reads. *Nucleic Acids Res* (2019) 47(8):e47. doi: 10.1093/nar/gkz114
17. Wöhner M, Tagoh H, Bilic I, Jaritz M, Poliakova DK, Fischer M, et al. Molecular Functions of the Transcription Factors E2A and E2-2 in Controlling Germinal Center B Cell and Plasma Cell Development. *J Exp Med* (2016) 213:1201–21. doi: 10.1084/jem.20152002
18. Béguelin W, Rivas MA, Calvo Fernández MT, Teater M, Purwada A, Redmond D, et al. EZH2 Enables Germinal Centre Formation Through Epigenetic Silencing of CDKN1A and an Rb-E2F1 Feedback Loop. *Nat Commun* (2017) 8(1):877. doi: 10.1038/s41467-017-01029-x
19. Zhang ZH, et al. A Comparative Study of Techniques for Differential Expression Analysis on RNA-Seq Data. *PLoS One* (2014) 9(8):e103207. doi: 10.1371/journal.pone.0103207
20. Love MI, Huber W, Anders S. Moderated Estimation of Fold Change and Dispersion for RNA-seq Data With Deseq2. *Genome Biol* (2014) 15:550. doi: 10.1186/s13059-014-0550-8
21. Zhu A, Ibrahim JG, Love MI. Heavy-Tailed Prior Distributions for Sequence Count Data: Removing the Noise and Preserving Large Differences. *Bioinformatics* (2018) 35(12):2084–92. doi: 10.1093/bioinformatics/bty895
22. Subramanian A, Tamayo P, Mootha VK, Mukherjee S, Ebert BL, Gillette MA, et al. Gene Set Enrichment Analysis: A Knowledge-Based Approach for Interpreting Genome-Wide Expression Profiles. *Proc Natl Acad Sci USA* (2005) 102:15545–50. doi: 10.1073/pnas.0506580102
23. Mootha VK, Lindgren CM, Ericksson KF, Subramanian A, Sihag S, Lehar J, et al. Pgc-1a-responsive Genes Involved in Oxidative Phosphorylation are Coordinately Downregulated in Human Diabetes. *Nat Genet* (2003) 34:267–73. doi: 10.1038/ng1180
24. Ackermann M, Strimmer K. A General Modular Framework for Gene Set Enrichment Analysis. *BMC Bioinf* (2009) 10:47. doi: 10.1186/1471-2105-10-47
25. Hung JH, Yang TH, Hu Z, Weng Z, DeLisi C. Gene Set Enrichment Analysis: Performance Evaluation and Usage Guidelines. *Brief Bioinform* (2012) 13 (3):281–91. doi: 10.1093/bib/bbr049
26. Schurch NJ, Schofield P, Gierlinski M, Cole C, Sherstnev A, Singh V, et al. How Many Biological Replicates are Needed in an RNA-seq Experiment and Which Differential Expression Tool Should You Use? *RNA* (2016) 22:839–51. doi: 10.1261/rna.053959.115
27. Costa-Silva J, Domingues D, Lopes FM. Rna-Seq Differential Expression Analysis: An Extended Review and a Software Tool. *PLoS One* (2017) 12:12e0190152. doi: 10.1371/journal.pone.0190152
28. Anders S, Huber W. Differential Expression Analysis for Sequence Count Data. *Genome Biol* (2010) 11:R106. doi: 10.1186/gb-2010-11-10-r106
29. Ricker E, Chinenov Y, Pannellini T, Flores-Castro D, Ye C, Gupta S, et al. Serine-Threonine Kinase ROCK2 Regulates Germinal Center B Cell Positioning and Cholesterol Biosynthesis. *J Clin Invest* (2020) 130:3654–70. doi: 10.1172/JCI132414
30. Badovinac VP, Haring JS, Harty JT. Initial T Cell Receptor Transgenic Cell Precursor Frequency Dictates Critical Aspects of the CD8(+) T Cell Response to Infection. *Immunity* (2007) 26:827–41. doi: 10.1016/j.immuni.2007.04.013
31. Le TV, Kim TH, Chaplin DD. Intraclonal Competition Inhibits the Formation of High-Affinity Antibody-Secreting Cells. *J Immunol* (2008) 181:6027–37. doi: 10.4049/jimmunol.181.9.6027
32. Abbott RK, Lee JH, Menis S, Skog P, Rossi M, Ota T, et al. Precursor Frequency and Affinity Determine B Cell Competitive Fitness in Germinal Centers, Tested With Germline-Targeting HIV Vaccine Immunogens. *Immunity* (2018) 48:133–46. doi: 10.1016/j.immuni.2017.11.023
33. Tas JM, Mesin L, Pasqual G, Targ S, Jacobsen JT, Mano YM, et al. Visualizing Antibody Affinity Maturation in Germinal Centers. *Science* (2016) 351:1048–54. doi: 10.1126/science.aad3439
34. Mesin L, Ersching J, Victora GD. Germinal Center B Cell Dynamics. *Immunity* (2016) 45:471–82. doi: 10.1016/j.immuni.2016.09.001
35. Sinclair LV, Barthelemy C, Cantrell DA. Single Cell Glucose Uptake Assays: A Cautionary Tale. *Immunometabolism* (2020) 2(4):e200029. doi: 10.20900/immunometab20200029

Conflict of Interest: The authors declare that the research was conducted in the absence of any commercial or financial relationships that could be construed as a potential conflict of interest.

frontiers in Immunology

REVIEW
published: 10 June 2021
doi: 10.3389/fimmu.2021.679909

T Follicular Regulatory Cells: Choreographers of Productive Germinal Center Responses

Yisi Lu[1] *and Joe Craft*[1,2*]

[1] Department of Immunobiology, Yale School of Medicine, New Haven, CT, United States, [2] Department of Internal Medicine, Yale School of Medicine, New Haven, CT, United States

T follicular regulatory cells, or Tfr cells, are a discernable population of regulatory T (Treg) cells that migrate to the B cell follicle and germinal center (GC) upon immune challenge. These cells express the transcription factor Bcl6, the master regulator required for development and differentiation of T follicular helper cells, and are among a group of previously described Treg cells that use T helper cell–associated transcription factors to adapt their regulatory function to diverse milieus for maintenance of immune homeostasis. While there is consensus that Tfr cells control B-cell autoreactivity, it has been unclear whether they regulate productive, antigen-specific GC responses. Accordingly, understanding the regulatory balancing that Tfr cells play in maintenance of B-cell tolerance while optimizing productive humoral immunity is crucial for vaccine-design strategies. To this end, we discuss recent evidence that Tfr cells promote humoral immunity and memory following viral infections, fitting with the accepted role of Treg cells in maintaining homeostasis with promotion of productive immunity, while mitigating that which is potentially pathological. We also propose models in which Tfr cells regulate antigen-specific B cell responses.

Keywords: autoimmunity, B cell follicle, Bcl6, germinal center, humoral immunity, T follicular helper cells, T follicular regulatory cells

OPEN ACCESS

Edited by:
Thierry Fest, University of Rennes 1, France

Reviewed by:
Wataru Ise, Osaka University, Japan
Bruce David Mazer, Research Institute of the McGill University Health Center (RI-MUHC), Canada

***Correspondence:**
Joe Craft
joseph.craft@yale.edu

Specialty section:
This article was submitted to B Cell Biology, a section of the journal Frontiers in Immunology

Received: *12 March 2021*
Accepted: *27 May 2021*
Published: *10 June 2021*

Citation:
Lu Y and Craft J (2021) T Follicular Regulatory Cells: Choreographers of Productive Germinal Center Responses. Front. Immunol. 12:679909. doi: 10.3389/fimmu.2021.679909

Antibodies form the first line of defense against invading pathogens and provide the basis for successful vaccines *via* humoral memory (1). Upon encounter with pathogens, naïve follicular B cells are activated and migrate into the T-B border of the spleen or interfollicular regions of lymph nodes, where they become fully activated upon further interaction with antigen-specific T cells (2–6). A subset of the activated B cells differentiates into short-lived plasmablasts secreting low-affinity antibodies in the splenic red pulp or medullary cords of lymph nodes, while in parallel, other B cells migrate back into follicle to seed early germinal centers (GCs) (7).

A subset of effector $CD4^+$ T cells, T follicular helper (Tfh) cells defined by expression of the transcriptional factor Bcl6, also migrate into the early GCs. Therein, B cells undergo proliferation and somatic hypermutation of their immunoglobulin (Ig) genes, followed by a process in which

the fittest B cells – those able to capture antigen *via* surface Ig and best present it on surface MHCII – are selected by follicular helper T (Tfh) cells (8). The strength of interaction between Tfh cells and GC B cells, which is proportional to the amount of antigen presented by GC B cells, drives the cyclic reentry and determines the cell cycle speed and number of division of GC B cell clones (9–11). The selected GC B cell clones then differentiate and mature into memory B cells and long-lived antibody-producing plasma cells, together forming the basis of humoral memory and associated pathogen protection. Upon pathogen re-exposure, high-affinity, protective antibodies secreted by LLPCs are a first line of protection; additionally, pathogen-specific memory B cells are activated and rapidly mature into plasmablasts to produce protective antibodies (12).

T follicular regulatory cells, or Tfr cells, express the germinal center (GC)-defining transcription factor Bcl6, and migrate to the B-cell follicle following immunization and infection, adding to the complexity of interplay between different cell types within the B cell follicle and GC and the heterogeneity of Treg cells that express T helper (Th) cell transcription factors (13–18). The localization of Tfr cells to the GC is believed to be dependent on the chemokine receptor CXCR5; however, a recent study showed that Tfr cells can access the GC in a CXCR5-independent manner, suggesting the possibility of other molecules, such as CXCR4 or S1PR2, playing a similar or redundant role of facilitating their migration (19). It is crucial to understand whether these Treg cells have acquired specialized function to regulate B cells responses and fine-tune their output, including development of humoral memory. Such insights will contribute to efforts in vaccine design.

Tfr cells differentiate from $CD25^{hi}$ $Foxp3^{+}$ Treg precursors (13, 20), while co-opting the developmental pathway of Tfh cells, dependent on the same signaling cues including CD28, signaling lymphocytic activation molecule (SLAM)-associated protein

(SAP), and inducible T cell co-stimulator (ICOS) (13, 14). One important aspect of the Tfr cell differentiation process is downregulation of CD25 expression (20–22), with these cells comprising both $CD25^{+}$ and $CD25^{-}$ populations with the former a transitional phenotype potentially because of their high CCR7 expression compared to their $CD25^{-}$ counterparts (21). The necessity of downregulation of CD25 in Tfr cells lies in that IL-2 signaling leads to phosphorylation of Stat5 and the downstream upregulation of Blimp1, which antagonizes Bcl6 (23, 24). Thus, in order to upregulate Bcl6 expression, Tfr cells downregulate CD25, possibly through a mechanism of upregulation of ASCL2 (21, 25). Yet, the expression of key functional molecules in Tfr cells, such as Foxp3 and CTLA-4, are similar between $CD25^{+}$ and $CD25^{-}$ populations (21).

Treg cells are crucial for the maintenance of tolerance and homeostasis. Seminal work from Shimon Sakaguchi showed that athymic nude mice lacking T cells developed autoimmunity in several organs upon adoptive transfer of T cells lacking the $CD4^{+}CD25^{+}$ Treg population (26). This work demonstrated the classical function of Treg cells, which is limiting inflammation mediated by T effector cells to minimize associated tissue damage and prevent autoimmunity. Since then, various mechanisms of action by which Treg cells function in maintenance of immune and tissue homeostasis have been elucidated, which have been extensively reviewed elsewhere (27–30).

Accumulating evidence suggests that Treg cells also actively promote productive immune responses upon immune challenge, rather than functioning merely as suppressors. Early after infection, Treg cells optimize the chemokine milieu to ensure recruitment of the appropriate effector cells to sites of infection, for example in a model of mucosal herpes simplex virus infection (31). By controlling the overproduction of chemokines (CCL-2/3/4/5) from antigen-presenting dendritic cells (DCs), Treg cells also promote the avidity of $CD8^{+}$ T cell primary responses by limiting priming of low-avidity $CD8^{+}$ T cells (32–34). Subsequently, the disruption of high-avidity $CD8^{+}$ T cell responses during the primary infection leads to an impaired $CD8^{+}$ memory response in a model of recombinant *Listeria monocytogenes* infection (32). Treg cells have been found to act as an IL-2 sink during priming of $CD8^{+}$ T cells to shield them from excessive IL-2 signaling, therefore favoring their differentiation into memory precursor effector cells rather than short-lived effector cells, thereby promoting effective secondary $CD8^{+}$ T cell responses (35, 36). In a like vein, Treg cell-mediated dampening of inflammation during the resolution phase of the infection is crucial for the maturation of $CD8^{+}$ T cell memory responses, mediated by Treg cell–derived IL-10 and CTLA-4 (37, 38). Treg cells additionally promote the formation of resident $CD8^{+}$ memory T cells through the production of TGF-β in a model of West Nile virus infection (39). Independent from their role in suppression, Treg cells support tissue protection in an influenza virus infection model (40), reminiscent of their tissue repair function in nonlymphoid tissues (41). These lines of evidence, among others, support the idea that Tregs are essential for development of protective immune responses.

In line with these findings, we propose that functions of Tfr cells can be categorized into maintaining self-tolerance as well as promoting effective humoral responses. There are necessary mechanisms to maintain self-tolerance as B cells mature to antibody-secreting cells (ASCs) or memory cells because of the propensity for development of self-reactivity, particularly within the GC due to rapid proliferation with somatic hypermutation (SHM) of the antigen-binding variable region of immunoglobulin genes (42). Tfr cells thus serve as an additional level of regulation. For example, in the absence of Tfr cells, there is development of self-reactive ASCs in models of influenza virus infection, suggesting that one of the functions of Tfr cells is to prevent the expansion of autoreactive B cell clones (20). Protein immunization also revealed autoreactive IgG and IgE in the serum of mice lacking Tfr cells (43). Tfr-deficient mice also spontaneously develop autoantibodies at older age (44, 45). The mode of action by which Tfr cells maintain tolerance is incompletely understood, with CTLA-4 being implicated (46, 47) based on known function of this molecule in regulating peripheral tolerance (48) and with neuritin produced by Tfr cells suppressing the development of autoantibodies and IgE class switching (45).

Whether and how Tfr cells optimize GC responses and promote effective humoral memory is incompletely understood. In an protein immunization model, adoptive transfers of CXCR5-deficient Treg cells and naïve wild type $CD4^+$ T cells into T-cell deficient recipients lead to enhanced antigen-specific antibody responses (14, 15). In genetically engineered mouse models lacking Tfr cells, antigen-specific B cell responses are elevated both *in vitro* and *in vivo* following immunization with protein-hapten conjugates and in a house dust mite challenge allergy model (43, 49), with other work revealing reduced antigen-specific IgE and IgG titers in Tfr-deficient mice in food allergen sensitization and immunization settings, respectively (50, 51). Different allergy models with distinct response kinetics and different Tfr-deficient animals were used in these two settings, which may potentially explain the contrasting results. In addition, depleting Tfr cells but not Tregs specifically using SAP KO (which do not form Tfh or Tfr cells but do form Treg cells) and Foxp3-DTR (which lack Tfr cells) mixed bone marrow chimeras as well as $Bcl6^{flox/flox}$ Foxp3-Cre animals following a similar protein immunization model resulted in decreased antigen-specific GC B cells (13, 45).

Yet, it is likely that the function of Tfr cells depends on the complexity of the antigen, and its potential for replication. The maintenance of diverse antigen-specific and non-antigen-specific B cell clones upon viral infection in which the antigen is complex with distinct epitopes and replicative persistence is distinct from an immunization model with simpler, non-replicative antigens (52). The complexity of the antigen determines the kinetics of competition among different clones within the GC and therefore the rate of achieving homogenizing selection (52, 53). It is possible that one of the functions of Tfr cells is to maintain the breath of the response as it allows more layers of regulation in the selection process. Such function would be more important when there are lots of competing clones and there is the need of maintaining non-immunodominant antibody clones as in the case of influenza virus infection. Equally likely is the possibility that different infection or immunization routes in distinct local immune microenvironments leads to distinct Tfr cell-mediated effects (*e.*g., mucosal *versus* systemic). Consistent with the latter is the finding that mice developed impaired antigen-specific antibody response in the lack of polyclonal Treg cells in a mucosal immunization model (54), with the idea that Tfr cells contributed to the observed phenotype.

Recent studies have used influenza virus infection models to study the function of Tfr cells (20, 44). The total numbers of Tfh cells and GC B cells were not affected in the absence of Tfr cells at either day 9 post infection (p.i.) (44) or day 30 p.i (20). At day 9 p.i., the difference of anti-influenza virus antibodies in mice with and without Tfr cells was not detectable, although there was enhanced immune protection in the absence of Tfr cells (44). At day 30 p.i., there was a trend of reduced influenza virus-specific antibodies in the Tfr-deficient animals compared to controls (20). This work pointed to the potential of Tfr cells in regulating viral-specific GC output and humoral memory.

Our work has demonstrated that Tfr-cell derived IL-10 driving GC B cell transcriptional programs was necessary to maintain B cell responses following acute infection with lymphocytic choriomeningitis virus (LCMV), exemplifying the role of Tfr cells in optimizing productive humoral immunity following pathogen challenge (55). We subsequently showed that Tfr cells promote antigen-specific germinal center B cell responses during the late course of intranasal influenza virus infection (56). In the absence of Tfr cells, using $Bcl6^{flox/flox}$ Foxp3-Cre animals, we observed alterations in the BCR repertoire, reduced numbers of virus-specific, long-lived plasma cells, as well as decreased antibody titers against both hemagglutinin (HA) and neuraminidase (NA), the two major influenza virus glycoproteins. To further investigate the functional relevance of Tfr cells during viral challenge, we utilized a sequential immunization model with repeated exposure of antigenically partially conserved strains of influenza viruses, revealing that Tfr cells promote recall antibody responses against the conserved HA stalk region. Thus, our studies in aggregate demonstrated that Tfr cells promote antigen-specific B cell responses and are essential for the development of effective long-term humoral memory.

These findings suggest that Tfr cells are necessary and sufficient to maintain the optimal antigen-specific humoral response, although the mechanism is unclear. How might Tfr cells necessarily suppress non-antigen specific or autoreactive GC B cells while sparing the antigen-specific ones? First, it is a model reminiscent of Treg cells optimizing $CD8^+$ T cell responses with Treg cells preferentially suppressing responses by T cells that have weak, lower-affinity interactions with their cognate antigen (also the reason that Treg cells control self-reactive T cells due to their low-affinity) while sparing high-affinity interactions (32). One can imagine a similar scenario for the selection process of antigen-specific B cells regulated by Tfr cells within the GC. Specifically, as a positive selection signal is directly proportional to the strength of interaction between Tfh cells and GC B cells, Tfr cells selectively inhibit non-antigen-specific and autoreactive GC B cells based on their low-strength interactions with Tfh cells, whereas antigen-specific GC B cells that engage in high-strength interactions with Tfh cells overcome this suppression (**Figure 1**). The expression of positive selection signal, such as mTORC and cMyc signaling which are upregulated in GC B cells having recently received Tfh cell help, is likely to serve as a proxy for the strength of interaction that can be regulated by Tfr cells (57, 58). Furthermore, over-proliferation and outgrowth of non-antigen specific B cell clones in the absence of Tfr cells can compete for limited Tfh cell help within a given GC, therefore resulting in impaired antigen-specific B cell responses.

A second model by which Tfr cells promote productive immunity is their capacity to employ trogocytosis to reduce peptide-MHCII complexes on the surface of GC B cells, in this case those that are not specific to the immunizing antigen (**Figure 1**). Treg cells have been demonstrated to deplete peptide-MHCII complex from dendritic cells through trogocytosis in an antigen-specific manner to limit antigen

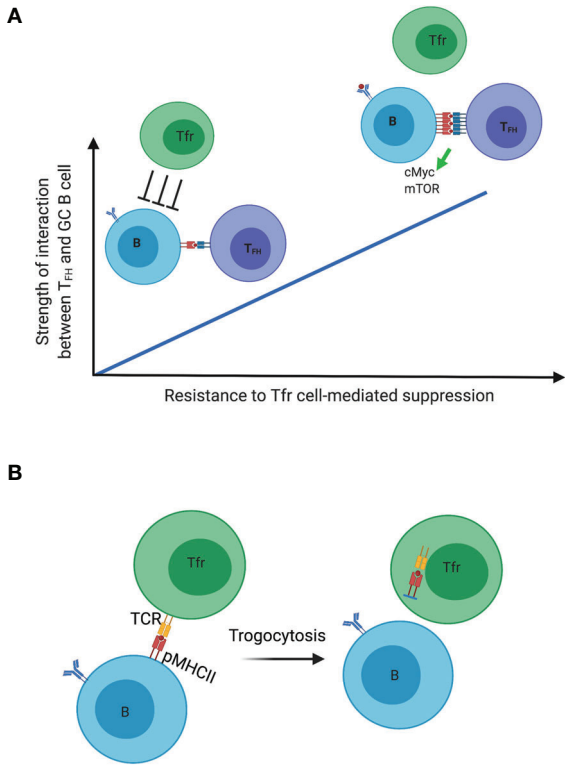

FIGURE 1 | Dynamic regulation of germinal center B cells mediated by Tfr cells. **(A)** Model 1; **(B)** Model 2. Created with BioRender.com.

presentation and subsequent effective priming of naïve antigen-specific T cells (59). Treg cells can also deplete CD80 and CD86 molecules on DCs in a similar fashion (60). If the specificity for Tfr cells is for self, and distinct from that of Tfh cells, the former may strip these antigens presented by GC B cells. With reduced antigen presentation, such GC B cells lose in the competition to other GC B cells presenting the immunizing antigen to elicit Tfh cell help. This would be another level of control to inhibit the outgrowth of autoreactive or non-antigen specific B cell clones. Our unpublished data show that Tfr cells indeed have higher surface expression of MHCII compared to that of non-follicular Treg cells at late time points following influenza virus infection (when the DC-Treg interaction is past the peak), which suggests the possibility of Tfr cells acquiring these molecules from the surface of GC B cells.

This second model is based on an assumption requiring further testing, that Tfr cells do not have specificity for the antigens of immune challenge or that the specificity for these is low. Treg cells can directly kill B cells through perforin and granzyme B in an antigen-specific manner (61); however, the specificity of Tfr cells is not well defined. There are contrasting results with work suggesting that Tfr cells can be specific for the immunizing antigen and the other data arguing that Tfr cells do not recognize the immunizing antigen with their repertoire distinct from that of Tfh cells which are antigen-specific (62, 63). One potential explanation for the distinct results is the differences in immunization models and immunizing antigens. Thus, it is important to examine the TCR specificity of Tfr cells in models using complex antigens in physiologically relevant models, such as influenza virus infection. Tfr cells differentiate from Treg cell precursors (13–15), so it is not surprising that there is substantial resemblance between the TCR repertoires of Tfr and Treg cells (63). However, it is not clear whether Treg cells recruited into the GC have specific TCR usage profile compared to the non-follicular Treg cells. The TCR repertoire analysis of Tfr cells following infection will answer questions of whether a particular subset of Treg precursors preferentially differentiate into Tfr cells and the polyclonality of these cells following influenza virus infection.

It will be of interest to identify Tfr-cell associated molecules (*e.g.*, cytokines, surface molecules) that might mediate the aforementioned proposed processes of optimizing antigen-specific B cell responses within the GC. Furthermore, it is important to study the interaction among Tfr cells, GC B cells and Tfh cells to better understand the mechanism by which Tfr cells regulate the selection process of GC B cells. While our work and that of others demonstrate that Tfr cells do not affect Tfh cell numbers during infection (44), there is also limited evidence indicating that Tfr cells directly interact with GC B cells (45, 64). Imaging analyses are necessary to address how Tfr cells may choreograph the intricate dance within the GC. Interestingly, observations from us and others point to a population of $Foxp3^+$ T cells in the follicles of lymphoid organs under steady state (65). It will be curious to explore whether these cells readily differentiate into Tfr cells and how they may regulate early responses in the follicles following infections.

AUTHOR CONTRIBUTIONS

Wrote the manuscript: YL and JC. All authors contributed to the article and approved the submitted version.

FUNDING

This work was supported by grants from the NIH [R37AR40072 and R01AR074545 and from the Lupus Research Alliance (JC), a Yale Gruber Fellowship (YL), and a Yale Gershon Fellowship (YL)]. The authors declare no competing financial interests.

ACKNOWLEDGMENTS

We would like to acknowledge current and past members of the Craft lab for helpful discussions.

REFERENCES

1. Nutt SL, Hodgkin PD, Tarlinton DM, Corcoran LM. The Generation of Antibody-Secreting Plasma Cells. *Nat Rev Immunol* (2015) 15:160–71. doi: 10.1038/nri3795
2. Okada T, Miller MJ, Parker I, Krummel MF, Neighbors M, Hartley SB, et al. Antigen-Engaged B Cells Undergo Chemotaxis Toward the T Zone and Form Motile Conjugates With Helper T Cells. *PloS Biol* (2005) 3:e150. doi: 10.1371/journal.pbio.0030150
3. Qi H, Cannons JL, Klauschen F, Schwartzberg PL, Germain RN. SAP-Controlled T-B Cell Interactions Underlie Germinal Centre Formation. *Nature* (2008) 455:764–9. doi: 10.1038/nature07345
4. Pereira JP, Kelly LM, Xu Y, Cyster JG. EBI2 Mediates B Cell Segregation Between the Outer and Centre Follicle. *Nature* (2009) 460:1122–6. doi: 10.1038/nature08226
5. Coffey F, Alabyev B, Manser T. Initial Clonal Expansion of Germinal Center B Cells Takes Place At the Perimeter of Follicles. *Immunity* (2009) 30:599–609. doi: 10.1016/j.immuni.2009.01.011
6. Kerfoot SM, Yaari G, Patel JR, Johnson KL, Gonzalez DG, Kleinstein SH, et al. Germinal Center B Cell and T Follicular Helper Cell Development Initiates in the Interfollicular Zone. *Immunity* (2011) 34:947–60. doi: 10.1016/j.immuni.2011.03.024
7. Allen CDC, Ansel KM, Low C, Lesley R, Tamamura H, Fujii N, et al. Germinal Center Dark and Light Zone Organization Is Mediated by CXCR4 and CXCR5. *Nat Immunol* (2004) 5:943–52. doi: 10.1038/ni1100
8. Victora GD, Nussenzweig MC. Germinal Centers. *Annu Rev Immunol* (2012) 30:429–57. doi: 10.1146/annurev-immunol-020711-075032
9. Victora GD, Schwickert TA, Fooksman DR, Kamphorst AO, Meyer-Hermann M, Dustin ML, et al. Germinal Center Dynamics Revealed by Multiphoton Microscopy With a Photoactivatable Fluorescent Reporter. *Cell* (2010) 143:592–605. doi: 10.1016/j.cell.2010.10.032
10. Gitlin AD, Shulman Z, Nussenzweig MC. Clonal Selection in the Germinal Centre by Regulated Proliferation and Hypermutation. *Nature* (2014) 509:637–40. doi: 10.1038/nature13300
11. Shulman Z, Gitlin AD, Weinstein JS, Lainez B, Esplugues E, Flavell RA, et al. Dynamic Signaling by T Follicular Helper Cells During Germinal Center B Cell Selection. *Science* (2014) 345(6200):1058–62. doi: 10.1126/science.1257861
12. De Silva NS, Klein U. Dynamics of B Cells in Germinal Centres. *Nat Rev Immunol* (2015) 15:137–48. doi: 10.1038/nri3804
13. Linterman MA, Pierson W, Lee SK, Kallies A, Kawamoto S, Rayner TF, et al. Foxp3(+) Follicular Regulatory T Cells Control the Germinal Center Response. *Nat Med* (2011) 17(8):975–82. doi: 10.1038/nm.2425
14. Chung Y, Tanaka S, Chu F, Nurieva RI, Martinez GJ, Rawal S, et al. Follicular Regulatory T Cells Expressing Foxp3 and Bcl-6 Suppress Germinal Center Reactions. *Nat Med* (2011) 17:983–8. doi: 10.1038/nm.2426
15. Wollenberg I, Agua-Doce A, Hernández A, Almeida C, Oliveira VG, Faro J, et al. Regulation of the Germinal Center Reaction by Foxp3+ Follicular Regulatory T Cells. *J Immunol* (2011) 187:4553–60. doi: 10.4049/jimmunol.1101328
16. Koch MA, Tucker-Heard G, Perdue NR, Killebrew JR, Urdahl KB, Campbell DJ. The Transcription Factor T-bet Controls Regulatory T Cell Homeostasis and Function During Type 1 Inflammation. *Nat Immunol* (2009) 10:595–602. doi: 10.1038/ni.1731
17. Ohnmacht C, Park J-H, Cording S, Wing JB, Atarashi K, Obata Y, et al. MUCOSAL IMMUNOLOGY. The Microbiota Regulates Type 2 Immunity Through RORγt+ T Cells. *Science* (2013) 349:989–93. doi: 10.1126/science.aac4263
18. Sefik E, Geva-zatorsky N, Oh S, Konnikova L, Zemmour D, Mcguire AM, et al. Individual Intestinal Symbionts Induce a Distinct Population of ROR G + Regulatory T Cells. *Science* (2015) 349(6251):993–7.
19. Vanderleyden I, Fra-Bido SC, Innocentin S, Stebegg M, Okkenhaug H, Evans-Bailey N, et al. Follicular Regulatory T Cells Can Access the Germinal Center Independently of CXCR5. *Cell Rep* (2020) 30:611–19.e4. doi: 10.1016/j.celrep.2019.12.076
20. Botta D, Fuller MJ, Marquez-Lago TT, Bachus H, Bradley JE, Weinmann AS, et al. Dynamic Regulation of T Follicular Regulatory Cell Responses by Interleukin 2 During Influenza Infection. *Nat Immunol* (2017) 18(11):1249–60. doi: 10.1038/ni.3837
21. Wing JB, Kitagawa Y, Locci M, Hume H, Tay C, Morita T. A Distinct Subpopulation of CD25 – T-follicular Regulatory Cells Localizes in the Germinal Centers. *Proc Natl Acad Sci USA* (2017) 114(31):E6400–E9. doi: 10.1073/pnas.1705551114
22. Ritvo PGG, Churlaud G, Quiniou V, Florez L, Brimaud F, Fourcade G, et al. Tfr Cells Lack IL-2R But Express Decoy IL-1R2 and IL-1Ra and Suppress the IL-1–dependent Activation of Tfh Cells. *Sci Immunol* (2017) 2:1–12. doi: 10.1126/sciimmunol.aan0368
23. Johnston RJ, Choi YS, Diamond JA, Yang JA, Crotty S. STAT5 is a Potent Negative Regulator of TFH Cell Differentiation. *J Exp Med* (2012) 209:243–50. doi: 10.1084/jem.20111174
24. Nurieva RI, Podd A, Chen Y, Alekseev AM, Yu M, Qi X, et al. STAT5 Protein Negatively Regulates T Follicular Helper (Tfh) Cell Generation and Function. *J Biol Chem* (2012) 287:11234–9. doi: 10.1074/jbc.M111.324046
25. Liu X, Chen X, Zhong B, Wang A, Wang X, Chu F, et al. Transcription Factor Achaete-Scute Homologue 2 Initiates Follicular T-Helper-Cell Development. *Nature* (2014) 507:513–8. doi: 10.1038/nature12910
26. Sakaguchi S, Sakaguchi N, Asano M, Itoh M, Toda M. Immunologic Self-Tolerance Maintained by Activated T Cells Expressing IL-2 Receptor Alpha-Chains (CD25). Breakdown of a Single Mechanism of Self-Tolerance Causes Various Autoimmune Diseases. *J Immunol* (1995) 155(3):1151–64.
27. Vignali DAA, Collison LW, Workman CJ. How Regulatory T Cells Work. *Nat Rev Immunol* (2008) 8:523–32. doi: 10.1038/nri2343
28. Sakaguchi S, Wing K, Onishi Y, Prieto-Martin P, Yamaguchi T. Regulatory T Cells: How do They Suppress Immune Responses? *Int Immunol* (2009) 21:1105–11. doi: 10.1093/intimm/dxp095
29. Shevach EM. Mechanisms of Foxp3+ T Regulatory Cell-Mediated Suppression. *Immunity* (2009) 30:636–45. doi: 10.1016/j.immuni.2009.04.010
30. Josefowicz SZ, Lu L-F, Rudensky AY. Regulatory T Cells: Mechanisms of Differentiation and Function. *Annu Rev Immunol* (2012) 30:531–64. doi: 10.1146/annurev.immunol.25.022106.141623
31. Lund JM, Hsing L, Pham TT, Rudensky AY. Coordination of Early Protective Immunity to Viral Infection by Regulatory T Cells. *Sci (80-)* (2008) 320:1220–4. doi: 10.1126/science.1155209
32. Pace L, Tempez A, Arnold-Schrauf C, Lemaitre F, Bousso P, Fetler L, et al. Regulatory T Cells Increase the Avidity of Primary Cd8+ T Cell Responses and Promote Memory. *Sci (80-)* (2012) 338:532–6. doi: 10.1126/science.1227049
33. Morlacchi S, Dal Secco V, Soldani C, Glaichenhaus N, Viola A, Sarukhan A. Regulatory T Cells Target Chemokine Secretion by Dendritic Cells Independently of Their Capacity to Regulate T Cell Proliferation. *J Immunol* (2011) 186(12):6807–14. doi: 10.4049/jimmunol.1003265
34. Dal Secco V, Soldani C, Debrat C, Asperti-Boursin F, Donnadieu E, Viola A, et al. Tunable Chemokine Production by Antigen Presenting Dendritic Cells in Response to Changes in Regulatory T Cell Frequency in Mouse Reactive Lymph Nodes. *PloS One* (2009) 4:e7696. doi: 10.1371/journal.pone.0007696
35. de Goër de Herve MG, Jaafoura S, Vallée M, Taoufik Y. FoxP3+ Regulatory CD4 T Cells Control the Generation of Functional CD8 Memory. *Nat Commun* (2012) 3:986. doi: 10.1038/ncomms1992
36. Kalia V, Sarkar S, Subramaniam S, Haining WN, Smith KA, Ahmed R. Prolonged Interleukin-2Ralpha Expression on Virus-Specific $Cd8^+$ T Cells Favors Terminal-Effector Differentiation *In Vivo*. *Immunity* (2010) 32:91–103. doi: 10.1016/j.immuni.2009.11.010
37. Laidlaw BJ, Cui W, Amezquita RA, Gray SM, Guan T, Lu Y, et al. Production of IL-10 by CD4+ Regulatory T Cells During the Resolution of Infection Promotes the Maturation of Memory CD8+ T Cells. *Nat Immunol* (2015) 8:871–9. doi: 10.1038/ni.3224
38. Kalia V, Penny LA, Yuzefpolskiy Y, Martin F, Kalia V, Penny LA, et al. Quiescence of Memory Cd8 + T Cells Is Mediated by Regulatory T Cells Through Inhibitory Receptor Article Quiescence of Memory Cd8 + T Cells Is Mediated by Regulatory T Cells Through Inhibitory Receptor Ctla-4. *Immuni* (2015) 42:1116–29. doi: 10.1016/j.immuni.2015.05.023
39. Graham JB, Da Costa A, Lund JM. Regulatory T Cells Shape the Resident Memory T Cell Response to Virus Infection in the Tissues. *J Immunol* (2014) 192(2):683–90. doi: 10.4049/jimmunol.1202153

40. Arpaia N, Green JA, Moltedo B, Arvey A, Hemmers S, Yuan S, et al. A Distinct Function of Regulatory T Cells in Tissue Protection. *Cell* (2015) 162:1078–89. doi: 10.1016/j.cell.2015.08.021
41. Burzyn D, Benoist C, Mathis D. Regulatory T Cells in Nonlymphoid Tissues. *Nat Immunol* (2013) 14:1007–13. doi: 10.1038/ni.2683
42. Brink R, Phan TG. Self-Reactive B Cells in the Germinal Center Reaction. *Annu Rev Immunol* (2018) 36:339–57. doi: 10.1146/annurev-immunol-051116-052510
43. Clement RL, Daccache J, Mohammed MT, Diallo A, Blazar BR, Kuchroo VK, et al. Follicular Regulatory T Cells Control Humoral and Allergic Immunity by Restraining Early B Cell Responses. *Nat Immunol* (2019) 10:1360–71. doi: 10.1038/s41590-019-0472-4
44. Fu W, Liu X, Lin X, Feng H, Sun L, Li S, et al. Deficiency in T Follicular Regulatory Cells Promotes Autoimmunity. *J Exp Med* (2018) 215(3):815–25. doi: 10.1084/jem.20170901
45. Gonzalez-Figueroa P, Roco JA, Papa I, Núñez Villacís L, Stanley M, Linterman MA, et al. Follicular Regulatory T Cells Produce Neuritin to Regulate B Cells. *Cell* (2021) 184:1775–89.e19. doi: 10.1016/j.cell.2021.02.027
46. Wing JB, Ise W, Kurosaki T, Sakaguchi S. Regulatory T Cells Control Antigen-Specific Expansion of Tfh Cell Number and Humoral Immune Responses Via the Coreceptor Ctla-4. *Immunity* (2014) 41:1013–25. doi: 10.1016/j.immuni.2014.12.006
47. Sage PT, Paterson AM, Lovitch SB, Sharpe AH. The Coinhibitory Receptor CTLA-4 Controls B Cell Responses by Modulating T Follicular Helper, T Follicular Regulatory, and T Regulatory Cells. *Immunity* (2014) 41:1026–39. doi: 10.1016/j.immuni.2014.12.005
48. Wing K, Onishi Y, Prieto-Martin P, Yamaguchi T, Miyara M, Fehervari Z, et al. CTLA-4 Control Over Foxp3+ Regulatory T Cell Function. *Science* (2008) 322:271–5. doi: 10.1126/science.1160062
49. Sage PT, Ron-Harel N, Juneja VR, Sen DR, Maleri S, Sungnak W, et al. Suppression by TFR Cells Leads to Durable and Selective Inhibition of B Cell Effector Function. *Nat Immunol* (2016) 12:1436–46. doi: 10.1038/ni.3578
50. Xie MM, Chen Q, Liu H, Yang K, Koh B, Wu H, et al. T Follicular Regulatory Cells and IL-10 Promote Food Antigen-Specific IgE. *J Clin Invest* (2020) 130:3820–32. doi: 10.1172/JCI132249
51. Wu H, Chen Y, Liu H, Xu L-L, Teuscher P, Wang S, et al. Follicular Regulatory T Cells Repress Cytokine Production by Follicular Helper T Cells and Optimize IgG Responses in Mice. *Eur J Immunol* (2016) 46(5):1152–61. doi: 10.1002/eji.201546094
52. Tas JMJ, Mesin L, Pasqual G, Targ S, Jacobsen JT, Mano YM, et al. Visualizing Antibody Affinity Maturation in Germinal Centers. *Sci (80-)* (2016) 351:1048–54. doi: 10.1126/science.aad3439
53. Mesin L, Ersching J, Victora GD. Germinal Center B Cell Dynamics. *Immunity* (2016) 45:471–82. doi: 10.1016/j.immuni.2016.09.001
54. Vendetti S, Davidson TS, Veglia F, Riccomi A, Negri DR, Lindstedt R, et al. Polyclonal Treg Cells Enhance the Activity of a Mucosal Adjuvant. *Immunol Cell Biol* (2010) 88:698–706. doi: 10.1038/icb.2010.76
55. Laidlaw BJ, Lu Y, Amezquita RA, Weinstein JS, Vander Heiden JA, Gupta NT, et al. Interleukin-10 From CD4+ Follicular Regulatory T Cells Promotes the Germinal Center Response. *Sci Immunol* (2017) 2:eaan4767. doi: 10.1126/sciimmunol.aan4767
56. Lu Y, Jiang R, Freyn AW, Wang J, Strohmeier S, Lederer K, et al. CD4+ Follicular Regulatory T Cells Optimize the Influenza Virus-Specific B Cell Response. *J Exp Med* (2021) 218(3):e20200547. doi: 10.1084/jem.20200547
57. Dominguez-Sola D, Victora GD, Ying CY, Phan RT, Saito M, Nussenzweig MC, et al. The Proto-Oncogene MYC is Required for Selection in the Germinal Center and Cyclic Reentry. *Nat Immunol* (2012) 13:1083–91. doi: 10.1038/ni.2428
58. Ersching J, Efeyan A, Mesin L, Jacobsen JT, Pasqual G, Grabiner BC, et al. Germinal Center Selection and Affinity Maturation Require Dynamic Regulation of Mtorc1 Kinase Germinal Center Selection and Affinity Maturation Require Dynamic Regulation of mTORC1 Kinase. *Immunity* (2017) 46:1045–58.e6. doi: 10.1016/j.immuni.2017.06.005
59. Akkaya B, Oya Y, Akkaya M, Al Souz J, Holstein AH, Kamenyeva O, et al. Regulatory T Cells Mediate Specific Suppression by Depleting Peptide–MHC Class II From Dendritic Cells. *Nat Immunol* (2019) 20:218–31. doi: 10.1038/s41590-018-0280-2
60. Gu P, Fang Gao J, D'Souza CA, Kowalczyk A, Chou K-Y, Zhang L. Trogocytosis of CD80 and CD86 by Induced Regulatory T Cells. *Cell Mol Immunol* (2012) 9:136–46. doi: 10.1038/cmi.2011.62
61. Zhao D-M, Thornton AM, DiPaolo RJ, Shevach EM. Activated Cd4+Cd25+ T Cells Selectively Kill B Lymphocytes. *Blood* (2006) 107:3925–32. doi: 10.1182/blood-2005-11-4502
62. Aloulou M, Carr EJ, Gador M, Bignon A, Liblau RS, Fazilleau N, et al. Follicular Regulatory T Cells can be Specific for the Immunizing Antigen and Derive From Naive T Cells. *Nat Commun* (2016) 7:10579. doi: 10.1038/ncomms10579
63. Maceiras AR, Almeida SCP, Mariotti-Ferrandiz E, Chaara W, Jebbawi F, Six A, et al. T Follicular Helper and T Follicular Regulatory Cells Have Different TCR Specificity. *Nat Commun* (2017) 8:15067. doi: 10.1038/ncomms15067
64. Benet ZL, Marthi M, Ke F, Wu R, Turner JS, Gabayre JB, et al. CCL3 Promotes Germinal Center B Cells Sampling by Follicular Regulatory T Cells in Murine Lymph Nodes. *Front Immunol* (2018) 9:1–13. doi: 10.3389/fimmu.2018.02044
65. Liu Z, Gerner MY, Van Panhuys N, Levine AG, Rudensky AY, Germain RN. Immune Homeostasis Enforced by Co-Localized Effector and Regulatory T Cells. *Nature* (2015) 528:225–30. doi: 10.1038/nature16169

Conflict of Interest: The authors declare that the research was conducted in the absence of any commercial or financial relationships that could be construed as a potential conflict of interest.

frontiers in Immunology

ORIGINAL RESEARCH
published: 17 August 2021
doi: 10.3389/fimmu.2021.716240

Coupled Antigen and BLIMP1 Asymmetric Division With a Large Segregation Between Daughter Cells Recapitulates the Temporal Transition From Memory B Cells to Plasma Cells and a DZ-to-LZ Ratio in the Germinal Center

Elena Merino Tejero[1‡], Danial Lashgari[1‡], Rodrigo García-Valiente[1], Jiaojiao He[2,3], Philippe A. Robert[4†], Michael Meyer-Hermann[4,5], Jeroen E. J. Guikema[6], Huub Hoefsloot[7] and Antoine H. C. van Kampen[1,7]*

[1] Bioinformatics Laboratory, Epidemiology and Data Science, Amsterdam Public Health Research Institute, Amsterdam Institute for Infection and Immunity, Amsterdam, Netherlands, [2] Bioinformatics and Systems Biology, Vrije Universiteit Amsterdam, Amsterdam, Netherlands, [3] Bioinformatics and Systems Biology, Institute for Life Sciences, University of Amsterdam, Amsterdam, Netherlands, [4] Department for Systems Immunology and Braunschweig Integrated Centre of Systems Biology, Helmholtz Centre for Infection Research, Braunschweig, Germany, [5] Institute for Biochemistry, Biotechnology and Bioinformatics, Technische Universität Braunschweig, Braunschweig, Germany, [6] Department of Pathology, Lymphoma and Myeloma Center Amsterdam (LYMMCARE), Amsterdam University Medical Centers, Amsterdam, Netherlands, [7] Biosystems Data Analysis, Swammerdam Institute for Life Sciences, University of Amsterdam, Amsterdam, Netherlands

Memory B cells and antibody-secreting plasma cells are generated within germinal centers during affinity maturation in which B-cell proliferation, selection, differentiation, and self-renewal play important roles. The mechanisms behind memory B cell and plasma cell differentiation in germinal centers are not well understood. However, it has been suggested that cell fate is (partially) determined by asymmetric cell division, which involves the unequal distribution of cellular components to both daughter cells. To investigate what level and/or probability of asymmetric segregation of several fate determinant molecules, such as the antigen and transcription factors (BCL6, IRF4, and BLIMP1) recapitulates the temporal switch and DZ-to-LZ ratio in the germinal center, we implemented a multiscale model that combines a core gene regulatory network for plasma cell differentiation with a model describing the cellular interactions and dynamics in the germinal center. Our simulations show that BLIMP1 driven plasma cell differentiation together with coupled asymmetric division of antigen and BLIMP1 with a large segregation between the daughter cells results in a germinal center DZ-to-LZ ratio and a temporal switch from memory B cells to plasma cells that have been observed in experiments.

Keywords: asymmetric division, germinal center, plasma cell differentiation, multiscale modeling, agent-based modeling

OPEN ACCESS

Edited by:
Said Aoufouchi, UMR 9019 Intégrité du Génome et Cancers, France

Reviewed by:
Ziv Shulman, Weizmann Institute of Science, Israel
Hong Zan, The University of Texas Health Science Center at San Antonio, United States

***Correspondence:**
Antoine H. C. van Kampen
a.h.vankampen@amsterdamumc.nl

†Present address:
Philippe A. Robert, Department of Immunology, University of Oslo, Oslo, Norway

‡*These authors share first authorship*

Specialty section:
This article was submitted to B Cell Biology, a section of the journal Frontiers in Immunology

Received: *28 May 2021*
Accepted: *26 July 2021*
Published: *17 August 2021*

Citation:
Merino Tejero E, Lashgari D, García-Valiente R, He J, Robert PA, Meyer-Hermann M, Guikema JEJ, Hoefsloot H and van Kampen AHC (2021) Coupled Antigen and BLIMP1 Asymmetric Division With a Large Segregation Between Daughter Cells Recapitulates the Temporal Transition From Memory B Cells to Plasma Cells and a DZ-to-LZ Ratio in the Germinal Center. Front. Immunol. 12:716240. doi: 10.3389/fimmu.2021.716240

INTRODUCTION

Memory B cells (MBCs) and antibody-secreting plasma cells (PCs) are generated within germinal centers (GCs) during affinity maturation in which B-cell proliferation, selection, differentiation, and self-renewal play important roles in the GC reaction (1). Positive selection of B cells is facilitated by collecting antigen (Ag) presented by follicular dendritic cells (FDCs) and subsequent engagement in T follicular helper (Tfh) cells contacts. B cells with higher-affinity receptors (BcRs) are thought to receive more help from Tfh cells due to increased presentation of pMHCII on their surface. Selected B cells recycle to the dark zone (DZ) to further divide and differentiate as output cells (OCs) or to enter a next cycle of selection (recycling).

The mechanisms behind MBC and PC differentiation into OCs from GCs are not well understood. However, in other systems, such as *Drosophila*, it has been suggested that cell fate is (partially) determined by asymmetric cell division, which involves the unequal distribution of cellular components to both daughter cells (2). Another study exclusively analyzed the distribution of Ag in *in vivo* and *in vitro* mouse B cells showing that accumulated Ag is maintained in a polarized distribution prior to the division in approximately 72% of the B cells and that this polarization is maintained during cell division resulting in an asymmetric division of Ag over both daughter cells (3). The daughter cell that receives more Ag as a result of asymmetric division was postulated to be more efficient in receiving T cell help, both at the B–T cell border and in the GC, which may affect cell fate (3). In the same issue, it was argued and shown by computational modeling that asymmetric division may largely affect the production of PCs (4). Later, a more comprehensive computational model of the GC reaction predicted that asymmetric division of Ag might codetermine B-cell fate, since inclusion of this mechanism resulted in GC transzone migration rates and DZ-to-LZ ratio in agreement with experimental data (5, 6). In addition to asymmetric Ag division, *in vitro* studies have shown that other B-cell fate-altering molecules, such as transcriptional regulator B-cell lymphoma 6 (BCL6) and the receptor for interleukin-21 (IL-21R), segregate asymmetrically in approximately 44% of mitotic GC B cells (7). In contrast, IRF4 was mostly symmetrically distributed (11% asymmetry comparable to tubulin). The same study suggested that CD40 signaling facilitates TF asymmetry by providing polarity cues to B cells. However, other polarity cues [e.g., cell–cell contacts (8)], TFs [e.g., BLIMP1 transcription (9)], and signaling pathways [e.g., nuclear factor kappa B (Nf-kB)] may drive asymmetric division and/or B-cell fate.

Regardless of the mechanism, asymmetric division has been shown to result in daughter cells with unequal amounts of Ag and/or TF. The amount of segregation seems to vary for different TFs, and this might be dependent on polarity cues, signaling pathways and strength, and/or stochastic events. We hypothesized that (the level of) Ag and TF (BCL6, IRF4, BLIMP1) segregation affects GC dynamics and B-cell fate in different ways or to different extents. To test this hypothesis, we implemented a multiscale model (MSM) that combines a core gene regulatory network for B cell of PC differentiation with a model describing the cellular interactions and dynamics in the GC.

Our simulations show that BLIMP1-driven PC differentiation coupled to asymmetric division of Ag and BLIMP1 with a large segregation between the daughter cells results in a GC transzone migration and a temporal switch from MBCs to PCs that are both observed in experiments (6, 10). Consequently, these computational results prompt for more direct experiments aimed to verify or falsify this mechanism for PC differentiation.

METHODS

Multiscale Model

To enable the investigation of cellular and molecular mechanisms involved in PC differentiation, we recently developed a multiscale model (MSM) (11) that integrates an agent-based model (ABM) of the GC reaction (5) with a gene regulatory network (GRN) involved in PC differentiation (12). We slightly modified this model to investigate the effect of asymmetric Ag and TF division. In brief, the ABM contains the main processes that take place in the GC reaction, which lasts for 21 days (504 h). B cells at the centroblast (CB) state divide in the DZ while accumulating SHMs in their BcR. They then differentiate to CCs and migrate to the LZ where they may encounter FDCs and Tfh cells. FDCs carry Ag in their membrane, which is internalized by CCs when in contact with an affinity-dependent rate. This provides CCs with survival signals that temporarily rescue them from apoptosis and allow them to undergo further encounter(s) with Tfh cells. CCs with higher internalized Ag, thus higher affinity for the Ag, will outcompete other CCs with less internalized Ag. CCs are then fully rescued from apoptosis and recycle back to the DZ as CBs. Recycled CBs further divide asymmetrically in 72% of the cases where all of the internalized Ag goes to one of the daughter cells. The GRN of PC differentiation comprises three TFs (BLIMP1, BCL6, and IRF4) that regulate each other and are affected by upstream BcR and CD40 signals. BCL6 is involved in maintaining GC B-cell phenotype, while IRF4 and BLIMP1 promote PC differentiation and exit from the GC. Initial TF concentration in founder CBs were based on microarray data (12) and defined as follows (BLIMP1 = 0, BCL6 = 5, and IRF4 = 0) to achieve the high BCL6 and low BLIMP1 and IRF4 steady state. CCs receive signals through BcR and CD40 respectively when in contact with FDCs or Tfh cells. In the model, BcR signal strength is assumed to be constant, while CD40 signal strength depends on affinity, which can range between 0 and 1, and determines the B-cell fate. The GRN is a bistable system with one state (BCL6 high, BLIMP1/IRF4 low) being the intracellular state of CBs, CCs, and MBCs and a second state (BLIMP1/IRF4 high, BCL6 low) representing the intracellular state of PCs. After dividing, recycled CBs that inherited all of the internalized Ag, and/or are in BLIMP1 high state, differentiate to OCs, either MBCs or PCs, while the remaining CBs differentiate to CCs and stay in the GC. Ag in the CCs is removed, giving no advantage in further rounds of selection.

Definition of Output Cells and Memory *Versus* PC Differentiation Fate

Table 1 shows the cell type definition based on Ag status and BLIMP1 level. Recycled CBs that finish dividing may differentiate to PCs at any time of the GC reaction (**Figure 1**) when BLIMP1 reaches the differentiation threshold ($\geq 8.10^{-8}$M) and become BLIMP1+ irrespective of its Ag status, and, consequently, PCs may either be Ag+ or Ag–. BLIMP1+ cells that are not (yet) OCs are annotated as PB (Ag+ or Ag–). Ag+/BLIMP1– OCs are considered to be MBCs. This definition correctly recapitulates the MBC dynamics as described in Weisel and coworkers (10). Finally, Ag-/BLIMP1– CBs stay in the GC and recycle back to the LZ as CCs.

TABLE 1 | Definition of OCs (PCs and MBCs) in terms of Ag status and BLIMP1 level.

PC	Ag+/BLIMP1+	Ag–/BLIMP1+
MBC	Ag+/BLIMP1–	

Modeling of Asymmetric Division

In the current model, we do not distinguish between different mechanisms that lead to asymmetry but only assume that Ag and TFs (BCL6, IRF4, BLIMP1) can be unequally distributed between the two daughter cells. Asymmetric division is parameterized by a probability (P) of asymmetric division and a polarity level (L) representing the extent of asymmetry. Following experimental observations from Thaunat and coworkers, we set the probability for asymmetric division of Ag to either $P_{Ag} = 0.0$ or $P_{Ag} = 0.72$ (3). The same study showed that Ag division can happened both symmetrically and asymmetrically, which is why we did not further investigate asymmetric Ag probabilities of 100%. Consequently, in 0% or 72% of the cell divisions, the Ag is distributed asymmetrically over the daughter cells. The probability of asymmetric division for TFs is unknown, and, therefore, we used three different probabilities: $P_{TF} = 0.0$, $P_{TF} = 0.72$, or $P_{TF} = 1.0$. Consequently, in 0%, 72%, or 100% of the cell divisions, the TFs are distributed asymmetrically over the daughter cells. In the current model, when the Ag and TFs are asymmetrically distributed in the same division, high Ag and TF

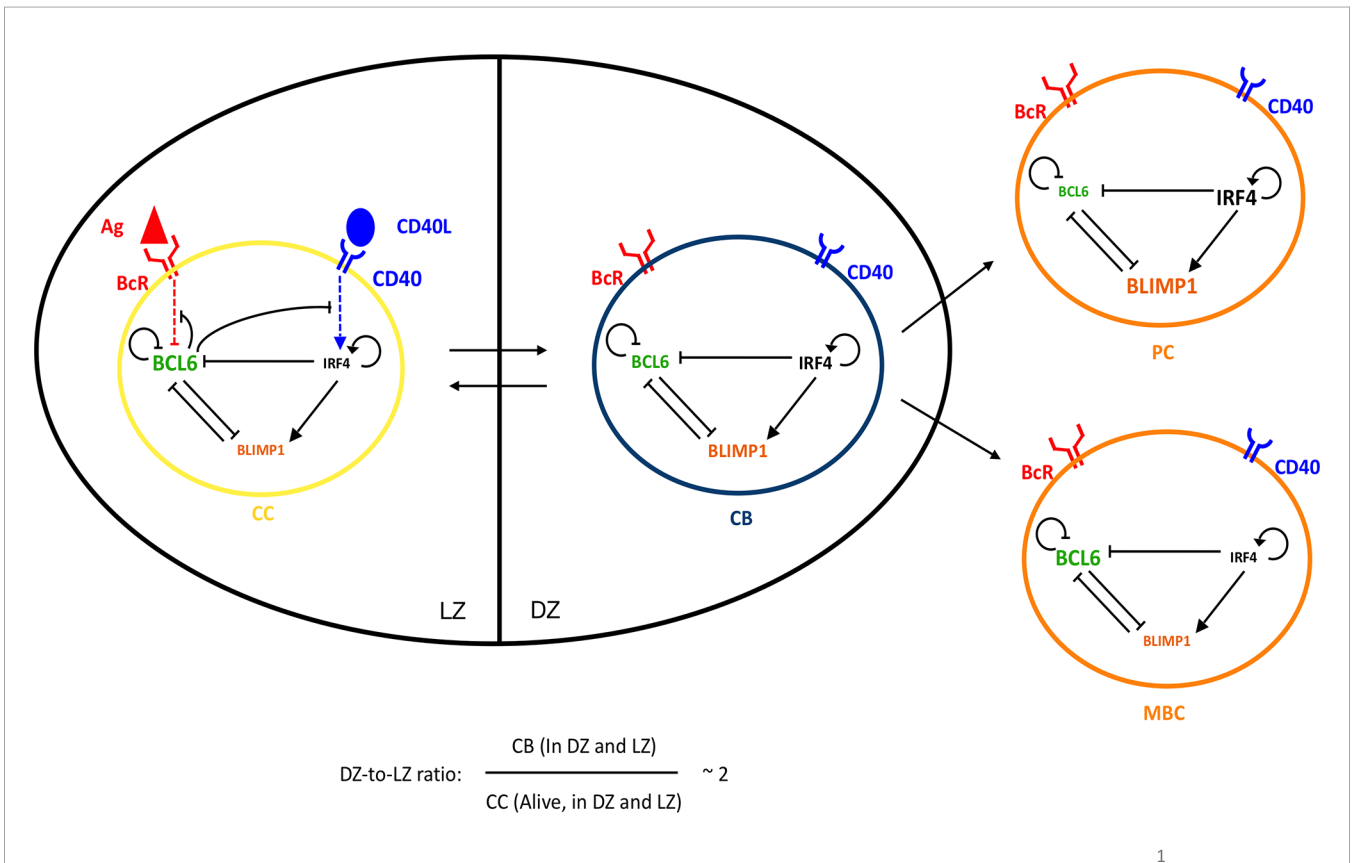

FIGURE 1 | Four GC B cells representing the PC differentiation process: CC (yellow), CB (blue), PC (orange), and MBC (orange). CBs are mainly present in the DZ and CCs in the LZ, while PCs and MBCs are mainly generated in the DZ and then exit the GC. Transition between CBs and CCs is reversible, while the transition between CBs and PCs or MBCs is irreversible. The DZ-to-LZ ratio is the ratio of CBs to non-apoptotic CCs present in both zones and fluctuates around 2. An intracellular GRN comprising three TFs is embedded in each B cell: BCL6 (green), IRF4 (black), and BLIMP1 (orange). The size of each TF represents the expression levels in the cell state. The CC BcR may bind to Ag (red) or the CD40L (blue) when receiving T-cell help, resulting in BcR and CD40 signaling, respectively, which changes the state of the network. Arrows between cells represent transition. Arrows between TFs, BcR, and/or CD40 indicate activation. Bar-headed lines denote inhibition.

polarity levels are directed towards the same daughter cell. Nevertheless, in this study, we are interested in simulating the effect of simultaneous asymmetric division of Ag and TFs.

The polarity level (L_{Ag} and L_{TF}) of asymmetry represents the concentration of Ag and TFs in one daughter cell expressed as the fraction of Ag and TFs in the parent cell; the second daughter cell, by definition, assumes a concentration of 1-polarity. Consequently, a polarity level of L = 0.5 represents symmetric division (the concentration of Ag and TFs in each daughter cell is 50% of the parent cell). An asymmetric division probability P = 0.0, by definition, corresponds to a polarity level (L = 0.5). A polarity level of L = 1.0 results in one daughter cell that has taken all Ag and/or TFs from the parent cell, while the other daughter cell will receive none. In the simulations, the TFs may segregate with a different polarity levels (L_{BLIMP1}, L_{BCL6}, L_{IRF4}).

Simulations

We performed two sets of GC simulations. In the first set of nine simulations (**Table 2**), the TFs cosegregate with equal polarity levels, while in the second set of 27 simulations (**Table 3**), the TFs may cosegregate with different polarity levels. Simulation 3 from the first set (**Table 2**) is considered the reference simulation in which there is asymmetric division of Ag (P_{Ag}) but always symmetric division of TFs. We consider this simulation as the reference since in the original LEDA model, no TFs were modeled, while asymmetric Ag division showed to result in a correct DZ-to-LZ ratio. The DZ-to-LZ ratio was calculated as the ratio of CBs to non-apoptotic CCs present in both zones (**Figure 1**). Since Simulations 1–3 from the second set of 27 simulations (**Table 3**) were the only cases to show differences in the MBC and PC dynamics, we repeated these simulations 15 times with different random seeds. **Supplementary Figures 1–3** show the results from these repetitions and demonstrate that there is a limited variability in the temporal dynamics. Therefore, we did not repeat the other simulations, since these are expected to give a similar amount of variation.

TABLE 2 | Simulated asymmetry of TF concentrations (polarity level L_{TF}) in daughter cells after division.

Simulation	Description	Mode Ag division	
		Asymmetric	Symmetric
		TF polarity level (L_{TF})	
1	(i) Symmetric Ag and TF division ($P_{Ag} = P_{TF} = 0$)	N.A.	0.5
2	(ii) Symmetric Ag division and asymmetric TF division ($P_{Ag} = 0$, $P_{TF} = 0.72$)	N.A.	1.0
3	(iii) Symmetric TF division and asymmetric Ag division (reference; $P_{Ag} = 0.72$, $P_{TF} = 0$)	0.5	0.5
4	(iv) Asymmetric TF division only if	1.0	0.5
5	mode of Ag division is asymmetric	0.9	0.5
6	(coupled asymmetric division; $P_{Ag} = P_{TF} = 0.72$)	0.75	0.5
7	(v) Always asymmetric TF division	1.0	1.0
8	regardless of mode of Ag division	0.9	0.9
9	(uncoupled asymmetric division; $P_{Ag} = 0.72$, $P_{TF} = 1.0$)	0.75	0.75

When mode of Ag division is asymmetric the probability and polarity level are $P_{Ag} = 0.72$; $L_{Ag} = 1.0$; otherwise, these are set to ($P_{Ag} = 0.0$; $L_{Ag} = 0.5$) for symmetric Ag division. In these nine simulations, BCL6, IRF4, and BLIMP1 are cosegregated.

TABLE 3 | Simulated asymmetry of TFs concentrations ($P_{TF} = 0.72$; polarity levels L_{BLIMP1}, L_{IRF4}, and L_{BCL6}) in daughter cells after asymmetric division.

	Mode Ag division			
	Asymmetric			Symmetric
	Polarity level (L_{TF})			
Simulations	BLIMP1 (L_{BLIMP1})	IRF4 (L_{IRF4})	BCL6 (L_{BCL6})	BLIMP1, IRF4, BCL6 ($L_{BLIMP1} = L_{IRF4} - L_{BCL6}$)
1–3		1.0	1.0	0.5
4–6		0.9	1.0	0.5
7–9		0.75	1.0	0.5
10–12	1.0	1.0	0.9	0.5
13–15	0.75	0.9	0.9	0.5
16–18	0.9	0.75	0.9	0.5
19–21		1.0	0.75	0.5
22–24		0.9	0.75	0.5
25–27		0.75	0.75	0.5

TFs divide asymmetrically if Ag divides asymmetrically ($P_{Ag} = P_{TF} = 0.72$; $L_{Ag} = 1.0$). In these 27 simulations, BCL6, IRF4, and BLIMP1 do not always cosegregate with same polarity levels.

In the first set of simulations, we studied different combinations of Ag and TF (a)symmetric division (**Table 2**). In these simulations, the TFs are cosegregated over the daughter cells according to the polarity levels (L_{TF}) shown in **Table 2**. The polarity level for the asymmetric Ag division is always $L_{Ag} = 1.0$. These nine simulations represent five scenarios: (i) TFs and Ag divide symmetrically ($P_{TF} = P_{Ag} = 0.0$); (ii) TFs divide asymmetrically with probability $P_{TF} = 0.72$, while Ag always divides symmetrically ($P_{Ag} = 0.0$; **Figure 2A**); (iii) TFs divide symmetrically ($P_{TF} = 0.0$), while Ag can divide asymmetrically ($P_{Ag} = 0.72$; reference); (iv) TFs divide asymmetrically ($P_{TF} = 0.72$) only when Ag divides asymmetric ($P_{Ag} = 1.0$; **Figure 2B**); and (5) TFs always divide asymmetrically ($P_{TF} = 1.0$), while Ag divides asymmetrically with probability $P_{Ag} = 0.72$ (**Figure 2C**).

In the second set of 27 simulations, the Ag is distributed asymmetrically in 72% of the recycled B-cell divisions ($P_{Ag} = 0.72$, $L_{Ag} = 1.0$; **Table 3**), since it was previously shown that this results in transzone migration rates in better agreement with experimental data (5). In these simulations, the TFs cosegregate with the Ag, since they only divide asymmetrically when the Ag divides asymmetrically ($P_{Ag} = P_{TF} = 0.72$). Moreover, TFs segregate with different polarity levels (L_{BLIMP1}, L_{BCL6}, L_{IRF4}) as shown in **Figure 2D**.

Simulation of Gene Regulatory Network

To facilitate the interpretation of the MSM, we additionally performed a set of GRN simulations to model TF dynamics. For these simulations, initial TF concentration of the mother cell was conceptually chosen to simulate an extreme condition of our MSM in which a mother PB, at the low BCL6 and high BLIMP1 and IRF4 steady state, underwent the last division before becoming a PC and exiting the GC. Subsequently, asymmetric division of the parent PB was simulated with the different

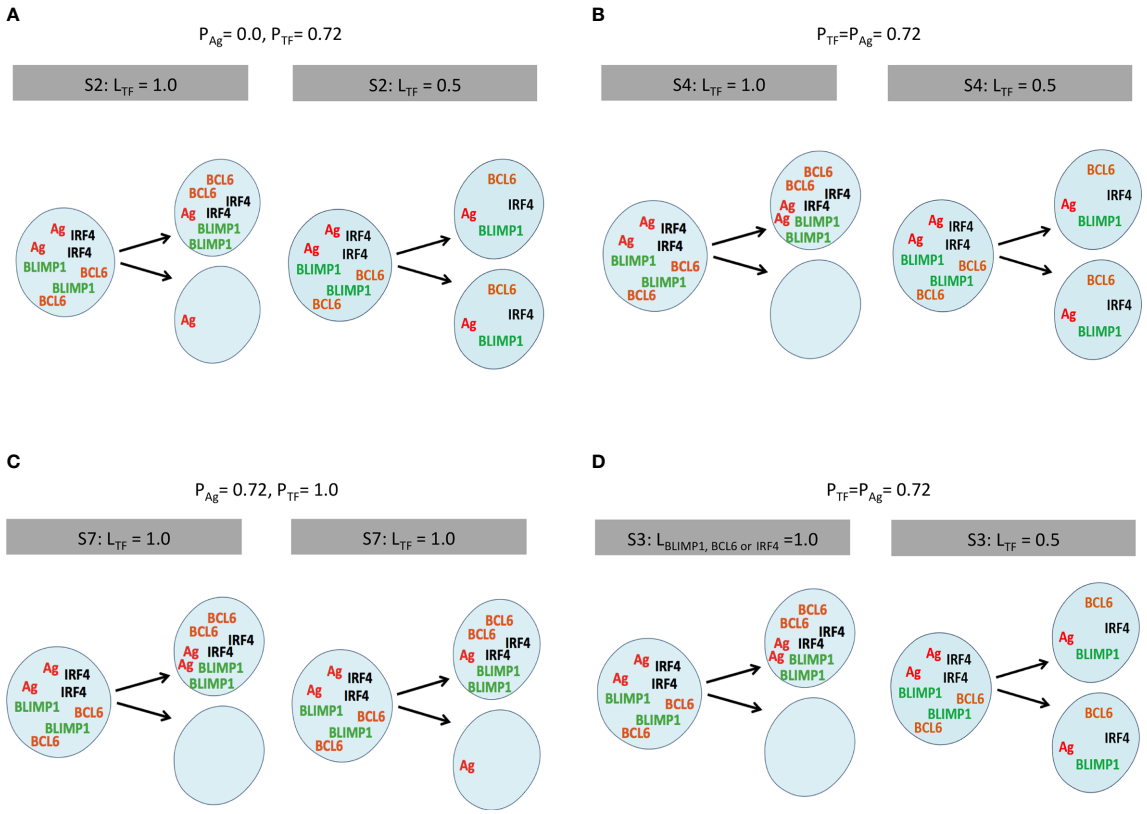

FIGURE 2 | Scheme of internalized Ag and TF division patterns modeled in a selection of simulations (**Tables 2**, **3**). **(A)** Simulation 2, symmetric Ag and asymmetric TF distribution (L_{TF} = 1.0). **(B)** Simulation 4, coupled asymmetric division (L_{TF} = 1.0). **(C)** Simulation 7, uncoupled asymmetric division (L_{TF} = 1.0), and **(D)** simulation 3, partial asymmetric co-segregation of TFs and Ag (P_{TF} = P_{Ag} = 0.72; L_{Ag} = 1.0) while varying the level of BLIMP1 (L_{BLIMP1} = 1.0). Internalized Ag (red) and TF (orange, green, black) are shown in the parent and two daughter cells. The probability and polarity levels are shown in the gray box.

combinations of L_{TFs} for the first set of simulations (**Table 2**). For the second set of simulations, we investigated representative L_{BLIMP1}, L_{BCL6}, and L_{IRF4} combinations (i.e., simulations 1–4, 7, 10, 19; **Table 3**). At the start of the simulation, we defined the concentrations of BLIMP1, BCL6, and IRF4 according to the polarity levels and, subsequently, simulate until a steady state was reached. This allowed us to determine if despite the concentration reduction, BLIMP1 concentration returned to its high level steady state (PC phenotype). Since we were simulating TF dynamics of CBs that do not interact with Ag presented by FDCs nor with Tfh cells, we set the CD40 and BcR signals to 0.

RESULTS

Symmetric TF and Ag Division

We first aimed to gain insight in the contribution of asymmetric division on GC dynamics and OCs. Therefore, we simulated the GC reaction without asymmetric Ag and TFs division (P_{TF} = P_{Ag} = 0.0, L_{TF} = L_{Ag} = 0.5; simulation 1, **Table 2**).

We found a DZ-to-LZ ratio that initially fluctuated between 5 and 15 and then increased to values up to 800 or the ratio became infinite due to low or zero CC counts, respectively (**Figure 3A**), strongly contradicting experimentally observed DZ-to-LZ ratio of 2. This is explained by a lack of recycled CBs without retained Ag, which led to no differentiation to CC state and a premature termination of the GC reaction. Thus, the number of accumulated OCs reached 1,417 cells at the end of the GC reaction (**Table 4** and **Figure 3B**). No MBCs were produced (**Figure 4A**), and all OCs were PCs (**Figure 4B**) due to the lack of Ag+ cells. Furthermore, 87% of PCs were generated within the first 6 days of the GC reaction, which contradicts a temporal switch from MBCs to PCs (**Supplementary Figure 3**).

Asymmetric TF Division and Symmetric Ag Division

Next, we aimed to establish the effect of asymmetric TF division while keeping symmetric Ag division (simulation 2, **Table 2**; P_{Ag} = 0.0, P_{TF} = 0.72, L_{Ag} = 0.5, L_{TF} = 1.0). Again, we find that the DZ-to-LZ ratio initially fluctuated between 5 and 15 and then increased until 400 or was infinite since no CCs were produced (**Figure 3A**) strongly contradicting experimentally observed DZ-to-LZ ratio of 2. In addition, the number of accumulated OCs reached 759 cells at the end of the GC reaction, none of them

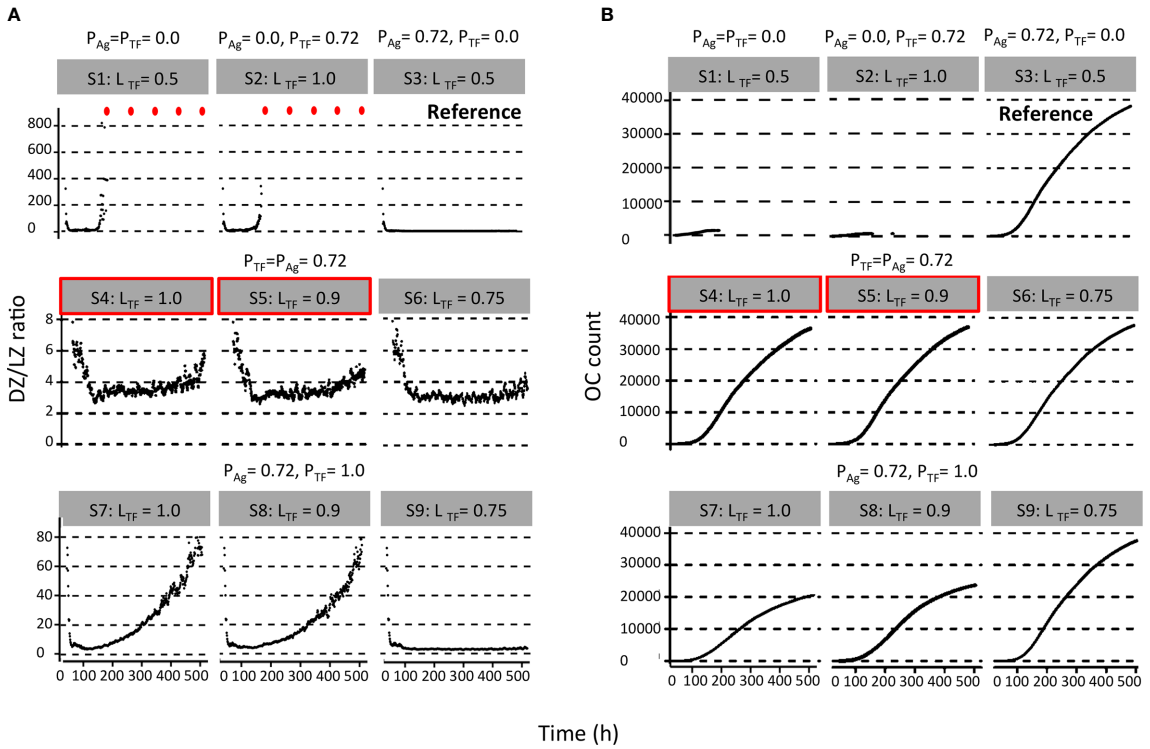

FIGURE 3 | Results from first set of simulations (**Table 2**). **(A)** DZ-to-LZ ratio and **(B)** accumulated OCs during the GC reaction. The probability of asymmetric division (P) is indicated above the gray box, and simulation number and polarity levels (L) are shown in the gray box. Red dots indicate DZ-to-LZ ratio values of infinity. First row of plots corresponds to (left column) symmetric division of Ag and TFs, (middle column) symmetric division of Ag and asymmetric division of TFs, and (right column) symmetric division of TFs and asymmetric division of Ag. Second row of plots corresponds to asymmetric TF division only if mode of Ag division is asymmetric. Red boxes indicate parameters that are closer to biological results. Third row of plots corresponds to always asymmetric TF division regardless of mode of Ag division.

being MBCs (**Table 4**; **Figures 3B**, **4**) Furthermore, 92% of PCs were generated within the first 6 days of the GC reaction (**Supplementary Figure 3**) again contradicting a temporal switch. Finally, asymmetric TF division led to approximately a twofold decrease in PC production compared to symmetric TF division (simulation 1) as shown in **Table 4**. This could be explained by analyzing the TF dynamics in isolation (**Figure 5**). Extreme TF polarity levels promoted the production of a daughter B cell in the low BLIMP1 state and another one in the high BLIMP1 state, yet symmetric TF polarities promoted the production of both daughter B cells in the high BLIMP1 state. We conclude that asymmetric division of TF only does not result in expected GC dynamics while also the number of OCs remains 50-fold lower than in the reference simulation.

Symmetric TFs Division and Asymmetric Ag Division (Reference)

We questioned whether or not symmetric cosegregation of TFs with asymmetric Ag division had an effect on GC B-cell dynamics (P_{TF} = 0.0, L_{TF} = 0.5, P_{Ag} = 0.72, L_{Ag} = 1.0; simulation 3, **Table 2**). We found the DZ-to-LZ ratio fluctuating between 2 and 4 (**Figure 3A**). This was a maximum of 2-fold increase in DZ-to-LZ ratio compared to previous observations of 2 (6) and similar to the affinity-based CD40

TABLE 4 | Number of OCs at day 21 originating from the first set of simulations (**Table 2**).

	P_{Ag}	0.0				0.72			
	P_{TF}	0.0	0.72	0.0		0.72		1.0	
	L_{TF}	0.5	1.0	0.5	1.0	0.9	0.75	1.0	0.9	0.75
	Simulation	**1**	**2**	**3 (ref)**	**4**	**5**	**6**	**7**	**8**	**9**
OCs	**PCs**	1,417	759	25,246	35,359	35,791	25,792	19,784	22,755	24,821
	MBCs	0	0	12,886	1,094	1106	12,704	824	948	12,787
	Total	1,417	759	38,132	36,453	36,898	38,496	20,608	23,703	37,608

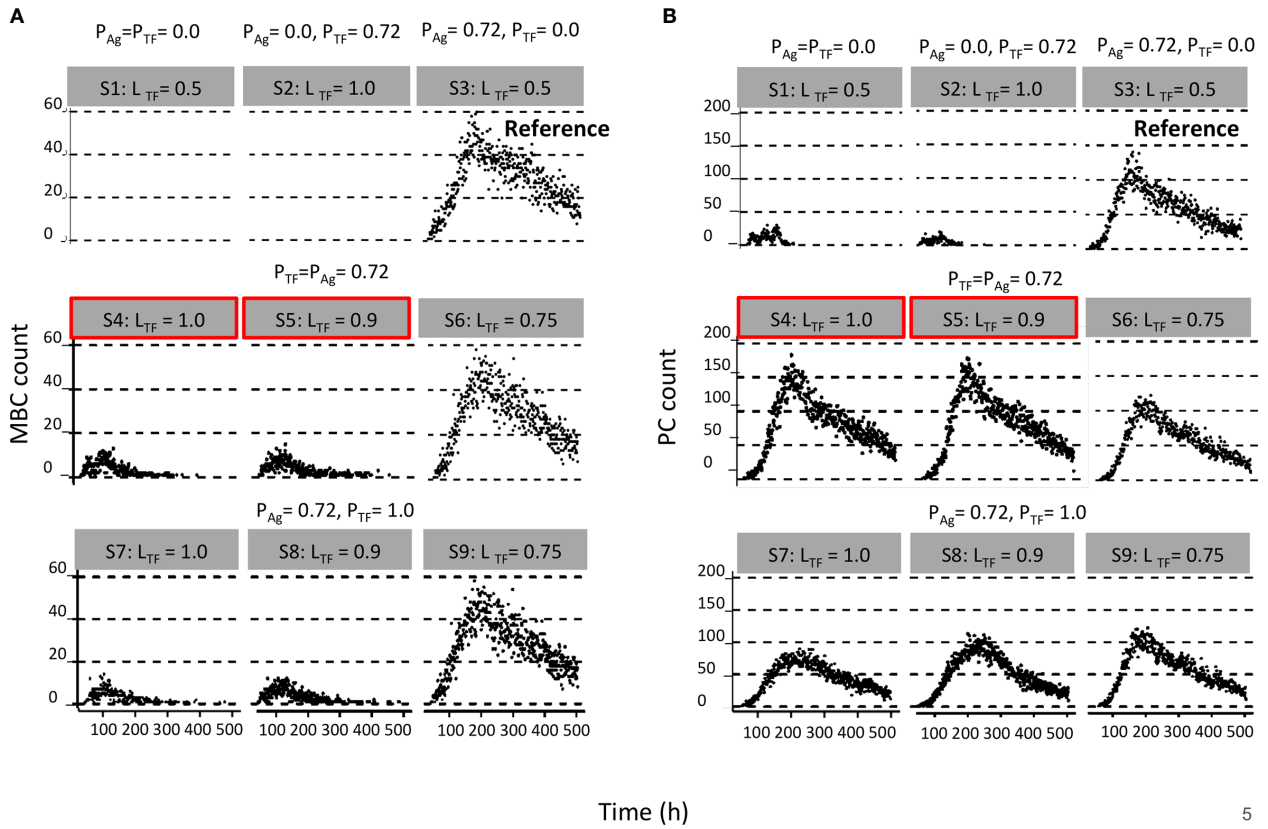

FIGURE 4 | Results from first set of simulations (**Table 2**). **(A)** Relative MBC and **(B)** PC count during the GC. The probability of asymmetric division (P) is indicated above the gray box and simulation number and polarity levels (L) are shown in the gray box. First row of plots corresponds to (left column) symmetric division of Ag and TFs, (middle column) symmetric division of Ag and asymmetric division of TFs, and (right column) symmetric division of TFs and asymmetric division of Ag. Second row of plots corresponds to asymmetric TF division only if mode of Ag division is asymmetric. Red boxes indicate parameters that are closer to biological results. Third row of plots corresponds to always asymmetric TF division regardless of mode of Ag division.

signaling simulation (Scenario 2) discussed in (11). The number of accumulated OCs reached 38,132 cells at the end of the GC reaction (**Table 4** and **Figure 3B**) of which 12,886 were MBCs (**Figure 4A**) and 25,246 were PCs (**Figure 4B**). Furthermore, MBCs were generated throughout the GC reaction, and 90% of PCs were generated after the peak (day 6) of the GC reaction (**Supplementary Figure 3**). We conclude that asymmetric Ag division is largely responsible for obtaining a DZ-to-LZ ratio close to experimental observations. Asymmetric TF division is not required. Asymmetric Ag division also re-establishes a larger number of OCs, but no temporal switch is observed.

Asymmetric TF Division Only if Mode of Ag Division Is Asymmetric (Coupled Asymmetric Division)

Next, we investigated a scenario (simulations 4–6, **Table 2**; P_{Ag} = P_{TF} = 0.72) that assumes that asymmetric TF and Ag division always happen simultaneously. Since we are mostly interested in the effect of the TFs, we assumed that in the case of asymmetric division, all Ag goes to a single daughter cell (L_{Ag} = 1.0) while we used different polarization levels for the TF (L_{TF} = 1.0, 0.9, and 0.75). All three simulations had similar DZ-to-LZ ratios and total number of OCs, which were also similar to the reference simulation (**Table 4** and **Figures 3A, B**). Nevertheless, low TF polarity levels showed approximately a 12-fold increase in MBCs, at the expense of PC output, compared to extreme TF polarity levels. Furthermore, low TF polarity levels showed similar MBC counts compared to the reference simulation (**Figure 4**). Interestingly, extreme TF polarity levels (L_{TF} = 1.0, 0.9) resulted in a temporal switch from MBCs to PCs, which was not the case for simulations with low TF polarity levels (L_{TF} = 0.75 nor L_{TF} = 0.5 in the reference simulation).

When analyzing the TF dynamics in the GRN, we found, as expected, that extreme TF polarity levels generated a high BLIMP1 state in one of the TF inheriting daughters (0 h, **Figure 5**) while leaving the other daughter B-cell in a low BLIMP1 state. Contrarily, low TF polarity levels promoted a slower progression to the high BLIMP1 state (4–8 h), which explains the increased number of MBCs (Ag+/BLIMP1−) in simulations 3 and 6. We conclude that simultaneous asymmetric division of Ag and TF results in DZ-to-LZ ratios similar to the reference simulation, but only extreme TF polarity levels resulted in a temporal switch.

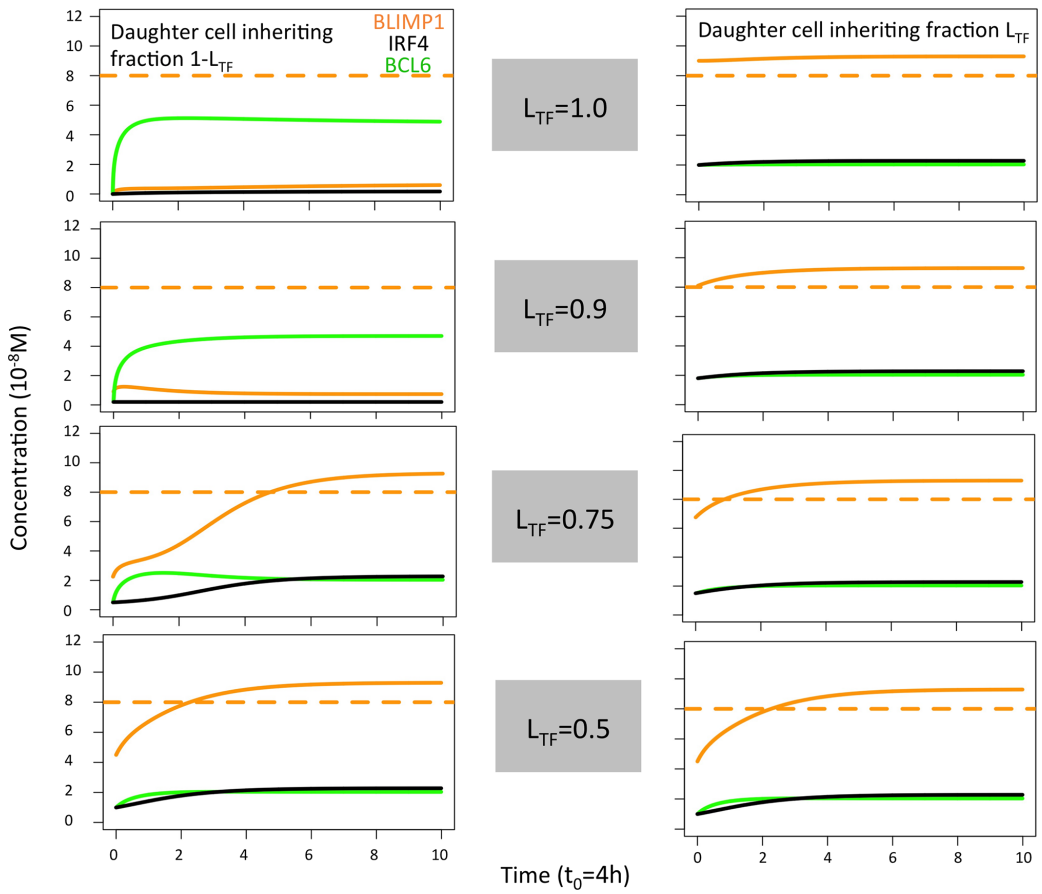

FIGURE 5 | Solution curves based on the GRN (ODE model) for BLIMP1 (orange), BCL6 (green), and IRF4 (black) in two daughter cells. The initial TF concentrations were based on the concentration of the parent cell (BLIMP1 = 8, BCL6 = 2, IRF4 = 2) and the different polarity levels (L_{TF} = 1.0, L_{TF} = 0.9, L_{TF} = 0.75, and L_{TF} = 0.5; **Table 2**).

Always Asymmetric TF Division Regardless of Mode of Ag Division (Uncoupled Asymmetric Division)

Since there is no *a priori* reason to suggest that asymmetric Ag and TF division are coupled (simulations 4–6), we performed three additional simulations in which TF always divide asymmetrically (P_{TF} = 1.0, L_{TF} = 1.0, L_{TF} = 0.9, and L_{TF} = 0.75) regardless of the model of Ag division (P_{Ag} = 0.72, L_{Ag} = 1.0; simulations 7–9, **Table 2**). We found that for extreme TF polarity levels (L_{TF} = 1.0, 0.9), the DZ-to-LZ ratio progressively increased up to a value of 80, which meant a 40-fold increase compared to the reference simulation (**Figure 3A**). Contrarily, low TF polarity levels (L_{TF} = 0.75) showed a DZ-to-LZ ratio that fluctuated between 2 and 4 similarly to the reference simulation (**Figure 3A**). Extreme TF polarity levels showed a 2-fold decrease in OC counts and a 12-fold increase in MBC counts compared to low TF polarity levels and the reference simulation (**Table 4** and **Figure 3B**). In extreme TF polarity levels, there was a 1.2-fold decrease in PC counts compared to low TF polarity levels and a 1.7-fold decrease in PC counts compared to simulations with coupled asymmetric Ag and TFs division (**Table 4** and **Figure 4**). While approximately 90% of PCs were generated after the peak (day 6) of the GC reaction for all TF polarity levels, low TF polarity levels produced MBCs during the entire GC reaction (**Supplementary Figure 4**). Thus, while low polarity levels resulted in similar DZ-to-LZ ratio and OC production as the reference simulation, it did not result in a temporal switch from MBCs to PCs.

The TF dynamics in the GRN, as described in the previous section (see above, **Figure 5**), explained the decreased OC count observed in simulations 7 and 8 compared to simulations 4–6 and 9. In addition, it could explain the similarity in OC count observed when comparing simulations 6 and 9.

We concluded that uncoupled Ag and TFs asymmetric division lead to a 40-fold increase in DZ-to-LZ ratios and a reduction in OC production for the extreme TF polarity levels. However, for these extreme polarities, a temporal switch is observed.

Collectively, the first set of simulations show that assuming that the decision for PC differentiation is fully based on BLIMP1 levels and that all TFs cosegregate during asymmetric division, then the simulated DZ-to-LZ ratio is close to those observed experimentally. Furthermore, a temporal switch from MBCs to PCs was only present in simulations with coupled Ag and TFs asymmetric division and extreme TF polarities L_{TF}.

Coupled Ag and TFs Asymmetric Division With Different Polarity Levels for Individual TFs

From the first set of simulations (simulations 1–9, **Table 2**), we showed that coupled Ag and TFs asymmetric division with extreme TF polarity levels resulted in a DZ-to-LZ ratio that was similar to the reference simulation and a temporal switch. However, in these simulations, we assumed that BCL6, IRF4, and BLIMP1 always distributed in equal amounts (L_{TF}) over the daughter cells. Based on previous research, this is unlikely (7, 8). Therefore, we performed 27 additional simulations (**Table 3**; $P_{TF} = P_{Ag} = 0.72$ and $L_{Ag} = 1.0$) in which TFs can be distributed in different amounts (L_{BLIMP1}, L_{IRF4}, and L_{BCL6}) to the daughter cells. In these simulations TFs are only asymmetrically distributed in case of asymmetric Ag division. For each simulation, we investigated the GC dynamics and OC production.

All simulations showed a DZ-to-LZ ratio that was similar to the reference simulation (data not shown). Furthermore, the number of OCs at the end of the GC reaction is similar for all 27 simulations (**Figure 6A**). **Figures 6B, C** show the number of MBCs and PCs produced for the 27 combinations of TF polarity levels. We observed that neither the polarity level of IRF4 nor BCL6 have a big influence on the number of OCs, MBCs, or PCs. However, there is a clear difference when comparing the extreme ($L_{BLIMP1} = 1.0$ and $L_{BLIMP1} = 0.9$; $L_{IRF4} = L_{BCL6} = 1.0$) and low ($L_{BLIMP1} = 0.75$; $L_{IRF4} = L_{BCL6} = 1.0$) BLIMP1 polarity levels. Low polarity levels resulted in a 12-fold increase in MBC counts and a 1.2-fold decrease in PC counts (**Supplementary Figures 5–7**).

When analyzing the TF dynamics in the GRN, we found that extreme IRF4 polarity levels ($L_{IRF4} = 1.0$, $L_{IRF4} = 0.9$; $L_{BLIMP1} = L_{BCL6} = 1.0$) immediately generated a high BLIMP1 state in one of the TF inheriting daughters while leaving the other daughter B cell in a low BLIMP1 state (**Figure 7**). Low IRF4 polarity levels ($L_{IRF4} = 0.75$; $L_{BLIMP1} = L_{IRF4} = 1.0$) generated both daughter B cells in the high BLIMP1 steady state. Nevertheless, in this situation, the daughter B cell that inherited 25% ($1 - L_{IRF4}$) of IRF4, along with 0% of BLIMP1 and BCL6 concentration, slowly progressed to the high BLIMP1 state within 20 h until BLIMP1 levels reached the PC differentiation threshold. Considering that after the last division, PBs are defined as PCs and exit the GC, this could explain why no difference in OC dynamics was observed when varying IRF4 polarity levels.

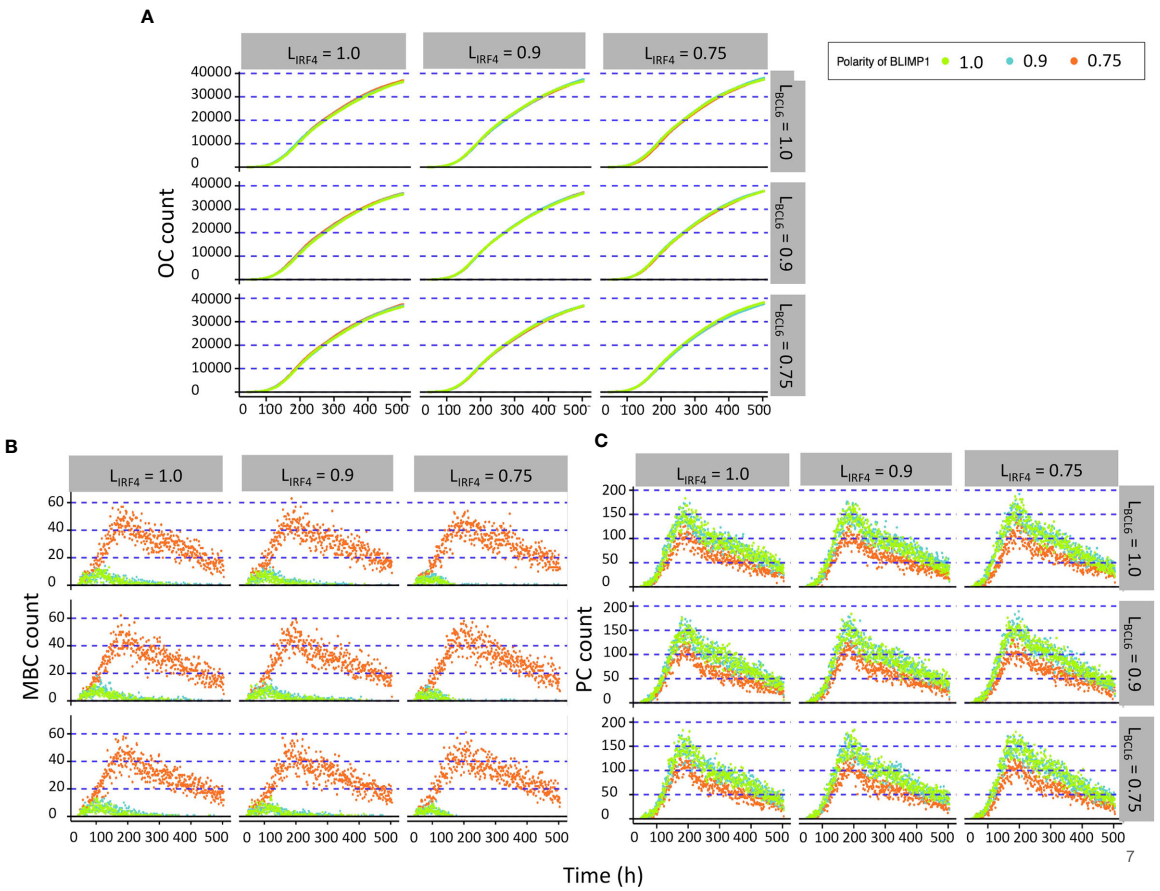

FIGURE 6 | Results from the second set of simulations (**Table 3**). **(A)** Accumulated OCs, **(B)** relative MBC, and **(C)** PC count during the GC reaction. At the top of each panel column, the IFR4 polarity level is indicated. To the right of each panel row, the BCL6 polarity level is indicated. The colors indicate the different BLIMP1 polarity levels.

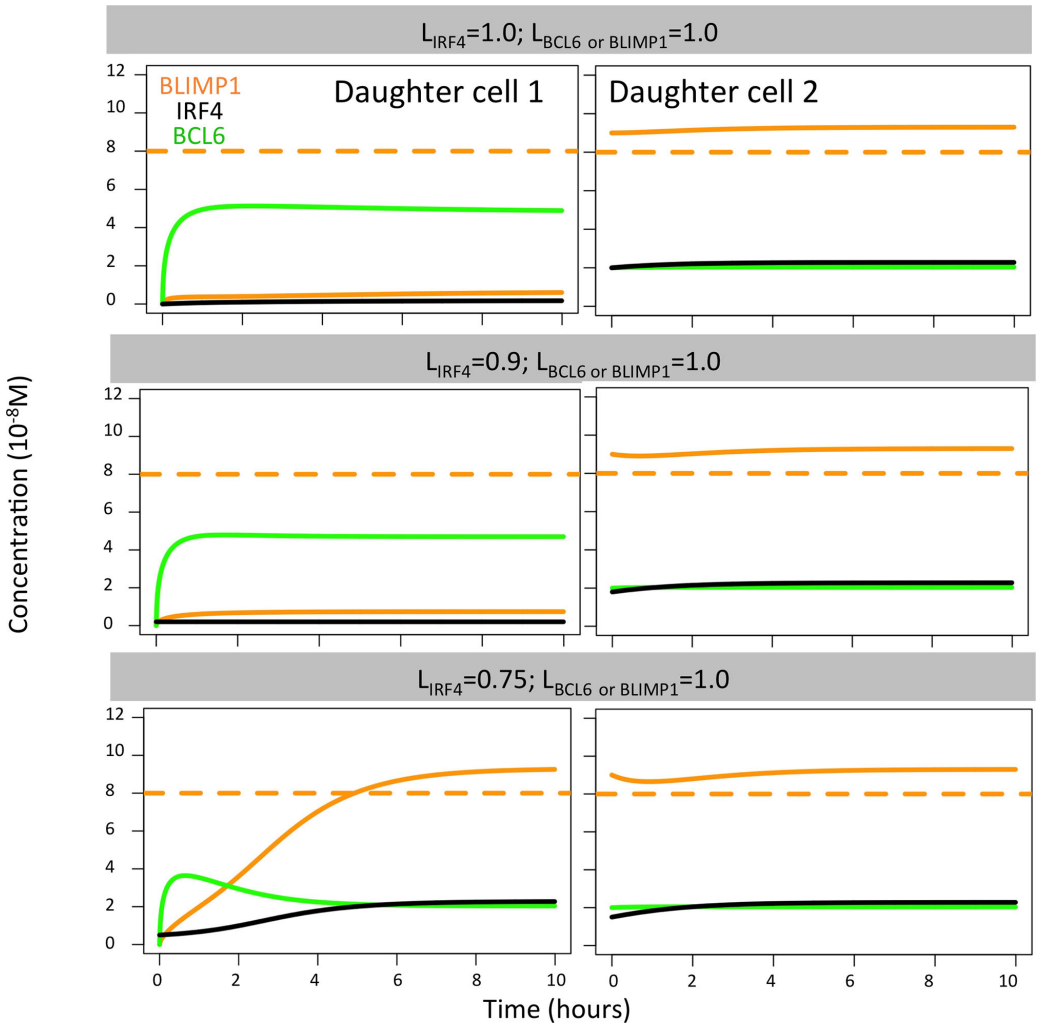

FIGURE 7 | BLIMP1 (orange), BCL6 (green), and IRF4 (black) dynamics in two theoretical daughter B cells. Their initial TF concentrations were set to simulate the asymmetric division of a parent cell (BLIMP1 = 8, BCL6 = 2, IRF4 = 2) with all different combinations of IRF4 levels (L_{IRF4} = 1.0, L_{IRF4} = 0.9, and L_{IRF4} = 0.75, as shown in **Table 2**). Levels of BCL6 and BLIMP1 were fixed (L_{BCL6} = L_{BLIMP1} = 1.0).

In the case of BCL6, we found that all polarity levels (L_{BCL6} = 1.0, L_{BCL6} = 0.9, L_{BCL6} = 0.75; L_{BLIMP1} = L_{IRF4} = 1.0) immediately generated a high BLIMP1 state in one of the TF inheriting daughters, leaving the other daughter B cell in a low BLIMP1 state (**Figure 8**). This is why no difference in OC dynamics was observed when varying BCL6 polarity levels. Such results were not surprising since changes in the BCL6 level as a result of BcR signaling are not sustained in time nor become large enough to switch the BLIMP1 from a high to low level.

Finally, we found extreme BLIMP1 polarity levels (L_{BLIMP1} = 1, L_{BLIMP1} = 0.9; L_{IRF4} = L_{BCL6} = 1.0) immediately generated a high BLIMP1 steady state in one of the TF inheriting daughters, leaving the other daughter B cell in a low BLIMP1 steady state (**Figure 9**). Low BLIMP1 polarity levels (L_{BLIMP1} = 0.75; L_{BCL6} = L_{IRF4} = 1.0) introduced a delay (4 h) in the progression of the high BLIMP1 inheriting daughter B cell to the high BLIMP1 state. This could explain the differences observed in OC dynamics when varying BLIMP1 polarity levels.

We conclude that the combined results from these 27 simulations and the first set of 9 simulations show that BLIMP1 driven PC differentiation together with coupled asymmetric division of Ag and BLIMP1 with a large segregation between the daughter cells results in a GC DZ-to-LZ ratio and a temporal switch from MBCs to PCs that are both observed in experiments (6, 10) However, future experimental validation of our findings remain necessary.

DISCUSSION

It has been shown experimentally that Ag and TFs can asymmetrically divide and that this may codetermine GC

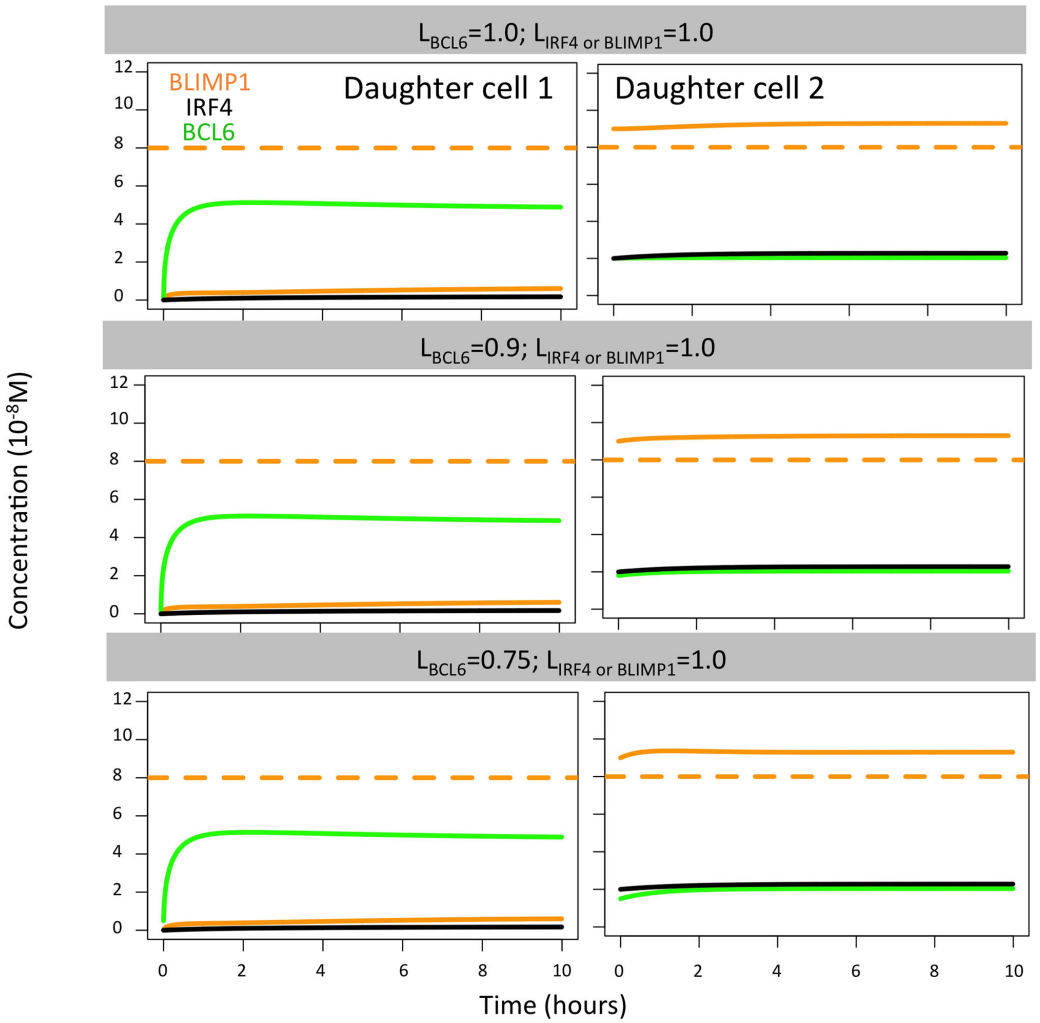

FIGURE 8 | BLIMP1 (orange), BCL6 (green), and IRF4 (black) dynamics in two theoretical daughter B cells. Their initial TF concentrations were set to simulate the asymmetric division of a parent cell (BLIMP1 = 8, BCL6 = 2, IRF4 = 2) with all different combinations of BCL6 levels (L_{BCL6} = 1.0, L_{BCL6} = 0.9, and L_{BCL6} = 0.75, as shown in **Table 2**). Levels of IRF4 and BLIMP1 were fixed (L_{IRF4} = L_{BLIMP1} = 1.0).

B-cell fate (3, 5, 7, 8). However, so far, this has not been proven experimentally. Based on a computational model of the GC, Meyer-Hermann and colleagues hypothesized that asymmetric division of Ag might play a role in PC differentiation, as this resulted in a DZ-to-LZ ratio in agreement with experimental data (5). However, using our MSM, we recently showed that asymmetric Ag division alone cannot explain PC differentiation, since it is not fully consistent with experimental observations that B cells with increased BLIMP1 levels differentiate to PCs, but we only considered one specific mode of coupled asymmetric division (i.e., P_{Ag} = P_{TF} = 0.72, L_{BLIMP1} = L_{IRF4} = L_{BCL6} = 1.0) (11). Therefore, in the current work, we investigated the putative effect of asymmetric division of Ag and TFs in more detail and hypothesized that this affects GC dynamics and B-cell dynamics and fate. From our simulations, we conclude that BLIMP1-driven PC differentiation together with coupled asymmetric division of Ag and BLIMP1 with extreme TF polarity levels for BLIMP1 segregation results in GC DZ-to-LZ ratio and a temporal switch from MBCs to PCs that are also observed in experiments (6, 10). This confirmed our previous finding that asymmetric Ag division alone is not sufficient to drive PC differentiation, but also asymmetric division of at least BLIMP1 is required.

An important insight from our model is the observation that outcomes of simulations with (uncoupled) symmetric division of Ag and/or TF do not agree with experimental observations (migrations rates, temporal switch). It is, however, important to emphasize that this result does not definitely exclude this scenario to be true. Although our GC model is the most sophisticated model currently available and based on a large range of experimental observations, we cannot exclude the possibility that other choices, assumptions, or parameter settings would

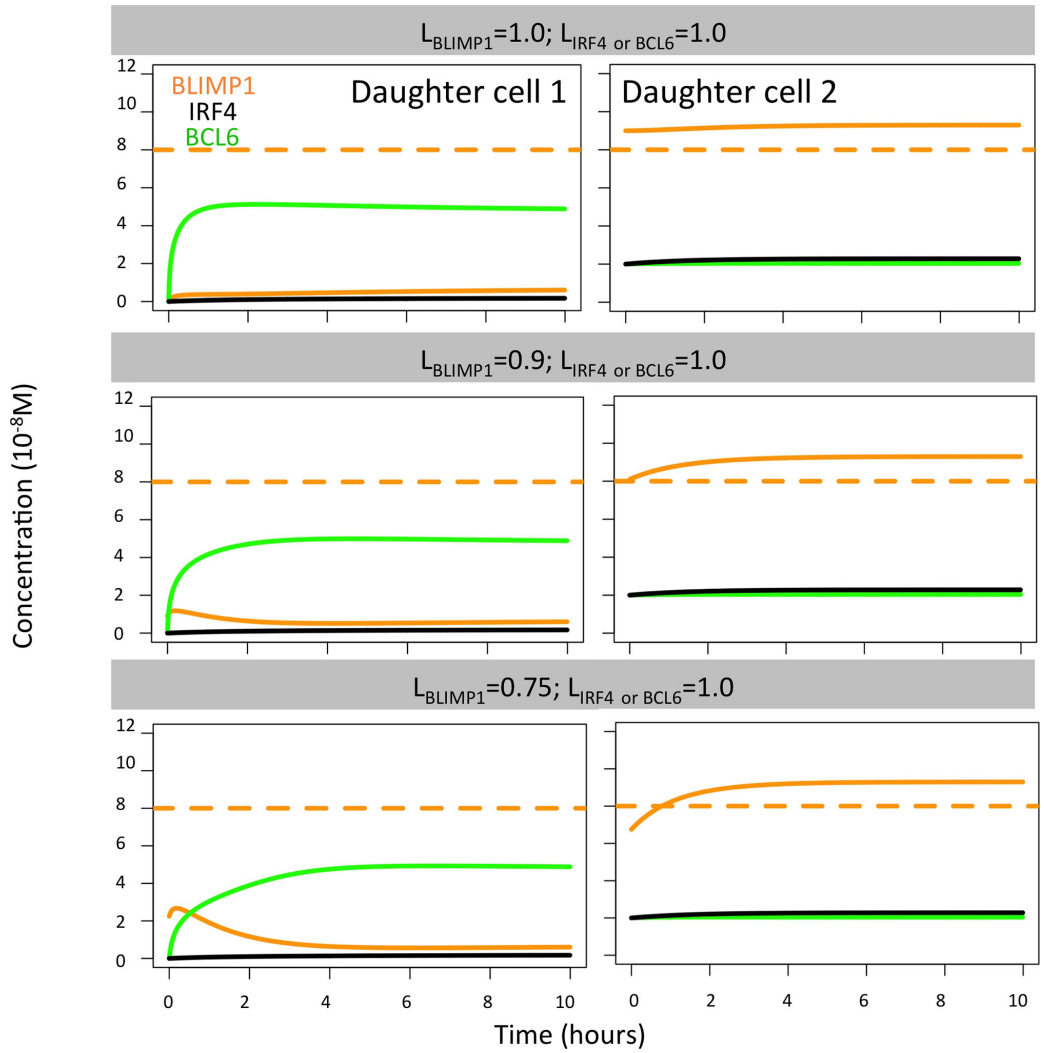

FIGURE 9 | BLIMP1 (orange), BCL6 (green), and IRF4 (black) dynamics in two theoretical daughter B cells. Their initial TF concentrations were set to simulate the asymmetric division of a parent cell (BLIMP1 = 8, BCL6 = 2, IRF4 = 2) with all different combinations of BLIMP1 levels (L_{BLIMP1} = 1.0, L_{BLIMP1} = 0.9, and L_{BLIMP1} = 0.75, as shown in **Table 2**). Levels of IRF4 and BCL6 were fixed (L_{IRF4} = L_{BCL6} = 1.0).

change our conclusion. Nevertheless, we think that our simulations provide at least some evidence that asymmetric division is involved in PC differentiation. Furthermore, prior studies have shown that unequal stimulation of signaling pathways, e.g., CD40 and PI3K, induced when B cells present Ag to and receive help from T_{FH} cells during the selection process in the GC reaction, can provide polarity cues that drive asymmetry division (7, 8). It was proposed that unequal inheritance of Ag transmembrane receptor, costimulation, and/or cytokine signaling could result in unequal activation of signaling pathways. Although this hypothesis was not experimentally tested, it is in line with our finding.

The observation that IRF4 asymmetric division had no effect of PC production was both interesting and surprising. On the one hand, *in vitro* data suggest that IRF4, and/or different levels of T help through Cd40/Nf-kB induction of IFR4, regulates MBC and PC differentiation in a concentration-dependent manner (13, 14). Furthermore, quantitative modeling of the terminal B-cell differentiation showed through parameter sensitivity analysis for bistability that kinetic parameters associated to IRF4 dynamics and CD40 induction of IRF4 were critical in promoting B-cell transition towards PC differentiation (12). Nevertheless, the same study showed that above a critical IRF4 concentration threshold (>1.10^{-8}M), CCs irreversibly differentiated to PCs. In our model, asymmetric division takes place at a late stage of B-cell development (PB) in which IRF4 concentration is close to the high IRF4 steady state (2.10^{-8}M). Thus, we found that even with low IRF4 polarity levels, when daughter B cells inherited 75% of IRF4 (L_{IRF4} = 0.75), this did not decrease IRF4 concentration below the above-mentioned critical

IRF4 threshold. This explained why we found no effect of IRF4 asymmetric division on PC differentiation. In addition, *in vitro* studies in conjoined sibling B cells showed that unequal IRF4 expression could drive branching of B-cell state prior to the loss of PAX5, a MBC promoter, hence at early stages of B-cell transition to PC. Furthermore, the levels of BLIMP1 in sibling B cells were not measured, leaving the open question of whether asymmetric BLIMP1 division could be the driver of PC differentiation and supporting the need to further investigate BLIMP1 asymmetric division at later stages of PC differentiation in the GCs.

Apart from model assumptions, our study has several limitations. First, our findings and conclusions remain to be validated or falsified in future experiments. We propose experiments to generate data about the (1) BLIMP1 probability of asymmetric division and polarity level in single PBs; (2) extent and/or role of the cosegregation of BLIMP1, BCL6 and IRF4; and (3) extent and/or role of (a)symmetric division of CD40 signaling in relation to B-cell fate. Second, the probability ($P_{Ag} = 0.72$) for asymmetric Ag division was based on experimental data (7). For asymmetric TF division, we used this same value in several simulations. However, probabilities of $P_{BCL6} = 0.44$ and $P_{IRF4} = 0.11$ have been reported (7), while for BLIMP1, such probability is unknown. Nevertheless, we here show that asymmetric division of IRF4 and BCL6 did not have an effect on the fate of the B cell, and thus, we believe that this would not change our main conclusion. Third, no data are available about the number of MBCs and PCs produced during a single GC reaction. Thus, we cannot substantiate which simulations are more realistic in terms of OC production. Fourth, as we have discussed previously (11), the current definition of MBCs as Ag+BLIMP1− cells should be improved, since it definition merely classifies OCs, which are not PCs to be MBCs. Nevertheless, we here showed that symmetric TF division did not agree with the observation of a temporal switch in the GC reaction. This could indicate that asymmetric TF division plays a role in MBC differentiation. Interestingly, PAX5 has been shown to asymmetrically segregate and always oppose asymmetric IRF4 distribution (8). Further experiments need to be carried out to validate this hypothesis since the effect of asymmetric PAX5 division on MBC formation was not addressed.

DATA AVAILABILITY STATEMENT

Publicly available datasets were analyzed in this study. This data can be found here: https://github.com/EDS-Bioinformatics-Laboratory/AsymmetricDivision.

AUTHOR CONTRIBUTIONS

EM, HH, and AK designed the study. EM, DL, MM-H, and PR implemented the software. JH, EM, DL, and AK carried out the simulations and analyses. All authors were involved in the interpretation of results. JG, HH, and AK supervised the study. All authors contributed to the article and approved the submitted version.

FUNDING

This work is supported by a CASyM Exchange Research Grant, COSMIC (www.cosmic-h2020.eu), which has received funding from the European Union's Horizon 2020 research and innovation programme under the Marie Skłodowska-Curie grant agreement No 765158, and by the Human Frontier Science Program 570 (RGP0033/2015).

ACKNOWLEDGMENTS

We thank Barbera van Schaik for setting up a Virtual Machine provided by the Dutch national e-infrastructure with the support of SURF Cooperative, to process large output files.

SUPPLEMENTARY MATERIAL

The Supplementary Material for this article can be found online at: https://www.frontiersin.org/articles/10.3389/fimmu.2021.716240/full#supplementary-material

REFERENCES

1. De Silva NS, Klein U. Dynamics of B Cells in Germinal Centres. *Nat Rev Immunol* (2015) 15(3):137–48. doi: 10.1038/nri3804
2. Neumüller RA, Knoblich JA. Dividing Cellular Asymmetry: Asymmetric Cell Division and its Implications for Stem Cells and Cancer. *Genes Dev* (2009) 23 (23):2675–99. doi: 10.1101/gad.1850809
3. Thaunat O, Granja AG, Barral P, Filby A, Montaner B, Collinson L, et al. Asymmetric Segregation of Polarized Antigen on B Cell Division Shapes Presentation Capacity. *Sci (80-)* (2012) 335(6067):457–79. doi: 10.1126/science.1214100
4. Dustin ML, Meyer-Hermann M. Antigen Feast or Famine. *Sci (80-)* (2012) 335(6067):408–9. doi: 10.1126/science.1218165
5. Meyer-Hermann M, Mohr E, Pelletier N, Zhang Y, Victora GD, Toellner KM. A Theory of Germinal Center B Cell Selection, Division, and Exit. *Cell Rep* (2012) 2(1):162–74. doi: 10.1016/j.celrep.2012.05.010
6. Victora GD, Schwickert TA, Fooksman DR, Kamphorst AO, Meyer-Hermann M, Dustin ML, et al. Germinal Center Dynamics Revealed by Multiphoton Microscopy With a Photoactivatable Fluorescent Reporter. *Cell* (2010) 143(4):592–605. doi: 10.1016/j.cell.2010.10.032
7. Barnett BE, Ciocca ML, Goenka R, Barnett LG, Wu J, Laufer TM, et al. Asymmetric B Cell Division in the Germinal Center Reaction. *Sci (80-)* (2012) 335(6066):342–4. doi: 10.1126/science.1213495
8. Lin W-HW, Adams WC, Nish SA, Chen Y-H, Yen B, Rothman NJ, et al. Asymmetric PI3K Signaling Driving Developmental and Regenerative Cell Fate Bifurcation. *Physiol Behav* (2015) 176(1):139–48. doi: 10.1016/j.celrep.2015.10.072
9. Radtke D, Bannard O. Expression of the Plasma Cell Transcriptional Regulator Blimp-1 by Dark Zone Germinal Center B Cells During Periods of Proliferation. *Front Immunol* (2019) 10(JAN):1–16. doi: 10.3389/fimmu.2018.03106
10. Weisel FJ, Zuccarino-Catania GV, Chikina M, Shlomchik MJ. A Temporal Switch in the Germinal Center Determines Differential Output of Memory B

and Plasma Cells. *Immunity* (2016) 44(1):116–30. doi: 10.1016/j.immuni.2015.12.004
11. Merino Tejero E, Lashgari D, García-Valiente R, Gao X, Crauste F, Robert PA, et al. Multiscale Modeling of Germinal Center Recapitulates the Temporal Transition From Memory B Cells to Plasma Cells Differentiation as Regulated by Antigen Affinity-Based Tfh Cell Help. *Front Immunol* (2021) 11 (620716):1–15. doi: 10.3389/fimmu.2020.620716
12. Martínez MR, Corradin A, Klein U, Álvarez MJ, Toffolo GM, Di Camillo B, et al. Quantitative Modeling of the Terminal Differentiation of B Cells and Mechanisms of Lymphomagenesis. *Proc Natl Acad Sci USA* (2012) 109 (7):2672–7. doi: 10.1073/pnas.1113019109
13. Sciammas R, Li Y, Warmflash A, Song Y, Dinner AR, Singh H. An Incoherent Regulatory Network Architecture That Orchestrates B Cell Diversification in Response to Antigen Signaling. *Mol Syst Biol* (2011) 7(495):1–15. doi: 10.1038/msb.2011.25
14. Laidlaw BJ, Cyster JG. Transcriptional Regulation of Memory B Cell Differentiation. *Nat Rev Immunol* (2020) 21. doi: 10.1038/s41577-020-00446-2

Conflict of Interest: The authors declare that the research was conducted in the absence of any commercial or financial relationships that could be construed as a potential conflict of interest.

Publisher's Note: All claims expressed in this article are solely those of the authors and do not necessarily represent those of their affiliated organizations, or those of the publisher, the editors and the reviewers. Any product that may be evaluated in this article, or claim that may be made by its manufacturer, is not guaranteed or endorsed by the publisher.

frontiers in Immunology

ORIGINAL RESEARCH
published: 01 September 2021
doi: 10.3389/fimmu.2021.705848

Brg1 Supports B Cell Proliferation and Germinal Center Formation Through Enhancer Activation

Dominik Schmiedel[*†‡], *Hadas Hezroni*[‡], *Amit Hamburg*[‡] *and Ziv Shulman*[*]

Department of Immunology, Weizmann Institute of Science, Rehovot, Israel

OPEN ACCESS

Edited by:
Michel Cogne,
University of Limoges, France

Reviewed by:
Mikael Sigvardsson,
Linköping University, Sweden
Hong Zan,
The University of Texas Health Science Center at San Antonio, United States

***Correspondence:**
Ziv Shulman
ziv.shulman@weizmann.ac.il
Dominik Schmiedel
dominik.schmiedel@izi.fraunhofer.de

†Present address:
Dominik Schmiedel,
Fraunhofer Institute for Cell Therapy and Immunology (IZI), Department of GMP development and ATMP design, Leipzig, Germany

‡These authors have contributed equally to this work

Specialty section:
This article was submitted to B Cell Biology, a section of the journal Frontiers in Immunology

Received: *06 May 2021*
Accepted: *11 August 2021*
Published: *01 September 2021*

Citation:
Schmiedel D, Hezroni H, Hamburg A and Shulman Z (2021) Brg1 Supports B Cell Proliferation and Germinal Center Formation Through Enhancer Activation. Front. Immunol. 12:705848. doi: 10.3389/fimmu.2021.705848

Activation and differentiation of B cells depend on extensive rewiring of gene expression networks through changes in chromatin structure and accessibility. The chromatin remodeling complex BAF with its catalytic subunit Brg1 was previously identified as an essential regulator of early B cell development, however, how Brg1 orchestrates gene expression during mature B cell activation is less clear. Here, we find that Brg1 is required for B cell proliferation and germinal center formation through selective interactions with enhancers. Brg1 recruitment to enhancers following B cell activation was associated with increased chromatin accessibility and transcriptional activation of their coupled promoters, thereby regulating the expression of cell cycle-associated genes. Accordingly, Brg1-deficient B cells were unable to mount germinal center reactions and support the formation of class-switched plasma cells. Our findings show that changes in B cell transcriptomes that support B cell proliferation and GC formation depend on enhancer activation by Brg1. Thus, the BAF complex plays a critical role during the onset of the humoral immune response.

Keywords: Brg1, BAF, SWI/SNF, chromatin remodeling, enhancer activation, B cells, germinal center, antibody-formation

INTRODUCTION

Long-lasting protection from harmful pathogens depends on the efficient generation of high-affinity antibodies (1). In response to vaccination or pathogen invasion, naive B cells that reside in follicles of secondary lymphoid organs interact with cognate antigens through their B cell receptors (BCRs) and present antigen-derived peptides on surface MHC class II to cognate T helper cells (2). At this stage, cognate T cells select B cells for the generation of short-lived plasmablasts or for differentiation into germinal center (GC) cells (3). GCs are microanatomical sites in which activated B cells rapidly divide and introduce somatic hypermutations (SHM) into their immunoglobulin genes followed by affinity-based-selection (4). The major function of the GC reaction is to produce memory and antibody-forming cells that depart the lymphoid organs and provide long-lasting immunity (5). The process of B cell activation and differentiation into GC, memory, or plasma cells (PCs) highly depends on changes in gene expression that is regulated at the transcriptional and post-transcriptional levels (6, 7). Whereas the specific transcription factors that drive B cell activation and differentiation were previously described, less is known about the regulation of gene expression through changes in chromatin accessibility and structure. /B cell state

transitions are guided by well-defined transcription factors such as BCL-6, BLIMP1, and PAX5 (8). However, in order to access their target sites, the chromatin structure must assume an accessible state, a process that is controlled by chromatin remodeling complexes (CRCs). The required establishment of nucleosome-depleted regions (NDRs) by shifting or evicting nucleosomes is one of the main functions of CRCs (9). NDRs are not only critical for transcription factor binding, but also for binding of cohesin and mediator complexes which create three-dimensional DNA structures, like the formation of loops between promoter regions and enhancers. These loop formations are a prerequisite for lineage-specific gene transcription as they bring transcription factors that bind distal enhancers in close proximity to the promoter of its target genes and are guided by the presence of histone modifications such as H3K4me1 or H3K27ac (10).

The BAF (BRG1/BRM-associated factor) CRC, also known as SWI/SNF complex, is particularly well-known for its capacity to form NDRs. This complex consists of up to 15 subunits and the incorporation of different subunits into it allows cell-specific functions (11, 12). The SWI/SNF complex possesses several subunits with DNA and histone recognition domains that can guide complex localization not only by DNA sequence recognition but predominantly by DNA architecture and pre-existing histone modifications (13, 14). The core of the complex is the ATPase subunit, which engages with the nucleosome-bound DNA and hydrolyzes ATP to induce a conformational change of the complex and enforces the nucleosome repositioning. Each complex possesses a single ATPase unit, which can be either Brm or Brg1 (encoded by *Smarca2* and *Smarca4*, respectively). Brg1 has a critical role in many physiological settings such as in maintaining pluripotency in stem cells (15, 16), neural development (17), and heart muscle development (18). On top, Brg1 and other complex subunits were found to be frequently mutated in diverse malignancies (13, 19), highlighting their essential role in maintaining transcriptional stability in a variety of tissues. Thus, Brg1 acts as both a tumor suppressor (18, 20) and a tumor driver (14, 21).

In the context of B cells, gene expression regulation by Brg1 was primarily studied in the process of B development in the bone marrow (BM) wherein the SWI/SNF complex plays a critical role (22). In developing B cells in the BM, Brg1 promotes fate decisions of lymphoid progenitor cells and has critical functions in pro- and pre-B cell stages. Specifically, Brg1 is required for the function of lineage-specific transcription factors like Ikaros and Pax5 through enabling access to enhancers, such as the Myc super-enhancer (23, 24). EBF1, a pioneering transcription factor, was shown to recruit Brg1 and promote phase separation and chromatin accessibility (25). Also, the contraction of the BCR heavy chain locus during the VDJ-recombination requires Brg1 functions (24).

Unlike in B cell development, understanding of the functions and mechanism of Brg1 in mature B cells remains less clear. A role for Brg1 in class-switch recombination and proliferation was previously suggested in a B cell line (26) and Srg1, a subunit of the SWI/SNF complex, was found to be required for GC formation (22). In contrast, a study that characterized changes in chromatin structure in B cells upon activation found only minor changes in Brg1 genomic occupancy, however, effects on gene expression were not examined (27). Thus, how Brg1 controls mature B cell activation and functions through chromatin modulation is not entirely solved.

Here, we find that Brg1 is critical for establishing the gene expression profile of activated B cells, by promoting chromatin accessibility at enhancers. This process allows Brg1 to activate the transcription of genes essential for cell cycle progression and ultimately GC formation. Thus, our findings define Brg1 as a key chromatin regulator that supports activation-induced transcription factors activity during the establishment of antibody-mediated immunity.

MATERIALS AND METHODS

Mice

$CD23^{Cre}$, $\gamma1^{Cre}$ and $Brg1^{fl/fl}$ (28) mice were purchased from the Jackson Laboratories. C57BL/6 wild-type mice were purchased from Envigo. All mice were bred and housed in specific-pathogen-free conditions. Littermate controls used as control animals were $Brg1^{+/+}$, $CD23^{+/+}$ or $\gamma1^{+/+}$. All experiments were approved by the Weizmann Institute Animal Care and Use Committee (IACUC) with animals aged between 7-14 weeks. For immunizations, NP-KLH was emulsified in complete Freud's adjuvant (CFA). Per mouse, 50 µl were subcutaneously injected close to the base of the tail. Animals were anesthetized with a mixture of ketamine, xylazine and acepromazine prior to the injection. 7 days after the immunization, inguinal lymph nodes were harvested and analyzed in flow cytometry.

Method Details

Enzyme-Linked Immunosorbent Assay

Serum was collected from unimmunized mice, by drawing blood into a heparin-coated microcapillary. Haematocrit was removed by centrifugation (800xg, 15 minutes, 4°C) and supernatant, which represents the serum fraction, was collected. Serum was then diluted 1: 40 000 in PBS, and IgM, IgG1, IgG3 antibodies were detected by ELISA using anti-mouse IgM-, anti-mouse IgG1-, or anti-mouse IgG3 horseradish peroxidase (HRP), using 1-step-TMB-ELISA substrate and stop solution. The optical density at 450 nm (OD450nm) was measured with a microplate reader (Tecan).

In Vitro Activation of B Cells

Splenic B cells were isolated by forcing the tissue through a filter mesh into PBS containing 2% fetal calf serum and 1 mM EDTA. The cell mixture was then subjected to erythrocyte lysis by ACK buffer for 10 min, then washed twice with PBS. B cells were isolated with the Ly-48 B cell isolation kit according to the manufacturer's instructions. Cells were cultivated in RPMI1640 medium including 25 mM HEPES, supplemented with 10% fetal calf serum (FCS), L-glutamine, pyruvate, non-essential amino acids, β-mercapto-ethanol, and activated with 10 µg/mL LPS and

20 ng/mL IL-4 for 72 or 96 hours. Cells were seeded in a density of 1 million per mL. If proliferation was examined, cells were stained with Cell Trace Violet dye according to the manufacturer's instructions prior to the activation.

Flow Cytometry

Spleens, lymph nodes and Peyer's patches were harvested and forced through a filter mesh into PBS containing 2% fetal calf serum and 1 mM EDTA. BM was collected from the hind limbs. Splenic single cell suspensions and BM samples were treated with ACK buffer in order to lyse erythrocytes. *In vitro* activated cells were mixed well, harvested and washed one with PBS.

On ice, single cell suspensions were subjected to 1 µg/ml anti-CD16/32 for 5 min in order to block nonspecific binding to FC receptors, then fluorescently labeled antibodies were added for another 25 min. Cells were gated as live and single according to their properties in FSC and SSC, then defined as follows: lymph node/Peyer's patch/spleen: B cells: B220+ CD138-, PCs: CD138+, germinal center B cells: B220+ CD38- FAS+; BM: B cells: B220+ CD138-, PCs: CD138+; *in vitro* activation - B220+; median fluorescence intensities plotted in all diagrams were either tested with student's t-test (2 groups) or one-way ANOVA with *post hoc* Tukey's multiple comparisons test. Statistics were calculated in Graph Pad Prism 8. Following p values are represented by the asterisks': $p<0.05$ = *; $p<0.01$ = **; $p<0.001$ = ***; $p<0.0001$ = ****, $p>0.05$ = ns (not significant). All antibodies were purchased from Biolegend.

For intracellular staining, cells were fixed after surface staining and fixed and permeabilized with the BD Cytofix/Cytoperm Kit according to the manufacturer's instructions and then stained with anti-Blimp-1-Alexa Fluor 647 and anti-IRF4-Alexa Fluor 488 (Biolegend).

Immunofluorescence

Immunized inguinal lymph nodes were excised, washed in PBS, and fixed with 4% paraformaldehyde for 16 hours at 4°C. The tissues were then subjected to 30% sucrose overnight, and then fresh sucrose solution for 4 more hours before being embedded in OCT freezing solution (Tissue-Tek). 10-mm sections were cut and dehydrated in acetone prior to freezing. Sections were rehydrated in PBS and incubated with 1% SDS in PBS for 5 min, then blocked in PBS with 0.05% Tween-20 and 3% BSA for at least one hour. Slides were probed with 1:100 rabbit-anti-mouse Brg1 (clone H-88) and 1:100 anti-mouse CD35-Biotin overnight, then washed three times and then stained with anti-rabbit Alexa Fluor-488, Alexa Fluor-647 conjugated streptavidin, anti-mouse IgD - PE (each 1:200) and in 1% BSA in PBST, incubated once more overnight. Slides were washed in PBS and nuclei were counterstained for 5 min with Hoechst 33342 (1:4000) (Thermo Fisher Scientific). Sections were mounted with a mounting medium (Sigma-Aldrich) and imaged with a Zeiss LSM 880 confocal microscope.

Quantitative PCR Analysis and RNA Sequencing Sample Preparation

Activated splenic B cells were harvested after 72 hours activation using LPS and IL-4. Polyadenylated RNA was isolated using Dynabeads mRNA Purification Kit (ThermoFisher) according to the manufacturer's instructions. For qPCR, total RNA was subjected to cDNA synthesis using qScript synthesis kit (Quantabio). qPCR mix was prepared using SYBR green (Roche) with primers specific for Brg1 (fw: CAAAGACAAG CATATCCTAGCCA; rv: CACGTAGTGTGTGTTAAGGACC) or Brm (fw: AGCCAGATGAGTGACCTGC: rv: TGCTTGGCA TCCTTTTCGGAA). Relative transcript expression was calculated using the ddCt method and all transcripts were normalized to Actin B. For RNA sequencing, libraries were generated for bulk sequencing using the MARSseq protocol as previously described.

RNAseq Data Analysis

Alignment and differential expression analysis were performed using the UTAP pipeline (29): Reads were trimmed using Cutadapt and mapped to the mm10 genome assembly using STAR (30) v2.4.2a with default parameters. The pipeline quantifies the genes annotated in Gencode, extended by 1,000 bases toward the 5′ edge and 100 bases in the 3′ direction. Counting of sequenced reads was done using htseq-count (31). Genes having a minimum of five UMI-corrected reads in at least one sample were included in the analysis. Normalization of the counts and differential expression analysis was performed using DESeq2 (32). Genes were considered differentially expressed if they had a FC ≥ 2 or ≤ 2, and padj < 0.05 in $Brg1^{fl/fl}$ cells compared to $Brg1^{fl/+}$ and littermate controls. Heatmap of differentially expressed genes was generated with the pheatmap R package.

Western Blot

In vitro cells were suspended with ice-cold RIPA buffer (10mM Tris-HCl, pH 8.0, 140mM NaCl, 1mM EDTA, 1% Triton X-100, 0.1% Sodium Deoxycholate, 0.1% SDS). Extracts were centrifuged (15,000 xg for 15 min at 4°C), and supernatants were boiled for 5 min in SDS sample buffer. Equal amounts of protein (30 µg/well) were loaded onto an 8% SDS-PAGE. After electrophoretic separation, proteins were transferred to a nitrocellulose membrane blocked for 1 h (5% nonfat dry milk and 0.5% Tween in Tris-buffered saline), and incubated overnight at 4°C with primary antibodies. After washing, membranes were then incubated with secondary anti-mouse or anti-rabbit horseradish peroxidase-conjugated Abs (Jackson ImmunoResearch Laboratories, West Grove, PA, USA) for 1 h and exposed to ECL reagent (Thermo Fisher Scientific, Waltham, MA, USA).

Antibodies that were used: rabbit anti-human Brg1 (1:500; Cell Signaling Technology, Danvers, Massachusetts, USA), mouse anti-human beta-Actin (1:1000; Thermo Fisher Scientific, Waltham, MA, USA).

ATAC-seq Library Preparation

ATAC-seq was performed as previously described (33) with minor adjustment. Cells were collected after 4 days of *in vitro* activation as mentioned above. 50,000 cells were centrifuged at 400 xg for 3 min, followed by a wash using 50 µL of cold PBS and centrifugation at 400 xg for 3 min. Cells were lysed using a cold lysis buffer (10 mM Tris-HCl, pH 7.4, 10 mM NaCl, 3 mM MgCl2 and 0.1% IGEPAL CA-630). Immediately after lysis, nuclei were spun at 400 xg for 10 min using a refrigerated centrifuge. Next, the pellet was resuspended in the transposase

reaction mix (25 μL 2 × TD buffer, 2.5 μL transposase (Illumina) and 22.5 μL nuclease-free water). The transposition reaction was carried out for 30 min at 37°C and immediately put on ice. Directly afterward, the sample was purified using a QIAGEN MinElute kit. Following purification, the library fragments were amplified using custom Nextera PCR primers 1 and 2 for a total of 12 cycles. Following PCR amplification, the libraries were purified using a QIAGEN MinElute kit and sequenced with paired-end sequencing using NovaSeq 6000.

ATAC-seq Data Analysis

Reads were aligned to the mm10 genome assembly using Bowtie2 (34). Normalized read coverage files were computed by deepTools (35). Peaks were called using MACS2 (36) and annotated using HOMER (37). Peaks from the eight analyzed datasets were combined. Read coverage in the peaks was computed using bigWigAverageOver bed UCSC utility (38). Differential accessibility was computed with DESeq2 (32).

ChIP-seq Data Analysis

A previously published Brg1 ChIP-seq dataset [GSE82144 (27)] was used for the identification of Brg1 binding sites. Reads were aligned to the mm10 genome assembly with Bowtie2 (34). Peak calling was done using MACS2 (36), and peaks were annotated using HOMER (37).

Functional Annotation of Brg1 Target Genes

Enriched GO terms within down- or upregulated Brg1 target genes were identified using GOrilla (39). Enriched GO terms were then summarized by REViGO (40). Gene Set Enrichment Analysis (GSEA) was performed using GSEA 4.1 (41). Gene names were converted to human gene symbols, and software was run with default parameters, using the "hallmark" signatures from the MSigDB database (42). Enrichment for transcription factors binding to promoters within down- or upregulated Brg1 targets was done using Enrichr (42, 43), with the Chea database (44).

Analysis of Brg1 Bound Enhancers

Heatmaps representing ChIP-seq signals for Brg1, H3K4me1 and H3K27ac were generated using deepTools (35). Bigwig files used heatmaps were downloaded from GEO (GSE82144). Genomic coordinates of FAIRE-seq and STARR-seq peaks, and of promoter-enhancer interactions were downloaded from GEO (GSE121753) (45). Overlap between Brg1 bound regions and enhancer regions was calculated using bedtools intersect. Signals of Brg1 over different genomic regions were generated using deepTools (35). Mean Brg1 coverage over different genomic regions was calculated using bigWigAverageOverBed.

RESULTS

Brg1 Controls Transcription Regulation in Activated B Cells

In order to examine how Brg1 controls the activation of mature B cells, we examined changes in gene expression patterns in B cells stimulated through TLR4 or the BCR. In this context, LPS stimulation or IgM crosslinking of B cells induced expression of Brg1 but not of Brm (**Figure 1A**). In order to examine the role of Brg1 in B cell immune responses, we crossed $Brg1^{fl/fl}$ mice to a transgenic mouse strain that expresses Cre specifically in mature B cells (CD23-Cre). In B cells derived from these mice, a significant reduction in Brg1 protein levels was observed (**Figure S1A**). As opposed to commonly used B cell-specific mouse models like CD19-Cre, deletion of genes in this mouse strain takes place during their final differentiation in the spleen after their departure from the BM (46). LPS-stimulated B cells derived from littermate control mice showed effective proliferation, whereas B cells lacking one *Smarca4* allele were moderately impaired, and the proliferation of B cells lacking both *Smarca4* alleles was significantly reduced (**Figure 1B**). Yet, Brg1-deficient B cells were able to respond to LPS stimulation as they showed CD86 upregulation 18 hours after activation (**Figure S1B**) and no reduction in cellular viability was observed (**Figure S1C**). To identify the genes and pathways affected by the loss of Brg1, LPS-activated B cells were subjected to RNA-seq. We found that 643 genes were downregulated and 1424 genes were upregulated by at least twofold in Brg1-deficient B cells compared to littermate controls (**Figure 1C**). Comparing our data to a dataset of gene expression following eight hours of LPS activation of splenic B cells (47), we found that genes that were induced following LPS activation were significantly downregulated in Brg1-deficient B cells, while genes that were repressed following LPS activation were upregulated in Brg1-deficient cells (**Figure 1D**). To characterize how genome-wide occupancy of Brg1 affects gene expression, we first examined a pre-existing dataset of Brg1 ChIP-seq of resting and LPS activated splenic B cells (27). Brg1 occupancy was abundant, with over 50,000 peaks in resting B cells and over 70,000 peaks in activated B cells. Similar to previous findings in pro-B cells (24), Brg1 peaks in mature activated B cells were localized mainly to introns and intergenic regions, while less than a third of the peaks were localized to gene promoters (**Figure 1E**). Analyzing the promoter-bound genes based on their transcriptional response to Brg1 loss, we found that 900 upregulated genes and 396 downregulated genes had Brg1 peaks in their promoters (**Figure 1F**), suggesting their transcription may be directly regulated by this chromatin remodeler. GO analysis and gene set enrichment analysis (GSEA) showed that downregulated Brg1 targets were enriched for cell cycle progression and anabolic process (**Figures 1G, H**), in agreement with the weak proliferation observed in stimulated Brg1-deficient B cells *in vitro*. Cdkn3 and E2f8, two regulators of cell cycle progression, were downregulated in Brg1-deficient B cells and showed Brg1 peaks in their promoters (**Figure 1** and **Figure S1D**). These findings demonstrate that Brg1-deficient cells fail to acquire the proper transcriptional program that promotes B cell activation in response to LPS. In addition, GSEA analysis showed downregulation of Myc and E2f target genes which are essential for proper B cell proliferation (**Figure S1E**). To examine whether Myc and E2f transcription factors directly regulate the expression of downregulated Brg1 targets, we

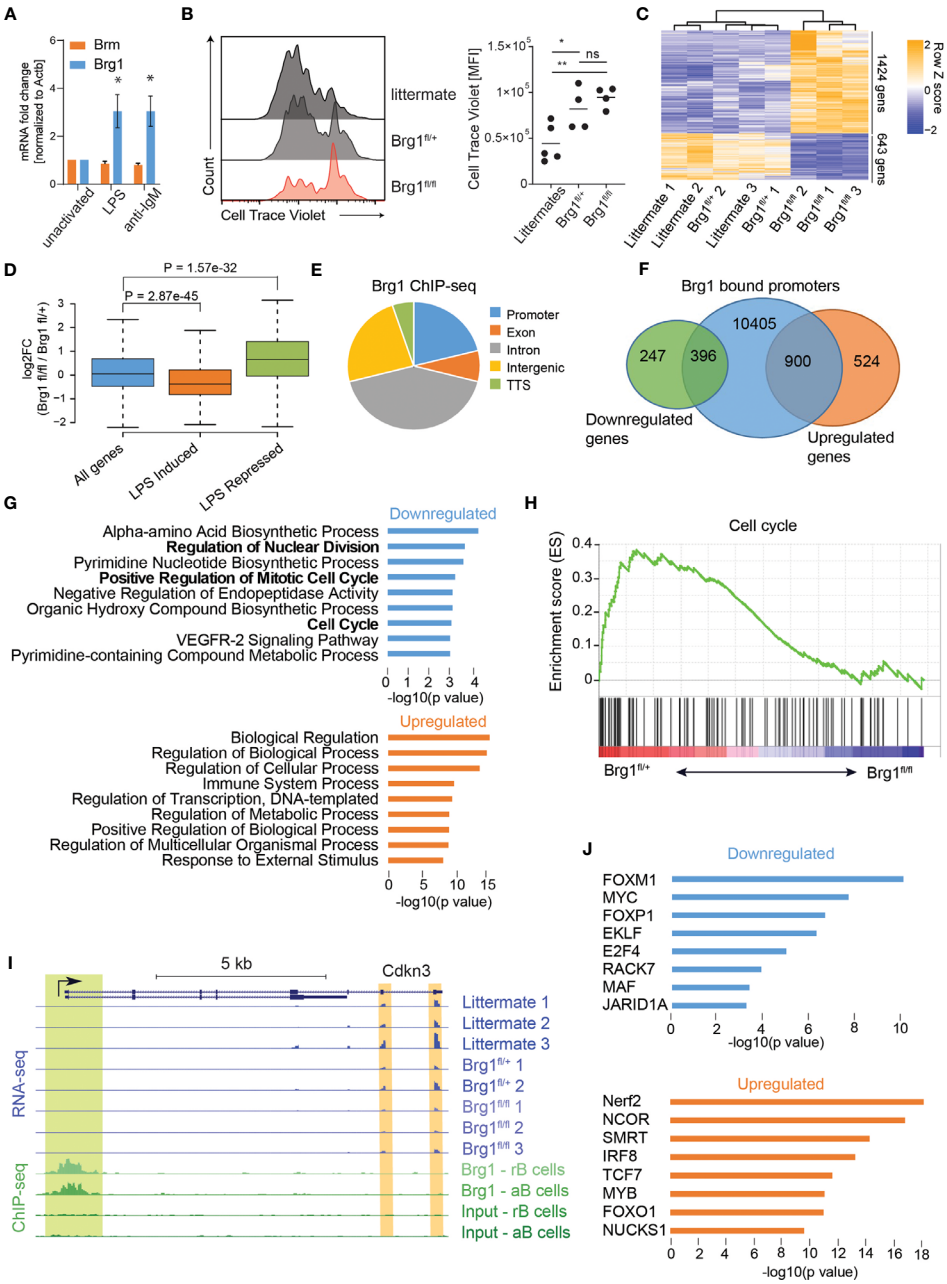

FIGURE 1 | Brg1 regulates the expression of cell cycle genes in activated B cells **(A)** qRT-PCR analysis of *Smarca2* and *Smarca4* mRNA levels of B cells following treatment with anti-IgM or LPS for 2 days, n = 3 mice, * p<0.05 in a one-sample t-test compared to unactivated cells. **(B)** Flow cytometric analysis of splenic B cell proliferation following 72 hours of LPS and IL-4 activation. MFI of CellTrace Violet cell tracker dye is shown and quantified. Each dot represents one mouse. Statistics were calculated with one-way ANOVA with *post hoc* Tukey's multiple comparisons test. p<0.05 = *; p<0.01 = **; p>0.05 = ns (not significant). **(C)** Heat map representation of clustering analysis of differentially expressed genes. All genes with padj<0.05 and fold change of at least 2 are shown. **(D)** Boxplots indicating the median, quartiles, and 5th and 95th percentiles of changes in expression levels of CD23-Cre Brg1$^{fl/fl}$ compared to Brg1$^{fl/+}$ B cells in genes induced or repressed following LPS activation compared to total genes. P value was calculated by a two-sided Wilcoxon rank sum test. **(E)** Distribution of 70,333 Brg1-binding sites across genomic regions in LPS activated B cells. TTS: transcription termination site. **(F)** Venn diagram showing overlap between 11,701 Brg1 bound promoters, 1,424 genes upregulated in Brg1$^{fl/fl}$ compared to Brg1$^{fl/+}$ cells, and 643 genes downregulated in Brg1$^{fl/fl}$ compared to Brg1$^{fl/+}$ cells. **(G)** GO terms which were enriched in genes whose promoters were bound by Brg1 and were down- or upregulated in CD23-Cre Brg1$^{fl/fl}$ compared to Brg1$^{fl/+}$ B cells. **(H)** Gene set enrichment plot for cell cycle genes from the hallmark gene sets. **(I)** UCSC genome browser tracks showing the locus of Cdkn3 (padj < 0.05). Tracks show the expression levels, measured by RNA-seq, in activated B cells and ChIP-seq signal of Brg1 in resting and activated B cells, compared to input controls. Green highlight: binding of Brg1 in the promoter region. Orange highlights: 3' end exons covered by RNA-seq. **(J)** Transcription factors enriched for binding the promoters of genes which were bound by Brg1 and were down- or upregulated in Brg1$^{fl/fl}$ compared to Brg1$^{fl/+}$ cells.

analyzed the promoters of these genes for binding by transcription factors using the Chea database, which contains ChIP-seq and ChIP-chip experiments for 199 transcription factors (44). We found that promoters of downregulated Brg1 targets were enriched for binding by Myc and E2f4, in addition to other transcription factors that play a role in cell cycle progression and cell proliferation including Foxm1 and Foxp1 (**Figure 1J**). Indeed, *E2f4* expression was reduced in Brg1-deficient B cells (**Figure S1F**). In contrast, despite the fact that MYC targets were less expressed in Brg1-deficient B cells, and that many downregulated Brg1 targets were regulated by MYC, the expression of *Myc* gene was not significantly reduced in Brg1-deficient cells compared to control cells (**Figure S1F**). These data suggest that in activated B cells, Brg1 doesn't control Myc expression directly. Upregulated Brg1 target genes were enriched for GO terms related to immune system processes and transcriptional regulation, including Bach2 transcriptional regulator (**Figure 1G** and **Figure S1C**). The promoters of these genes were enriched for binding by NCOR and SMRT (**Figure 1J**), two transcriptional repressors which are known to act in Brg1 containing complexes (48) that play important roles in transcription regulation in B cells (49, 50). Taken together, these data suggest that Brg1 plays important roles in transcriptional regulation in activated B cells, both through activation of genes required for cell proliferation and in repression of genes that are downregulated in response to LPS activation.

Brg1 Promotes Enhancer Chromatin Accessibility in Activated B Cells

Brg1 was previously reported to activate cell-type-specific enhancers by facilitating the depletion of nucleosomes in pro-B cells (24) and in mesoderm lineage commitment (51). In activated B cells, Brg1 bound regions were marked by H3K4me1 and H3K27ac, two histone modifications that typically mark enhancers (**Figure 2A**). In order to study whether Brg1 affects gene expression through enhancer activation, we utilized previously published datasets, including enhancer regions that were mapped by FAIRE-seq and tested for functionality using STARR-seq, and enhancer-promoter interactions mapped by Hi-C (45). FAIRE-seq peaks define regions of open and accessible chromatin. STARR-seq peaks define regions that are both accessible and were shown to act as functional enhancers using a high-throughput screen. Open chromatin regions that were not validated as functional enhancers might represent poised enhancers with the potential to rapidly become activated under specific cellular contexts (45). We found that Brg1 was bound to most poised and active enhancers (represented by FAIRE-seq and STARR-seq peaks, respectively), and to even larger fractions of enhancer-promoter pairs (as detected by Hi-C analysis) (**Figure 2B**). Brg1 signal was stronger in resting B cells compared to their activated counterparts, and stronger in STARR-seq validated enhancers compared to all FARE-seq regions (**Figures 2C**, **S1G**). We also found that the Brg1 signal was stronger in enhancers that interact with multiple promoters (**Figure 2D** and **Figure S1H**), which were reported to have increased chromatin accessibility, suggesting that Brg1 preferentially interacts with enhancers that show higher activity. In order to examine the effect of Brg1 deficiency on the chromatin landscape we used ATAC-seq to map accessible chromatin regions. We compared B cell-derived from CD23-Cre $Brg1^{fl/fl}$ and CD23-Cre $Brg1^{fl/+}$ that showed similar gene expression patterns as Brg1-sufficient littermates in RNA-seq analysis (**Figure 1C**). We obtained 16,464 peaks representing open chromatin regions, and for each peak computed the average ratio of read coverage between Brg1-deficient and control B cells. 752 peaks showed significantly reduced chromatin accessibility in Brg1-deficient B cells, and 340 of those peaks overlapped with activated B cells enhancers (**Figure S1I**). 322 peaks showed a significant increase in chromatin accessibility in Brg1-deficient B cells, and only 20 of these peaks overlapped enhancer regions (**Figure S1I**). Nearly all of the observed peaks with reduced chromatin accessibility were also bound by Brg1 according to the ChIP-seq data, while only a third of the peaks that showed increased accessibility was bound by Brg1 (**Figure S1J**). While peaks overlapping promoters were not affected by the loss of Brg1, peaks overlapping enhancer regions, as well as peaks overlapping Brg1 binding sites, had significantly reduced chromatin accessibility in Brg1-deficient B cells (**Figure 2E**). Taken together, these data suggest that Brg1 preferentially binds enhancers in activated B cells and promotes chromatin accessibility.

We next examined specifically the expression levels of genes whose promoters interact with enhancers bound by Brg1 and found that these genes were significantly less expressed in Brg1-deficient cells (**Figure 2F**). We also found that the expression of genes that were bound by more than four enhancers was downregulated to a larger extent compared to genes bound by up to four enhancers (**Figure 2G**). Importantly, genes bound by multiple enhancers were reported to have enhanced levels of nascent transcripts compared to genes bound by single enhancers (45). An example of a gene whose promoter interacts with multiple Brg1 bound enhancers is E2f4, a transcription factor regulating cell cycle progression whose expression was downregulated in Brg1-deficient cells (**Figure S1F**). Hi-C analysis identified seven enhancers interacting with the promoter of E2f4, and our data show that these enhancers were bound by Brg1 and had decreased chromatin accessibility in Brg1-deficient cells (**Figure 2H**). These data suggest that Brg1 recruitment to multiple enhancers promotes transcriptional activation of their coupled promoters.

Effective Antibody-Mediated Immune Response Depends on Brg1

To evaluate how Brg1 functions at the chromatin level translate to effects on B cell immune responses, we examined immunoglobulin titers in the serum of unimmunized littermate control and CD23-Cre $Brg1^{fl/fl}$ mice. This analysis revealed a significant reduction in all of the antibody isotypes in Brg1-deficient mice (**Figures 3A**). The generation of IgG1 antibodies is primarily promoted by a T cell-dependent B cell activation response and generation of GCs (52). Therefore, we also

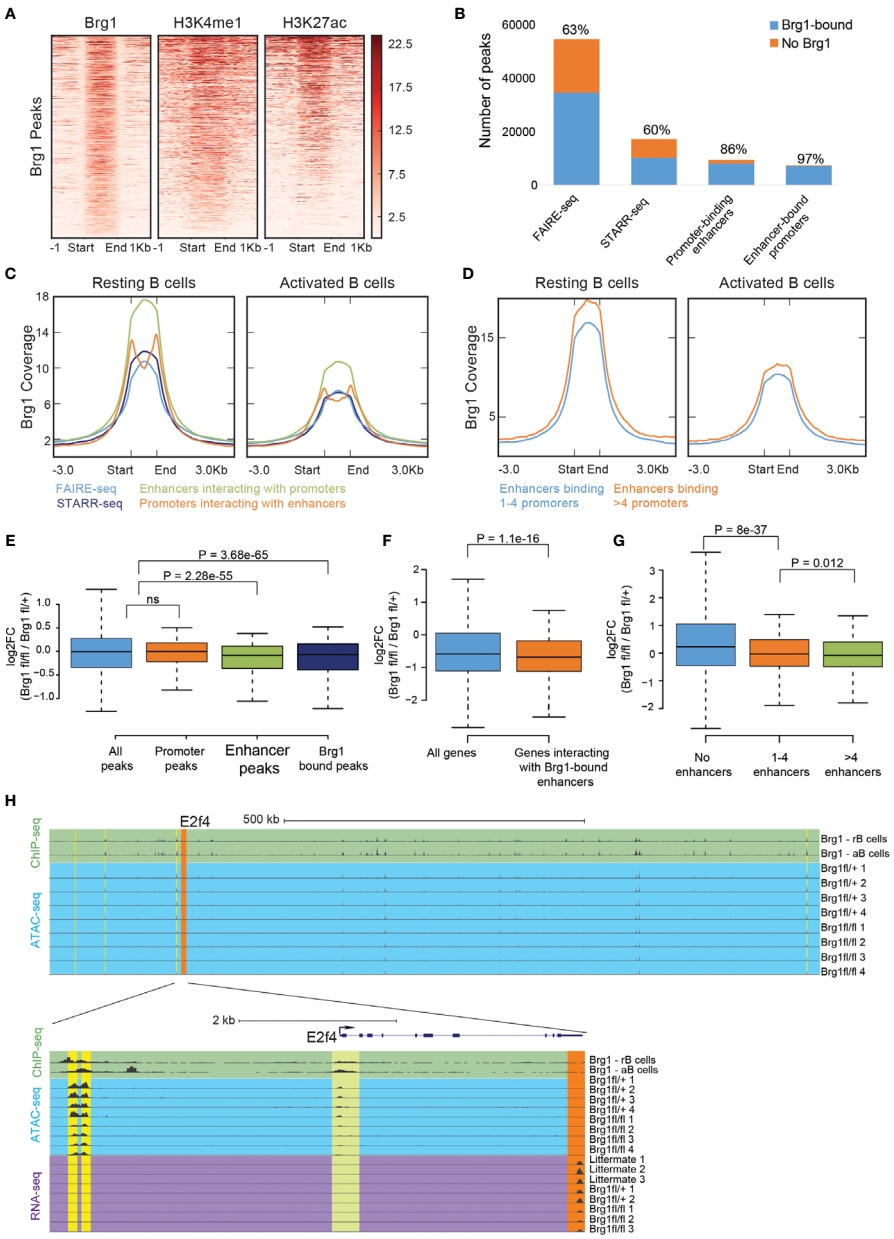

FIGURE 2 | Brg1 recruitment to multiple enhancers is associated with transcriptional activation of their coupled promoters. **(A)** Density of ChIP-seq reads for Brg1, H3K4me1, and H3K27ac in activated B cells. Plots show ±1 kb around the midpoint of each Brg1-enriched region ranked according to Brg1 density. **(B)** The numbers of FAIRE-seq peaks, STARR-seq peaks, promoter-binding enhancers, and enhancer-bound promoters, and the fraction of each group that overlaps Brg1 bound genomic regions. **(C)** Averaged tag densities of Brg1 are plotted across all FAIRE–seq peaks, STARR-seq peaks, promoter-binding enhancers, and enhancer-bound promoters, in resting and activated B cells. **(D)** Averaged tag densities of Brg1 are plotted across enhancers binding 1-4 promoters compared to enhancers binding >4 promoters, in resting and activated B cells. **(E)** Boxplots indicating the median, quartiles, and 5th and 95th percentiles of changes in ratios of ATAC-seq signal for the indicated group of peaks, comparing CD23-Cre $Brg1^{fl/fl}$ cells to $Brg1^{fl/+}$ B cells; p>0.05 = ns (not significant). **(F)** Boxplots indicating the median, quartiles, and 5th and 95th percentiles of changes in expression levels of $Brg1^{fl/fl}$ cells compared to $Brg1^{fl/+}$ cells in genes whose promoters interact with Brg1 bound enhancers compared to all genes. P-value was calculated by the two-sided Wilcoxon rank-sum test. **(G)** Boxplots indicating the median, quartiles, and 5th and 95th percentiles of changes in expression levels of CD23-Cre $Brg1^{fl/fl}$ cells compared to $Brg1^{fl/+}$ cells in genes whose promoters interact with 1-4 enhancers or with more than 4 enhancers, compared to genes whose promoters were not found to interact with active enhancers. P values were calculated by a two-sided Wilcoxon rank-sum test. **(H)** Top: UCSC genome browser tracks showing the area around the E2f4 gene, which was significantly downregulated in $Brg1^{fl/fl}$ cells (padj < 0.05). Tracks show the ChIP-seq signal of Brg1 in resting and activated B cells and ATAC-seq coverage in activated B cells. Orange highlight: E2f4 gene. Yellow highlights: enhancers which were found to interact with the promoter of E2f4. Bottom: zoom-in to the E2f4 locus, showing ChIP-seq signal of Brg1 in resting and activated B cells, ATAC-seq coverage and expression levels measured by RNA-seq. Green highlight: binding of Brg1 in the promoter region of E2f4. Orange highlight: 3' end exons covered by RNA-seq. Yellow highlights: enhancers which were found to interact with the promoter of E2f4. rB cells, resting B cells. aB cells, activated B cells.

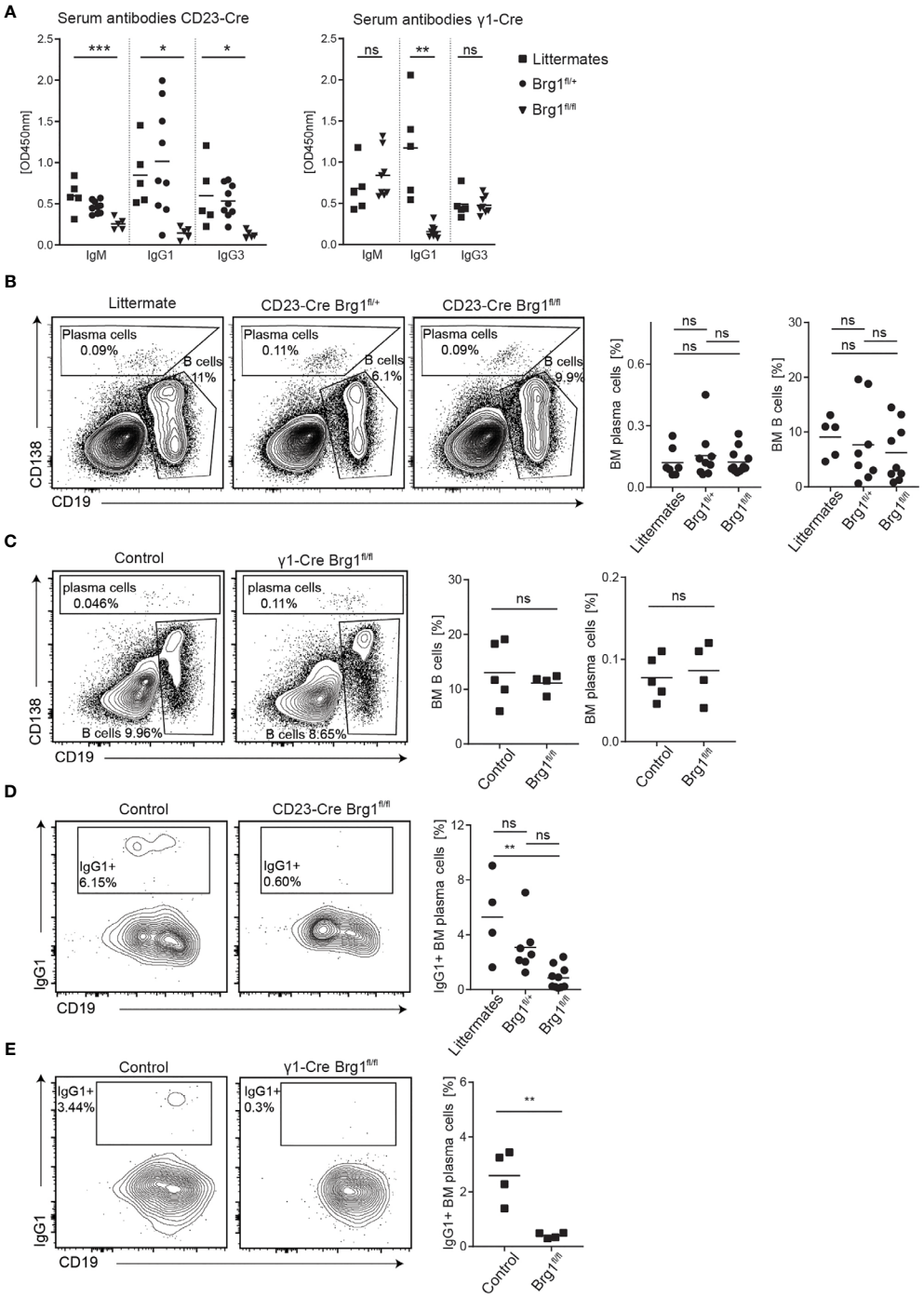

FIGURE 3 | Brg1-deficiency in B cells causes a reduction in serum antibodies and class-switched plasma cells. **(A)** ELISA for IgM, IgG1, and IgG3 in the serum of unimmunized CD23-Cre and γ1-Cre littermate, Brg1$^{fl/+}$ and Brg1$^{fl/fl}$ mice. One-way ANOVA with *post hoc* Tukey's multiple comparisons test. Following p values are represented by the asterisks': p<0.05 = *; p<0.01 = **; p<0.001 = ***; p>0.05 = ns (not significant). **(B)** Analysis of BM B cells and CD138$^+$ cells in CD23-Cre mice by flow cytometry. **(C)** Analysis of BM B cells and CD138$^+$ cells in γ1-Cre mice by flow cytometry. **(D)** Assessment of IgG1-class-switched BM CD138$^+$ cells in CD23-Cre mice using intracellular staining. **(E)** Assessment of IgG1-class-switched BM CD138$^+$ cells in γ1-Cre mice using intracellular staining.

examined antibody generation in mice in which Cre is expressed during B cell activation and CSR. For this purpose, we crossed the $Brg1^{fl/fl}$ mice to a mouse strain that expresses Cre after B cell activation during transcription of the sterile transcript of IgG1 (γ1-Cre mice (53),). In these mice, a significant reduction in IgG1 levels was observed whereas IgM and IgG3 titers were not affected (**Figures 3A**). We conclude that an effective generation of antibodies depends on Brg1.

The majority of long-lived PCs reside in the BM, where they can survive for long periods in specific niches and continuously secrete antibodies (54). Therefore, we assessed the frequency of total and $IgG1^+$ BM PCs in littermates and CD23-Cre $Brg1^{fl/fl}$ by flow cytometry analyses (**Figure S2A**). We found that the frequency of overall PCs was not different between the groups of mice. Overall the B cell fractions did not significantly change in CD23-Cre $Brg1^{fl/fl}$ and γ1-Cre $Brg1^{fl/fl}$ mouse strains within the BM (**Figures 3B, C**), although a small reduction was observed in the heterozygote mice. Nonetheless, the frequency of IgG1 class-switched PCs was significantly decreased, in the CD23-Cre $Brg1^{fl/fl}$ mice and nearly undetectable in γ1-Cre $Brg1^{fl/fl}$ mice (**Figures 3D, E**). To examine if Brg1 directly affects the expression of genes that are associated with plasma cell differentiation, we examined the expression of Irf4 and Blimp-1 in Brg1-deficient B cells following LPS activation. The expression of both of these transcription factors was intact suggesting that direct activation of plasma cell differentiation program is not dependent on Brg1 (**Figure S2B**). Collectively, we conclude that Brg1 in B cells is indirectly essential for the generation of $IgG1^+$ PCs.

Brg1 Is Required for the Generation of Germinal Center B Cells

Since IgG1 antibodies typically carry SHM, the GC reaction is their primary source. Thus, we examined the possibility that the observed reduction in PC frequencies in both mouse models is a result of defects in GC formation. First, we verified that Brg1 is expressed in GC B cells. For this purpose, we purified naive, light zone (LZ) and dark zone (DZ) GC B cells from immunized mice and examined Brg1 expression by qRT-PCR. Brg1 RNA (encoded by *Smarca4*) was primarily expressed in DZ B cells (**Figure 4A**). Accordingly, we detected Brg1 expression primarily in the DZ of the GC by immunohistochemistry (**Figure 4B**). To examine if Brg1 plays a role in PC generation during a T cell-dependent immune response, CD23-Cre $Brg1^{fl/+}$, CD23-Cre $Brg1^{fl/fl,}$ and littermates control mice were injected with KLH in CFA and the frequency of $CD138^+$ cells was examined in draining lymph nodes (LNs). Whereas a clear antibody-secreting cells (ASCs) population was detected in littermate controls and CD23-Cre $Brg1^{fl/+}$, these cells were undetectable in LNs derived from CD23-Cre $Brg1^{fl/fl}$ mice (**Figure 4C**, gating in **Figure S2C**). The absence of ASCs can be a result of either reduced levels of mature B cells or an inability to form GCs. The frequency of naive B cells was significantly reduced in CD23-Cre $Brg1^{fl/fl}$ mice compared to control, however, they still hosted substantial amounts of B cells (**Figure 4C**). ASCs were not detected in the LNs of CD23-Cre $Brg1^{fl/fl}$ and a similar trend was observed in γ1-Cre $Brg1^{fl/fl}$ mice, although in some mice ASCs were observed in this model (**Figures 4C, D**). Most importantly, GC B cells were not detected in the LNs of immunized CD23-Cre $Brg1^{fl/fl}$ and γ1-Cre $Brg1^{fl/fl}$ mice (**Figures 4E, F**). We conclude that the deficiency in the generation of ASCs in response to immunization is primarily due to a severe defect in GC formation.

To further substantiate our findings, we examined the role of Brg1 in immune responses within Peyer's patches, lymphoid organs that constantly host GCs driven by gut-derived antigens. In CD23-Cre $Brg1^{fl/fl}$ the frequency of GC B cells in PPs was severely reduced, although in most mice, a clear GC cell population could be detected (**Figure 4G**). Remarkably, nearly all of the remaining GC B cells in PPs of $Brg1^{fl/fl}$ mice carried an IgA BCR and very few cells were $IgG1^+$ (**Figure 4H**). These findings reveal that Brg1 is important for effective formation of $IgG1^+$ GC B cells in response to gut-derived antigens whereas IgA^+ GC B cells are less dependent on Brg1. Analysis of PP GCs in γ1-Cre $Brg1^{fl/fl}$ mice showed normal frequency of GC cells (**Figure S3A**) but nearly no $IgG1^+$ B cells were detected (**Figure S3B**). In γ1-Cre mice, Cre-mediated recombination in IgA^+ B cells in PPs is very ineffective and thus the IgA B cell compartment cannot be considered as Brg1-deficient (53). To validate a role for Brg1 in CSR, we performed *in vitro* activation of CD23-Cre splenic B cells using LPS and IL-4 and observed a significant reduction in $IgG1^+$ Brg1-deficient B cells (**Figure S3C**). Collectively, we conclude that Brg1 is required for the formation of $IgG1^+$ GC B cells in immune responses that are driven by gut-derived antigens within PPs.

DISCUSSION

In this study, we examined how Brg1 regulates gene expression through chromatin modulation in B cells. We have mapped the transcriptional response, chromatin landscape and Brg1 interactions with promoters and enhancers during B cell activation and found several hundred genes that are directly and indirectly regulated by Brg1. The majority of these genes were activation-induced genes, associated with cell cycle functions, that support B cell expansion. Specifically, we find that Brg1 promotes chromatin accessibility in enhancer regions, leading to transcriptional activation of genes that are essential for proper B cell proliferation. Accordingly, regulation of B cell activation by Brg1 is essential for GC formation and the establishment of long-lasting immunity.

What are the mechanistic details of Brg1 in regulating those genes? Our data show that Brg1 predominantly binds promoter and enhancer regions of the genes it regulates, defined by histone marks H3K27ac and H3K4me1 that occur concomitantly with Brg1 binding. These genes are then activated by diverse activating transcription factors which were previously shown to critically affect GC functions including Myc, which is essential for B cell proliferation and affinity-based selection (55, 56). In line with the binding of activating and inhibitory transcription factors at sites of Brg1 binding, we identified a subset of genes that are not induced in absence of Brg1, and also an additional

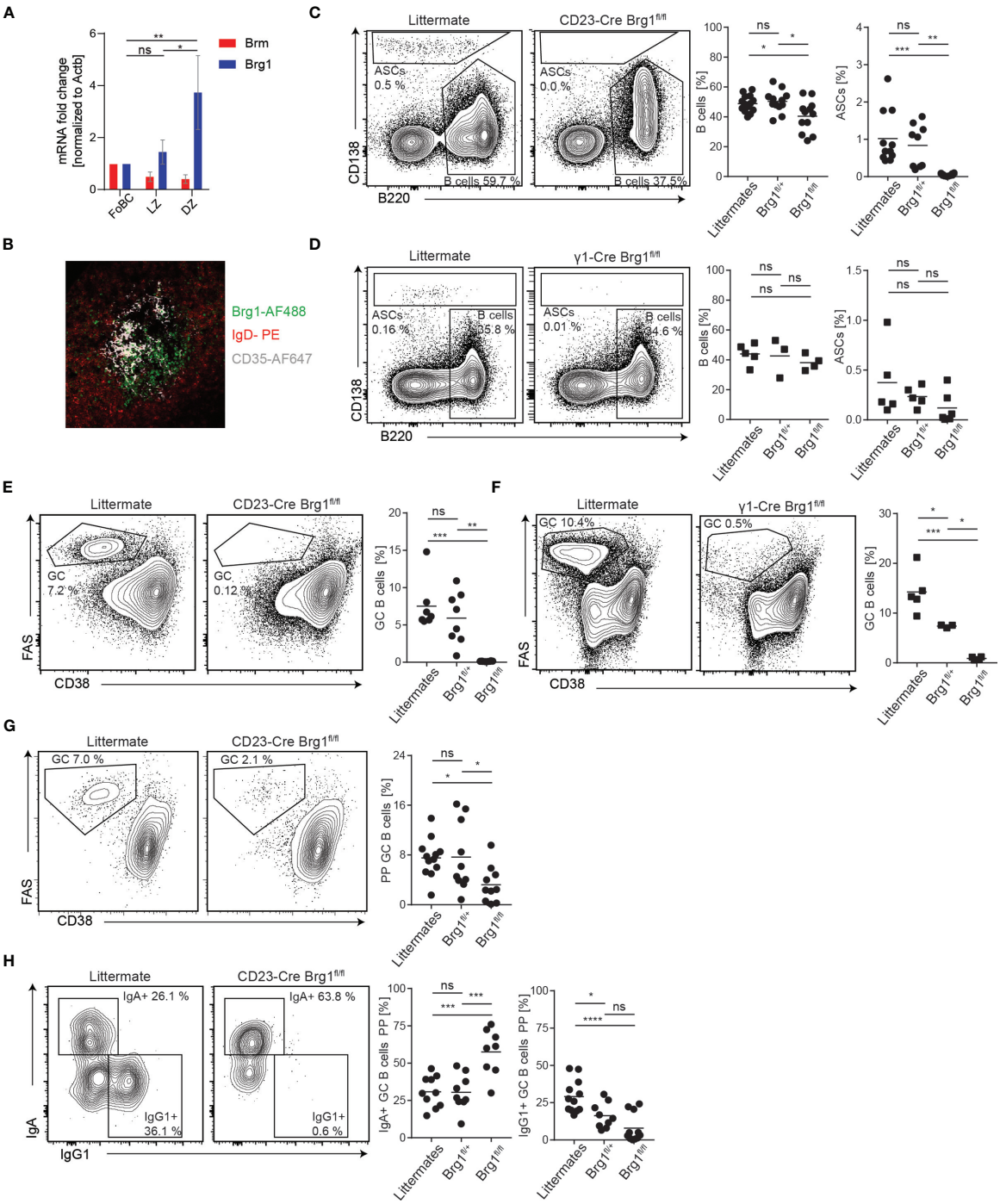

FIGURE 4 | Formation of germinal centers depends on Brg1. **(A)** qRT-PCR analysis of Brm and Brg1 RNA levels relative to Actin B levels in follicular B cells (FoBC), light zone (LZ), and dark zone (DZ) B cells; n = 5 mice. One-way ANOVA with *post hoc* Tukey's multiple comparisons test was performed, following p values for differences in Brg1 RNA levels are represented by the asterisks': $p<0.05$ = *; $p<0.01$ = **. Changes in Brm RNA levels were not significant. **(B)** Staining for IgD-PE (naive B cells), CD35-AF647 (follicular dendritic cells in the LZ) and Brg1 (clone H-88, detected with an anti-rabbit-IgG-AF488 secondary antibody) in LN-derived from immunized mouse **(C)** Naive B cell and ASC percentages in inguinal LN determined by flow cytometry, 7d after injection of KLH in CFA. Each dot represents one mouse, n = 9 - 12 mice per group. One-way ANOVA with post hoc Tukey's multiple comparisons test was used for statistical analysis. Following p values are represented by the asterisks' in this figure: $p<0.05$ = *; $p<0.01$ = **; $p<0.001$ = ***; $p<0.0001$ = ****; $p>0.05$ = ns (not significant). **(D)** Naive B cell and ASC percentages in inguinal LN determined by flow cytometry 7d after injection of KLH in CFA. **(E)** The fraction of GC B cells in inguinal LN determined by flow cytometry, 7d after injection of KLH in CFA. **(F)** GC B cells in inguinal LN determined by flow cytometry in immunized γ1-Cre littermate, $Brg1^{fl/+}$ and $Brg1^{fl/fl}$ mice, 7d after injection of KLH in CFA. **(G)** Flow cytometric analysis of PP GCs in CD23-Cre littermate, $Brg1^{fl/+}$ and $Brg1^{fl/fl}$ mice. **(H)** Quantification of IgA^+ and $IgG1^+$ B cells in PP in CD23-Cre littermate, $Brg1^{fl/+}$ and $Brg1^{fl/fl}$ mice.

subset of genes that are not sufficiently suppressed. Of note, in mature B cells, Brg1 does not play a role in the regulation of *Myc* as previously shown in developing B cells in the BM (24). Nonetheless, plenty of MYC downstream targets were downregulated in absence of Brg1, suggesting that this chromatin remodeling complex creates NRDs to enable MYC binding and function. Therefore, we define a new additional mechanism of action of the BAF complex that regulates MYC targets within the same cell lineage.

Our data show that Brg1 binds the majority of open-chromatin regions and active enhancers in activated B cells and that genes whose promoters interact with Brg1-bound enhancers are downregulated in Brg1-deficient cells. These findings support previous studies showing that Brg1 is required for enhancer activation through eviction of nucleosomes (24) and robust acetylation of chromatin (51) at enhancer regions.

We found that Brg1 recruitment to enhancers was more frequent in resting B cells than in activated B cells, suggesting Brg1 might be required for the initial activation of these enhancers, allowing the cells to acquire the proper transcriptional response to LPS activation. This is similar to H3K4me1, which marks poised enhancers and was reported to be diminished following B cell LPS activation (45). In addition, we found increased Brg1 occupancy in enhancers that interact with multiple promoters. Through these interactions, Brg1 can be involved in coordinated control over multiple genes, which can explain the strong impact of Brg1 loss on the expression of hundreds of genes. Although the possibility of a secondary effect cannot be completely excluded, the fact that we observe changes in genes whose promoters and enhancers are Brg1 targets, strongly suggests a direct effect.

Given the cell cycle-centered genetic profile related to Brg1-mediated functions, it is unsurprising that Brg1 is predominantly expressed in the DZ of the GC, as this is the primary site where GC B cells proliferate. Accordingly, both of our mouse models lack GC reactions which explain the strong defect in antibody formation. Yet, Brg1 was not essential for the generation of all bone-marrow resident PCs. Furthermore, the Brg1-deficient GC B cells observed in PPs were class-switched to IgA whereas IgG1 class-switched cells, which highly depend on T cell help, were not detected. Since IgA is less dependent on T cell help (52), these findings suggest that Brg1 might not be essential for T cell-independent responses. Thus, whereas IgG1 responses are Brg1-dependent it is most likely that the PP GCs are defective as well, further investigation to expose the role of Brg1 in CSR to IgA is required.

Collectively, our data highlight new mechanistic insights into the mode of action of Brg1 in B cell activation and raise the hypothesis that the main role of this chromatin remodeler, also in other physiological contexts, lies in the guidance of enhancer-promoter pairings. On the one hand, this would explain its striking role in the differentiation of diverse tissues, as lineage-specific transcription factors frequently bind enhancers remotely apart from their target genes. Without Brg1, the pairing of promoters and enhancers might be impaired and therefore gene transcription cannot be properly induced. On the other hand, this hypothesis also fits the seemingly contradicting roles for Brg1 in different cancer cells, both previously described as a tumor suppressor and oncogene. As Brg1 does not exert transcriptional regulation by itself but rather enables functions of other transcription factors, the impacts of a Brg1 loss depend on the transcription factor expression in a given tumor cell. Together, our findings provide an explanation for how Brg1 regulates multiple genetic programs that support cell proliferation and differentiation in healthy and pathological conditions.

DATA AVAILABILITY STATEMENT

All sequencing data have been deposited in GEO (accession number GSE180994). The data is publicly available using following link: https://www.ncbi.nlm.nih.gov/geo/query/acc.cgi?acc=GSE180994.

ETHICS STATEMENT

The animal study was reviewed and approved by The Weizmann Institute IACUC committee.

AUTHOR CONTRIBUTIONS

Conceptualization, DS, HH, and ZS. Investigation, DS and AH. Formal analysis, DS and HH. Resources, DS and AH. Visualization: DS and HH, Software, HH. Data curation, DS and HH. Writing - original draft, DS and HH. Writing – review and editing, DS, HH and ZS, Supervision, project administration management, and funding acquisition, ZS. All authors contributed to the article and approved the submitted version.

FUNDING

ZS is supported by the Israel Science Foundation (ISF) grant no. 1090/18 and the Morris Kahn Institute for Human Immunology. ZS is also supported by grants from The Benoziyo Endowment Fund for the Advancement of Science, The Sir Charles Clore Research Prize, Comisaroff Family Trust, Irma & Jacques Ber-Lehmsdorf Foundation, Gerald O. Mann Charitable Foundation and David M. Polen Charitable Trust. ZS is a member of the European Molecular Biology Organization (EMBO) Young Investigator Program.

SUPPLEMENTARY MATERIAL

The Supplementary Material for this article can be found online at: https://www.frontiersin.org/articles/10.3389/fimmu.2021.705848/full#supplementary-material

Supplementary Figure 1 | Brg1 is required for proper expression of cell-cycle-related genes in LPS-stimulated B cells. **(A)** Western Blot analysis for Brg1 protein levels in splenic B cells of littermate and Brg1$^{fl/fl}$ CD23-Cre mice. B cells were activated for 4 days with LPS and IL-4. β-Actin serves as loading control. **(B, C)** Flow cytometric analysis of the live-dead marker 7-AAD as well as B cell activation marker CD86 after 18 hours of activation with LPS and IL-4. Background staining was determined from CD86-PE on B220-negative splenic cells (non-B cells). **(D)** UCSC genome browser tracks showing the loci of E2f8, which was significantly downregulated in CD23-Cre Brg1$^{fl/fl}$ B cells, and Bach2, which was significantly upregulated in CD23-Cre Brg1$^{fl/fl}$ cells. Tracks show the expression levels of the genes, measured by RNA-seq, in activated B cells from littermates, CD23-Cre Brg1$^{fl/+}$, and Brg1$^{fl/fl}$ mice, and ChIP-seq signal of Brg1 in resting and activated B cells, compared to input control. Green highlight: binding of Brg1 in the promoter regions. Orange highlights: 3' end exons covered by RNA-seq. rB cells, resting B cells. aB cells, activated B cells. **(E)** Gene set enrichment plots for Myc targets and E2f targets from the hallmark gene sets. **(F)** Expression levels of E2f4 and Myc, measured by RNA seq, in control samples, including CD23-Cre Brg1$^{fl/fl}$ and littermate controls. Normalization of reading counts and calculation of p value were done using Deseq2. **(G)** Boxplots indicating the median, quartiles, and 5th and 95th percentiles of mean Brg1 coverage across all FAIRE-seq and STARR-seq peaks in resting B cells. P values were calculated by a two-sided Wilcoxon rank-sum test. **(H)** Boxplots indicating the median, quartiles, and 5th and 95th percentiles of mean Brg1 coverage across all enhancers binding 1-4 promoters and enhancers binding more than 4 enhancers, in resting and activated B cells. P values were calculated by a two-sided Wilcoxon rank-sum test. **(I)** Venn diagram showing overlap between 5,841 ATAC-seq peaks overlapping activated B cells enhancers, 752 ATAC-seq peaks with significantly reduced chromatin accessibility in Brg1-deficient cells, and 322 ATAC-seq peaks with significantly increased chromatin accessibility in Brg1-deficient cells. **(J)** Venn diagram showing overlap between 13,890 Brg1 bound ATAC-seq peaks, 752 ATAC-seq peaks with significantly reduced chromatin accessibility in Brg1-deficient cells, and 322 ATAC-seq peaks with significantly increased chromatin accessibility in Brg1-deficient cells.

Supplementary Figure 2 | Brg1 is not critical for the expression of Blimp-1 and IRF4 in B cells following LPS activation. **(A)** Gating strategy used for analysis of PCs in BM samples. **(B)** Analysis of IRF4 and Blimp-1 protein levels assessed by intracellular flow cytometry in CD23-Cre littermates or Brg1$^{fl/fl}$ splenic B cells before and after 4 days activation with LPS and IL-4. Statistics were calculated with students' t-test. **(C)** Gating strategy applied to detect GC B cells in lymph nodes and PPs.

Supplementary Figure 3 | Brg1 is required for the generation of IgG1+ germinal centers B cells in Peyer's patches. **(A)** Analysis of germinal center size in PPs of γ1-Cre control (littermate or Brg1$^{fl/+}$) or Brg1$^{fl/fl}$ mice analyzed by flow cytometry. Statistic s were calculated with students' t-test. **(B)** Analysis of class-switch recombination to IgA and IgG1 in Peyer's patches of γ1-Cre control (littermate or Brg1$^{fl/+}$) or Brg1$^{fl/fl}$ mice analyzed by flow cytometry. Statistics were calculated with students' t-test. **(C)** Analysis of class-switch recombination to IgG1 in splenic B cells derived from littermate, Brg1$^{fl/+}$ or Brg1$^{fl/fl}$ CD23-Cre mice after 4 days activation with LPS and IL-4. Statistics were calculated using one-way ANOVA with *post hoc* Tukey's multiple comparisons. CellTrace Violet staining indicates the magnitude of B cell proliferation.

REFERENCES

1. Nutt SL, Hodgkin PD, Tarlinton DM, Corcoran LM. The Generation of Antibody-Secreting Plasma Cells. *Nat Rev Immunol* (2015) 15:160–71. doi: 10.1038/nri3795
2. Victora GD, Nussenzweig MC. Germinal Centers. *Annu Rev Immunol* (2012) 30:429–57. doi: 10.1146/annurev-immunol-020711-075032
3. Elsner RA, Shlomchik MJ. Germinal Center and Extrafollicular B Cell Responses in Vaccination, Immunity, and Autoimmunity. *Immunity* (2020) 53:1136–50. doi: 10.1016/j.immuni.2020.11.006
4. Cyster JG, Allen CDC. B Cell Responses: Cell Interaction Dynamics and Decisions. *Cell* (2019) 177:524–40. doi: 10.1016/j.cell.2019.03.016
5. Pritchard GH, Pepper M. Memory B Cell Heterogeneity: Remembrance of Things Past. *J Leukocyte Biol* (2018) 103(2):269–74. doi: 10.1002/jlb.4mr0517-215r
6. Shi W, Liao Y, Willis SN, Taubenheim N, Inouye M, Tarlinton DM, et al. Transcriptional Profiling of Mouse B Cell Terminal Differentiation Defines a Signature for Antibody-Secreting Plasma Cells. *Nat Immunol* (2015) 16:663–73. doi: 10.1038/ni.3154
7. Turner M, Díaz-Muñoz MD. RNA-Binding Proteins Control Gene Expression and Cell Fate in the Immune System. *Nat Immunol* (2018) 19:120–9. doi: 10.1038/s41590-017-0028-4
8. Basso K, Dalla-Favera R. Germinal Centres and B Cell Lymphomagenesis. *Nat Rev Immunol* (2015) 15:172–84. doi: 10.1038/nri3814
9. Struhl K, Segal E. Determinants of Nucleosome Positioning. *Nat Struct Mol Biol* (2013) 20:267–73. doi: 10.1038/nsmb.2506
10. Ren G, Jin W, Cui K, Rodrigez J, Hu G, Zhang Z, et al. CTCF-Mediated Enhancer-Promoter Interaction Is a Critical Regulator of Cell-To-Cell Variation of Gene Expression. *Mol Cell* (2017) 67:1049–58.e6. doi: 10.1016/j.molcel.2017.08.026
11. He S, Wu Z, Tian Y, Yu Z, Yu J, Wang X, et al. Structure of Nucleosome-Bound Human BAF Complex. *Science* (2020) 367:875–81. doi: 10.1126/science.aaz9761
12. Centore RC, Sandoval GJ, Soares LMM, Kadoch C, Chan HM. Mammalian SWI/SNF Chromatin Remodeling Complexes: Emerging Mechanisms and Therapeutic Strategies. *Trends Genet* (2020) 36:936–50. doi: 10.1016/j.tig.2020.07.011
13. Alfert A, Moreno N, Kerl K. The BAF Complex in Development and Disease. *Epigenet Chromatin* (2019) 12:19. doi: 10.1186/s13072-019-0264-y
14. Wilson BG, Roberts CWM. SWI/SNF Nucleosome Remodellers and Cancer. *Nat Rev Cancer* (2011) 11:481–92. doi: 10.1038/nrc3068
15. Zhang X, Li B, Li W, Ma L, Zheng D, Li L, et al. Transcriptional Repression by the BRG1-SWI/SNF Complex Affects the Pluripotency of Human Embryonic Stem Cells. *Stem Cell Rep* (2014) 3:460–74. doi: 10.1016/j.stemcr.2014.07.004
16. Kidder BL, Palmer S, Knott JG. SWI/SNF-Brg1 Regulates Self-Renewal and Occupies Core Pluripotency-Related Genes in Embryonic Stem Cells. *Stem Cells* (2009) 27:317–28. doi: 10.1634/stemcells.2008-0710
17. Sokpor G, Xie Y, Rosenbusch J, Tuoc T. Chromatin Remodeling BAF (SWI/SNF) Complexes in Neural Development and Disorders. *Front Mol Neurosci* (2017) 10:243. doi: 10.3389/fnmol.2017.00243
18. Hang CT, Yang J, Han P, Cheng H-L, Shang C, Ashley E, et al. Chromatin Regulation by Brg1 Underlies Heart Muscle Development and Disease. *Nature* (2010) 466:62–7. doi: 10.1038/nature09130
19. Hodges C, Kirkland JG. The Many Roles of BAF (mSWI/SNF) and PBAF Complexes in Cancer. *Cold Spring Harb Perspect Med* (2016) 6(8):a026930. doi: 10.1101/cshperspect.a026930
20. Strobeck MW, Knudsen KE, Fribourg AF, DeCristofaro MF, Weissman BE, Imbalzano AN, et al. BRG-1 is Required for RB-Mediated Cell Cycle Arrest. *Proc Natl Acad Sci U S A* (2000) 97:7748–53. doi: 10.1073/pnas.97.14.7748
21. Wu Q, Lian JB, Stein JL, Stein GS, Nickerson JA, Imbalzano AN. The BRG1 ATPase of Human SWI/SNF Chromatin Remodeling Enzymes as a Driver of Cancer. *Epigenomics* (2017) pp:919–31. doi: 10.2217/epi-2017-0034
22. Choi J, Ko M, Jeon S, Jeon Y, Park K, Lee C, et al. The SWI/SNF-Like BAF Complex is Essential for Early B Cell Development. *J Immunol* (2012) 188:3791–803. doi: 10.4049/jimmunol.1103390
23. Gao H, Lukin K, Ramírez J, Fields S, Lopez D, Hagman J. Opposing Effects of SWI/SNF and Mi-2/NuRD Chromatin Remodeling Complexes on Epigenetic Reprogramming by EBF and Pax5. *Proc Natl Acad Sci U S A* (2009) 106:11258–63. doi: 10.1073/pnas.0809485106
24. Bossen C, Murre CS, Chang AN, Mansson R, Rodewald H-R, Murre C. The Chromatin Remodeler Brg1 Activates Enhancer Repertoires to Establish B Cell Identity and Modulate Cell Growth. *Nat Immunol* (2015) 16:775–84. doi: 10.1038/ni.3170
25. Wang Y, Zolotarev N, Yang C-Y, Rambold A, Mittler G, Grosschedl R. A Prion-Like Domain in Transcription Factor EBF1 Promotes Phase Separation and Enables B Cell Programming of Progenitor Chromatin. *Immunity* (2020) 53:1151–67.e6. doi: 10.1016/j.immuni.2020.10.009

26. Husain A, Begum NA, Taniguchi T, Taniguchi H, Kobayashi M, Honjo T. Chromatin Remodeller SMARCA4 Recruits Topoisomerase 1 and Suppresses Transcription-Associated Genomic Instability. *Nat Commun* (2016) 7:10549. doi: 10.1038/ncomms10549
27. Kieffer-Kwon K-R, Nimura K, Rao SSP, Xu J, Jung S, Pekowska A, et al. Myc Regulates Chromatin Decompaction and Nuclear Architecture During B Cell Activation. *Mol Cell* (2017) 67:566–78.e10. doi: 10.1016/j.molcel.2017.07.013
28. Bultman S, Gebuhr T, Yee D, La Mantia C, Nicholson J, Gilliam A, et al. A Brg1 Null Mutation in the Mouse Reveals Functional Differences Among Mammalian SWI/SNF Complexes. *Mol Cell* (2000) 6:1287–95. doi: 10.1016/S1097-2765(00)00127-1
29. Kohen R, Barlev J, Hornung G, Stelzer G, Feldmesser E, Kogan K, et al. UTAP: User-Friendly Transcriptome Analysis Pipeline. *BMC Bioinf* (2019) 20:154. doi: 10.1186/s12859-019-2728-2
30. Dobin A, Davis CA, Schlesinger F, Drenkow J, Zaleski C, Jha S, et al. STAR: Ultrafast Universal RNA-Seq Aligner. *Bioinformatics* (2013) 29:15–21. doi: 10.1093/bioinformatics/bts635
31. Anders S, Pyl PT, Huber W. HTSeq–A Python Framework to Work With High-Throughput Sequencing Data. *Bioinformatics* (2015) 31:166–9. doi: 10.1093/bioinformatics/btu638
32. Love MI, Huber W, Anders S. Moderated Estimation of Fold Change and Dispersion for RNA-Seq Data With Deseq2. *Genome Biol* (2014) 15:550. doi: 10.1186/s13059-014-0550-8
33. Buenrostro JD, Giresi PG, Zaba LC, Chang HY, Greenleaf WJ. Transposition of Native Chromatin for Fast and Sensitive Epigenomic Profiling of Open Chromatin, DNA-Binding Proteins and Nucleosome Position. *Nat Methods* (2013) 10:1213–8. doi: 10.1038/nmeth.2688
34. Langmead B, Trapnell C, Pop M, Salzberg SL. Ultrafast and Memory-Efficient Alignment of Short DNA Sequences to the Human Genome. *Genome Biol* (2009) 10:R25. doi: 10.1186/gb-2009-10-3-r25
35. Ramírez F, Ryan DP, Grüning B, Bhardwaj V, Kilpert F, Richter AS, et al. deepTools2: A Next Generation Web Server for Deep-Sequencing Data Analysis. *Nucleic Acids Res* (2016) 44:W160–5. doi: 10.1093/nar/gkw257
36. Zhang Y, Liu T, Meyer CA, Eeckhoute J, Johnson DS, Bernstein BE, et al. Model-Based Analysis of ChIP-Seq (MACS). *Genome Biol* (2008) 9:R137. doi: 10.1186/gb-2008-9-9-r137
37. Heinz S, Benner C, Spann N, Bertolino E, Lin YC, Laslo P, et al. Simple Combinations of Lineage-Determining Transcription Factors Prime Cis-Regulatory Elements Required for Macrophage and B Cell Identities. *Mol Cell* (2010) 38:576–89. doi: 10.1016/j.molcel.2010.05.004
38. Karolchik D, Hinrichs AS, Kent WJ. The UCSC Genome Browser. *Curr Protoc Hum Genet* (2011) 71:18.6.1–33. doi: 10.1002/0471142905.hg1806s71
39. Eden E, Navon R, Steinfeld I, Lipson D, Yakhini Z. GOrilla: A Tool for Discovery and Visualization of Enriched GO Terms in Ranked Gene Lists. *BMC Bioinf* (2009) 10:48. doi: 10.1186/1471-2105-10-48
40. Supek F, Bošnjak M, Škunca N, Šmuc T. REVIGO Summarizes and Visualizes Long Lists of Gene Ontology Terms. *PLoS One* (2011) 6:e21800. doi: 10.1371/journal.pone.0021800
41. Subramanian A, Tamayo P, Mootha VK, Mukherjee S, Ebert BL, Gillette MA, et al. Gene Set Enrichment Analysis: A Knowledge-Based Approach for Interpreting Genome-Wide Expression Profiles. *Proc Natl Acad Sci U S A* (2005) 102:15545–50. doi: 10.1073/pnas.0506580102
42. Liberzon A, Subramanian A, Pinchback R, Thorvaldsdóttir H, Tamayo P, Mesirov JP. Molecular Signatures Database (MSigDB) 3.0. *Bioinformatics* (2011) 27:1739–40. doi: 10.1093/bioinformatics/btr260
43. Chen EY, Tan CM, Kou Y, Duan Q, Wang Z, Meirelles GV, et al. Enrichr: Interactive and Collaborative HTML5 Gene List Enrichment Analysis Tool. *BMC Bioinf* (2013) 14:128. doi: 10.1186/1471-2105-14-128
44. Lachmann A, Xu H, Krishnan J, Berger SI, Mazloom AR, Ma'ayan A. ChEA: Transcription Factor Regulation Inferred From Integrating Genome-Wide ChIP-X Experiments. *Bioinformatics* (2010) 26:2438–44. doi: 10.1093/bioinformatics/btq466
45. Chaudhri VK, Dienger-Stambaugh K, Wu Z, Shrestha M, Singh H. Charting the Cis-Regulome of Activated B Cells by Coupling Structural and Functional Genomics. *Nat Immunol* (2020) 21:210–20. doi: 10.1038/s41590-019-0565-0
46. Kwon K, Hutter C, Sun Q, Bilic I, Cobaleda C, Malin S, et al. Instructive Role of the Transcription Factor E2A in Early B Lymphopoiesis and Germinal Center B Cell Development. *Immunity* (2008) 28:751–62. doi: 10.1016/j.immuni.2008.04.014
47. Tesi A, de Pretis S, Furlan M, Filipuzzi M, Morelli MJ, Andronache A, et al. An Early Myc-Dependent Transcriptional Program Orchestrates Cell Growth During B-Cell Activation. *EMBO Rep* (2019) 20:e47987. doi: 10.15252/embr.201947987
48. Trotter KW, Archer TK. The BRG1 Transcriptional Coregulator. *Nucl Recept Signal* (2008) 6:e004. doi: 10.1621/nrs.06004
49. Ahmad KF, Melnick A, Lax S, Bouchard D, Liu J, Kiang C-L, et al. Mechanism of SMRT Corepressor Recruitment by the BCL6 BTB Domain. *Mol Cell* (2003) 12:1551–64. doi: 10.1016/S1097-2765(03)00454-4
50. Hatzi K, Jiang Y, Huang C, Garrett-Bakelman F, Gearhart MD, Giannopoulou EG, et al. A Hybrid Mechanism of Action for BCL6 in B Cells Defined by Formation of Functionally Distinct Complexes at Enhancers and Promoters. *Cell Rep* (2013) 4:578–88. doi: 10.1016/j.celrep.2013.06.016
51. Alexander JM, Hota SK, He D, Thomas S, Ho L, Pennacchio LA, et al. Brg1 Modulates Enhancer Activation in Mesoderm Lineage Commitment. *Development* (2015) 142:1418–30. doi: 10.1242/dev.109496
52. Biram A, Winter E, Denton AE, Zaretsky I, Dassa B, Bemark M, et al. B Cell Diversification Is Uncoupled From SAP-Mediated Selection Forces in Chronic Germinal Centers Within Peyer's Patches. *Cell Rep* (2020) pp:1910–22.e5. doi: 10.1016/j.celrep.2020.01.032
53. Casola S, Cattoretti G, Uyttersprot N, Koralov SB, Seagal J, Hao Z, et al. Tracking Germinal Center B Cells Expressing Germ-Line Immunoglobulin Gamma1 Transcripts by Conditional Gene Targeting. *Proc Natl Acad Sci U S A* (2006) 103:7396–401. doi: 10.1073/pnas.0602353103
54. Tangye SG. Staying Alive: Regulation of Plasma Cell Survival. *Trends Immunol* (2011) 32:595–602. doi: 10.1016/j.it.2011.09.001
55. Dominguez-Sola D, Victora GD, Ying CY, Phan RT, Saito M, Nussenzweig MC, et al. The Proto-Oncogene MYC Is Required for Selection in the Germinal Center and Cyclic Reentry. *Nat Immunol* (2012) 13:1083–91. doi: 10.1038/ni.2428
56. Calado DP, Sasaki Y, Godinho SA, Pellerin A, Köchert K, Sleckman BP, et al. The Cell-Cycle Regulator C-Myc is Essential for the Formation and Maintenance of Germinal Centers. *Nat Immunol* (2012) 13:1092–100. doi: 10.1038/ni.2418
57. Karolchikz D, Hinrichs AS, Kent WJ. The UCSC Genome Browser. *Current Protocols in Human Genetics* (2011) 71:18.6.1–33. doi: 10.1002/0471142905.hg1806s71

Conflict of Interest: The authors declare that the research was conducted in the absence of any commercial or financial relationships that could be construed as a potential conflict of interest.

Publisher's Note: All claims expressed in this article are solely those of the authors and do not necessarily represent those of their affiliated organizations, or those of the publisher, the editors and the reviewers. Any product that may be evaluated in this article, or claim that may be made by its manufacturer, is not guaranteed or endorsed by the publisher.

frontiers in Immunology

REVIEW
published: 14 September 2021
doi: 10.3389/fimmu.2021.738216

Long-Range Control of Class Switch Recombination by Transcriptional Regulatory Elements

*Audrey Dauba and Ahmed Amine Khamlichi**

Institut de Pharmacologie et de Biologie Structurale, IPBS, Université de Toulouse, CNRS, Université Paul Sabatier, Toulouse, France

Immunoglobulin class switch recombination (CSR) plays a crucial role in adaptive immune responses through a change of the effector functions of antibodies and is triggered by T-cell-dependent as well as T-cell-independent antigens. Signals generated following encounter with each type of antigen direct CSR to different isotypes. At the genomic level, CSR occurs between highly repetitive switch sequences located upstream of the constant gene exons of the immunoglobulin heavy chain locus. Transcription of switch sequences is mandatory for CSR and is induced in a stimulation-dependent manner. Switch transcription takes place within dynamic chromatin domains and is regulated by long-range regulatory elements which promote alignment of partner switch regions in CSR centers. Here, we review recent work and models that account for the function of long-range transcriptional regulatory elements and the chromatin-based mechanisms involved in the control of CSR.

Keywords: *IgH* locus, class switch recombination, switch transcription, enhancer, insulator, long-range interactions, chromatin loop extrusion

OPEN ACCESS

Edited by:
Michel Cogne, University of Limoges, France

Reviewed by:
Patricia Johanna Gearhart, National Institutes of Health (NIH), United States
Duane R. Wesemann, Brigham and Women's Hospital and Harvard Medical School, United States

***Correspondence:**
Ahmed Amine Khamlichi
ahmed.khamlichi@ipbs.fr
orcid.org/0000-0002-6523-2035

Specialty section:
This article was submitted to B Cell Biology, a section of the journal Frontiers in Immunology

Received: *08 July 2021*
Accepted: *17 August 2021*
Published: *14 September 2021*

Citation:
Dauba A and Khamlichi AA (2021) Long-Range Control of Class Switch Recombination by Transcriptional Regulatory Elements. Front. Immunol. 12:738216. doi: 10.3389/fimmu.2021.738216

1 OUTLINE OF CSR IN AND OUT OF GERMINAL CENTERS

B lymphocytes have a remarkable ability to somatically alter their immunoglobulin (*Ig*) loci at different stages of their development. In developing B cells, *Ig* loci undergo V(D)J recombination catalyzed by the RAG1/RAG2 (RAG) complex. V(D)J recombination targets the variable regions of both Ig heavy chain (*IgH*) and Ig light chain (*IgL*) loci and lies at the basis of the vast primary antibody repertoire (1–4). Upon antigen challenge, mature B cells can further diversify the variable regions of *IgH* and *IgL* genes through somatic hypermutation (SHM) and the constant (C_H) genes of the *IgH* locus through class switch recombination (CSR). The enzyme activation-induced cytidine deaminase (AID) is absolutely required for SHM and CSR and initiates these processes *via* transcription-dependent cytosine deamination of single-stranded DNA targets (5–9).

Depending on the type of the eliciting antigen, humoral responses are classically categorized in T-cell-dependent and T-cell-independent responses. SHM is a hallmark of affinity maturation featuring an increase in the affinity of antibodies (Abs), as an outcome of SHM in germinal centers (GCs) in the context of T-cell-dependent responses (5, 10). In a typical GC response, SHM generates a pool of mutated B cells that compete for a variety of signals required for their survival, delivered by the other GC-resident cells in an affinity-dependent manner. Positively selected B cells, with higher-affinity B-cell receptors, ultimately produce memory B cells and long-lived Ab secreting plasma cells, which provide effective protection against future reinfection (10).

CSR occurs *in vivo* following immunization or infection and enables antigen-activated, IgM^+-expressing B cells to change the constant domains of Igμ heavy chains, hence the expression of novel isotypes (IgG, IgE, or IgA) with different effector functions (11–13). Switching from IgM to other isotypes depends on the nature of antigen, the cytokines produced by other immune cell types, and the interactions engaging activated B cells with the other immune cell types (helper T cells, dendritic cells…) (11–13). The signals received by the B cell trigger different signaling pathways that induce a complex interplay between 3D conformational changes of the *IgH* locus, epigenetic modifications, and transcriptional programs that mobilize a set of transcription factors that induce or suppress transcription of C_H genes (6, 8, 14–17).

Besides CSR induced in T-cell-independent responses which do not involve GC formation, CSR in the context of T-cell-dependent responses has long been assimilated to GCs (10, 18). However, seminal observations on the kinetics of switch transcripts appearance and CSR [e.g., (19–21)] suggested that CSR occurs outside GCs. This notion recently gained support from the analyses of the earliest stages of an immune response, showing CSR at the early onset of GC formation, prior to SHM (22).

CSR is usually triggered *in vitro* by culturing splenic B cells in the presence of various cocktails of cytokines and/or mitogens which induce both AID and CSR. For instance, mouse B cells are typically induced to switch to IgG3 and IgG2b when activated with lipopolysaccharide (LPS) and to IgG1 and IgE in the presence of LPS+IL4 or anti-CD40+IL4. These culture systems allow the investigators to address B-cell-autonomous mechanisms that are more difficult to tackle in the context of the complex molecular processes and cellular interactions triggered *in vivo* by antigens (6).

Most, if not all, of our knowledge on the transcriptional elements that control CSR derives from the use of cultured splenic B2 B cells, the main B-cell population in the spleen. However, CSR can also take place in B1 B cells, which form the major population in the pleural and peritoneal cavities. B1 B cells have a distinct antigen specificity, display different cell surface markers, and switch to IgA preferentially (23, 24). However, the transcriptional mechanisms involved in CSR in B1 B cells have just begun to be investigated.

CSR is not restricted to activated mature B cells. It has long been known that it can occur in developing B cells, though at a low frequency. Indeed, various studies described CSR events in Abelson murine leukemia virus (A-MuLV)-transformed pro-B lines [e.g., (25–29)] and early primary B cells as well [e.g., (30–35)]. In fact, seminal discoveries on the importance of transcriptional mechanisms in CSR were made by using pro-B and pre-B lines [e.g., (36–38)]. Nonetheless, here too, there is still much to learn about the transcriptional elements that control CSR.

Regardless of the developmental stage, CSR occurs between highly repetitive switch (S) sequences, located upstream of the C_H gene exons, whose transcription is mandatory for CSR, and is driven by specific promoters (called I promoters) in a signal-dependent manner (6, 8, 14) (**Figure 1**). Switch transcription (ST) targets AID activity, which initiates DNA cleavage by deaminating exposed cytosines into uracils at the universal donor, Sμ region, and the activated downstream S region. The uracils are processed by the base excision and mismatch repair pathways, ultimately leading to double-strand break (DSB) intermediates. The DSBs are taken in charge by the DNA damage response pathway and repaired by the classical and alternative non-homologous end joining pathways (9, 39, 40).

ST is controlled by various distant *cis*-acting elements, described in detail below. This control often involves long-range interactions that juxtapose transcribed partner S sequences and promote CSR initiation. In this review, we mainly summarize recent work and models on the activity of these regulatory elements and on the long-range chromatin-based mechanisms that control ST and CSR.

2 *IgH* TRANSCRIPTIONAL ELEMENTS THAT CONTROL CSR

The critical transcriptional elements involved in ST and CSR have long been thought to be confined within the C_H region, bordered by the Eμ enhancer and the 3' CTCF binding elements (3'CBEs) (**Figure 1**). However, recent studies involved additional remote non-*IgH* elements in the control of CSR. Here, we will focus on the role of enhancers and CTCF insulators as revealed by mutational studies on the endogenous murine *IgH* locus.

2.1 The Lingering Mystery of Eμ Enhancer

The Eμ enhancer comprises the core enhancer (cEμ) flanked by matrix attachment regions (41) (**Figure 2**). The cEμ coincides with Iμ promoter, which likely explains the constitutive transcriptional activity of Iμ (65, 66), contrasting in this regard with the inducible activity of downstream I promoters.

Deletion of Eμ led to a dramatic decrease of IgM^+ population in Peyer's patches but did not affect the number of B cells engaged in the GC reaction (45). In the spleen, the number of follicular (FO) B cells was significantly reduced, whereas the number of marginal zone (MZ) B cells was unaffected. Nonetheless, surface staining revealed that MZ and FO B cells expressed comparable levels of IgM, suggesting that Eμ deletion did not impact μ heavy chain (HC) gene expression in mature B cells (45). Slightly reduced IgG1 serum levels were found in Eμ-deleted mice, which otherwise exhibited normal response upon immunization (45).

The role of Eμ enhancer in CSR is far from clear since deletion of either cEμ or Eμ enhancer only marginally affected CSR (43–45). In particular, cEμ deletion markedly reduced Iμ transcript levels (44) but had no apparent effect on ST of acceptor S regions (67), on surface Ig expression or *IgH* isotype serum levels (43, 44) (**Figure 2** and associated table). The moderate effect of Eμ enhancer on CSR is surprising as Eμ activates the universal donor Sμ and interactions with the 3'RR and other essential elements for CSR (see below), suggesting the presence of redundant elements that render Eμ enhancer dispensable in activated mature B cells.

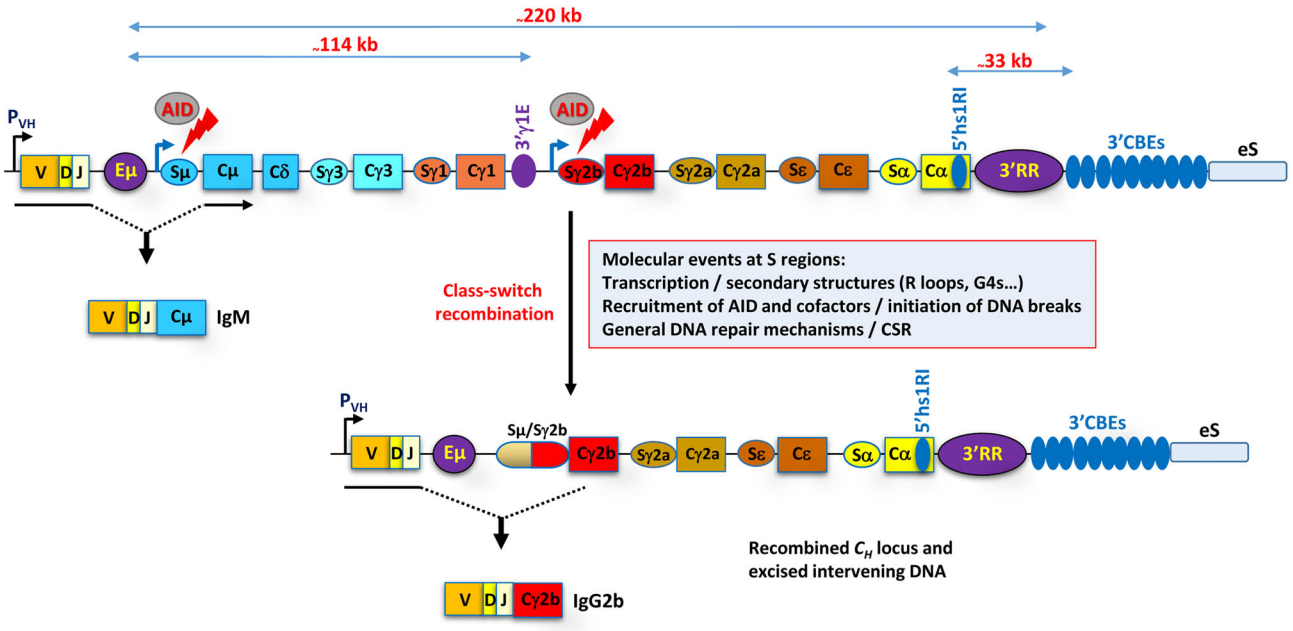

FIGURE 1 | Rearranged mouse *IgH* locus. The various regulatory elements, Eμ, 3'γ1E, 5'hs1RI, and 3'RR, and the 3' CTCF binding elements (3'CBEs) are depicted. Approximate distances are indicated on the top of the scheme. The promoter of the rearranged V(D)J gene is indicated by a black arrow. With the exception of *Cδ*, the C_H genes are structurally similar. They are composed of an I promoter followed by an I exon; highly repetitive, GC-rich S regions; and C_H exons (not depicted). The core S sequences vary in size, the shortest being Sε (~1 kb) and the largest Sγ1 (~10 kb), and contain characteristic repeated motifs including AID target motifs. The Iμ promoter is constitutive and coincides with the core Eμ enhancer, while the other I promoters are signal dependent and have typically no enhancer function. The constitutive Iμ promoter and (in this example) the induced Iγ2b promoter drive the transcription of Sμ and Sγ2b, respectively (blue arrows). AID targets the transcribed Sμ and Sγ2b regions (red arrows) and initiates DSBs. Repair of the breaks ultimately leads to CSR (fused Sμ/Sγ2b oval). Consequently, the IgM^+-expressing B cell switches to the expression of IgG2b (in this example) with novel effector functions. The eS region downstream of the 3'CBEs stands for ectopic S-like region (see main text for details and the table associated with **Figure 2**).

2.2 The *IgH* Locus Got Its Super-Enhancer: The 3' Regulatory Region

The major *IgH* control element in mature B cells is a long-range super-enhancer termed 3' regulatory region (3'RR) (17, 68) (**Figure 2**). The 3'RR (~28 kb) is composed of four B-cell-specific enhancers, hs3a, hs1,2, hs3b, and hs4, that act in synergy. hs1,2 is flanked by inverted repeated intervening sequences (IRISs) and lies at the center of a large palindromic region bordered by two inverted copies of hs3, hs3a and hs3b, whereas the distal hs4 enhancer is located outside of the palindrome (17, 68).

Beyond its key role in CSR discussed below, the 3'RR was also shown to control SHM (69) and *IgH* expression (51, 55), thus revealing the centrality of the 3'RR in the major molecular processes that take place at the *IgH* locus in activated mature B cells and plasma cells.

Deletion of the 3'RR markedly reduced the number of MZ B cells with no obvious effect on FO B cells. Nonetheless, the deletion impacted surface IgM expression on both populations (70). Among the 3'RR enhancers, hs4 appears to maintain μ gene expression in unstimulated MZ and FO B cells. However, upon antigen activation, hs4 is no longer required for this maintenance (53). Instead, the upstream 3'RR enhancers jointly gain a prominent role and control SHM, CSR, and Ig production (53).

Deletion of individual 3'RR enhancers had no effect on B-cell proliferation, ST, CSR, Ig serum isotype production, percentage of FO and MZ B cells in the spleen, or antigen-specific responses, suggesting a redundancy between these elements (48–50). In contrast, joint deletion of hs3b/hs4 severely impaired ST and CSR to all isotypes except for IgG1, which was only reduced (51). When the whole 3'RR was deleted, ST of and CSR to all isotypes were inhibited, with notable exception of Sγ1 ST and IgG1 CSR, which were severely reduced but readily detectable. Sμ transcript levels were also reduced in 3'RR-deleted B cells, though the reduction was moderate compared with downstream switch regions (55) (**Figure 2**).

An important question concerning the function of the 3'RR relates to the relative contribution of the core enhancers *versus* the whole structure of the 3'RR, in particular its large palindrome. In this regard, removal of the proximal hs3a-left IRIS-hs1,2 region reduced Sγ3, Sγ2b, and Sγ2a transcription (**Figure 2**). Ig production of all isotypes was significantly reduced *in vitro*, while only IgG3 and IgG2a serum levels were reduced (17, 52). When the left IRIS alone was deleted, but leaving intact hs3a and hs1,2 enhancers, only Sγ2a transcription

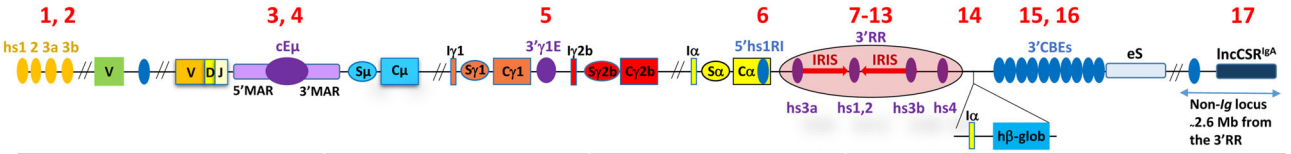

Mouse model	ST at acceptor S regions	Effect on CSR	Reference
1: Deletion of hs1	Not assayed	Not detectable	Perlot et al. 2010 (42)
2: Deletion of the hs1, 2, 3a, 3b cluster	Not assayed	Not detectable	Perlot et al. 2010 (42)
3: Deletion of cEμ	Moderate	Moderate	Sakai et al. 1999 (43); Perlot et al. 2005 (44)
4: Deletion of Eμ (cEμ+MARs)	Not assayed	Moderate	Sakai et al. 1999 (43); Marquet et al. 2014 (45)
5: Deletion of the 3'γ1^{E}	Reduced Sγ3, Sγ2b, Sγ2a	Reduced IgG3, IgG2b, IgG2a	Amoretti-Villa et al. 2019 (46)
6: Deletion of the 5'hs1RI	Sγ3, Sγ2b, Sγ2a in resting B cells Increased Sγ2b in activated B cells	Reduced IgG3, increased IgG2b	Braikia et al. 2017 (47)
7: Deletion of individual hss	Not detectable	Not detectable	Manis et al. 1998 (48); Vincent-Fabert et al. 2009 (49); Bébin et al. 2010 (50)
8: Deletion of hs3b and hs4	Reduced (except Sγ1)	Reduced (except IgG1)	Pinaud et al. 2001 (51)
9: Deletion of hs3a-IRIS-hs1,2	Reduced Sγ3, Sγ2b, Sγ2a	Reduced IgG3, IgG2b, IgG2a	Saintamand et al. 2015 (52)
10: Deletion of 5'IRIS (inverted residual hs3a)	Reduced Sγ2a	Reduced IgG2a	Saintamand et al. 2015 (52)
11: Deletion of palindrome+hs3a, hs1.2, hs3b	Reduced Sγ3, Sγ1, Sγ2a	Reduced IgG3, IgG1, IgG2a	Garot et al. 2016 (53)
12: core 3'RR replacement	Moderate decrease (± Sγ1)	Moderate (except IgG1)	Le Noir et al. 2017 (54)
13: Deletion of the whole 3'RR	Strong decrease (± Sγ1)	Strong decrease (± IgG1)	Vincent-Fabert et al. 2010 (55)
14: Duplication of Iα promoter	Reduced Sγ1, Sγ2b*, Sγ2a, Sε	Reduced IgG1, IgG2b*, IgG2a, IgE, IgA	Santos et al. 2018 (56)
15: Deletion of 8 out of 10 of the 3'CBEs	Not detectable	Not detectable (± increased IgG1)	Volpi et al. 2012 (57)
16: Deletion of all the 3'CBEs	Reduced (except Sγ1) (eS transcribed)	Reduced (except IgG1)	Zhang et al. 2021 (58)
17: Deletion of the IncCSR^{IgA}	Not assayed	Reduced IgG2b and IgA**	Rothschild et al. 2020 (59)
CH12F3 cell line	**Effect on Sα transcription**	**Effect on IgA CSR**	**Reference**
- Deletion of the 3'γ1E	Not detectable	Reduced	Amoretti-Villa et al. 2019 (46)
- Deletion of Iα promoter	± Increased on Sx (abolished for Sα)	± Increased IgX (abolished for IgA)	Santos et al. 2019 (60); Zhang et al. 2019 (61)
- Deletion of the whole 3'RR	± Reduced	Reduced	Kim et al. 2016 (62)
- Core 3'RR replacement	Not detectable	Normal to increased	Kim et al. 2016 (62)
- Deletion of all the 3'CBEs	Reduced	Reduced	Vian et al. 2018 (63)
- Deletion of the IncCSR^{IgA}	Reduced	Reduced	Pefanis et al. 2015 (64); Rothschild et al. 2020 (59)

FIGURE 2 | Effects of the mutations of the *IgH* and non-*Ig* regulatory elements on ST and CSR. The various mutations in mice and in CH12 cell line are numbered in the upper scheme. At the 5' part of the locus, hs1, hs2, hs3a, and hs3b are a cluster of four DNase I hypersensitive sites located some 30 kb upstream of the most distal V_H gene segment. hs1 is pro-B specific, binds various transcription factors, and exhibits a moderate repressive transcriptional activity as detected in transient transfection assays. The core enhancer Eμ (cEμ) and the flanking matrix attachment regions (MARs) are depicted. Within the 3'RR, the hs1,2 enhancer lies at the center of a large palindrome. The palindrome is bordered by inverted copies of hs3 enhancer. hs4, in contrast, lies outside the palindrome. hβ-glob stands for the human β-globin exon whose transcription is driven by the mouse Iα promoter (see main text for details). The table is a summary of the targeted mutations outlined in the upper scheme and their effect. ± indicates low to moderate. The asterisk on γ2b in mutation 14 means that Sγ2b transcription and IgG2b CSR are reduced following LPS stimulation but are normal upon TGF-β stimulation. The two asterisks on IgA in mutation 17 indicate that CSR to IgG2b and IgA are reduced in activated splenic B cells, while in Peyer's patch B cells, only IgA CSR is reduced. Sx and IgX stand for Sγ3, Sγ1, Sγ2b, Sγ2a, Sε, and the corresponding isotypes, respectively, and eS stands for ectopic S-like region [updated from (17)].

and IgG2a surface expression were reduced, while IgG3 and IgG2a serum titers were reduced (52). Overall, when the large proximal deletion encompasses hs3a and hs1,2, there is a strong reduction of ST and CSR to a subset of S regions, while deletion of the IRIS alone preferentially targets Sγ2a.

When the entire palindrome (including hs3a, hs1,2 and hs3b) was deleted, Sγ3 and, to a lesser extent, Sγ1 and Sγ2a transcription, and CSR to the corresponding isotypes were impaired (53) (**Figure 2**). Interestingly, replacement of the whole endogenous 3'RR by the four core enhancers led to an overall moderate defect in ST of all isotypes (54) (**Figure 2**). Thus, the palindrome appears to be required for efficient ST and CSR.

In another mouse line, Iα promoter was inserted downstream of the 3'RR (47), preserving the integrity of the 3'RR (**Figure 2**). Of the ectopic and the endogenous Iα promoters, only the ectopic promoter was active in resting B cells. Following stimulation, the ectopic Iα was further induced, together with the endogenous Iα (47, 56). The duplication reduced Sγ1, Sγ2a, and Sε transcription and CSR to the corresponding isotypes. Surprisingly, IgA CSR was reduced despite apparently normal Sα transcript levels. The pattern of Sγ2b activation depended on the type of stimulation. LPS stimulation reduced Sγ2b transcripts and IgG2b CSR levels. In contrast, TGF-β stimulation (which also activates Iα) led to normal Sγ2b transcripts and IgG2b CSR levels (56).

Nonetheless, as discussed (17), a potential caveat in these studies relates to 3'RR transcription and associated enhancer RNAs (eRNAs) which correlate with its activity (71–73). It is still unknown whether and how a large deletion of an IRIS or a close alignment of the core enhancers affects 3'RR eRNA structure, stability, and function (see below). It is possible that the effect on ST and CSR results from missing or destabilized eRNAs rather than from the absence of an IRIS per se. Similarly, whether the active ectopic Iα promoter perturbs the architecture of the 3'RR or interferes with transcription elongation within or downstream of the 3'RR remains to be investigated (17).

In conclusion, the whole 3'RR is the master element in the control of ST, CSR, SHM, and *IgH* expression. The 3'RR controls CSR by regulating ST, but this correlation is not absolute. Components of the 3'RR may display some isotype preference. Overall, the 3'RR only moderately impacts ST at Sμ region.

The 3'RR core enhancers display redundancy but act in synergy for efficient CSR, and the global structure of the 3'RR seems to contribute to its full activity (17).

2.2.1 When the *IgH* Locus Starts to Transvect: The 3'RR and Inter-Allelic Recombination

Most of the mutational studies conducted on the endogenous *IgH* locus concluded to a *cis*-regulation of ST and CSR by the 3'RR through a long-range effect on I promoters (17). However, the possibility remained that inter-allelic recombination could contribute to CSR. The bi-allelic nature of ST (74–76), the long-known frequent occurrence of CSR on both chromosomes [e.g., (77, 78)] and the recurrent involvement of switch regions in chromosomal translocations (79), made such scenario plausible. Besides the peculiar case of rabbit, featuring 13 *Cα* genes (80, 81), detection of presumably infrequent inter-allelic switch recombination at the endogenous *IgH* locus of other species required special genetic tools.

In a mouse model in which one *IgH* allele was engineered so that VDJ-Cμ transcription was suppressed (and *trans*-splicing prevented), sequencing of cDNAs revealed that inter-allelic recombination accounted for up to 7% of recombination events to *Cα* in Peyer's patches and up to 13% to *Cγ3* in LPS-activated splenic B cells (82). Upon crossing with mice devoid of hs3b/hs4, hence deficient in CSR (51), and sequencing of switch junctions in activated hemizygous B cells, it was found that the CSR-deficient allele (with deleted hs3b/hs4) could complement the excluded allele (with suppressed VDJ-Cμ transcription) through inter-allelic recombination (83). Another mouse model bearing a wild-type allele and a 3'RR-deficient allele enabled the same group to tackle directly the *trans*-effect of the 3'RR. It was found that the 3'RR of the wild-type allele could promote SHM and CSR on the second, 3'RR-deficient allele (on which both SHM and CSR are deficient) (84).

Thus, in addition to its established role as a major *cis*-regulatory element of SHM and CSR, the 3'RR can also operate in *trans* to control these processes in a fraction of activated B cells.

2.2.2 When B Cells Become Suicidal: The 3'RR and Locus Suicide Recombination

The observation that the 3'RR was highly enriched in switch-like repeats (85) and that it was transcribed upon activation of mature B cells for CSR (73) raised the possibility that the 3'RR could be the target of a CSR-like process (17). Unlike classical CSR, however, recombination between Sμ and the 3'RR would delete the whole C_H region and part of or the whole 3'RR (73), leading to the loss of surface Ig expression required for B-cell survival. It was thus proposed that this CSR-like process was important for B effector cell differentiation and homeostasis, for instance by counterselecting activated mature B cells with harmful Ig specificities (73). This phenomenon, termed locus suicide recombination (LSR) (73), was reported in both mice and humans and was AID dependent (73, 86). The binding profiles of AID and RNA polymerase II (RNAPII) at the 3'RR and flanking sequences were similar (73, 87). LSR was initially reported to occur at levels approaching classical CSR by PCR/Southern blot on excised episomal circles (73), though not by more sensitive techniques (58, 88, 89).

It is presently unclear if LSR is an active and autonomous process driven by specific mechanisms that co-opt classical CSR. Alternatively, LSR could be a by-product of bona fide CSR, resulting from an accidental attack of the transcribed 3'RR by AID. Further studies are required to elucidate the mechanisms that underlie LSR and its physiological significance.

2.2.3 The 3'RR and the Curious Case of IgD

It has long been established that IgD was co-expressed with IgM on the surface of naive mature B cells and that δ HC production resulted from alternative splicing of a long primary transcript encompassing Cμ and Cδ exons (90, 91). IgD CSR is a rare event and was mostly studied in humans in whom IgD CSR is relatively abundant in B cells that populate the upper aerodigestive mucosa-associated lymphoid tissues (91). The *Cδ* gene is unique in that it has no canonical switch sequence. Nonetheless, the gene has a switch-like sequence termed σδ, upstream of Cδ exons, that can recombine with Sμ (91). IgD CSR is rare in mouse and is not detectable in splenic B cells but was readily detected in mouse mesenteric lymph nodes (92). Surprisingly, IgD CSR was found to be 3'RR independent (92), contrasting in this regard with CSR to other isotypes. The transcriptional elements that control CSR to IgD remain to be identified.

2.2.4 The 3'RR and CSR in B1 B Cells: It May Depend on Which B Cell You Are

A plethora of mutational studies established the central role of the 3'RR in activated B2 B cells with the unspoken assumption that this role extended to the B1 B cells as well. However, in contrast to B2 B cells, IgA CSR in activated B1 B cells was reported to be 3′RR independent (93). Surface expression of IgA was normal in *in vitro*-activated 3'RR-deficient B1 B cells, but IgA titers were markedly reduced in culture supernatants, and this correlated with decreased Iμ-Cα post-switch transcript levels (93). Nonetheless, it is unclear if Sα pre-switch transcription was affected. Thus, it was proposed that though dispensable for IgA CSR in B1 B cells, the 3'RR was required for efficient transcription of the switched *Cα* gene (93).

2.3 The 3'γ1E Enhancer: Better Few Constant Genes Than Nothing

Previous 4C-Seq analyses identified a PAX5-dependent hs site downstream of *Cγ1* gene (hereafter 3'γ1E) that bound multiple transcription factors in *Rag2*-deficient pro-B cells (94). In particular, the 3'γ1E exhibited a pro-B-cell-specific enhancer activity (95) and bound the MED1 subunit of the Mediator complex (95, 96).

In activated mature B cells, the 3'γ1E also bound MED1 and MED12 subunits of the Mediator complex and was transcribed (97). 4C-Seq experiments revealed that the 3'γ1E interacted with Eμ and the 3'RR (97). In 3'γ1E-deficient mice, activated B cells displayed defective ST across Sγ3, Sγ2b, and Sγ2a and CSR to the corresponding isotypes (**Figure 2**) (46).

Thus, the 3'γ1E emerges as a novel element that regulates CSR in an isotype-specific manner (46), adding an additional layer of complexity to the long-range mechanisms that operate at the *IgH* constant locus.

2.4 CTCF Binding Elements: Guardians of the Temple and Insiders

CTCF is a multivalent 11 zinc finger (ZF) protein thought to bind uncommonly long and diverse DNA sequences through different combinations of its 11 ZFs (98). These combinations are not arbitrary. Extensive mutational and ChIP-Seq analyses of ~50,000 genomic sites in primary B lymphocytes found that CTCF reads sequence diversity through ZF clustering by grouping contiguous ZFs into distinct binding subdomains (99). Broadly outlined, the central ZFs 4–7 were found to anchor CTCF to ~80% of CBEs containing the core motif. Peripheral ZFs associate with non-conserved flanking DNA sequences as functional clusters and modulate CTCF binding *in vivo* (99). CTCF was involved in various processes ranging from transcriptional regulation and insulator activity to chromatin boundary formation (17, 100). Its role in chromatin loop formation during CSR is discussed below.

The role of CTCF in CSR was investigated through a conditional knockout of the mouse *Ctcf* gene (101). Interestingly, CTCF loss led to increased transcript levels of Sγ3, Sγ1, and Sγ2b in unstimulated but not in activated splenic B cells, associated with an apparently increased CSR to IgG3, IgG1, and IgG2b. In contrast, CTCF depletion had no significant effect on Sμ transcription or AID expression (101).

These findings strongly suggest that CTCF acts, at least in part, by preventing premature activation of I promoters (101).

2.4.1 The 5'hs1RI Insulator

A hs was identified within the last intron of the *Cα* gene (102), which binds CTCF and cohesin in resting B cells (103), but evicts CTCF though not cohesin upon activation (47, 101, 103). This element, termed 5'hs1RI (**Figure 1**), is conserved in the human *Cα1* and *Cα2* genes (17, 47).

In 5'hs1RI-deleted mice, Sγ3 and, to a lesser extent, Sγ2b and Sγ2a transcripts were specifically upregulated in unstimulated splenic B cells (47). In activated B cells, increased CSR to IgG2b correlated with increased Sγ2b transcription; however, CSR to IgG3 were defective despite abundant Sγ3 transcripts. It is still unclear whether this is due to promoter interference or to other mechanisms (47). Notwithstanding, the data strongly suggest that 5′hs1RI is involved in the transcriptional silencing of Iγ3, Iγ2b, and Iγ2a, but not of Iγ1, Iε, and Iα promoters.

Overall, the 5'hs1RI emerges as an inducible CTCF insulator that regulates the temporal expression of a subset of C_H genes, by blocking premature activation of their promoters prior to B-cell activation (47).

2.4.2 The *IgH* Super-Anchor: 3'CTCF Binding Elements

Multiple hs elements were identified downstream of hs4 enhancer, some of them exhibiting insulator activity *in vitro* (104). This region, also termed super-anchor, consists of 10 CBEs (57, 105). Deletion of the first eight CBEs in mice had at best a modest increase of CSR to IgG1 (63) (**Figure 2**), and the crosslinking frequencies (by 3C assays) of the 3'RR with Eμ or with I promoter regions were not altered (63). However, the fact that the deletion spared two CBEs prevented a definitive conclusion on the role of the super-anchor in CSR and the architecture of the locus.

This issue was solved in two systems. Deletion of the 10 3′ CBEs in CH12F3 B lymphoma cell line led to ~2-fold decrease of CSR to IgA and a moderate decrease of Sα transcript levels, suggesting a role for the 3'CBEs in 3'RR/Iα promoter interactions (106). Nonetheless, because activated CH12 cells switch exclusively to IgA (upon stimulation with TGFβ-containing cocktails), the impact of the 3'CBEs on the other isotypes remained unclear.

In this regard, deletion of the whole 3'CBEs cluster was recently performed in chimeric mice generated by RAG2-deficient blastocyst complementation (58) and CSR assayed by CSR-HTGTS. Except for Sγ1 transcripts and CSR to IgG1 whose levels were unaffected, CSR to all other isotypes was reduced, and this correlated with varying degrees of reduced ST of the corresponding S regions (58).

Together, the data from CH12 cells (106) and chimeric mice (58) revealed that the 3'CBEs promote ST of and CSR to all downstream S regions with the exception of Sγ1.

Interestingly, GRO-Seq analysis revealed that, upon deletion of the 3'CBEs, the 30-kb region just downstream [termed ectopic S (eS) region] (**Figure 1**) becomes transcriptionally active in both sense and antisense orientations in unstimulated splenic B cells (58). Following activation, the eS region is further transcribed, generating convergent transcription that may facilitate AID recruitment. 3C-HTGTS data showed that the eS region interacts with the Eμ–Sμ region, suggesting a synapsis between Sμ and eS regions (58). Accordingly, CSR-like junctions involving Sμ and sequences within the first 6 kb of the eS region were detected and accounted for 1%–3% of all CSR-related junctions (58).

Thus, the 3'CBEs act as an insulator that prevents transcriptional activation of the eS region and its recombination with Sμ region during CSR.

3 SIGNALS AND REGULATORY ELEMENTS THAT CONTROL SWITCH RECOMBINATION IN DEVELOPING B CELLS

Various studies involved signaling through Toll-like receptors in the induction of AID expression and CSR in early B cells [e.g., (31, 32, 107)]. Recently, interleukin 7 (IL7) was involved in the control of ST by repressing Iγ3 and, to a lesser extent, Iγ2b promoter in cultured wild-type pro-B cells (108). Nonetheless, LPS stimulation induced Sγ3 and Sγ2b transcription and CSR to Sγ3 and Sγ2b, respectively (108). Sγ1 and Sε transcript levels, though undetectable in cultured pro-B cells, were also increased following LPS+IL4 stimulation (108).

With regard to transcriptional elements, the 5'hs1RI suppressed Sγ3 and, to a lesser extent, Sγ2b transcription in unstimulated pro-B and pre-B cells (47). Interestingly, removal of 5'hs1RI led to increased levels of Sγ3 and Sγ2b transcripts in the absence of detectable 3'RR eRNAs (47). Along similar lines, duplication of Iα promoter downstream of the 3'RR led to a premature activation of the ectopic Iα at the pro-B-cell stage, while the endogenous Iα promoter remained silent (47). These observations indicate that the 3′RR activity at the pro-B-cell stage does not require 3′RR transcription (i.e., 3'RR eRNAs) (47). Together, the above findings strongly suggest that IL7/IL7R pathways and the 5'hs1RI are part of active processes that operate in developing B cells to keep in check, through yet unknown mechanisms, ST and CSR (108).

4 LONG-RANGE REGULATION BY *IgH* CONTROL ELEMENTS: THE PROBLEM IS NOT THE DISTANCE

4.1 Compete or Not Compete for the Control of CSR

An important question in the field of transcriptional regulation is whether promoters compete for, or are co-regulated by, a shared (and often distant) regulatory element. In the specific case of the 3'RR, it was known that activation of primary B-cell populations often induces more than one I promoter, the prevailing interpretation being that I promoters compete for 3′RR activity [e.g., (47, 48, 109–111)]. However, whether competition applied to I promoters located on the same chromosome and that responded to the same stimulus remained uncertain. The issue was complicated by the finding that ST can occur on both alleles (74–76), so that even the use of single cells does not settle this issue.

The use of mouse models with engineered endogenous *IgH* locus, polymorphic allelic differences, and a single allele-specific RT-qPCR assay revealed that the type of stimulation largely determined which mode of *cis*-activation, competition or co-activation, prevailed (112). In the presence of IL4, the majority of alleles displayed promoter competition, but Sγ1 single expressers prevailed over Sε single expressers. In the presence of TGF-β, there was also competition between Iγ2b and Iα, but the percentages of single Sγ2b- and Sα-expressing alleles were similar (112). In contrast, Iγ3 and Iγ2b promoters were co-activated upon LPS stimulation. Moroever, Iγ2b promoter was often activated on alleles with pre-activated Iγ3. These findings strongly suggest that 3′RR activity, RNAPII, and transcription factors and co-factors are not limiting during I promoter activation and that initial activation of one promoter does not prevent activation of the other (17, 112). In particular, the Iγ2b promoter, which is induced by both LPS and TGF-β, was co-activated with Iγ3 in the vast majority of alleles upon LPS stimulation, but was almost never co-activated with Iα after TGF-β stimulation (112). It was speculated that co-activation and competition reflect two kinetics of the activation of I promoters: co-activation of Iγ3 and Iγ2b promoters in the rapidly responding MZ B cells during T-independent responses and competition between the other I promoter pairs in FO B cells during the relatively delayed T-dependent responses (112).

The single-chromosome approach also solved the long-standing issue of the polarity of the 3'RR, i.e., if the 3'RR activity was exclusively oriented toward the upstream I promoters or if it could also target a downstream promoter (17). In this regard, analysis at the single-chromosome level of activated B cells with duplicated Iα promoter downstream of the 3'RR (47) (**Figure 2**) revealed that the 3′RR activated both the ectopic and the endogenous Iα promoters, which points to a bidirectional activity (112).

The above studies revealed that the 3'RR has a bi-directional activity, and that the type of stimulation largely determines which mode of cis-activation, competition or co-activation, prevails.

4.2 Transcriptional and Epigenetic Regulation by the 3'RR

Mammalian genomes are predominantly methylated at cytosines in CpG dinucleotides. In general, unmethylated CpGs are associated with active promoters, while methylated CpGs are closely associated with transcriptionally silent promoters (113). The methylation patterns of various *cis*-acting elements at the *IgH* constant region were determined in primary B cells by bisulfite sequencing. Unexpectedly, the methylation profiles of almost all the *cis*-acting elements were established and faithfully maintained independently of B-cell activation or ST (114). The unmethylated pattern of Eμ and 3'γ1E and the hypermethylated pattern of 5'hs1RI did not change following B-cell activation or insulation of the 3'RR. Surprisingly, induction of ST did not impact the methylation profiles of I promoters: Iγ3 and Iγ2b were unmethylated in resting as well as in LPS-activated splenic B cells, while the hypermethylated profile of Iε for instance did not vary upon activation. The only exception was Iγ1 whose demethylation was induced. Importantly, the 3'RR-dependent Iγ3 and Iγ2b promoters remained unmethylated following insulation of the 3'RR, which fully repressed the two promoters. This implies that the long-range activation of these promoters by the 3'RR involves mechanisms that do not rely on DNA methylation (114).

A remarkable aspect of transcription elongation across switch regions relates to the marked stalling of RNAPII (66, 115) and the peculiar pattern of chromatin activating modifications (115–117) at these regions. In particular, induced histone acetylation and H3K4me3 mark extended over the entire switch regions irrespective of their length and dropped at C_H exons (115, 117). In contrast, these patterns were observed in the constitutively transcribed Sμ region in resting B cells and did not vary upon activation (115, 117).

Catalysis of methylation marks on H3K4 is effected by PTIP (PAX interaction with transcription activation domain protein), a component of the mixed-lineage leukemia 3 (MLL3)/MLL4 complex (118). Activated PTIP-deficient B cells exhibited a defect in Sγ3, Sγ1 and Sγ2b and CSR to IgG3, IgG1, and IgG2b; the effect on Sγ1 transcription was milder, whereas Sε transcript and IgE CSR were unaffected (117, 119, 120). On the other hand, the chromatin profiles of Sμ and the 3'RR were

essentially unaffected (117). It was proposed that PTIP promotes ST by bridging the 3'RR to I promoters, as 3'RR/I promoter interactions are disrupted in activated PTIP-deficient B cells (119).

Transcriptional and epigenetic analyses of mice devoid of the 3'RR revealed a dramatic decrease of transcription initiation along the downstream Ix–Sx–Cx regions, while the Iμ–Sμ–Cμ region was only minimally affected (121). Similarly, while the deposition of H3Ac and H3K4me3 marks was severely reduced along the downstream S regions, the Iμ–Sμ–Cμ region was essentially unaffected (121). This trend was not seen for H4Ac deposition which remained intact in activated 3'RR deficient (121).

Thus, the 3'RR is the central element in the control of ST initiation and histone modifications at acceptor S regions. Nonetheless, some epigenetic modifications, illustrated by H4Ac mark and DNA methylation, are 3'RR independent.

4.3 The Cohesin and the Mediator Complexes and Long-Range Interactions in CSR

It is now admitted that the chromatin interaction landscape plays an important role in the epigenetic control of gene expression. Interactions between enhancers and target promoters generally take place within submegabase-sized topologically associating domains (TADs), where these interactions occur at higher frequency than with elements of different TADs (122, 123). Chromatin interactions between boundary elements that bind CTCF (CBEs) and the Cohesin complex tether the bases of loops and separate the TADs from each other, thus preventing ectopic enhancer–promoter interactions (122–125). However, this is not an absolute rule as long-range interactions are not always blocked by CTCF and Cohesin binding to CBEs (126), and some of these sites can rather facilitate gene activation (122–124). Various studies revealed that juxtaposition of TAD boundaries by CTCF is strongly biased toward convergent CBEs (127–130). Within TADs, the Cohesin and the Mediator complexes are important for the formation of enhancer/promoter chromatin loops. Cohesin is loaded at these loops by the cohesin-loading factor NIPBL, which also binds the Mediator complex (131–133).

In pro-B cells, it was shown that the *IgH* locus spans a multi-megabase-sized TAD divided into three sub-TADs; one of these sub-TADs extends from the proximal V_H domain to the 3'CBEs (134). It is in that sub-TAD that most events pertinent to ST and CSR take place and, for the most parts, in the domain extending from the Eμ region to the 3'CBEs (**Figure 2**). In this chromatin domain, Eμ enhancer associates with the 3'RR in both unstimulated and activated B cells (67). Surprisingly, cEμ deletion only marginally impacted Eμ/3'RR association (67). In resting B cells, Eμ, the 3'RR, and I promoters, especially Iγ3, were poised for ST activation, and it was proposed that this poised configuration facilitates I promoter activation (67). Depending on the nature of stimulation, I promoters were recruited to the Eμ/3'RR complex leading to a juxtaposition of Sμ and the downstream switch partner (67).

Subsequent analyses by ChIP-Seq found that CTCF and Cohesin were recruited to the 3'CBEs in unstimulated B cells, with no significant enrichment at the Eμ region. Following stimulation, Cohesin was recruited to the Sμ–Cμ region, though not to Eμ, in a CTCF-independent manner (103). In the CH12 line, knockdown of SMC1 and SMC3 core subunits of the Cohesin complex or of NIPBL and WAPAL loader/unloader subunits reduced IgA CSR, a clear indication that the Cohesin complex was required for CSR (103).

The Mediator complex was also involved in ST and CSR. In unstimulated B cells, the MED1 and MED12 subunits were specifically recruited to Eμ enhancer and 3'RR (97). Following stimulation, the two subunits were recruited to Eμ, 3'RR, 3'γ1E, and the induced I promoter, in a stimulation-dependent manner (97). A conditional knockout of *Med1* led to reduced ST of all acceptor S regions and CSR to the corresponding isotypes in activated B cells. These findings strongly suggested that the Mediator complex promoted ST at downstream S regions (97). In agreement with previous findings on unstimulated B cells (67), 4C-Seq experiments detected strong interactions between Eμ and the 3'RR as well as a preferential association with the Iγ3 region (97). Upon stimulation, interactions between Eμ, 3'RR, 3'γ1E, and the activated I promoter were readily detected, and the pattern of these interactions correlated with MED1 and MED12 recruitment. Accordingly, Eμ/3'γ1E/I promoter interactions were reduced in MED1-depleted B cells (97). Altogether, these findings suggested that the Mediator and the Cohesin complexes promoted ST of downstream switch regions and were required for the long-range interactions between the *IgH* transcriptional *cis*-acting elements (97).

4.4 A Role for Non-Coding RNAs in the Long-Range Control of CSR

4.4.1 Regulation of the Transcriptional Activity of the 3'RR

Enhancer transcripts (eRNAs) have (relatively) recently emerged as potentially essential for enhancer activity. These non-coding RNAs have been involved in the regulation of gene expression at different levels, for instance by stabilizing or trapping factors that bind enhancers, by generating and/or stabilizing chromatin loops that facilitate interactions between enhancer and target promoters, and by releasing paused RNAPII for productive transcriptional elongation (135). Yet, the mechanisms of action of eRNAs are still unclear. Moreover, whether it is the act of transcribing the enhancer or the eRNAs themselves that are crucial for enhancer activity has not been definitively solved. The transcriptional activity of the 3'RR has been mentioned previously. Here, we summarize recent findings on the relationship between 3'RR transcriptional activity and its regulatory function.

The zinc finger MYND-type containing 8 (ZMYND8) protein is a histone mark reader that associates with enhancers and promoters and can mediate transcriptional activation or repression in a context-dependent manner (72). ZMYND8 was recently identified as a critical regulator that binds both Eμ and the 3'RR (72). Conditional deletion of the mouse *Zmynd8* gene severely reduced ST and CSR to all isotypes but had no effect on Sμ transcription (72). Significantly, the loss of ZMYND8 led to a substantial increase of RNAPII loading as well as transcription at the 3'RR (notably at hs1,2 and hs3b enhancers) (72).

These findings suggested that ZMYND8-mediated control of the 3'RR function was effected through downregulation of its transcriptional activity, and it was proposed that by suppressing RNAPII loading on the 3'RR, ZMYND8 would suppress competition for transcription factors, thus favoring ST (72).

Another study addressed the role of 3'RR transcription and its eRNAs in the control of ST by using a conditional knockout enabling depletion of the general RNAPII elongation factor SPT5 (136), previously shown to be required for AID recruitment (137). Depletion of SPT5 severely reduced nascent transcription and RNAPII occupancy at downstream S regions but had only a moderate effect at the Sμ region (136). 3C-qPCR assays revealed reduced Eμ/3'RR/Iγ1 interaction frequencies in IL4-activated splenic B cells (136). The apparent decrease of 3'RR transcription in activated SPT5-depleted B cells did not affect its chromatin accessibility or H3K27Ac levels. The depletion also did not significantly impact Mediator and Cohesin recruitment at Eμ, 3'RR, and Iγ1 promoter.

These and other findings suggested that the 3'RR chromatin was in an active state; nonetheless, the weakly transcribed 3'RR was unable to physically interact with its target promoters. This indicated that SPT5-mediated transcription of the 3'RR was required for 3'RR interactions (136). Restoration of transcription through dCas9-VPR at one or two 3'RR enhancers additively rescued 3'RR/Iγ1 promoter interactions and Sγ1 transcription (136). Pharmacological inhibition of transcription initiation or elongation in activated wild-type B cells led to a significant decrease of 3'RR eRNAs. Surprisingly, 3'RR interaction frequencies as assayed by 3C-qPCR assays tended to increase. These findings suggested that transcription elongation within the 3'RR may rather disrupt 3'RR interactions (136).

It was thus proposed that SPT5-mediated transcription of the 3'RR is actually required for the initiation of 3'RR/promoter interactions. Once established, these interactions no longer require 3'RR transcription for their maintenance. Overall, transcription of the 3'RR, but not eRNAs themselves, would be important for 3'RR interactions (136).

4.4.2 The *lncCSR*^{IgA} Locus: Controlling the *IgH* Locus From Within May not Be Enough

The eRNA levels are generally lower than the messenger RNA levels of their target genes, which complicates the analysis of the eRNA function(s). Fortunately, a subset of eRNAs are sensitive to the RNA surveillance machinery, the RNA exosome complex, and can therefore be more easily studied in the absence of the RNA exosome (64). In this context, recent analyses of the role of RNA exosome in B cells revealed a novel mechanism that influences CSR, involving long-range interactions between a non-*Ig* locus and the 3'RR. The non-*Ig* locus was termed *lncCSR*^{IgA} and is located some 2.6 Mb downstream of the 3'RR (59) (**Figure 2**).

The *lncCSR*^{IgA} locus is a divergent eRNA-expressing element which, as detected by 3C assay, interacted with hs4 enhancer of the 3'RR (59). In CH12 cells, deletion of the *lncCSR*^{IgA} locus reduced Sα transcription and IgA CSR and decreased the interaction frequency between hs4 enhancer and the deleted locus (59). In *lncCSR*^{IgA}-deficient mice, no difference in the distribution of MZ B cells and FO B cells was seen in the spleen. However, activated splenic B cells displayed CSR defect to both IgG2b and IgA, while Peyer's patch B cells had reduced IgA CSR specifically (138). Based on its DNase I hypersensitivity, MED1 binding, and enrichment in H3K27Ac and H3K4me1 marks, the *lncCSR*^{IgA} locus was suggested to act as an enhancer-like element (138).

The *lncCSR*^{IgA} is flanked in particular by a CTCF- and Cohesin-binding element, and lies within a TAD that is separated from the *IgH* TAD by other non-*Ig* TADs. The CBE of the *lncCSR*^{IgA} locus interacted in particular with the hs4 region of the 3′RR. Accordingly, interaction frequency between hs4 and the CBE dropped following deletion of the *lncCSR*^{IgA} locus (138). Various genetic and biochemical analyses pointed toward a pivotal role of the *lncCSR*^{IgA} CBE in the intra-TAD$^{\text{lncCSRIgA}}$ interactions required for optimal IgA CSR (138). These findings led to a model positing that the transcribed enhancer-like *lncCSR*^{IgA} locus produces a lncRNA that facilitates the recruitment of regulatory proteins such as the Cohesin subunit SMC3 to the neighboring CBE. This recruitment alters in turn the interactions that take place within the TAD$^{\text{lncCSRIgA}}$ as well as interactions with the 3′RR (138).

The precise mechanism by which CSR is impaired in the absence of the lncCSR$^{\text{IgA}}$ RNA remains unclear. Nonetheless, these investigations reveal an unanticipated mechanism whereby the 3'RR-mediated control of CSR within the *IgH* TAD is influenced by chromatin interactions that take place within a different and distant TAD.

4.5 Chromatin Loop Extrusion and CSR Center: A Center at Last

The standard loop extrusion model (130, 139–142) stipulates that the ring-shaped cohesin complex binds and passes chromatin through its lumen to form a loop. The process continues until chromatin reaches a CTCF homodimer, at convergent CBEs, which generally blocks loop extrusion (122, 123, 125). In this process, Cohesin not only associates with CBE-bound CTCF but plays an active role within the chromatin loop by promoting for instance enhancer/promoter interactions (122, 123). Additionally, Cohesin may escape the constrains of the CTCF loops, by moving past CTCF anchors, and promote long-range interactions between compartmental domains (122, 123).

Recent studies (61, 143) involved specific transcribed, Cohesin-binding elements in the mechanism that underlie the long-range control of CSR through Cohesin-based impediment of loop extrusion. In one study (61), the V(D)J recombination center (144) of an A-MuLV pro-B line that constitutively transcribes Sγ2b was engineered so that RAG scanning activity (145) was directed toward the C_H region (61). The detected Eμ/Sγ2b/3'CBE interactions were associated with RAD21 binding at the 3'CBEs and a rather low accumulation at Eμ–Sμ and Iγ2b-Sγ2b regions (61). The transcribed Sγ2b region impeded loop extrusion and RAG scanning activity, the latter being specifically detected at the transcribed Sγ2b and the weakly transcribed 3'CBEs. Removal of the active Iγ2b promoter suppressed Sγ2b transcription, RAG scanning, Eμ interactions, and RAD21

accumulation at Sγ2b, but RAG activity now increased at the 3'CBEs (61). These and other findings led to a model stipulating that transcription of the Sγ2b region impedes both upstream and downstream loop extrusions (17, 61).

The other study (143) investigated the mechanism of CSR in splenic B cells and CH12 cells, both in an AID-deficient background. In unstimulated B cells, robust transcription took place at the Eμ region and the 3'RR essentially, and the Eμ region/3'RR/3'CBE interactions formed what was called a CSR center (CSRC) (17, 143, 146). RAD21 and NIPBL were shown to accumulate at the Eμ region, 5'hs1RI, 3'RR, and 3'CBEs (143). Upon stimulation, Eμ/3'RR/3'CBE interactions now included the transcribed switch regions, with a marked accumulation of Cohesin at switch regions (143). This suggests that Cohesin loading at transcribed switch regions contributes to ongoing 3'RR–3'CBE domain extrusion that promotes switch region alignment to initiate CSR (143).

In both unstimulated and stimulated AID-deficient CH12 cells, interactions between the constitutively transcribed Iμ–Cμ, Iα–Cα, 3'RR, and proximal 3'CBE regions were detected, and NIPBL and Cohesin markedly accumulated at the active Iα promoter but not at the other (silent) I promoters (17, 143). Deletion of Iα promoter suppressed the transcription of Sα and IgA CSR and led to a low to moderate increase in upstream S regions' transcription (60, 143). This resulted in the loss of Eμ- and hs4-mediated CSRC interactions with the Sα region. In contrast, interactions of Eμ and hs4 with the newly transcribed sequences upstream of the Sα region were now increased (143).

These and other genetic and mechanistic analyses (17, 143, 146) led to a general model positing that Eμ and 3'RR enhancers, as Cohesin-loading sites, act as dynamic impediments to loop extrusion (**Figure 3**).

As discussed (17), the role of Eμ enhancer in this process and its relevance for CSR remain unclear, as ST, CSR, and 3'RR/Sμ region interactions are only marginally affected in its absence (43–45, 67). Moreover, a role for CBEs upstream of Eμ cannot presently be excluded (17). Whether the functions of Eμ as a transcriptional enhancer and as a loop extrusion impediment involve the same mechanisms remains to be elucidated. On the other hand, the 3'γ1E and 5'hs1RI, which control ST of and CSR to specific isotypes (46, 47), are also Cohesin-loading elements. Whether they are involved in loop extrusion impediment is still unclear. Thus, the mechanisms that regulate loop extrusion during CSR remain to be investigated and more so because not all loops are Cohesin-dependent (147).

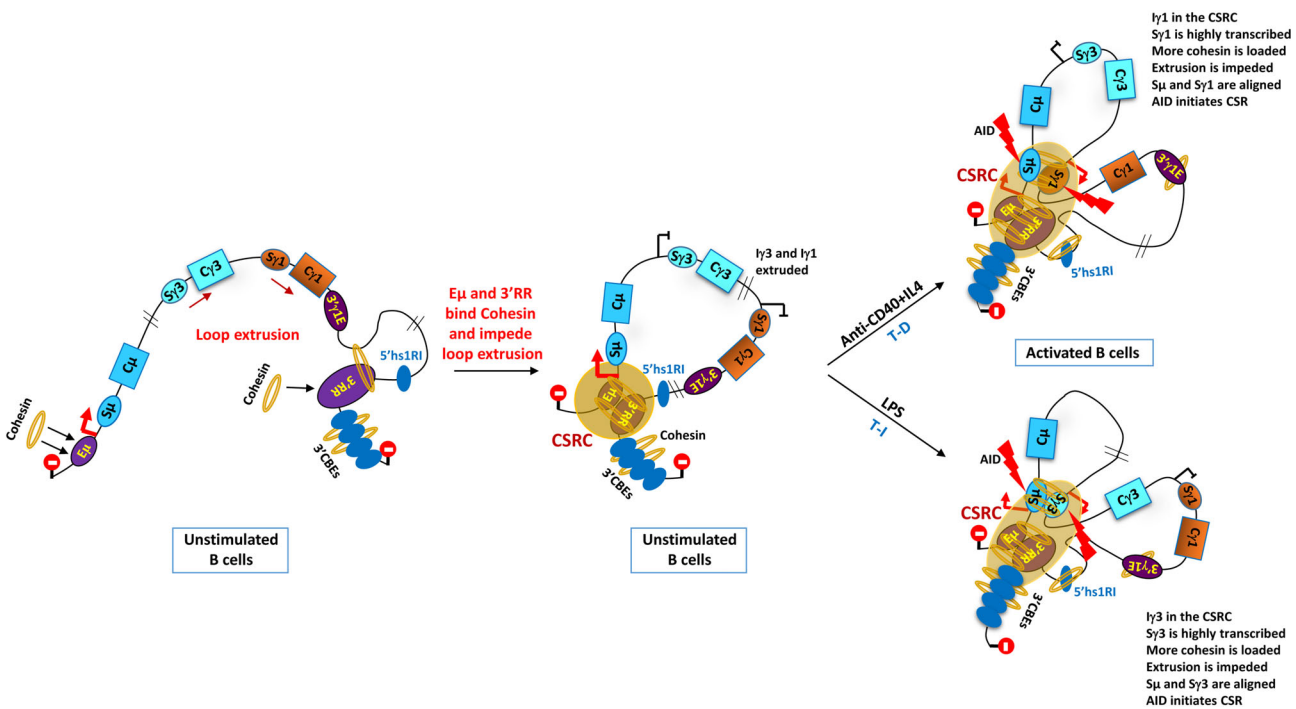

FIGURE 3 | Outline of loop extrusion and class switch recombination center (CSRC) model. The model stipulates that Eμ and 3'RR act as dynamic impediments to loop extrusion thanks to their function as Cohesin-loading sites. The Eμ region impedes upstream extrusion and the 3'RR (potentially assisted by the 3'CBEs) impedes downstream extrusion (illustrated by the stop signals). Chromatin extrusion ultimately leads to a juxtaposition of the Eμ–Sμ region with the 3'RR and 3'CBEs to form a CSRC. Signal-dependent promoters, Iγ1 and Iγ3 (in this example), are primed following anti-CD40+IL4 and LPS stimulations respectively, which mimic T-dependent (T-D) and T-independent (T-I) immune responses, respectively. Ongoing extrusion brings the associated transcribed S regions close to the 3'RR in the CSRC. There, the highly transcribed S regions load more Cohesin and impede chromatin extrusion ultimately aligning the partner S region with Sμ. AID is recruited by the transcribed S regions and initiates bona fide CSR [see (17, 143) for more details]. The 3'γ1E and 5'hs1RI are also Cohesin-loading sites, but their potential role in loop extrusion and CSRC is still unclear [adapted from (17)].

In this context, a recent study involved the RNA exosome complex in the regulation of chromatin loop extrusion. By generating a conditional mutant mouse line to induce loss of the DIS3 RNase subunit of the RNA exosome complex, it was shown in particular that this loss led to decreased binding of CTCF and Cohesin (RAD21) at the 3'CBEs and 5'hs1RI, which was often associated with accumulated eRNAs (148). Interestingly, this overlap between reduced CTCF/Cohesin occupancy and accumulated eRNAs correlated with an accumulation of DNA/RNA hybrids at the 3'CBEs, 3'RR, and switch regions, particularly at the Sμ region. These findings, together with the observation that 3'RR/Eμ interactions were reduced upon loss of DIS3 activity, suggested that the accumulation of DNA/RNA hybrids at specific transcribed sequences impeded Cohesin-mediated chromatin loop extrusion during CSR (148).

Thus, by processing non-coding RNAs at critical transcribed sequences, the RNA exosome complex emerges as an important factor in the mechanisms that regulate chromatin loop extrusion.

5 PERSPECTIVES

The last decade witnessed important advances in our understanding of the transcriptional and epigenetic mechanisms involved in the long-range control of CSR. Elucidation of the function of newly identified regulatory elements and the role of *trans*-acting factors in CSR added new layers to the complexity of the mechanisms involved. The development of various genome editing approaches as illustrated by CRISPR/Cas9-based techniques as well as high-throughput technologies made it possible to tackle and to further our knowledge of the long-range chromatin interactions that take place during CSR.

As usual, any new knowledge raises new questions and paths. For instance, the question of why do some long-range regulatory elements target specific promoters remains to be investigated. The signals that trigger chromatin loop formation and their collapse and the precise relationship between (presumably) large chromatin loops and the fine details of transcriptional and epigenetic control are still unclear. In the context of Cohesin-based loop extrusion/CSRC model, the role of other transcriptional/architectural factors remains to be investigated. Moreover, one should bear in mind that *IgH* chromatin domains are defined in resting or activated B-cell populations and, therefore, display averaged interactions [e.g., (149)] that do not necessarily reflect interactions on a single-cell or single-chromosome basis. Correlatively, it is presently unclear to what extent the long-range mechanisms identified in *in vitro*-activated B-cell populations operate during genuine T-cell-dependent and T-cell-independent responses. Though technically challenging, it will be of outmost importance to develop new approaches and models to tackle these mechanisms on a single B-cell or chromosome basis during immune responses.

AUTHOR CONTRIBUTIONS

AK wrote the manuscript. AD contributed to the writing of the manuscript and checked the references and figures. All authors contributed to the article and approved the submitted version.

FUNDING

This work was supported by the Agence Nationale de la Recherche (ANR-16-CE12-0017), the Institut National du Cancer (INCA_9363, PLBIO15-134), the Fondation ARC pour la Recherche sur le Cancer (PJA 20191209515), and the Ligue Contre le Cancer (Ligue Régionale: comités de l'Ex Région Midi-Pyrénées).

ACKNOWLEDGMENTS

We apologize to our colleagues whose work could not be cited for space constraints.

REFERENCES

1. Kumari G, Sen R. Chromatin Interactions in the Control of Immunoglobulin Heavy Chain Gene Assembly. *Adv Immunol* (2015) 128:41–92. doi: 10.1016/bs.ai.2015.08.001
2. Proudhon C, Hao B, Raviram R, Chaumeil J, Skok JA. Long-Range Regulation of V(D)J Recombination. *Adv Immunol* (2015) 128:123–82. doi: 10.1016/bs.ai.2015.07.003
3. Teng G, Schatz DG. Regulation and Evolution of the RAG Recombinase. *Adv Immunol* (2015) 128:1–39. doi: 10.1016/bs.ai.2015.07.002
4. Khamlichi AA, Feil R. Parallels Between Mammalian Mechanisms of Monoallelic Gene Expression. *Trends Genet* (2018) 34:954–71. doi: 10.1016/j.tig.2018.08.005
5. Di Noia JM, Neuberger MS. Molecular Mechanisms of Antibody Somatic Hypermutation. *Annu Rev Biochem* (2007) 76:1–22. doi: 10.1146/annurev.biochem.76.061705.090740
6. Stavnezer J, Guikema JE, Schrader CE. Mechanism and Regulation of Class Switch Recombination. *Annu Rev Immunol* (2008) 26:261–92. doi: 10.1146/annurev.immunol.26.021607.090248
7. Yeap LS, Meng FL. Cis- and Trans-Factors Affecting AID Targeting and Mutagenic Outcomes in Antibody Diversification. *Adv Immunol* (2019) 141:51–103. doi: 10.1016/bs.ai.2019.01.002
8. Yu K, Lieber MR. Current Insights Into the Mechanism of Mammalian Immunoglobulin Class Switch Recombination. *Crit Rev Biochem Mol Biol* (2019) 54:333–51. doi: 10.1080/10409238.2019.1659227
9. Feng Y, Seija N, Di Noia JM, Martin A. AID in Antibody Diversification: There and Back Again. *Trends Immunol* (2020) 41:586–600. doi: 10.1016/j.it.2020.04.009
10. Mesin L, Ersching J, Victora GD. Germinal Center B Cell Dynamics. *Immunity* (2016) 45:471–82. doi: 10.1016/j.immuni.2016.09.001
11. Lu LL, Suscovich TJ, Fortune SM, Alter G. Beyond Binding: Antibody Effector Functions in Infectious Diseases. *Nat Rev Immunol* (2018) 18:46–61. doi: 10.1038/nri.2017.106
12. Higgins BW, McHeyzer-Williams LJ, McHeyzer-Williams MG. Programming Isotype-Specific Plasma Cell Function. *Trends Immunol* (2019) 40:345–57. doi: 10.1016/j.it.2019.01.012
13. Bournazos S, Gupta A, Ravetch JV. The Role of IgG Fc Receptors in Antibody-Dependent Enhancement. *Nat Rev Immunol* (2020) 20:633–43. doi: 10.1038/s41577-020-00410-0
14. Chaudhuri J, Basu U, Zarrin A, Yan C, Franco S, Perlot T, et al. Evolution of the Immunoglobulin Heavy Chain Class Switch Recombination Mechanism. *Adv Immunol* (2007) 94:157–214. doi: 10.1016/S0065-2776(06)94006-1
15. Chen Z, Wang JH. Signaling Control of Antibody Isotype Switching. *Adv Immunol* (2019) 141:105–64. doi: 10.1016/bs.ai.2019.01.001

16. Methot SP, Di Noia JM. Molecular Mechanisms of Somatic Hypermutation and Class Switch Recombination. *Adv Immunol* (2017) 133:37–87. doi: 10.1016/bs.ai.2016.11.002
17. Oudinet C, Braikia FZ, Dauba A, Khamlichi AA. Mechanism and Regulation of Class Switch Recombination by IgH Transcriptional Control Elements. *Adv Immunol* (2020) 147:89–137. doi: 10.1016/bs.ai.2020.06.003
18. Klein U, Dalla-Favera R. Germinal Centres: Role in B-Cell Physiology and Malignancy. *Nat Rev Immunol* (2008) 8:22–33. doi: 10.1038/nri2217
19. Jacob J, Kassir R, Kelsoe G. In Situ Studies of the Primary Immune Response to (4-Hydroxy-3-Nitrophenyl)Acetyl. I. The Architecture and Dynamics of Responding Cell Populations. *J Exp Med* (1991) 174:1165–75. doi: 10.1084/jem.173.5.1165
20. Toellner KM, Gulbranson-Judge A, Taylor DR, Sze DM, MacLennan IC. Immunoglobulin Switch Transcript Production *In Vivo* Related to the Site and Time of Antigen-Specific B Cell Activation. *J Exp Med* (1996) 183:2303–12. doi: 10.1084/jem.183.5.2303
21. Pape KA, Kouskoff V, Nemazee D, Tang LH, Cyster JG, Tze LE, et al. Visualization of the Genesis and Fate of Isotype-Switched B Cells During a Primary Immune Response. *J Exp Med* (2003) 197:1677–87. doi: 10.1084/jem.20012065
22. Roco JA, Mesin L, Binder SC, Nefzger C, Gonzalez-Figueroa P, Canete PF, et al. Class-Switch Recombination Occurs Infrequently in Germinal Centers. *Immunity* (2019) 51:337–50. doi: 10.1016/j.immuni.2019.07.001
23. Ehrenstein MR, Notley CA. The Importance of Natural IgM: Scavenger, Protector and Regulator. *Nat Rev Immunol* (2010) 10:778–86. doi: 10.1038/nri2849
24. Tung JW, Herzenberg LA. Unraveling B-1 Progenitors. *Curr Opin Immunol* (2007) 19:150–5. doi: 10.1016/j.coi.2007.02.012
25. Alt FW, Rosenberg N, Casanova RJ, Thomas E, Baltimore D. Immunoglobulin Heavy-Chain Expression and Class Switching in a Murine Leukaemia Cell Line. *Nature* (1982) 296:325–31. doi: 10.1038/296325a0
26. Akira S, Sugiyama H, Yoshida N, Kikutani H, Yamamura Y, Kishimoto T. Isotype Switching in Murine Pre-B Cell Lines. *Cell* (1983) 34:545–56. doi: 10.1016/0092-8674(83)90387-2
27. Burrows PD, Beck-Engeser GB, Wabl MR. Immunoglobulin Heavy-Chain Class Switching in a Pre-B Cell Line Is Accompanied by DNA Rearrangement. *Nature* (1983) 306:243–6. doi: 10.1038/306243a0
28. Kubagawa H, Mayumi M, Crist WM, Cooper MD. Immunoglobulin Heavy-Chain Switching in Pre-B Leukaemias. *Nature* (1983) 301:340–2. doi: 10.1038/301340a0
29. Sugiyama H, Maeda T, Akira S, Kishimoto S. Class-Switching From Mu to Gamma 3 or Gamma 2b Production at Pre-B Cell Stage. *J Immunol* (1986) 136:3092–7.
30. Edry E, Koralov SB, Rajewsky K, Melamed D. Spontaneous Class Switch Recombination in B Cell Lymphopoiesis Generates Aberrant Switch Junctions and Is Increased After VDJ Rearrangement. *J Immunol* (2007) 179:6555–60. doi: 10.4049/jimmunol.179.10.6555
31. Edry E, Azulay-Debby H, Melamed D. TOLL-Like Receptor Ligands Stimulate Aberrant Class Switch Recombination in Early B Cell Precursors. *Int Immunol* (2008) 20:1575–85. doi: 10.1093/intimm/dxn117
32. Han JH, Akira S, Calame K, Beutler B, Selsing E, Imanishi-Kari T. Class Switch Recombination and Somatic Hypermutation in Early Mouse B Cells Are Mediated by B Cell and Toll-Like Receptors. *Immunity* (2007) 27:64–75. doi: 10.1016/j.immuni.2007.05.018
33. Hasan M, Polic B, Bralic M, Jonjic S, Rajewsky K. Incomplete Block of B Cell Development and Immunoglobulin Production in Mice Carrying the muMT Mutation on the BALB/c Background. *Eur J Immunol* (2002) 32:3463–71. doi: 10.1002/1521-4141(200212)32:12<3463::AID-IMMU3463>3.0.CO;2-B
34. Kumar S, Wuerffel R, Achour I, Lajoie B, Sen R, Dekker J, et al. Flexible Ordering of Antibody Class Switch and V(D)J Joining During B-Cell Ontogeny. *Genes Dev* (2013) 27:2439–44. doi: 10.1101/gad.227165.113
35. Seagal J, Edry E, Keren Z, Leider N, Benny O, Machluf M, et al. A Fail-Safe Mechanism for Negative Selection of Isotype-Switched B Cell Precursors Is Regulated by the Fas/FasL Pathway. *J Exp Med* (2003) 198:1609–19. doi: 10.1084/jem.20030357
36. Lutzker S, Rothman P, Pollock R, Coffman R, Alt FW. Mitogen- and IL-4-Regulated Expression of Germ-Line Ig Gamma 2b Transcripts: Evidence for Directed Heavy Chain Class Switching. *Cell* (1988) 53:177–84. doi: 10.1016/0092-8674(88)90379-0
37. Rothman P, Li SC, Gorham B, Glimcher L, Alt F, Boothby M. Identification of a Conserved Lipopolysaccharide-Plus-Interleukin-4-Responsive Element Located at the Promoter of Germ Line Epsilon Transcripts. *Mol Cell Biol* (1991) 11:5551–61. doi: 10.1128/MCB.11.11.5551
38. Xu L, Gorham B, Li SC, Bottaro A, Alt FW, Rothman P. Replacement of Germ-Line Epsilon Promoter by Gene Targeting Alters Control of Immunoglobulin Heavy Chain Class Switching. *Proc Natl Acad Sci USA* (1993) 90:3705–9. doi: 10.1073/pnas.90.8.3705
39. Stavnezer J, Bjorkman A, Du L, Cagigi A, Pan-Hammarstrom Q. Mapping of Switch Recombination Junctions, a Tool for Studying DNA Repair Pathways During Immunoglobulin Class Switching. *Adv Immunol* (2010) 108:45–109. doi: 10.1016/B978-0-12-380995-7.00003-3
40. Boboila C, Alt FW, Schwer B. Classical and Alternative End-Joining Pathways for Repair of Lymphocyte-Specific and General DNA Double-Strand Breaks. *Adv Immunol* (2012) 116:1–49. doi: 10.1016/B978-0-12-394300-2.00001-6
41. Ernst P, Smale ST. Combinatorial Regulation of Transcription II: The Immunoglobulin Mu Heavy Chain Gene. *Immunity* (1995) 2:427–38. doi: 10.1016/1074-7613(95)90024-1
42. Perlot T, Pawlitzky I, Manis JP, Zarrin AA, Brodeur PH, Alt FW. Analysis of Mice Lacking DNaseI Hypersensitive Sites at the 5' End of the IgH Locus. *PLoS One* (2010) 5:e13992. doi: 10.1371/journal.pone.0013992
43. Sakai E, Bottaro A, Davidson L, Sleckman BP, Alt FW. Recombination and Transcription of the Endogenous Ig Heavy Chain Locus Is Effected by the Ig Heavy Chain Intronic Enhancer Core Region in the Absence of the Matrix Attachment Regions. *Proc Natl Acad Sci USA* (1999) 96:1526–31. doi: 10.1073/pnas.96.4.1526
44. Perlot T, Alt FW, Bassing CH, Suh H, Pinaud E. Elucidation of IgH Intronic Enhancer Functions via Germ-Line Deletion. *Proc Natl Acad Sci USA* (2005) 102:14362–7. doi: 10.1073/pnas.0507090102
45. Marquet M, Garot A, Bender S, Carrion C, Rouaud P, Lecardeur S, et al. The Emu Enhancer Region Influences H Chain Expression and B Cell Fate Without Impacting IgVH Repertoire and Immune Response *In Vivo*. *J Immunol* (2014) 193:1171–83. doi: 10.4049/jimmunol.1302868
46. Amoretti-Villa R, Rogier M, Robert I, Heyer V, Reina-San-Martin B. A Novel Regulatory Region Controls IgH Locus Transcription and Switch Recombination to a Subset of Isotypes. *Cell Mol Immunol* (2019) 16:887–9. doi: 10.1038/s41423-019-0267-4
47. Braikia FZ, Oudinet C, Haddad D, Oruc Z, Orlando D, Dauba A, et al. Inducible CTCF Insulator Delays the IgH 3' Regulatory Region-Mediated Activation of Germline Promoters and Alters Class Switching. *Proc Natl Acad Sci USA* (2017) 114:6092–7. doi: 10.1073/pnas.1701631114
48. Manis JP, van der Stoep N, Tian M, Ferrini R, Davidson L, Bottaro A, et al. Class Switching in B Cells Lacking 3' Immunoglobulin Heavy Chain Enhancers. *J Exp Med* (1998) 188:1421–31. doi: 10.1084/jem.188.8.1421
49. Vincent-Fabert C, Truffinet V, Fiancette R, Cogné N, Cogné M, Denizot Y. Ig Synthesis and Class Switching do Not Require the Presence of the Hs4 Enhancer in the 3' IgH Regulatory Region. *J Immunol* (2009) 182:6926–32. doi: 10.4049/jimmunol.0900214
50. Bébin AG, Carrion C, Marquet M, Cogné N, Lecardeur S, Cogné M, et al. *In Vivo* Redundant Function of the 3' IgH Regulatory Element HS3b in the Mouse. *J Immunol* (2010) 184:3710–7. doi: 10.4049/jimmunol.0901978
51. Pinaud E, Khamlichi AA, Le Morvan C, Drouet M, Nalesso V, Le Bert M, et al. Localization of the 3' IgH Locus Elements That Effect Long-Distance Regulation of Class Switch Recombination. *Immunity* (2001) 15:187–99. doi: 10.1016/S1074-7613(01)00181-9
52. Saintamand A, Vincent-Fabert C, Garot A, Rouaud P, Oruc Z, Magnone V, et al. Deciphering the Importance of the Palindromic Architecture of the Immunoglobulin Heavy-Chain 3' Regulatory Region. *Nat Commun* (2016) 7:10740. doi: 10.1038/ncomms10730
53. Garot A, Marquet M, Saintamand A, Bender S, Le Noir S, Rouaud P, et al. Sequential Activation and Distinct Functions for Distal and Proximal Modules Within the IgH 3' Regulatory Region. *Proc Natl Acad Sci USA* (2016) 113:1618–23. doi: 10.1073/pnas.1514090113
54. Le Noir S, Boyer F, Lecardeur S, Brousse M, Oruc Z, Cook-Moreau J, et al. Functional Anatomy of the Immunoglobulin Heavy Chain 3′ Super-

Enhancer Needs Not Only Core Enhancer Elements But Also Their Unique DNA Context. *Nucleic Acids Res* (2017) 45:5829–37. doi: 10.1093/nar/gkx203
55. Vincent-Fabert C, Fiancette R, Pinaud E, Truffinet V, Cogné N, Cogné M, et al. Genomic Deletion of the Whole IgH 3' Regulatory Region (Hs3a, Hs1,2, Hs3b, and Hs4) Dramatically Affects Class Switch Recombination and Ig Secretion to All Isotypes. *Blood* (2010) 116:1895–8. doi: 10.1182/blood-2010-01-264689
56. Santos JM, Braikia F-Z, Oudinet C, Haddad D, Conte C, Dauba A, et al. Duplication of a Germline Promoter Downstream of the IgH 3' Regulatory Region Impairs Class Switch Recombination. *Sci Rep* (2018) 8:9164. doi: 10.1038/s41598-018-27448-4
57. Benner C, Isoda T, Murre C. New Roles for DNA Cytosine Modification, eRNA, Anchors, and Superanchors in Developing B Cell Progenitors. *Proc Natl Acad Sci USA* (2015) 112:12776–81. doi: 10.1073/pnas.1512995112
58. Zhang X, Yoon HS, Chapdelaine-Williams AM, Kyritsis N, Alt FW. Physiological Role of the 3'igh CBEs Super-Anchor in Antibody Class Switching. *Proc Natl Acad Sci USA* (2021) 118:e2024392118. doi: 10.1073/pnas.2024392118
59. Pefanis E, Wang J, Rothschild G, Lim J, Kazadi D, Sun J, et al. RNA Exosome-Regulated Long non-Coding RNA Transcription Controls Super-Enhancer Activity. *Cell* (2015) 161:774–89. doi: 10.1016/j.cell.2015.04.034
60. Santos JM, Oudinet C, Schone L, Dauba A, Khamlichi AA. Essential Role of the Initial Activation Signal in Isotype Selection Upon Deletion of a Transcriptionally Committed Promoter. *Sci Rep* (2019) 9:18543. doi: 10.1038/s41598-019-54929-x
61. Zhang Y, Zhang X, Ba Z, Liang Z, Dring EW, Hu H, et al. The Fundamental Role of Chromatin Loop Extrusion in Physiological V(D)J Recombination. *Nature* (2019) 574:600–4. doi: 10.1038/s41586-019-1547-y
62. Kim A, Han L, Santiago GE, Verdun RE, Yu K. Class-Switch Recombination in the Absence of the IgH 3' Regulatory Region. *J Immunol* (2016) 197:2930–5. doi: 10.4049/jimmunol.1600530
63. Volpi SA, Verma-Gaur J, Hassan R, Ju Z, Roa S, Chatterjee S, et al. Germline Deletion of Igh 3' Regulatory Region Elements Hs 5, 6, 7 (Hs5-7) Affects B Cell-Specific Regulation, Rearrangement, and Insulation of the Igh Locus. *J Immunol* (2012) 188:2556–66. doi: 10.4049/jimmunol.1102763
64. Nair L, Chung H, Basu U. Regulation of Long non-Coding RNAs and Genome Dynamics by the RNA Surveillance Machinery. *Nat Rev Mol Cell Biol* (2020) 21:123–36. doi: 10.1038/s41580-019-0209-0
65. Li SC, Rothman PB, Zhang J, Chan C, Hirsh D, Alt FW. Expression of I Mu-C Gamma Hybrid Germline Transcripts Subsequent to Immunoglobulin Heavy Chain Class Switching. *Int Immunol* (1994) 6:491–7. doi: 10.1093/intimm/6.4.491
66. Rajagopal D, Maul RW, Ghosh A, Chakraborty T, Khamlichi AA, Sen R, et al. Immunoglobulin Switch Mu Sequence Causes RNA Polymerase II Accumulation and Reduces dA Hypermutation. *J Exp Med* (2009) 206:1237–44. doi: 10.1084/jem.20082514
67. Wuerffel R, Wang L, Grigera F, Manis J, Selsing E, Perlot T, et al. S-S Synapsis During Class Switch Recombination Is Promoted by Distantly Located Transcriptional Elements and Activation-Induced Deaminase. *Immunity* (2007) 27:711–22. doi: 10.1016/j.immuni.2007.09.007
68. Bruzeau C, Moreau J, Le Noir S, Pinaud E. Panorama of Stepwise Involvement of the IgH 3' Regulatory Region in Murine B Cells. *Adv Immunol* (2021) 149:95–114. doi: 10.1016/bs.ai.2021.03.004
69. Rouaud P, Vincent-Fabert C, Saintamand A, Fiancette R, Marquet M, Robert I, et al. The IgH 3' Regulatory Region Controls Somatic Hypermutation in Germinal Center B Cells. *J Exp Med* (2013) 210:1501–7. doi: 10.1084/jem.20130072
70. Saintamand A, Rouaud P, Garot A, Saad F, Carrion C, Oblet C, et al. The IgH 3' Regulatory Region Governs μ Chain Transcription in Mature B Lymphocytes and the B Cell Fate. *Oncotarget* (2015) 6:4845–52. doi: 10.18632/oncotarget.3010
71. Braikia FZ, Conte C, Moutahir M, Denizot Y, Cogné M, Khamlichi AA. Developmental Switch in the Transcriptional Activity of a Long-Range Regulatory Element. *Mol Cell Biol* (2015) 35:3370–80. doi: 10.1128/MCB.00509-15
72. Delgado-Benito V, Rosen DB, Wang Q, Gazumyan A, Pai JA, Oliveira TY, et al. The Chromatin Reader ZMYND8 Regulates Igh Enhancers to Promote Immunoglobulin Class Switch Recombination. *Mol Cell* (2018) 72:636–49.e638. doi: 10.1016/j.molcel.2018.08.042
73. Péron S, Laffleur B, Denis-Lagache N, Cook-Moreau J, Tinguely A, Delpy L, et al. AID-Driven Deletion Causes Immunoglobulin Heavy Chain Locus Suicide Recombination in B Cells. *Science* (2012) 336:931–4. doi: 10.1126/science.1218692
74. Delpy L, Le Bert M, Cogné M, Khamlichi AA. Germ-Line Transcription Occurs on Both the Functional and the non-Functional Alleles of Immunoglobulin Constant Heavy Chain Genes. *Eur J Immunol* (2003) 33:2108–13. doi: 10.1002/eji.200323969
75. Casola S, Cattoretti G, Uyttersprot N, Koralov SB, Seagal J, Hao Z, et al. Tracking Germinal Center B Cells Expressing Germ-Line Immunoglobulin Gamma1 Transcripts by Conditional Gene Targeting. *Proc Natl Acad Sci USA* (2006) 103:7496–01. doi: 10.1073/pnas.0602353103
76. Wu YL, Stubbington MJ, Daly M, Teichmann SA, Rada C. Intrinsic Transcriptional Heterogeneity in B Cells Controls Early Class Switching to IgE. *J Exp Med* (2017) 214:183–96. doi: 10.1084/jem.20161056
77. Lang RB, Stanton LW, Marcu KB. On Immunoglobulin Heavy Chain Gene Switching: Two Gamma 2b Genes Are Rearranged *via* Switch Sequences in MPC-11 Cells But Only One Is Expressed. *Nucleic Acids Res* (1982) 10:611–30. doi: 10.1093/nar/10.2.611
78. Radbruch A, Müller W, Rajewsky K. Class Switch Recombination Is IgG1 Specific on Active and Inactive IgH Loci of IgG1-Secreting B-Cell Blasts. *Proc Natl Acad Sci USA* (1986) 83:3954–7. doi: 10.1073/pnas.83.11.3954
79. Zhang Y, Gostissa M, Hildebrand DG, Becker MS, Boboila C, Chiarle R, et al. The Role of Mechanistic Factors in Promoting Chromosomal Translocations Found in Lymphoid and Other Cancers. *Adv Immunol* (2010) 106:93–133. doi: 10.1016/S0065-2776(10)06004-9
80. Burnett RC, Hanly WC, Zhai SK, Knight KL. The IgA Heavy-Chain Gene Family in Rabbit: Cloning and Sequence Analysis of 13 C Alpha Genes. *EMBO J* (1989) 8:4041–7. doi: 10.1002/j.1460-2075.1989.tb08587.x
81. Kingzette M, Spieker-Polet H, Yam PC, Zhai SK, Knight KL. Trans-Chromosomal Recombination Within the Ig Heavy Chain Switch Region in B Lymphocytes. *Proc Natl Acad Sci USA* (1998) 95:11840–5. doi: 10.1073/pnas.95.20.11840
82. Reynaud S, Delpy L, Fleury L, Dougier HL, Sirac C, Cogné M. Interallelic Class Switch Recombination Contributes Significantly to Class Switching in Mouse B Cells. *J Immunol* (2005) 174:6176–83. doi: 10.4049/jimmunol.174.10.6176
83. Dougier HL, Reynaud S, Pinaud E, Carrion C, Delpy L, Cogné M. Interallelic Class Switch Recombination can Reverse Allelic Exclusion and Allow Trans-Complementation of an IgH Locus Switching Defect. *Eur J Immunol* (2006) 36:2181–91. doi: 10.1002/eji.200535529
84. Le Noir S, Laffleur B, Carrion C, Garot A, Lecardeur S, Pinaud E, et al. The IgH Locus 3' Cis-Regulatory Super-Enhancer Co-Opts AID for Allelic Transvection. *Oncotarget* (2017) 8:12929–40. doi: 10.18632/oncotarget.14585
85. Chauveau C, Cogné M. Palindromic Structure of the IgH 3'locus Control Region. *Nat Genet* (1996) 14:15–6. doi: 10.1038/ng0996-15
86. Dalloul I, Boyer F, Dalloul Z, Pignarre A, Caron G, Fest T, et al. Locus Suicide Recombination Actively Occurs on the Functionally Rearranged IgH Allele in B-Cells From Inflamed Human Lymphoid Tissues. *PLoS Genet* (2019) 15:e1007721. doi: 10.1371/journal.pgen.1007721
87. Yamane A, Resch W, Kuo N, Kuchen S, Li Z, Sun HW, et al. Deep-Sequencing Identification of the Genomic Targets of the Cytidine Deaminase AID and Its Cofactor RPA in B Lymphocytes. *Nat Immunol* (2011) 12:62–9. doi: 10.1038/ni.1964
88. Meng FL, Du Z, Federation A, Hu J, Wang Q, Kieffer-Kwon KR, et al. Convergent Transcription at Intragenic Super-Enhancers Targets AID-Initiated Genomic Instability. *Cell* (2014) 159:1538–48. doi: 10.1016/j.cell.2014.11.014
89. Qian J, Wang Q, Dose M, Pruett N, Kieffer-Kwon KR, Resch W, et al. B Cell Super-Enhancers and Regulatory Clusters Recruit AID Tumorigenic Activity. *Cell* (2014) 159:1524–37. doi: 10.1016/j.cell.2014.11.013
90. Blattner FR, Tucker PW. The Molecular Biology of Immunoglobulin D. *Nature* (1984) 307:417–22. doi: 10.1038/307417a0
91. Gutzeit C, Chen K, Cerutti A. The Enigmatic Function of IgD: Some Answers at Last. *Eur J Immunol* (2018) 48:1101–13. doi: 10.1002/eji.201646547

92. Rouaud P, Saintamand A, Saad F, Carrion C, Lecardeur S, Cogné M, et al. Elucidation of the Enigmatic IgD Class-Switch Recombination *via* Germline Deletion of the IgH 3' Regulatory Region. *J Exp Med* (2014) 211:975–85. doi: 10.1084/jem.20131385
93. Issaoui H, Ghazzaui N, Saintamand A, Carrion C, Oblet C, Denizot Y. The IgH 3' Regulatory Region Super-Enhancer Does Not Control IgA Class Switch Recombination in the B1 Lineage. *Cell Mol Immunol* (2018) 15:289–91. doi: 10.1038/cmi.2017.103
94. Medvedovic J, Ebert A, Tagoh H, Tamir IM, Schwickert TA, Novatchkova M, et al. Flexible Long-Range Loops in the VH Gene Region of the Igh Locus Facilitate the Generation of a Diverse Antibody Repertoire. *Immunity* (2013) 39:229–44. doi: 10.1016/j.immuni.2013.08.011
95. Predeus AV, Gopalakrishnan S, Huang Y, Tang J, Feeney AJ, Oltz EM, et al. Targeted Chromatin Profiling Reveals Novel Enhancers in Ig H and Ig L Chain Loci. *J Immunol* (2014) 192:1064–70. doi: 10.4049/jimmunol.1302800
96. Whyte WA, Orlando DA, Hnisz D, Abraham BJ, Lin CY, Kagey MH, et al. Master Transcription Factors and Mediator Establish Super-Enhancers at Key Cell Identity Genes. *Cell* (2013) 153:307–19. doi: 10.1016/j.cell.2013.03.035
97. Thomas-Claudepierre AS, Robert I, Rocha PP, Raviram R, Schiavo E, Heyer V, et al. Mediator Facilitates Transcriptional Activation and Dynamic Long-Range Contacts at the IgH Locus During Class Switch Recombination. *J Exp Med* (2016) 213:303–12. doi: 10.1084/jem.20141967
98. Ohlsson R, Lobanenkov V, Klenova E. Does CTCF Mediate Between Nuclear Organization and Gene Expression? *Bioessays* (2010) 32:37–50. doi: 10.1002/bies.200900118
99. Nakahashi H, Kieffer Kwon KR, Resch W, Vian L, Dose M, Stavreva D, et al. A Genome-Wide Map of CTCF Multivalency Redefines the CTCF Code. *Cell Rep* (2013) 3:1678–89. doi: 10.1016/j.celrep.2013.04.024
100. Ong C-T, Corces VG. CTCF: An Architectural Protein Bridging Genome Topology and Function. *Nat Rev Genet* (2014) 15:234–46. doi: 10.1038/nrg3663
101. Marina-Zárate E, Perez-Garcia A, Ramiro AR. CCCTC-Binding Factor Locks Premature IgH Germline Transcription and Restrains Class Switch Recombination. *Front Immunol* (2017) 8:1076. doi: 10.3389/fimmu.2017.01076
102. Kakkis E, Mercola M, Calame K. Strong Transcriptional Activation of Translocated C-Myc Genes Occurs Without a Strong Nearby Enhancer or Promoter. *Nucleic Acids Res* (1988) 16:77–96. doi: 10.1093/nar/16.1.77
103. Thomas-Claudepierre A-S, Schiavo E, Heyer V, Fournier M, Page A, Robert I, et al. The Cohesin Complex Regulates Immunoglobulin Class Switch Recombination. *J Exp Med* (2013) 210:2495–502. doi: 10.1084/jem.20130166
104. Garrett FE, Emelyanov AV, Sepulveda MA, Flanagan P, Volpi S, Li F, et al. Chromatin Architecture Near a Potential 3' End of the Igh Locus Involves Modular Regulation of Histone Modifications During B-Cell Development and *In Vivo* Occupancy at CTCF Sites. *Mol Cell Biol* (2005) 25:1511–25. doi: 10.1128/MCB.25.4.1511-1525.2005
105. Aiden EL, Casellas R. Somatic Rearrangement in B Cells: It's (Mostly) Nuclear Physics. *Cell* (2015) 162:708–11. doi: 10.1016/j.cell.2015.07.034
106. Vian L, Pękowska A, Rao SSP, Kieffer-Kwon K-R, Jung S, Laura Baranello L, et al. The Energetics and Physiological Impact of Cohesin Extrusion. *Cell* (2018) 174:1165–78. doi: 10.1016/j.cell.2018.03.072
107. Swaminathan S, Klemm L, Park E, Papaemmanuil E, Ford A, Kweon SM, et al. Mechanisms of Clonal Evolution in Childhood Acute Lymphoblastic Leukemia. *Nat Immunol* (2015) 16:766–74. doi: 10.1038/ni.3160
108. Dauba A, Braikia FZ, Oudinet C, Khamlichi AA. Interleukin 7 Regulates Switch Transcription in Developing B Cells. *Cell Mol Immunol* (2021) 18:776–8. doi: 10.1038/s41423-020-0430-y
109. Cogné M, Lansford R, Bottaro A, Zhang J, Gorman J, Young F, et al. A Class Switch Control Region at the 3' End of the Immunoglobulin Heavy Chain Locus. *Cell* (1994) 77:747–7. doi: 10.1016/0092-8674(94)90057-4
110. Seidl KJ, Manis JP, Bottaro A, Zhang J, Davidson L, Kisselgof A, et al. Position-Dependent Inhibition of Class-Switch Recombination by PGK-Neor Cassettes Inserted Into the Immunoglobulin Heavy Chain Constant Region Locus. *Proc Natl Acad Sci USA* (1999) 96:3000–5. doi: 10.1073/pnas.96.6.3000
111. Oruc Z, Boumediene A, Le Bert M, Khamlichi AA. Replacement of Igamma3 Germ-Line Promoter by Igamma1 Inhibits Class-Switch Recombination to Igg3. *Proc Natl Acad Sci USA* (2007) 104:20484–9. doi: 10.1073/pnas.0608364104
112. Santos JM, Braikia FZ, Oudinet C, Dauba A, Khamlichi AA. Two Modes of Cis-Activation of Switch Transcription by the IgH Superenhancer. *Proc Natl Acad Sci USA* (2019) 116:14708–13. doi: 10.1073/pnas.1902250116
113. Jones PA. Functions of DNA Methylation: Islands, Start Sites, Gene Bodies and Beyond. *Nat Rev Genet* (2012) 13:484–92. doi: 10.1038/nrg3230
114. Oudinet C, Braikia FZ, Dauba A, Santos JM, Khamlichi AA. Developmental Regulation of DNA Cytosine Methylation at the Immunoglobulin Heavy Chain Constant Locus. *PLoS Genet* (2019) 15:e1007930. doi: 10.1371/journal.pgen.1007930
115. Wang L, Wuerffel R, Feldman S, Khamlichi AA, Kenter AL. S Region Sequence, RNA Polymerase II, and Histone Modifications Create Chromatin Accessibility During Class Switch Recombination. *J Exp Med* (2009) 206:1817–30. doi: 10.1084/jem.20081678
116. Wang L, Whang N, Wuerffel R, Kenter AL. AID-Dependent Histone Acetylation Is Detected in Immunoglobulin S Regions. *J Exp Med* (2006) 203:215–26. doi: 10.1084/jem.20051774
117. Daniel JA, Santos MA, Wang Z, Zang C, Schwab KR, Jankovic M, et al. PTIP Promotes Chromatin Changes Critical for Immunoglobulin Class Switch Recombination. *Science* (2010) 329:917–23. doi: 10.1126/science.1187942
118. Daniel JA, Nussenzweig A. The AID-Induced DNA Damage Response in Chromatin. *Mol Cell* (2013) 50:309–21. doi: 10.1016/j.molcel.2013.04.017
119. Schwab KR, Patel SR, Dressler GR. Role of PTIP in Class Switch Recombination and Long-Range Chromatin Interactions at the Immunoglobulin Heavy Chain Locus. *Mol Cell Biol* (2011) 31:1503–11. doi: 10.1128/MCB.00990-10
120. Callen E, Di Virgilio M, Kruhlak MJ, Nieto-Soler M, Wong N, Chen H-T, et al. 53BP1 Mediates Productive and Mutagenic DNA Repair Through Distinct Phosphoprotein Interactions. *Cell* (2013) 153:1266–80. doi: 10.1016/j.cell.2013.05.023
121. Saintamand A, Rouaud P, Saad F, Rios G, Cogné M, Denizot Y. Elucidation of IgH 3' Region Regulatory Role During Class Switch Recombination *via* Germline Deletion. *Nat Commun* (2015) 6:7084. doi: 10.1038/ncomms8084
122. Dekker J, Mirny L. The 3d Genome as Moderator of Chromosomal Communication. *Cell* (2016) 164:1110–21. doi: 10.1016/j.cell.2016.02.007
123. Rowley MJ, Corces VG. Organizational Principles of 3D Genome Architecture. *Nat Rev Genet* (2018) 19:789–800. doi: 10.1038/s41576-018-0060-8
124. Hnisz D, Day DS, Young RA. Insulated Neighborhoods: Structural and Functional Units of Mammalian Gene Control. *Cell* (2016) 167:1188–200. doi: 10.1016/j.cell.2016.10.024
125. Schoenfelder S, Fraser P. Long-Range Enhancer-Promoter Contacts in Gene Expression Control. *Nat Rev Genet* (2019) 20:437–55. doi: 10.1038/s41576-019-0128-0
126. Sanyal A, Lajoie BR, Jain G, Dekker J. The Long-Range Interaction Landscape of Gene Promoters. *Nature* (2012) 489:109–13. doi: 10.1038/nature11279
127. Rao SS, Huntley MH, Durand NC, Stamenova EK, Bochkov ID, Robinson JT, et al. A 3D Map of the Human Genome at Kilobase Resolution Reveals Principles of Chromatin Looping. *Cell* (2014) 159:1665–80. doi: 10.1016/j.cell.2014.11.021
128. de Wit E, Vos ES, Holwerda SJ, Valdes-Quezada C, Verstegen MJ, Teunissen H, et al. CTCF Binding Polarity Determines Chromatin Looping. *Mol Cell* (2015) 60:676–84. doi: 10.1016/j.molcel.2015.09.023
129. Guo Y, Xu Q, Canzio D, Shou J, Li J, Gorkin DU, et al. CRISPR Inversion of CTCF Sites Alters Genome Topology and Enhancer/Promoter Function. *Cell* (2015) 162:900–10. doi: 10.1016/j.cell.2015.07.038
130. Sanborn AL, Rao SS, Huang SC, Durand NC, Huntley MH, Jewett AI, et al. Chromatin Extrusion Explains Key Features of Loop and Domain Formation in Wild-Type and Engineered Genomes. *Proc Natl Acad Sci USA* (2015) 112:E6456–6465. doi: 10.1073/pnas.1518552112
131. Allen BL, Taatjes DJ. The Mediator Complex: A Central Integrator of Transcription. *Nat Rev Mol Cell Biol* (2015) 16:155–66. doi: 10.1038/nrm3951
132. Heinz S, Romanoski CE, Benner C, Glass CK. The Selection and Function of Cell Type-Specific Enhancers. *Nat Rev Mol Cell Biol* (2015) 16:144–54. doi: 10.1038/nrm3949
133. Soutourina J. Transcription Regulation by the Mediator Complex. *Nat Rev Mol Cell Biol* (2018) 19:262–74. doi: 10.1038/nrm.2017.115

134. Montefiori L, Wuerffel R, Roqueiro D, Lajoie B, Guo C, Gerasimova T, et al. Extremely Long-Range Chromatin Loops Link Topological Domains to Facilitate a Diverse Antibody Repertoire. *Cell Rep* (2016) 14:896–906. doi: 10.1016/j.celrep.2015.12.083
135. Li W, Notani D, Rosenfeld MG. Enhancers as non-Coding RNA Transcription Units: Recent Insights and Future Perspectives. *Nat Rev Genet* (2016) 17:207–23. doi: 10.1038/nrg.2016.4
136. Fitz J, Neumann T, Steininger M, Wiedemann EM, Garcia AC, Athanasiadis A, et al. Spt5-Mediated Enhancer Transcription Directly Couples Enhancer Activation With Physical Promoter Interaction. *Nat Genet* (2020) 52:505–15. doi: 10.1038/s41588-020-0605-6
137. Pavri R, Gazumyan A, Jankovic M, Di Virgilio M, Klein I, Ansarah-Sobrinho C, et al. Activation-Induced Cytidine Deaminase Targets DNA at Sites of RNA Polymerase II Stalling by Interaction With Spt5. *Cell* (2010) 143:122–33. doi: 10.1016/j.cell.2010.09.017
138. Rothschild G, Zhang W, Lim J, Giri PK, Laffleur B, Chen Y, et al. Noncoding RNA Transcription Alters Chromosomal Topology to Promote Isotype-Specific Class Switch Recombination. *Sci Immunol* (2020) 5:eaay5864. doi: 10.1126/sciimmunol.aay5864
139. Nasmyth K. Disseminating the Genome: Joining, Resolving, and Separating Sister Chromatids During Mitosis and Meiosis. *Annu Rev Genet* (2001) 35:674–745. doi: 10.1146/annurev.genet.35.102401.091334
140. Alipour E, Marko JF. Self-Organization of Domain Structures by DNA-Loop-Extruding Enzymes. *Nucleic Acids Res* (2012) 40:11202–12. doi: 10.1093/nar/gks925
141. Nichols MH, Corces VG. A CTCF Code for 3D Genome Architecture. *Cell* (2015) 162:703–5. doi: 10.1016/j.cell.2015.07.053
142. Fudenberg G, Imakaev M, Lu C, Goloborodko A, Abdennur N, Mirny LA. Formation of Chromosomal Domains by Loop Extrusion. *Cell Rep* (2016) 15:2038–49. doi: 10.1016/j.celrep.2016.04.085
143. Zhang X, Zhang Y, Ba Z, Kyritsis N, Casellas R, Alt FW. Fundamental Roles of Chromatin Loop Extrusion in Antibody Class Switching. *Nature* (2019) 575:385–9. doi: 10.1038/s41586-019-1723-0
144. Schatz DG, Ji Y. Recombination Centres and the Orchestration of V(D)J Recombination. *Nat Rev Immunol* (2011) 11:251–63. doi: 10.1038/nri2941
145. Lin SG, Ba Z, Alt FW, Zhang Y. RAG Chromatin Scanning During V (D)J Recombination and Chromatin Loop Extrusion Are Related Processes. *Adv Immunol* (2018) 139:93–135. doi: 10.1016/bs.ai.2018.07.001
146. Yu K. An Insulator That Regulates Chromatin Extrusion and Class Switch Recombination. *Proc Natl Acad Sci USA* (2021) 118:e2026399118. doi: 10.1073/pnas.2026399118
147. Rao SSP, Huang SC, Glenn St Hilaire B, Engreitz JM, Perez EM, Kieffer-Kwon KR, et al. Cohesin Loss Eliminates All Loop Domains. *Cell* (2017) 171:305–20. doi: 10.1016/j.cell.2017.09.026
148. Laffleur B, Lim J, Zhang W, Chen Y, Pefanis E, Bizarro J, et al. Noncoding RNA Processing by DIS3 Regulates Chromosomal Architecture and Somatic Hypermutation in B Cells. *Nat Genet* (2021) 53:230–42. doi: 10.1038/s41588-020-00772-0
149. Luppino JM, Park DS, Nguyen SC, Lan Y, Xu Z, Yunker R, et al. Cohesin Promotes Stochastic Domain Intermingling to Ensure Proper Regulation of Boundary-Proximal Genes. *Nat Genet* (2020) 52:840–8. doi: 10.1038/s41588-020-0647-9

Conflict of Interest: The authors declare that the research was conducted in the absence of any commercial or financial relationships that could be construed as a potential conflict of interest.

Publisher's Note: All claims expressed in this article are solely those of the authors and do not necessarily represent those of their affiliated organizations, or those of the publisher, the editors and the reviewers. Any product that may be evaluated in this article, or claim that may be made by its manufacturer, is not guaranteed or endorsed by the publisher.

frontiers in Immunology

ORIGINAL RESEARCH
published: 21 September 2021
doi: 10.3389/fimmu.2021.688493

Cohesin Core Complex Gene Dosage Contributes to Germinal Center Derived Lymphoma Phenotypes and Outcomes

Martin A. Rivas[1], Ceyda Durmaz[2†], Andreas Kloetgen[3†], Cristopher R. Chin[4,5], Zhengming Chen[6], Bhavneet Bhinder[4,5,7], Amnon Koren[8], Aaron D. Viny[9,10], Christopher D. Scharer[11], Jeremy M. Boss[11], Olivier Elemento[4,5,7], Christopher E. Mason[4,5,12,13] and Ari M. Melnick[1]**

[1] Division of Hematology and Medical Oncology, Department of Medicine, Weill Cornell Medicine, New York, NY, United States, [2] Graduate Program on Physiology, Biophysics & Systems Biology, Weill Cornell Medicine, New York, NY, United States, [3] Department of Computational Biology of Infection Research, Helmholtz Centre for Infection Research, Braunschweig, Germany, [4] Department of Physiology and Biophysics, Weill Cornell Medicine, New York, NY, United States, [5] The HRH Prince Alwaleed Bin Talal Bin Abdulaziz Al-Saud Institute for Computational Biomedicine, Weill Cornell Medicine, New York, NY, United States, [6] Division of Biostatistics and Epidemiology, Department of Population Health Sciences, Weill Cornell Medical College, New York, NY, United States, [7] Caryl and Israel Englander Institute for Precision Medicine, Weill Cornell Medicine, New York, NY, United States, [8] Department of Molecular Biology and Genetics, Cornell University, Ithaca, NY, United States, [9] Division of Hematology/Oncology, Department of Medicine, Columbia University Irving Medical Center, New York, NY, United States, [10] Columbia Stem Cell Initiative, Department of Genetics & Development, Columbia University, New York, NY, United States, [11] Department of Microbiology and Immunology, School of Medicine, Emory University, Atlanta, GA, United States, [12] The WorldQuant Initiative for Quantitative Prediction, Weill Cornell Medicine, New York, NY, United States, [13] The Feil Family Brain and Mind Research Institute, Weill Cornell Medicine, New York, NY, United States

The cohesin complex plays critical roles in genomic stability and gene expression through effects on 3D architecture. Cohesin core subunit genes are mutated across a wide cross-section of cancers, but not in germinal center (GC) derived lymphomas. In spite of this, haploinsufficiency of cohesin ATPase subunit *Smc3* was shown to contribute to malignant transformation of GC B-cells in mice. Herein we explored potential mechanisms and clinical relevance of *Smc3* deficiency in GC lymphomagenesis. Transcriptional profiling of *Smc3* haploinsufficient murine lymphomas revealed downregulation of genes repressed by loss of epigenetic tumor suppressors *Tet2* and *Kmt2d*. Profiling 3D chromosomal interactions in lymphomas revealed impaired enhancer-promoter interactions affecting genes like *Tet2*, which was aberrantly downregulated in *Smc3* deficient lymphomas. *Tet2* plays important roles in B-cell exit from the GC reaction, and single cell RNA-seq profiles and phenotypic trajectory analysis in *Smc3* mutant mice revealed a specific defect in commitment to the final steps of plasma cell differentiation. Although *Smc3* deficiency resulted in structural abnormalities in GC B-cells, there was no increase of somatic mutations or structural variants in *Smc3* haploinsufficient lymphomas, suggesting that cohesin deficiency largely induces lymphomas through disruption of enhancer-promoter interactions of terminal differentiation and tumor suppressor genes. Strikingly, the presence of the *Smc3* haploinsufficient GC B-cell transcriptional signature in human

OPEN ACCESS

Edited by:
Michel Cogne, University of Limoges, France

Reviewed by:
Rushad Pavri, Research Institute of Molecular Pathology (IMP), Austria
Brice Laffleur, Columbia University, United States
Bernardo Reina-San-Martin, Institut de Génétique et de Biologie Moléculaire et Cellulaire (IGBMC), France

***Correspondence:**
Martin A. Rivas
mar2091@med.cornell.edu
Ari M. Melnick
amm2014@med.cornell.edu

†These authors have contributed equally to this work

Specialty section:
This article was submitted to B Cell Biology, a section of the journal Frontiers in Immunology

Received: *30 March 2021*
Accepted: *24 August 2021*
Published: *21 September 2021*

Citation:
Rivas MA, Durmaz C, Kloetgen A, Chin CR, Chen Z, Bhinder B, Koren A, Viny AD, Scharer CD, Boss JM, Elemento O, Mason CE and Melnick AM (2021) Cohesin Core Complex Gene Dosage Contributes to Germinal Center Derived Lymphoma Phenotypes and Outcomes. Front. Immunol. 12:688493. doi: 10.3389/fimmu.2021.688493

patients with GC-derived diffuse large B-cell lymphoma (DLBCL) was linked to inferior clinical outcome and low expression of cohesin core subunits. Reciprocally, reduced expression of cohesin subunits was an independent risk factor for worse survival int DLBCL patient cohorts. Collectively, the data suggest that *Smc3* functions as a bona fide tumor suppressor for lymphomas through non-genetic mechanisms, and drives disease by disrupting the commitment of GC B-cells to the plasma cell fate.

Keywords: cohesin, lymphoma, B-cell, chromosomal architecture, Hi-C, Tet2 gene, GCB-subtype DLBCL

INTRODUCTION

Cohesin proteins form a ring-shaped complex that plays a key role in 3D architectural organization of the genome, and is composed of Smc3, Smc1a, Stag1 or Stag2 and Rad21 subunits. Cohesin functions include maintaining sister chromatids cohesion until the end of mitosis, as well as maintaining chromatids aligned when DNA-damage occurs (1). Acting in concert with CCCTC-binding factor (CTCF), the cohesin complex forms chromatin regulatory structures, such topologically associated domains, and long distance interactions between gene regulatory elements such as enhancers with gene promoters, thus contributing transcriptional regulatory states and cell phenotypes (2).

Germinal centers (GC) are transient structures that form within secondary lymphoid tissues in response to T-cell dependent antigenic stimulation. GCs are initially established by highly proliferative centroblasts that form the GC dark zone and undergo immunoglobulin somatic hypermutation (3). After several rounds of division these cells migrate towards a region rich in T follicular helper cells (TFH) as non-dividing centrocytes, to form the GC light zone. B-cells with increased affinity for cognate antigen will receive T-cell help, which will enable them to either return to the DZ for more rounds of somatic hypermutation, or exit the GC reaction to become plasma cells or memory B-cells (4). GC B-cells undergo massive changes in their transcriptional, epigenetic and 3D architectural states, which is required for them to manifest their distinctive phenotype (5). Along these lines, conditional knockout of the ATPase subunit of the cohesin complex, Smc3, showed that cohesin dosage regulates B cell transit through GCs (6). *Smc3* haploinsufficient ($Smc3^{wt/-}$) mice display GC hyperplasia, with increased proliferation, accumulation of centrocytes and impairment of plasma cell differentiation. Chromosomal architecture analysis by Hi-C revealed that $Smc3^{wt/-}$ centrocytes have decreased long-range chromosomal interactions between enhancers and promoters, and reduced expression of tumor suppressor genes linked to lymphomagenesis in humans. Consistent with these findings, *Smc3* haploinsufficiency accelerated lymphomagenesis in mice engineered for constitutive expression of the Bcl6 oncoprotein, which drives formation of diffuse large B-cell lymphomas (DLBCLs) (6).

Cohesin complex mutations are common in human cancers (7) including myeloid malignancies (8–10). Curiously, although *Smc3* behaves as a haploinsufficient tumor suppressor in GC B-cells, it is rarely if ever affected by somatic mutations in patients with GC-derived lymphomas. Yet *SMC3* dosage may still be relevant to human GC derived lymphomas since it was shown that patients with low *SMC3* expression experience inferior clinical outcomes (6). Therefore, to gain insight into how *SMC3* dosage might contribute to malignant lymphoma phenotypes we explored its transcriptional, architectural and genomic effects in murine B-cell and lymphoma models with *Smc3* haploinsufficiency, with correlations to human DLBCL patients.

METHODS

Conditional Smc3-Deficient Mice

The Research Animal Resource Center of the Weill Cornell Medical College approved all mouse procedures. The *Smc3* allele was deleted by targeting exon 4 in a construct obtained from the EUCOMM consortium [$Smc3^{tm1a(EUCOMM)Wtsi}$ (8)]. The generated mice ($Smc3^{fl/fl}$) were crossed to B6.129P2(Cg)-$Ighg1^{tm1(cre)Cgn}$/J mice (11) ($C\gamma1^{cre}$; The Jackson Laboratory) to generate germinal center specific heterozygous deletion of *Smc3*. $C\gamma1^{cre/cre}$;$Smc3^{wt/-}$ mice were further crossed to $Ighm^{wt/tm1(Bcl6)Rdf}$ mice [*IμBcl6* (12)].

Induced Germinal Center B Cell Culture System

Induced GC B cell (iGCB) cultures were performed as reported elsewhere (13). Briefly, splenic $CD43^-$ cells were co-cultured with irradiated 40LB cells (13) in the presence of 1 ng/mL IL-4. Four days after plating, iGCBs were incubated for 1 h in the presence of demecolcine 0.01 μg/ml, and iGCBs were separated by carefully collecting the cells in suspension and used in karyotyping analysis.

Karyotyping Analysis

Induced GCB-like cells from culture systems were treated for 1 h with 0.01 μg/mL *N*-methyl-*N*-deacetyl-colchicine. Following 45 min incubation at 37°C, the cultures were resuspended in pre-warmed 0.075 M KCl, incubated for an additional 10 min at 37°C and fixed in methanol:acetic acid (3:1). The fixed cell suspension was then dropped onto slides, stained in 0.08 μg/ml DAPI in 2 × SSC for 5 min and mounted in antifade solution (Vectashield, Vector Labs). Metaphase spreads were captured using a Nikon Eclipse E800 epifluorescence microscope equipped with GenASI Cytogenetic suite (Applied Spectral Imaging). For each sample a minimum of 50 inverted DAPI-stained metaphases were fully karyotyped and analyzed.

Flow Cytometry

Single-cell suspensions from mouse spleens and were stained using the following fluorescence-labeled anti-mouse antibodies: from BD Biosciences, FITC anti-CD38 (BD558813; clone 90; dilution 1:500), BV421 anti-CD95/Fas (BD562633; clone Jo2; dilution 1/500), PE-Cy7 anti-CD86 (BD560582; clone GL1; dilution 1:400), PE anti-CD184/CXCR4 (BD561734; 2B11; dilution 1:250); from BioLegend, APC-Cy7 anti-B220 (103224; clone RA3-6B2; dilution 1:750) and AlexaFluor647 anti-pSer139-H2AX (613407; clone 2F3, dilution 1:200). For internal markers, cells were fixed and permeabilized with the BD Cytofix/Cytoperm fixation/permeabilization solution kit (BD Biosciences). Data were acquired on a BD FACSCanto II flow cytometer (BD Biosciences) and analyzed using the FlowJo software package (BD Biosciences).

Patient Data

For survival analysis we used publicly available gene expression data from 322 DLBCL patients from British Columbia Cancer Agency, BCCA (14). Additional analysis have been done in 243 patients from an NCI cohort (15). For univariable and multivariable Cox analysis, we used data from the British Columbia Cancer Agency cohort, and from publicly available gene expression data of 757 DLBCL patients, an independent cohort from our institution (16–19). All patient data used in this manuscript has been previously de-identified.

Whole-Exome Sequencing and Identification of Somatic Variants

Genomic DNA from tumors was extracted from the mouse Smc3/Bcl6 or Bcl6 tumors and the germline tail (wild type) using DNeasy Blood Tissue kit (Qiagen). 1 μg of the genomic DNA was used to prepare the whole exome sequencing libraries with the Agilent SureSelect kit (SureSelect Mouse All Exon Kit). Using the NovaSeq6000 platform (Illumina), paired end sequencing was performed on the Smc3/Bcl6 (n=10) and Bcl6 tumors (n=5), and the wild type specimens (n=4). The average sequencing converge in the targeted regions was >40X except for one wild-type sample where the average coverage was 18X; this sample was excluded from further analysis. The whole exome sequencing reads were aligned to the Mouse reference genome GRCm38/mm10 using bwa mem and the PCR duplicates were marked and removed using Picard. The aligned and de-duplicated reads were then realigned around the indels, mates fixed and recalibrated to be used for downstream analysis. Somatic mutations were called using a consensus approach, where point mutations and indels were identified using Strelka2, MuTect and VarScan, and variants called by minimum two tools were retained for further analysis. Additional filtering steps excluded variants with total read depth < 30, number of reads supporting the variant < 5, tumor variant allele frequency (VAF) < 10% and germline VAF > 1%. The somatic mutations were annotated using the Variant Effect Predictor (VEP) and known mouse dbSNPs were filtered out while retaining only the missense, silent and truncating mutations. Copy number alterations were identified using the CNVkit. The percent genome altered (gain or loss) was calculated as the percentage of the copy number segments altered based on the size of the mouse genome. For the calculation of the altered segments, copy number segments with log2 ratio threshold of <-0.1 and >0.1 was used to quantify loss and gains, respectively. All statistical tests for significance were performed using the Wilcoxon rank sum test in R.

Whole Genome Sequencing Analysis

Primary naïve B cells isolated from *Smc3*$^{wt/wt}$ (n=3) or *Smc3*$^{wt/-}$ were cultured ex vivo to produce iGCs as explained (13). Genomic DNA was used to produce whole genome sequencing libraries using the KAPA LTP Library Preparation kit following manufacturer's directions. Sequencing was done in NextSeq500 instrument using a 75 bp single-read sequencing cell. We used TIGER (20) to infer DNA copy number values at 1Kb windows in mm10 coordinates. TIGER separates continuous and low-amplitude signals of DNA replication timing from the larger and sharper changes caused by copy number alterations. For genome-wide visualization of raw DNA copy number values, every 40 consecutive windows were merged. For DNA replication timing, outlier segments representing putative copy number alterations were filtered out by TIGER, and the remaining data was smoothed, normalized to units of standard deviation, and plotted.

RNA Sequencing

mRNA-seq Library Preparation and RNA-seq libraries were prepared using the Illumina TruSeq RNA sample kits, according to the manufacturer. Libraries were validated using the Agilent Technologies 2100 Bioanalyzer and Quant-iT dsDNA HS Assay (Life Technologies) and 8–10 pM sequenced on HiSeq2000 sequencer. RNA-seq data was processed using the nf-core/rnaseq pipeline (v1.4.2) (21). Reads were aligned to mm10 and Gencode M12 (22) transcripts using STAR (v2.6.1) (23). Gene expression quantified by featureCounts (v1.6.4) (24) to counts and normalized to Transcripts per Million (TPM) (25). Differentially expressed genes between Smc3wt/– and Smc3wt/wt were identified using count data with a negative binomial model with the DESeq2 package (26). Pathway enrichment was calculated by using GSEA (27) and FGSEA (v1.14.0) (28) on the $\log_2$ fold change ranking results from DESeq2 output (26) with gene signature databases from literature, using murine and human orthologs of genes as necessary.

Hi-C and Virtual 4C

1.5×10^6 flow sorted mouse GC B cells from Cγ1$^{wt/cre}$;Smc3$^{wt/wt}$ (n=3) and Cγ1$^{wt/cre}$;Smc3$^{wt/-}$ (n=3) were fixed in 1% formaldehyde for 10 min. Fixation was quenched by the addition of 0.125 M glycine for 10 min. In situ Hi-C was performed as described (29). Briefly, nuclei were permeabilized and DNA was digested overnight with 100 U DpnII (New England BioLabs). The ends of the restriction fragments were labeled using biotin-14-dATP and ligated in 1 mL final volume. After reversal of crosslinks, ligated DNA was purified and sheared to a length of ~400 bp, at which point ligation

junctions were pulled down with streptavidin beads, DNA fragments repaired, dA-tailed and Illumina adapters ligated. Library was produced by 6-10 cycles of PCR amplification. Sequencing was performed in a HiSeq2500 Illumina Sequencer, pair-end 50 bp, in the Weill Cornell Medicine Epigenomics Core.

All Hi-C data were processed using the hic-bench platform (30). In short, reads were aligned against the mouse genome (mm10) with bowtie (31) and multi-mapped, single-sided, duplicated, low quality and self-ligated reads were filtered with genomic-tools (32). Contact matrices were built with hic-bench at 20kb and 100kb resolution. Compartment analysis was performed with the c-score tool (33) at 100kb resolution, and A and B compartments were defined with the help of H3K27ac information. Compartment differences were defined as the difference in c-scores, called delta c-score. Loop analysis was performed with the mango loop calling approach (34), using a negative binomial test per diagonal in the 20kb resolution contact matrix, followed by multiple testing correction. Only loops with FDR<0.1 and CPM>30 were kept as significant loops. Differential loop analysis reported the $\log_2$ fold-change between CPM values per significant loop called in either sample. Protein-coding gene promoters and enhancer information were overlapped with all loop anchors, and promoter-enhancer loops were defined if one anchor holds at least one protein-coding gene promoter and the other anchor holds at least one enhancer. Virtual 4C analysis was performed based on the filtered reads. Filtered read pairs for which one read maps within +/– 10kb around the virtual viewpoint of the *Tet2* promoter (chr3:133,544,706) were extracted. Next, the genome was binned in successive overlapping windows of 20kb, and all adjacent windows are overlapping by 95% of their length (that is 19kb). We then added a count to all overlapping bins in which the second mapped read mate aligned. Read counts were then normalized to the total sequencing depth of the respective sample by edgeR reporting counts-per-million (CPM) per bin. Rad21 ChIP-seq in the CH12.LX mouse lymphoma cell line was downloaded from ENCODE (35, 36).

Single-Cell RNA Sequencing

Splenic cells were sorted from *Smc3*$^{wt/wt}$ (n=6) and *Smc3*$^{wt/-}$ (n=3) mice 8 days after SRBC immunization. Sorted cells were subjected to single cell RNA-seq using the 10X Genomics Chromium platform. Library preparation for single cell 3' RNA-seq v2, sequencing and post-processing of the raw data was performed at the Epigenomics Core at Weill Cornell Medicine. Libraries were prepared according to 10X Genomics specification and clustered on HiSeq4000. Sequencing data was processed with Cell Ranger from the 10X Genomics Cell Ranger Single Cell Software suite v3.0.2 (https://support.10xgenomics.com/single-cell-gene-expression/software/pipelines/latest/what-is-cell-ranger) using the manufacturer parameters to generate a sparse matrix file of features by barcodes. This sparse matrix data was then loaded into R (v4.0.2) using the R package Seurat (v4.0.0) (37). Additional wild-type 10X single-cell RNA-seq data was integrated with the Smc3 single-cell dataset to reduce batch effect. To identify genes and cells suitable for inclusion in the analysis, standard quality control was run to remove cells with few genes or an over representation of mitochondria reads. Data was then scaled and normalized. Linear dimensional reduction was performed by calculation of PCA from the most variable genes. Cells were then clustered using a resolution value of 0.5 and visualized by UMAP. Module scores were calculated using the AddModuleScore function with a control value of 5. Individual genes and gene signatures were projected and used to manually classify clusters. Centroblast (CB) and centrocyte (CC) cell clusters were identified using gene signatures defined by germinal center microarrays of DZ and LZ genes (38). Transitioning centroblast to centrocyte (CB → CC) clusters were classified by overlap of both DZ and LZ markers. The transitioning centrocyte to centroblast (Recycling) cluster was classified by a light zone DECP upregulated signature (39). Plasma cell (PC) clusters were identified using gene signatures from RNA-seq data (40), and the plasma blast (PB) cluster was identified as expressing c-Myc and S phase genes in addition to PC gene signatures. Prememory B cells (Pre-MBC) clusters were identified using transcriptional gene markers (41), and were subset into naive B cells (NB/Pre-MBC) and memory B cells (Pre-MBC/MBC) based on IgD^+ gene expression and Ccr6 gene signatures respectively. Cell division signatures from RNA-seq were derived from Scharer et al. (42) data by determining significantly upregulated (padj < 0.05, log2FC > 1) genes between cells that underwent 8 cell divisions (D8) and express CD138 (D8 $CD138^+$) or not (D8 $CD138^-$), and cells that did not divide (division 0, D0) as assessed by the CTV fluorescence by flow cytometry (42). These signatures were then used to calculate module scores, project onto UMAP, and downstream analysis. RNA trajectory analysis was performed using Slingshot (v1.6.1). This package was used to create a pseudotime based on a combination of PCA 1 and 2 calculated by Seurat, using the cells identified as Centroblasts as the anchor point. Three lineages were generated (Lineage 1: CB → CC → MBC, Lineage 2: CB → Recycling, Lineage 3: CB → PC), and Lineage 3 was projected onto UMAP and used in downstream analysis. Pseudotime density plots were generated by cell cluster using the ggplot2 (v3.3.2) geom_density function. Pseudotime scatter plots were generated by genotype using the geom_point function.

Quantitative RT-PCR

RNA was prepared by TRIzol extraction (Invitrogen). cDNA was prepared using the Verso cDNA synthesis kit (Thermo Fisher Scientific) and detected by Fast SYBR Green (Thermo Fisher Scientific) on a QuantStudio 6 Flex Real-Time PCR System (Thermo Fisher Scientific). We normalized gene expression to that of *Hprt1* and expressed values relative to control using the ΔΔCT method. Results were represented as fold expression with the s.d. for two series of triplicates. The following primers were used in qPCR experiments: Smc3_F, 5'-GGCTTCCGAAGT TACCGAGA-3'; Smc3_R, 5'-CAATCGCTGCTCTGGACG-3'; Tet2_F, 5'-TAGCTTTGCGTCAGTGGAGA-3'; Tet2_R, 5'-TAGGGATGGCTGGCTCAAAA-3'; Hprt1_F, 5′-AGGACCTCTCGAAGTGTTGG-3′; Hprt1_R, 5′-TTG CAGATTCAACTTGCGCT-3′.

Quantification and Statistical Analysis

The overall survival of DLBCL patients was estimated by Kaplan-Meier method. The mRNA expression levels of genes in the Smc3_*vs*_WT:CC_UP_logFC_0.56 gene signature [human orthologs: *H1F0*, *RP1L1*, *GSTT2B*, *GSTT2*, *THYN1*, *ALAD*, *IRAK1BP1*, *RANBP17*, *UBE2C*, *RET*, *GNB4*, *USP2*, *MFGE8*, *LGALS1*, *EMP2*, *TMED6*, *GCSAM*, *BFSP2*, *MYL4*, *GNAZ*, *TBXA2R*, *CPNE5*, *LRRC49*, *CCNB2*, *PAFAH1B3*, *CDC20*, *SCCPDH*, *AVIL*, *PI4KB*, *SSR2*, *CDKN3*, *NREP*, *TMOD4* (6)] were used for unsupervised hierarchical clustering on DLBCL patient cohorts. The differences of overall survival between two resulting clusters were tested by log-rank test. The univariable and multivariable Cox proportional hazard regression were also used to confirm the findings, while adjusting for age, sex and subtype. Statistical analyses were performed in statistical software R Version 3.6.0 (R Foundation for Statistical Computing, Vienna, Austria).

RESULTS

Aberrant Transcriptional Programming in *Smc3* Haploinsufficient Lymphomas

Smc3 haploinsufficiency drives accelerated lymphomagenesis in *IμBcl6* transgenic mice (6). To explore whether this aggressive phenotype was linked to aberrant transcriptional programming, we performed RNA-seq from mesenteric lymph node lymphoma cells from the $Smc3^{wt/wt}$;$C\gamma1^{wt/cre}$;*IμBcl6* (Bcl6) and $Smc3^{wt/-}$;$C\gamma1^{wt/cre}$;*IμBcl6* (Smc3/Bcl6) mice, verifying the expected reduced expression of *Smc3* (**Figure 1A**, **Supplementary Table 1**, and **Supplementary Figure 1A**). Unsupervised analyses did not yield strong differences between these lymphomas (**Supplementary Figures 1B, C**), and no difference in other cohesin subunit or related genes (**Supplementary Figure 1D**). However, naturally occurring primary lymphomas are often highly heterogeneous including in the context of *IuBcl6*

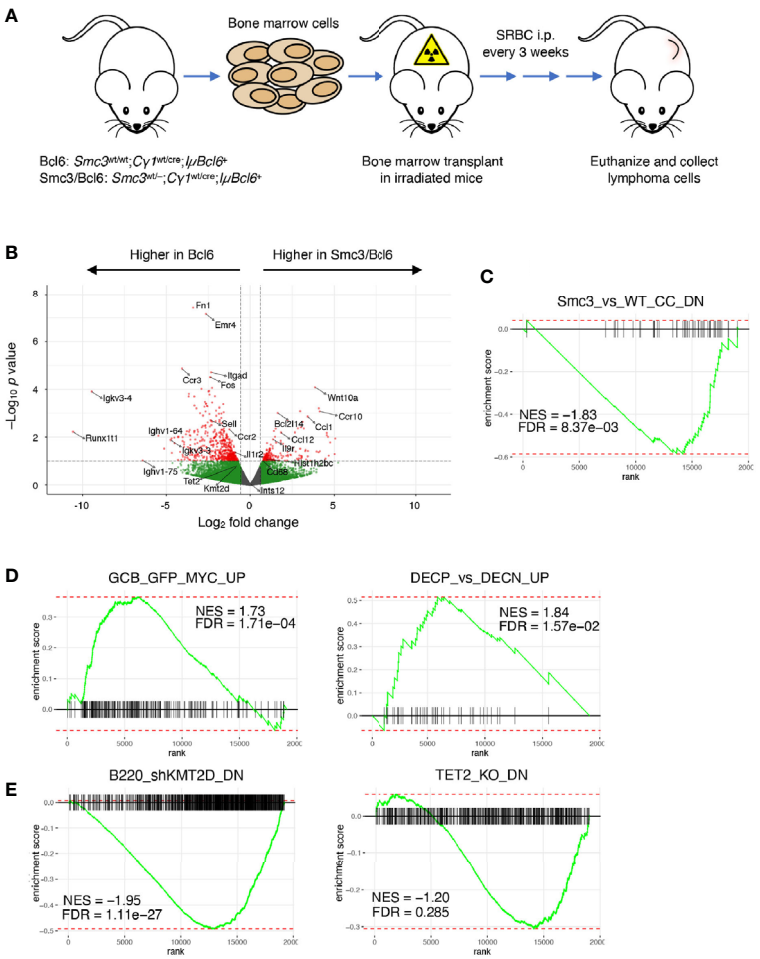

FIGURE 1 | Aberrant gene expression program in Smc3 haploinsufficient tumors. **(A)** Development and experimental design for study of lymphomas in Bcl6 and Smc3/Bcl6 mice, where conditional heterozygous deletion of Smc3 was directed towards B-cells entering the GC reaction by crossing to the Cγ1-Cre strain. **(B)** Volcano plot showing differentially expressed genes in Bcl6 and Smc3/Bcl6 tumor cell RNA-sequencing. **(C–E)** Gene set enrichment analysis plots in Bcl6 *vs* Smc3/Bcl6 RNA-sequencing. Smc3_*vs*_WT_CC_DN (6), DECP_*vs*_DECN_UP, GCB_GFP_MYC_UP (39), B220_shKMT2D_DN (43) and TET2_KO_DN (44).

mice (12, 45, 46), which might interfere with our ability to appreciate changes in gene expression. Along these lines, a supervised analysis indeed revealed only subtle differences in the transcriptional programs of Bcl6 *versus* Smc3/Bcl6 mice with 199 genes upregulated and 537 genes downregulated in Smc3/Bcl6 tumors (pval < 0.1, |log2FC| > 0.56 used, **Figure 1B**), that were not captured using higher stringency parameters. In spite of this there was evident perturbation of transcriptional programming in these tumors, as noted by performing GSEA analysis, which revealed significant down regulation of genes that were previously shown to be repressed in *Smc3*$^{wt/-}$ centrocytes (6) (**Figure 1C**). More critically and consistent with the observed aggressive tumor phenotype, Smc3/Bcl6 lymphomas featured induction of canonical GC-associated MYC target gene sets (**Figure 1D**). We also found evidence of tumor suppressor effects, such as negative enrichment for genes down regulated in *Kmt2d* or *Tet2* deficient GCs (**Figure 1E**). Both of these genes are tumor suppressors in human DLBCLs (47), and *Tet2* loss of function was also shown to induce lymphomagenesis in *IuBcl6* mice (44). Overall these transcriptional perturbations similar to those caused by *Smc3* haploinsufficiency in GC B-cells, suggest that persistence of these effects contributes to its role in lymphomagenesis.

Cohesin Haploinsufficiency Induces Loss of Tumor Suppressor Gene Promoter-Enhancer Interactions

In order to explore whether these changes in gene expression or other aspects of the malignant phenotype might be linked to 3D architectural effects, we performed *in situ* Hi-C in lymphoma cells collected from involved mesenteric lymph node tumors of moribund Bcl6 (n=3) and Smc3/Bcl6 (n=3) mice. Hi-C contact maps revealed little difference globally between Smc3/Bcl6 *vs* Bcl6 tumor interactivity profiles (**Supplementary Figure 2A**). This is consistent with genomic chromatin compartmentalization being independent of cohesin subunit dose, as previously reported (48). Indeed further examination of chromatin compartment distribution in Smc3/Bcl6 *vs* Bcl6 and tumor cells showed very little difference between these genotypes (**Figure 2A** and **Supplementary Figure 2B**). In contrast, there were significant compartment changes among these lymphomas as compared to normal centrocytes (**Figure 2B**). Hence aberrant chromatin compartmentalization in these lymphomas must occur through a cohesin independent manner as well. Focusing instead on differential chromatin interactivity, we found a significant bias towards reduction in chromatin loop strength in Smc3/Bcl6 *vs* Bcl6 lymphomas (**Figure 2C**). There was also significant difference in loop strength when comparing all murine lymphomas to normal centrocytes (**Figure 2D**). Examining differential chromatin interactions in more detail revealed reduction in loop strength of enhancer-promoter loops as well as other chromatin interactions (**Supplementary Figure 2C**). Among genes with reduced enhancer-promoter loops were known tumor suppressors such as *Tet2*, *Dusp4*, as well as MHC class II genes. Conversely genes such as *Cdk6, Btk* and *Irak1* were among those with stronger enhancer to promoter looping. Decreased loop interactivity in Smc3/Bcl6 *versus* Bcl6 tumors was also appreciated by performing aggregate peak analysis (**Supplementary Figure 2D**).

The reduction of *Tet2* enhancer promoter loop strength observed in this global analysis prompted us to look more closely at this tumor suppressor gene. For this we performed virtual 4C analysis using our Hi-C data (**Figure 2E**), anchored at the *Tet2* promoter and observed marked reduction of its interactivity with upstream and downstream regions (**Figure 2E**). These sites overlapped with putative enhancers defined by the presence of H3K27Ac peaks identified by Mint-ChIP-seq from GC B-cells (6) and with cohesin subunit Rad21ChIP-seq peaks in murine CHX.12 lymphoma cells (35). Strikingly, this reduction in *Tet2* promoter to enhancer looping was associated with reduced abundance of *Tet2* mRNA in Smc3/Bcl6 *vs* Bcl6 lymphomas from qPCR experiments performed in independent lymphoma specimens (**Figure 2F**). Tumor suppressor genes *Kmt2d* and *Dusp4* showed similar loss of interactivity of their promoters with putative H3K27Ac rich loci (**Supplementary Figures 2E, F**) in Smc3/Bcl6 tumors. Taken together with our transcriptional profiling showing enrichment for *Tet2* and Kmt2d deficient signatures, these data suggest that reduced levels of *Smc3* in lymphomas impairs expression and functionality of tumor suppressor genes through disruption of enhancer-promoter interactions.

Smc3 Haploinsufficiency Specifically Impairs Terminal Steps of Plasma Cell Differentiation

Conditional deletion of *Smc3* in GC B-cells results in impaired plasma cell differentiation (6). Our data shown above suggest that this effect persists in *Smc3* haploinsufficient lymphomas, pointing to plasma cell differentiation as a key vulnerability for malignant transformation. However, this is a step-wise and complex process, and the precise point in plasma cell differentiation where the *Smc3* function becomes critical is not known. Along these lines, Scharer et al. revealed that mature B cells induced to form plasma cells undergo ~8 cell divisions prior to acquiring the full plasma cell phenotype (42). Scharer et al. performed RNA-seq at sequential cell divisions in selected populations based on cell cycle dye exclusion and CD138 staining, as well as single cell RNA-seq of activated B cells to precisely map plasma cell differentiation trajectory. This trajectory was complex and included a critical cell fate decision that took place upon the last (8^{th}) cell division, whereupon B-cells either committed to the final plasma cell phenotype or remained in a less defined B-cell state (**Figure 3A**) (42).

To define the point along this trajectory that was specifically dependent on *Smc3* dosage, we performed single cell RNA-seq in *Smc3*$^{wt/-}$ and *Smc3*$^{wt/wt}$ GC B cells. We defined cell clusters by unsupervised analysis using Seurat and then projected canonical GC and post-GC related signatures from centroblasts (DZ), centrocytes (LZ), plasma cells (PC), memory B-cells (MB), and MYC^{+} GC B-cells (selected by T-cell help) onto these transcriptional profiles. This allowed us to assign clusters of cells to these various cell subpopulations (**Figures 3B–D**).

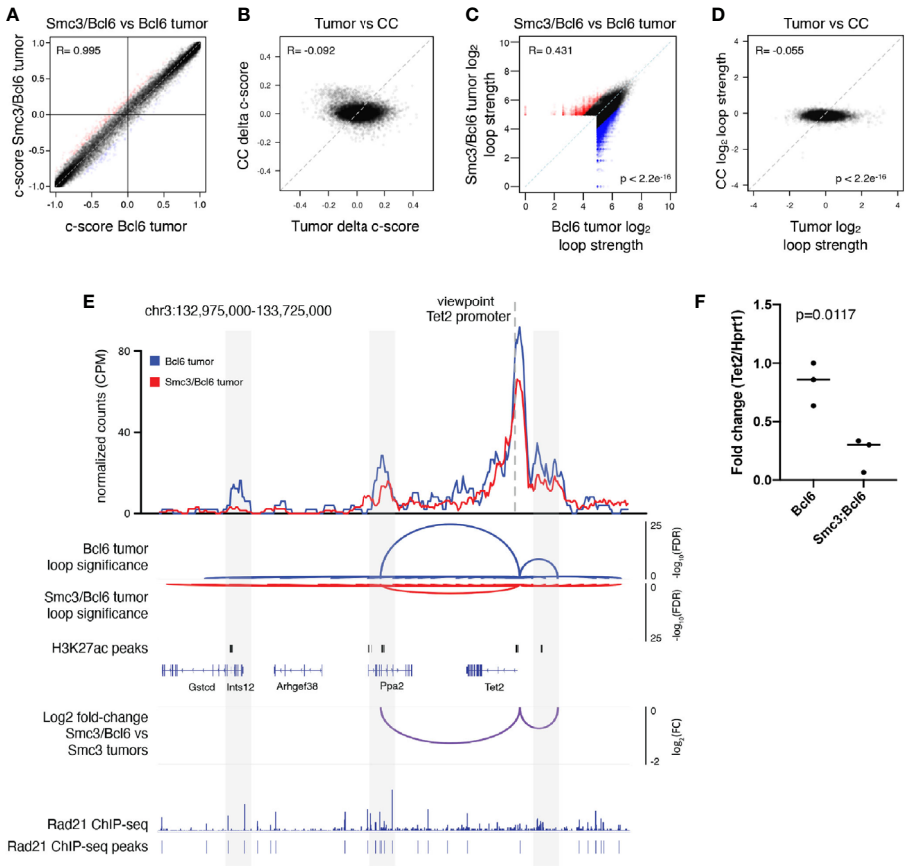

FIGURE 2 | Cohesin haploinsufficiency induces loss of interactivity of promoter-enhancers at tumor suppressor genes. **(A)** Correlation plot between the compartment c-scores of Smc3/Bcl6 *versus* Bcl6 tumor cells at 100kb resolution. **(B)** Correlation plot for the change in compartment c-scores of Smc3/Bcl6 *versus* Bcl6 tumor cells and the change in compartment c-scores of *Smc3*$^{wt/-}$ *versus* *Smc3*$^{wt/wt}$ centrocytes (CC) at 100kb resolution. **(C)** Correlation plot for the log_2 normalized loop interactivity of Smc3/Bcl6 *versus* Bcl6 tumor cells at 20kb resolution. **(D)** Correlation plot for the log_2 fold change of normalized loop interactivity of Smc3/Bcl6 *versus* Bcl6 tumor cells and the log_2 fold change of normalized loop interactivity of *Smc3*$^{wt/-}$ *versus* *Smc3*$^{wt/wt}$ centrocytes (CC) at 20kb resolution. **(E)** Virtual 4C analysis showing normalized interactions with the *Tet2* promoter for Bcl6 tumors (blue line) and Smc3/Bcl6 tumors (red line) at 20kb resolution. Loop calling significance following the mango approach are shown for Bcl6 and Smc3/Bcl6 tumors with $-log_{10}$(FDR). Enhancers were defined as H3K27Ac peaks mapped in germinal center B cells by Mint-ChIP. Rad21 ChIP-seq was performed in the mouse lymphoma cell line CH12.LX (35). The differences between normalized interactions with the *Tet2* promoter are shown as log_2 fold-change between Bcl6 and Smc3/Bcl6 tumors. **(F)** RT-qPCR for *Tet2* mRNA in Bcl6 (n=3) and Smc3/Bcl6 (n=3) tumors, normalized to *Hprt1* mRNA expression.

Plasma cells were further subdivided into plasmablasts *vs* plasma cells based on the former expressing MYC-associated and S phase genes (**Figure 3C**). Other cell clusters were assigned as intermediate between DZ and LZ, possibly reflecting cells transitioning from DZ to LZ. In addition to MB cells, we identified cell clusters enriching for a mixture of cells with pre-MB signature, with IgD$^+$ naïve B-cells.

We then projected the RNA-seq signatures derived from the data from Scharer et al. (42), by comparing their division 8 (D8) CD138$^+$ or D8 CD138$^-$ profiles with those from baseline (day 0) mature B-cells (**Figure 3E**). D8 CD138$^+$ cells largely overlapped with plasmablast and plasma cells, whereas D8 CD138$^-$ overlapped with centrocytes and memory/pre-memory B cells (**Figure 3E**). Examining the plasmablast and plasma cell populations from our single cell RNA-seq dataset we observed depletion of D8 CD138$^+$ signature gene scores among *Smc3*$^{wt/-}$ cells (**Figure 3F**), whereas in contrast these cells scored more highly for D8 CD138$^-$ signature gene expression (**Figure 3G**). Performing pseudotime analysis to distribute cells according to their differentiation state from centroblast towards plasma cell transcriptional programming (**Supplementary Figure 3**), we observed impaired acquisition of the D8 CD138$^+$ signature among *Smc3*$^{wt/-}$ haploinsufficient plasma cells, suggesting defective engagement of the late-stage plasma cell commitment program (**Figure 3H**). In contrast, the D8 CD138$^-$ signature scored higher among *Smc3*$^{wt/-}$ plasma cells, suggesting a strong bias away from the final stages of plasma cell commitment and preferential maintenance of B-cell transcriptional signatures. This branching point may represent a particularly vulnerable architectural checkpoint for malignant transformation.

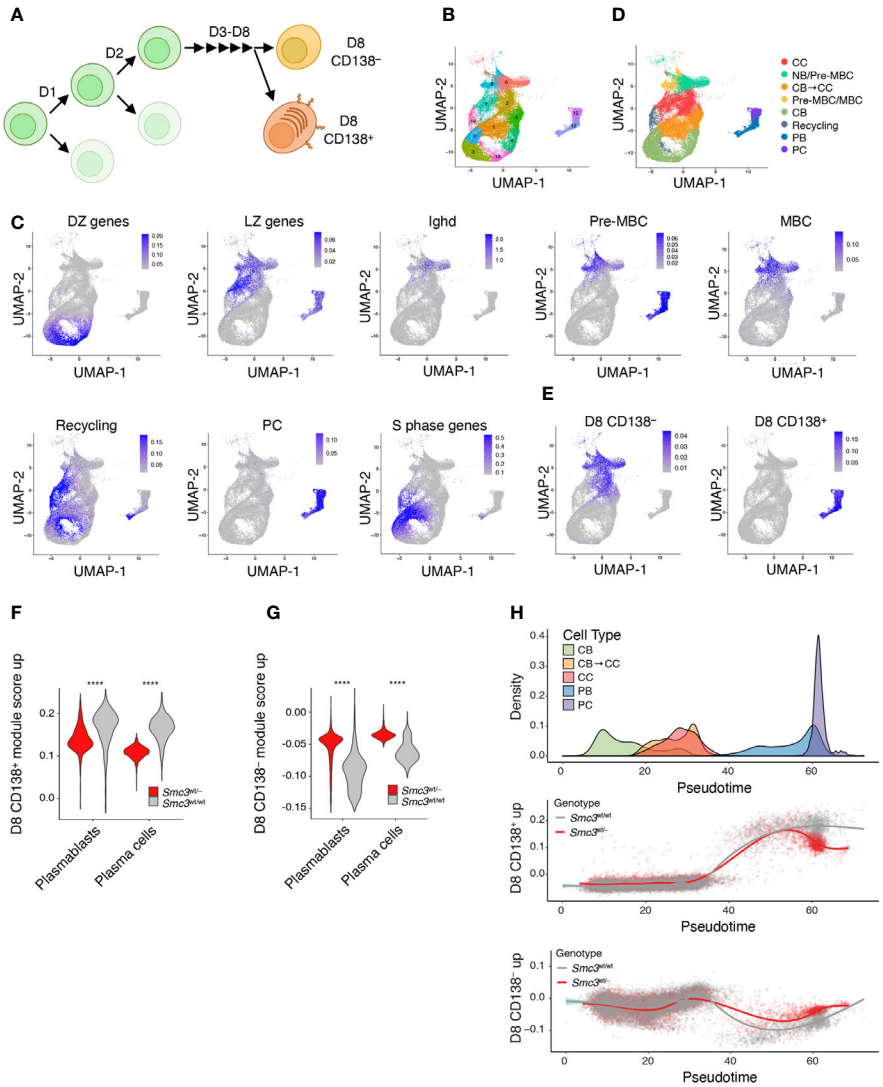

FIGURE 3 | Smc3 haploinsufficient cells undergo proliferation burst but fail to differentiate into plasma cells. **(A)** Scheme depicting mature B cell differentiation leading to the plasma cell phenotype. **(B)** Uniform Manifold Approximation and Projection (UMAP) applied to single cell RNA-seq populations of germinal center and post germinal center populations. **(C)** UMAP projections of gene expression cell signatures used to classify clusters. **(D)** Applying previously defined gene expression signatures, Seurat clusters were manually defined as centrocyte (CC), pre-memory B cells (Pre-MBC), transitioning centroblast to centrocyte (CB → CC), transitioning centrocyte to centroblast (Recycling), memory B cells (MBC), plasmablast (PB), and plasma cells (PC). **(E)** UMAP showing the projections of *in vivo* LPS-stimulated CFSE stained B cells that divided 8 times expressing CD138 (D8 CD138$^+$) or not (D8 CD138$^-$). **(F)** Violin plots showing expression levels of D8 CD138$^+$ for PB and PC clusters. **(G)** Violin plots showing expression levels of D8 CD138$^-$ for PB and PC clusters. **(H)** Cell densities for pseudotime lineage (CB → CB to CC → CC → PB → PC, top plot) and scatter plots of cells by genotype across pseudotime lineage expressing D8 CD138$^+$ (middle panel) or D8 CD138$^-$ (lower panel) profiles. ****p < 0.00001.

Smc3 Haploinsufficiency Increase DNA Damage in Germinal Center B Cells

Given that GC B-cells are exposed to considerable DNA damage stress (49, 50) and cohesin complex is reported to play important roles in DNA damage response (51, 52), we wondered whether *Smc3* haploinsufficiency might also contribute to lymphomagenesis through accumulation of DNA damage. Phosphorylation of Ser-139 residue of histone H2AX, forming γH2AX, is an early cellular response to the induction of DNA double-strand breaks that has been shown to be dependent on the loop extrusion activity of cohesin (53). We therefore used flow cytometry to measure γH2AX staining in total splenic B cells (live B220$^+$ cells) or GC B-cells (B220$^+$FAS$^+$CD38$^-$) from *Smc3*$^{wt/-}$ or *Smc3*$^{wt/wt}$ mice, eight days after immunization (**Supplementary Figures 4A, B**). Notably, although we did not observe differences in total live B cells (**Figure 4A**), we observed a significant reduction of γH2AX$^+$ staining in *Smc3*$^{wt/-}$ GC B-cells (**Figure 4B**). Notably the reduced abundance of γH2AX was evident in both centroblasts (B220$^+$FAS$^+$CD38$^-$CXCR4$^+$CD86$^-$) and centrocytes (B220$^+$FAS$^+$CD38$^-$CXCR4$^-$CD86$^+$, **Figures 4C, D**). *Smc3*

haploinsufficiency did not result in differential apoptosis in GC B cells (6). The lack of apoptosis along with the reduced γH2AX suggested that there might be impaired DNA damage detection in Smc3 haploinsufficient cells.

For more direct assessment of DNA damage, we performed karyotype analysis in proliferating *Smc3*$^{wt/-}$ *and Smc3*$^{wt/wt}$ GC B cells. Since obtaining abundant actively proliferating GC B cells from murine lymphoid tissue is not possible, we instead used the induced GC B cell (i-GCB) co-culture system, to produce high numbers of proliferating iGCB cells (**Supplementary Figure 4C**) (13). Karyotyping analysis was used to identify chromosomal aberrations (**Figure 4E**). Examining metaphase spreads from these cells revealed significantly higher abundance of lesions such as centromeric fusions or chromosomal breaks in *Smc3*$^{wt/-}$ GC B-cells (**Figures 4F–I** and **Supplementary Figure 4D**). Notably, centromeric fusions were completely absent from wild type iGCB cells, suggesting these are highly cohesin dose dependent. Whole genome sequencing in i-GC failed to demonstrate detectable

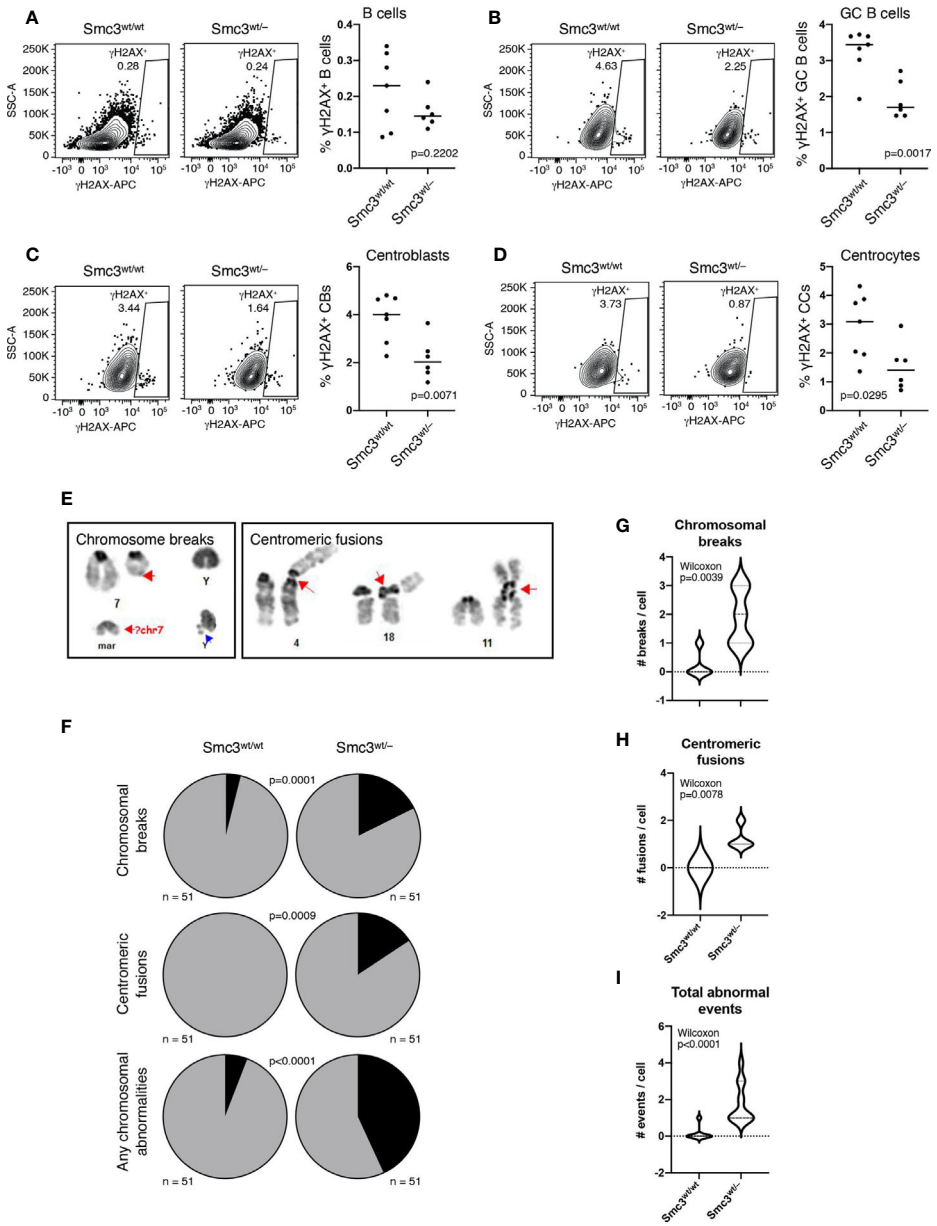

FIGURE 4 | Smc3 haploinsufficiency increases DNA damage in germinal center B cells. **(A–D)** Gating strategy used to detect phospho-γH2AX by flow cytometry (left) and quantification (right) in B cells **(A)**, germinal centers **(B)**, centroblasts **(C)**, and centrocytes **(D)**. **(E)** Identification and classification of chromosomal aberrations in induced GC B cells (iGC). **(F)** Quantification of the frequency of chromosomal breaks and centromeric fusions in iGCs of Smc3$^{wt/wt}$ (n=3) and Smc3$^{wt/-}$ (n=3) mice, and **(G),** quantification of chromosomal breaks, **(H),** centromeric fusions per cell, or **(I)** total events per cell. Experiment shown is a representative one from 3 performed. P values calculated using a binomial test for expected *versus* observed frequencies **(F)** and Wilcoxon rank test for count distribution **(G-I)**.

structural lesions or differences in replication fork usage or activation (**Supplementary Figures 5A, B**).

These observations prompted us to perform exome capture for mutation profiling in Smc3/Bcl6 *vs* Bcl6 lymphoma cells, obtained from lymphoid tissues of moribund animals. Although Smc3/Bcl6 tumors showed higher variability in the total numbers of somatic mutations, these were not significantly different than tumor cells from the Bcl6 (Wilcoxon p=0.24, **Figure 5A**). Copy number gains and losses quantified as the percent mouse genome altered were also not significantly different between the Smc3/Bcl6 and the Bcl6 mouse models (**Figure 5B**). Activation induced cytosine deaminase (AICDA) is the main source of mutations in germinal center B-cells during the process of somatic hypermutation (3). We thus analyzed the mutation frequency of 125 off-target genes (i.e. non-immunoglobulin, **Supplementary Table 2**) in Bcl6 and Smc3/Bcl6 tumors. Interestingly, we found that only 8 genes were mutated in at least one Bcl6 tumor, while 119 of them were mutated in at least one Smc3/Bcl6 tumor. The identity of those genes was also different between the tumors, with *Traf6* and *Pim1* being amongst the most frequently mutated genes in Bcl6 tumors, and *Mycbp2* and *Brca1* amongst Smc3/Bcl6 tumors (**Figure 5C** and **Supplementary Table 2**). Overall, the lack of a clear gain in structural genomic variants in Smc3/Bcl6 lymphomas suggests that the types of lesions induced by Smc3 deficiency in GC B-cells may not yield efficient trajectories for malignant transformation, although the reduced DNA damage sensing may lead to accumulation of mutations in AICDA off-target genes.

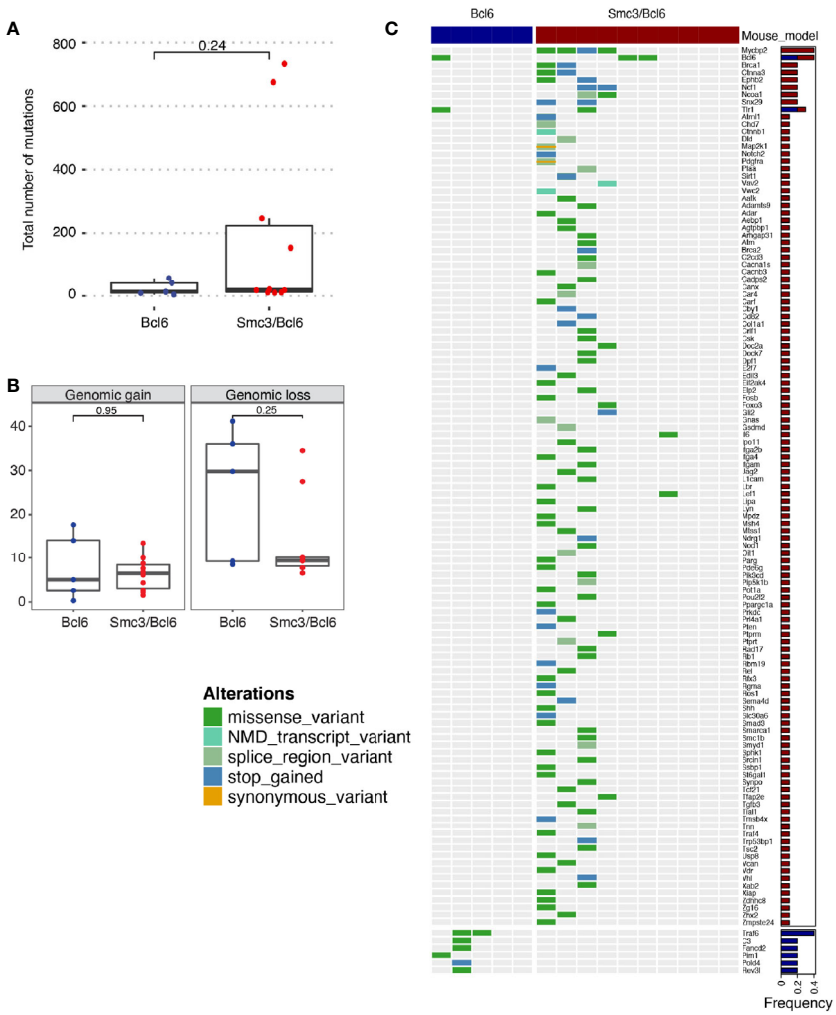

FIGURE 5 | Mutational analysis of Smc3/Bcl6 tumors. **(A, B)** Mutational burden of Bcl6 and Smc3/Bcl6 tumors assessed by exon capture analysis. **(A)** number of mutations per tumor. **(B)** Genomic gain and loss in Bcl6 and Smc3/Bcl6 tumors. **(C)** Oncoprint depicting AID-induced mutations in 125 non-immunoglobulin genes in Bcl6 (n=5) and Smc3/Bcl6 (n=10) tumors. Mutation frequency is shown in the right bar plot for Bcl6 (blue) and Smc3/Bcl6 (red). Mutations were classified as missense mutations, nonsense-mediated decay transcript variants, splice regions variants, stop gained, or synonymous variants, as indicated by the color key on the left of the oncoprint.

Decreased Cohesin Levels Predict Poor Survival in DLBCL Patients

The enrichment of *Smc3*$^{wt/-}$ centrocyte transcriptional signature in accelerated lymphomas induced by *Smc3* haploinsufficiency, prompted us to explore whether these profiles are linked to clinical outcome DLBCL patients. Examining the RNA-seq profiles of 322 newly diagnosed DLBCL patients, we performed unsupervised clustering to define DLBCL patient clusters with high and low expression of human ortholog genes that are repressed in *Smc3*$^{+/-}$ centrocytes (**Supplementary Figure 6A**). Cluster 1 contained 237 DLBCL patients and cluster 2 contained 85 DLBCL patients. Remarkably, patients in cluster 2 manifested significantly inferior overall survival (Log-rank test p=0.013, HR=1.69, 95% CI=1.11-2.2, **Figure 6A**) and inferior progression-free survival (Log-rank test: p=0.006, HR=1.6, 95% CI=1.16-2.22, **Figure 6B**) compared to those in cluster 1. To determine whether *Smc3* haploinsufficiency signature was associated with reduced expression of cohesin complex genes we examined the relative expression of *SMC3*, *SMC1A*, *RAD21*, *STAG1* and *STAG2* in our DLBCL patient cohort. Strikingly, all five of these genes were significantly reduced among the patients in cluster 2 (**Supplementary Figure 6B**). When DLBCL tumors were classified according to their gene expression profiles as belonging to the germinal center B cell-like subtype (GCB, n=186) or activated B cell-like subtype (ABCs, n=108), we observed that the cohesin low cluster 2 still displayed decreased overall survival (Log-rank test p= 0.002, HR=2.11, 95% CI=1.34-3.33, **Figure 6C**), and decreased progression-free survival (Log-rank test p=0.006, HR=2.13, 95% CI=1.39-3.27, **Figure 6D**) in the GCB subtype, but not among the ABC-DLBCLs (overall survival Log-rank test p=0.86, HR=1.05, 95% CI=0.63-1.72, **Supplementary Figure 6C**, and progression-free survival Log-rank test p=0.931, HR=0.98, 95% CI=0.6-1.59, **Supplementary Figure 6D**).

We validated these findings in an independent cohort of 243 DLBCL patients (15), where unsupervised clustering using the *Smc3* haploinsufficient gene signature defined two clusters, of 156 and 87 patients, respectively (**Supplementary Figure 6E**). In striking similarity, cluster 2 displayed decreased expression of all five cohesin core subunits (**Supplementary Figure 6F**) and a significantly shorter overall survival (Log-rank test p=0.0174, HR=1.64, 95% CI=1.10-2.45, **Supplementary Figure 6G**) compared to cluster 1.

Consistent with our findings, lower abundance of *Smc3* mRNA was shown to be associated with worse clinical outcome (6), but our data suggest a broader association of clinical outcomes with cohesin subunit expression. We therefore performed univariate Cox regression for cohesin subunits *SMC1A*, *RAD21*, *STAG1* and *STAG2*, and found a similar inverse correlation with overall survival across two independent cohorts of 322 and 757 DLBCL patients, with the exception of *STAG1* (**Figure 6E**). This effect was still observed in multivariate Cox analysis that include age, sex and DLBCL subtype (**Figure 6F**). These results strongly link reduced cohesin dosage with more aggressive disease among DLBCL patients, in line with observations of lymphomagenesis in *Smc3* haploinsufficient mice (6).

DISCUSSION

Recent pan-cancer studies have shown that cohesin and its regulators are among the most frequently mutated genes in cancer. Mutations in genes encoding cohesin subunits were first reported in colorectal cancer (54), and later in glioblastoma, Ewing sarcoma and melanoma (55). Chromosome missegregation has been suggested as a mechanism of cohesin dysfunction to tumorigenesis. Yet sequencing of acute myeloid leukemia (AML) patient specimens revealed the presence of recurrent mutations in all four core cohesin subunits but not associated with cytogenetic abnormalities (56). The correlation between STAG2 mutations and aneuploidy in bladder cancer is also unclear (57, 58). Even though somatic mutations of core cohesin genes in GC derived lymphomas are exceptionally rare, it was previously shown that *Smc3* could still function as a tumor suppressor in these cells (6). Herein was explored potential mechanisms through which this might occur and examined this from both the genomic stability and transcriptional regulatory standpoints (**Figure 7**).

Notably we did observe chromosomal structural aberrances in cohesin haploinsufficient GC cells, in contrast to what has been reported in myeloid cells (59). This might be explained by the fact that GCB cells are already at increased genotoxic stress compared to other cells types. For example, it is well established that the critical GCB transcription factor BCL6 represses checkpoint and DNA damage response genes (49, 50). Therefore, it is possible in this context that DNA damage due to reduced cohesin dosage is not properly sensed or repaired, tipping the balance towards accumulation of DNA damage. In spite of this, we did not observe increased abundance of DNA damage in *Smc3* haploinsufficient murine lymphomas. Perhaps this may be due to cells experiencing major chromosomal structural aberrancies being negatively selected during the transformation process. Nonetheless, taking together the apparent impairment in DNA damage sensing that we observed in Smc3$^{wt/-}$ GC B-cells and more frequent mutations in AICDA off-target genes in Smc3/Bcl6 lymphomas does suggest a potential genetic contribution of Smc3 deficiency to lymphomagenesis, pointing to the need for further investigation into this possibility. Along these lines, a recent publication revealed a role for the cohesin complex during DNA damage and γH2AX mark deposition (53). According to that model, cohesin complex loop-extrusion activity plays a critical role in detection of double strand breaks and topologically associating domains are the functional units of the DNA damage response, being instrumental for the correct establishment of γH2AX–53BP1 chromatin domains in a manner that involves one-sided cohesin-mediated loop extrusion on both sides of the double strand break. The authors proposed that H2AX-containing nucleosomes are rapidly phosphorylated as they actively pass by double strand breaks-anchored cohesin. Here, we speculate that cohesin haploinsufficiency attenuates detection of double strand breaks. This would explain both the decreased levels of γH2AX and increased chromosomal aberrations observed in Smc3$^{wt/-}$ GC B-cells.

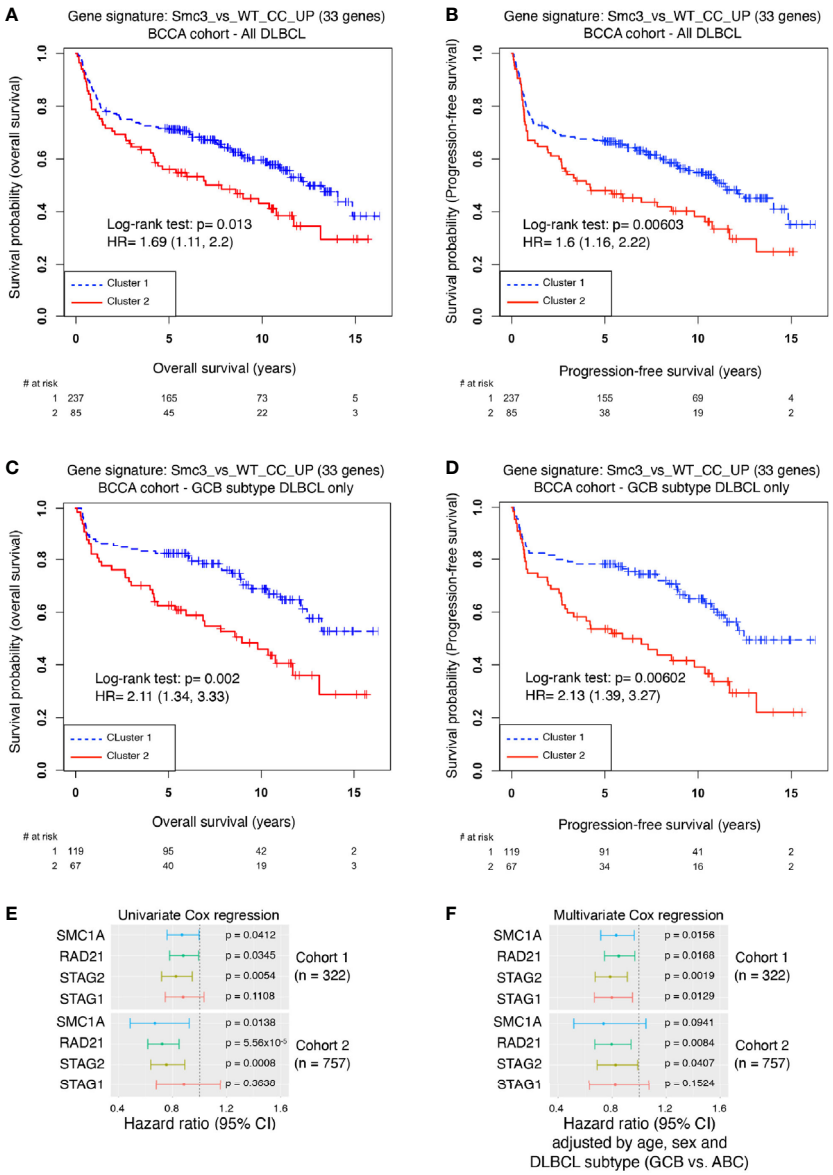

FIGURE 6 | Decreased cohesin levels predict poor survival in DLBCL patients. **(A)** Kaplan-Meier overall survival curves for DLBCL patients (n=322) in BCCA cohort clustered with the *Smc3* haploinsufficient gene signature (6). **(B)** Kaplan-Meier progression-free survival curves for DLBCL patients (n=322) in BCCA cohort clustered with the *Smc3* haploinsufficient gene signature (6). **(C)** Kaplan-Meier overall survival curves for GCB-subtype DLBCL patients (n=186) in cluster 1 and 2. **(D)** Kaplan-Meier progression-free survival curves for GCB-subtype DLBCL patients (n=186) in cluster 1 and 2. **(E)** Univariate Cox regression analysis, and **(F)** multivariate Cox regression analysis were performed in two cohorts of DLBCL patients (cohort 1, n = 322 individuals; cohort 2, n = 757 individuals). In both cases, *SMC1A*, *RAD21*, *STAG2* and *STAG1* expression levels were used as a continuous variable. Multivariate analysis was adjusted by age, sex and DLBCL subtype of the individual. Error bars represent 95% confidence intervals of the hazard ratio.

On the other hand, *Smc3* haploinsufficient lymphomas did manifest transcriptional and architectural perturbations consistent with those observed in *Smc3* haploinsufficient centrocytes. This includes repression of genes that are also aberrantly repressed by loss of function of two DLBCL epigenetic tumor suppressor genes *TET2* and *KMT2D*. *Tet2* normally mediates enhancer cytosine hydroxymethylation whereas *Kmt2d* mediates enhancer H3K4 mono and demethylation (60, 61). Loss of function of these genes leads to impaired enhancer function with repression of the respective genes and accelerated lymphomagenesis in mice (43, 44). This is reminiscent of and consistent with the impaired enhancer-promoter interactions that we observe by Hi-C in $Smc3^{wt/-}$ murine lymphomas. The phenotype of $Tet2^{-/-}$ GCs is especially similar to that of $Smc3^{wt/-}$ and *Tet2* deficiency also cooperates with *Bcl6* to induce accelerated lymphomagenesis (44). The finding that the *Tet2* gene itself showed impaired connectivity with upstream and downstream enhancers and

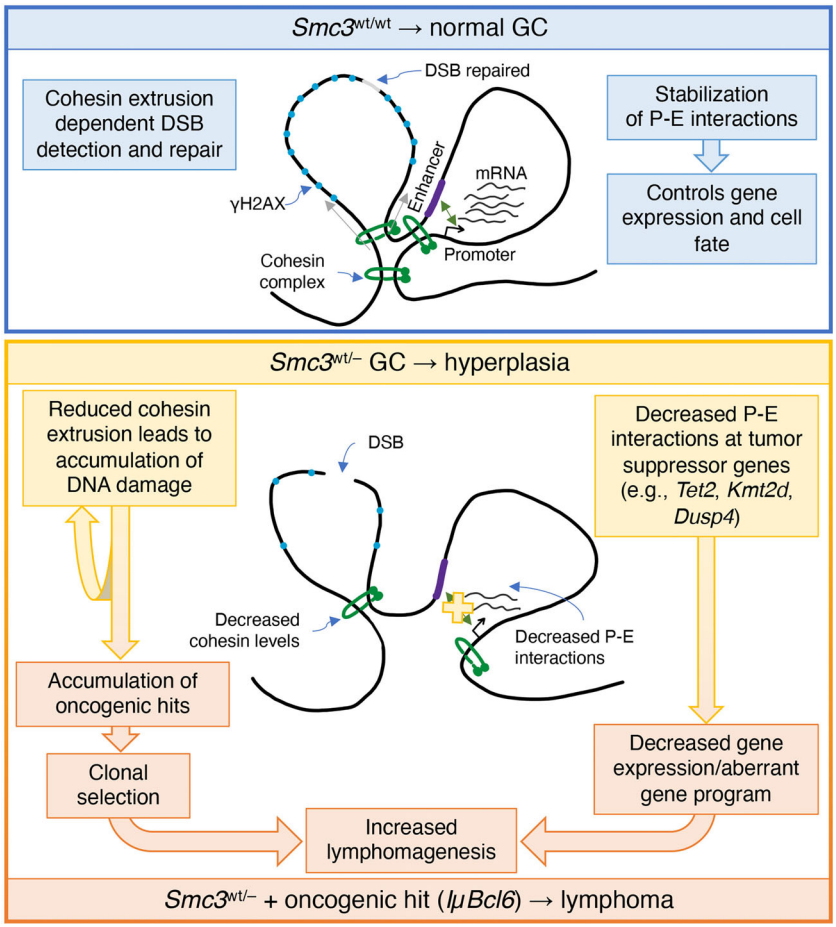

FIGURE 7 | Model of cohesin haploinsufficiency induced lymphomagenesis. Biallelic dosage of the *Smc3* cohesin subunit enables promoter-enhancer (P-E) interactions of critical genes for cell identity and cell fate. In addition, the extrusion function of cohesin plays an important role in detection of double strand breaks (DSB) and establishment of phosphorylated histone H2AX (γH2AX). In *Smc3* haploinsufficient GCs, decreased promoter-enhancer interactions in tumor suppressor genes such as *Tet2*, *Kmt2d* and *Dusp4*, result in decreased gene expression and/or alteration of the gene program. Defective detection of DSB leads to accumulation of chromosomal aberrations that are mechanistically linked to reduced abundance of Smc3 protein and hence fewer cohesin loop extrusion complexes, both of which may play a role in lymphomagenesis.

reduced expression in $Smc3^{wt/-}$ murine lymphomas further underlines the potential mechanistic and biological links between *Tet2* and cohesin complex in GC lymphomagenesis. Along these lines, it is notable that $Smc3^{wt/-}$ signature is linked to reduced expression of cohesin complex genes and is most clinically significant in GCB-subtype DLBCL, where *Tet2* and *Kmt2d* loss of function are most clearly deleterious (44, 62). Although tumors derived from *Smc3* haploinsufficient B cells display a *Kmt2d* loss of function-like transcriptional profile, we did not detect consistent downregulation of *Kmt2d* mRNA itself in tumor cells. Whether the transcriptional profile observed is due to an earlier downregulation of *Kmt2d* and epigenetic maintenance of the aberrant transcriptional status or if it is simply due to overlap with *Tet2* loss of function signature remains unknown. Taken together, these findings, suggest that the oncogenic impact of cohesin loss of function in GC B-cells is mainly due its transcriptional and architectural effect related to gene enhancers, and not to genomic instability. It is interesting to speculate to what extent cohesin complexes might act in a coordinate manner with *KMT2D* and *TET2* to control enhancer functions.

Our data point to the lymphomagenic effect of *Smc3* deficiency manifesting specifically during late stages of GC exit when B-cells undergo terminal stages of plasma cell commitment. In general, differentiation requires that cells undergo various rounds of cell division. As cells exit from mitosis, cohesin is recruited to chromatin and regenerates the architectural features optimal for cell context dependent transcriptional programs to be maintained (63). Presumably post-mitotic architectural reconfiguration of the genome provides an opportunity to favor new architectural settings required for differentiation. Along these lines it is notable that we traced the effect of Smc3 haploinsufficiency to crucial, late cell divisions that give rise either to $CD138^{+}$ plasma cells or $CD138^{-}$ B-cells. This is consistent with a previous report showing that early events during PC differentiation, such as induction of *Irf4*,

remain intact in *Smc3*$^{wt/-}$ B-cells, but late events such as *Prdm1* upregulation are impaired (6). We speculate that this leads to accumulation of greater numbers of mutated post GC B-cells, which may serve as the cell of origin of lymphomas observed in these mice. Hence it is possible that our findings could reflect loss of asymmetric division in B-cells as a potential mechanism of malignant transformation.

Finally, our results suggest that cohesin dose reduction contributes to lymphoma phenotypes in humans, in spite of the fact that cohesin mutations are uncommon in DLBCL. This is supported by the fact that DLBCLs enriched for lower expression of genes downregulated by *Smc3* haploinsufficiency also features reduced expression of cohesin core subunits as well as inferior clinical outcomes, an effect that was reproducible across two, large independent cohorts of patients. Moreover, and consistent with a previous report indicating that *Smc3* expression is a negative prognostic factor in DLBCL (6), we showed that reduction in the four core subunits *SMC3*, *STAG2*, *SMC1A* and *RAD21* are all independent adverse risk factors. What remains to be determined is the mechanism through which cohesin expression is suppressed in these tumors, as well as the reason why this may be the preferred rout to cohesin impairment instead of somatic mutations. Regardless, our data strongly support the notion that cohesin complex does play critical roles in lymphomagenesis and warrants further in-depth mechanistic study and consideration of potential therapeutic vulnerabilities.

DATA AVAILABILITY STATEMENT

The datasets presented in this study can be found in online repositories. The names of the repository/repositories and accession number(s) can be found below: https://www.ncbi.nlm.nih.gov/geo/, GSE172332.

ETHICS STATEMENT

Ethical review and approval was not required for the study on human participants in accordance with the local legislation and institutional requirements. Written informed consent for participation was not required for this study in accordance with the national legislation and the institutional requirements. The animal study was reviewed and approved by Weill Cornell Medicine.

AUTHOR CONTRIBUTIONS

MR conceptualized, designed and performed research, analyzed and interpreted data, drafted the manuscript and supervised the study. CD analyzed RNA-sequencing, and single cell RNA-sequencing with the help of CC. AKl analyzed Hi-C. ZC analyzed patient data. BB analyzed exome capture. AKo analyzed whole genome sequencing. AV provided the Smc3 mouse model. CS and JB performed the RNA-sequencing of LPS-induced plasma cells. OE and CM provided expertise and resources for data analysis. AM participated in the study conceptualization, interpretation of data, drafting of the manuscript, acquisition of funds and supervision of the project. All authors contributed to the article and approved the submitted version.

FUNDING

MR was a recipient of a postdoctoral fellowship grant from the Lymphoma Research Foundation and is funded by an NHLBI 5 T32 HL135465-3 training grant. AM is supported by NCI/NIH R35 CA220499, NCI/NIH P01 CA229086-01A1, LLS-SCOR 7012-16, LLS-TRP 6572-19, the Samuel Waxman Cancer Research Foundation, the Follicular Lymphoma Consortium and the Chemotherapy Foundation. AV is supported by NCI K08 CA215317, the William Raveis Charitable Fund Fellowship of the Damon Runyon Cancer Research Foundation (DRG 117-15) and an Evans MDS Young Investigator grant from the Edward P. Evans Foundation. CM thanks the Scientific Computing Unit, XSEDE Supercomputing Resources as well as the Starr Cancer Consortium (I7-A765, I9-A9- 071 and I13-0052) and acknowledges funding from the WorldQuant Foundation, The Pershing Square Sohn Cancer Research Alliance, the NIH (grants R01 CA249054, R01 AI151059, P01 CA214274, R01 AI125416-03 and R21 AI129851-02) and Leukemia and Lymphoma Society grants LLS 9238-16 and LLS MCL-982. AKo is supported by DP2GM123495 from the National Institutes of Health.

ACKNOWLEDGMENTS

Sequencing was performed in the Epigenomics Core and the Genomics Core at Weill Cornell Medicine. The authors thank J. McCormick and T. Baumgartner from the Flow Cytometry Core Facility at Weill Cornell Medicine and G. Nanjangud from the Molecular Genetics Core at Memorial Sloan Kettering Cancer Center for expert assistance with protocols.

SUPPLEMENTARY MATERIAL

The Supplementary Material for this article can be found online at: https://www.frontiersin.org/articles/10.3389/fimmu.2021.688493/full#supplementary-material

Supplementary Figure 1 | Aberrant gene expression program in Smc3 haploinsufficient tumors. **(A)** RT-qPCR for Smc3 mRNA in Bcl6 (n=3) and Smc3/Bcl6 (n=3) tumors, normalized to Hprt1 mRNA expression. **(B)** Principal component analysis for Bcl6 and Smc3/Bcl6 tumor cell RNA-sequencing. **(C)** Dendrogram of unsupervised hierarchical clustering for Bcl6 and Smc3/Bcl6 tumor cell RNA-sequencing. **(D)** Normalized counts for cohesin subunits, cohesin regulators and Ctcf in Bcl6 (n=3) and Smc3/Bcl6 (n=6) tumors.

Supplementary Figure 2 | Cohesin haploinsufficiency induces loss of interactivity of promoter-enhancers at tumor suppressor genes. **(A)** Contact maps at 100kb

resolution for Bcl6 and Smc3/Bcl6 tumors depicting chromosomal interactions for the whole chromosome 14 (top panels) and for nucleotides 92 to 107 Mb in chromosome 14. **(B)** A (red) and B (blue) compartments genome wide (top panel) and for chromosome 14 in Bcl6 and Smc3/Bcl6 tumors (bottom panel), each at 100kb resolution. **(C)** Differential loop analysis ranked by $\log_2$ fold change showing either all significantly called loops genome wide (violet line) or all promoter-enhancer loops (black line). A normal distribution with mean equals 0 and standard deviation equals the standard deviation of all promoter-enhancer loops is depicted as green line. Top up and down regulated loops in Smc3/Bcl6 tumors are highlighted for promoter-enhancer loops. **(D)** Aggregate peak analysis (APA) of Hi-C-identified loops from Bcl6 (left) and Smc3/Bcl6 (right) tumor cells. The heatmaps were generated by using the raw chromatin interaction frequency**. (E)** Virtual 4C analysis showing normalized interactions with the *Kmt2d* or **(F)** *Dusp4* promoter for Bcl6 tumors (blue line) and Smc3/Bcl6 tumors (red line) at 20kb resolution. Loop calling significance following the Mango approach are shown for Bcl6 and Smc3/Bcl6 tumors with $-\log_{10}$(FDR). Enhancers were defined as H3K27Ac peaks mapped in germinal center B cells by Mint-ChIP. Rad21 ChIP-seq was performed in the mouse lymphoma cell line CH12.LX. The differences between normalized interactions with the *Kmt2d* **(E)** or *Dusp4* **(F)** promoter are shown as $\log_2$ fold-change between Bcl6 and Smc3/Bcl6 tumors. **(G)** RPKM values for *Ints12* gene in Bcl6 and Smc3/Bcl6 tumors. NS, non-significant differences.

Supplementary Figure 3 | Smc3 haploinsufficient cells undergo proliferation burst but fail to differentiate into plasma cells. UMAP depicting cell lineage from CB → PC.

Supplementary Figure 4 | Smc3 haploinsufficiency increases DNA damage in germinal center B cells. **(A)** Gating strategy used to detect phospho-γH2AX by flow cytometry in B cells, germinal centers, centroblasts, and centrocytes. **(B)** Freshly isolated resting B cells (control) and 90 Gy irradiated resting B cells (irradiated) were stained with anti- γH2AX antibodies and analyzed by FACS. Averages of percent positivity for γH2AX control and irradiated are shown in the plot below. **(C)** Scheme depicting the induced GC B cell culture system. **(D)** Representative karyotype arrangement produced from iGC B cells.

Supplementary Figure 5 | Copy number and replication fork usage analysis in primary *Smc3* haploinsufficient germinal center B cells. **(A)** DNA copy number for mouse chromosomes 1 to 19 and ChrX in $Smc3^{wt/wt}$ (upper plot), $Smc3^{wt/-}$ (middle plot), and the difference (lower plot). **(B)** DNA replication timing for Chr 2 calculated by assessing the DNA copy number along the whole chromosome for $Smc3^{wt/wt}$ (blue line) and $Smc3^{wt/-}$ (green line).

Supplementary Figure 6 | Decreased cohesin levels predict poor survival in DLBCL patients. **(A)** Dendrogram showing assignment of patients from the BCCA cohort to clusters 1 and 2, defined by unsupervised hierarchical clustering using the *Smc3* haploinsufficient gene signature. **(B)** Expression levels of cohesin core subunits in cluster 1 and cluster 2 in the BCCA cohort. **(C)** Kaplan-Meier overall survival curves for ABC-subtype DLBCL patients (n=108) in BCCA cohort clustered with the *Smc3* haploinsufficient signature (6). **(D)** Kaplan-Meier progression-free survival curves for ABC-subtype DLBCL patients (n=108) in BCCA cohort clustered with the *Smc3* haploinsufficient signature (6). **(E)** Dendrogram showing assignment of patients from the NCI cohort to clusters 1 and 2, defined by unsupervised hierarchical clustering using the *Smc3* haploinsufficient gene signature. **(F)** Expression levels of cohesin core subunits in cluster 1 and cluster 2 in the NCI cohort. **(G)** Kaplan-Meier overall survival curves for DLBCL patients (n=243) in NCI cohort clustered with the *Smc3* haploinsufficient gene signature (6).

REFERENCES

1. Losada A. Cohesin in Cancer: Chromosome Segregation and Beyond. *Nat Rev Cancer* (2014) 14:389–93. doi: 10.1038/nrc3743
2. Merkenschlager M, Nora EP. CTCF and Cohesin in Genome Folding and Transcriptional Gene Regulation. *Annu Rev Genomics Hum Genet* (2016) 17:17–43. doi: 10.1146/annurev-genom-083115-022339
3. Victora GD, Nussenzweig MC. Germinal Centers. *Annu Rev Immunol* (2012) 30:429–57. doi: 10.1146/annurev-immunol-020711-075032
4. Mesin L, Ersching J, Victora GD. Germinal Center B Cell Dynamics. *Immunity* (2016) 45:471–82. doi: 10.1016/j.immuni.2016.09.001
5. Bunting KL, Soong TD, Singh R, Jiang Y, Beguelin W, Poloway DW, et al. Multi-Tiered Reorganization of the Genome During B Cell Affinity Maturation Anchored by a Germinal Center-Specific Locus Control Region. *Immunity* (2016) 45:497–512. doi: 10.1016/j.immuni.2016.08.012
6. Rivas MA, Meydan C, Chin CR, Challman MF, Kim D, Bhinder B, et al. Smc3 Dosage Regulates B Cell Transit Through Germinal Centers and Restricts Their Malignant Transformation. *Nat Immunol* (2021) 22:240–53. doi: 10.1038/s41590-020-00827-8
7. Hill VK, Kim JS, Waldman T. Cohesin Mutations in Human Cancer. *Biochim Biophys Acta* (2016) 1866:1–11. doi: 10.1016/j.bbcan.2016.05.002
8. Viny AD, Ott CJ, Spitzer B, Rivas M, Meydan C, Papalexi E, et al. Dose-Dependent Role of the Cohesin Complex in Normal and Malignant Hematopoiesis. *J Exp Med* (2015) 212:1819–32. doi: 10.1084/jem.20151317
9. Mullenders J, Aranda-Orgilles B, Lhoumaud P, Keller M, Pae J, Wang K, et al. Cohesin Loss Alters Adult Hematopoietic Stem Cell Homeostasis, Leading to Myeloproliferative Neoplasms. *J Exp Med* (2015) 212:1833–50. doi: 10.1084/jem.20151323
10. Mazumdar C, Shen Y, Xavy S, Zhao F, Reinisch A, Li R, et al. Leukemia-Associated Cohesin Mutants Dominantly Enforce Stem Cell Programs and Impair Human Hematopoietic Progenitor Differentiation. *Cell Stem Cell* (2015) 17:675–88. doi: 10.1016/j.stem.2015.09.017
11. Casola S, Cattoretti G, Uyttersprot N, Koralov SB, Seagal J, Hao Z, et al. Tracking Germinal Center B Cells Expressing Germ-Line Immunoglobulin Gamma1 Transcripts by Conditional Gene Targeting. *Proc Natl Acad Sci USA* (2006) 103:7396–401. doi: 10.1073/pnas.0602353103
12. Cattoretti G, Pasqualucci L, Ballon G, Tam W, Nandula SV, Shen Q, et al. Deregulated BCL6 Expression Recapitulates the Pathogenesis of Human Diffuse Large B Cell Lymphomas in Mice. *Cancer Cell* (2005) 7:445–55. doi: 10.1016/j.ccr.2005.03.037
13. Nojima T, Haniuda K, Moutai T, Matsudaira M, Mizokawa S, Shiratori I, et al. In-Vitro Derived Germinal Centre B Cells Differentially Generate Memory B or Plasma Cells In Vivo. *Nat Commun* (2011) 2:465. doi: 10.1038/ncomms1475
14. Jiang Y, Ortega-Molina A, Geng H, Ying HY, Hatzi K, Parsa S, et al. CREBBP Inactivation Promotes the Development of HDAC3-Dependent Lymphomas. *Cancer Discovery* (2017) 7:38–53. doi: 10.1158/2159-8290.CD-16-0975
15. Wright GW, Huang DW, Phelan JD, Coulibaly ZA, Roulland S, Young RM, et al. A Probabilistic Classification Tool for Genetic Subtypes of Diffuse Large B Cell Lymphoma With Therapeutic Implications. *Cancer Cell* (2020) 37:551–568 e14. doi: 10.1016/j.ccell.2020.03.015
16. Hummel M, Bentink S, Berger H, Klapper W, Wessendorf S, Barth TF, et al. A Biologic Definition of Burkitt's Lymphoma From Transcriptional and Genomic Profiling. *N Engl J Med* (2006) 354:2419–30. doi: 10.1056/NEJMoa055351
17. Jais JP, Haioun C, Molina TJ, Rickman DS, de Reynies A, Berger F, et al. The Expression of 16 Genes Related to the Cell of Origin and Immune Response Predicts Survival in Elderly Patients With Diffuse Large B-Cell Lymphoma Treated With CHOP and Rituximab. *Leukemia* (2008) 22:1917–24. doi: 10.1038/leu.2008.188
18. Lenz G, Wright G, Dave SS, Xiao W, Powell J, Zhao H, et al. Stromal Gene Signatures in Large-B-Cell Lymphomas. *N Engl J Med* (2008) 359:2313–23. doi: 10.1056/NEJMoa0802885
19. Shaknovich R, Geng H, Johnson NA, Tsikitas L, Cerchietti L, Greally JM, et al. DNA Methylation Signatures Define Molecular Subtypes of Diffuse Large B-Cell Lymphoma. *Blood* (2010) 116:e81–9. doi: 10.1182/blood-2010-05-285320
20. Koren A, Massey DJ, Bracci AN. TIGER: Inferring DNA Replication Timing From Whole-Genome Sequence Data. *Bioinformatics* (2021). doi: 10.1093/bioinformatics/btab166
21. Ewels PA, Peltzer A, Fillinger S, Patel H, Alneberg J, Wilm A, et al. The Nf-Core Framework for Community-Curated Bioinformatics Pipelines. *Nat Biotechnol* (2020) 38:276–8. doi: 10.1038/s41587-020-0439-x
22. Harrow J, Frankish A, Gonzalez JM, Tapanari E, Diekhans M, Kokocinski F, et al. GENCODE: The Reference Human Genome Annotation for The ENCODE Project. *Genome Res* (2012) 22:1760–74. doi: 10.1101/gr.135350.111

23. Dobin A, Davis CA, Schlesinger F, Drenkow J, Zaleski C, Jha S, et al. STAR: Ultrafast Universal RNA-Seq Aligner. *Bioinformatics* (2013) 29:15–21. doi: 10.1093/bioinformatics/bts635
24. Liao Y, Smyth GK, Shi W. Featurecounts: An Efficient General Purpose Program for Assigning Sequence Reads to Genomic Features. *Bioinformatics* (2014) 30:923–30. doi: 10.1093/bioinformatics/btt656
25. Li B, Ruotti V, Stewart RM, Thomson JA, Dewey CN. RNA-Seq Gene Expression Estimation With Read Mapping Uncertainty. *Bioinformatics* (2010) 26:493–500. doi: 10.1093/bioinformatics/btp692
26. Love MI, Huber W, Anders S. Moderated Estimation of Fold Change and Dispersion for RNA-Seq Data With Deseq2. *Genome Biol* (2014) 15:550. doi: 10.1186/s13059-014-0550-8
27. Subramanian A, Tamayo P, Mootha VK, Mukherjee S, Ebert BL, Gillette MA, et al. Gene Set Enrichment Analysis: A Knowledge-Based Approach for Interpreting Genome-Wide Expression Profiles. *Proc Natl Acad Sci USA* (2005) 102:15545–50. doi: 10.1073/pnas.0506580102
28. Korotkevich G, Sukhov V, Budin N, Shpak B, Artyomov MN, Sergushichev A. Fast Gene Set Enrichment Analysis. *bioRxiv* (2021). doi: 10.1101/060012
29. Rao SS, Huntley MH, Durand NC, Stamenova EK, Bochkov ID, Robinson JT, et al. A 3D Map of the Human Genome at Kilobase Resolution Reveals Principles of Chromatin Looping. *Cell* (2014) 159:1665–80. doi: 10.1016/j.cell.2014.11.021
30. Lazaris C, Kelly S, Ntziachristos P, Aifantis I, Tsirigos A. HiC-Bench: Comprehensive and Reproducible Hi-C Data Analysis Designed for Parameter Exploration and Benchmarking. *BMC Genomics* (2017) 18:22. doi: 10.1186/s12864-016-3387-6
31. Langmead B, Salzberg SL. Fast Gapped-Read Alignment With Bowtie 2. *Nat Methods* (2012) 9:357–9. doi: 10.1038/nmeth.1923
32. Imakaev M, Fudenberg G, McCord RP, Naumova N, Goloborodko A, Lajoie BR, et al. Iterative Correction of Hi-C Data Reveals Hallmarks of Chromosome Organization. *Nat Methods* (2012) 9:999–1003. doi: 10.1038/nmeth.2148
33. Zheng X, Zheng Y. CscoreTool: Fast Hi-C Compartment Analysis at High Resolution. *Bioinformatics* (2018) 34:1568–70. doi: 10.1093/bioinformatics/btx802
34. Phanstiel DH, Boyle AP, Heidari N, Snyder MP. Mango: A Bias-Correcting ChIA-PET Analysis Pipeline. *Bioinformatics* (2015) 31:3092–8. doi: 10.1093/bioinformatics/btv336
35. Davis CA, Hitz BC, Sloan CA, Chan ET, Davidson JM, Gabdank I, et al. The Encyclopedia of DNA Elements (ENCODE): Data Portal Update. *Nucleic Acids Res* (2018) 46:D794–801. doi: 10.1093/nar/gkx1081
36. Bishop GA, Haughton G. Induced Differentiation of a Transformed Clone of Ly-1+ B Cells by Clonal T Cells and Antigen. *Proc Natl Acad Sci USA* (1986) 83:7410–4. doi: 10.1073/pnas.83.19.7410
37. Satija R, Farrell JA, Gennert D, Schier AF, Regev A. Spatial Reconstruction of Single-Cell Gene Expression Data. *Nat Biotechnol* (2015) 33:495–502. doi: 10.1038/nbt.3192
38. Victora GD, Dominguez-Sola D, Holmes AB, Deroubaix S, Dalla-Favera R, Nussenzweig MC. Identification of Human Germinal Center Light and Dark Zone Cells and Their Relationship to Human B-Cell Lymphomas. *Blood* (2012) 120:2240–8. doi: 10.1182/blood-2012-03-415380
39. Ersching J, Efeyan A, Mesin L, Jacobsen JT, Pasqual G, Grabiner BC, et al. Germinal Center Selection and Affinity Maturation Require Dynamic Regulation of Mtorc1 Kinase. *Immunity* (2017) 46:1045–1058 e6. doi: 10.1016/j.immuni.2017.06.005
40. Agirre X, Meydan C, Jiang Y, Garate L, Doane AS, Li Z, et al. Long Non-Coding RNAs Discriminate the Stages and Gene Regulatory States of Human Humoral Immune Response. *Nat Commun* (2019) 10:821. doi: 10.1038/s41467-019-08679-z
41. Laidlaw BJ, Schmidt TH, Green JA, Allen CD, Okada T, Cyster JG. The Eph-Related Tyrosine Kinase Ligand Ephrin-B1 Marks Germinal Center and Memory Precursor B Cells. *J Exp Med* (2017) 214:639–49. doi: 10.1084/jem.20161461
42. Scharer CD, Patterson DG, Mi T, Price MJ, Hicks SL, Boss JM. Antibody-Secreting Cell Destiny Emerges During the Initial Stages of B-Cell Activation. *Nat Commun* (2020) 11:3989. doi: 10.1038/s41467-020-17798-x
43. Ortega-Molina A, Boss IW, Canela A, Pan H, Jiang Y, Zhao C, et al. The Histone Lysine Methyltransferase KMT2D Sustains a Gene Expression Program That Represses B Cell Lymphoma Development. *Nat Med* (2015) 21:1199–208. doi: 10.1038/nm.3943
44. Dominguez PM, Ghamlouch H, Rosikiewicz W, Kumar P, Beguelin W, Fontan L, et al. TET2 Deficiency Causes Germinal Center Hyperplasia, Impairs Plasma Cell Differentiation, and Promotes B-Cell Lymphomagenesis. *Cancer Discov* (2018) 8:1632–53. doi: 10.1158/2159-8290.CD-18-0657
45. De Paepe P, De Wolf-Peeters C. Diffuse Large B-Cell Lymphoma: A Heterogeneous Group of Non-Hodgkin Lymphomas Comprising Several Distinct Clinicopathological Entities. *Leukemia* (2007) 21:37–43. doi: 10.1038/sj.leu.2404449
46. Zhang J, Grubor V, Love CL, Banerjee A, Richards KL, Mieczkowski PA, et al. Genetic Heterogeneity of Diffuse Large B-Cell Lymphoma. *Proc Natl Acad Sci USA* (2013) 110:1398–403. doi: 10.1073/pnas.1205299110
47. Isshiki Y, Melnick A. Epigenetic Mechanisms of Therapy Resistance in Diffuse Large B Cell Lymphoma (DLBCL). *Curr Cancer Drug Targets* (2021) 21(4):274–82. doi: 10.2174/1568009620666210106122750
48. Schwarzer W, Abdennur N, Goloborodko A, Pekowska A, Fudenberg G, Loe-Mie Y, et al. Two Independent Modes of Chromatin Organization Revealed by Cohesin Removal. *Nature* (2017) 551:51–6. doi: 10.1038/nature24281
49. Ranuncolo SM, Polo JM, Dierov J, Singer M, Kuo T, Greally J, et al. Bcl-6 Mediates the Germinal Center B Cell Phenotype and Lymphomagenesis Through Transcriptional Repression of the DNA-Damage Sensor ATR. *Nat Immunol* (2007) 8:705–14. doi: 10.1038/ni1478
50. Phan RT, Dalla-Favera R. The BCL6 Proto-Oncogene Suppresses P53 Expression in Germinal-Centre B Cells. *Nature* (2004) 432:635–9. doi: 10.1038/nature03147
51. Watrin E, Peters JM. The Cohesin Complex is Required for the DNA Damage-Induced G2/M Checkpoint in Mammalian Cells. *EMBO J* (2009) 28:2625–35. doi: 10.1038/emboj.2009.202
52. Caron P, Aymard F, Iacovoni JS, Briois S, Canitrot Y, Bugler B, et al. Cohesin Protects Genes Against Gammah2ax Induced by DNA Double-Strand Breaks. *PloS Genet* (2012) 8:e1002460. doi: 10.1371/journal.pgen.1002460
53. Arnould C, Rocher V, Finoux AL, Clouaire T, Li K, Zhou F, et al. Loop Extrusion as a Mechanism for Formation of DNA Damage Repair Foci. *Nature* (2021) 590:660–5. doi: 10.1038/s41586-021-03193-z
54. Barber TD, McManus K, Yuen KW, Reis M, Parmigiani G, Shen D, et al. Chromatid Cohesion Defects may Underlie Chromosome Instability in Human Colorectal Cancers. *Proc Natl Acad Sci USA* (2008) 105:3443–8. doi: 10.1073/pnas.0712384105
55. Solomon DA, Kim T, Diaz-Martinez LA, Fair J, Elkahloun AG, Harris BT, et al. Mutational Inactivation of STAG2 Causes Aneuploidy in Human Cancer. *Science* (2011) 333:1039–43. doi: 10.1126/science.1203619
56. Welch JS, Ley TJ, Link DC, Miller CA, Larson DE, Koboldt DC, et al. The Origin and Evolution of Mutations in Acute Myeloid Leukemia. *Cell* (2012) 150:264–78. doi: 10.1016/j.cell.2012.06.023
57. Balbas-Martinez C, Sagrera A, Carrillo-de-Santa-Pau E, Earl J, Marquez M, Vazquez M, et al. Recurrent Inactivation of STAG2 in Bladder Cancer is Not Associated With Aneuploidy. *Nat Genet* (2013) 45:1464–9. doi: 10.1038/ng.2799
58. Guo G, Sun X, Chen C, Wu S, Huang P, Li Z, et al. Whole-Genome and Whole-Exome Sequencing of Bladder Cancer Identifies Frequent Alterations in Genes Involved in Sister Chromatid Cohesion and Segregation. *Nat Genet* (2013) 45:1459–63. doi: 10.1038/ng.2798
59. Thota S, Viny AD, Makishima H, Spitzer B, Radivoyevitch T, Przychodzen B, et al. Genetic Alterations of the Cohesin Complex Genes in Myeloid Malignancies. *Blood* (2014) 124:1790–8. doi: 10.1182/blood-2014-04-567057
60. Rasmussen KD, Helin K. Role of TET Enzymes in DNA Methylation, Development, and Cancer. *Genes Dev* (2016) 30:733–50. doi: 10.1101/gad.276568.115
61. Froimchuk E, Jang Y, Ge K. Histone H3 Lysine 4 Methyltransferase KMT2D. *Gene* (2017) 627:337–42. doi: 10.1016/j.gene.2017.06.056
62. Karube K, Enjuanes A, Dlouhy I, Jares P, Martin-Garcia D, Nadeu F, et al. Integrating Genomic Alterations in Diffuse Large B-Cell Lymphoma Identifies New Relevant Pathways and Potential Therapeutic Targets. *Leukemia* (2018) 32:675–84. doi: 10.1038/leu.2017.251
63. Peters JM, Tedeschi A, Schmitz J. The Cohesin Complex and Its Roles in Chromosome Biology. *Genes Dev* (2008) 22:3089–114. doi: 10.1101/gad.1724308

Conflict of Interest: MR is a scientific advisor of NuRevelation, Inc. OE is supported by Janssen, Johnson and Johnson, Volastra Therapeutics, AstraZeneca and Eli Lilly research grants. He is scientific advisor and equity holder in Freenome, Owkin, Volastra Therapeutics and One Three Biotech. CM is a cofounder and board member for Biotia and Onegevity Health as well as an advisor or compensated speaker for Abbvie, Acuamark Diagnostics, ArcBio, Bio-Rad, DNA Genotek, Genialis, Genpro, Karius, Illumina, New England BioLabs, Qiagen, Whole Biome and Zymo Research. AM receives research funding from Janssen Pharmaceuticals, Sanofi and Daiichi Sankyo, has consulted for Epizyme and Constellation and is on the scientific advisory board of KDAC pharmaceuticals.

The remaining authors declare that the research was conducted in the absence of any commercial or financial relationships that could be construed as a potential conflict of interest.

Publisher's Note: All claims expressed in this article are solely those of the authors and do not necessarily represent those of their affiliated organizations, or those of the publisher, the editors and the reviewers. Any product that may be evaluated in this article, or claim that may be made by its manufacturer, is not guaranteed or endorsed by the publisher.

frontiers in Immunology

ORIGINAL RESEARCH
published: 28 October 2021
doi: 10.3389/fimmu.2021.737427

UnAIDed Class Switching in Activated B-Cells Reveals Intrinsic Features of a Self-Cleaving IgH Locus

*Iman Dalloul[1], Brice Laffleur[2], Zeinab Dalloul[1], Batoul Wehbi[1], Florence Jouan[2], Baptiste Brauge[2], Paco Derouault[3], Jeanne Moreau[1], Sven Kracker[4], Alain Fischer[4], Anne Durandy[4], Sandrine Le Noir[1] and Michel Cogné[1,2]**

[1] Institut National de la Santé et de la Recherche Médicale (INSERM) U1262, Centre National de la Recherche Scientifique (CNRS) Unité Mixte de Recherche (UMR) 7276, Limoges University, Limoges, France, [2] Institut National de la Santé et de la Recherche Médicale (INSERM) U 1236, Rennes1 University, Rennes, France, [3] Centre Hospitalier Universitaire (CHU) Dupuytren, Limoges, France, [4] Institut National de la Santé et de la Recherche Médicale (INSERM) Unité Mixte de Recherche (UMR) 1163, Laboratory of Human Lympho-hematopoiesis, Imagine Institute, Université de Paris, Paris, France

OPEN ACCESS

Edited by:
Peter Daniel Burrows,
University of Alabama at Birmingham,
United States

Reviewed by:
Jeroen EJ Guikema,
Academic Medical Center,
Netherlands
Javier Marcelo Di Noia,
Montreal Clinical Research Institute
(IRCM), Canada
Jiazhi Hu,
Peking University, China

***Correspondence:**
Michel Cogné
michel.cogne@inserm.fr

Specialty section:
This article was submitted to
B Cell Biology,
a section of the journal
Frontiers in Immunology

Received: 06 July 2021
Accepted: 11 October 2021
Published: 28 October 2021

Citation:
Dalloul I, Laffleur B, Dalloul Z, Wehbi B, Jouan F, Brauge B, Derouault P, Moreau J, Kracker S, Fischer A, Durandy A, Le Noir S and Cogné M (2021) UnAIDed Class Switching in Activated B-Cells Reveals Intrinsic Features of a Self-Cleaving IgH Locus. Front. Immunol. 12:737427. doi: 10.3389/fimmu.2021.737427

Activation-induced deaminase (AID) is the major actor of immunoglobulin (Ig) gene diversification in germinal center B-cells. From its first description, it was considered as mandatory for class switch recombination (CSR), and this discovery initiated a long quest for all of the AID-interacting factors controlling its activity. The mechanisms focusing AID-mediated DNA lesions to given target sequences remain incompletely understood with regards the detailed characterization of optimal substrates in which cytidine deamination will lead to double strand breaks (DSBs) and chromosomal cleavage. In an effort to reconsider whether such CSR breaks absolutely require AID, we herein provide evidence, based on deep-sequencing approaches, showing that this dogma is not absolute in both human and mouse B lymphocytes. In activated B-cells from either AID-deficient mice or human AID-deficient patients, we report an intrinsic ability of the *IgH* locus to undergo "on-target" cleavage and subsequent synapsis of broken regions in conditions able to yield low-level CSR. DNA breaks occur in such conditions within the same repetitive S regions usually targeted by AID, but their repair follows a specific pathway with increased usage of microhomology-mediated repair. These data further demonstrate the role of AID machinery as not initiating *de novo* chromosomal cleavage but rather catalyzing a process which spontaneously initiates at low levels in an appropriately conformed *IgH* locus.

Keywords: B lymphocyte, class switch DNA recombination (CSR), AICDA, immunoglobulin, class switch

INTRODUCTION

Germinal center B-cells actively undergo remodeling of their immunoglobulin (Ig) loci while being selected for antigen binding. This results in the emergence of cells carrying a B-cell receptor with higher affinity for antigen after somatic hypermutation (SHM) of rearranged Ig V(D)J genes and which undergo class switch recombination (CSR) of Ig heavy chain (*IgH*) constant (C_H) genes. SHM

and CSR are initiated by activation-induced deaminase (AID), a member of the AID/APOBEC family of enzymes deaminating cytidines into uridines. By initiating DNA lesions in the repetitive S regions that precede C_H regions, AID is the key enzyme responsible for the CSR of C_H genes (1, 2). In some conditions, it can also initiate complete deletion of the constant gene cluster and locus suicide recombination (3, 4).

The targeting of *Ig* genes by AID requires preexisting chromatin accessibility and transcription, which expose single-stranded DNA within transcription bubbles and R-loops. In such Ig target sequences, AID deamination is focused on WRC motifs (W = A/T, R = A/G) (5). Off-target lesions are also found at a much lower frequency in some non-Ig genes transcribed in B-cells and can eventually contribute to lymphomagenesis (6, 7).

The C_H regions of Ig genes usually escape AID lesions while being transcribed by RNA polymerase II (RNAPII) in its elongating form (phosphorylated on the C-terminal domain at Ser2) and carrying the histone marks H4K20me1 and H3K36me3, which recruit histone acetyltransferases (8). In contrast, the S regions are enriched for hyperacetylated (Ac) H3K9 and trimethylated histone H3 on lysine 4 (H3K4me3), with local recruitment of histone deacetylases (8, 9). Sμ is additionally enriched in trimethylated histone H3 at lysine 9 (H3K9me3), which recruits KRAB domain-associated protein 1 and heterochromatin protein 1 (HP1) (10). On its main targets, i.e., V and S regions, AID interacts with stalled RNAPII phosphorylated at Ser5 and bound by the transcription elongation factor Spt5 (11). Additional RNAPII-associated factors (PAF) also help recruit AID (12). Both V and S regions are locations for paused RNAPII, but this is increased within S regions by the local abundance of DNA repeats, secondary structures, and R-loops where transcribed RNA remains associated with the DNA template strand (13). AID preferentially binds to structured DNA, notably G-quadruplex (G4) structures, with also a likely contribution of G4-rich transcripts in AID recruitment (14, 15). In mammals, dense G4 structures present on the non-template strand of S-regions promote the formation of R-loops, and pharmacological G4 ligands were shown to inhibit CSR (16). To access both strands of transcribed Ig genes *in vivo*, AID requires a prior activity of the RNA exosome complex, tethered to RNAPII by Spt5/Spt6 (17). Within R-loops, the RNA exosome removes RNA from the template strand, which provides equivalent accessibility of both DNA strands to cytosine deamination by AID and also participates in the correct conformation of the topologically associating domain (17, 18). The S regions have specific transcription patterns, with abundant antisense transcription and the presence of multiple alternate transcription start sites (19). The location of S regions within spliced introns is an additional prerequisite for CSR and might promote the interactions of AID and Spt5 with spliceosome-associated factors, such as CTNNBL1 (9, 20).

These features altogether engender an abundant occurrence of DNA lesions along extended domains of the target S regions, where staggered AID-initiated single-strand cleavages affecting either DNA strand are followed by DSBs. While such breaks are often considered as totally AID dependent, we wished to reconsider whether they could occur at low levels in the absence of AID.

MATERIALS AND METHODS

Patients

DNA from AID-deficient human patients included in this study included one tonsil DNA sample (patient P4) and DNA from three peripheral blood samples (patients P3, P5, and P6). Biallelic mutations within the AICDA coding sequence were identified in all patients. Patient P3 carried a nonsense W68X mutation at the beginning of the AICDA exon 3 (which encodes the catalytic domain of AID) on one allele and a complete deletion of exon 3 on the other allele. Patients P4 and P5 were family relatives, and both carried the same W68X nonsense mutation within exon 3 on one allele and a three-codon deletion affecting exon 3 on the other allele. These three patients have been described in detail, including for clinical manifestations and immune phenotype in the initial report from Revy et al. (2). Besides serum IgM at 1, 1.5, and 2.4 mg/ml, respectively, in patients P3, P4, and P5, those three patients had serum levels of class-switched IgG and IgA below the detection threshold, except for a low but detectable level (0.4 mg/ml) of serum IgG in patient P4 (2). Patient P6 is previously unpublished and carried a homozygous K22X nonsense mutation terminating the AID coding sequence within exon 2. The serum Ig levels in this patient were as follows: IgM, 0.65 mg/ml; IgG, 0.10 mg/ml; and IgA below 0.01 mg/ml. The AID alterations in patients are summarized in **Supplementary Figure S1**. Patients P3 and P6 are clearly affected on both alleles with loss-of-function (LOF) mutations severely truncating or deleting the catalytic domain. Patients P4 and P5 carry a clear LOF mutation on one allele, while it is debatable whether partial enzymatic activity could remain for the allele affected with the three-codon deletion.

Samples were obtained after receiving informed consent from the parents of patients.

Mice

Our research was conducted under ethical agreement APAFIS no. APAFIS#16689-2018091017202113 v3. The wild-type (WT), homozygous RAG2-deficient (referred to as $Rag^{-/-}$), and homozygous AID-deficient (referred to as $AID^{-/-}$) mice (a kind gift from Pr. T. Honjo) used for our experiments were maintained at 21–23°C with a 12-h light/dark cycle.

Ovalbumin and Sheep Red Blood Cells

WT, Rag, and AID-deficient mice were injected intraperitoneally with an emulsion of 50% V/V complete Freund's adjuvant (Sigma-Aldrich) and 1 mg/ml ovalbumin (Sigma-Aldrich). The mice were sacrificed at day 14.

The WT, Rag, and AID-deficient mice were injected intraperitoneally with 200 μl sheep red blood cells (SRBC) at day 0 and were boosted with 200 μl SRBC at day 7. The mice were sacrificed at day 17.

Sample and Cell Preparations

Blood samples were recovered from WT, RAG, and AID-deficient mice at days 0, 7, and 14 after ovalbumin (OVA) immunization and at days 0, 7, and 17 after SRBC

immunization with heparinized needles. Plasma samples were recovered by centrifugation and stored at -20°C until use.

Splenocytes were collected at sacrifice, red blood cells were lysed, and B-cells were isolated using EasySep™ Mouse B-cell Isolation Kit (Stem cell). B-cells were cultured for 4 days in RPMI containing 10% fetal calf serum with lipopolysaccharide (LPS) (1 μg/ml) (Invivogen) + IL-4 (20 ng/ml) (Peprotech). Supernatants were recovered and stored at -20°C until use.

For immunofluorescence, sections (18μm thick) of frozen spleen fixed with acetone, were labeled with fluorescent Abs (Jackson immunoresearch, Alexa 647 Goat Anti-Mouse IgG1, ref 115-605-205 and Alexa 488 Goat Anti- IgG2b, ref 115-545-207). Nuclei were stained with DAPI.

Class-Specific ELISA

ELISA was performed on sera or supernatants from *in vitro* stimulated primary B-cells for the detection of various Ig classes and subclasses. Plates were coated overnight with monoclonal antibodies specific for IgM, IgA, IgG1, and total IgG (Southern Biotech). Anti-OVA-specific Abs produced *in vivo* after immunization were evaluated in sera by coating the plates with 10 μg/ml OVA. Sera or supernatants were added and incubated for 2 h at 37°C. After washing, alkaline phosphatase (AP) conjugates of goat anti-mouse IgM, IgG1, IgA, and total IgG (Southern Biotech) were incubated for 1 h at 37°C. Following washing and addition of AP substrate (Sigma), absorbance was measured at 405 nm. The specificity of the anti-sera used in ELISA for the identification of class-switched Ig was checked by verifying the absolute lack of signal yielded in the assays when using four different monoclonal mouse IgM clones [mouse IgM isotype control clone 11E10 (Southern Biotechnologies) and anti-ABO mouse IgM clones BHS17, AY144, and E11 (French National Blood Center)] as negative controls (**Supplementary Figure S2**). The specificity of class-switched Ig ELISA detection was further indicated by a polyclonal internal control, observing that serum from a naive mouse with spontaneously high IgM was not producing detectable IgG or IgA prior to immunization (**Supplementary Figure S2**).

Amplification of Sμ/Sγ Junctions for Sequencing by CSRseq

DNA from SRBC immunized B-cells isolated from spleens of *WT* and AID-deficient mice was extracted using GenElute Mammalian Genomic DNA miniprep Kit (Sigma Aldrich). Murine Sμ/Sγ junctions were amplified in triplicate by nested PCR with 100 ng DNA (Phusion HF polymerase, BioLabs) using the following primers: Sμ Nest1 For (5′-A GAGACCTGCAGTTGAGGCC-3′) and Sγ consensus1 Rev (5′-TCAGGGAARTAVCCYTTGACCAGGCA-3′) for PCR1 Sμ/Sγ ju nctions and Sμ Nest2 For (5′-CCAGCCACAGTAATGACCCAG-3′) and Sγ consensus2 Rev (5′-CCARKGGATAGACHGATGGG G-3′) for PCR2.

Human Sμ/Sγ junctions were amplified as previously described (4). Each library was prepared using 200 ng of PCR2 product. Barcoded libraries with 200-bp read lengths were prepared using Ion Xpress plus Fragment Library Kit (Thermo Fisher Scientific) according to the instructions of the manufacturer. Each barcoded library was mixed in equal amounts and diluted to 100 pM. The libraries were run on chip 540 on the Ion S5 sequencer (Life Technologies). Data were analyzed using the CSReport software (21). This algorithm first aligns sequences with Sμ (set for identities higher than 90% and longer than 40 nucleotides) and explores identities to downstream S regions when the alignment with Sμ stops (again tracking identities higher than 90% and longer than 40 bp). The annotated IgH locus switch sequences considered for aligning mouse and human sequences are provided in **Supplementary Table S1**.

Quality controls for the whole CSRseq procedure process were done by processing non-lymphoid DNA samples (embryonic stem cell DNA for mouse assays and DNA from the human carcinoma cell line Hep2 for human assays). For both human and mouse assays, no CSR junction was obtained from such non-lymphoid samples, validating that the protocol safely identifies true CSR junctions from the template DNA and not PCR-built assemblies.

Data Accessibility

Raw sequencing data and a table reporting processed data from the CSreport algorithm have been deposited on GEO.

RESULTS

We evaluated the AID dependence of B-cell responses using a colony of homozygous AID-deficient mice that had been bred for at least two generations.

Circulating Ig levels were quantified in blood from 8–10-week-old animals. Total Ig levels from AID-deficient mice were compared to those from either wild-type or RAG2-/- immunodeficient mice. Circulating IgM in mice bred in specific and opportunistic-free conditions did not significantly differ from wild-type controls, in agreement with the lack of overt hyper-IgM previously documented by Honjo and colleagues in 10-week-old AID-deficient mice (22). By contrast, the total IgA level was below the detection threshold, while class-switched IgG was very low, with a mean ± standard deviation of 55 ± 35 ng/ml, but still clearly detectable (**Figure 1A**).

A similar profile was obtained when evaluating Ig production *in vitro* in supernatants of B-cells activated with either LPS+TGFβ (**Figure 1B**, right panel) or LPS+IL4 (**Figure 1B**, left panel), which respectively yielded no IgA but a low level of IgG1, together with IgM secreted in amounts similar to WT B-cells. Basal IgG production thus remains possible both *in vivo* in mice and *in vitro* in stimulated B-cells, in conditions of complete AID deficiency.

Since the functional role of Ig is to bind specific antigens as antibodies, we evaluated the dynamic process of the humoral response following immunization of AID-proficient compared to AID-deficient animals and to RAG-deficient mice. We monitored total IgM, IgG1, or IgA after immunization with the particulate Ag SRBC. In WT mice, total serum IgM and total serum IgA did not significantly vary from day 0 to 17 (**Figure 2A**, left panel), while at a much lower level, AID-deficient mice, by

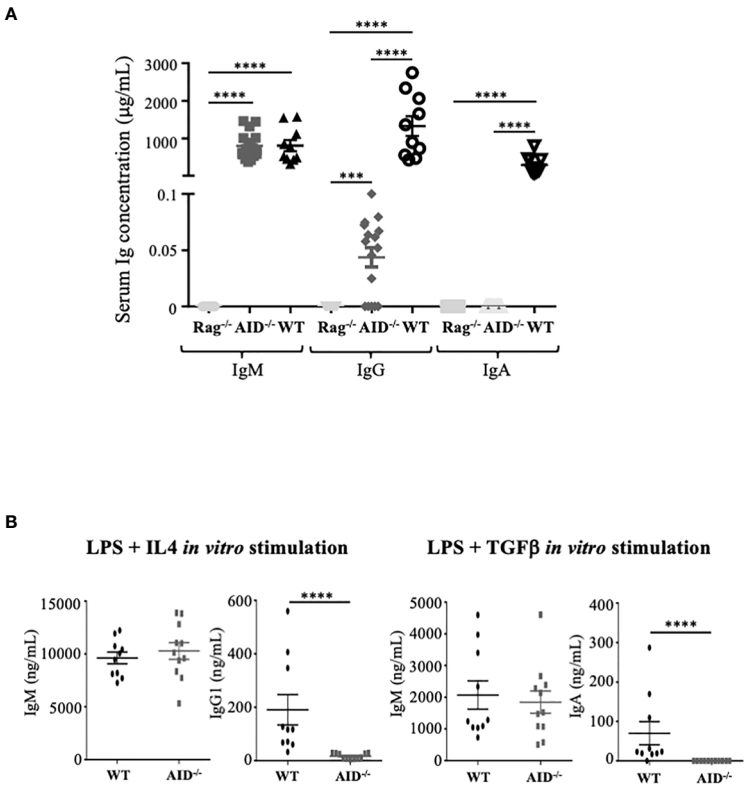

FIGURE 1 | Ig secretion by activation-induced deaminase (AID)-deficient mice. **(A)** Basal serum level of Ig in non-immunized mice. **(B)** *In vitro* secretion of Ig in B-cells from wild-type (WT) and AID-deficient mice stimulated for 4 days with lipopolysaccharide and IL-4 (left) or with LPS+TGFβ (right). The supernatants were quantified by ELISA for IgM, IgG1, and IgA. The data represent mean concentrations ± SEM from two independent experiments with at least three WT and five AID-deficient mice. Mann–Whitney test was used for significance. ****p < 0.0001.

contrast, displayed about an eightfold increase in total IgG during the same time period, reaching a mean of 0.4 ± 0.38 µg/ml, and total IgA which was initially undetectable but finally reached a mean of 0.7 ± 0.65 µg/ml at day 17 (**Figure 2A**, middle and right panels). The validity of these evaluations of switched Ig classes, without cross-reaction with IgM, was further attested by the lack of correlation with total IgM levels (**Supplementary Figure S3**). As expected, all Ig levels remained undetectable in control RAG-deficient mice immunized in parallel.

Immune stimulation with a more strictly defined protein Ag, OVA, resulted in the same profile but with a weaker impact on total IgG levels and with no detectable induction of serum IgA (**Figure 2B**). The latter condition of OVA immunization yielded anti-OVA IgM at normal levels in AID-deficient mice but was also associated with anti-OVA IgG1 at low but significant levels, clearly above the background obtained in non-responding RAG-deficient mice (**Figure 2C**).

The switched Ig produced in low amounts in AID-deficient mice was thus not just bystander products secreted after random recombination events in B-cells but dynamically followed B-cell stimulation and included Ag-specific switched IgG after immunization.

In order to explore the type of recombination occurring in activated B-cells from AID-deficient mice, we used the high-throughput CSRseq method to identify sequences of Sµ–Sγ junctions amplified through long-distance PCR. Sequencing reads showing identical junctions were assembled into clusters which were comparatively quantified for abundance and structure. Experiments using similar inputs (100 ng) of spleen DNA from immunized mice scored much more abundant CSR clusters in WT animals than in AID-deficient mice (mean 569 ± 282 instead of 32 ± 29, $p = 0.0001$), but CSR junctions were thus still clearly detectable and diversified in the latter (**Figure 3A**, top). The CSR defect in AID-deficient B-cells is thus incomplete, and CSR detected in such polyclonal cells remains diversified in terms of breakpoint positions, suggesting that it does not correspond to rare accidental breaks.

We also had the opportunity to analyze DNA from one tonsil and three peripheral blood samples from four immunodeficient patients with a class-switching defect involving biallelic germline mutations located upstream or within the AICDA exon 3 which encodes the catalytic domain of AID. Similar to AID deficient-mice and although in lower abundance than in tonsil DNA from an AID-proficient control, diversified Sµ–Sγ junction sequences were detectable in all four patients (**Figure 3A**, bottom).

The structures of CSR DNA junctions in lymphoid tissues from AID-deficient mice and patients were compared with regards to repair and the relative occurrence of either flush

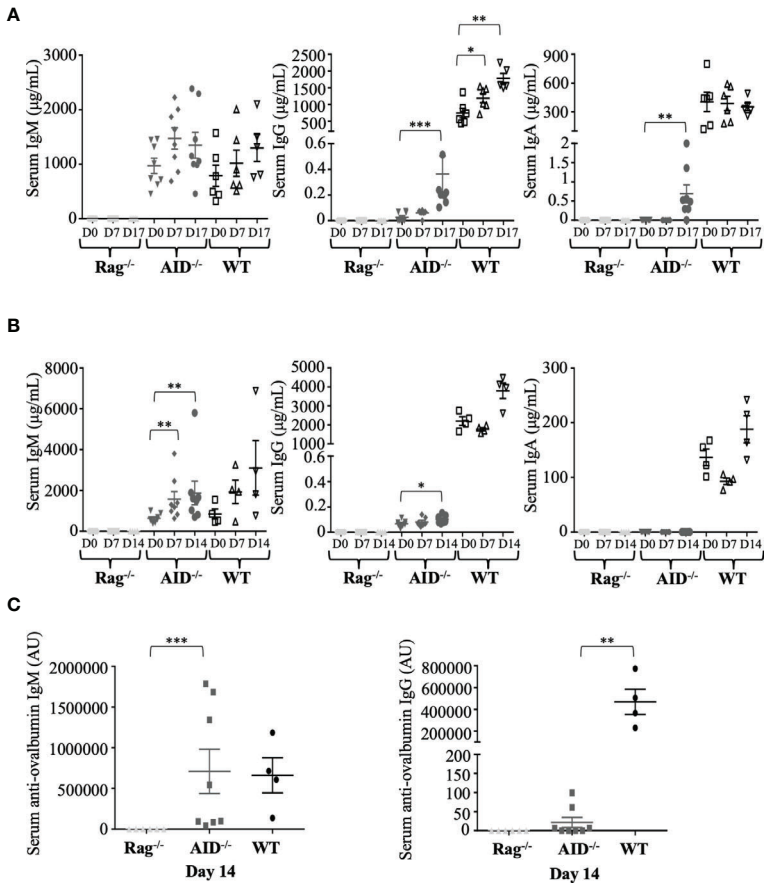

FIGURE 2 | Dynamic induction of Ig production after mouse immunization. **(A)** Total IgM, IgG, and IgA concentrations in serum from immunized mice were evaluated by ELISA before and at 17 days after immunization with sheep red blood cells (samples were taken at days 0, 7, and 17, with booster immunization at day 7). **(B)** Total IgM, G, and A concentrations in serum from immunized mice were evaluated by ELISA before and at 14 days after ovalbumin (OVA) immunization at days 0, 7, and 14. **(C)** Ag-specific IgG1 and IgM antibodies were evaluated by ELISA after 14 days of intraperitoneal OVA immunization. The data in **(A)** represent mean concentrations ± SEM from five RAG-deficient, eight activation-induced deaminase (AID)-deficient, and six wild-type (WT) mice. Mann–Whitney test was used for significance. The data in **(B, C)** represent mean concentrations ± SEM from six RAG-deficient, eight AID-deficient mice, and four WT mice. Mann–Whitney test was used for significance. *p < 0.05; **p < 0.01; ***p < 0.001.

junctions or junctions revealing short insertions or microhomologies between both DNA ends. In both mice (**Figure 3B**, left) and humans (**Figure 3B**, right), junctions characterized in AID-deficient conditions revealed a lower occurrence of flush junctions which directly corresponded to the ligation of blunt ends and an increased occurrence of microhomology between both ends. Sequences from all reads, including junctions and their detailed analysis using CSreport, have been deposited on GEO (GSE183034); examples of junctions obtained in human patients and controls are provided in **Supplementary Table S2**.

The examination of junction sequences also determined the distance between the positions of DNA breaks and sites corresponding to classical AID target sites. This distance was significantly increased in junctions from AID-deficient mice compared to wild-type mice (mean 2.97 *vs.* 2.23 nt, $p < 0.01$), showing that DNA breaks were not focused on WRCY motifs but, more probably, randomly affected the fragile portions of S regions (**Figure 4**). Indeed we also compared the distance between DNA break positions in a WT context and in *in silico* simulated events (*i.e.*, DNA breaks randomly simulated within the *Sμ* region), and we observed that the WT pattern of breaks differed from the simulated random distribution ($p < 0.0001$). By contrast, the AID-deficient pattern and the simulated random breaks did not significantly differ.

That the CSR defect in AID-deficient B-cells is only incomplete, both in AID-deficient mice and AID-deficient patients, is thus confirmed at the gene level by the occurrence of DNA junctions ligating the usual target regions of CSR, Sμ; and Sγ, but with a random pattern of breaks and an altered pattern of DNA repair suggesting the increased usage of microhomology-mediated end-joining.

Finally, in order to check whether the rarely occurring CSR persisting in AID-deficient B lymphocytes might reach a

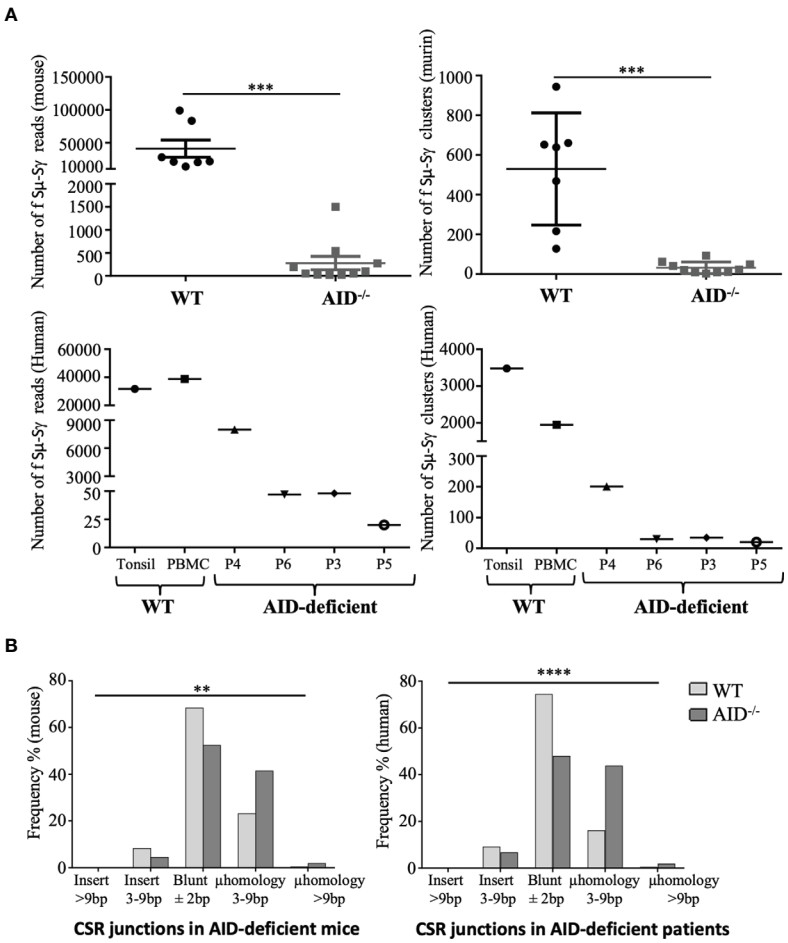

FIGURE 3 | Class switch recombination (CSR) in murine and human activation-induced deaminase (AID)-deficient samples. **(A)** Sμ-Sγ murine CSR junctions were PCR-amplified and sequenced from spleen B-cells at 17 days after sheep red blood cell immunization, comparing mutant and control mice (top). Sμ-Sγ human CSR junctions were also PCR-amplified and sequenced from blood and tonsils from AID-deficient human samples (bottom). Numbers of independent reads including Sμ–Sγ junctions are shown on the left graph. Independent reads including the same CSR breakpoint were assembled and considered as clusters; numbers of independent clusters are shown on the right graph. Junction structures were analyzed using CSReport. **(B)** Structures of repaired junctions were analyzed depending on the mean number of inserted nucleotides and length of microhomologies between the broken ends of Sμ-Sγ junctions in WT and AID-deficient samples. χ^2 test was used for significance of IgG CSR structure analysis. **p < 0.01; ***p < 0.001; ****p < 0.0001.

sufficient level for the detection of class-switched cells in lymphoid tissues, we explored the presence of plasma cells producing IgG1 or IgG2b in spleen sections from immunized AID-deficient mice by conventional immunohistochemistry. In agreement with the presence of secreted IgG in serum and of Sμ–Sγ junctions in lymphoid tissue DNA, cells staining for intracellular IgG and with the typical aspect of plasma cells were readily identified in such conditions (**Figure 5**).

DISCUSSION

The S regions harbor a repetitive structure favorable for clustered AID-mediated DNA lesions and frequent occurrence of close single-strand gaps on opposite strands leading to staggered DSBs. Their structure is unique in terms of primary sequence, architectural organization, and chromatin marks. We hypothesized that such structures might, by themselves, promote DSBs even in the absence of AID lesions, either due to co-transcriptional R-loops and/or due to repeated and overlapping motifs which may favor DNA polymerase slipping during replication and result in transient single-stranded structures. However, AID deficiency is classically considered to abrogate CSR.

This paradigm might, however, overlook a residual level of class-switched Ig produced even in the absence of AID, and, noticeably, the initial report of AID knock-out mice in fact mentioned low but still detectable levels of serum IgG1 and IgG2a (around 1 μg/ml) (22). In some human patients, such as patient P4 in the study by Revy et al. (2) or patient P6 in the current report, low serum IgG also remained detectable at 0.4 and 0.1 mg/ml, respectively. This is

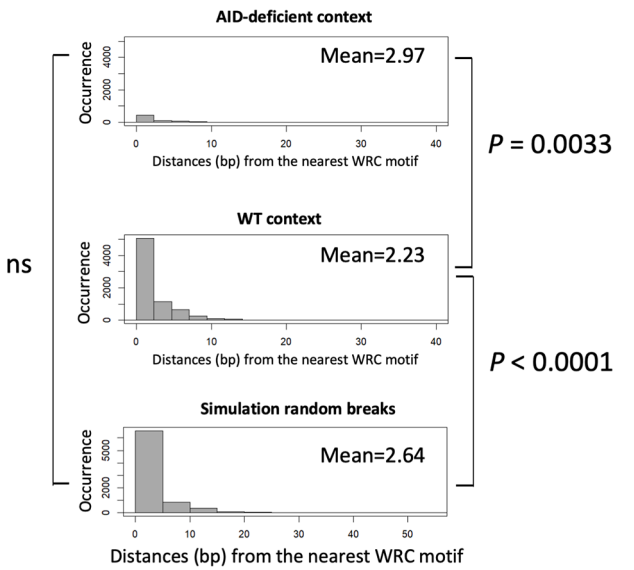

FIGURE 4 | Comparison of distances between CSR breaks and nearest activation-induced deaminase (AID) target sites. Distances between the position of DNA breaks and nearby WRCY sites were scored in either junctions from wild type B-cells, AID-deficient B-cells, or a control reference distribution of random breaks (4,000 junctions). An approximate permutation distribution test built from 100,000 random permutations was performed. ns, non significant.

especially intriguing in such patients affected with mutations which truncate AID upstream or within its catalytic domain: our patient P6 notably carried a homozygous nonsense mutation as early as codon 22 of the AID coding sequence.

To explore the hypothesis that a low rate of CSR junctions could be dynamically induced in activated B-cells in the absence of AID, we used sensitive methods to measure residual CSR in AID-deficient B-cells.

IgG production by AID-deficient mice was indeed detected *in vivo* and strongly increased after immunization, with plasma cells producing switched IgG detectable in tissues from immunized animals. We also observed that these switched Ig could be detected as Ag-specific antibodies in low amounts but dynamically increasing after immunization, *i.e.*, with kinetics resembling normal immune humoral responses and not bystander production after random recombination.

Characterization of switch junctions at the DNA level confirmed the occurrence of DNA breaks within the classical target Sμ and Sγ regions and also revealed an altered pattern of repair, suggesting the lesser involvement of non-homologous end-joining, rather yielding flush junctions, and with increased involvement of non-classical alternate end-joining, which is supported by short microhomologies between DNA ends.

Whether such breaks in the S regions, responsible for basal CSR, constitute an intrinsic property of S regions by behaving as fragile sites will remain to be determined. Noticeably, the process remains inducible, showing that such an intrinsic "fragility" is not simply related to the DNA structure but also needs B-cell activation, germline transcription of S regions, and all of the processes usually considered to facilitate the recruitment and processivity of AID for mediating DNA lesions. In this regard, the G4 richness of S regions might expose DNA to breaks, as it was shown to favor non-B DNA structures and to confer transcription-dependent instability to S regions transferred in yeast (23). The active transcription of S-regions in Ag-stimulated B-cells is thus likely to facilitate transcription–replication conflicts (TRCs) and the occurrence of single-strand DNA breaks at the positions of the G4 DNA and R-loops, notably due to the activity of helicases and of endonucleases like XPG and CtIP or of the exonuclease Exo1, all previously reported to promote the occurrence of breaks at R-loops or TRCs (24–27).

The chromosomal context of S regions might also intrinsically expose them to AID-independent breaks. Prior to any AID activity, the S regions are under the control of their upstream cytokine-dependent germline promoters and of the *cis*-acting 3′ RR superenhancer (28–31). This promotes major dynamic changes, marked by germline S region transcription, a modified histone mark landscape, and 3D remodeling including local co-transcriptional R-loops and the long-range cohesin-dependent loop extrusion process, which is driven by IgH promoters and the 3′RR superenhancer and finally juxtaposes distant transcribed S regions (30, 32, 33).

Although AID is considered mandatory for CSR and SHM, it is also questionable whether other cytidine deaminases of the APOBEC family might target DNA at low levels and not only RNA.

Low levels of DNA cytidine deamination have been described for APOBEC 3 and APOBEC1 (34, 35), and although their activity has never been demonstrated in Ig genes nor shown to induce DSBs, it is conceivable that, as for AID, staggered single-strand breaks induced after deamination in S regions might promote DSBs and CSR.

AID deamination occurs in the G1 phase, where 53BP1 and γH2AX protect SSBs and lead to repair through classical NHEJ (36, 37). Beyond G1, RPA associates with unrepaired ends in an ATM-dependent manner and favors repair by micro-homology-dependent alternate NHEJ (A-NHEJ). Finally, DNA breaks persisting in the S/G2 phase recruit higher amounts of Rad51 and are preferentially repaired by error-free homologous recombination (38). Increased repair through A-NHEJ is thus an indication that AID-independent breaks occur later in the cell cycle. Such breaks might also lack the intervention of AID and of downstream factors such as UNG in promoting synapsis and repair (39). While IgH breaks joined to *c-myc* were previously reported in AID-deficient mice after pristane-induced lymphomagenesis, they were, however, not shown to affect the S regions (40). Noticeably, while AID strongly contributes to DNA breaks with legitimate repair and CSR, it also supports illegitimate repair with non-Ig loci during GC-derived lymphomagenesis (41).

Our work is reminiscent of previous studies where experimental genomic breaks elicited by nucleases identified AID-independent hotspots as partners for repair, which included Sμ and Sγ regions in activated B-cells (42). The AID defects result in severe immunodeficiency, and its role comes on

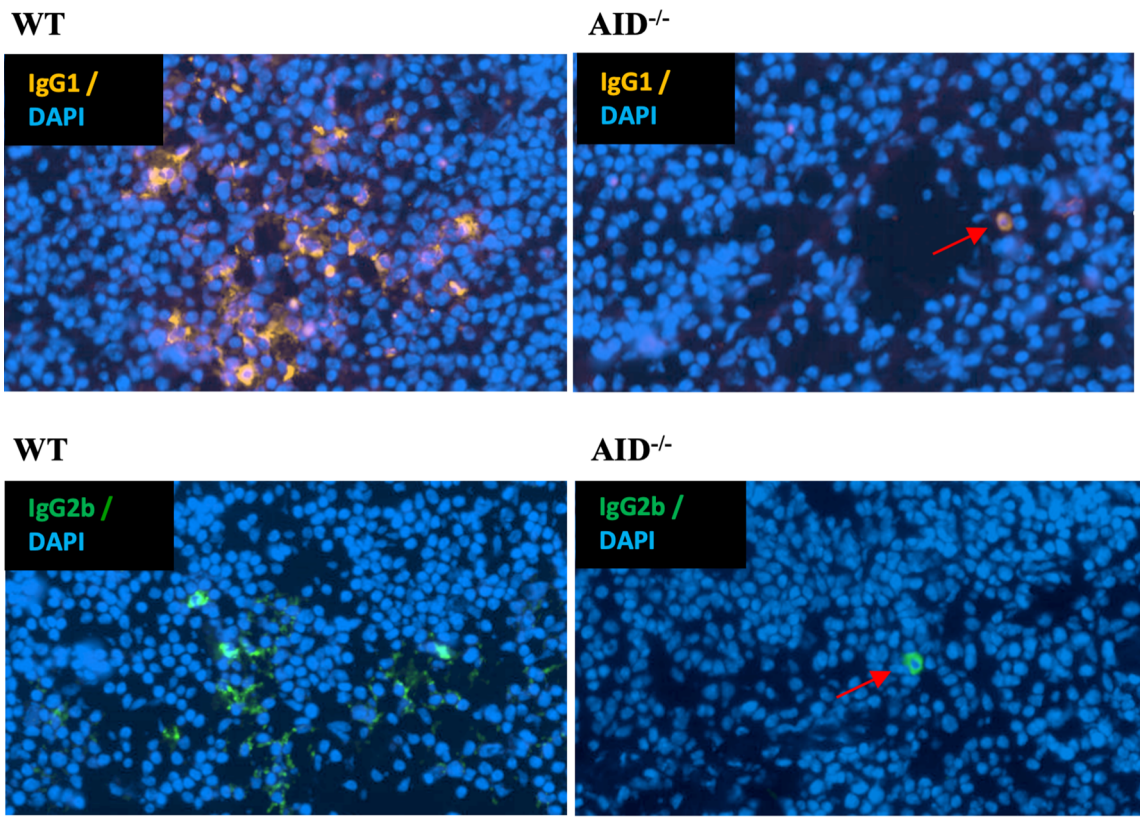

FIGURE 5 | Identification of rare cells producing class-switched Ig in spleens from immunized animals. Representative microscopy fields from slides of spleen tissues obtained from either WT (left) or AID-deficient (right) immunized mice, stained either for mouse IgG1 (top) or IgG2b (bottom). Red arrows indicate rare switched plasma cells in spleen tissue from an AID-deficient mouse.

top of several processes shaping Ig loci as optimal substrates for AID lesions and occurrence of DNA breaks. Even in the absence of AID, it is thus not unexpected that some accessibility to breaks remains. AID has multiple interactions with factors regulating its nuclear location and activity. This includes nuclear factors involved in transcription elongation and pausing, RNA splicing and degradation, DNA repair, heterochromatin-specific factors, and components of nucleoli: eEF1A, the Spt5/RNAPII/PAF complex, CTNNBL1, GANP, the nascent RNA-degrading exosome complex, RNF126, REG-γ, RPA (bound to pSer38-AID), and the heterochromatin factors Kap/HP1 (binding H3K9me3 on Sμ), nucleolin, nucleophosmin, and 14-3-3 (binding WRCY repeats and helping recruit CSR co-factors together with AID) (43). All the functional roles of AID interactions with other partners have not yet been elucidated. While some factors interact with AID after the occurrence of SSBs, others are recruited on Ig genes prior to AID. This is notably the case of factors binding the structural features of transcribed S regions loaded with paused RNAPII (Spt5/RNAPII/PAF complex, 14-3-3, GANP, the nascent RNA-degrading exosome or the heterochromatin factors Kap/HP1, RPA, *etc.*). Whether such factors might, by themselves, contribute to the occurrence of DNA lesions independently of AID will remain to be determined.

DATA AVAILABILITY STATEMENT

The datasets presented in this study can be found in online repositories. The names of the repository/repositories and accession number(s) can be found below: (https://www.ncbi.nlm.nih.gov/), GEO Accession GSE183034.

ETHICS STATEMENT

The studies involving human participants were reviewed and approved by Comité de protection des personnes Ile de France. Written informed consent to participate in this study was provided by the participants' legal guardian/next of kin. The animal study was reviewed and approved by Ministère de la recherche, l'enseignement supérieur et l'innovation (APAFIS#16689-2018091017202113 v3).

AUTHOR CONTRIBUTIONS

ID, ZD, and BW participated in investigation, methodology, and writing of the original draft (supporting). BL participated in data curation and writing of the original draft (supporting). FJ and BB

participated in methodology. PD participated in formal analysis. JM participated in writing—review. SK, AF, and AD participated in providing samples from patients and writing of the original draft (supporting). SN participated in data curation and formal analysis. MC led the conceptualization, data curation, funding acquisition, writing of the original draft, and review and editing as well as participated in formal analysis. All authors contributed to the article and approved the submitted version.

FUNDING

This work was supported by grants from Agence Nationale de la Recherche (grants ANR-16-CE15-0019-01 and 18-CE18-0022-02) and Fondation ARC (grant PGA1 RF20180207070).

ACKNOWLEDGMENTS

We thank Claire Carrion and Sandrine Lecardeur for technical help and the staff from the Limoges University core animal facility for animal care. We thank Dr. Yannic Danger and Franck Vérité, at the French Blood Center, for providing mouse monoclonal IgM. SLN and SK are Centre National de la Recherche Scientifique staff investigators.

SUPPLEMENTARY MATERIAL

The Supplementary Material for this article can be found online at: https://www.frontiersin.org/articles/10.3389/fimmu.2021.737427/full#supplementary-material

REFERENCES

1. Muramatsu M, Sankaranand VS, Anant S, Sugai M, Kinoshita K, Davidson NO, et al. Specific Expression of Activation-Induced Cytidine Deaminase (AID), a Novel Member of the RNA-Editing Deaminase Family in Germinal Center B Cells. *J Biol Chem* (1999) 274:18470–6. doi: 10.1074/jbc.274.26.18470
2. Revy P, Muto T, Levy Y, Geissmann F, Plebani A, Sanal O, et al. Activation-Induced Cytidine Deaminase (AID) Deficiency Causes the Autosomal Recessive Form of the Hyper-IgM Syndrome (HIGM2). *Cell* (2000) 102:565–75. doi: 10.1016/S0092-8674(00)00079-9
3. Péron S, Laffleur B, Denis-Lagache N, Cook-Moreau J, Tinguely A, Delpy L, et al. AID-Driven Deletion Causes Immunoglobulin Heavy Chain Locus Suicide Recombination in B Cells. *Science* (2012) 336:931–4. doi: 10.1126/science.1218692
4. Dalloul I, Boyer F, Dalloul Z, Pignarre A, Caron G, Fest T, et al. Locus Suicide Recombination Actively Occurs on the Functionally Rearranged IgH Allele in B-Cells From Inflamed Human Lymphoid Tissues. *PloS Genet* (2019) 15: e1007721. doi: 10.1371/journal.pgen.1007721
5. Maul RW, Gearhart PJ. AID and Somatic Hypermutation. *Adv Immunol* (2010) 105:159–91. doi: 10.1016/S0065-2776(10)05006-6
6. Staszewski O, Baker RE, Ucher AJ, Martier R, Stavnezer J, Guikema JEJ. Activation-Induced Cytidine Deaminase Induces Reproducible DNA Breaks at Many non-Ig Loci in Activated B Cells. *Mol Cell* (2011) 41:232–42. doi: 10.1016/j.molcel.2011.01.007
7. Liu M, Duke JL, Richter DJ, Vinuesa CG, Goodnow CC, Kleinstein SH, et al. Two Levels of Protection for the B Cell Genome During Somatic Hypermutation. *Nature* (2008) 451:841–5. doi: 10.1038/nature06547
8. Wang L, Wuerffel R, Feldman S, Khamlichi AA, Kenter AL. S Region Sequence, RNA Polymerase II, and Histone Modifications Create Chromatin Accessibility During Class Switch Recombination. *J Exp Med* (2009) 206:1817–30. doi: 10.1084/jem.20081678
9. Kenter AL. AID Targeting is Dependent on RNA Polymerase II Pausing. *Semin Immunol* (2012) 24:281–6. doi: 10.1016/j.smim.2012.06.001
10. Jeevan-Raj BP, Robert I, Heyer V, Page A, Wang JH, Cammas F, et al. Epigenetic Tethering of AID to the Donor Switch Region During Immunoglobulin Class Switch Recombination. *J Exp Med* (2011) 208:1649–60. doi: 10.1084/jem.20110118
11. Pavri R, Gazumyan A, Jankovic M, Di Virgilio M, Klein I, Ansarah-Sobrinho C, et al. Activation-Induced Cytidine Deaminase Targets DNA at Sites of RNA Polymerase II Stalling by Interaction With Spt5. *Cell* (2010) 143:122–33. doi: 10.1016/j.cell.2010.09.017
12. Willmann KL, Milosevic S, Pauklin S, Schmitz K-M, Rangam G, Simon MT, et al. A Role for the RNA Pol II-Associated PAF Complex in AID-Induced Immune Diversification. *J Exp Med* (2012) 209:2099–111. doi: 10.1084/jem.20112145
13. Maul RW, Gearhart PJ. Controlling Somatic Hypermutation in Immunoglobulin Variable and Switch Regions. *Immunol Res* (2010) 47:113–22. doi: 10.1007/s12026-009-8142-5
14. Zheng S, Vuong BQ, Vaidyanathan B, Lin J-Y, Huang F-T, Chaudhuri J. Non-Coding RNA Generated Following Lariat Debranching Mediates Targeting of AID to DNA. *Cell* (2015) 161:762–73. doi: 10.1016/j.cell.2015.03.020
15. Qiao Q, Wang L, Meng F-L, Hwang JK, Alt FW, Wu H. AID Recognizes Structured DNA for Class Switch Recombination. *Mol Cell* (2017) 67:361–73.e4. doi: 10.1016/j.molcel.2017.06.034
16. Dalloul Z, Chenuet P, Dalloul I, Boyer F, Aldigier J-C, Laffleur B, et al. G-Quadruplex DNA Targeting Alters Class-Switch Recombination in B Cells and Attenuates Allergic Inflammation. *J Allergy Clin Immunol* (2018) 142:1352–5. doi: 10.1016/j.jaci.2018.06.011
17. Basu U, Meng F-L, Keim C, Grinstein V, Pefanis E, Eccleston J, et al. The RNA Exosome Targets the AID Cytidine Deaminase to Both Strands of Transcribed Duplex DNA Substrates. *Cell* (2011) 144:353–63. doi: 10.1016/j.cell.2011.01.001
18. Laffleur B, Lim J, Zhang W, Chen Y, Pefanis E, Bizarro J, et al. Noncoding RNA Processing by DIS3 Regulates Chromosomal Architecture and Somatic Hypermutation in B Cells. *Nat Genet* (2021) 53:230–42. doi: 10.1038/s41588-020-00772-0
19. Kato L, Stanlie A, Begum NA, Kobayashi M, Aida M, Honjo T. An Evolutionary View of the Mechanism for Immune and Genome Diversity. *J Immunol* (2012) 188:3559–66. doi: 10.4049/jimmunol.1102397
20. Lorenz M, Jung S, Radbruch A. Switch Transcripts in Immunoglobulin Class Switching. *Science* (1995) 267:1825–8. doi: 10.1126/science.7892607
21. Boyer F, Boutouil H, Dalloul I, Dalloul Z, Cook-Moreau J, Aldigier J-C, et al. CSReport: A New Computational Tool Designed for Automatic Analysis of Class Switch Recombination Junctions Sequenced by High-Throughput Sequencing. *J Immunol Baltim Md 1950* (2017) 198:4148–55. doi: 10.4049/jimmunol.1601924
22. Muramatsu M, Kinoshita K, Fagarasan S, Yamada S, Shinkai Y, Honjo T. Class Switch Recombination and Hypermutation Require Activation-Induced Cytidine Deaminase (AID), a Potential RNA Editing Enzyme. *Cell* (2000) 102:553–63. doi: 10.1016/S0092-8674(00)00078-7
23. Kim N, Jinks-Robertson S. Guanine Repeat-Containing Sequences Confer Transcription-Dependent Instability in an Orientation-Specific Manner in Yeast. *DNA Repair* (2011) 10:953–60. doi: 10.1016/j.dnarep.2011.07.002
24. Yasuhara T, Kato R, Hagiwara Y, Shiotani B, Yamauchi M, Nakada S, et al. Human Rad52 Promotes XPG-Mediated R-Loop Processing to Initiate Transcription-Associated Homologous Recombination Repair. *Cell* (2018) 175:558–70.e11. doi: 10.1016/j.cell.2018.08.056
25. Sartori AA, Lukas C, Coates J, Mistrik M, Fu S, Bartek J, et al. Human CtIP Promotes DNA End Resection. *Nature* (2007) 450:509–14. doi: 10.1038/nature06337
26. Makharashvili N, Arora S, Yin Y, Fu Q, Wen X, Lee J-H, et al. Sae2/CtIP Prevents R-Loop Accumulation in Eukaryotic Cells. *eLife* (2018) 7:e42733. doi: 10.7554/eLife.42733
27. Keijzers G, Liu D, Rasmussen LJ. Exonuclease 1 and its Versatile Roles in DNA Repair. *Crit Rev Biochem Mol Biol* (2016) 51:440–51. doi: 10.1080/10409238.2016.1215407
28. Cogné M, Lansford R, Bottaro A, Zhang J, Gorman J, Young F, et al. A Class Switch Control Region at the 3' End of the Immunoglobulin Heavy Chain Locus. *Cell* (1994) 77:737–47. doi: 10.1016/0092-8674(94)90057-4
29. Pinaud E, Khamlichi AA, Le Morvan C, Drouet M, Nalesso V, Le Bert M, et al. Localization of the 3' IgH Locus Elements That Effect Long-Distance Regulation of Class Switch Recombination. *Immunity* (2001) 15:187–99. doi: 10.1016/S1074-7613(01)00181-9

30. Wuerffel R, Wang L, Grigera F, Manis J, Selsing E, Perlot T, et al. S-S Synapsis During Class Switch Recombination is Promoted by Distantly Located Transcriptional Elements and Activation-Induced Deaminase. *Immunity* (2007) 27:711–22. doi: 10.1016/j.immuni.2007.09.007
31. Rouaud P, Saintamand A, Saad F, Carrion C, Lecardeur S, Cogné M, et al. Elucidation of the Enigmatic IgD Class-Switch Recombination *via* Germline Deletion of the IgH 3' Regulatory Region. *J Exp Med* (2014) 211:975–85. doi: 10.1084/jem.20131385
32. Zhang X, Zhang Y, Ba Z, Kyritsis N, Casellas R, Alt FW. Fundamental Roles of Chromatin Loop Extrusion in Antibody Class Switching. *Nature* (2019) 575:385–9. doi: 10.1038/s41586-019-1723-0
33. Saintamand A, Rouaud P, Saad F, Rios G, Cogné M, Denizot Y. Elucidation of IgH 3' Region Regulatory Role During Class Switch Recombination *via* Germline Deletion. *Nat Commun* (2015) 6:7084. doi: 10.1038/ncomms8084
34. Caval V, Suspène R, Vartanian J-P, Wain-Hobson S. Orthologous Mammalian APOBEC3A Cytidine Deaminases Hypermutate Nuclear DNA. *Mol Biol Evol* (2014) 31:330–40. doi: 10.1093/molbev/mst195
35. Caval V, Jiao W, Berry N, Khalfi P, Pitré E, Thiers V, et al. Mouse APOBEC1 Cytidine Deaminase can Induce Somatic Mutations in Chromosomal DNA. *BMC Genomics* (2019) 20:858. doi: 10.1186/s12864-019-6216-x
36. Bothmer A, Robbiani DF, Di Virgilio M, Bunting SF, Klein IA, Feldhahn N, et al. Regulation of DNA End Joining, Resection, and Immunoglobulin Class Switch Recombination by 53BP1. *Mol Cell* (2011) 42:319–29. doi: 10.1016/j.molcel.2011.03.019
37. Reina-San-Martin B, Difilippantonio S, Hanitsch L, Masilamani RF, Nussenzweig A, Nussenzweig MC. H2AX is Required for Recombination Between Immunoglobulin Switch Regions But Not for Intra-Switch Region Recombination or Somatic Hypermutation. *J Exp Med* (2003) 197:1767–78. doi: 10.1084/jem.20030569
38. Yamane A, Robbiani DF, Resch W, Bothmer A, Nakahashi H, Oliveira T, et al. RPA Accumulation During Class Switch Recombination Represents 5'-3' DNA-End Resection During the S-G2/M Phase of the Cell Cycle. *Cell Rep* (2013) 3:138–47. doi: 10.1016/j.celrep.2012.12.006
39. Begum NA, Stanlie A, Doi T, Sasaki Y, Jin HW, Kim YS, et al. Further Evidence for Involvement of a Noncanonical Function of Uracil DNA Glycosylase in Class Switch Recombination. *Proc Natl Acad Sci U S A* (2009) 106:2752–7. doi: 10.1073/pnas.0813252106
40. Kovalchuk AL, duBois W, Mushinski E, McNeil NE, Hirt C, Qi C-F, et al. AID-Deficient Bcl-xL Transgenic Mice Develop Delayed Atypical Plasma Cell Tumors With Unusual Ig/Myc Chromosomal Rearrangements. *J Exp Med* (2007) 204:2989–3001. doi: 10.1084/jem.20070882
41. Pasqualucci L, Bhagat G, Jankovic M, Compagno M, Smith P, Muramatsu M, et al. AID is Required for Germinal Center-Derived Lymphomagenesis. *Nat Genet* (2008) 40:108–12. doi: 10.1038/ng.2007.35
42. Chiarle R, Zhang Y, Frock RL, Lewis SM, Molinie B, Ho Y-J, et al. Genome-Wide Translocation Sequencing Reveals Mechanisms of Chromosome Breaks and Rearrangements in B Cells. *Cell* (2011) 147:107–19. doi: 10.1016/j.cell.2011.07.049
43. Xu Z, Fulop Z, Wu G, Pone EJ, Zhang J, Mai T, et al. 14-3-3 Adaptor Proteins Recruit AID to 5′-AGCT-3′–Rich Switch Regions for Class Switch Recombination. *Nat Struct Mol Biol* (2010) 17:1124–35. doi: 10.1038/nsmb.1884

Conflict of Interest: The authors declare that the research was conducted in the absence of any commercial or financial relationships that could be construed as a potential conflict of interest.

frontiers in Immunology

ORIGINAL RESEARCH
published: 02 December 2021
doi: 10.3389/fimmu.2021.744573

Committed Human CD23-Negative Light-Zone Germinal Center B Cells Delineate Transcriptional Program Supporting Plasma Cell Differentiation

Kathleen Santamaria[1‡], *Fabienne Desmots*[1,2‡], *Simon Leonard*[1,3‡], *Gersende Caron*[1,2‡], *Marion Haas*[1,2], *Céline Delaloy*[1], *Fabrice Chatonnet*[1,2], *Delphine Rossille*[1,2], *Amandine Pignarre*[1,2], *Céline Monvoisin*[1], *Marine Seffals*[4], *Claire Lamaison*[1], *Michel Cogné*[1,2†], *Karin Tarte*[1,2] *and Thierry Fest*[1,2*†]

[1] UMR 1236, University of Rennes 1, INSERM, Établissement Français du Sang Bretagne, Rennes, France, [2] Pôle de Biologie, Rennes University Medical Center, Rennes, France, [3] LabEx IGO "Immunotherapy, Graft, Oncology", Nantes, France, [4] University of Rennes 1, UMS Biosit, H2P2 Platform, Rennes, France

B cell affinity maturation occurs in the germinal center (GC). Light-zone (LZ) GC B cells (B_{GC}-cells) interact with follicular dendritic cells (FDCs) and compete for the limited, sequential help from T follicular helper cells needed to escape from apoptosis and complete their differentiation. The highest-affinity LZ B_{GC}-cells enter the cell cycle and differentiate into PCs, following a dramatic epigenetic reorganization that induces transcriptome changes in general and the expression of the *PRDM1* gene in particular. Human PC precursors are characterized by the loss of IL-4/STAT6 signaling and the absence of CD23 expression. Here, we studied the fate of human LZ B_{GC}-cells as a function of their CD23 expression. We first showed that CD23 expression was restricted to the GC LZ, where it was primarily expressed by FDCs; less than 10% of tonsil LZ B_{GC}-cells were positive. Sorted LZ B_{GC}-cells left in culture and stimulated upregulated CD23 expression but were unable to differentiate into PCs – in contrast to cells that did not upregulate CD23 expression. An in-depth analysis (including single-cell gene expression) showed that stimulated CD23-negative LZ B_{GC}-cells differentiated into plasmablasts and time course of gene expression changes delineates the transcriptional program that sustains PC differentiation. In particular, we identified a B cell proliferation signature supported by a transient *MYC* gene expression. Overall, the CD23 marker might be of value in answering questions about the differentiation of normal B_{GC}-cells and allowed us to propose an instructive LZ B_{GC}-cells maturation and fate model.

Keywords: germinal center (GC), germinal center (GC) B cells, CD23+ B cells, B cell differentiation, plasmablasts/plasma cells, GC Light-Zone B cells

OPEN ACCESS

Edited by:
Stefano Casola, IFOM - The FIRC Institute of Molecular Oncology, Italy

Reviewed by:
Dinis Pedro Calado, Francis Crick Institute, United Kingdom
Dirk Mielenz, University of Erlangen Nuremberg, Germany

***Correspondence:**
Thierry Fest
thierry.fest@univ-rennes1.fr

***ORCID:**
Thierry Fest
orcid.org/0000-0002-6437-4189
Michel Cogné
orcid.org/0000-0002-8519-4427

*These authors have contributed equally to this work and share first authorship

Specialty section:
This article was submitted to B Cell Biology, a section of the journal Frontiers in Immunology

Received: *20 July 2021*
Accepted: *15 November 2021*
Published: *02 December 2021*

Citation:
Santamaria K, Desmots F, Leonard S, Caron G, Haas M, Delaloy C, Chatonnet F, Rossille D, Pignarre A, Monvoisin C, Seffals M, Lamaison C, Cogné M, Tarte K and Fest T (2021) Committed Human CD23-Negative Light-Zone Germinal Center B Cells Delineate Transcriptional Program Supporting Plasma Cell Differentiation. Front. Immunol. 12:744573. doi: 10.3389/fimmu.2021.744573

HIGHLIGHTS

- Only human light-zone GC B cells that fail to express CD23 after appropriate stimulation are likely to differentiate into plasma cells
- Light-zone GC B cells heterogeneity through use of the CD23 marker allow to decipher gene expression changes during B cell differentiation

INTRODUCTION

Within the secondary lymphoid organs, the germinal center (GC) is the primary site for the maturation of B-cell affinity. Iterative rounds of proliferation (associated with activation-induced cytidine (AID) enzyme activity) and positive selection of B-cell receptors (BCRs) with high affinity for their cognate antigens (Ags) ultimately lead to the production of memory B cells (MBCs) and plasma cells (PCs). Fully developed GCs comprise two functional zones, each of which contains a distinct GC B cell (B_{GC}-cell) subtype. Firstly, the dark zone (DZ) is close to the T-zone and is where centroblasts proliferate in bursts. Secondly, the light zone (LZ) mainly contains non-proliferating centrocytes, some of them testing their BCR against the Ags displayed by follicular dendritic cells (FDCs) and thus competing for limited, sequential help from T follicular helper (Tfh) cells (1–3). Once the Ag is captured by the BCR, the cell receives a survival signal; the Ag is subsequently internalized, processed and presented on the cell surface as a class II MHC-peptide complex, which in turn leads to interaction with cognate Tfh cells. Hence, Tfh-derived signals enable B-cell proliferation, differentiation and isotype switching (3). MBCs tend to emerge earlier from a low-affinity compartment in the LZ, while PCs appear later during the immune response, committed B cells require strong Tfh cell help, and accumulate somatic hypermutation (4–6). Positively selected LZ B_{GC}-cells escape from apoptosis, upregulate transiently their *MYC* expression, re-enter the cell cycle and travel to the DZ for further cell division and AID activity (7–9). It has been estimated that between 10% and 30% of the B cells that reach the LZ are selected and possibly re-enter the DZ; the remainder die mainly by apoptosis (9). Cognate B cell-T cell contact and help signal strength (both of which depend on BCR affinity) are likely to determine B cell fate. Medium-affinity cells express high levels of the BACH2 transcription factor and replenish the MBC pool, while the highest-affinity LZ B_{GC}-cells are preferentially selected for cell cycle entry and differentiation into PCs (10, 11). With regard to this process, the results of a computational model of B_{GC}-cell fate suggested that B cells that have been positively selected by successful Ag processing return to the DZ for asymmetric division, and that Ag affinity is inherited by only one of the daughter cells (12). On the other hand, PC precursors can exit the GC reaction *via* the DZ due to acquisition of CXCR4 expression leading cells to move to the CXCL12 rich DZ stromal environment. There is some experimental evidence to support this theory – notably the presence of PC precursors in the DZ (5, 13).

Committed B cells differentiate into plasmablasts (PBs) during an S phase in which specific oxidation of 5-methylcytosine (5mC) residues at given genomic positions leads to the expression of PC identity genes (14). Recently, we used an *in vitro* naïve B cell (NBC) differentiation model to demonstrate that human PC precursors are characterized by the loss of IL-4/STAT6 signaling and the absence of expression of CD23 [a pSTAT6-induced, low-affinity receptor for IgE (15)], although they are still imprinted by the previous IL-4 activation. In humans, low expression of the CD23 marker is reported in B_{GC}-cells (16) and LZ B_{GC}-cells (17), and the downregulation of CD23 is associated with PC commitment (18, 19). In mice, follicular B cells express CD23 (encoded by the *Fcer2a* gene), and CD23 expression is more intense on LZ follicular B_{GC}-cells than on DZ B_{GC}-cells (4, 20). In addition, B cell differentiation into PCs is accompanied by the loss of CD23 expression (21) and in contrast, recently reportedly that early positively selected $cMyc^+$ murine LZ B_{GC}-cells express the *Fcer2a* gene besides genes associated with both BCR signaling and immunological synapse suggesting a very recent activation following BCR engagement and GC B: Tfh interaction (20).

The objective of the present study was to assess the fate of human LZ B_{GC}-cells as a function of their CD23 expression. In immune-histochemistry assessments, we determined the CD23 expression pattern in tonsillar GCs. Staining was restricted to the LZ, with strong expression by FDCs. By flow cytometry, we found less than 10% of tonsil LZ B_{GC}-cells positive for CD23. However, most LZ B_{GC}-cells expressed CD23 *in vitro* after productive Tfh cell help or appropriate cytokine stimulation. An in-depth analysis (including single-cell gene expression) showed that LZ B_{GC}-cells $CD23^+$ obtained after stimulation are unable to differentiate into PCs - unlike the cells that remain $CD23^-$. Time course of single-cell gene expression changes during the differentiation of $CD23^-$ LZ B_{GC}-cells sheds new light on the final transcriptional switch that take place when human B cells metamorphosis into PBs characterized by the upregulation of *PRDM1* expression.

RESULT

In GCs, Only a Small Proportion of B Cells Expresses the CD23 Marker

To determine the CD23 cell surface marker's expression patterns, sections of human tonsil tissue were stained with several combinations of antibodies in immunohistofluorescence experiments. In GCs, CD23 staining was restricted to the LZ. In line with the literature data (22, 23), $CD21L^+$ FDCs were intensely stained (**Supplemental Figure S1A**). Using antibodies against CD23, PAX5 and PD1, we possibly distinguished $CD23^+$ LZ B_{GC}-cells located near $PD1^+$ Tfh but without certainty due to the FDC labeling (**Figure 1A** and **Supplemental Figure S1B**). Indeed, CD23 staining of frozen tissue sections showed that the FDCs' extensions formed a dense mesh around B and T cells (**Figure 1B** and **Supplemental Figure S1C**). Overall, our data show that FDCs in LZ are strongly positive for CD23, which makes it harder to detect $CD23^+$ B_{GC}-cells, in contrast to NBCs in the mantle zone. (**Supplemental Figure S1A**).

To determine the proportion of $CD23^+$ B cells in GCs, we used flow cytometry to analyze cell suspensions obtained from tonsils

and reactive lymph nodes (rLNs). Unlike NBCs and IgD$^+$ B_{GC}-cells, IgD$^-$ B_{GC}-cells, PBs and MBCs were predominantly CD23-negative (**Figure 1C** and **Supplemental Figure S1D**). Centrocytes are defined as CXCR4$^-$ B_{GC}-cells; they belong to the LZ compartment where B cells were also described as CD83$^+$ (1, 17). The mean ± standard deviation of CD23-expressing LZ B_{GC}-cells was 6.99% ± 1.45 in tonsils and 7.7% ± 3.99 in rLNs (**Figure 1D** and **Supplemental Figure S1E**). In B cells, CD23 expression is induced by Tfh-derived cytokines in general and by IL-4/STAT6 signaling in particular. CD23$^+$ and CD23$^-$ LZ B_{GC}-cells expressed similar levels of IL-21 and IL-4 receptors, CD40 and Ki-67, however, we found a significantly higher proportion of CCR6$^+$ cells in the

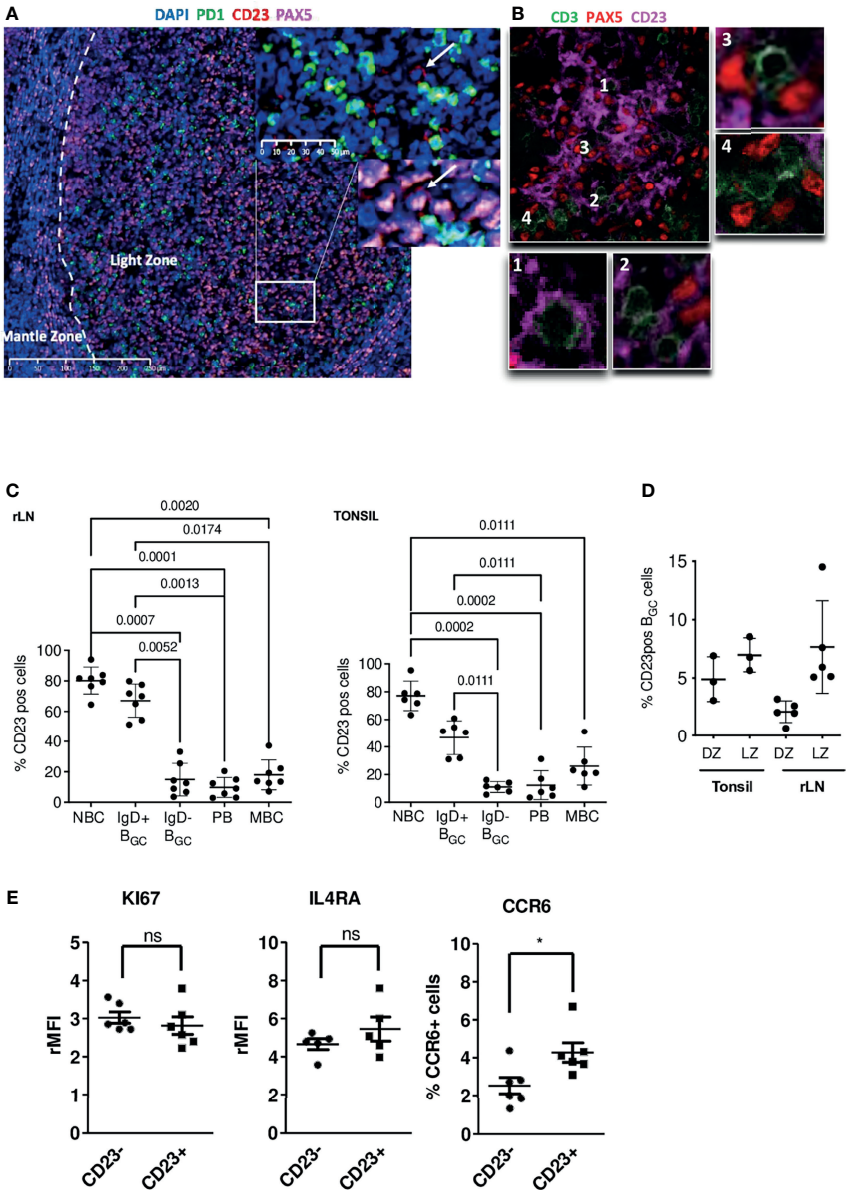

FIGURE 1 | In the GC, CD23 is expressed in the LZ, mainly by FDCs but also by some B cells. **(A)** Immunofluorescence staining of CD23 (red), PAX5 (pink) and PD1 (green) in paraffin-embedded tonsil tissues; the white arrow shows a CD23$^+$ B cell located in front of a PD1$^+$ Tfh cell. **(B)** Immunofluorescence staining of CD23 (pink), PAX5 (red) and CD3 (green) on frozen tonsil tissues; the PAX5 staining pattern for B cells does not really match the CD23 marker; panels 1 & 2 show T cells surrounded by CD23$^+$ dendritic extensions, and panels 3 & 4 show T cells in the vicinity of CD23$^-$ B cells. **(C)** The proportion of CD23-expressing B cells was determined by flow cytometry in different B cell populations in tonsils (Right panel) and rLNs (Left panel): CD19$^+$CD38$^-$IgD$^+$ naïve B cells (NBCs), CD19$^+$CD38$^+$IgD$^+$ & IgD$^-$ B_{GC}-cells, CD19$^+$CD38^{++}IgD$^-$ plasmablasts (PBs), and CD19$^+$CD38$^-$IgD$^-$CD27$^+$ memory B cells (MBCs) (one-way Anova & Kruskal-Wallis multiple comparisons test). **(D)** The proportion of CD23-positive cells in CXCR4^{hi}CD83^{lo} DZ B_{GC}-cells and CXCR4^{lo}CD83^{hi} LZ B_{GC}-cells in tonsils and rLNs. **(E)** Flow cytometry analysis of KI67, IL4RA and CCR6 in tonsil CD23$^+$ and CD23$^-$ LZ B_{GC}-cells. Results are expressed as the relative mean fluorescence intensity (rMFI) or the percentage of positive cells (*$P \leq .05$; "ns" for non significant; Mann-Whitney test).

$CD23^+$ subset consistent with Duan et al. (24) in mice. These cells could correspond to memory B cell precursors (**Figure 1E** and **Supplemental Figure S1F**) (25).

Given that CD23 expression is signaling-dependent, we hypothesized that $CD23^+$ LZ B_{GC}-cells correspond to B_{GC}-cells that had recently engaged in a productive synapse with cognate Tfh and might therefore harbor a more restricted BCR repertoire than their $CD23^-$ counterparts. We assessed common CDR3 clusters and variable (V) gene usage for both IgM and IgG BCRs in $CD23^+$ and $CD23^-$ LZ BGC-cells isolated from rLNs of three different subjects. We found common CDR3 clusters in all three subjects, with no significant differences in V gene usages between IgMs and IgGs. Interestingly, for one subject we noticed and enrichment for somatic mutations in CDR1, 2 & 3 in $CD23^+$ cells compared to $CD23^-$ counterparts. No definitive conclusion can be drawn, however, these results showed that $CD23^+$ and $CD23^-$ LZ B_{GC}-cells have very similar repertoires and so probably share a common initial activation pathway (**Supplemental Figure S1G**).

An Analysis of *FCER2*/CD23 Expression Reveals Heterogeneities in LZ B_{GC}-Cells

In humans, the CD23 protein is encoded by the *FCER2* gene. To detect possible transcriptional differences between LZ B_{GC}-cells as a function of *FCER2* expression, we compared previously published single-cell (sc) RNA-seq data obtained from tonsil-derived B_{GC}-cells (26). A comparison of 8,465 DZ cells and 11,118 LZ B_{GC}-cells revealed a highly significant difference between the proportions of *FCER2*-expressing cells (2.9% and 15.3%, respectively) (**Supplemental Figure S2A**, *Left panel*). Among the 11,118 LZ B_{GC}-cells, 2,360 (21%) had a proliferative signature (i.e., S-G2-M genes expression) and among them, only 231 (9.8%) cells (primarily in the S phase cluster) expressed *FCER2* (**Supplemental Figure S2A**, *Right panel*). To investigate the heterogeneity of *FCER2* expression in the LZ compartment and follow the same rationale as Holmes et al. (26), we focused our analysis on 8,758 nonproliferating LZ B_{GC}-cells (i.e., those in the G0-G1 stage of the cell cycle) which presented 1,465 (16.8%) cells expressing *FCER2* (**Figures 2A, B**). The uniform manifold approximation and projection (UMAP) representation of the original 12 specific clusters allowed to detect the projection of *FCER2*-positive cells and revealed that this gene expression was significantly associated with cell activation clusters and two BCR engagement clusters. In contrast, five clusters presented significantly weaker expression; they included the PB signature, two clusters associated with B_{GC}-cell transition between the DZ and the LZ, and one Ribosome cluster (**Figure 2B**).

Taken as a whole, these data showed that the majority of $FCER2^+$ cells belong to a small number of activated, non-proliferating LZ B_{GC}-cells that might have been diverted from a PC fate. In contrast, *FCER2*-negative LZ B_{GC}-cells were more heterogeneous in their distribution and presented a relative prevalence in the PB subset by taking into account the significant low number of *FCER2*-positive cells in this compartment. In mice, it has been suggested that most pre-plasmablasts are derived from positively selected cells i.e., expressing *MYC* gene (13, 20), we found among the 1,518 human MYC-positive LZ B_{GC}-cells from Holmes et al. (26) dataset that 316 (21%) and 1,202 (79%) were, respectively, positive and negative for *FCER2* expression. This result was consistent with data obtained recently in mice (24). Altogether, these data suggest that *FCER2*-negative LZ B_{GC}-cells were either unable to express *FCER2* or had not received sufficient Tfh cell help to express it. In particular, *FCER2*-negative LZ B_{GC}-cells might include activated B cells that have been committed to PB differentiation and therefore have switched off the IL-4/STAT6 pathway, thereby preventing the expression of *FCER2*/CD23 (19).

In order to complete this *in silico* analysis we explored the heterogeneity of the LZ B_{GC}-cell compartment by comparing CD23-negative and CD23-positive cells freshly sorted from tonsils, and $CD19^+IgD^-CD38^{bright}$ PBs were included in the analysis (gating strategy, in **Supplemental Figure 2B**). We applied a sensitive sc-qRT-PCR approach to profile the expression of a set of selected genes from our previous study (**Supplemental Material, Method & Tables, Table 2**) (19). An unsupervised clustering analysis revealed three gene clusters linked to specific cell functions identified with GeneMANIA (https://genemania.org/): cell cycle regulation, B cell activation and PC signature (**Figure 2C**). Only a few genes in each cluster were significantly differentially expressed between $CD23^+$ and $CD23^-$ cells, including *FCER2* and B cell activation markers *CD86* and *NFKB1* (**Supplemental, Material, Method & Tables, Table 6**). Note that *PRDM1* and *IRF4* genes linked to PC differentiation were not differentially expressed (**Figure 2D**). However, $CD23^-$ compared to $CD23^+$ LZ B_{GC}-cells expressed higher levels of cell proliferation *E2F1* and *MKI67* genes (**Figure 2D**). The cell proliferation signature was primarily attributed to a group of $CD23^-$ LZ B_{GC}-cells that also expressed *MYC* (**Figure 2C**). To complete our exploration on a higher number of analyzed cells, differentiation-associated transcription factors assessed by flow cytometry showed a significant enrichment in BCL6-negative and Blimp1-positive cells in $CD23^-$ LZ B_{GC}-cells. In contrast, both subsets expressed similar levels of c-MYC and phospho-p70 S6 kinase (pS6), two markers related to B-cell selection (**Figure 2E**) (7, 8, 27). Altogether, these findings suggest that the $CD23^-$ population comprises B cells committed to PC differentiation.

CD23 Expression of LZ B_{GC}-Cells Depends on Response to Tfh-Driven Stimulation

To study the effect of Tfh cell help on the membrane expression of CD23 on LZ B_{GC}-cells, we first cultured LZ B_{GC}-cells for 12 h with IL-4, CD40, IL-21 or combinations of these. IL-4 alone, CD40 alone and especially a combination of IL-4 and CD40 were effective in inducing the significant upregulation of CD23 expression (**Figure 3A**). Despite similar expression levels of IL-4R, CD40 and IL-21R on post-stimulated $CD23^+$ and $CD23^-$ LZ B_{GC}-cells, pSTAT6 was only induced in $CD23^+$ B cells, and chemical inhibition of pSTAT6 blocked the CD23 expression (**Figure 3B** and **Supplemental Figures S3A, B**). Since the production of IL-21 and IL-4 by Tfh cells predominantly

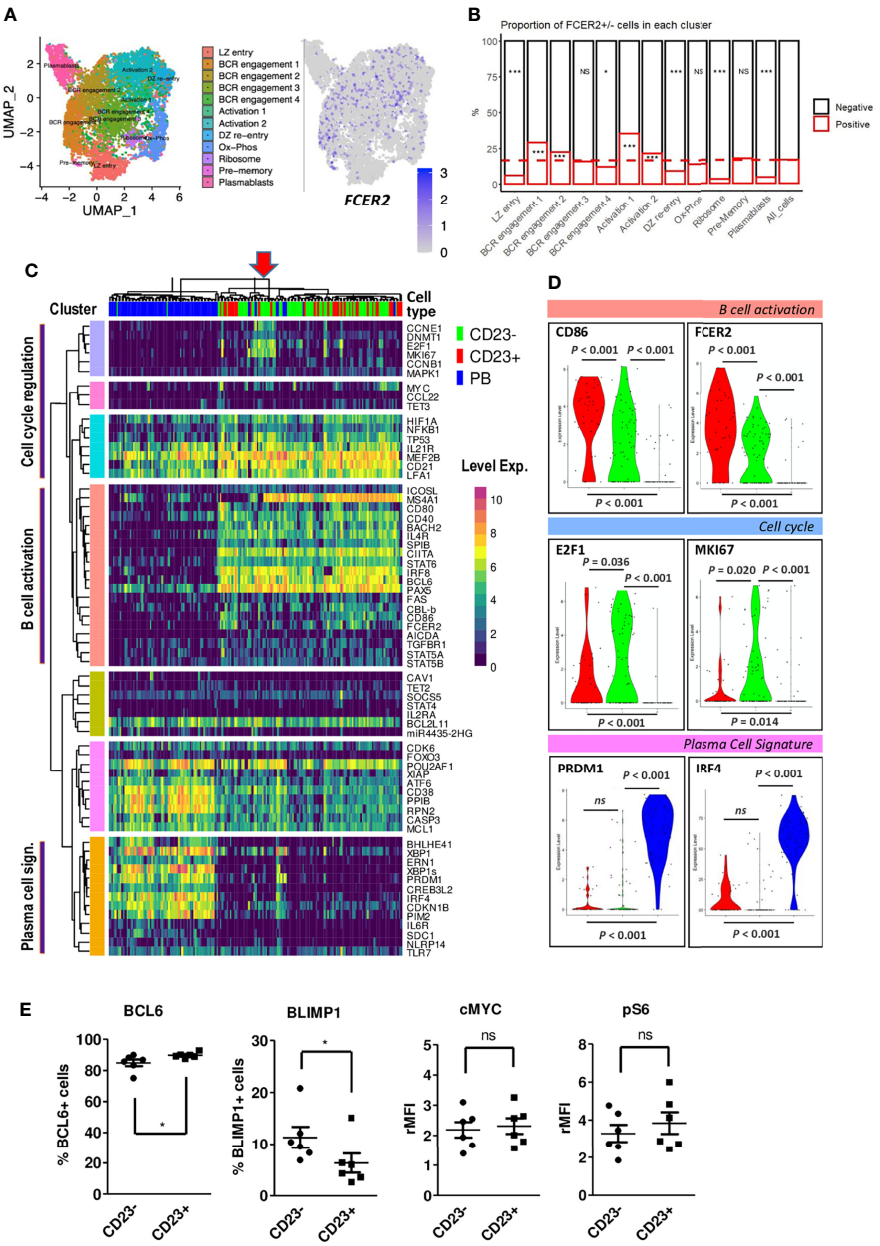

FIGURE 2 | *FCER2*/CD23 expression delineates specific LZ B_{GC}-cell subsets. **(A, B)** Single-cell RNA-seq data for human tonsil-derived CXCR4^{lo}CD83^{hi} LZ B_{GC}-cells in the G0-G1 phase of the cell cycle, from Holmes et al., 2020. **(A)** UMAP of the 12 specific clusters defined by Holmes et al. and expression of *FCER2* in these clusters. **(B)** Distribution of *FCER2*$^+$ (red) and *FCER2*$^-$ (black) non-proliferating LZ B_{GC}-cells, in the 12 clusters. Dotted line represent the mean value of positive cells for all clusters (last barplot named All_cells) (Chi2 test for each population vs. total cells (*$P < 0.05$, ***$P < 0.001$; significant test are indicated in the barplot of enriched CD23-negative or -positive populations accordingly). **(C)** Selected view of the heatmap with unsupervised clustering of single-cell RT-qPCR data comparing paired cell-sorted CD23$^+$ and CD23$^-$ LZ B_{GC}-cells (CD19$^+$IgD$^-$CD10$^+$CD38$^+$CXCR4^{lo}) and PBs (CD19$^+$IgD$^-$CD38^{bright}). Annotation of three clusters of genes linked to specific cell functions identified with GeneMANIA related to PCs, B cell activation and cell proliferation. The red arrow on the top of the heatmap indicate in cluster of cycling cells, mostly CD23$^-$ LZ B_{GC}-cells, that are positive for *MYC* expression represented in the Y-axis pink cluster. **(D)** Violin plot comparisons of the expression of few selected genes in CD23$^+$, CD23$^-$ LZ B_{GC}-cells and PBs. **(E)** Flow cytometry analysis of BCL6, BLIMP1, c-MYC and pS6 in tonsil CD23$^+$ and CD23$^-$ LZ B_{GC}-cells. Results are expressed as the percentage of positive cells or the relative mean fluorescence intensity (rMFI) (*$P \leq .05$; "ns" for non significant; Mann-Whitney test).

supports B_{GC}-cells (along with CD40L) (28, 29), we used these three stimuli in our subsequent experiments on primary LZ B_{GC}-cells. The data were reproducible, up to 50% of the cells were CD23$^+$ after 12 h of culture, cell viability was over 70% (data not shown) and cell proliferation was similar in CD23$^+$ and CD23$^-$ cells (**Supplemental Figure S3C**). We next co-cultured LZ B_{GC}-cells with paired autologous CD4$^+$CXCR5$^+$ICOS$^+$PD1$^+$ Tfh cells for 24 h and then analyzed CD23 expression in three

independent experiments. Only a weak increase in CD23 expression was observed. In contrast, when Tfh cells were activated either with α-CDA/α-CD28 antibodies or staphylococcal enterotoxin B protein, the CD23 expression increased markedly; 13.6+/-7.4% and 39.4+/-9.0% of the B cells were $CD23^+$, respectively (**Figure 3C**).

Taken as a whole, our present data suggest that the low number of $CD23^+$ LZ B_{GC}-cells is linked to a lack of effective, complete Tfh cell help in GCs - a key limiting resource for which the B cells compete (29). After early B cell-Tfh cell contact and in the absence of sustained Tfh support, $CD23^+$ B_{GC}-cells might also undergo apoptosis; this has been described *in vivo* for B_{GC}-cells after 24 h of antigen recognition and *in vitro* for $CD23^+$ post-activated B cells (19, 30). We confirmed the latter observation and showed that only $CD23^+$ LZ B_{GC}-cells were more numerous when the pan-caspase inhibitor QVD-OPH was added to the culture for 12 h (**Supplemental Figure S3D**).

Since IL-4 signaling goes through the STAT6 pathway, we next determined the number of B cells receiving Tfh-derived IL-4 in a contact dependent manner at a given point in time. To this end, we looked for nuclear expression of pSTAT6 in $CD20^+$ B_{GC}-cells by staining tonsil tissue sections. Tfh cells were detected by staining for PD1. By using a machine learning approach to automatically detect cells on microscopy images, we estimated that approximately 2 to 3% of B_{GC}-cells were $pSTAT6^+CD20^+$ (**Figure 3D** and **Supplemental Figure S3E**). By replacing CD20 with PAX5, we could estimate the number of $pSTAT6^+$ cells in the vicinity of $PD1^+$ T cells for three tonsils. Overall, among the average of 2880 $PAX5^+$/$pSTAT6^+$ B cells per tonsil, we found 18 (min 13- max 32) and 84 (min 62- max 124) of these cells located, respectively, within 10µm and 20µm of $PD1^+$ T cells. This corresponds to an average of 1.2% and 5.2% of B cells in less than 10µm or within 20µm proximity of T cells that may sufficient to favor contact between cognate B and T cells (**Figures 3E, F**). For the reasons mentioned above, we could not use the CD23 marker in parallel.

$CD23^-$ Activated LZ B_{GC}-Cells Contain PC Precursors

Since the LZ B_{GC}-cell compartment was heterogeneous with regard of CD23 expression after stimulation, we decided to study $CD23^-$ and $CD23^+$ LZ B_{GC}-cells obtained after 12 h of culture in the combined presence of IL-21, IL-4 and CD40L (hereafter referred to as $pcCD23^-$ or $pcCD23^+$ LZ B_{GC}-cells, where "pc" indicates "post-culture"). The gating strategy for cell sorting is presented in **Supplemental Figure S4A**. A comparison of these two subsets showed that *FCER2* expression was elevated only in $pcCD23^+$ LZ B_{GC}-cells (**Supplemental Figure S4B**). With regard to the four characteristic transcription factors involved in PC differentiation, there were no differences between the subsets in *BCL6, PAX5* and *XBP1* expression but *PRDM1* was significantly upregulated in $pcCD23^-$ LZ B_{GC}-cells (**Figure 4A**). Flow cytometry analysis showed significantly higher BCL6 expressing cells in the $CD23^+$ subset while the $CD23^-$ counterpart contained more $BLIMP1^+$ cells (**Figure 4B**).

We then evaluated the subsets' ability to differentiate into PBs ($CD38^{bright}$) and PCs ($CD138^+$). To that end, $pcCD23^-$ and $pcCD23^+$ LZ B_{GC}-cells were cultured separately for 48 h in the presence of IL-2, IL-4 and IL-10. Statistically significant results showed that only $pcCD23^-$ LZ B_{GC}-cells were able to give rise to a significant number of $CD38^{bright}$ and $CD138^+$ differentiated cells (**Figure 4C**).

The stimulation experiments were performed on total LZ B_{GC}-cells. However, to further specifically explore the $CD23^+$ minority compartment of LZ B_{GC}-cells, sorted tonsillar $CD23^+$ LZ B_{GC}-cells (**Supplemental Figure S2B**) were cultured for 24 h under the same conditions as above and analyzed by sc-qRT-PCR. No marker related to PC differentiation was detected after stimulation (**Supplemental Figure S4C**).

Activated $CD23^-$ LZ B_{GC}-cells Follow a Continuous, Homogeneous Trajectory Towards PBs

Our *in vitro* results and the literature data on LZ B_{GC}-cells (19) confirmed that the $CD23^+$ and $CD23^-$ subsets contained cells with distinct cell fates. To further explore this difference, we tracked spatiotemporally gene expression in stimulated LZ B_{GC}-cells. To this end, selected genes (**Supplemental Material, Method & Tables, Table 2**) (19) were analyzed using sc-qRT-PCR at different time points of the culture. Thus, tonsil sorted PBs were compared with paired LZ B_{GC}-cells after 4 h and 24 h of culture with IL-21, IL-4 and CD40L. For the 24 h time point, $CD23^+$ and $CD23^-$ cells were sorted (**Figure 5A**). To investigate the time course of changes in cell populations, we applied the Monocle trajectory inference algorithm (https://doi.org/10.1038/nbt.2859). UMAP reduction of the five cell populations highlighted two clusters that differed in their cell fate as a function of CD23 expression (**Supplemental Figure S5**). Only 24 h $CD23^-$ LZ B_{GC}-cells followed continuous, homogeneous trajectory *via* expression of the *BCL6, PAX5, IRF4, XBP1* and *PRDM1* genes associated with differentiation into PBs (**Figures 5B, C**). However, some LZ B_{GC}-cells had started to migrate along the differentiation trajectory as early as 4 h, and clustered with PBs. Using Monocle, the UMAP projection was color-coded according to the pseudo-time; this showed a well-ordered progression in quadrants from LZ B_{GC}-cells to PBs (**Figure 5D**).

The Time Course of Gene Expression Changes During the Differentiation of $CD23^-$ LZ B_{GC}-Cells

The expression heatmap for Monocle-ordered cells showed a sequential transition from $CD19^+IgD^-CD38^+CD10^+CXCR4^-$ LZ B_{GC}-cells to $CD19^+IgD^-CD38^{bright}$ PBs (**Figure 6A**). This situation enabled us to analyze changes over time in gene expression from one quadrant to the next and excluded T24h $CD23^+$ B_{GC} cells in agreement with the above result (**Supplemental Figure S5**). Each quadrant is enriched with a specific subset of cells (**Figure 6B**). The computed clustering allowed to identify six gene modules annotated by GeneMANIA (**Figure 6C**) characterized by a specific expression time course and linked to transcription factors, cell identity factors, and cell functions (**Supplemental Material, Method & Tables, Table 5**). Modules 1 and 2 were linked to PC identity genes. Modules 3, 5 & 6 were linked to a B cell activation state. In fact, Module 3 encompassed several transcription factors (including MYC) and preceded Module 6, which was linked to transient cell cycle entry prior to extinction in

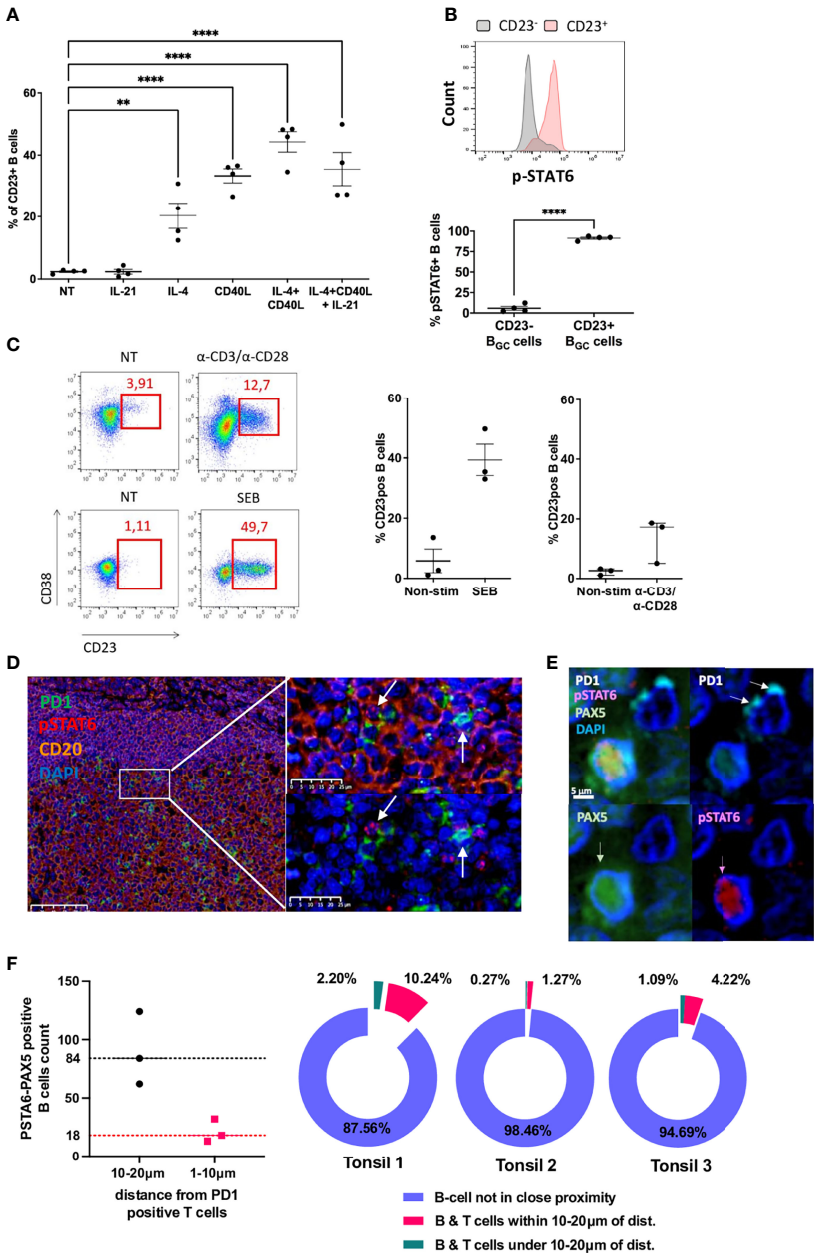

FIGURE 3 | CD23 expression of LZ B_{GC}-cells depends on response to Tfh-driven stimulation. **(A)** Flow cytometry analysis of $CD23^+$ LZ B_{GC}-cells obtained after 12 h of culture with IL-4, CD40L and IL-21 alone or in combinations (**$P < .01$; ****$P < .0001$; one-way multiple comparisons test). **(B)** Flow cytometry analysis of pSTAT6 induction on post-stimulation $CD23^+$ and $CD23^-$ LZ B_{GC}-cells, in four independent experiments: Upper panel, a representative flow histogram; Lower panel, quantitative and statistically significant analysis. **(C)** LZ B_{GC}-cells and Tfh cells were co-cultured without treatment (NT) or with aCD3/aCD28 or staphylococcal enterotoxin B (SEB) protein for 24 h and subsequently analyzed for CD23 and CD38 expression, using flow cytometry: left panel, representative flow graphs; right panel, results of three independent experiments. **(D)** GC immunohistostaining on paraffin-embedded tonsil sections with DAPI (blue), CD20 (yellow), PD1 (green), and pSTAT6 (red) presenting two high magnification views, showing $pSTAT6^+$ B cells in the proximity of $PD1^+$ Tfh cells (white arrows). **(E)** An image compatible with a cognate B cell-Tfh cell contact characterized by $pSTAT6^+$ B cell in contact with $PD1^+$ Tfh cell; immunohistostaining on paraffin-embedded tonsil sections with DAPI (blue), PAX5 (green), PD1 (white), and pSTAT6 (red). **(F)** Number of pSTAT6-PAX5 positive cells in three tonsils in the vicinity of PD1-positive T cells (left panel) and proportion of B cells closed to T cells among total of pSTAT6/PAX5-positive cells (right panel) in each tonsil.

the fourth quadrant (Q4). In Module 4, a transient expression pattern peaked during Q3 - probably in response to upstream factors such as MYC. It included the expression of *ATF5*, a transcription factor involved in the CREB3L2-ATF5-MCL1 survival pathway and which acts as a stress sensor (31). Module 5 featured a transient decline in the expression of B cell identity genes in Q1, a sharp increase in Q2 and Q3, and a drastic fall in Q4.

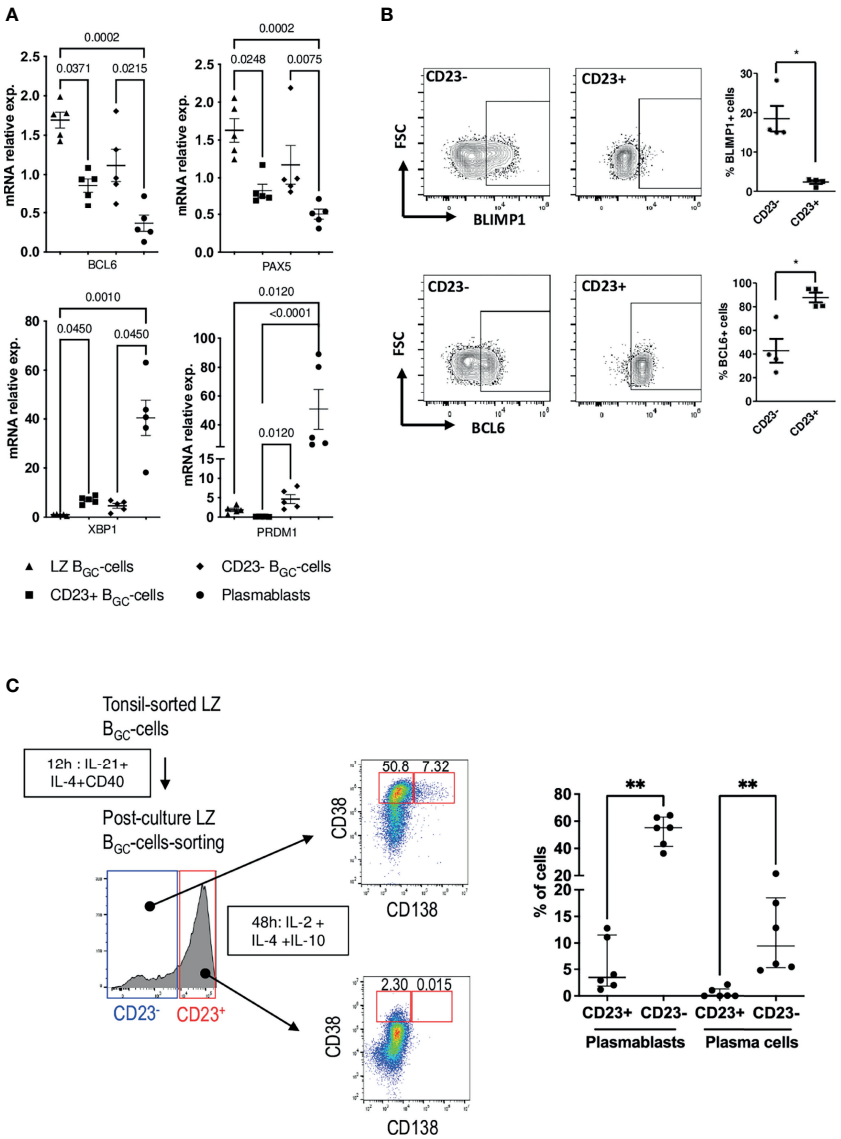

FIGURE 4 | CD23$^-$ LZ B_{GC}-cells contain PB precursors. **(A)** *BCL6*, *PAX5*, *XBP1* and *PRDM1* gene expression after 12 h culture in the presence of IL-4, CD40L and IL-21 for LZ B_{GC}-cells *vs*. freshly sorted, paired LZ B_{GC}-cells and PBs (one-way Anova & Kruskal-Wallis multiple comparisons test). **(B)** Flow cytometry analysis of BLIMP1 and BCL6 expression in post-culture CD23+ and CD23- LZ B_{GC}-cells: Left panel, representative flow graphs; Right panel, results of four independent experiments (*$P \leq .05$; Mann-Whitney test. **(C)** Post-culture CD23$^+$ and CD23$^-$ LZ B_{GC}-cells were subsequently maintained for 48 h in the presence of IL-2, IL-4 and IL-10 prior to flow cytometry analysis, in order to detect CD38^{bright}CD138$^-$ PBs and CD38^{bright}CD138$^+$ PCs. Left panel, graphical representation of the experiment and right panel, detected percentages of PBs and PCs for six independent experiments (**$P \leq .01$; Mann-Whitney test).

Our model of LZ B_{GC}-cell differentiation as a function of CD23 expression makes it possible to calculate how levels of transcription factors change in space and over time. The changes over time observed here were in line with the literature data (**Figure 6D**) (32). The *IRF4* gene was expressed in two phases, with an initial peak preceding the increase in expression of the B cell identity genes *PAX5, BCL6, BACH2*, and *SPIB*. The second peak occurred when the four factors were no longer expressed. *PAX5* expression showed a striking increase and peaked at the end of Q3 before dropping sharply and thus de-repressing the expression of *PRDM1*. This result is consistent with the fact that LZ B_{GC}-cells enter an activation state before they switch to the PB differentiation pathway (32). Although *PRDM1* and *XBP1s* are late transcription factors that seal the commitment to PBs, *XBP1* expression starts as soon as B cells activate. Furthermore, our model highlights the MYC imprint involved in the differentiation of B cells; our results are in agreement with MYC's description as a mediator of B_{GC}-cell survival and cell-cycle re-entry and as a marker of positive selection (7, 32, 33, 34). *MYC* expression is absent in sorted LZ B_{GC}-cells but rises quickly in the timeline followed by the expression of early MYC-target genes

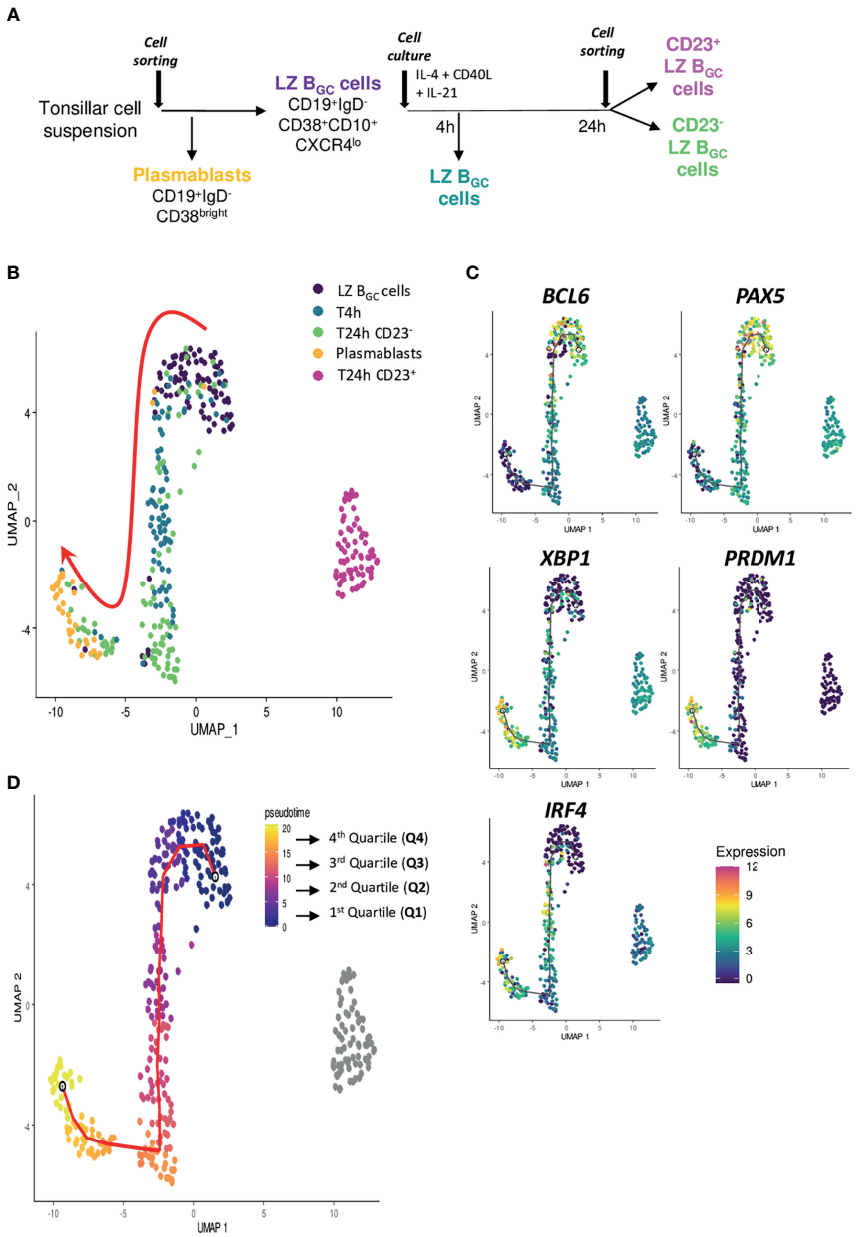

FIGURE 5 | Cell destiny of human LZ B_{GC}-cells after Tfh-like stimulation. **(A)** The experimental plan, with five different cell populations (colored script) analyzed using sc-RTqPCR. **(B)** The UMAP representation (colored according to the experimental conditions) highlighted two different fates as a function of CD23 expression. **(C)** Projection of B cell identity genes (*BCL6* and *PAX5*) and PC identity genes (*PRDM1*, *XBP1*, and *IRF4*) onto the UMAP representation. **(D)** The UMAP representation (colored according to the Monocle pseudotime), showing an ordered, progression in four quadrants from LZ B_{GC}-cells to PBs.

TP53, *CDK4* and *CDK6* (**Figure 6E**) (35, 36) and then the proliferative genes from Module 6 plus *CCNB1* (Module 4) – marking cell cycle re-entry.

Overview of IL-4 Signature Integration in LZ B_{GC}-Cells

The pseudo-time inferred from the Monocle algorithm provided an overview of the signal delivered by IL-4 (present in our differentiation cocktail) through the expression of *STAT6*, *IL4R*, *FCER2* and the well-established IL-4/STAT6 target *CCL22* (37) (**Figure 7A**). In line with our previous results (19), LZ B_{GC}-cells are unable to upregulate *FCER2* once they have committed to the PBs pathway but do produce a clear *STAT6* response marked by the expression of *IL4R* and *CCL22*. We then positioned on the sc-RNA-seq UMAP plot of total B_{GC}-cells from Holmes et al. (26) genes a B cell-specific IL-4 response signature (**Figure 7B**) (38). Positive cells for this signature were predominantly located in an area between pre-MBC and PB clusters, the latter two representing the two

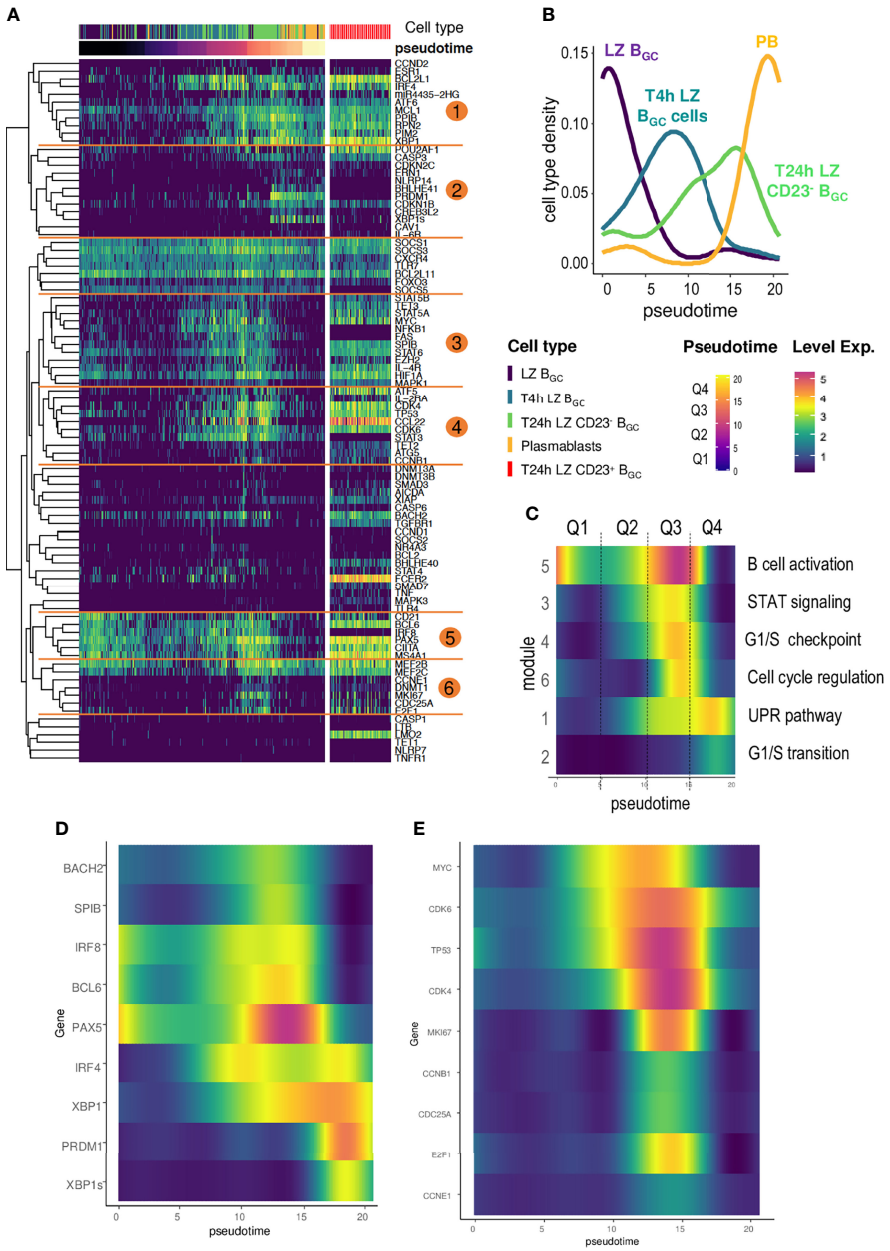

FIGURE 6 | The time course of gene analysis during LZ B_{GC}-cell differentiation. **(A)** A heatmap computed for Monocle-ordered cells (LZ B_{GC}-cells, PBs, T4h LZ B_{GC}-cells, T24h $CD23^+$ LZ B_{GC}-cells, and $CD23^-$ LZ B_{GC}-cells), showing six different gene modules annotated with GeneMANIA. The pseudotime scale was calculated from the gene expression data. **(B)** Density of cell subsets in each quadrant of the pseudotime. **(C)** Smooth analysis of the time course of each module by pseudotime quadrant (Q1 to Q4) for all cell subsets except T24h $CD23^+$ LZ B_{GC}-cells. **(D)** The time course of gene expression during B cell activation and differentiation into PCs showing (i) a bimodal expression of *IRF4*, (ii) a striking peak for *PAX5*, (iii) *PRDM1* elevation synchronized with *PAX5* decline, and (iv) the specific expression of *XBP1s* in the last quadrant of the pseudotime compared to *XBP1*. **(E)** Gene expression during the differentiation of $CD23^-$ LZ B_{GC}-cells for Monocle-ordered cells showing a sequential transition from LZ B_{GC}-cells to PBs for *MYC* expression, MYC-target genes and gene involved in cell cycle re-entry.

distinct fates for B_{GC}-cells (**Figure 7C**). A similar distribution was obtained for cells expressing *FCER2* with higher density on the far right of the map, drawing a ridge line extending from the intermediate (INT) 6 cluster to the pre-MBC cluster (**Figure 7D**). Statistical analysis showed a striking enrichment for the IL-4 signature in INT5, INT6, light-zone (LZ) and pre-memory clusters compared to other clusters (**Figure 7E**). IL-4 signaling was significantly enriched in $FCER2^+$ cells compared to $FCER2^-$ counterparts in some clusters including INT6, LZ and pre-memory (**Figure 7F**). Interestingly, these three latter also exhibited the highest proportion of $FCER2^+$ cells compared to other clusters (**Figure 7G**). Finally, unlike pre-MBCs, most differentiated PBs were

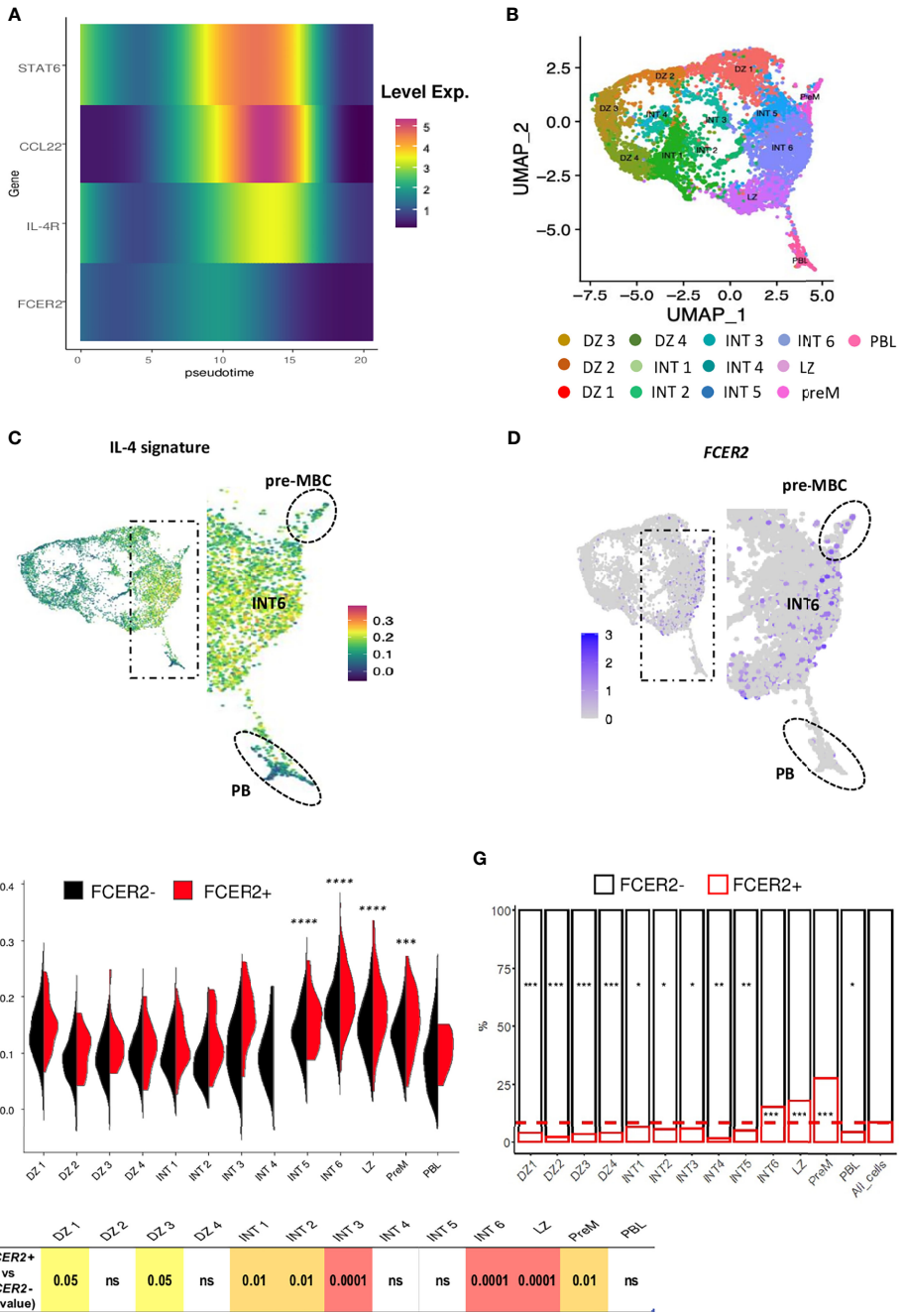

FIGURE 7 | Overview of the IL-4 signature in LZ B_{GC}-cells. **(A)** The time course of expression of IL-4-induced genes by quadrant showing a difference between the almost flat *FCER2* expression and the strong *CCL22* expression. **(B–G)** Single-cell RNA-seq data for human tonsil-derived total B_{GC}-cells, from Holmes et al., 2020**. (B)** UMAP representation of the 13 specific clusters defined by Holmes et al. ***(C)*** UMAP showing cell expression of the IL-4 signature, noteworthy that positive cells are located in the right part of the map mainly in intermediate 6 (INT6) cluster (enlarged view) with an expression maintained in pre-MBCs (Top, dotted circle) while PBs are negative (Bottom, dotted circle). **(D)** UMAP showing *FCER2*$^+$ cells; the enlarged view shows the preferential enrichment of these cells on the far right of the map depicting a ridge line extending from the INT6 cluster to the pre-MBC cluster (top, dotted line circle). **(E)** Violin plots comparing IL-4 signature expression in each of the 13 GC B cell clusters for *FCER2*$^+$ (red) and *FCER2*$^-$ (black) cells (Pairwise t-test for IL-4 signature comparison between clusters is indicated above the plot; ***$P < .001$; ****$P < .0001$). **(F)** Table of *P* values of Wilcox test comparing *FCER2*$^+$ and *FCER2*$^-$ B_{GC}-cells for IL-4 signature in each of the 13 clusters. **(G)** Percentage of *FCER2*$^+$ and *FCER2*$^-$ B_{GC}-cells in the 13 clusters. Dotted line represent the mean value of positive cells for all clusters (last barplot named All_cells). Chi2 test for each population compared to total cells (*p < 0.05, **p < 0.01, ***p < 0.001, "ns" for non significant); significant test are indicated in the barplot of enriched FCER2 neg or pos populations accordingly.

negative for both IL-4 signature and *FCER2* expression, confirming that in last steps of the PB commitment, cells turned off their IL-4/STAT6/FCER2 signaling (19).

DISCUSSION

In the present study, we investigated the functional diversity of human LZ B_{GC}-cells collected at a single point in time from tonsils and rLNs. We found that the PC precursors are contained within the CD23-negative LZ B_{GC}-cell compartment. Based on our findings, time course gene expression analysis provided new information on the LZ B_{GC}-cells' commitment to differentiation and, in particular, on the kinetics and interconnexion between transcription factors.

Conventionally, it has been thought that like in mice, human B_{GC}-cells express CD23 in response to molecules produced by Tfh cells (19). Our results show that less than 10% of tonsil B_{GC}-cells expressed this protein, this number increasing when considering only LZ B_{GC}-cells. In contrast, in rLNs, LZ B_{GC}-cells express much higher levels of CD23 positive cells reflecting likely that unlike chronically inflamed tonsils, rLN tissues are produced in an acute response to a more limited number of antigens. In addition, our study confirmed previous data by showing that LZ stromal FDCs express very high levels of the CD23 receptor (22, 23). Complementing very recently published data from Cyster's team showing that FDC restricted IL-4 availability in the GC (24) and our work revealing the expression of IL-4 receptor and CD40 by FDCs (39), it is tempting to speculate that FDCs activate CD23 expression by trapping molecules produced by Tfh cells in the LZ and then titrating them. In such a case, the LZ B_{GC}-cells require effective, lasting contact with Tfh cells for activation leading notably in B cells by the recruitment of the IL-4/STAT6 signaling and CD23 expression (19). Our pSTAT6 protein staining is consistent with the detection of the CD23 marker and the single-cell data on *FCER2* expression; these findings indicate that only a small proportion of LZ B_{GC}-cells are engaged in B cell-Tfh cell contacts at a given point in time. These results also agree with (i) the transient, dynamic interactions between B_{GC}-cells and Tfh cells observed in GCs (providing opportunities for competition between B cells) and (ii) the fact that up to half of the B_{GC}-cells undergo apoptosis every 6 hours due to the absence of active positive selection and irrespective of the BCR affinity (34). *In silico* reanalyzed data from Holmes et al. (26) shows that *FCER2*-expressing LZ B_{GC}-cells are activated, BCR^+ cells that might upregulate *CD86* - a gene whose expression in MBCs is induced by IL-21 (40). In addition, flow cytometry detects significantly more $CCR6^+$ cells in $CD23^+$ than $CD23^-$ LZ B_{GC}-cells. The sc-qRT-PCR experiment shows no upregulation of genes related to PC differentiation after stimulation of sorted $CD23^+$ LZ B_{GC}-cells as well as absence of cells downregulating the *FCER2* expression. Overall, our findings support the hypothesis whereby CD23 expression characterizes Tfh-instructed, post-activated LZ B_{GC}-cells diverted from a PC fate (40, 41). However, some activated LZ B_{GC}-cells may decrease the density of the membrane-bound form of CD23 – a probable reason for the expression of the *FCER2* gene in some $CD23^-$ tonsillar LZ B_{GC}-cells sorted by flow cytometry – after release as a freely soluble molecule due to ADAM10 sheddase (42, 43). This point may contribute to our BCR repertoire results where $CD23^+$ and $CD23^-$ subsets are clonally related, which do not exclude that clonal evolution could possibly stand at different stages of their differentiation. Collectively, our data demonstrate that $CD23^-$ LZ B_{GC}-cells are heterogeneous and contain both stimulated and unstimulated B cells as well as B cells having committed to the PB pathway. In these committed B cells, the IL-4 signal is removed and the *FCER2* gene can no longer be upregulated, the PBs being totally negative for this signaling and this marker. Interestingly, committed $CD23^-$ LZ B_{GC}-cells maintain a transient ability to upregulate IL-4/pSTAT6-dependent *CCL22* after stimulation; this observation is consistent with the finding that CCL22 promotes positive selection in murine GCs by increasing the chance of productive Tfh help (44). Thus, in the committal step of PB generation, IL-4/STAT6 signaling is definitively repressed before a switch into a PC gene expression pattern during the S phase of the cell cycle (14, 19). In agreement with a recent study, we used a sensitive sc-RT-qPCR to detect proliferating $CD23^-$ LZ B_{GC}-cells that steadily increased their expression of *MYC* - an indicator of positive selection (45)- after *in vitro* stimulation (20). The computed cell trajectory showed that some LZ B_{GC}-cells reached the PB site after just 4 h and indicated that some cells were ready to recycle and differentiate after appropriate stimulation. This finding is consistent with previous data on high-affinity LZ B_{GC}-cells that migrate to the DZ and can differentiate into PCs, depending on the amount of CD40 signal captured (13, 46). Overall, the trajectory of $CD23^-$ LZ B_{GC}-cells (i) sheds light on the time course in gene expression during commitment to the PC pathway, and (ii) enables comparisons with regard to various genes and possible interdependencies. For example, transient expression of IRF4 sustains the expression of *BCL6* and *POU2AF1* (47); *POU2AF1* expression is consistent with its ability to activate B_{GC}-cells and induce GC formation by (at least in part) underpinning the IL-4 response (48) and then enhancing the generation of PCs (49).

Overall, the CD23 marker might be of value in answering questions about the differentiation of normal B_{GC}-cells. Based on extensive data in the literature including our previously published data (14, 50, 51) and present results complemented by explorations on previous scRNA-seq (26) as well as recent results of Duan et al. (24), we propose an instructive model of the maturation and fate of human B_{GC}-cells in LZ (**Figure 8**). The majority of B_{GC}-cells are CD23-negative, progress in an affinity-based proliferation and compete for Tfh help leading to a productive IL-4/pSTAT6 response. B cells committed in PB differentiation first lose their capacity to express the CD23 marker, then IL-4/pSTAT6 signaling and finally trigger final PC programming supported by a specific demethylation process (14). In this context, CD23-negative committed B cells correspond to pre-PBs, diverted from cell death, they transiently express *MYC* which triggers the cell cycle and gives rise to a metamorphosis of B cells into PBs. The cell fate split

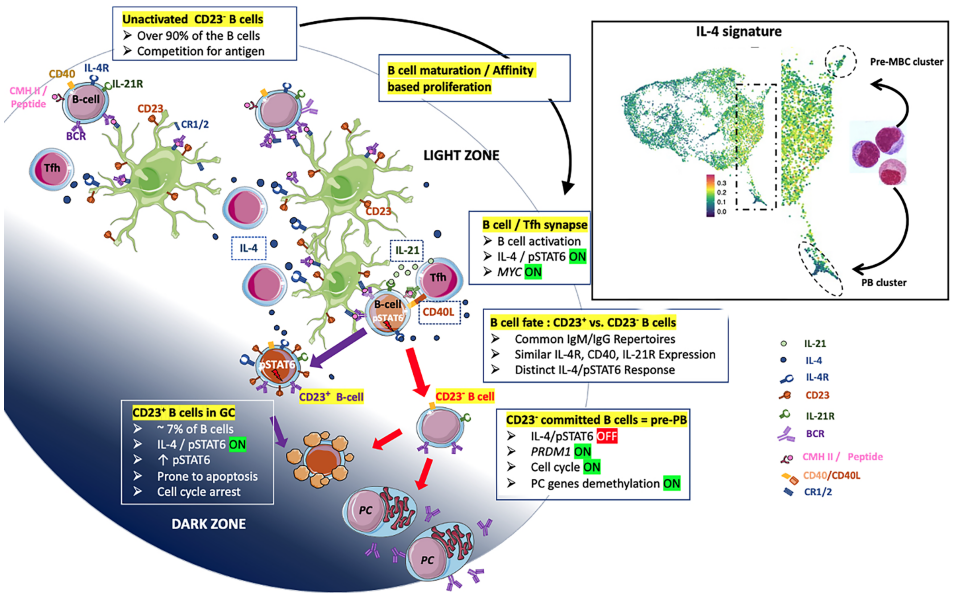

FIGURE 8 | Proposal of an instructive differentiation model of LZ B_{GC}-cells integrating the expression of the CD23 marker. B_{GC}-cells are predominantly $CD23^-$ compete for antigen (Ag) when only limited amount of Ag is available (top-left B cells). Fit cells proliferate, retrieve Ag deposited on follicular dendritic cells (FDCs) and receive survival signals from stromal cells (top-middle part). Note that FDCs express IL-4R and may take available IL-4 cytokine - in a non-directed manner [IL-4 broadcasting as called in (24)] – produced by Tfh. Both, high and low-affinity cells process Ag and present - in proportion to its affinity - peptide-MHC complex which supports the interaction with cognate Tfh and the delivery of crucial molecules including IL-21, CD40L and IL-4 leading to pSTAT6 expression (right-middle part). The split of the B cell fate depends on the integration of sufficient signals which impacts the maintenance or extinction of the IL-4/pSTAT6 signaling pathway. B cells that have quenched the IL-4/STAT6 signal are unable to express the CD23 marker and progress further to the PB axis of differentiation (bottom-right). These $CD23^-$ LZ B_{GC}-cells correspond to pre-PB described previously (19) which express transiently *MYC* leading to cell cycle and the committal step of differentiation described elsewhere (14). In contrast, $CD23^+$ LZ B_{GC}-cells which have maintained IL-4/STAT6 signaling are prone to apoptosis or give rise to pre-MBCs; the maintenance of CD23 expression depends on the presence of IL-4 and CD40 stimuli (bottom-middle). In the right square, a view of the **Figure 7C** concerning scRNA-seq data for B_{GC}-cells representing the fate of activated LZ B_{GC}-cells between pre-MBC or PB outputs.

between pre-MBC and PB destinies may take place in the INT6 cluster of B_{GC}-cells. There, B cells express the IL-4/STAT6 signature and then migrate either to the pre-MBC group or after their IL-4/STAT6 signaling has been turned off, to the PB cluster. Taken as a whole, the present results have implications for the design of future studies on the differentiation of both normal human B_{GC}-cells and their malignant counterparts. Indeed, in patients with follicular lymphoma, the survival was significantly better in patients carrying $CD23^+$ FL B cells (52).

MATERIALS AND METHODS

Human Samples and Primary B Cell Purification

Tonsils obtained from children undergoing routine tonsillectomy were obtained following approval by the French Ministry of Higher Education and Research (reference: AC-2014-2315). The children's parents provided their informed consent to use of the samples for research purposes. The study was performed in accordance with the principles of the Declaration of Helsinki. Tonsil-derived B_{GC}-cells were enriched by negative selection *via* magnetic cell separation, using the MojoSort Human Pan B Cell Isolation Kit (Biolegend, San Diego, CA) with the addition of biotinylated IgD antibody (BD Biosciences, San Jose, CA) and the AutoMACS deplete program (Miltenyi Biotech, Bergisch Gladbach, Germany). LZ B_{GC}-cells ($CD19^+IgD^-CD10^+CD38^+CXCR4^{lo}$) and PBs ($CD19^+IgD^-CD38^{bright}$) were then sorted using a FACSAria system (BD Biosciences). All antibodies used for flow cytometry are listed in **Supplemental Material, Method & Tables, Table 1**.

Single-Cell qPCR Experiments

Single-cell experiments were performed using the Fluidigm® C1™systems according to manufacturer instructions., Briefly, sorted cells were captured with CI Single-Cell Auto Prep integrated fluidic circuits (IFC) 5-10 µm (Fluidigm; 100-5757). Cells were then lysed, and reversed transcription and pre-amplification (Ambion Single cell-to-Ct Kit; 4458237) was done within the C1 system. Gene expression levels was then assessed by qPCR for selected taqman assays using Taqman Gene expression master mix Life technologies; 4369016) on 96.96 Dynamic Arrays IFC (Fluidigm; BMK-M-96.96) within the Fluidigm BioMark™ HD system. The list of TaqMan assay-on-Demand™ used is provided in **Supplemental Material, Method & Tables, Table 2**.

Histo-Immunofluorescence Staining

Human tonsils and reactive lymph nodes were embedded in Optimal Cutting Temperature Compound (OCT, Sakura) and conserved at -80°C. Cryostat sections (18 µm thick) were fixed with 4% paraformaldehyde for 15 min at room temperature (RT). Sections were then incubated during 1 h with a blocking solution (PBS, 2% Bovine Serum Albumin, 4% donkey serum and 0.1% saponin) at RT and incubated in a humidified chamber overnight at 4° C with primary antibodies. Sections were washed with PBS 0.1% saponin and incubated with secondary antibodies for 1 h at RT. Finally, tissue sections were mounted with Mowiol (Merck) antifade reagent containing 20µM of SytoxBlue nucleic acid stain (Thermo Fischer) and analyzed by confocal microscopy on a SP8 (Leica Microsystems). ImageJ software (National Institutes of Health) was used for image analysis. The list of primary and secondary antibodies used for immunohistofluorescence is provided in **Supplemental Material, Method & Tables, Tables 3, 4**.

For multiplex fluorescence microscopy and analysis, three FFPE samples of human tonsil were provided by the Pathology department of Rennes. Four-micrometer-thick whole-slide sections, obtained with a microtome (Histocore multicut Leicabiosystems, Nanterre, France) from FFPE tissue, were transferred onto plus-charged slides (VWR international), followed by multiplex immunofluorescence staining with a U DISCOVERY 5 plex immunofluorescence (Roche Diagnostics, Meylan, France). Four sequential rounds of staining were performed each including heat deactivation step, followed by incubation with primary antibody and corresponding HRP secondary antibody. Hence, primary antibodies expressions (as described in **Supplemental Material, Method & Tables, Table 3**) were visualized on the same section. HRP enzyme mediated deposition of the tyramide; coupled to respectively rhodamine, DCC, cyanine-5 and FAM fluorophores species (kits Ventana Medical Systems, Tucson, Arizona) that covalently bound to the tissue at the site of the reaction. After four sequential reactions, sections were counterstained with DAPI and cover slipped using fluoromount (Enzo Life Sciences, Farmingdale, NY, USA). Visualization was performed with the Nanozoomer (Hamamatsu Photonics, Massy, France) equipped with the multicolor fluorescence module.

For the pSTAT6-positive B_{GC}-cell percentage assessment, an automated analysis by machine learning with the HALO software was performed. After cell segmentation and nuclear detection pSTAT6, CD20, PAX5 and PD1 threshold intensities were set up. Six GCs in three different tonsils were analyzed. Double CD20 or PAX5 and pSTAT6-positive cells and total CD20- or PAX5-positive cells were quantified and a percentage of positive pSTAT6 B cells was assessed.

Information About RNA-Seq Datasets Used Throughout the Paper

Bulk RNAseq datasets used to select genes analyzed by sc-qPCR in this study are available in the Gene Expression Omnibus database under accession no. GSE136990.

Single-cell-RNAseq datasets from Holmes et al.'s paper (26) are available in the Gene Expression Omnibus database under accession no. GSE139833. sc-gene expression data are available under accession no. GSE139891.

Statistical Analysis

Quantitative variables were expressed as the mean ± standard deviation (SD). Statistical analyses were performed with Prism software (version 5, GraphPad Software, San Diego, CA) and R software (version 3.6.0). Statistical significance was assessed using the Mann-Whitney nonparametric U test and a one-way Anova and Kruskal-Wallis multiple comparison test ($^{*}P \leq .05$; $^{**}P < .01$; $^{***}P < .001$; $^{****}P < .0001$).

DATA AVAILABILITY STATEMENT

Publicly available datasets were analyzed in this study. These data can be found here: 1) The dark zone and light zone bulk single-cell RNAseq gene expression data are available in the Gene Expression Omnibus database under accession no. GSE139833. sc-gene expression data are available under accession no. GSE139891; 2) CD23-positive and CD23-negative RNA-seq data have been deposited in the Gene Expression Omnibus: GSE136990.

ETHICS STATEMENT

Ethical review and approval was not required for the study on human participants in accordance with the local legislation and institutional requirements. The ethics committee waived the requirement of written informed consent for participation.

AUTHOR CONTRIBUTIONS

KS performed experiments, designed some experiments, analyzed data. FD analyzed and integrated omics data, created tools for analysis, supervised KS for some experiments and helped draft the manuscript. GC performed and designed experiments, reviewed the paper. SL analyzed single-cell transcriptome data., MH, CD, and AP performed experiments to characterize CD23 marker expression on the various B cell populations. FC analyzed and integrated omics data and created tools for analysis. DR and MC analyzed B cell repertoires. CM performed single-cell experiments. MS and CL performed histology and immunofluorescence experiments. KT analyzed stromal cell staining and B cell-Tfh cell cocultures. TF designed the study, performed transcriptome analysis, supervised the project and wrote the manuscript. All authors read and approved the manuscript.

FUNDING

This research was funded by an internal grant from the Hematology Laboratory (Pôle de Biologie, CHU de Rennes, Rennes, France) and two grants from the *Association pour la Recherche contre le Cancer* (ARC, PJA 20181207839 and PJA3 2020060002221).

ACKNOWLEDGMENTS

Cell sorting was performed at the Biosit Flow Cytometry and Cell Sorting Facility (CytomeTRI, University of Rennes 1, Rennes, France). Histologic immunofluorescence analyses were performed at the Biosit H2P2 and PRISM facilities (University of Rennes 1, Rennes, France). We thank L. Deleurme and A. Saintamand for technical assistance, and I. Papa for discussions. KS received a doctoral fellowship from the University of Rennes 1. SL is funded by the chair "Cancer & Innovation" of the Rennes 1 Foundation and the LabEx IGO project (reference: ANR-11-LABX-0016-01). MH received a doctoral fellowship from the FHU CAMIn, university hospital of Rennes, Fance. We thank David Fraser at Biotech Communication for editing services.

SUPPLEMENTARY MATERIAL

The Supplementary Material for this article can be found online at: https://www.frontiersin.org/articles/10.3389/fimmu.2021.744573/full#supplementary-material

REFERENCES

1. Caron G, Gallou SL, Lamy T, Tarte K, Fest T. CXCR4 Expression Functionally Discriminates Centroblasts *Versus* Centrocytes Within Human Germinal Center B Cells. *J Immunol* (2009) 182(12):7595–602. doi: 10.4049/jimmunol.0804272
2. MacLennan IC. Germinal Centers. *Annu Rev Immunol* (1994) 12:117–39. doi: 10.1146/annurev.iy.12.040194.001001
3. Vinuesa CG, Linterman MA, Yu D, MacLennan ICM. Follicular Helper T Cells. *Annu Rev Immunol* (2016) 34(1):335–68. doi: 10.1146/annurev-immunol-041015-055605
4. Victora GD, Schwickert TA, Fooksman DR, Kamphorst AO, Meyer-Hermann M, Dustin ML, et al. Germinal Center Dynamics Revealed by Multiphoton Microscopy With a Photoactivatable Fluorescent Reporter. *Cell* (2010) 143(4):592–605. doi: 10.1016/j.cell.2010.10.032
5. Kräutler NJ, Suan D, Butt D, Bourne K, Hermes JR, Chan TD, et al. Differentiation of Germinal Center B Cells Into Plasma Cells Is Initiated by High-Affinity Antigen and Completed by Tfh Cells. *J Exp Med* (2017) 214 (5):1259–67. doi: 10.1084/jem.20161533
6. Weisel FJ, Zuccarino-Catania GV, Chikina M, Shlomchik MJ. A Temporal Switch in the Germinal Center Determines Differential Output of Memory B and Plasma Cells. *Immunity* (2016) 44(1):116–30. doi: 10.1016/j.immuni.2015.12.004
7. Dominguez-Sola D, Victora GD, Ying CY, Phan RT, Saito M, Nussenzweig MC, et al. The Proto-Oncogene MYC Is Required for Selection in the Germinal Center and Cyclic Reentry. *Nat Immunol* (2012) 13(11):1083–91. doi: 10.1038/ni.2428
8. Calado DP, Sasaki Y, Godinho SA, Pellerin A, Köchert K, Sleckman BP, et al. The Cell-Cycle Regulator C-Myc Is Essential for the Formation and Maintenance of Germinal Centers. *Nat Immunol* (2012) 13(11):1092–100. doi: 10.1038/ni.2418
9. Mesin L, Ersching J, Victora GD. Germinal Center B Cell Dynamics. *Immunity* (2016) 45:471–82. doi: 10.1016/j.immuni.2016.09.001
10. Shinnakasu R, Inoue T, Kometani K, Moriyama S, Adachi Y, Nakayama M, et al. Regulated Selection of Germinal-Center Cells Into the Memory B Cell Compartment. *Nat Immunol* (2016) 17(7):861–9. doi: 10.1038/ni.3460
11. Shinnakasu R, Kurosaki T. Regulation of Memory B and Plasma Cell Differentiation. *Curr Opin Immunol* (2017) 45:126–31. doi: 10.1016/j.coi.2017.03.003
12. Meyer-Hermann M, Mohr E, Pelletier N, Zhang Y, Victora GD, Toellner K-M. A Theory of Germinal Center B Cell Selection, Division, and Exit. *Cell Rep* (2012) 2(1):162–74. doi: 10.1016/j.celrep.2012.05.010
13. Ise W, Fujii K, Shiroguchi K, Ito A, Kometani K, Takeda K, et al. T Follicular Helper Cell-Germinal Center B Cell Interaction Strength Regulates Entry Into Plasma Cell or Recycling Germinal Center Cell Fate. *Immunity* (2018) 48 (4):702–15.e4. doi: 10.1016/j.immuni.2018.03.027
14. Caron G, Hussein M, Kulis M, Delaloy C, Chatonnet F, Pignarre A, et al. Cell-Cycle-Dependent Reconfiguration of the DNA Methylome During Terminal Differentiation of Human B Cells Into Plasma Cells. *Cell Rep* (2015) 13 (5):1059–71. doi: 10.1016/j.celrep.2015.09.051
15. Tinnell SB, Jacobs-Helber SM, Sterneck E, Sawyer ST, Conrad DH. STAT6, NF-Kappab and C/EBP in CD23 Expression and Ige Production. *Int Immunol* (1998) 10(10):1529–38. doi: 10.1093/intimm/10.10.1529
16. Colombo M, Cutrona G, Reverberi D, Bruno S, Ghiotto F, Tenca C, et al. Expression of Immunoglobulin Receptors With Distinctive Features Indicating Antigen Selection by Marginal Zone B Cells From Human Spleen. *Mol Med* (2013) 19(1):294–302. doi: 10.2119/molmed.2013.00069
17. Victora GD, Dominguez-Sola D, Holmes AB, Deroubaix S, Dalla-Favera R, Nussenzweig MC. Identification of Human Germinal Center Light and Dark Zone Cells and Their Relationship to Human B-Cell Lymphomas. *Blood* (2012) 120(11):2240–8. doi: 10.1182/blood-2012-03-415380
18. Kolar GR, Mehta D, Pelayo R, Capra JD. A Novel Human B Cell Subpopulation Representing the Initial Germinal Center Population to Express AID. *Blood* (2006) 109(6):2545–52. doi: 10.1182/blood-2006-07-037150
19. Pignarre A, Chatonnet F, Caron G, Haas M, Desmots F, Fest T. Plasmablasts Derive From CD23– Activated B Cells After the Extinction of IL-4/STAT6 Signaling and IRF4 Induction. *Blood* (2021) 137(9):1166–80. doi: 10.1182/blood.2020005083
20. Nakagawa R, Toboso-Navasa A, Schips M, Young G, Bhaw-Rosun L, Llorian-Sopena M, et al. Permissive Selection Followed by Affinity-Based Proliferation of GC Light Zone B Cells Dictates Cell Fate and Ensures Clonal Breadth. *Proc Natl Acad Sci USA* (2021) 118(2):e2016425118–12. doi: 10.1073/pnas.2016425118
21. Shinall SM, Gonzalez-Fernandez M, Noelle RJ, Waldschmidt TJ. Identification of Murine Germinal Center B Cell Subsets Defined by the Expression of Surface Isotypes and Differentiation Antigens. *J Immunol* (2000) 164(11):5729–38. doi: 10.4049/jimmunol.164.11.5729
22. Allen CDC, Cyster JG. Follicular Dendritic Cell Networks of Primary Follicles and Germinal Centers: Phenotype and Function. *Semin Immunol* (2008) 20 (1):14–25. doi: 10.1016/j.smim.2007.12.001
23. Tjin EPM, Bende RJ, Derksen PWB, van Huijstee A-P, Kataoka H, Spaargaren M, et al. Follicular Dendritic Cells Catalyze Hepatocyte Growth Factor (HGF) Activation in the Germinal Center Microenvironment by Secreting the Serine Protease HGF Activator. *J Immunol* (2005) 175(5):2807–13. doi: 10.4049/jimmunol.175.5.2807
24. Duan L, Liu D, Chen H, Mintz MA, Chou MY, Kotov DI, et al. Follicular Dendritic Cells Restrict Interleukin-4 Availability in Germinal Centers and Foster Memory B Cell Generation. *Immunity* (2021) 54:2256–72.e6. doi: 10.1016/j.immuni.2021.08.028
25. Suan D, Kräutler NJ, Maag JLV, Butt D, Bourne K, Hermes JR, et al. CCR6 Defines Memory B Cell Precursors in Mouse and Human Germinal Centers, Revealing Light-Zone Location and Predominant Low Antigen Affinity. *Immunity* (2017) 47(6):1142–53.e4. doi: 10.1016/j.immuni.2017.11.022
26. Holmes AB, Corinaldesi C, Shen Q, Kumar R, Compagno N, Wang Z, et al. Single-Cell Analysis of Germinal-Center B Cells Informs on Lymphoma Cell of Origin and Outcome. *J Exp Med* (2020) 217:e20200483. doi: 10.1084/jem.20200483
27. Ersching J, Efeyan A, Mesin L, Jacobsen JT, Pasqual G, Grabiner BC, et al. Germinal Center Selection and Affinity Maturation Require Dynamic Regulation of Mtorc1 Kinase. *Immunity* (2017) 46(6):1045–58.e6. doi: 10.1016/j.immuni.2017.06.005

28. Weinstein JS, Herman EI, Lainez B, Licona-Limón P, Esplugues E, Flavell R, et al. TFH Cells Progressively Differentiate to Regulate the Germinal Center Response. *Nat Immunol* (2016) 17(10):1197–205. doi: 10.1038/ni.3554
29. Crotty S. T Follicular Helper Cell Biology: A Decade of Discovery and Diseases. *Immunity* (2019) 50(5):1132–48. doi: 10.1016/j.immuni.2019.04.011
30. Akkaya M, Traba J, Roesler AS, Miozzo P, Akkaya B, Theall BP, et al. Second Signals Rescue B Cells From Activation- Induced Mitochondrial Dysfunction and Death. *Nat Immunol* (2018) 19(8):871–84. doi: 10.1038/s41590-018-0156-5
31. Sheng Z, Li L, Zhu LJ, Smith TW, Demers A, Ross AH, et al. A Genome-Wide RNA Interference Screen Reveals an Essential CREB3L2-ATF5-MCL1 Survival Pathway in Malignant Glioma With Therapeutic Implications. *Nat Med* (2010) 16(6):671–7. doi: 10.1038/nm.2158
32. Willis SN, Nutt SL. Sciencedirect New Players in the Gene Regulatory Network Controlling Late B Cell Differentiation. *Curr Opin Immunol* (2019) 58:68–74. doi: 10.1016/j.coi.2019.04.007
33. Luo W, Weisel F. Shlomchik MJ. B Cell Receptor and CD40 Signaling Are Rewired for Synergistic Induction of the C-Myc Transcription Factor in Germinal Center B Cells. *Immunity* (2018) 48(2):313–26.e5. doi: 10.1016/j.immuni.2018.01.008
34. Mayer CT, Gazumyan A, Kara EE, Gitlin AD, Golijanin J, Viant C, et al. The Microanatomic Segregation of Selection by Apoptosis in the Germinal Center. *Sci (New York NY)* (2017) 358(6360):eaao2602–10. doi: 10.1126/science.aao2602
35. Zindy F, Eischen CM, Randle DH, Kamijo T, Cleveland JL, Sherr CJ, et al. Myc Signaling *via* the ARF Tumor Suppressor Regulates P53-Dependent Apoptosis and Immortalization. *Gene Dev* (1998) 12(15):2424–33. doi: 10.1101/gad.12.15.2424
36. Hermeking H, Rago C, Schuhmacher M, Li Q, Barrett JF, Obaya AJ, et al. Identification of CDK4 as a Target of C-MYC. *Proc Natl Acad Sci* (2000) 97 (5):2229–34. doi: 10.1073/pnas.050586197
37. Takemura M, Nakahara T, Hashimoto-Hachiya A, Furue M, Tsuji G. Glyteer, Soybean Tar, Impairs IL-4/Stat6 Signaling in Murine Bone Marrow-Derived Dendritic Cells: The Basis of Its Therapeutic Effect on Atopic Dermatitis. *Int J Mol Sci* (2018) 19(4):1169. doi: 10.3390/ijms19041169
38. Lu X, Nechushtan H, Ding F, Rosado MF, Singal R, Alizadeh AA, et al. Distinct IL-4-Induced Gene Expression, Proliferation, and Intracellular Signaling in Germinal Center B-Cell-Like and Activated B-Cell-Like Diffuse Large-Cell Lymphomas. *Blood* (2005) 105(7):2924–32. doi: 10.1182/blood-2004-10-3820
39. Mourcin F, Verdiére L, Roulois D, Amin R, Lamaison C, Sibut V, et al. Follicular Lymphoma Triggers Phenotypic and Functional Remodeling of the Human Lymphoid Stromal Cell Landscape. *Immunity* (2021) 54(8):1788–806.e7. doi: 10.1016/j.immuni.2021.05.019
40. Attridge K, Kenefeck R, Wardzinski L, Qureshi OS, Wang CJ, Manzotti C, et al. IL-21 Promotes CD4 T Cell Responses by Phosphatidylinositol 3-Kinase–Dependent Upregulation of CD86 on B Cells. *J Immunol* (2014) 192(5):2195–201. doi: 10.4049/jimmunol.1302082
41. Good KL, Avery DT, Tangye SG. Resting Human Memory B Cells Are Intrinsically Programmed for Enhanced Survival and Responsiveness to Diverse Stimuli Compared to Naive B Cells. *J Immunol* (2009) 182(2):890–901. doi: 10.4049/jimmunol.182.2.890
42. Weskamp G, Ford JW, Sturgill J, Martin S, Docherty AJP, Swendeman S, et al. ADAM10 Is a Principal "Sheddase" of the Low-Affinity Immunoglobulin E Receptor CD23. *Nat Immunol* (2006) 7(12):1293–8. doi: 10.1038/ni1399
43. Lemieux GA, Blumenkron F, Yeung N, Zhou P, Williams J, Grammer AC, et al. The Low Affinity Ige Receptor (CD23) Is Cleaved by the Metalloproteinase ADAM10*. *J Biol Chem* (2007) 282(20):14836–44. doi: 10.1074/jbc.M608414200
44. Liu B, Lin Y, Yan J, Yao J, Liu D, Ma W, et al. Affinity-Coupled CCL22 Promotes Positive Selection in Germinal Centres. *Nature* (2021) 592 (7852):133–7. doi: 10.1038/s41586-021-03239-2
45. Finkin S, Hartweger H, Oliveira TY, Kara EE, Nussenzweig MC. Protein Amounts of the MYC Transcription Factor Determine Germinal Center B Cell Division Capacity. *Immunity* (2019) 51(2):324–36.e5. doi: 10.1016/j.immuni.2019.06.013
46. Gitlin AD, Shulman Z, Nussenzweig MC. Clonal Selection in the Germinal Centre by Regulated Proliferation and Hypermutation. *Nature* (2014) 509 (7502):637–40. doi: 10.1038/nature13300
47. Ochiai K, Maienschein-Cline M, Simonetti G, Chen J, Rosenthal R, Brink R, et al. Transcriptional Regulation of Germinal Center B and Plasma Cell Fates by Dynamical Control of IRF4. *Immunity* (2013) 38(5):918–29. doi: 10.1016/j.immuni.2013.04.009
48. Nutt SL, Hodgkin PD, Tarlinton DM, Corcoran LM. The Generation of Antibody-Secreting Plasma Cells. *Nat Rev Immunol* (2015) 15(3):160–71. doi: 10.1038/nri3795
49. Emslie D, D'Costa K, Hasbold J, Metcalf D, Takatsu K, Hodgkin PO, et al. Oct2 Enhances Antibody-Secreting Cell Differentiation Through Regulation of IL-5 Receptor α Chain Expression on Activated B Cells. *J Exp Med* (2008) 205(2):409–21. doi: 10.1084/jem.20072049
50. Gallou SL, Caron G, Delaloy C, Rossille D, Tarte K, Fest T. IL-2 Requirement for Human Plasma Cell Generation: Coupling Differentiation and Proliferation by Enhancing MAPK-ERK Signaling. *J Immunol* (2012) 189 (1):161–73. doi: 10.4049/jimmunol.1200301
51. Hipp N, Symington H, Pastoret C, Caron G, Monvoisin C, Tarte K, et al. IL-2 Imprints Human Naive B Cell Fate Towards Plasma Cell Through ERK/ELK1-Mediated BACH2 Repression. *Nat Commun* (2017) 8(1):1443. doi: 10.1038/s41467-017-01475-7
52. Olteanu H, Fenske TS, Harrington AM, Szabo A, He P, Kroft SH, et al. CD23 Expression in Follicular Lymphomaclinicopathologic Correlations. *Am J Clin Pathol* (2011) 135(1):46–53. doi: 10.1309/AJCP27YWLIQRAJPW

Conflict of Interest: The authors declare that the research was conducted in the absence of any commercial or financial relationships that could be construed as a potential conflict of interest.

Advantages of publishing in Frontiers

OPEN ACCESS
Articles are free to read for greatest visibility and readership

FAST PUBLICATION
Around 90 days from submission to decision

HIGH QUALITY PEER-REVIEW
Rigorous, collaborative, and constructive peer-review

TRANSPARENT PEER-REVIEW
Editors and reviewers acknowledged by name on published articles

Frontiers
Avenue du Tribunal-Fédéral 34
1005 Lausanne | Switzerland

Visit us: www.frontiersin.org
Contact us: frontiersin.org/about/contact

REPRODUCIBILITY OF RESEARCH
Support open data and methods to enhance research reproducibility

DIGITAL PUBLISHING
Articles designed for optimal readership across devices

FOLLOW US
@frontiersin

IMPACT METRICS
Advanced article metrics track visibility across digital media

EXTENSIVE PROMOTION
Marketing and promotion of impactful research

LOOP RESEARCH NETWORK
Our network increases your article's readership